Tectonic evolution of the Himalayas constrained by a detrital investigation of the Siwalik Group molasse in SW Nepal.

A.G. Szulc

Joint PhD
The University of Edinburgh
and The Université Joseph Fourier, Grenoble
2005



Declaration of originality

This thesis, composed by A.G. Szulc, represents the author's own work and has not been submitted for any other degree or professional qualification.

Signed:

A.G. Szulc

Abstract

In order to constrain models for Himalayan evolution three contemporaneous Neogene molasse deposits of the Siwalik Group were sampled at 1 Myr intervals for ^{40}Ar-^{39}Ar dating of single white micas, petrography/heavy mineral analysis, and whole-rock Nd-Sr geochemistry. The sedimentary successions are exposed in three road and river sections through the Sub-Himalayan Zone of central-southern Nepal (from east to west: Tinau Khola section (12-6.3 Ma), Surai Khola section (12-1 Ma), and Karnali section (16-5 Ma)). Whilst providing further insight into the exhumation history of the central Himalayas, the work was designed to test the consistency of detrital signals between the three time-equivalent sections. Fission-track dating of zircons and apatites from Ordovician aged samples within the Main Boundary Thrust sheet was also carried out for the purpose of timing movement along the structure. The Siwalik Group in Nepal conforms well with descriptions of the succession throughout the length of the Himalayan foreland basin. From bottom to top the Siwaliks consist of mudstones, sandstones and conglomerates, representing distal to proximal deposition within a fluvial fan environment. Laser fusion ^{40}Ar-^{39}Ar ages from 1415 single detrital white micas show a peak of ages between 20-15 Ma with a mode of 16.8 Ma, corresponding to the period of most extensive exhumation of the Greater Himalaya. The shortest lag-time (host sediment depositional age minus mineral cooling age) occurs in sediment deposited at 16 Ma, reflecting the 16.8 Ma mode. Lag-times of less than 5 Myr persist until 10 Ma, indicating Greater Himalayan exhumation rates of up to 2.6 mm/yr using 1D thermal modelling. There are few micas younger than 12 Ma, no lag-times of less than 5 Myr after 10 Ma, and a significant provenance change at 12 Ma (as indicated by petrography and geochemistry data) indicating erosion from the Lesser Himalaya at this time. These changes suggest that a switch in the dynamics of the orogen took place during the 12-10 Ma period whereby most strain began to be accommodated by structures within the Lesser Himalaya rather than the Main Central Thrust-South Tibetan Detachment system. The increased sediment flux from the new area of uplift above the Lesser Himalayan Duplex resulted in a rapid increase in sedimentation rates across the foreland basin and the Bay of Bengal between 11-9 Ma. My conclusions are supported by consistent data from all three sections, suggesting a lateral continuity in tectonic evolution for the central Himalayas and the absence of geomorphic processes that can hinder the use of the detrital technique to unravel hinterland tectonism, such as sediment ponding and drainage diversion.

Résumé

Dans le but de contraindre des modèles d'évolution de la Chaîne de l'Himalaya, trois dépôts molassiques contemporains et d'âge néogène ont été échantillonnés au niveau du groupe des Siwaliks, suivant des intervalles de temps de 1 Ma. Ont été effectuées à partir de cet échantillonnage diverses études analytiques: datations ^{40}Ar-^{39}Ar sur minéraux séparés de micas blancs, études pétrographique et minéralogique sur minéraux lourds ainsi que des analyses isotopiques Sr et Nd sur roche totale. Les successions sédimentaires sont exposées suivant trois profils au niveau de routes et rivières à travers la zone Sub-Himalayenne du Népal du Centre et du Sud (d'Est en Ouest: coupes de Tinau Khola (12 - 6,3 Ma), Surai Khola (12 – 1 Ma) et Karnali (16 – 5 Ma)). Bien que cette étude fournisse de nouveaux apports quant à la compréhension des processus d'exhumation de l'Himalaya Central, son but était de tester la cohérence des signaux détritiques entre ces trois profils de même âge. La datation par traces de fission de zircons et apatites provenant d'échantillons d'âge Ordovicien, prélevés au sein de la nappe du MBT a également été réalisée afin de contraindre l'évolution temporelle des mouvements verticaux le long de la structure. Le Groupe des Siwaliks au Népal est en bonne conformité avec les successions décrites le long du bassin d'avant-pays Himalayen. De bas en haut, les Siwaliks sont constitués d'argiles, grès et conglomérats, correspondant aux dépôts distaux à proximaux d'un cône de déjection. Des âges ^{40}Ar-^{39}Ar réalisés par fusion laser sur 1415 minéraux de micas blancs montrent des pics d'âges entre 15 et 20 Ma, avec un mode pour 16,8 Ma. Des décalages temporels de moins de 5 millions d'années persistent jusqu'à 10 Ma, indiquant ainsi des taux d'exhumation du Greater Himalaya de plus de 2,6 mm/an estimés par modélisation thermique 1D. Il y a peu de micas plus jeunes que 12 Ma, pas de décalages temporels de moins de 5 millions d'années après 10 Ma, et un changement significatif de leur provenance se produit à 12 Ma, démontrant un processus d'érosion du Lesser Himalaya actif à cette période (à partir de données pétrographiques et géochimiques). Ces variations suggèrent qu'un changement dans la dynamique de l'orogène s'est produit entre 12 et 10 Ma alors que la plupart des contraintes commençaient à être accomodées par les structures au sein du Lesser Himalaya plutôt qu'au niveau du détachement MBT-Sud Tibet. L'augmentation du flux sédimentaire depuis la nouvelle zone de soulèvement au-dessus du duplex du Lesser Himalaya résulta en une augmentation rapide des taux de sédimentation au sein du bassin d'avant-pays et de la Baie du Bengale entre 11 et 9 Ma. Nos conclusions sont confirmées par l'obtention de données cohérentes sur l'ensemble des trois profils, suggérant une continuité latérale dans l'évolution tectonique de l'Himalaya Central. Elles sont également validées par l'absence de processus géomorphologiques qui pourraient entraver l'utilisation de techniques d'analyses sur minéraux détritiques pour comprendre la tectonique d'arrière-pays, par exemple la formation de lacs par accumulations sédimentaires et des divergences de drainages.

CONTENTS

1. INTRODUCTION 1

1.1. Context 1

1.2. Aims and objectives 2

1.3. The detrital technique 5
1.3.1. Advantages 5
1.3.2. Development 6
1.3.3. Application to the Himalayas 8

1.4. Overview of Himalayan evolution 13

1.5. Field area – SW Nepal 17

1.6. Methods and materials 19

Figures 21-30

Plates 31-32

2. BACKGROUND GEOLOGY 33

2.1. Introduction 33

2.2. Tibetan Himalayan Zone 34
2.2.1. Lithologies 34
2.2.2. Structure 36
2.2.3. The South Tibetan Detachment 37
2.2.4. The North Himalayan Gneiss Domes 38

2.3. Greater Himalayan Zone 41
2.3.1. Lithologies 41
2.3.1.1. Formation I 42
2.3.1.2. Formation II 42
2.3.1.3. Formation III 43
2.3.1.4. Leucogranites 43
2.3.1.5. Greater Himalayan protolith 45
2.3.2. Tectono-metamorphic history 46

2.4. Main Central Thrust **51**

2.5. Lesser Himalayan Zone **57**
2.5.1. Inner and Outer Lesser Himalaya 59
2.5.2. Crystalline Thrust Sheets 60
2.5.3. Lesser Himalayan Duplex 63

2.6. Main Boundary Thrust **64**

2.7. Sub-Himalayan Zone **67**

2.8. Main Frontal Thrust **69**

2.9. Foreland basin sediments **70**
2.9.1. Palaeogene sediments 70
2.9.1.1. Unconformity *73*
2.9.2. Neogene sediments 75

Figures **77-90**

Plates **91**

3. THE HIMALAYAN FORELAND BASIN AND DRAINAGE SYSTEM **92**

3.1. Introduction **92**

3.2. Provenance limitations **94**

3.3. Foreland basin morphology **95**
3.3.1. Present drainage configuration 97
3.3.1.1. Field area *99*

3.4. Himalayan drainage through time **101**

3.5. Modelling drainage evolution using ArcInfo **106**
3.5.1. Introduction 106
3.5.2. Limitations 110
3.5.3. Previous Work 111
3.5.4. Methodology 116
3.5.5. Results 116
3.5.6. Discussion 118

3.6. Conclusion **121**

Figures **122-128**

4. SEDIMENTOLOGY **129**

4.1. Introduction **129**
4.1.1. Siwalik Group subdivisions 129

4.2. Previous work **130**
4.2.1. Modern and ancient fluvial system 131
4.2.2. Facies characteristics in Nepal 133
4.2.3. Sedimentation rates 134

4.3. Magnetostratigraphy problems **136**
4.3.1. General sources of error 136

4.4. Results **139**
4.4.1. Facies type 1. 140
4.4.1.1. Facies type 1. interpretation (small channel facies) *141*
4.4.2. Facies type 2. 142
4.4.2.1. Facies type 2. interpretation (palaeosol facies) *143*
4.4.3. Facies type 3. 144
4.4.3.1. Facies type 3. interpretation (crevasse splay facies) *145*
4.4.4. Facies type 4. 146
4.4.4.1. Facies type 4. interpretation (floodplain facies) *146*
4.4.5. Facies type 5. 147
4.4.5.1. Facies type 5. interpretation (meandering channel facies) *149*
4.4.6. Facies type 6. 150
4.4.6.1. Facies type 6. interpretation (braided channel facies) *151*

4.5. Palaeoflow **153**

4.6. Facies models **156**

4.7. Provenance **160**

4.8. Sedimentation rates **162**
4.8.1. Comparison with Himalayan erosion rates 163

Figures **165-173**

Plates **174-181**

5. PETROGRAPHY AND HEAVY MINERALS **182**

5.1. Introduction **182**

5.2. Limitations **182**

5.3. Previous work **183**

5.3.1. Timing of India-Eurasia collision 183
5.3.2. Himalayan evolution 186

5.4. Methodology **191**

5.5. Results **192**
5.5.1. Modern rivers 194

5.6. Discussion **195**
5.6.1. Modern Rivers 198
5.6.2. Comparison with Siwalik sediments along-strike 199

Figures **201-205**

6. GEOCHEMISTRY **206**

6.1. Introduction **206**

6.2. Limitations **207**

6.3. Previous Work **208**
6.3.1. Depositional relationships 208
6.3.2. Structural mapping 209
6.3.3. Provenance and tectonic evolution 210
6.3.4. Climate 212
6.3.4.1. Global seawater geochemistry *212*

6.4. Methodology **215**

6.5. Results **216**

6.6. Discussion **220**

Figures **223-229**

7. ^{40}AR-^{39}AR THERMOCHRONOLOGY **230**

7.1. Introduction **230**

7.2. The lag-time concept **233**

7.3. Limitations **234**
7.3.1. Transport times 235
7.3.2. Number of grains 236
7.3.3. Interpretation of ages 237

7.3.4. Types of white mica 238
7.3.5. Geothermal gradient 239
7.3.6. Closure temperature 241

7.4. Previous work **241**
7.4.1. Exhumation studies 241
7.4.1.1. Modern Rivers *245*
7.4.2. Other uses of detrital ^{40}Ar-^{39}Ar ages 245

7.5. Methodology **247**

7.6. Results **248**
7.6.1. Tinau Khola section 250
7.6.2. Surai Khola section 251
7.6.3. Karnali section 251

7.7. Discussion **252**

Figures **255-266**

8. FISSION-TRACK DATING **267**

8.1. Introduction **267**

8.2. Limitations **268**

8.3. Methodology **270**

8.4. Results **271**

8.5. Discussion **274**

Figures **278-281**

9. DISCUSSION AND CONCLUSIONS **282**

9.1. Introduction **282**
9.1.1. Provenance of the Siwalik Group 282
9.1.2. Exhumation of Siwalik Group source area 286
9.1.3. Drainage evolution 290

9.2. Conclusions - Neogene evolution of the Himalayas **291**

9.3. Further work **293**

Figures 294-296

Acknowledgements 297

Bibliography 298-344

Appendix 345
I Sample lists 346-351
II ArcInfo Aml's 352-353
III Detailed logs 354-424
IV Whole-rock Nd-Sr geochemistry notes 425-426
V ^{40}Ar-^{39}Ar dating notes 427-429
VI Fission-track dating notes 430-431

CD in back cover includes: Petrography and heavy mineral data file
Petrography and heavy mineral key file
All mica ages file
Step-heating data file
Papers folder
Thesis (digital copy)

1. Introduction

1.1. Context

The Himalaya-Tibet orogenic system is the planet's most exquisite example of continent-continent collision. Boasting the highest peaks, the largest terrestrial foreland basin, the greatest submarine fans, and some of the most active tectonics on the planet, the Himalayas represent an unrivalled opportunity for understanding the orogenic process. Whilst being the type example on which our geodynamic models of crustal deformation and strain accommodation are based, the Himalayas are also held responsible for major changes in late Cretaceous and Cenozoic oceanography, climate, and faunal extinctions (Flynn & Jacobs, 1982; Barry et al., 1985; Prell et al., 1988; Awasthi & Prasad, 1989; Kroon et al., 1991; Prell & Kutzbach, 1992; Raymo & Ruddiman, 1992; Burbank et al., 1993; Harrison et al., 1993; Kutzbach et al., 1993; Beck et al., 1995; Quade et al., 1989, 1995, 1997; Konomatsu, 1997; Dettman et al., 2001). They therefore offer an important insight into the profound effect mountain building has on the planet. The key to understanding the feedback between mountain growth, climate and oceanography is the bulk-rock kinematic history of the Himalayan thrust belt and the evolving distribution of rock-types and sediment sources. Determination of the timing and rates of vertical tectonic activities are also fundamental to the assessment of virtually all geophysical processes during orogeny. Various ideas have been proposed for the tectonic evolution of the Himalayas based on bedrock studies (e.g. Coward & Butler, 1985; England & Houseman, 1988, 1989; Searle, 1991; Schelling, 1992; Zhao et al., 1993; Ratschbacher et al., 1994; Srivastava & Mitra, 1994; Hauck et al., 1998; Hodges, 2000; Beaumont et al., 2001;

DeCelles et al., 2001; Tapponnier et al., 2001; Robinson et al., 2003). However, a single robust model has yet to be realised. Since each evolutionary model makes different predictions regarding the timing of uplift and consequent denudation, a possible key to distinguish when these various mechanisms operated may be locked within foreland basin sedimentary deposits. Analysis of this sedimentary fill with the purpose of constraining tectonic, geomorphologic, or climatic models for the Himalayas comes under the auspices of the detrital technique.

The Ganges River and its tributaries which flow across northern India to debouch into the Bay of Bengal are the modern equivalents of a drainage network that for ~ 45 Ma (DeCelles et al., 1998a) has transported well-mixed detritus from all tectonic zones of the central Himalayas across the adjacent foreland basin. Because the Himalayas are a young, currently active mountain belt, this syntectonic molasse has been well preserved. The molasse is also easily accessible, being gradually uplifted and exposed as the fold-thrust belt encroaches on the foreland basin. Furthermore, determining the provenance of this sediment is made easier by the fact that the Himalayas are zoned in terms of lithology, age and geochemistry (Fig. 1.1.). All of these factors make the Himalayas ideally suited to the detrital technique.

1.2. Aims and objectives

The aim of this thesis is to place constraints on Himalayan evolutionary models by providing further information about the timing, rates, and episodicity of uplift and erosion as preserved in syntectonic foreland basin sediments exposed in SW Nepal. ^{40}Ar-^{39}Ar dating of single detrital white micas (Chapter 7), petrography (Chapter 5),

and whole-rock Nd-Sr geochemistry (Chapter 6) have been employed with the objective of deducing the provenance of these sediments and to decipher the sequence of tectonic reorganisation that the relevant source areas underwent. When compared with host sediment depositional ages (determined by magnetostratigraphy; Ojha et al., 2001; Gautam & Fujiwara, 2000; Ojha, personal communication, 2002) ^{40}Ar-^{39}Ar dating of single detrital white micas provides information about source-area exhumation rates. Petrography and whole-rock geochemistry allow an assessment of when rocks with characteristic composition or geochemical signatures were first exposed in the hinterland. Detailed sedimentologic investigation of the Siwalik Group (Chapter 4) also forges a direct link between hinterland thrust emplacement and the foreland basin sedimentary response.

I focus on three contemporaneous sections, calibrated using magnetostratigraphy (Ojha, personal communication, 2002; Gautam & Fujiwara, 2000), through the Siwalik Group molasse (Tinau Khola (12-6.3 Ma), Surai Khola (12-1 Ma), and Karnali (16-5 Ma)). Analyses were performed on samples taken at 1 Myr intervals along each section (see Appendix I for sample list). The sections are at least catchment-width apart in an attempt to highlight possible lateral variations in the detrital signal. Such variation could reflect sediment ponding or drainage diversion rather than tectonics. Therefore, incorporating three along-strike sections adds weight to my interpretations and provides a test of the technique which has been absent from similar previous studies. This is linked to a study of the modern-day controls on drainage diversion adjacent to the foreland basin (Chapter 3), a process that has the potential to hamper the detrital approach by producing local tectonic

signal anomalies. I focus on modelling the controls governing river capture behind thrust-cored anticline uplift along the front of the range. A better understanding of the modern fluvial system will allow a deeper understanding of the ancient fluvial sedimentary record.

The detrital investigation is combined with fission-track dating from hinterland bedrock with the objective of constraining the history of displacement across a major Himalayan structure (the Main Boundary Thrust) (Chapter 8). This was designed to complement the Siwalik study with the possibility of a correlation between fission-track ages and a shift in detrital signals.

Crucial questions concerning the Himalayas are when rapid exhumation of the metamorphic core (Greater Himalayan Zone) ceased and thrusting was transferred south to the Lesser Himalayan Zone and whether or not there has been recent reactivation of the Main Central Thrust. The time frame of Siwalik deposition (~ 16 Ma to recent) focuses this effort on the Neogene history of the Main Central Thrust and Main Boundary Thrust and the exhumation of their hanging wall lithologies, comprising the Greater and Lesser Himalayan Zones respectively. Analysis of Siwalik Group rocks therefore offers an insight into two of the most important structural features accommodating collision during the Neogene.

This work provides new insight into the timing, rates, and source of uplift of the central Himalayas during the Neogene whilst emphasising the utility of the detrital approach with regard to understanding hinterland tectonics in general. Additionally, comparing these results with previous detrital studies, focused mainly in the western

Himalayas, enables a greater appreciation of any lateral variation or otherwise in the tectonic evolution of the mountain belt. By combining numerous catchment-scale detrital investigations along-strike an orogen-wide understanding of Himalayan evolution can be constructed.

1.3. The detrital technique

1.3.1. Advantages

The sedimentary fill of a foreland basin reflects the evolution of the fold-thrust belt to which it is genetically linked. This record is not only potentially inaccessible in hinterland bedrock due to extreme relief, vegetation, or glaciation, but is also gradually lost through either denudation or metamorphism. Furthermore, whilst traditional bedrock studies enable an accurate assessment of structural characteristics and exhumation history, they are restricted to particular regions. Such limitations can be potentially side-stepped by applying the same techniques to sediment that has been shed from the growing mountain belt throughout its evolution (Fig. 1.2.). Therefore the detrital technique can offer a unique contribution to orogenic studies because sediment derived from either a local or regional area can be sampled with ease, eliminating the restrictions of bedrock inaccessibility. Because sediment can be sampled at various stratigraphic ages, the constituent minerals represent the rocks that were exposed on the hinterland surface at those particular times. Additionally, long transport distances mean foreland basin deposits often preserve a well-mixed average of sediment generated by collisional orogenic belts. Detrital thermochronology can therefore potentially encapsulate the full spectrum of bedrock

cooling ages in a particular catchment (Brandon & Vance, 1992; Garver et al., 1999). In one catchment study, it is thus possible to obtain detailed information regarding the evolution of a considerable region of hinterland through time. Furthermore, analysis of the environment of deposition of the foreland basin sediments provides a direct link between tectonics, surface processes and climate. The morphology of bedrock rivers are directly coupled with orogenic style and both are heavily influenced by the prevailing climatic conditions. The detrital technique therefore encompasses previously isolated disciplines whilst complementing traditional bedrock studies.

1.3.2. Development

Molasse deposits have long been recognised as important in the analysis of orogenic histories (Allen et al., 1986 and references therein). Indeed, the utility of sediments in establishing a tectonic context for basin development is evidenced by the continuing refinements of techniques to decipher this record (e.g. Dickinson, 1974; Ingersoll, 1988). Initial studies were concerned with determining the provenance of the sediment in question. This is fundamental if tectonic interpretations derived from a detrital investigation are to be tied to a specific hinterland area. It was found that quantitative analysis of sandstone petrography (by point counting of thin sections) can be used to determine the tectonic setting and provenance of foreland basin sediments (Dickinson, 1974; Graham et al., 1976; Dickinson & Valloni, 1980; Dickinson, 1985). Whilst bulk detrital modes are indicative of provenance, the occurrence of different clast types or diagnostic heavy mineral assemblages in the sedimentary succession allows an evaluation of the hinterland unroofing history as

deeper structural levels are brought to the surface. In this way orogenic molasse can provide insight into the timing of uplift and metamorphic history of a particular source region.

Following the success of petrographic studies other methods were soon added to the detrital technique repertoire. Pearce & Cann (1971, 1973) were the first to utilise the geochemistry of volcanic rocks to discriminate their original tectonic environment. This approach was subsequently expanded to include sedimentary rocks whereby detrital whole-rock geochemistry was found to be a useful provenance tool (Schwab, 1986 and references therein). Trace elements and rare earth elements (REE) in particular have very low concentrations in sea and river waters, low residence times in the ocean and element ratios which are unaffected by diagenesis and metamorphism (Rollinson, 1993). They are thus transported exclusively in the terrigenous component of a sediment and reflect the chemistry of their source (Fleet, 1984; McLennan, 1989). In cases where the hinterland has distinct variations in regional geochemical signatures the provenance of foreland sediments can be well constrained. An important study by Cullers et al. (1987), on the effect of sedimentary sorting on REE concentrations, found that the REE pattern of the source was most faithfully represented in the clay-sized fraction of sediment. The majority of subsequent work has therefore focused on fine-grained lithologies. Nesbitt et al. (1990) also found that the major and trace element chemistry of modern muds reflects the degree of weathering in their source and so the composition of ancient muds could be used to infer past weathering conditions.

Detrital thermochronology relies on techniques that allow the dating of single grains. With the advent of high-sensitivity isotopic techniques, it became possible to date grains in relatively fine-grained rocks to reveal isotopic variations with high precision. Individual detrital grains were therefore able provide information regarding the age of the source and its cooling history (e.g. Froude et al., 1983). Whilst there are numerous methods, the most commonly used are U-Pb dating of zircon (e.g. DeCelles et al., 1998b, 2000); $^{40}Ar/^{39}Ar$ dating of white mica (e.g. Copeland & Harrison, 1990; Harrison et al., 1993; Najman et al., 1997; White et al., 2002), and fission-track dating of apatite and zircon (e.g. Cerveny et al., 1988; Garver et al., 1999; Carter et al., 2000).

1.3.3. Application to the Himalayas

The detrital techniques described previously have all been successfully applied to the Himalayas (Fig. 1.3.). Conventional analysis of bulk-composition detrital modes has proved a powerful tool in reconstructing Himalayan evolution (e.g. Garzanti et al., 1996). Other studies have utilised the variability of detrital Nd-Sr isotopic values as an additional provenance tool and a means to infer the timing of uplift of hinterland source areas (e.g. France-Lanord et al., 1993; Najman et al., 2000; Huyghe et al., 2001; Robinson et al., 2001). Detrital thermochronology, particularly ^{40}Ar-^{39}Ar dating of white mica, has helped to determine when periods of rapid Himalayan exhumation occurred and to quantify exhumation rates through time (e.g. White et al., 2002).

The first comprehensive model to describe the relationships between tectonism and sedimentation in the Himalayas was proposed by Curray & Moore (1971) and Graham et al. (1975) who envisaged long distance dispersal of detritus from the suture belt through foreland basins and remnant-ocean basins. Since then a number of successful investigations have used molasse and flysch detritus as a proxy for understanding the timing and rates of tectonic events within the hinterland (e.g. Cerveny et al., 1988; Copeland & Harrison, 1990; Harrison et al., 1993; Najman et al., 1993, 1997, 2001; Garzanti et al., 1996; Huyghe et al., 2001; White et al., 2002). These studies have both supported previous models based on bedrock investigations and broken new ground where bedrock data has proved insufficient in elucidating a precise tectonic history. Whilst providing insight into the timing and rates of uplift of specific source areas, Himalayan detritus has also been fundamental in deriving an accurate age for India-Eurasia collision and assessing its potential diachroneity (Rowley, 1996; DeCelles et al., 2004).

Many detrital studies have focused on the Indus Molasse (e.g. Garzanti & Van Haver, 1988; Searle et al., 1990; Sinclair & Jaffey, 2001). This is a pre- and syn-tectonic sedimentary sequence situated in the suture zone of the western Himalaya. Because sedimentation took place during collision these deposits are well placed to record the evolving uplift and erosion history of the incipient orogen. Garzanti and Van Haver (1988) studied the petrography and geochemistry of the Indus Molasse and underlying successions, and demonstrated that in latest Palaeocene times (start of Indus Molasse deposition) there was a transition from marine to predominantly continental sedimentation. The final termination of marine sedimentation in early

Eocene times is interpreted to record the initiation of continental collision (Searle et al., 1987). Clift et al. (2001) combined Pb isotopic analysis of K-feldspars with Nd analysis of clay to help constrain the source of the Indus Molasse. Nd isotope signatures vary greatly between Himalayan tectonic zones as do the isotopic compositions of K-feldspars, reflecting differing degrees of recycling of older continental crust during petrogenesis. They conclude that a post-collisional change in palaeoflow and provenance reflects the initiation of the Indus River during the Early Eocene. The same approach was used by Clift et al. (2002) on sand from the tributaries of the modern Indus River in northern Pakistan to ascertain source areas for the sediment. They found that the inferred source areas reflected both the area and modern uplift rates within the drainage basin.

The Indus and Bengal Fans have proved fertile ground for the detrital technique. Ingersoll & Suczek (1979) analysed the petrology of the Bengal Fan to determine its provenance. Suczek & Ingersoll (1985) applied the same approach to the Indus Fan. Copeland & Harrison (1990) conducted ^{40}Ar-^{39}Ar dating of single detrital K-feldspar and white mica grains from the Bengal Fan. From the ages they concluded that the Himalayas were undergoing rapid uplift at some point within the orogen throughout the last 18 Ma. Based on the ratio of calcic amphibole grains in total heavy minerals from Bengal Fan cores, Amano & Taira (1992) suggest this uplift was expressed in two main pulses, the first between 10.9 and 7.5 Ma and the second after 0.9 Ma. Further evidence for uplift episodicity was found by Hovan & Rea (1992) who estimated mass sediment accumulation rates for the Bengal Fan and found a sharp increase in influx after 12 Ma, with two depositional pulses between 9-6 Ma, and

between 4-2 Ma which they attribute to Himalayan uplift. France-Lanord et al. (1993) applied Sr, Nd, O, and H isotopic analyses and calculated clay mineral abundances for Bengal Fan sediments. They found that Sr (~ 0.741), ε_{Nd} (~ -16), and $\delta^{18}O$ (~ 12.8 ± 0.5 ‰) values define a narrow range over the past 18 Ma and concluded that the source of the sediments had not changed since the Early Miocene. This conclusion requires the Himalayas to have been a significant topographic feature since at least the Early Miocene, and is supported by subsequent detrital work (Galy et al., 1996; Derry & France-Lanord, 1996). France-Lanord & Derry (1994) analysed $\delta^{13}C$ in organic matter from the Bengal Fan and found that C_4 plants became abundant in the source area after 7 Ma, a change which may have required a climatic shift.

Whilst Indus and Bengal Fan studies give insight into the Himalayas as a whole, more focused single catchment studies within the foreland are required to limit the number of potential source areas and therefore provide greater detail for particular hinterland regions. Several studies have therefore focused on sections through foreland basin sediments closer to the mountain range. The most complete stratigraphic record is exposed in the NW Himalaya, preserved within structural re-entrants. Therefore most detrital work has focused on that region, including the pioneering fission-track study by Cerveny et al. (1988) which reported evidence for rapid exhumation of the Himalayas in northern Pakistan during the last few million years. Critelli & Garzanti (1994) used the petrography of Himalayan molasse in the Kashmir-Hazara Syntaxis to infer the early stages of orogenic development. In a similar study further east in India Najman & Garzanti (2000) used petrographic

analysis of foreland basin sediments to constrain the timing of India-Eurasia collision and foreland basin development. White et al. (2002) combined detrital petrography, geochemistry, and thermochronology techniques in a study of Indian foreland basin sediments to provide a more complete picture of provenance and hinterland evolution.

Although the majority of Himalayan detrital work has been carried-out in Pakistan and India, recent palaeomagnetic work has calibrated some of the better-exposed sections in Nepal and thus made them amenable to detrital investigation (e.g. Johnson et al., 1982, 1985; Appel et al., 1991; Gautam & Appel, 1994; Roesler et al., 1997; Roesler & Appel, 1998; Gautam & Fujiwara, 2000; Ojha personal communication 2002). Among these studies much detrital work has been conducted on the three sections that are the focus of this thesis: Tinau Khola (Dahal et al., 1997; Tanaka, 1997; Konomatsu & Awasthi, 1999; Ulak & Nakayama, 2001), Surai Khola (Awasthi & Prasad, 1989; Sarkar, 1989; Prasad & Awasthi, 1994; Quade et al., 1995; Kotlia & Mathur, 1997; DeCelles et al., 1998b; Sah, 1998; Gurung, 1998; Nakayama & Ulak, 1999; Tamrakar, 2000; Hoorn et al., 2000; Corvinus & Rimal, 2001; Robinson et al., 2001), and Karnali (Huyghe et al., 2001). Harrison et al. (1993) conducted ^{40}Ar-^{39}Ar dating of detrital K-feldspars on the Siwalik Group (Bakiya Khola section) in south-central Nepal and found evidence for rapid exhumation of the source area between 11-5 Ma. Robinson et al. (2001) were the first to conduct isotopic studies within foreland basin sediments. This helped to establish the value of Nd isotopes in distinguishing between lithotectonic zones and permitted an estimation of the timing of exposure of these zones in the hinterland. Further

geochemical work on the Siwalik Group of Nepal has enabled an estimation of the tectonic evolution of the hinterland (e.g. Huyghe et al., 2001). Quade et al. (1997) found a rise in the $^{87}Sr/^{86}Sr$ ratio of pedogenic carbonate nodules within foreland basin sediments of Nepal at ~ 9 Ma which has been related to the tectonic evolution of the hinterland (DeCelles et al., 2001). Additionally, carbon isotope studies of these sediments indicate a biomass transition from C_3 ($\delta^{13}C$: c. -10.5 ‰) to C_4 ($\delta^{13}C$: c. 0 ‰) plants between 7-8 Ma (Harrison et al., 1993; Quade et al., 1995). Quade et al. (1995) interpret this as a shift from semitropical evergreen forests to monsoonal grasslands. A major climate change like this has important implications for tectonic models of the Himalaya and also the timing of Tibetan Plateau uplift.

1.4. Overview of Himalayan evolution

At ~ 52 Ma the northern margin of the Indian continental plate collided with the Andean-type southern margin of Eurasia (Garzanti et al., 1987, 1996; Klootwijk et al., 1992; DeCelles et al., 2004). The consequent Himalayan mountain chain has accommodated an estimated one-third to one-half (Hodges, 2000 and references therein) of the ~ 1800-2750 km of post-collision shortening between India and Eurasia (Dewey et al., 1989). Following closure of the Tethys Ocean and subduction of the Indian plate beneath Eurasia, orogenesis involved southwards progression of thrusting and exhumation. This has divided the fold-thrust belt into a series of NW to SE-trending lithotectonic zones (Gansser, 1964; Valdiya, 1980). These zones and their fault boundaries can be traced the full ~ 2500 km along the length of the orogen (Fig. 1.1. & 1.4.).

Starting in the north, the site of collision is marked by the Indus-Yarlung Suture Zone which contains ophiolites and flysch material as exposed in Ladakh, NW India (Searle, 1983; Garzanti & Van Haver, 1988). These were thrust southwards onto the north Indian passive continental margin, represented by the Tibetan Himalayan Zone (Garzanti, 1999). The Tibetan Himalayan Zone is a fold and thrust belt and in the Zanskar Range of NW India it contains Proterozoic metasediments, Cambro-Ordovician granitoids and Palaeozoic and Mesozoic sediments (Fuchs, 1982; Gaetani & Garzanti, 1991). Work in Tibet suggests thrusting and uplift of these rocks took place during Eocene to early Miocene time (Searle, 1991; Ratschbacher et al., 1994) and eclogite facies metamorphism had occurred by 49 Ma in northern Pakistan (Pognante & Spencer, 1991; Tonarini et al., 1993). Extension within this compressional setting also facilitated the development of a series of metamorphic core complexes (The North Himalayan Gneiss Domes) within the Tibetan Himalaya (Chen et al., 1990; Lee et al., 1999). This extension also resulted in a series of low-angle north-dipping normal detachment faults in southern Tibet collectively referred to as the South Tibetan Detachment along the southern boundary of the Tibetan Himalayan Zone (Searle, 1995). These faults place Palaeozoic sediments at the base of the Tibetan Himalaya on top of high-grade Greater Himalayan Zone gneisses. The South Tibetan Detachment accommodates several tens of km of top-to-the-north displacement and was active from ~ 22 Ma to ~ 16 Ma or younger (Burg & Chen, 1984; Burchfiel et al., 1992; Coleman, 1996; Hodges et al., 1994; 1996; Searle et al., 1997; Dezes et al., 1999; Walker et al., 1999; Searle & Godin, 2003).

South of the South Tibetan Detachment the Greater Himalayan Zone comprises medium- to high-grade gneiss and leucogranites, forming the metamorphic core of the Himalayas. Multiple phases of thrusting and normal faulting (often synchronous) have been documented within the Greater Himalaya of Nepal (Searle, 1999), which was thrust southwards over the Lesser Himalayan Zone along the Main Central Thrust. Greater Himalayan rocks underwent prograde Barrovian metamorphism between ~ 40-30 Ma as they were subducted beneath Eurasia (Treloar & Rex, 1990; Vance & Harris, 1999; Walker et al., 1999; Simpson et al., 2000). Subsequently, the high-grade rocks of the Main Central Thrust sheet were being shortened and uplifted in the ductile regime by ~ 23-20 Ma in Nepal (e.g. Hubbard & Harrison, 1989; Harrison et al., 1992; Hodges et al., 1996). The Main Central Thrust is therefore thought to have been coeval with the South Tibetan Detachment, together facilitating ductile channel flow extrusion of the Greater Himalaya (Nelson et al., 1996; Grujic et al., 1996, 2002; Beaumont et al., 2001; Hodges et al., 2001; Searle & Szulc, 2005). Whilst the inception age of the Main Central Thrust has been well constrained, the age of cessation or suggestions that it may have undergone late-stage reactivation are still matters for debate (e.g. Harrison et al., 1997; Catlos et al., 2001).

The Lesser Himalayan Zone in India and Nepal comprises unmetamorphosed or low-grade Palaeoproterozoic to Tertiary metasediments and carbonates with volcanic and granitic components (Valdiya, 1980; Sakai, 1983). The older Lesser Himalayan units are thought to represent the proximal equivalents of Tibetan Himalayan Indian margin deposits. Structurally complex, the Lesser Himalayan Zone in Nepal is thought to have undergone duplex growth in the north following Main Central Thrust

cessation (~ 16-11 Ma) with the Himalayan Basal Detachment and Ramgarh Thrust acting as the floor and roof thrusts respectively (DeCelles et al., 1998b). Complex synformal klippen, or Crystalline Thrust Sheets, have also been thrust southward over the less metamorphosed Lesser Himalayan rocks and are widely regarded as erosional outliers of the Greater Himalaya (Valdiya, 1980; Schelling, 1992; Upreti, 1996). All of these Lesser Himalayan rocks have been thrust southwards over the Sub-Himalayan Zone along the Main Boundary Thrust. Displacement along the Main Boundary Thrust is thought to have occurred during Late Miocene-Pliocene time along the length of the Himalayas but there is poor age control for this episode (e.g. Meigs et al., 1995; Burbank et al., 1996; DeCelles et al., 1998b, 2001).

The Sub-Himalayan Zone in southern Nepal is comprised entirely of the Siwalik Group foreland basin sediments. These have been repeated in a series of Tertiary sediment thrust slices beneath the Main Boundary Thrust (Fig. 1.3.c). From river terraces in central-southern Nepal, Lavé & Avouac (2000) calculated current uplift rates of ~ 15 mm/yr above these thrust slices. The Sub-Himalayan Zone has been carried above Quaternary deposits of the modern foreland along the currently active Main Frontal Thrust. The Main Frontal Thrust is the surface expression of the Himalayan Basal Detachment which dips ~ 10° north and progressively ramps up-section to the south (Zhao et al., 1993; Nelson et al., 1996). All major Himalayan structures south of the South Tibetan Detachment are thought to root in this detachment (Brown et al., 1996; Hodges, 2000). Active seismicity and maximum uplift/convergence rates in the Himalayas is also concentrated at depths of 5-20 km along a ramp in the Basal Detachment (Ni & Barazangi, 1984; Zhao et al., 1993,

Pandey et al., 1995). The locus of most modern-day shortening along the front of the belt is in the subsurface beneath the northern Indo-Gangetic Plain (Mugnier et al., 1993). At present the Indian craton moves north-northeast at a rate of 44-61 mm/yr relative to Eurasia/Siberia (DeMets et al., 1990; Bilham et al., 1997).

These estimates of the timing, duration and displacement of thrusting episodes are largely based on metamorphic and geochronological data, resticted to the presently exposed rocks. Such information does not fully answer critical questions concerning the rates of exhumation and identity of the separate source zones and the significance of the major faults in controlling the evolution of the Himalayan orogen. There is also continued uncertainty regarding the distribution of strain within the crustal and mantle parts of the lithosphere, particularly the relative roles of major thrust-faults, strike-slip faults, and distributed strain (e.g. Tapponier & Molnar, 1975; England & McKenzie, 1982; Houseman & England, 1986; Molnar, 1988). It is therefore possible that the findings of previous bedrock studies can be enhanced by application of the detrital technique. The age of Siwalik Group deposition (~ 16 Ma to Recent) focuses the current effort on the timing of movement across the Main Central Thrust and Main Boundary Thrust and the exhumation history of their hanging wall lithologies.

1.5. Field area – SW Nepal

This thesis is focused on the Siwalik Group foreland basin sediments of the Sub-Himalayan Zone in SW Nepal. Although exposure generally worsens towards the eastern Himalayas (due to an increase in monsoon-related vegetation cover) a

number of classic sections expose the Siwaliks either along rivers or roads as they cut through the Dundwa and Churia ranges of southern Nepal (Plate 1.1.). The bulk of this thesis is based on the analysis of three such sections. These lie between the towns of Butwal and Chispani, situated along the dramatic juncture between Himalayan foothills and Indo-Gangetic Plain (Fig. 1.5.). From west to east these are: the Karnali section (16-5.2 Ma), the Surai Khola section (12-1 Ma), and the Tinau Khola section (12-6.3 Ma). The Tinau Khola section (Khola means small river in Nepali) is exposed along the modern-day Tinau River and along the Butwal to Pokhara road (Fig. 1.6. & Plate 1.2.). The Surai Khola section is exposed along the King Mahendra Highway as it cuts through the Dundwa Range north of Bhagwanpur (Fig. 1.7.). The Surai Khola section lies within the southernmost imbricate slice of the Sub-Himalayan Zone, bounded by the Main Frontal Thrust in the south and the Rangsing Thrust in the north. This represents the southernmost of four slices that constitute a ~ 25 km wide imbricate thrust package of Siwalik rocks south of the Main Boundary Thrust. The Karnali section is exposed along the modern Karnali River north of Chisapani town in far-western Nepal (Fig. 1.8.). The base of the Siwalik Group is not exposed along these three sections and the youngest units at the top of the sections terminate in thrusts. The Surai Khola and Karnali sections offer the most continuous exposure of Siwalik rocks in Nepal. Relatively few Siwalik sections extend to times earlier than ~ 13 Ma, and only two sections in Pakistan date back to ~ 18 Ma so the early stages of Siwalik deposition are poorly documented. Therefore the ~ 16 Myr old Karnali section provides an excellent opportunity to extend detailed detrital work further back in time.

The three sections used in this study were chosen for a number of reasons. Most importantly they have been accurately dated using magnetostratigraphy (Gautam & Fujiwara, 2000; Ojha, personal communication, 2002), the age of sedimentation being a prerequisite for the detrital technique (Fig. 1.9.). These depositional ages overlap between the three sections, which means the sections can be correlated and also span the maximum age-range of the Siwalik Group. Furthermore, Siwalik sedimentation occurred throughout much of the Neogene and models for Himalayan tectonics remain contentious for this time period. The sections also provide suitable exposure for sampling and detailed sedimentology and are tectonically uncomplicated. Finally, there is a horizontal distance of ~ 240 km separating the Karnali and Surai Khola sections and ~ 60 km between the Surai Khola and Tinau Khola sections. This means the study covers a significant total potential catchment area and the sections are at least catchment-width apart so any lateral variations in tectonic signal will be highlighted. Such variation could reflect sediment ponding or drainage diversion rather than tectonics. However, whereas a change in tectonic regime would be expected to be recorded in all three sections, drainage capture is more likely to occur on a local catchment-scale. Incorporating three adjacent sections thus adds weight to our interpretations and provides a test of the detrital technique which has been absent from similar previous studies.

1.6. Methods and materials

Fieldwork was carried-out over two 8- to 10-week periods that commenced in January of 2002 and 2003. The 2002 field season was based in the towns of Butwal and Chandrauta in central Nepal from where the Tinau Khola and Surai Khola

sections were accessed (Fig. 1.5.). Two trips were also taken to localities in the hanging wall of the Main Boundary Thrust sheet along the Butwal to Pokhara road and also along the Birpur to Sandhikharka road where the structure sharply places contorted Lesser Himalayan carbonates upon the tectonised Siwaliks. The purpose of these trips was to sample for apatites and zircons within hanging wall lithologies for fission-track analysis. The 2003 field season was based in the town of Chisapani in western Nepal from where the Karnali section was accessed.

Each section was subject to detailed cm-scale sedimentary logging and a large palaeoflow data set was accumulated (Fig. 1.9). Sandstone samples donated by an agreed collaborator (Dr P. DeCelles) were supplemented by fresh samples. The sections were sampled at 1 Myr intervals using previous magnetostratigraphy data (Gautam & Fujiwara, 2000; Ojha, personal communication, 2002). Mudstone was sampled for Nd and Sr whole-rock isotopic analysis and sandstone was sampled for ^{40}Ar-^{39}Ar dating of detrital white mica and petrographic analysis. Samples of sediment from the modern-day rivers flowing through the sections were also collected for petrography, Nd-Sr whole-rock geochemistry and ^{40}Ar-^{39}Ar thermochronology work. A detailed methodology will be discussed for each of these techniques in the relevant chapter.

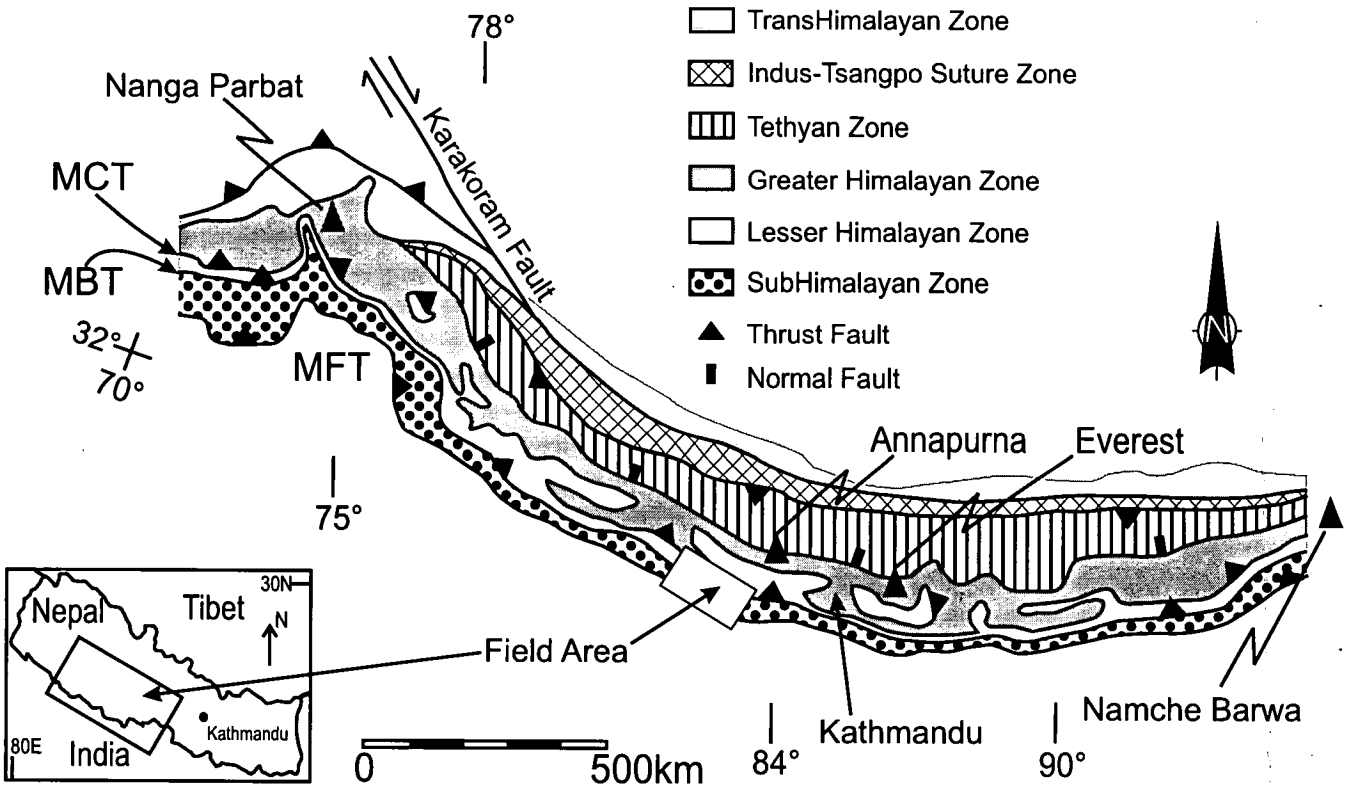


Figure 1.1. General geology map of the Himalayas showing main tectonostratigraphic zones and bounding structures. MCT - Main Central Thrust, MBT - Main Boundary Thrust, MFT - Main Frontal Thrust.

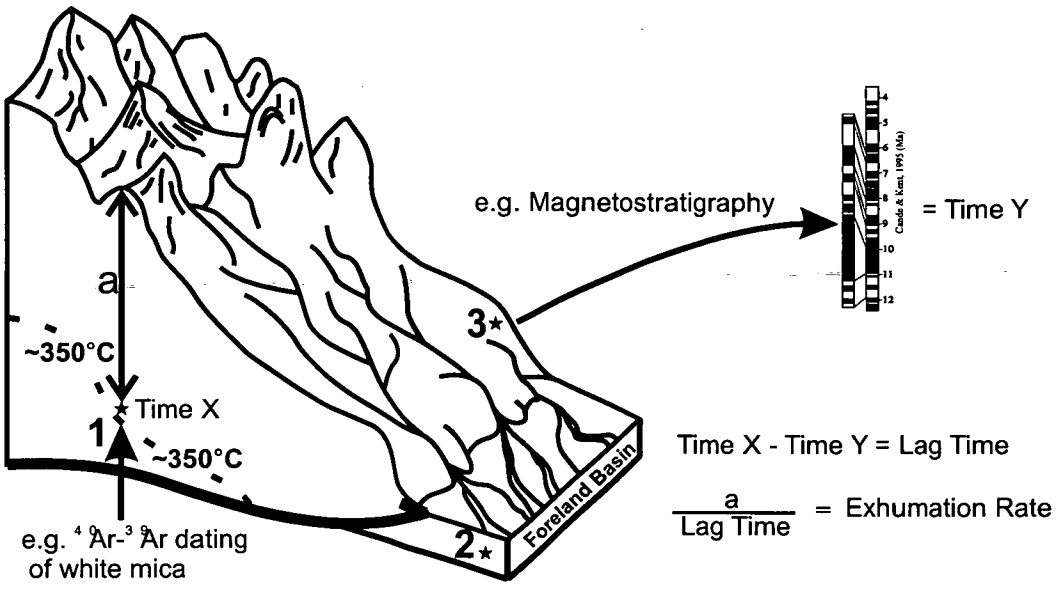


Figure 1.2. Cartoon explanation of detrital thermochronology. Numbers 1-3 track the transport of a single grain of white mica from the time of cooling through the mineral closure temperature, to arriving in the foreland basin, to being uplifted and exposed in the thrust front and then amenable to detrital investigation. This technique assumes subaerial transport times are geologically insignificant.

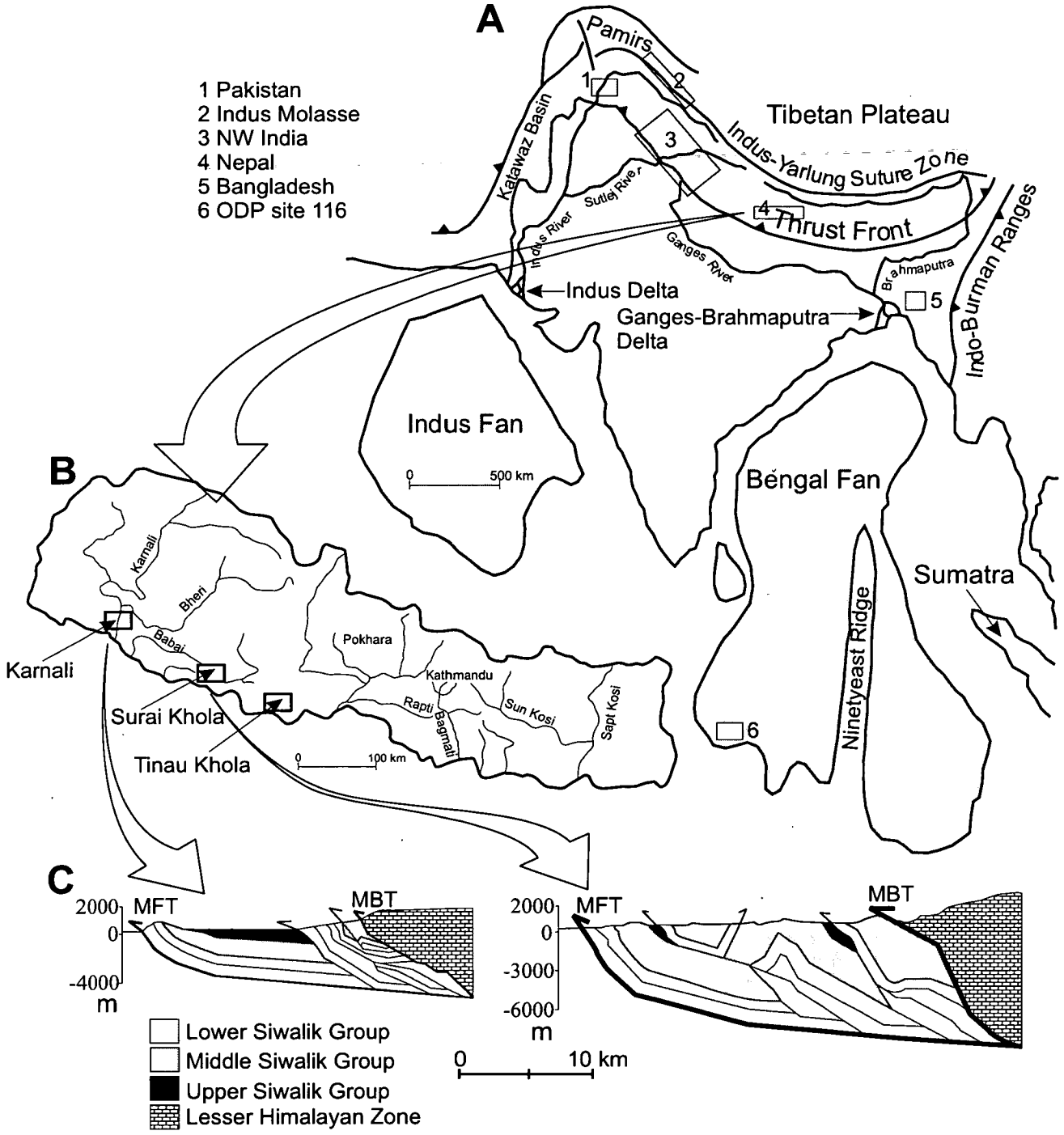


Figure 1.3. Caption on next page.

Figure 1.3. A - Map of Himalayan region showing locations of selected detrital studies, adapted from Quayyum et al., 2001. **B** - Larger map of Nepal highlights major drainage systems and location of Siwalik sections in this study. **C** - Cross-sections through the Sub-Himalayan Zone at locations indicated by arrows, from Mugnier et al. (1999); MBT (Main Boundary Thrust), MFT (Main Frontal Thrust). Pre-eminent detrital studies at **1** = Garzanti et al., 1987; Cerveny et al., 1988; Bossart & Ottiger, 1989; Burbank & Beck, 1991; Gaetani & Garzanti, 1991; Critelli & Garzanti, 1994; Abbasi & Friend, 2000; Quayyum et al., 2001; Clift et al., 2002. **2** = Van Haver, 1984; Garzanti & Van Haver, 1988; Searle et al., 1990; Clift et al., 2001; Sinclair & Jaffey, 2001. **3** = Chaudhri, 1975; Parkash et al., 1980; Najman et al., 1993, 1997; Najman & Garzanti, 2000; White et al., 2002. **4** = Harrison et al., 1993; Quade et al., 1995, 1997; DeCelles et al., 1998a,b; Nakayama & Ulak, 1999; Brewer et al., 2003; Robinson et al., 2001; Huyghe et al., 2001. **5** = Uddin & Lundberg, 1998. **6** = Suczek & Ingersoll, 1985; Copeland & Harrison, 1990; Corrigan & Crowley, 1990; Amano & Taira, 1992; France-Lanord et al., 1993, 1994.

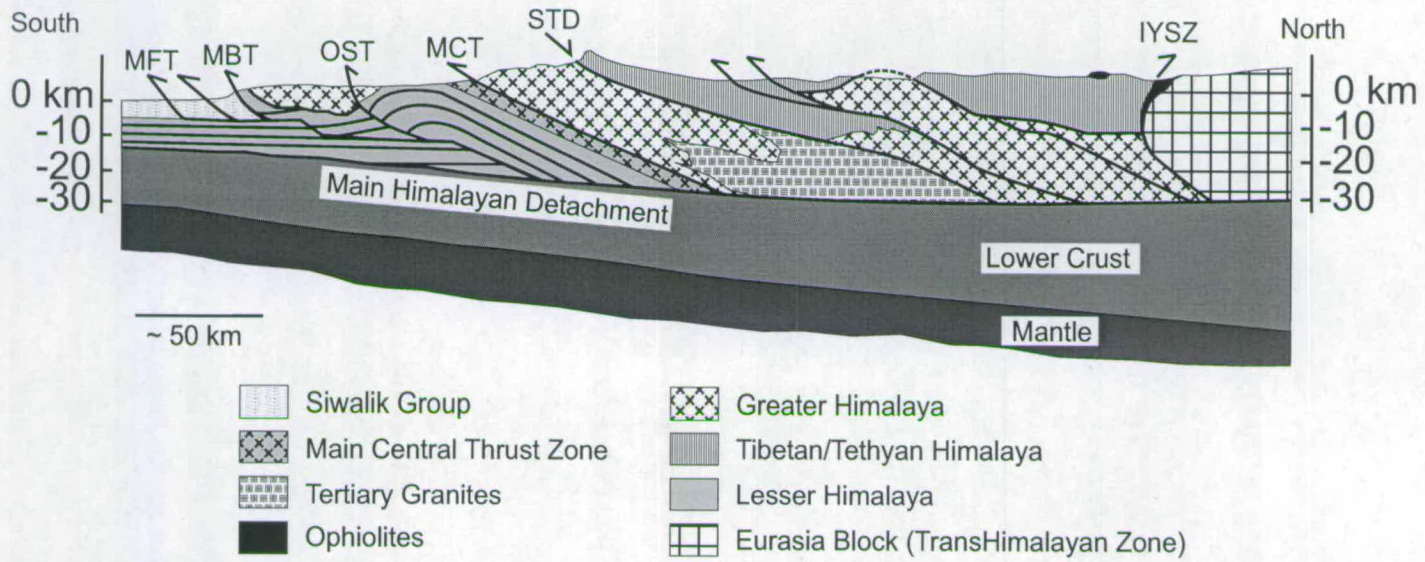


Figure 1.4. Schematic cross-section through the central Himalaya, from Arita et al. (1997). MFT - Main Frontal Thrust, MBT - Main Boundary Thrust, OST - Out of Sequence Thrust, MCT - Main Central Thrust, STD - South Tibetan Detachment, IYSZ - Indus-Yarlung Suture Zone.

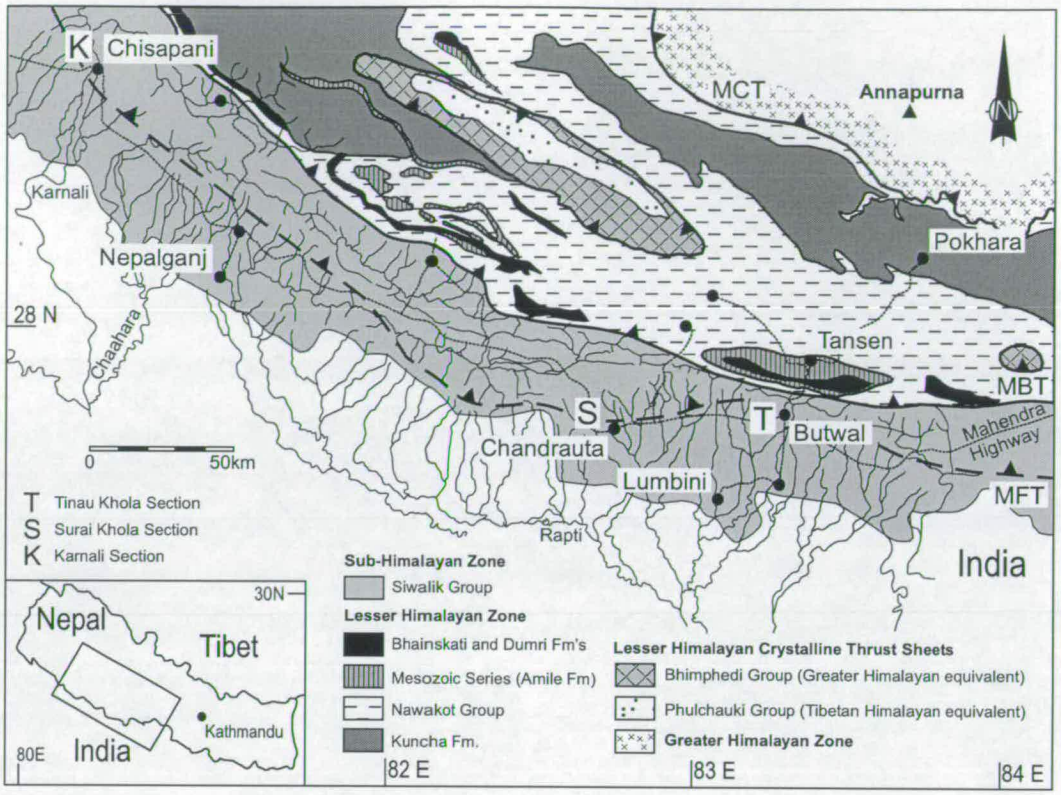


Figure 1.5. Geological map of SW Nepal, inset shows map location. Locations of the three sections under investigation are highlighted. MCT - Main Central Thrust, MBT - Main Boundary Thrust, MFT - Main Frontal Thrust. Modified from Amatya & Jnawali (1994).

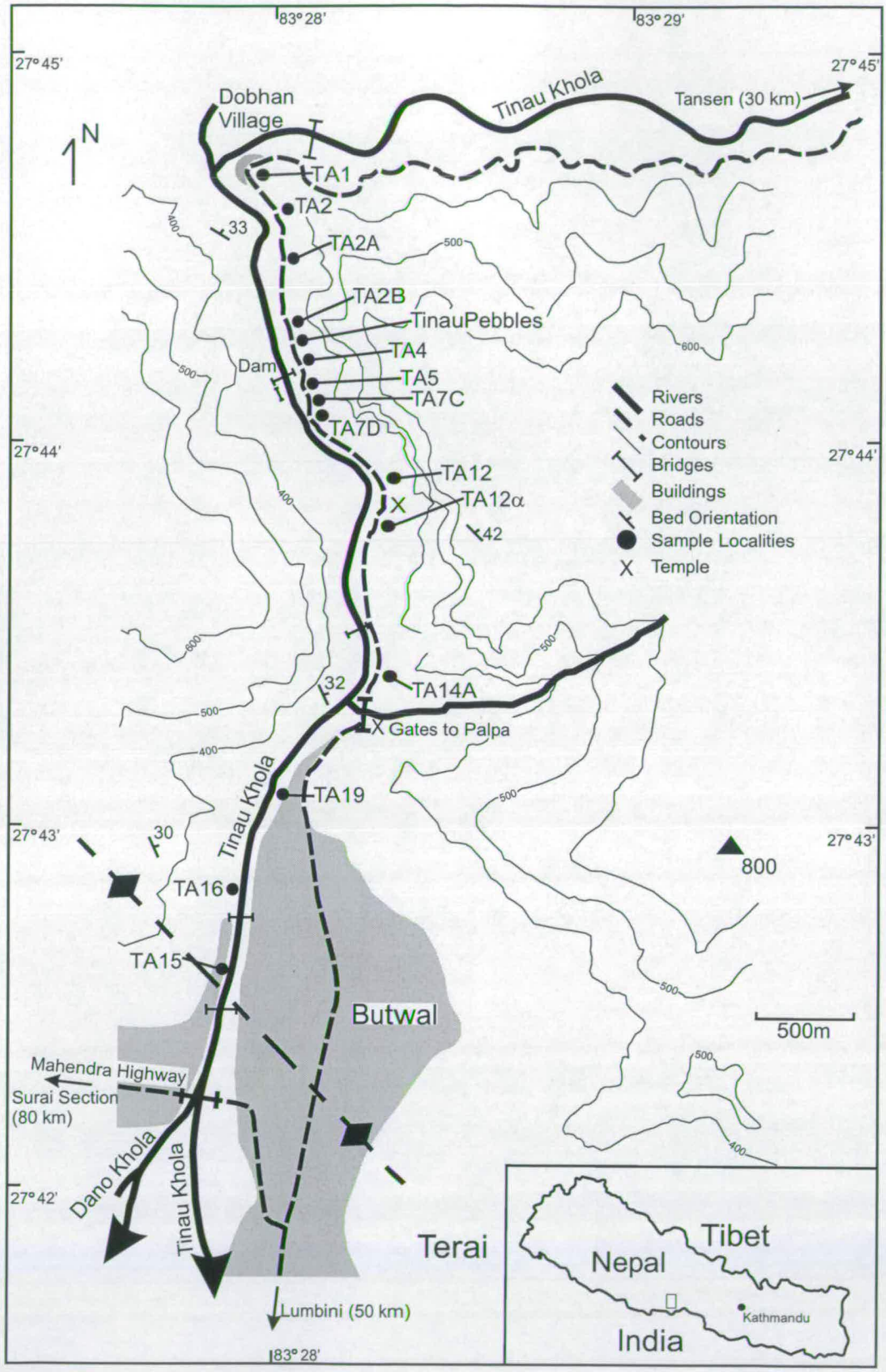


Figure 1.6. Simplified map of the Tinau Khola section showing sample localities. Adapted from the Survey department map, His Majesty's Government of Nepal, 1997.

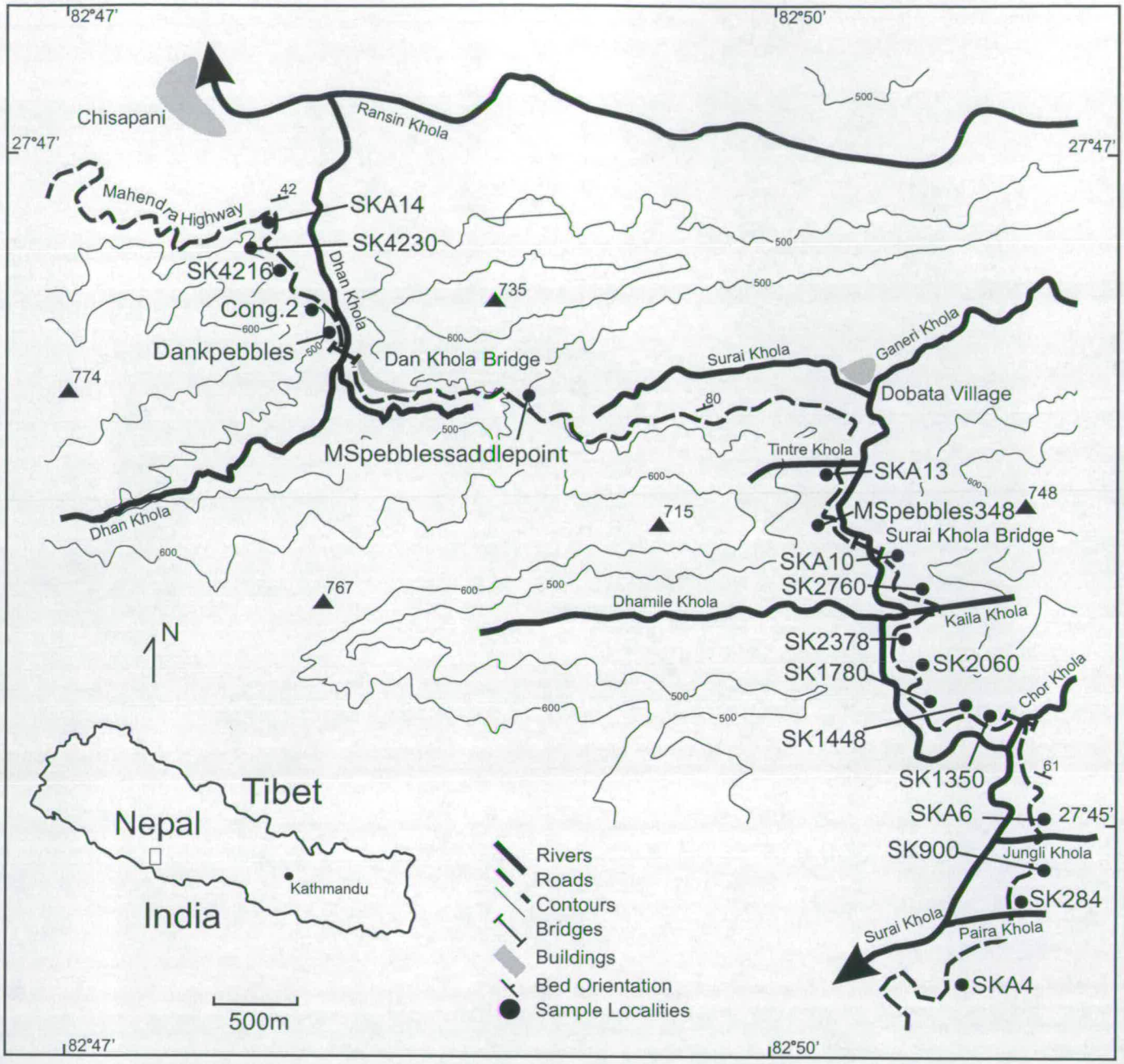


Figure 1.7. Simplified map of the Surai Khola section showing sample localities. Adapted from the Survey department map, His Majesty's Government of Nepal, 1997.

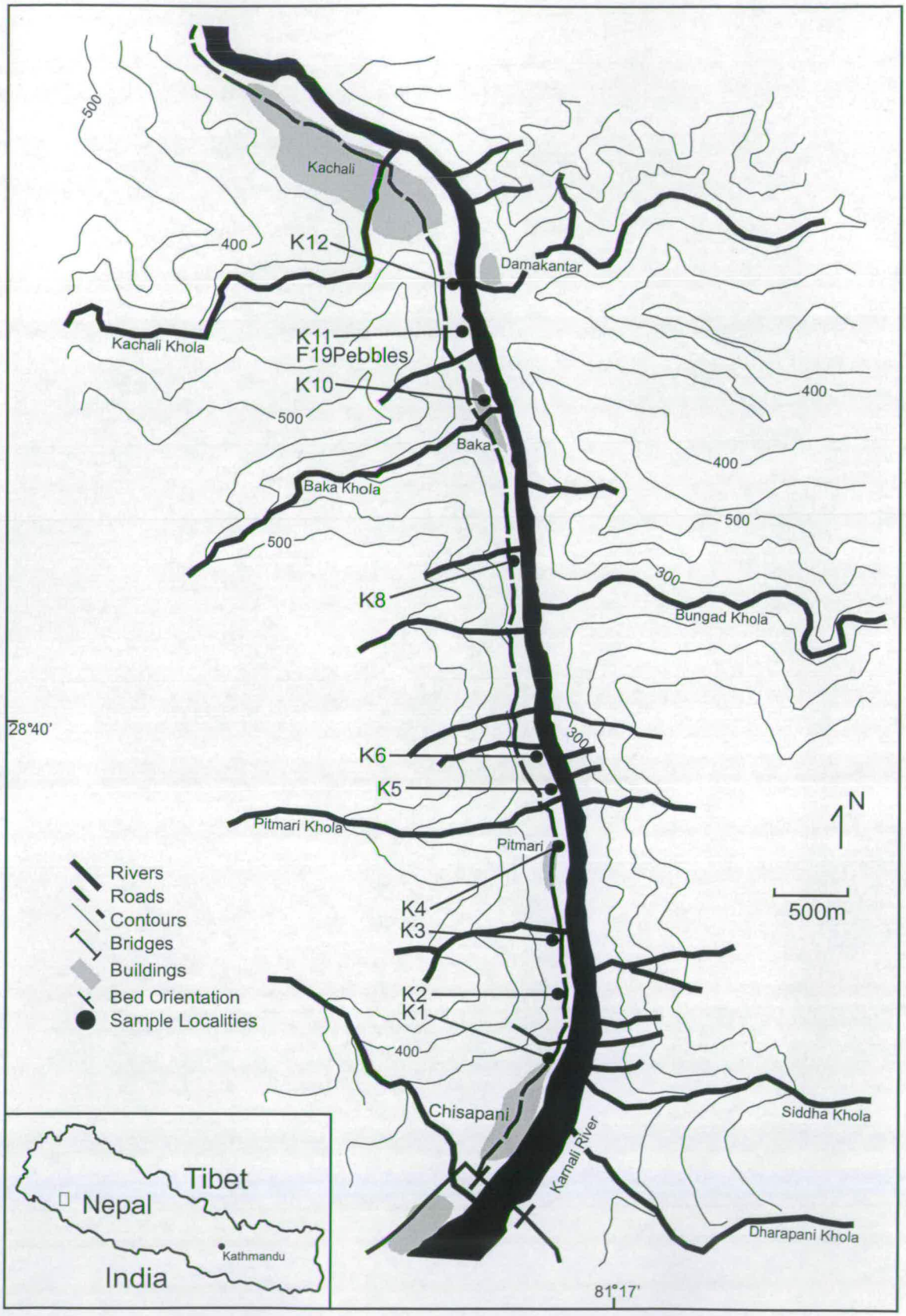


Figure 1.8. Simplified map of the Karnali section showing sample localities. Adapted from the Survey department map, His Majesty's Government of Nepal, 1997.

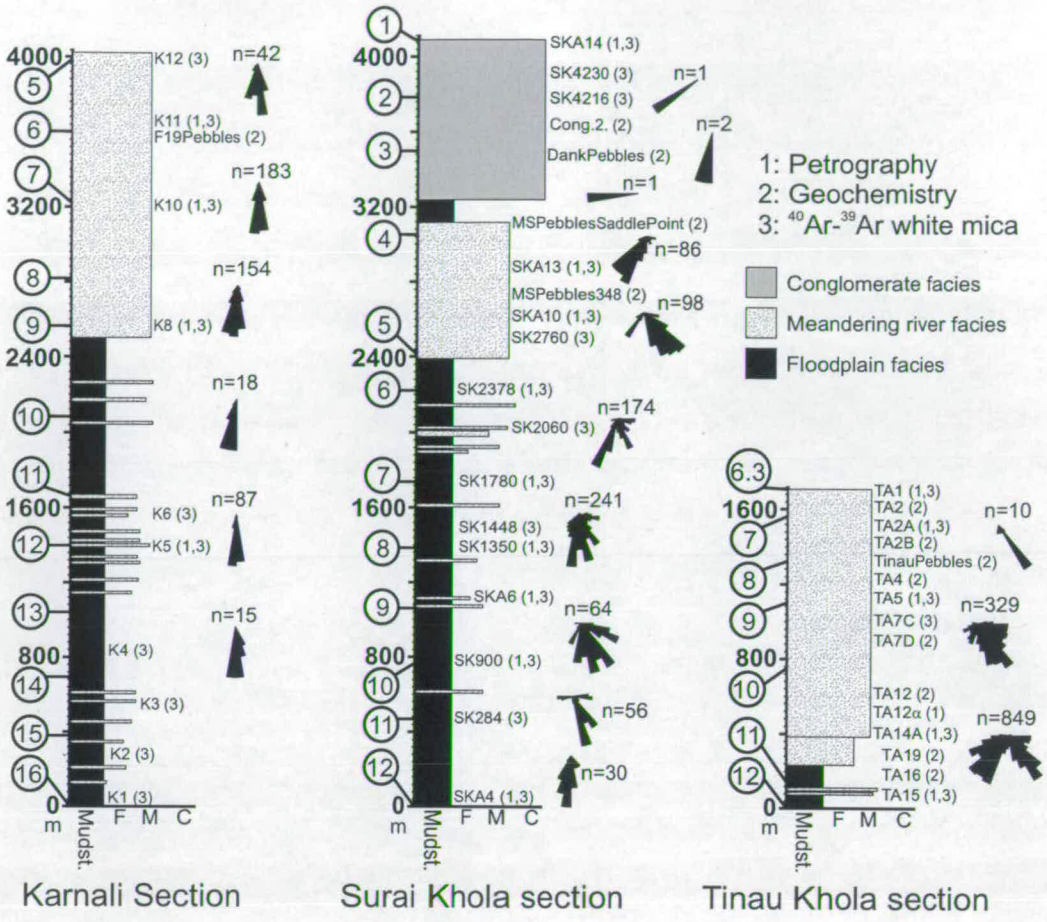


Figure 1.9. Simplified logs for the three Siwalik Group sections used in this study. Magnetostratigraphic ages are shown in circles. Palaeoflow rosettes group data into 400 m intervals. The magnetic data are from Gautam & Fujiwara (2000) (Karnali) and Ojha et al. (personal communication, 2002) (Tinau Khola and Surai Khola) and ages are based on the geomagnetic time scale of Cande & Kent (1995). Sample locations are shown with types of analyses in brackets. The Tinau Khola and Surai Khola sections are incomplete due to thrusting, the top of the Karnali section was not accessible at the time of research. Samples K15 (1), K13 (3), and K13Pebbles (2) taken from the Karnali section are not indicated because they were sampled above the top of the log, which ends with the youngest available magnetostratigraphic age. The ages for these samples were thus inferred from their stratigraphic position.



Plate 1.1. Looking north up the modern Tinau River where it exits the Himalayan foothills at Butwal, the base of the Tinau Khola section is in the middle distance.

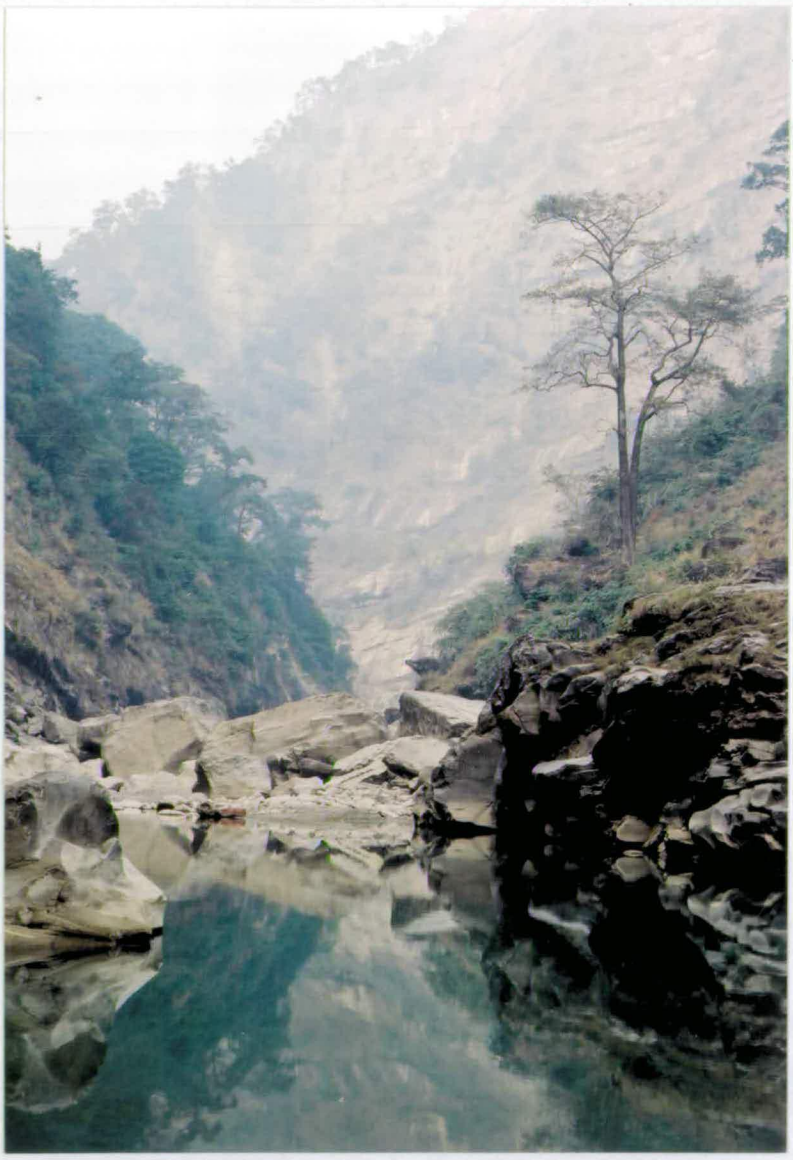


Plate 1.2. Looking north up the modern Tinau River showing exposure of the Tinau Khola section along the river and along the road in the distance.

2. Background Geology

2.1. Introduction

Knowledge of the geology and tectonic evolution of potential hinterland source zones is fundamental before the results of a detrital investigation can be properly interpreted. The time frame of Siwalik deposition (16-1 Ma for the sediment in question) focuses this work on the latter stages of Greater Himalayan exhumation and the transference of thrusting into the Lesser Himalaya and the Main Boundary Thrust, along with the emplacement of the Crystalline Thrust Sheets and the subsequent unroofing of Lesser Himalayan lithologies. This section offers a detailed description of the relevant source zones (from north to south: the Tibetan Himalayan Zone, Greater Himalayan Zone, Lesser Himalayan Zone, and Sub-Himalayan Zone) and related boundary structures (South Tibetan Detachment, Main Central Thrust, Main Boundary Thrust, and Main Frontal Thrust) that have controlled the bulk-composition detrital modes, whole-rock geochemistry and white mica ages of foreland basin sediment during the 16-1 Ma period. Emphasis is placed on the central Himalayas and, in particular, Nepal because these areas comprise the most likely provenance zones for the sediments that are the focus of this thesis.

Within the Himalayan zones south of the South Tibetan Detachment there are separate thrust systems that, along with the Main Central Thrust and Main Boundary Thrust, have controlled the regional geology of Nepal and so must be mentioned. These are the Lesser Himalayan Duplex, the Lesser Himalayan Crystalline Thrust Sheets, and the Ramgarh Thrust (Fig. 2.1.). Zones to the north of the Tibetan

Himalayan Zone (Indus-Yarlung Suture Zone and Trans-Himalayan Zone) are unlikely to have contributed much, if any, sediment during Siwalik deposition. This is because the topographic barrier of the Himalaya coincides with the Greater Himalayan Zone and therefore the majority of post-Miocene foreland basin sediment has been derived from the southern flank of the range (France-Lanord et al., 1993; Garzanti et al., 1996). Although larger rivers such as the Karnali and Rapti in Nepal or the Ganges in India cut back through the high mountains and drain zones north of the Greater Himalaya, the proportion of detritus from these areas in relation to the total detritus which reaches the foreland basin is minimal. These zones are also not so relevant in terms of the tectonic evolution of the hinterland during Siwalik deposition and thus are excluded here.

2.2. Tibetan Himalayan Zone

2.2.1. Lithologies

The Tibetan Himalayan Zone contains a nearly complete stratigraphic record of the northern continental margin of India over the Palaeozoic-Eocene interval (Gaetani & Garzanti, 1991). This is well exposed in the Mustang-Manang area of Nepal where the zone comprises mainly fossiliferous sandstones, mudstones and limestones that are generally unmetamorphosed (Garzanti, 1999). However, in some areas thrust imbrication and large-scale back-folding has produced low- to medium-grade metamorphic assemblages (Schneider & Masch, 1993; Godin et al., 1999). Higher-grade exceptions include amphibolite-facies rocks present within horses of the South Tibetan Detachment and in the carapaces of the North Himalayan Gneiss Domes (see

below) (Hodges, 2000 and references therein). Numerous studies have resulted in a detailed lithostratigraphy for the Tibetan Himalayan Zone (e.g. Bordet et al., 1975; Fuchs, 1977; Searle, 1983; Gaetani et al., 1985; Fuchs et al., 1988; Gaetani & Garzanti, 1991; Gradstein et al., 1992; Liu & Einsele, 1994; Willems et al., 1996; Jadoul et al., 1998; Garzanti, 1999). A review of the plethora of facies and formation names contained within the Tibetan Himalaya is beyond the scope of this thesis but Garzanti (1999) offers a concise summary. The oldest exposed units are Lower Cambrian shallow-marine, terrigenous rocks in Zanskar, NW India. These pass upwards into Middle- to Upper-Cambrian deep marine strata (Gaetani & Garzanti, 1991). Shallow-marine to coastal deposition continued from Ordovician time until the Late Carboniferous-Permian disruption of Gondwana and the opening of Neo-Tethys (Sengor et al., 1988). Evidence for this rifting is witnessed by Permian basalts and alkali granites which inject the Tibetan Himalaya (Spring et al., 1993; Garzanti, 1999). Subsequent Upper Permian to Lower Jurassic strata record Neo-Tethys passive margin development which produced extensive carbonate platforms (Gaetani & Garzanti, 1991). Tibetan Himalayan lithologies suggest these marine conditions persisted on the Indian margin until Early Eocene time when red beds of ophiolitic provenance first appeared in the succession to mark the onset of collision with Eurasia (Gaetani & Garzanti, 1991).

2.2.2. Structure

Ratshbacher et al. (1994) reported ~ 51-47 Ma ^{40}Ar-^{39}Ar ages from the suture zone which date the early phases of thrusting and tectonic burial in the Tibetan Himalaya. Tibetan Himalayan Zone rocks near the suture zone are deformed by upright folds and steep reverse faults whilst southward folds and thrusts dip more shallowly northward (Hodges, 2000). The oldest Tibetan Himalayan structures are south-vergent thrust and fold nappes of Late Cretaceous to Palaeocene age (Proto-Himalayan) which apparently formed during ophiolite obduction (Chen et al., 1990). For example, Proto-Himalayan structures found in Zanskar are related to the obduction of the Spontang ophiolite over the Tibetan Himalaya (Searle, 1986). These fold-and-thrust nappes carried the Tibetan Himalayan units southwards with a minimum of ~ 135 km of shortening in central-southern Tibet (Burg & Chen, 1984; Searle, 1986; Ratschbacher et al., 1994; DeCelles et al., 1998a). Eocene-Miocene structures related to collision include shallowly dipping south-vergent thrust faults and steeply dipping north-vergent backthrusts (Chen et al., 1990). At least three major Eocene fold-and-thrust nappes have been identified within the Tibetan Himalaya of eastern Ladakh (Steck et al., 1998). Such structures may have facilitated the rise of the North Himalayan Gneiss Domes (Hodges, 2000). In the southern outcrop of the Tibetan Himalayan Zone, structures exhibit classical ramp-flat geometries characteristic of foreland fold-and-thrust belts (Searle et al., 1988; McElroy et al., 1990; Hodges, 2000). In north-central Nepal the Tibetan Himalayan Zone is characterised by regional-scale NE-verging folds that record some of the earliest Himalayan contraction (Godin et al., 1999). Palinspastic reconstructions of the Tibetan Himalaya in Ladakh suggest significantly more than 100 km of Eocene

shortening (Searle, 1986; Searle et al., 1997; Steck et al., 1998). Eocene-Oligocene thrusting is also inferred from the detrital unroofing record of Nepal (DeCelles et al., 2001).

North-dipping normal faults and related folds of Early Miocene age have been found throughout the Himalayas but most commonly within the Tibetan Himalayan Zone, the most famous of which being the South Tibetan Detachment (Burchfield et al., 1992; Hodges, 2000). Additionally, a series of prominent north-trending rifts in southern Tibet, along-which there is current seismicity, suggest east-west extension is the dominant deformation mechanism in the modern plateau region (Molnar & Tapponnier, 1975, 1978; Ni & York, 1978; Chen et al., 1990). Although these rifts are attributed to gravitational spreading of Tibet following the attainment of maximum altitude, the idea of a Tibetan "collapse" is controversial (Harrison et al., 1992; Molnar et al., 1993).

2.2.3. The South Tibetan Detachment

The South Tibetan Detachment is a major Himalayan structure and has been mapped along a 2000 km length of the mountain chain from Zanskar (NW India) to Bhutan (Burchfiel & Royden, 1985; Searle & Rex, 1989; Searle, 1999; Searle et al., 1999; Walker et al., 1999) (Fig. 2.2.). The South Tibetan Detachment comprises north-dipping ductile shear zones and brittle low-angle extensional faults, many of which form complex fault splays (Hodges et al., 1992; Pognante & Benna, 1993; Searle, 1999). These faults tend to display a normal sense of shear to the NE or NW (Burchfiel et al., 1992). The basal detachment of this fault system, which typically

separates unmetamorphosed Tibetan Himalayan sediments in the hanging wall from upper-amphibolite facies gneisses and leucogranites of the Greater Himalaya in the footwall, is exposed very near the crest of the Himalaya. A sub-parallel mylonitic carapace overlies the basal detachment in the uppermost 500-1000 m of the footwall (Hodges, 2000). The age of fault movement has been largely determined by U-Th-Pb crystallisation ages of leucogranites which are restricted to the footwall. Leucogranites have been used extensively to determine the timing of normal faulting depending on their relationship with the fault zone. From such work it is likely much of the South Tibetan Detachment has been active episodically over the Miocene-Holocene interval, although the precise timing of these episodes is poorly understood (Burg & Chen, 1984; Burchfiel et al., 1992; Coleman, 1996; Hodges et al., 1994; 1996; Searle et al., 1997; Dezes, 1999; Walker et al., 1999; Searle & Godin, 2003). Indeed, in north-central Nepal there is clear evidence for multiple displacement episodes (Stutz & Steck, 1986; Pecher, 1991; Coleman, 1996). During the Miocene-Holocene time period it is estimated that the South Tibetan Detachment accommodated several tens of kilometres of top-to-the-north displacement (Burg & Chen, 1984; Burchfiel et al., 1992; Coleman, 1996).

2.2.4. The North Himalayan Gneiss Domes

The North Himalayan Gneiss Domes form a series of eleven domal stuctures along the hanging wall of the Kangmar Thrust, a large-scale break-back thrust (Searle, 1995). The domal structures formed as a consequence of the same regional extensional deformation that resulted in the South Tibetan Detachment (Chen et al., 1990). Burchfiel et al. (1992) suggested all of the domes may be metamorphic core

complexes but more recent work relates exposure of the domes to a North Himalayan antiform, which would suggest the domes represent a northern exposure of Greater Himalayan rocks (e.g. Zhang et al., 2004). Most domes occur within the northern half of the Tibetan Himalayan Zone but they are also present within the suture zone. Although metamorphic rocks are not abundant within the Tibetan Himalayan sediments, the rocks of the gneiss domes were subject to high-grade metamorphic episodes. All domes display an upwards- and outwards-decreasing metamorphic grade (Burg et al., 1984; Searle et al., 1987; Chen et al., 1990). The largest dome, at over 1200 km^2, is the Tso Morari dome of Ladakh, which has early eclogite-facies assemblages that are overprinted by amphibolite-facies assemblages (Guillot et al., 1995; De Sigoyer et al., 1997). Early Eocene (~ 55-44 Ma) high- and ultrahigh-pressure eclogite-facies (18-22 kbar; 500-600°C) metamorphism is recorded in a number of these western Himalayan domes (Pognante & Spencer, 1991; Guillot et al., 1995; De Sigoyer, 1997, 2000). Sm-Nd and U-Pb geochronology suggests a 44-49 Ma age for eclogite-facies metamorphism in Pakistan (Tonarini et al., 1993; Lombardo et al., 2000). Evidence for the eclogite event has also been found in the eastern Himalaya (Lombardo et al., 1998).

^{40}Ar-^{39}Ar dates for phengites and biotites from these high-pressure rocks suggest cooling below ~ 350°C by ~ 30 Ma (De Sigoyer et al., 1997). Dome rocks were therefore exhumed to mid-crustal levels at a rate of over 5 mm/yr by ~ 47 Ma and to upper crustal levels at ~ 1.2 mm/yr by ~ 30 Ma (De Sigoyer, 2000). Other domes display basement complexes of variably deformed orthogneisses and paragneisses with Early Ordovician or older protolith ages (Hodges, 2000 and references therein).

Muscovite and biotite give Early- to Middle-Miocene cooling ages (Maluski et al., 1988), which is roughly concomitant with the Greater Himalayan leucogranites (see below). Granites from the core of the gneiss domes give an age range of 21-9 Ma (Searle, 1995 and references therein).

Another well-studied dome is the Kangmar Dome of southern Tibet. Burg et al. (1984) showed that the core of the Kangmar Dome consists of deformed augen orthogneiss. The dome is mantled by progressively less metamorphosed Carboniferous-Triassic rocks of the Tibetan Himalaya. The gneiss core yielded a U-Pb zircon age of 562 ± 4 Ma (Scharer et al., 1986). The gneiss is mantled by metasedimentary and sedimentary rocks of Palaeozoic-Jurassic age along a detachment which displays ductile shearing and brecciation (Chen et al., 1990). The exhumation history of the Kangmar Dome shows cooling between 15-11 Ma (mica cooling ages), cooling of 10-30°C/Ma between 11.5-10 Ma (from K-feldspar diffusion models), and cooling below the apatite fission-track closure temperature (~ 75-125°C) at ~ 5.5 Ma (Lee et al., 1999). Many domes in south-central Xizang, Tibet, are dominated by muscovite-biotite granites and leucogranites of Cenozoic age (Burg et al., 1984; Debon et al., 1986) with U-Th-Pb monazite ages ranging from ~ 9.5 Ma to 17.6 Ma (Scharer et al., 1986; Harrison et al., 1997).

2.3. Greater Himalayan Zone

2.3.1. Lithologies

The Greater Himalayan Zone is a northwards-dipping layer of medium- to high-grade metamorphic rocks, migmatites, and crustal melt granites, forming the metamorphic core of the Himalayas (Gansser, 1964; Searle & Godin, 2003). No unambiguous Greater Himalayan fossils have been recovered and so its age remains poorly constrained. U-Pb and Sm-Nd studies of zircon grains show the sedimentary provenance of the Greater Himalaya is ~ 1 Ga younger than that of the Lesser Himalaya (Parrish & Hodges, 1996). A compilation of Sm-Nd isotope analyses on metasedimentary rocks and granitoids indicates depleted-mantle model ages (T_{DM}) of 2300-2600 Ma (ε_{Nd} = -23 to -26) for the Lesser Himalaya and 1500-2200 Ma (ε_{Nd} = -10 to -18) for most of the Greater Himalayan samples (Ahmad et al., 2000 and references therein). DeCelles et al. (2000) used U-Pb zircon ages of 800-1700 Ma to suggest that protoliths of the Greater Himalaya were shed from the northern end of the East African orogen during the Late Proterozoic pan-African orogen (DeCelles et al., 2000). The gneiss of the Greater Himalaya forms a thick continuous sequence of about 5 to 15 km (Guillot, 1999). Thermobarometric data from Nepal suggests some 26 km of overburden has been removed from the top of the Greater Himalaya since ~ 23 Ma to exhume the rocks currently exposed at the surface (Searle, 1995). Throughout much of the range, the Greater Himalaya are divided into three formations known simply as Formations I to III (Pêcher and Le Fort, 1986). Whilst it has proved hard to map these three formations outside of the central Himalayas,

their constituent lithologies are dominant throughout the Greater Himalaya in varying proportions.

2.3.1.1. Formation I

Formation I represents the base of the Greater Himalayan Zone. It is comprised predominantly of clastic metasedimentary rocks and dominated by biotite-muscovite gneiss with additional mica schists and phyllites, quartzites, para-amphibolites, and impure marbles. Mineral assemblages are typically consistent with middle- to upper-amphibolite facies metamorphism. The uppermost part of the unit contains magmatic gneisses with abundant leucosomes or discrete leucogranitic dikes and sills. Parrish & Hodges (1996) showed Formation I rocks from the central Himalaya contain abundant detrital zircons with 0.8-1 Ga ages and therefore the formation must have a Neoproterozoic or younger depositional age. Formation I is regarded as an intact crustal section with a thickness of 1 km to over 15 km along-strike (Le Fort, 1975). Such lateral thickness variation can be attributed to low-angle structural discontinuities and also lateral ramping of the Main Central Thrust (e.g. Burg et al., 1984, Grujic et al., 1996; Searle, 1999; Hodges, 2000).

2.3.1.2. Formation II

This middle formation comprises middle- to upper-amphibolite facies calcareous rocks. Banded calc-silicate gneiss is predominant whilst other lithologies include marble, calc-schist, psammitic schist, para-amphibolite, and orthoquartzite (Guillot, 1999; Hodges, 2000). The contact with Formation I is sharp and parallel to compositional layering, and the lack of any metamorphic discontinuity or local

tectonic fabrics suggests Formations I and II are a conformable package (e.g. Colchen et al., 1986; Hodges, 2000). Formation II is missing from several central Himalayan sections, particularly in Eastern Nepal, probably due to South Tibetan Detachment displacements.

2.3.1.3. Formation III

This is a near homogeneous augen orthogneiss horizon with a few metasedimentary intercalations and is usually present within the upper part of Formation II or where Formation II is absent (Guillot, 1999; Hodges, 2000 and references therein). This formation is thought to be Cambro-Ordovician in age from Rb-Sr isotopic studies (Frank et al., 1977; Ferrara et al., 1983; Pognante et al., 1990). However U-Pb dating has also yielded ages consistent with either early Palaeozoic or Neogene crystallisation (Hodges et al., 1996). Formation III can be traced almost continuously from eastern to central Nepal (Le Fort et al., 1986) and similar rocks occur at the same structural level as far as Bhutan in the east (Gansser, 1983) and Zanskar in the west (Pognante et el., 1990).

2.3.1.4. Leucogranites

A major feature of the Himalayas, and a suite of rocks that play a key role in models of orogenic evolution, are the Greater Himalayan leucogranites. Discrete leucogranite bodies can be found within all Greater Himalayan units and rarely in basal Tibetan Himalayan strata and were intruded mainly along the South Tibetan Detachment (Dietrich & Gansser, 1981; Le Fort et al., 1987; Burchfiel et al., 1992; Guillot et al., 1993; Searle, 1995; Hodges et al., 1996). They range from cm-scale

sills and dikes to plutons with dimensions of several hundreds of kilometres with the typical mineral assemblage: Qtz + K-feld + Plag + Musc + Biot ± Tourm ± Gnt ± Sill ± Ky (Hodges, 2000). U-Th-Pb ages for the central Himalayan leucogranites range from ~ 23 Ma to ~ 12 Ma (Harrison et al., 1995; Hodges et al., 1996; Edwards & Harrison, 1997; Coleman, 1998; Wu et al., 1998; Searle et al., 1999). The youngest leucogranites (< 4 Ma) are exposed at the east (Namche Barwa) and west (Nanga Parbat) syntaxes (Zeitler et al., 1993; Burg et al., 1998). The leucogranites were produced by high-temperature, low-pressure (~ 4-5 kbar, 14-18 km depth; Searle & Szulc, 2005) anatectic melting of Greater Himalayan Zone rocks during orogenesis (Le Fort et al., 1987). The heat source for this melting is still being debated. Some workers favour water-saturated anatexis of Greater Himalayan rocks with shear heating along the Main Central Thrust as the cause of leucogranite generation (LeFort, 1975, 1981; England et al., 1992). Others propose fluid-absent muscovite dehydration, induced by decompression during uplift and exhumation along the South Tibetan Detachment footwall (Harris et al., 1995; Massey, 1994; Searle & Godin, 2003). Searle & Szulc (2005) argue that because leucogranite extrusion was largely horizontal along the low-angle South Tibetan Detachment, decompression melting cannot be invoked as an origin for the leucogranites. They propose the heat source for such widespread shallow-level melting can only be explained by having a highly radioactive protolith of Indian plate Proterozoic sediments. Nevertheless PTt constraints show that decompression took place at the time of melt formation and thus was an important mechanism in leucogranite formation but not necessarily the initial cause (Harris et al., 2004). Whilst there is no evidence for leucogranite emplacement during the last few million years, deep seismic reflection profiling

across southern Tibet (Zhao et al., 1993; Nelson et al., 1996) along with earthquake and magnetotelluric data (Wei et al., 1997) indicate the presence of partial melts and/or aqueous fluids in the middle crust of southern Tibet at 15-20 km depth (Nelson et al., 1996; Alsdorf & Nelson, 1999) (Fig. 2.3.). It has been proposed that these "bright spots" represent leucogranites forming today (Nelson et al., 1996), at a similar structural horizon and depth to the Greater Himalayan leucogranites (Searle et al., 1993; Searle, 1999).

2.3.1.5. Greater Himalayan protolith

Whilst dominantly metamorphosed, the Greater Himalayan Zone also has a number of low-grade tectonostratigraphic cover units, which are interpreted to represent unmetamorphosed to weakly metamorphosed protolith material. Two prominent examples are the variously named Haimantas, Kade Formation, or Chamba sequence in NW India (Thakur, 1980, 1987, 1998; Pognante et al., 1990; Walker et al., 1999; White et al., 2002) and the Sanctuary Formation of Nepal (Colchen et al., 1986). In NW India the Haimantas is separated from the metamorphosed Greater Himalaya by the Miyar Thrust (Pognante et al., 1990). The unit consists of low-grade meta-greywackes and metapelites. The Sanctuary Formation outcrops along the length of Nepal (maximum width of ~ 15 km), occuring above Formation III and the South Tibetan Detachment and below the Annapurna Yellow Formation of the Tibetan Himalaya. It consists of folded black schists, sandstones and limestones with some levels of tuffs and basic volcanics (Colchen et al., 1986). Greywacke is most abundant and there are calcareous and dolomitic levels. It is increasingly likely

further back in time that there were larger areas of this sedimentary and low-grade Greater Himalayan protolith material.

2.3.2. Tectono-metamorphic history

Post-collision prograde Barrovian metamorphism of the Greater Himalayan Zone took place between ~ 40 Ma to ~ 14 Ma or younger (Searle, 1995). A number of workers have noted a 10-20 Myr west to east diachroneity in age data. Guillot (1999) suggests counter-clockwise rotation of India between 50-40 Ma produced later nappe stacking in the eastern Himalaya. However, the idea of diachronous collision is still a matter for debate (Catlos et al., 2002, DeCelles et al., 2004).

Subduction of Greater Himalayan protoliths beneath the southern edge of Asia culminated in peak metamorphic conditions (~ 8-10 kbar, 550-700°C) between ~ 40-30 Ma (Le Fort, 1986; Treloar & Rex, 1990; Vance & Harris, 1999; Walker et al., 1999; Foster et al., 2000; Simpson et al., 2000; Godin et al., 2001; Catlos et al., 2002) (Fig. 2.4.). This was followed by decompression and an initial increase in temperature (~ 4-7 kbar, 650-750°C) then isobaric cooling from ~ 22 Ma, contemporaneous with the inception of the South Tibetan Detachment-Main Central Thrust system. Additional out-of-sequence thrusts of Miocene age have been mapped near the top of the Greater Himalayan slab in Nepal and Bhutan (Brun et al., 1985; Grujic et al., 1996; Hodges et al., 1996; Vannay & Hodges, 1996; Searle, 1999). Decompression is associated with crustal melting and migmatisation, which resulted in leucogranite production (Guillot, 1999). Leucogranites lubricated shear zones and triggered rapid unroofing of the Greater Himalaya by horizontal extrusion

(Searle & Szulc, 2005). This involved ductile channel flow processes (Nelson et al., 1996; Grujic et al., 1996, 2002; Beaumont et al., 2001; Hodges et al., 2001; Searle & Szulc, 2005) (Fig. 2.5.). Although emplacement of the Greater Himalaya initiated rapid cooling, temperatures remained high at least until ~ 17 Ma (Searle et al., 2003). When cooling commenced ductile extrusion ceased, effectively "freezing" the Main Central Thrust-South Tibetan Detachment system, and thrusting propagated down-section into the Lesser Himalaya. Geophysical data show that the faults bounding the Greater Himalaya (South Tibetan Detachment and Main Central Thrust) converge at depth (Nelson et al., 1996), which supports the ductile extrusion model and suggests compressional and gravitational forces compete for control of the orogenic profile. It is now believed ductile extrusion has entered a period of stagnation whereby orogenic evolution has been focused to the front of the mountain belt (Main Boundary Thrust and Main Frontal Thrust). The precise timing of this switch in critical wedge evolution and subsequent thrusting is a matter of controversy.

Along the Marsyandi transect in central Nepal, Greater Himalayan monazites near the Main Central Thrust record ~ 18-22 Ma ages whilst those from near the South Tibetan Detachment yield ~ 30-50 Ma ages (Catlos et al., 2001). According to the model of Harrison et al. (1998), samples from the South Tibetan Detachment area are from shallower levels and travelled along the thrust flat, preserving their Eocene-Oligocene origin, whereas those near the Main Central Thrust were exhumed from the deep crust along the thrust ramp and thus reset. K-Ar and ^{40}Ar-^{39}Ar mica cooling age data from Greater Himalayan bedrock also show that ages young from the South

Tibetan Detachment (~ 22 Ma) in the north to the Main Central Thrust (~ 8-2 Ma) in the south. This younging trend has been related to a combination of rapid upper Greater Himalayan cooling during Miocene decompression followed by slow cooling which produced the younger ages (Macfarlane, 1993; Searle et al., 1999). There is also an apparent northward declining pressure gradient within the Greater Himalaya from ~ 8-10 kbar near the Main Central Thrust to ~ 4 kbar near the South Tibetan Detachment (Harrison et al., 1999; Guillot, 1999). This has been associated with duplex growth within the Lesser Himalaya following Main Central Thrust cessation (Robinson et al., 2003).

Mineral cooling ages at the top of the Greater Himalaya suggest ductile deformation had ceased by ~ 18 Ma (Copeland et al., 1991; Parrish & Hodges, 1993; Hodges et al., 1996). Guillot et al. (1994) also report ^{40}Ar-^{39}Ar mica plateau ages from the Manaslu Leucogranite in Nepal of ~ 18 Ma. This is supported by leucogranite U-Th-Pb crystallisation ages throughout the Himalayas, which generally vary between 17-24 Ma (Searle et al., 2003 and references therein). Coleman & Hodges (1998) obtained 15-16 Ma mean ^{40}Ar-^{39}Ar ages on biotite from the Greater Himalayan Zone. Indeed, bedrock micas give ages between 10-25 Ma for much of the Greater Himalaya and suggest the entire slab had cooled below the muscovite closure temperature (~ 400-350°C; within the ductile strain field of Sibson (1977)) by 15-13 Ma (Vannay & Hodges, 1996; Coleman & Hodges, 1998; Walker et al., 1999; Godin et al., 2001; Searle et al., 2003).

However, a number of younger (Late Miocene-Pliocene) ages found along the Main Central Thrust and within the Greater and Lesser Himalayan Formations (Fig. 2.2.) challenge the traditional view that Greater Himalayan exhumation had ceased by ~ 15-17 Ma (e.g. Honegger et al., 1982; Maluski et al., 1988; Hubbard & Harrison, 1989; Godin et al., 2001). A 10.8 Ma ^{40}Ar-^{39}Ar mica age from the Kula Kangri leucogranite and 12-13 Ma U-Th-Pb ages from leucogranites in Bhutan are exceptions to the general leucogranite age trend (Edwards & Harrison, 1997; Daniel et al., 2003). These may reflect exposure of deeper Greater Himalayan rocks or younger tectonism in the eastern Himalaya and may indicate that exhumation along the South Tibetan Detachment persisted until ~ 10 Ma (Edwards & Harrison, 1997). Catlos et al. (2002) also report Th-Pb ages of 10-14 Ma from monazite inclusions in garnet in the Sikkim Greater Himalayan Zone. An east to west diachroneity in leucogranite cooling ages has long been recognised. Diachroneity is however by no means clear-cut and young ages have been found further west. For example Maluski et al. (1988) reported ^{40}Ar-^{39}Ar mica cooling ages of ~ 11 Ma from the Kula Kangri leucogranite (Bhutan) and a biotite plateau age of 11.8 ± 0.3 Ma from micaschists along a section in Nepal between the Main Central Thrust and Mt. Everest. They also report younger ~ 4-9 Ma mica ages derived from gneiss and migmatite along the same section. Godin et al. (2001) found ages as young as 13-11 Ma from the hanging wall of the Annapurna Detachment in Nepal. Metamorphism may even have extended (not necessarily continuously) to Pleistocene time in the syntaxial regions of the Himalayas (Zeitler et al., 1982; Sverdrup et al., 1993; Treloar et al., 1991, 2000; Chamberlain et al., 1995; Burchfiel et al., 2000; Hodges, 2000; Ding et al., 2001). Apatite U-Th/He ages from upper structural levels of the Greater

Himalaya and upper Lesser Himalaya vary between 6-0.8 Ma (Hubbard & House, 2000). Therefore low temperature thermochronometers indicate continued exhumation of Greater Himalayan rocks until recent times.

It has been proposed that these young ages arose from post-16 Ma rapid Greater Himalayan cooling in the Late Miocene due to either Lesser Himalayan Duplex growth, movement over a ramp on the Main Boundary Thrust, Main Central Thrust reactivation during late Miocene-Pliocene time or a combination of these (Copeland et al., 1991; Macfarlane, 1993; Arita & Paudel, 1997; Harrison et al., 1997; Catlos et al., 2001; DeCelles et al., 2001; Robinson et al., 2003). Vance et al. (2003) calculated modern Greater Himalayan erosion rates of 2.7 ± 0.3 mm/yr using cosmogenic nuclides (^{10}Be & ^{26}Al), higher than exhumation rates calculated from ^{40}Ar-^{39}Ar muscovite ages. They therefore propose that either climatic forcing or tectonic diachroneity resulted in a three- to six-fold increase in exhumation rates within the last few million years. This is in agreement with the age data supporting relatively young exhumation. Models associated with the young ages have yet to be fully accepted however, due to the limited data set and the suggestions that hydrothermal activity may have resulted in mineral resetting rather than tectonics.

2.4. Main Central Thrust

The Main Central Thrust is a 3-5 km thick ductile shear zone with top-to-the south sense of shear (Searle et al., 2003). It is defined by the occurrence of high temperature, upper amphibolite facies gneisses of the Greater Himalayan Zone above lower temperature, greenschist and amphibolite facies Lesser Himalayan rocks. The fault zone stretches for nearly 2500 km along strike from Bhutan in the east to the Kashmir region in the west and is the dominant thickening structure in the Himalayas.

Heim & Gansser (1939) first defined the Main Central Thrust zone as the Greater-Lesser Himalaya boundary. However, the history of displacement and origin of its footwall inverted metamorphic sequence are still matters for debate (Le Fort, 1975; Jaupart & Provost, 1985; Searle & Rex, 1989; England et al., 1992; Grujic et al., 1996; Grasemann & Vannay, 1999; Kohn et al., 2001; Robinson et al., 2003). Workers have faced a challenge in even locating the Main Central Thrust, which is a tectonic melange of Greater and Lesser Himalayan units and presents no definite structural or metamorphic discontinuity (Valdiya, 1980; Ahmad et al., 2000). Rather than mapping a single detachment, Arita (1983) places two thrusts (MCT I and MCT II) on each side of the shear zone. These roof and sole thrusts dip moderately northward, sub-parallel to intense shear fabrics internal to the zone (Schelling, 1992; Hodges, 2000).



Inverted metamorphic isograds in the footwall, progressing from chlorite- to kyanite/staurolite-grade in a northward direction are an enigmatic feature of the Main Central Thrust (e.g. Pecher, 1989; Harrison et al., 1998). Temperatures tend to increase from the Main Central Thrust zone into the lower portion of the Greater Himalaya (350-750°C), and then trend lower from the middle of the Greater Himalaya to the top (750-450°C) (Pognante & Benna, 1993; Hubbard, 1989) (Fig. 2.6.). Pressure has also been found to increase up-section in central Nepal (Vannay & Hodges, 1996; Kohn et al., 2001), Garhwal (Metcalf, 1993), and Kishtwar (Stephenson, 2000). Pressures then decrease upwards above the kyanite isograd. In eastern Nepal, pressures decrease from 7-8 kbar near the Main Central Thrust to 2-4 kbar near the South Tibetan Detachment (Brunel & Kienast, 1986; Hubbard, 1989).

Estimates for the amount of slip along the Main Central Thrust vary between 140-600 km (Molnar, 1984; Lyon-Caen & Molnar, 1985; Brunel & Kienast, 1986; Schelling & Arita, 1991; Schelling, 1992; Srivastava & Mitra, 1994). Muscovite and K-feldspar K-Ar cooling ages along the thrust zone in Nepal show an average unroofing rate of 1.2 ± 0.6 mm/yr (Hubbard et al., 1991). The pressure conditions recorded by the rim of a garnet (7 kbar), the precise age of its monazite inclusion (13.9 Ma) and a lithostatic gradient (0.27 kbar/km) suggest the exhumation rate of the thrust zone in eastern Nepal was ~ 2 mm/yr (Catlos et al., 2002). Since the Main Central Thrust is parallel to the regional fabrics of the footwall and hanging-wall this implies the fault juxtaposes a hanging-wall flat with a footwall flat (Robinson et al., 2003). Therefore the current steep northwards dip of the structure probably

developed after the main phase of movement and perhaps during passive uplift above the Lesser Himalayan Duplex (DeCelles et al., 2001; Robinson et al., 2003).

The Main Central Thrust has an inception age of ~ 23-20 Ma and is thought to have been most active around this time (Kaneoka & Kono, 1981; Hubbard & Harrison, 1989; Harrison et al., 1992; Hodges et al., 1996; Daniel et al., 2003). DeCelles et al. (2000) also entertain a large amount of pre-Tertiary displacement and there is abundant evidence for additional southward displacement along less well defined shear zones that developed at garnet-grade and lower metamorphic conditions (Brunel & Kienast, 1986; Hodges et al., 1996; Macfarlane et al., 1992; Wyss et al., 1999). The age of cessation is not as clear-cut, with some workers favouring a 15-13 Ma maximum age for displacement (Stephenson et al., 2000; Daniel et al., 2003) whilst others argue for later-stage reactivation (Macfarlane et al., 1992; Harrison et al., 1997; Catlos et al., 2001, 2002; Kohn et al., 2001).

Srivastava & Mitra (1994) report crosscutting relationships that indicate the Main Central Thrust may have had a major episode of out-of-sequence displacement. The thrust has also yielded many Late Miocene-Pliocene mineral cooling ages (Copeland et al., 1991; Macfarlane, 1993; Metcalf, 1993; Edwards, 1995; Oliver et al., 1995; Harrison et al., 1997; Catlos et al., 2001, 2002). Indeed, Pliocene ^{40}Ar-^{39}Ar mica ages characterise the shear zone (Copeland et al., 1991; Macfarlane, 1993; Edwards, 1995) whilst Late-Miocene-Pliocene monazite ages are characteristic of rocks within the inverted metamorphic sequence. These monazites decrease in age down-section between the MCT-I and MCT-II from ~ 22 Ma to 3.3 Ma (Metcalf, 1993; Catlos et

al., 2001) (Fig. 2.7. & 2.12). The young ages have been interpreted as indicating fault reactivation at ~ 6-8 Ma following ~ 10 Myr of inactivity and imply 20 km of exhumation since then (Harrison et al., 1997). Furthermore, Catlos et al. (2001) purport ~ 3.3 Ma movement along the Main Central Thrust in central Nepal from Th-Pb ion-microprobe dating of Lesser Himalayan synkinematic monazites. From this they infer ~ 30 km of slip along the Main Central Thrust during the last 3 Myr with exhumation rates of > 10 mm/yr. Along the Everest transect in eastern Nepal Krummenacher et al. (1978) obtained biotite K-Ar ages from Greater Himalayan gneiss within the Main Central Thrust of between 9 ± 0.5 Ma and 3.4 ± 0.1 Ma. Hubbard & Harrison (1989) also report a ^{40}Ar-^{39}Ar age of 12 ± 0.2 Ma for muscovite and 8 ± 0.2 Ma for K-feldspar along the same section. The youngest mica ages include those from the Lesser Himalaya of central Nepal (2.9 ± 0.1 Ma; Edwards, 1995). Johnson et al. (2001) disagree with studies that suggest slip on the Main Central Thrust was completed by ~ 18 Ma (Hodges et al., 1996; Coleman, 1998) and propose high-temperature ductile slip continued until ~ 14 Ma. They also accept late Miocene-Pliocene reactivation suggestions. In central Nepal, along the Darondi Khola, Kohn et al. (2001) derived Th-Pb ion microprobe ages of monazites as young as 7.9 ± 0.2 Ma in the high strain zone.

However, whether the Late Miocene-Pliocene ages reflect brittle faulting or resetting by hydrothermal fluids, despite several of the monazites occurring as inclusions in garnet, is a matter for debate, (e.g. Searle et al., 2002). The fact that the regional structure where the ion microprobe studies have been executed is not well documented complicates matters. As with the Greater Himalayan Zone, passive

uplift above a duplex within the Lesser Himalaya could also explain the young ages whilst conveniently explaining the inverted metamorphic gradient (DeCelles et al., 1998b, 2001; Robinson et al., 2003). Catlos et al. (2001) propose the distribution of ages and P-T histories across the Main Central Thrust are consistent with the inverted metamorphism having formed by the transposition of right-way-up metamorphic sequences during Late Miocene-Pliocene shearing with the accretion of successive tectonic slices of the Lesser Himalaya to the hanging-wall. This is in agreement with the thermo-kinematic model of Harrison et al. (1998) who, along with Hubbard & Harrison (1989), invoke out-of-sequence thrusts to explain the reheating of the Greater Himalaya. The successive southwards emplacement of duplex thrust sheets could explain the N-S decreasing age of metamorphism (~ 21 Ma to ~ 7 Ma 7 km south of the Main Central Thrust) within the Lesser Himalayan rocks of the Main Central Thrust in central Nepal, documented by Harrison et al. (1997, 1998) and Catlos et al. (2001) from Th-Pb ages of monazite inclusions (Fig. 2.7. & 2.12.). The age data already discussed, together with numerous models that have been put forward, indicate the inverted metamorphism is indeed a late-stage phenomenon, favouring rapid unroofing in late Miocene-Pliocene time. Reported ages suggest reactivation occurred contemporaneously along-strike at least between Garhwal and central Nepal. This indicates the rotation of India model proposed by Guillot et al. (1999) to explain the apparent east to west diachroneity of age data had ceased to be a factor by Late Miocene time (Catlos et al., 2002).

The young muscovite ages cited above could be due to recrystallisation through localised shear partitioning within the Main Central Thrust Zone but the monazite

ages are harder to explain (Metcalf, 1993). No structural or textural evidence is cited to show that the garnet growths were associated with Himalayan thrusts. Additionally, from monazite and ^{40}Ar-^{39}Ar mica dates, the section between the MCT-I and MCT-II cooled below 350°C at ~ 3–5 Ma and therefore, contrary to Kohn et al. (2001), was too cold to permit garnet growth (3.3 Ma and T > 500°C, Catlos et al., 2001) in the underlying rocks (Johnson & Harley, 2003). The temperature at which the garnets grew and the process which enabled the generation late-stage high temperatures remains unknown. More work is thus required to test the validity of the young monazite ages.

There have been suggestions of current movement along the Main Central Thrust (geodetic data, Bilham et al., 1997; Hodges et al., 2001) and the South Tibetan Detachment (^{14}C ages of river terraces, Hurtado et al., 2001). It is possible that strain accumulation along a ramp in the basal detachment below the Main Central Thrust could explain the geodetic data (Jackson & Bilham, 1994). Using ^{40}Ar-^{39}Ar ages of synkinematic muscovite and river channel steepness changes, Hodges et al. (2004) invoke passive uplift over this ramp to explain the presence of out-of-sequence thrusts, active during the last 4 Ma, within the Lesser Himalaya adjacent to the Main Central Thrust. Additionally, the spatial association of the Main Central Thrust with an abrupt physiographic transition, where rivers display sharp knick-points, could suggest current movement (Seeber & Gornitz, 1983). But once again there are counter arguments and a fault-ramp has been proposed for the origin for this phenomenon (Cattin & Avouac, 2000). There is also a cluster of landslide and hydrothermal activity along the thrust zone and a ~ 50 km wide zone of moderate

earthquakes located in the Lesser Himalaya south of the Main Central Thrust (Seeber et al., 1981; Valdiya, 1992; Kayal, 1996). So although there are arguments that disagree, all of the associations outlined above seem to favour recent movement along the Main Central Thrust and elsewhere.

2.5. Lesser Himalayan Zone

The Lesser Himalaya comprise Proterozoic to Tertiary low-grade metasediments and carbonates that were originally deposited on the north Indian passive margin (Fuchs, 1977; Stöcklin, 1980; Valdiya, 1980; Sakai, 1983; Bashyal, 1986; Upreti, 1996, 1999; Garzanti, 1999; Paudel & Arita, 2000; Myrow et al., 2003). The majority of rocks are however Mesoproterozoic to Early Cambrian in age (Brasier & Singh, 1987; Brookfield, 1993; Parrish & Hodges, 1996; Singh et al., 1999). Although the entire succession is ~ 8-10 km thick (e.g. Schelling, 1992), detailed information about the thickness of individual formations is not available. Lesser Himalayan rocks contain few fossils and consequently have been difficult to date and correlate regionally, resulting in a long list of formation names and hindering research (Fig. 2.8.). However, some of this confusion has been alleviated by U-Pb dating of detrital zircons (Parrish & Hodges, 1996; DeCelles et al., 2000). The lower half of the Lesser Himalaya is dominated by siliciclastic rocks which are joined by carbonates in the upper half (Le Fort, 1975; Stöcklin, 1980; DeCelles et al., 2001). The lower Lesser Himalayan sequence (Kushma, Ranimata, Ulleri Formations and equivalents) is Palaeo- and Meso-Proterozoic in age (1.86-1.83 Ga) (Parrish & Hodges, 1996; Gehrels et al., 1999; DeCelles et al., 2000). The upper sequence comprises Permian to Palaeocene Gondwanas and Eocene to Miocene foreland basin units (Sakai, 1983).

The metamorphic grade of Lesser Himalayan rocks increases towards the Main Central Thrust at higher structural levels whilst Lower amphibolite grade rocks exist within the thrust zone (i.e. upper Lesser Himalaya) and the Crystalline Thrust Sheets. Kyanite and sillimanite gneisses are also found within the Main Central Thrust Zone.

At least five phases of deformation have given the Lesser Himalayan Zone a structural complexity, two of which are pre-Himalayan (Paudel & Arita, 2000) (Fig. 2.9.). The Lesser Himalayan Zone also underwent granite intrusion at 1800 Ma (Trivedi et al., 1984). Another series of granite plutons of Early Palaeozoic age (e.g. Mandi Granite, NW India) reflect emplacement during Pan-African magmatism (Le Fort et al., 1980, 1983; Le Fort, 1995). Two white mica ages from an augen gneiss and a meta-conglomerate of the Kuncha Formation in Nepal gave staircase age spectra with high-temperature steps reaching 1400 Ma (Copeland et al., 1991). Additionally, K-Ar whole-rock ages of Lesser Himalayan units show peak metamorphic temperatures were reached in Permian Strata by 209-157 Ma and in Proterozoic-Palaeozoic samples from 486-74 Ma (Johnson & Oliver, 1990; Oliver et al., 1995). Indeed, most mica plateau ages from Lesser Himalayan units fall in the range 1200-800 Ma (Frank et al., 1995). However, in Garhwal (NW India) the Lesser Himalaya underwent a Pre- to Upper-Palaeocene low-grade metamorphic event (Johnson & Oliver, 1990; Morrison & Oliver, 1993). Peak metamorphism thus occurred prior to Himalayan orogenesis which was then followed by Himalayan diagenetic to garnet-grade metamorphism (Oliver et al., 1995; Paudel & Arita, 2000). Along with the lack of evidence for any Himalayan ages, illite crystallinity indicates

most of the Lesser Himalaya has not been heated above 350°C since collision except those rocks adjacent to the Main Central Thrust (Oliver et al., 1995).

2.5.1. Inner and Outer Lesser Himalaya

The Lesser Himalayan Zone is divided into inner and outer zones (Valdiya, 1995) by the Bari Gad – Kali Gandaki Fault in Nepal (Arita et al., 1984; Sakai, 1985) and by the Tons Thrust in the Garhwal-Kumaon Region (Srivastava & Mitra, 1994; Ahmad et al., 2000) (Fig. 2.10.). These zones are defined by differing ε_{Nd} values (see Chapter 6) whereby the Outer Lesser Himalaya yield consistent Greater Himalayan-type values and the Inner Lesser Himalaya yield consistent Lesser Himalayan-type values (Ahmad et al., 2000). In Nepal the outer belt is a para-autochthonous unit and is distributed mainly in the southern Lesser Himalaya along the Main Boundary Thrust. The inner belt comprises two thrust sheets (Paudel & Arita, 2000) and extends north to the Main Central Thrust. Ahmad et al. (2000) discovered the Outer Lesser Himalaya has a Rb-Sr array aligned along a 500 Ma reference line. This early Palaeozoic age for Outer Lesser Himalayan deposition is consistent with the ages proposed on the basis of lithostratigraphic correlation (Valdiya, 1995; Oliver et al., 1995). The Outer Lesser Himalaya and the Greater Himalaya form a set on a Th-Sc-Zr ternary element plot, indicating a strong similarity in source area, which is distinct from the Inner Lesser Himalaya (Ahmad et al., 2000). Ahmad et al. (2000) suggest the Outer Lesser Himalaya and Greater Himalaya were deposited between 1900 Ma (youngest model age) and 500 Ma (age of partial resetting of Sr isotopes) whereas the Inner Lesser Himalaya were deposited between 2300-1800 Ma. They discuss the possibility of the Outer Lesser Himalaya representing a low-grade Greater

Himalayan equivalent. The Tons Thrust in Garhwal would then be an out-of-sequence thrust with sufficient displacement to elevate Lesser Himalayan rocks in the north to the structural level of the unmetamorphosed Greater Himalayan equivalents in the south (Ahmad et al., 2000). There is as yet, however, no stratigraphic link between the Outer Lesser Himalaya and the Greater Himalaya.

2.5.2. Crystalline Thrust Sheets

Lying structurally above the rocks of the Lesser Himalayan Zone are several synformal klippen or Crystalline Thrust Sheets, Pre-Cambrian to Mid-Palaeozoic in age (Gansser, 1964; DeCelles et al., 1998b; Hodges, 2000). In Nepal these include, from west to east, the Dadeldhura, Karnali, Jajarkot, and Kathmandu Crystalline Thrust Sheets (Gansser, 1964; Valdiya, 1980). These have a Greater Himalayan affinity and are generally recognised as Greater Himalayan outliers having been emplaced along the Main Central Thrust (Gansser, 1964; Stocklin, 1980; Valdiya, 1980; Schelling, 1992; Upreti, 1996; Upreti & Le Fort, 1999). However, the location of their root zones remains contentious. It is possible the Crystalline Thrust Sheets represent a separate tectonic unit that was carried along a thrust other than the true Main Central Thrust, with an inception age younger than the Main Central Thrust but older than the Main Boundary Thrust (Upreti & LeFort, 1999) (Fig. 2.11). The fact that many of the largest thrust sheets (e.g. the Almora Thrust Sheet in NW India and the Kathmandu Thrust Sheet in Nepal) have an internal stratigraphy unlike that of the Greater Himalayan Zone supports the latter hypothesis (Hodges, 2000). The Crystalline Thrust Sheets consist of garnet- to biotite-grade schist and orthogneiss in the lower part (Greater Himalayan affinity) and low-grade meta-sedimentary to

sedimentary units in the upper part (Tibetan Himalayan affinity). Late Cambrian to Early Ordovician plutons of two-mica, cordierite-bearing granite are also present in several of the Thrust Sheets.

The Dadeldhura Crystalline Thrust Sheet in west Nepal is the eastern continuation of the Almora Crystalline Thrust Sheet in Kumaon, NW India (Valdiya, 1980; Srivastava & Mitra, 1994) and forms a NW- to SE-trending synform (DeCelles et al., 1998b). This is a remnant of an extensive thrust sheet that must have covered the entire Lesser Himalayan Zone to the north of the presently exposed synform. The thrust sheet contains a large Cambro-Ordovician granitic pluton (Dadeldhura Granite) and ~ 10 km of Pre-Cambrian phyllite, quartzite, slate, schist, augen gneiss, and local meta-volcanic units (Bashyal, 1986; Upreti, 1996). The Dadeldhura Thrust Sheet was emplaced on to the Ranimata Formation of the Lesser Himalaya during the Early Miocene (Main Central Thrust phase). An ^{40}Ar-^{39}Ar muscovite plateau age of 21.36 ± 0.09 Ma from the north limb of the Dadeldhura Thrust Sheet dates its initial emplacement (DeCelles et al., 2001) (Fig. 2.2.). Also, in west Nepal the Dadeldhura Thrust cuts the Dumri Formation foreland basin succession (deposited ~ 20 Ma) and so must have had a major phase of displacement (tens of kilometres) that post-dates Dumri deposition (~ 20-15 Ma) (DeCelles et al., 1998b). The Dadeldhura Crystalline Thrust Sheet is thought to have been passively folded by Lesser Himalayan Duplex growth and again in latest Miocene-Pliocene time by transport of the Main Boundary Thrust over an ~ 8 km-high footwall ramp (DeCelles et al., 1998b).

In central and eastern Nepal the equivalent of the Dadeldhura Thrust is the Mahabarat Thrust which carries the structurally analogous Kathmandu Crystalline Thrust Sheet (Lal et al., 1981; Mohan et al., 1989) and is considered to be the southern continuation of the Main Central Thrust (Stocklin, 1980; Rai et al., 1998; Johnson et al., 2001). Due to a shallower level of erosion, the Kathmandu Crystalline Thrust Sheet and Main Central Thrust still cover most of the Lesser Himalaya in eastern Nepal (e.g. Schelling, 1992; Upreti & Le Fort, 1999). This suggests at least ~ 15 km of rock was eroded from the hanging-wall of the Dadeldhura Thrust between its present northern trace and the Main Central Thrust (DeCelles et al., 1998b). Thermochronologic data from the Kathmandu Crystalline Thrust Sheet indicate cooling through the muscovite blocking temperature between 22-14 Ma (Copeland et al., 1996; Johnson et al., 2001). The cooling rate over the 22-14 Ma period was ~ 20°C/Ma, giving an exhumation rate of ~ 1.9 mm/yr (Johnson et al., 2001). Due to a lack of younger muscovite cooling ages within the Crystalline Thrust Sheets it seems likely that the proposed reactivation of the Main Central Thrust only affected the Greater Himalaya and not the outlying nappes. Johnson et al. (2001) explain this using thermobarometry data, which indicate that the high-grade rocks of the Kathmandu Crystalline Thrust Sheet and Greater Himalaya detached at a deep level in the crust. Arita & Ganzawa (1997) obtained zircon fission-track ages of ~ 9 Ma from granites within the Kathmandu Crystalline Thrust Sheet and calculate an average denudation rate of 0.8 mm/yr for the last ~ 9 Myr. They relate this late-stage cooling to passive uplift above the Lesser Himalayan Duplex.

2.5.3. Lesser Himalayan Duplex

The rocks of the northern Lesser Himalaya have been repeated by a foreland-propagating duplex structure resulting in steep and overturned folds and imbricated panels of the Lower and Upper Nawakot units and the overlying Gondwanan and Tertiary units (Fig. 2.1.). In central and western Nepal the duplex has a hinterland-dipping, antiformal geometry (Robinson et al., 2003). Whilst the Himalayan basal detachment forms the floor thrust to the Lesser Himalayan Duplex, the Ramgarh Thrust forms the roof thrust. In western Nepal it is thought duplex growth commenced with emplacement of the Ramgarh Thrust (DeCelles et al., 1998b). The Ramgarh Thrust is a major fault system which roots beneath the Main Central Thrust and places greenschist-grade rocks of the Kushma and Ranimata Formations (Lower Lesser Himalayan Zone) on top of less metamorphosed Lesser Himalayan rocks (Valdiya, 1980). Structurally, the Ramgarh Thrust rests on top of Upper Nawakot and/or Tertiary rocks and beneath the Dadeldhura Crystalline Thrust Sheet. Duplex growth has been linked to the folding of the overlying Crystalline Thrust Sheets. Therefore, inception of the Ramgarh Thrust and subsequent duplex growth is thought to post-date the emplacement of the Crystalline Thrust Sheets (~ 15-10 Ma) (Srivastava & Mitra, 1994; DeCelles et al., 1998a; Paudel & Arita, 2000; Robinson et al., 2003). Because the ~ 20-15 Ma Dumri Formation (foreland basin sediments) is contained within some of the duplex horses, DeCelles et al. (1998b) support an ~ 11 Ma age for duplex initiation. Additional structural, stratigraphic, and geochemical arguments indicate Lesser Himalayan rocks were not exposed in the thrust belt until this time (Quade et al., 1997; DeCelles et al., 1998b). Thrust sheets of Lesser Himalayan rocks were subsequently incorporated into the duplex, passively uplifting

and folding the Greater Himalaya, Crystalline Thrust Sheets, and underlying Ramgarh Thrust into a broad antiform (DeCelles et al., 1998b; Robinson et al., 2003) (Fig. 2.12.). Although the presence of the Lesser Himalayan Duplex in eastern Nepal has been disputed, DeCelles et al. (2001) have recognised the Ramgarh Thrust in central and eastern Nepal along the southern limb of the Kathmandu Crystalline Thrust Sheet. The location of maximum seismicity, convergence and uplift in the modern-day Himalayas is located along a ramp in the basal detachment below the Lesser Himalayan Duplex (Bilham et al., 1997; DeCelles et al., 1998b).

2.6. Main Boundary Thrust

The Main Boundary Thrust is a major Himalayan structure that runs roughly parallel to the Main Central Thrust but can be traced for even further distances along-strike (Gansser, 1983; Valdiya, 1992; Meigs et al., 1995) (Fig. 2.2.). Good outcrops of the fault are only found in the western Himalayas where it is generally marked by a narrow zone (~ 100 m) of cataclasis (Schelling, 1992; Valdiya, 1992). The Main Boundary Thrust is thought to be the most recently active of the thrusts that root beneath the Lesser Himalayan Duplex and there is evidence for current seismicity along the structure (Ye et al., 1981; Molnar, 1988; Valdiya, 1992). In fact, based on seismic activity and fault-plane solutions Baranowski et al. (1984) suspect the thrust to be active today. The Main Boundary Thrust is composed of discrete faults and narrow shear zones which are offset by transverse faults (Treloar et al., 1992; DeCelles et al., 1998b; Upreti, 1999). Rocks within the Main Boundary Thrust sheet are generally not metamorphosed or are metamorphosed only to lower greenschist facies. Although the hanging-wall of the Main Boundary Thrust generally comprises

Mesozoic and/or Palaeozoic strata, it is often in close proximity (1-10 km) to a hinterlandward thrust carrying a thick succession of Pre-Cambrian metasedimentary rocks in the hanging-wall, such as the Cherat Fault in Pakistan (McDougal & Khan, 1990) or the Panjal Thrust in Kashmir (Wadia, 1931).

The history of the Main Boundary Thrust is far less constrained than that of the Main Central Thrust despite tens of kilometres of estimated N-S shortening across the structure (Powell & Conaghan, 1973; Molnar, 1984, 1988; Schelling, 1992; Treloar et al., 1992; Srivastava & Mitra, 1994; DeCelles et al., 1998b). This is due to inferior exposure, a dearth of radiometric dates and a lack of displaced units or crosscutting relations that closely define its deformation history. Erosion has removed those strata directly associated with the thrust that could unambiguously record its motion (Burbank et al., 1988; Burbank, 1992).

The Main Boundary Thrust folds the Main Central Thrust in places and cuts Quaternary sedimentary rocks in the foreland, thus it must have formed sometime between the present and ~ 20-25 Ma (Meigs et al., 1995). The kinematic history of the Himalayan thrust belt is generally considered to involve southward progression of thrusting from Eocene to present (Ratschbacher et al., 1994; DeCelles et al., 2001). Therefore it is thought that the main phase of Main Central Thrust movement had ceased prior to Main Boundary Thrust inception. Harrison et al. (1998) estimate a ~ 15 Ma age for this transition on the basis of estimates for the age of cessation of slip along the Main Central Thrust. Meigs et al. (1995) propose a similar age based on three lines of evidence. They interpret regional changes in depositional

characteristics and accumulation rates in the foreland basin between 11 and 9.5 Ma as reflecting new hinterland loading due to Main Boundary Thrust inception. They also found an 8.7 Ma conglomerate from the Jawalamukhi foreland basin section in Himachal Pradesh that was derived from the Main Boundary Thrust Sheet. Assuming a gravel progradation rate of 3 cm/yr this age would suggest the Main Boundary Thrust hanging-wall was uplifting prior to 10 Ma. Meigs et al. (1995) also report apatite fission-track ages from structures at the leading edge of the Main Boundary Thrust in the Kohat region of NW Pakistan that indicate rapid cooling between 10-8 Ma. This probably followed bedrock uplift and erosion that began 1-2 Ma earlier. They entertain the idea that the Main Boundary Thrust may have been coeval with late Main Central Thrust movement and propose synchronous along-strike inception of the Main Boundary Thrust with a displacement rate of ~ 10 mm/yr. An ~ 11 Ma inception age is also suggested by Burbank et al. (1996) based on foreland basin depositional characteristics and Najman et al. (2004) based on apatite fission-track data from the Kangra and Subathu sub-basins in NW India. DeCelles et al. (1998b, 2001), however, argue that the Main Boundary Thrust in Nepal must post-date emplacement of the Crystalline Thrust Sheets (~ 10 Ma) because the latter were folded by growth of the Lesser Himalayan Duplex which fed slip southward into the Main Boundary Thrust. They therefore favour a Pliocene age for Main Boundary Thrust inception and suggest an age earlier than ~ 5 Ma is unlikely since most shortening was accommodated by duplex growth until that time. A minimum age limit can also be derived from sediment deposited and preserved in intermontane basins blocked by hanging-wall uplifts. Burbank & Johnson (1983) used the age of the Karewa strata in Kashmir to suggest Main Boundary Thrust

activity by 4-5 Ma. In fact, whatever the age of the Main Boundary Thrust, uplift of the Karewas by 1.5-3 km indicates several kilometres of shortening along the structure during Pleistocene time. Similarly, the fill of the Peshawar intermontane basin of Pakistan indicates Main Boundary Thrust movement commenced prior to ~ 3 Ma (Burbank et al., 1986). Although these younger ages have been supported by other studies (Macfarlane, 1993; Huyghe et al., 2001; Johnson et al., 2001), there still remains confusion as to the precise age of Main Boundary Thrust inception.

2.7. Sub-Himalayan Zone

The Sub-Himalayan Zone, comprising foreland basin sediment of the Siwalik Group south of the Main Boundary Thrust, represents the currently active thrust-front (10-25 km wide) of the Himalayas and forms the hanging wall of the Main Frontal Thrust. In India and Nepal the Sub-Himalayan Zone is narrower than in Pakistan, reflecting the absence of evaporites (which lubricate the Salt Range) and a steeper slope of the basement towards the hinterland (Yeats & Lillie, 1991). A series of concatenated faults and duplexes of Pliocene age between the Main Boundary Thrust and Main Frontal Thrust repeat the north-dipping Siwalik Group rocks and divide the Sub-Himalayan Zone into tectonic slices in southern Nepal (Mugnier et al., 1999). These faults run roughly parallel to the mountain front and are commonly manifested in antiformal ridges of uplift. The Sub-Himalayan Zone thrusts indicate the presence of a regional detachment in the lowermost Siwalik units at a depth of ~ 5-6 km (Schelling & Arita, 1991; Schelling, 1992; Srivastava & Mitra, 1994; Mugnier et al., 1993; DeCelles et al., 1998b). Most of these thrust sheets have a top-to-the-SSW sense of shear and have generally experienced less than 10 km of shortening

(Burbank et al., 1996; Mugnier et al., 1999). They carry Siwalik Group rocks (4-10 km thick) of Pliocene age and younger and must therefore be younger than ~ 3 Ma. Progressively rotated syn-tectonic strata indicate the thrusts began to disrupt this part of the foreland during Late Pliocene time (Burbank et al., 1996). Mugnier et al. (1998) calculated a shortening rate of 11-17 mm/yr during the last 2.4 Ma for one of the Sub-Himalayan Zone thrusts (Main Dun Thrust) whereas only 4 mm/yr for the Main Frontal Thrust during the same period. This indicates that the Sub-Himalayan Zone faults have experienced out-of-sequence reactivation and episodic pulses of displacement (DeCelles et al., 2001; Mugnier et al., 1998, 1999, 2001). The Siwaliks have consequently been uplifted and tilted by fault-bend-folds (e.g. Suppe, 1983), with uplift rates of up to 15 mm/yr (Lavé & Avouac, 2000; Mugnier et al., 2004). This has produced the Siwalik/Churia Hills which vary between 600-1500 m in height and provide the best exposure of Siwalik rocks. The Siwalik strata often reveal a subtle antiformal geometry (Plate 2.1.).

Schelling & Arita (1991) calculated ~ 17 km of total shortening for the Sub-Himalayan Zone in central Nepal. The overall rate of crustal shortening accommodated within the Lesser Himalaya and Sub-Himalaya since ~ 11 Ma is ~ 21 mm/yr (DeCelles et al., 2001). This is comparable to modern convergence rates determined from GPS geodetic studies (Bilham et al., 1997; Jouanne et al., 1999). A similar value has been reached by other studies that have utilised Sub-Himalayan structures (Mugnier et al., 2002), deformed Quaternary terraces (Lavé & Avouac, 2000), balanced cross-sections (Powers et al., 1998), and the velocity of the flexural wave across the foreland basin during Oligocene-Neogene time (Lyon-Caen &

Molnar, 1985; DeCelles et al., 1998b). It is estimated that 20 % of Indo-Asian convergence has been accommodated by thin-skinned thrusting within the Himalayan foreland (Burbank et al., 1996).

2.8. Main Frontal Thrust

The Main Frontal Thrust is the youngest major Himalayan structure and is located at the topographic break of the Himalayan foothills where Siwalik rocks overlie Quaternary gravels of the modern foreland basin. There is no direct geologic evidence for the age of the Main Frontal Thrust but it is assumed to be a Pliocene-Holocene structure (Molnar, 1984). The fault cuts Siwalik strata in places and is often manifested as anticline growth but actual outcrops are rare, as evidenced from the dashed line in Figure 1.5. (Nakata, 1989; Schelling, 1992; Yeats et al., 1992; Mugnier et al., 1993; Powers et al., 1998; Wesnousky et al., 1999; Lavé & Avouac, 2000). Cross-sections typically depict the Main Frontal Thrust as a decollement thrust with no basement involvement at least as far back as the Main Boundary Thrust system (Fig. 2.1.). It has been estimated that the Main Frontal Thrust has a shortening rate of 9-16 mm/yr (Lyon-Caen & Molnar, 1983; Yeats et al., 1992; Powers et al., 1998). A study of Quaternary terraces in central Nepal suggests the Main Frontal Thrust is accommodating most of the present-day India-Eurasia convergence (Lavé & Avouac, 2000).

2.9. Foreland basin sediments

2.9.1. Palaeogene sediments

Palaeogene sediments comprise the first products of Himalayan erosion and the earliest foreland basin deposits. These are variably exposed in the Sub-Himalayan Zone and piggy-back basins. In Nepal these deposits are restricted to the hanging-wall of the Main Boundary Thrust, in the Lesser Himalaya (Sakai, 1983; DeCelles et al., 1998b). The restricted regional extent of these deposits, their exposure as thrust complexes, and the difficulty of correlation in what are largely unfossiliferous rocks has led to a plethora of local formation names (Fig. 2.13.). The Palaeogene sedimentary record is fragmentary due to uplift and erosion. These sediments were most likely over-thrust during shortening along the Main Boundary Thrust and other Lesser Himalayan structures.

The oldest Himalayan detritus consists of Palaeocene to Early-Middle Eocene carbonate deposits, mudstone, and fine sandstone (e.g. Chulung La Formation in Ladakh, Critelli & Garzanti, 1994; Patala Formation in northern Pakistan, Najman et al., 2002; Subathu Formation in NW India, Najman et al., 2000). These have detrital mineralogy and Nd-Sr isotopic systematics characteristic of Indus-Yarlung Suture Zone rocks (Najman & Garzanti, 2000; Najman et al., 2000). In Nepal, the oldest foreland basin sediments comprise the Amile Formation which was derived from the Indian Shield (DeCelles et al., 1998a). The overlying Bhainskati Formation is correlated with the Subathu Formation of northern India and the Patala Formation of northern Pakistan on the basis of marine faunas, although formation boundaries are

diachronous along strike (Fig. 2.13.). The Bhainskati Formation consists of organic-rich shale, thin quartzose sandstone and conglomerate and thin limestone beds (DeCelles et al., 1998a).

Unconformably overlying the Bhainskati Formation is the Dumri Formation, which consists of a thick unit of fluvial sandstone and red mudstone and is the youngest and stratigraphically highest unit in the hanging-wall of the Main Boundary Thrust (Sakai, 1983; DeCelles et al., 1998a, 1998b). Stratigraphic thickness reaches ~ 700 m at the Dumri Bridge type-section in central Nepal but its upper part is everywhere concealed (DeCelles et al., 1998a). Dumri facies have been interpreted as fluvial channel, crevasse splay, and over-bank deposits and the sandstone to mudstone ratio decreases up-section (Sakai, 1989; DeCelles et al., 1998a). The Dumri has yet to be reliably dated. Regional lithostratigraphic correlations suggest an Early Miocene age for deposition (Sakai, 1983, 1989) although Gautam (1989) inferred a Late Eocene age on the basis of palaeomagnetic inclination data. Using Najman et al's (1997) ^{40}Ar-^{39}Ar ages of detrital white mica from the Dagshai and Kasauli Formations of NW India (Dumri-equivalents), it is likely the Dumri was deposited after ~ 25 Ma. DeCelles et al. (2001) found ^{40}Ar-^{39}Ar detrital mica ages in the Dumri Formation in western Nepal of ~ 20 Ma and detrital fission-track data suggests deposition was younger than 30 Ma (Najman et al., 2005). Additionally, magnetostratigraphy places Dumri deposition between 21-16 Ma (Ojha, personal communication, 2002). The youngest age limit of the Dumri Formation is also poorly known because the top is either faulted or eroded (DeCelles et al., 1998b). Dumri rocks are very different in terms of petrography, lithofacies and palaeoflow from the Siwalik Group lithologies

(DeCelles et al., 1998a). Therefore, the Dumri Formation is probably entirely older than the Siwalik Group.

The Balakot Formation overlies the Palaeocene shallow marine Patala Formation and is the first evidence for Himalayan derived foreland basin detritus in northern Pakistan (Critelli & Garzanti, 1994). This is a > 8 km fossil-free clastic red bed succession and equivalent to the Dumri Formation in Nepal. ^{40}Ar-^{39}Ar dating of detrital muscovites indicate the Balakot Formation was deposited after ~ 37 Ma (Najman et al., 2001). In India, the Subathu Formation is overlain by the Dharamsalas in the Kangra sub-basin, which are divided into the older Daghshai (Dumre equivalent) and overlying Kasauli Formations in the Subathu sub-basin (Najman et al., 1993, 1994, 1997; White et al., 2002). The Dagshai Formation has been poorly dated but ^{40}Ar-^{39}Ar detrital white mica ages and zircon fission-track ages (25-32 Ma) date units within the Dagshai as younger than Middle Oligocene (Najman et al., 1997, 2004). The Dagshai Formation comprises laminated upward-fining sandstone and shale with abundant plant debris, interpreted as having been deposited in a meandering river environment (Najman et al., 2004). These units show SW- to SE-directed palaeoflow (Najman et al., 1993). The Kasauli Formation is dated as younger than 22-32 Ma (Early- to Mid-Miocene), again from ^{40}Ar-^{39}Ar ages of detrital white mica (Najman et al., 1997). Multistoried and amalgamated grey sandstones dominate the Kasauli Formation, suggesting braided fluvial deposition on a wide floodplain (Najman et al., 2004). In Pakistan, fluvial red beds of the Murree Formation (Dumri equivalents) bear a close resemblance to the

Kasauli Formation and are considered to be of Early Miocene age (Burbank et al., 1996).

2.9.1.1. Unconformity

A Late Eocene-Oligocene regional unconformity within Himalayan Palaeogene sediments from Nepal to Pakistan has long been recognised by many workers (DeCelles et al., 1998a and references therein). The ~ 31 ± 2 Ma age for the Dagshai Formation and Early Eocene age for the top of the Subathu Formation beneath shows conclusively the unconformable nature of the Subathu-Dagshai contact, spanning more than 12 Ma (Najman et al., 2004). Similar depositional patterns are witnessed along strike. The equivalent Bainskati-Dumri Formation contact in Nepal is thought to represent a ~ 15-20 Ma unconformity (DeCelles et al., 1998a). Again, in the Hazara-Kashmir syntaxis of Pakistan, shallow marine facies of the Patala Formation (55-53 Ma, Critelli & Garzanti, 1994) are overlain by continental facies of the Balakot Formation (< 37 Ma, Najman et al., 2001). This unconformity is also recorded in the Kohat and Potwar plateaus (Najman et al., 2002 and references therein). DeCelles et al. (1998a) relate the unconformity to migration of the Himalayan forebulge (Fig. 2.14.). They suggest the shallow-marine Bhainskati Formation (Eocene) was the first erosional product of Himalayan orogeny in Nepal and accumulated in a back-bulge depozone (DeCelles et al., 1998a). Forebulge migration then resulted in the ~ 15-20 Ma regional unconformity between the Bhainskati and Dumri Formations. The Dumri and Siwaliks were deposited in the southwards-migrating foredeep and therefore overlapped the Bhainskati. In northern India a well-documented backbulge depozone is not apparent, perhaps because of the

high flexural rigidity of Indian lithosphere in this region (Lyon-Caen & Molnar, 1985). Najman & Garzanti (2000) also propose that the unconformity may relate to choking of the continental subduction zone due to arrival of thicker Indian crust at that time (Najman & Garzanti, 2000)

In terms of the detrital technique the unconformity represents a fundamental gap in our knowledge of Himalayan evolution. In an attempt to account for the missing sediments DeCelles et al. (1998a) propose that there may be proximal equivalents of the Bhainskati Formation rocks which are now preserved in the Tibetan Himalayan Zone of Nepal and that previous workers have documented these units (Liu & Einsele, 1994; Willems et al., 1996). The corresponding missing distal sediments were probably deposited in the Katawaz remnant ocean basin to the west, which represents an Eocene-Oligocene analogue of the Neogene to Holocene Indus delta and fan system (Qayyum et al., 1997).

2.9.2. Neogene sediments

Neogene deposits are much more complete than the Palaeogene detritus and are comprised of continental fluvial sediments. The youngest foreland basin sediments, overlying the Dumri Formation in Nepal (although the two have not been documented in stratigraphic contact), are represented by the > 5 km thick Siwalik Group. In India the Kasauli Formation grades conformably into the Siwalik Group. The Siwalik Group is Mid-Miocene to Pleistocene in age and crops-out along the entire 2500 km of Himalayan foothills from Pakistan to Assam (Gansser, 1964; Parkash et al., 1980; Burbank et al., 1996 and references therein). Siwalik strata are best exposed in the thrust sheets and folds of the proximal foreland (Sub-Himalayan Zone). In contrast to Eocene-Oligocene rocks, considerable chronostratigraphic data exist for the Neogene strata of the foreland. Early discoveries of numerous vertebrate fossils, including hominids, in Siwalik strata led to intensive fossil prospecting and development of detailed biostratigraphies at several localities (e.g. Johnson et al., 1983; Barry et al., 1985; Corvinus & Rimal, 2001). Subsequently, radiometric dating of volcanic ashes and an extensive and ongoing programme of magnetostratigraphic sampling have created numerous well-calibrated stratigraphic successions (Johnson et al., 1982b; Burbank et al., 1996 and references therein; Ojha et al., 2000; Gautam & Fujiwara, 2000). The base of the Siwalik Group has not been found in outcrop in Nepal and so could be older than the ~ 16 Ma currently oldest dated unit (Karnali section, Gautam & Fujiwara, 2000). Palaeocurrent and modal petrographic data from the Siwalik Group indicate these rocks were derived from the developing fold-thrust belt and deposited within the Himalayan flexural foredeep (Critelli & Ingersoll, 1994; DeCelles et al., 1998a). There is a systematic trend of

decreasing quartz content and increasing lithic grain content from the Amile and Bhainskati Formations to the Dumri Formation, and increasing total feldspar content from the Dumri Formation to the Siwalik Group (DeCelles et al., 1998a).

The classic peripheral foreland basin depositional model involves a progression from "underfilled" (deep-water facies), through "filled" (shallow-marine and distal continental facies) to "overfilled" (wholly continental facies) stage, reflecting the changing balance between subsidence and sediment supply (Covey, 1986; Allen et al., 1991; Sinclair et al., 1991). The absence of a deep-water facies in the Himalayan foreland basin is therefore intriguing. The relatively rigid nature of the old, cold Indian crust has been cited as an explanation (Garzanti et al., 1987). However there is modern along-strike variation in rigidity and the Indian crust loaded during the early stages of collision was likely to be weaker than that of today (Lyon-Caen & Molnar, 1985; Burbank et al., 1996). Flysch deposits and deep marine sediments could potentially have been deposited in a proximal position and therefore can now be found in the Tibetan Himalayan Zone or have been concealed by overthrusting. If the Indian crust was weaker during initial subduction (younger rocks and also highly extended passive margin) a deeper and narrower foreland basin should have resulted (Turcotte & Schubert, 1982). Indeed, some of the oldest and most northerly of the preserved foreland strata (Eocene Murree Formation in the Kashmir-Hazara syntaxis, Bossart & Ottiger, 1989) are also some of the thickest successions (~ 8 km).

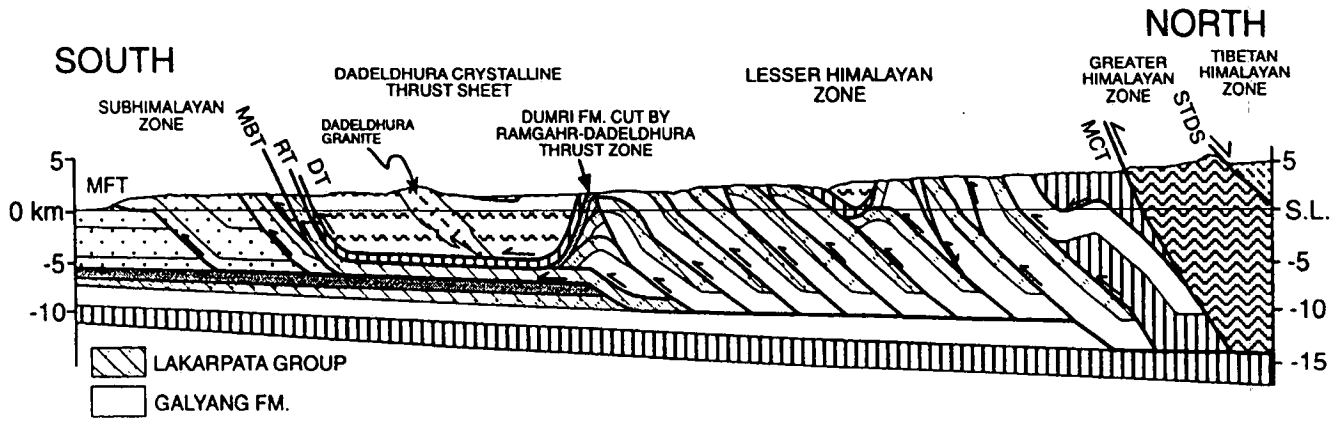


Figure 2.1. Structural cross-section of the Himalayas in far west Nepal showing main features including Lesser Himalayan Duplex, from DeCelles et al. (1998b). MFT - Main Frontal Thrust, MBT - Main Boundary Thrust, RT - Ramgarh Thrust, DT - Dadeldhura Thrust, MCT - Main Central Thrust, STDS - South Tibetan Detachment System.

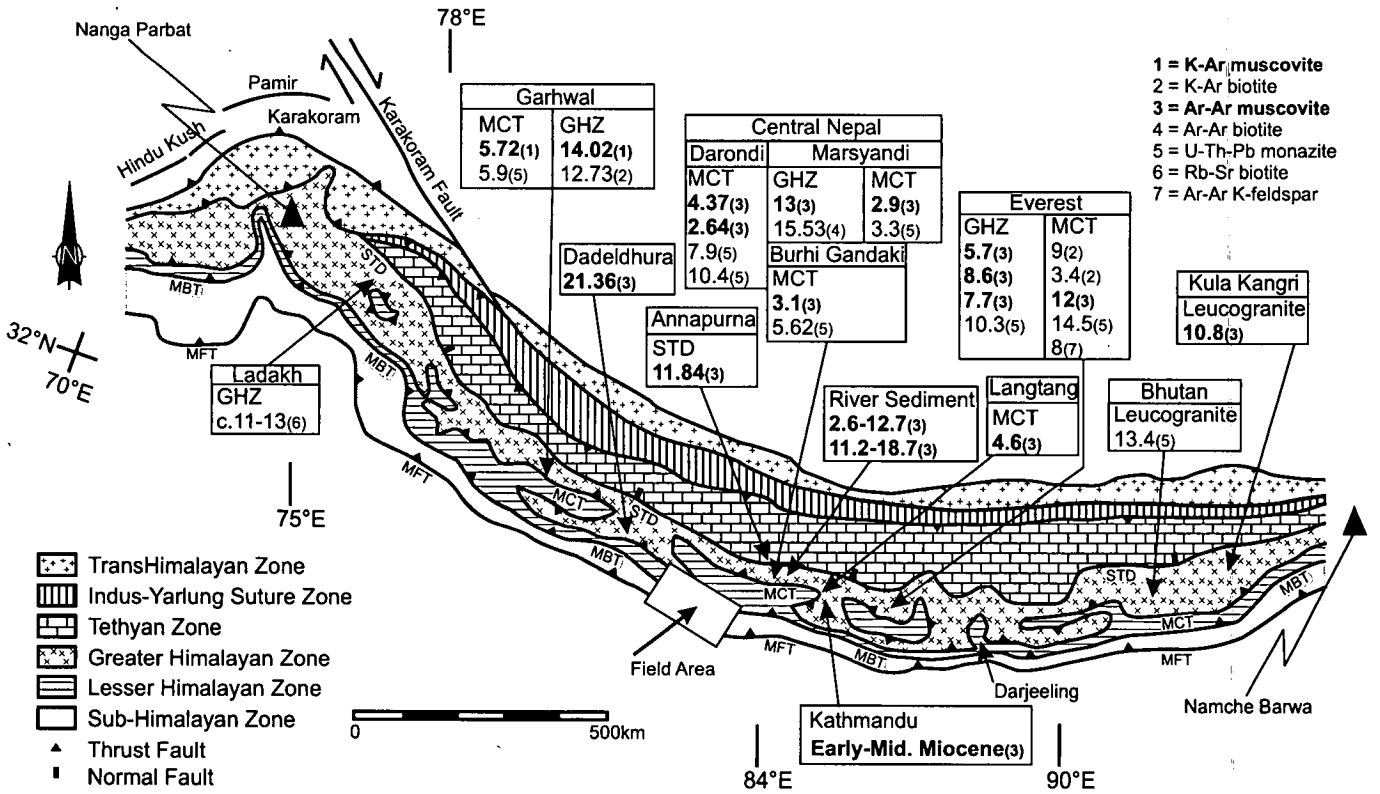


Figure 2.2. Geological map of the Himalaya, adapted from Searle et al. (2003), showing selected young age data as evidence for most recent tectonics. Relevant dating technique is shown in key. Data sources: Ladakh (Honegger et al., 1982), Garhwal (Metcalf, 1993; Catlos et al., 2002), Dadeldhura (DeCelles et al., 2001), Annapurna (Godin et al., 2001), Central Nepal (Copeland et al., 1991; Edwards, 1995; Vannay & Hodges, 1996; Harrison et al., 1997; Coleman & Hodges, 1998; Catlos et al., 2001; Kohn et al., 2001), river sediment (Brewer et al., 2003), Langtang (Macfarlane, 1993), Everest (Catlos et al., 2002), Bhutan (Daniel et al., 2003), Kula Kangri (Maluski et al., 1988). STD: South Tibetan Detachment, MCT: Main Central Thrust, MBT: Main Boundary Thrust, MFT: Main Frontal Thrust.

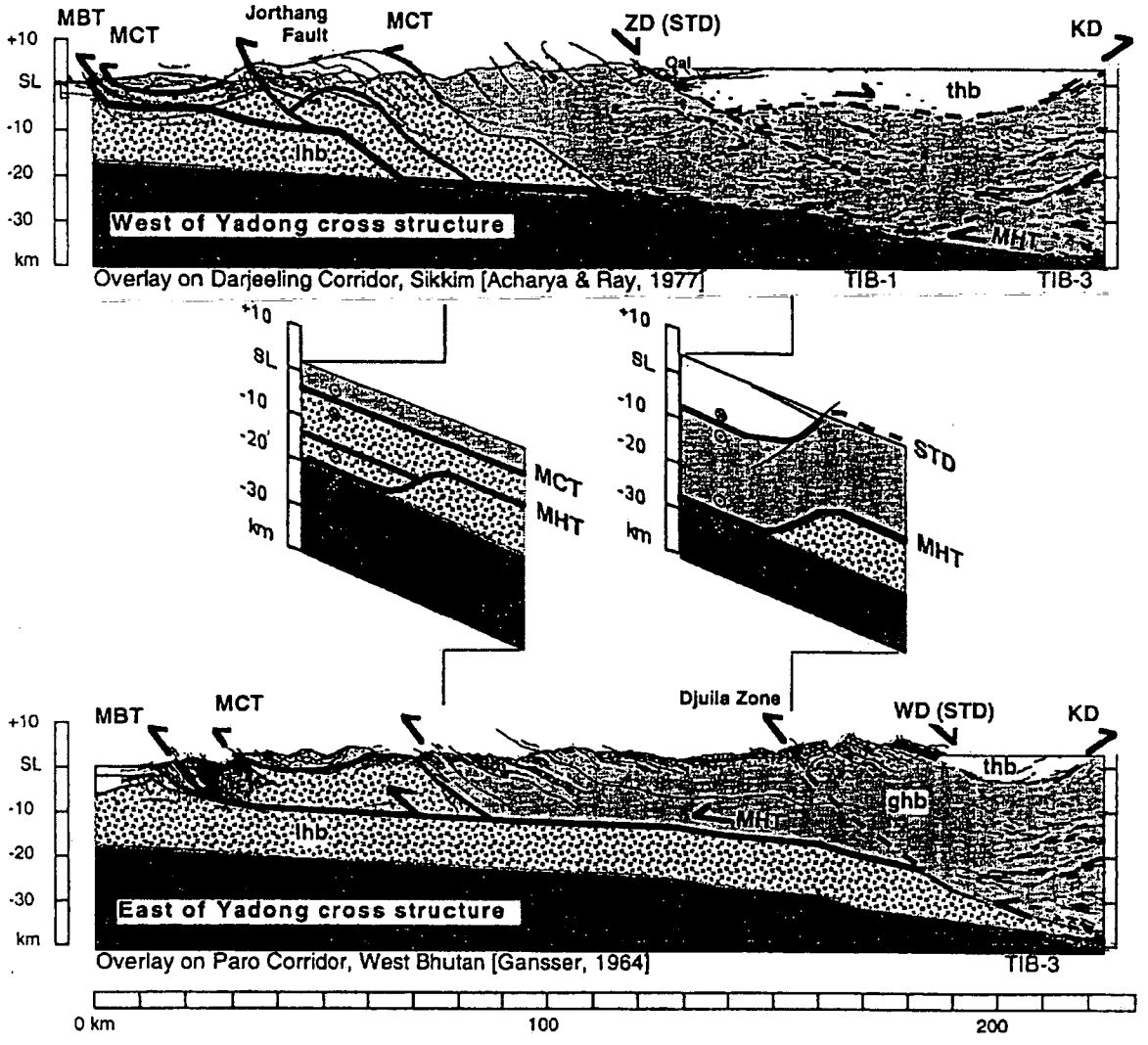


Figure 2.3. Interpretive geological cross-section based on INDEPTH data, from Searle & Szulc (2005). lhb - Lesser Himalayan belt, ghb - Greater Himalayan belt, thb - Tibetan Himalayan belt, MHT - Main Himalayan Thrust or basal detachment, ZD - Zherger-la detachment, WD - Wagye-la detachment (both local names for strands of the South Tibetan Detachment (STD)).

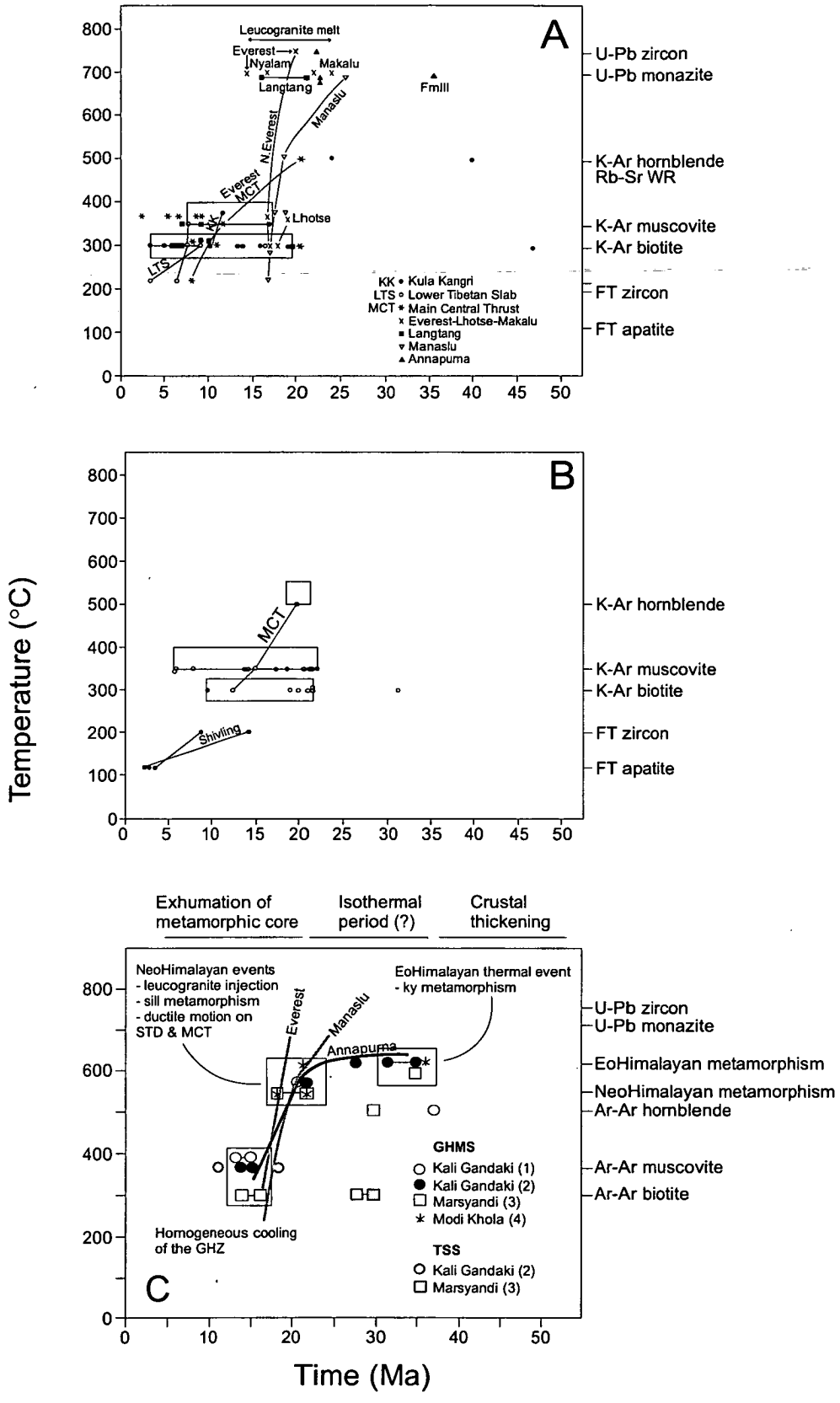


Figure 2.4. Caption on next page.

Figure 2.4. Temperature-time plots for the central Nepal Himalaya (A), Garhwal Himalaya (B), and Annapurna-Manaslu Himalaya (C) from Searle (1996) and Searle & Godin (2003). The solid lines show T-t cooling paths. MCT - Main Central Thrust, STD - South Tibetan Detachment, GHZ - Greater Himalayan Zone, GHMS - Greater Himalayan Metamorphic Sequence, TSS - Tibetan Sedimentary Sequence, ky - kyanite.

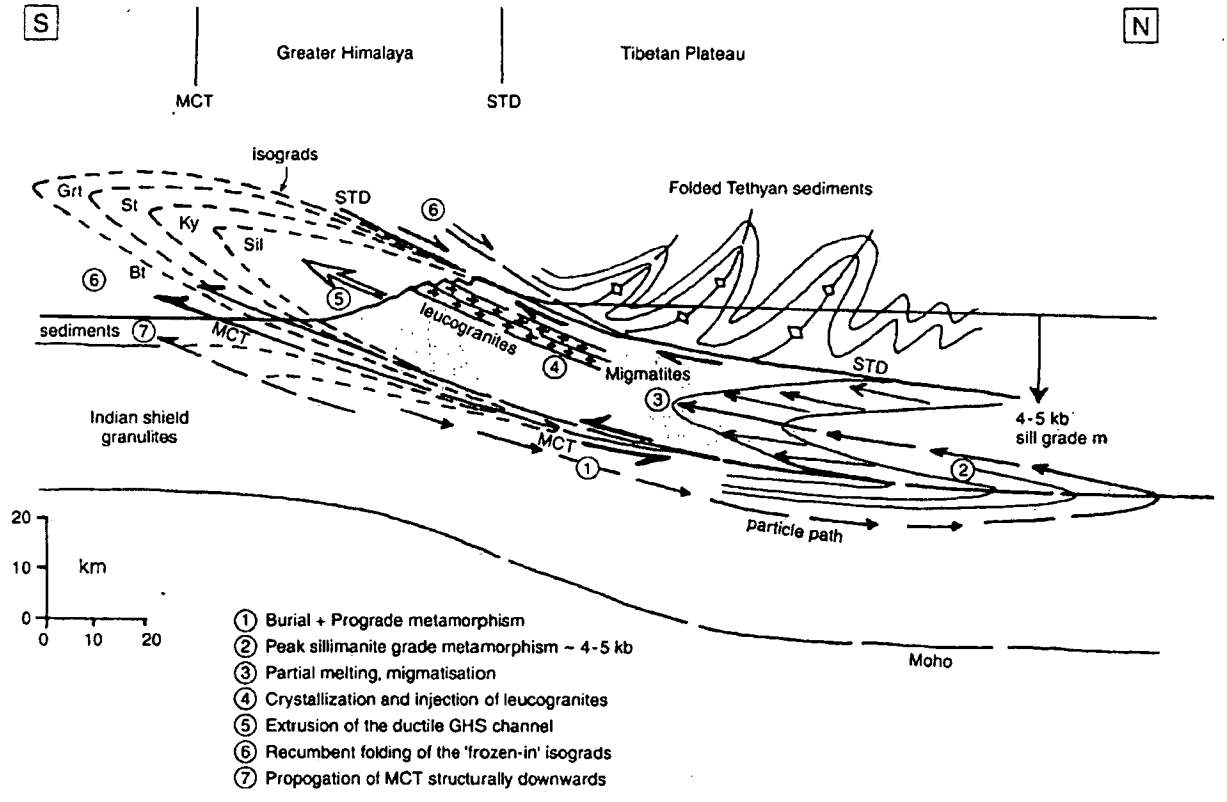


Figure 2.5. The Searle & Szulc (2005) model for channel flow and ductile extrusion of the Greater Himalaya, showing stages in burial at 1, metamorphism, melting and exhumation history until final exposure and erosion at 6. The depth to the South Tibetan detachment during peak metamorphism is constrained by pressures of 4-5 kbar in sillimanite grade gneisses. The model shows how the metamorphosed Greater Himalaya was extruded between the coeval Main Central Thrust (MCT) and South Tibetan Detachment (STD). Sil - sillimanite, Ky - kyanite, St - staurolite, Grt - garnet, Bt - biotite.

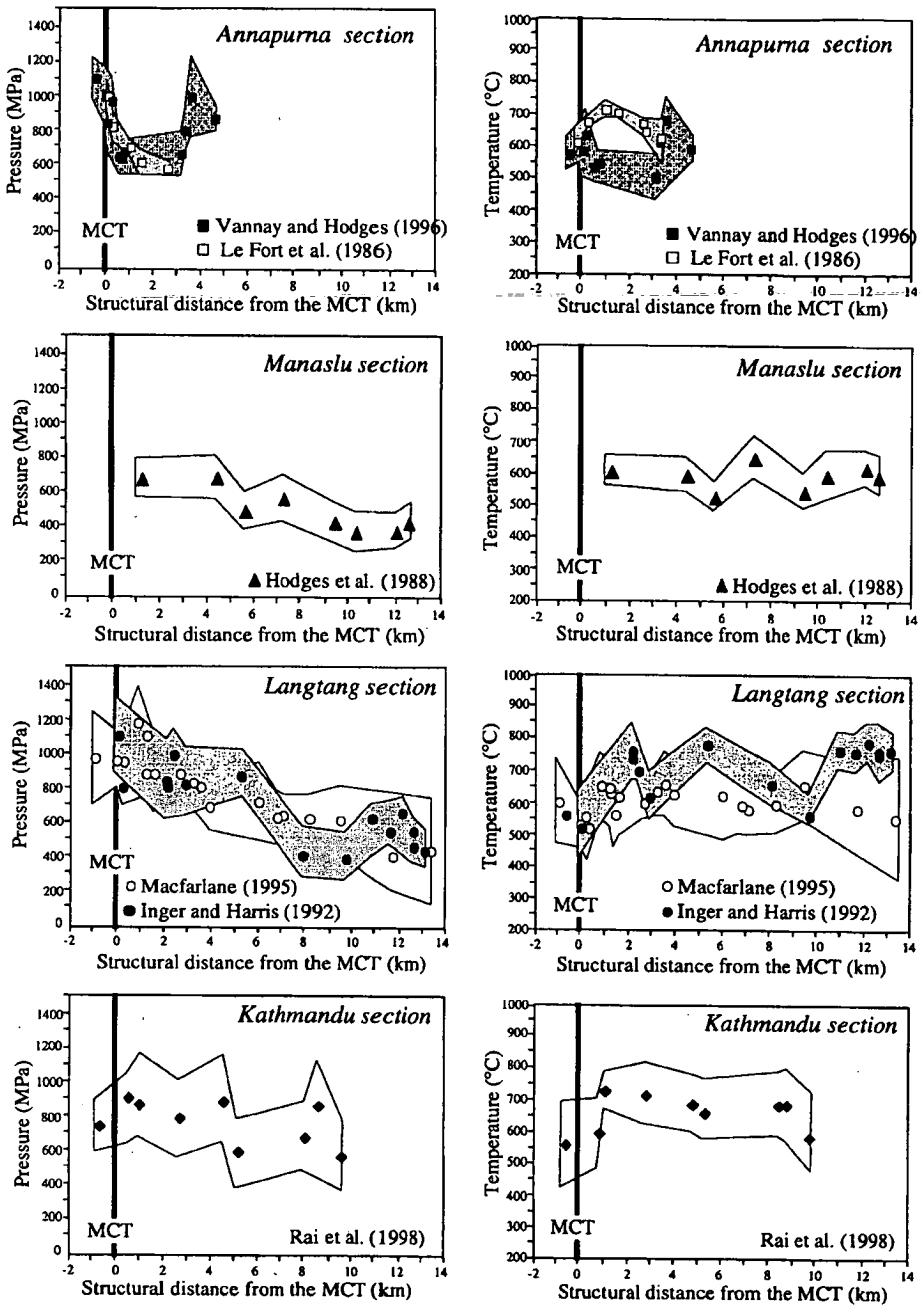


Figure 2.6. Pressure and temperature (with 2σ uncertainties) versus distance from the Main Central Thrust (MCT) along different sections in central Nepal, from Guillot (1999).

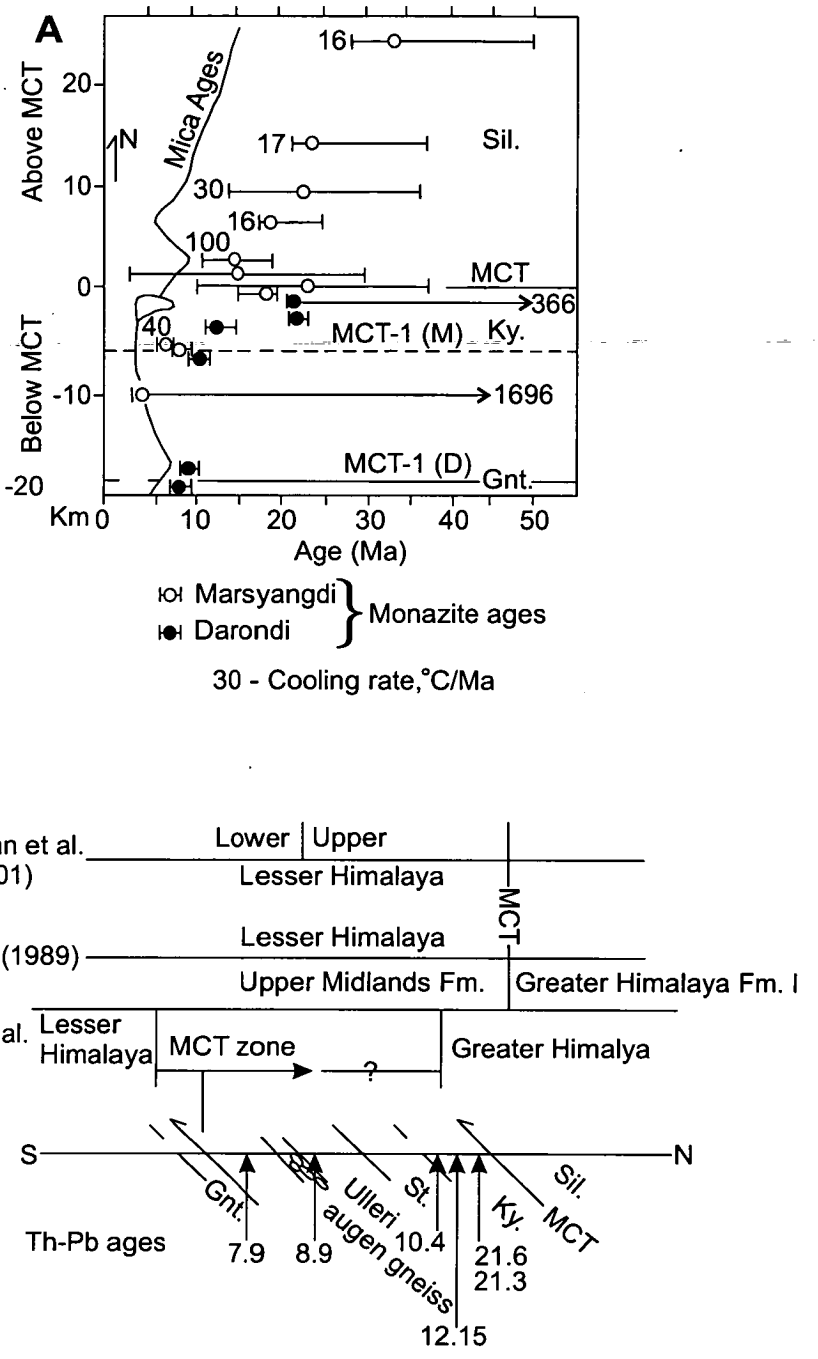


Figure 2.7. A - shows Th-Pb monazite and ^{40}Ar-^{39}Ar mica ages in relation to the Main Central Thrust along the Marsyangdi (M) and Darondi (D) rivers, from Johnson & Harley (2003). Data from Catlos et al. (2001) and Robinson et al. (2003). Circles show weighted mean ages. Sil. - sillimanite, Ky. - kyanite, Gnt. - garnet. **B** - shows Th-Pb monazite ages along the Darondi Khola in Nepal, in relation to the Main Central Thrust, from Searle et al. (2002). Data from Kohn et al. (2001).

Age	Kumaun-Garhwal, India	Western Nepal		Central Nepal	
Miocene	Dagshai Fm.	Dumri Fm.		Dumri Fm.	
		Unconformity			
Eocene	Subathu Fm.	Bhainskati Fm.		Bhainskati Fm.	
Permian-Cretaceous	Krol Fm.	Gondwanas		Gondwanas	
		Unconformity			
Middle Proterozoic	Mandhari Fm.	Upper N. Gr.	Lakarpata Fm.	Upper K. G. Gr.	Robang Fm. Kerabari Fm. Benighat Fm.
	Deoban Fm.		Syangia Fm.	Mid. K. G. Gr.	Nourpul Fm.
	Rautgara Fm.	Lower Nawakot Gr.	Galyang Fm.		Dandagaon Fm.
			Sangram Fm.		Fagfog Fm.
Early Proterozoic	Chandpur Fm.		Ranimata Fm.	L. Kali Gandaki Gr.	Kuncha Fm.
			Kushma Fm.		

Figure 2.8. Chart showing regional correlation of Lesser Himalayan formations between Kumaon-Garhwal (Valdiya, 1980), western Nepal (DeCelles et al., 2001), and Central Nepal (Sakai, 1985; Upreti, 1996).

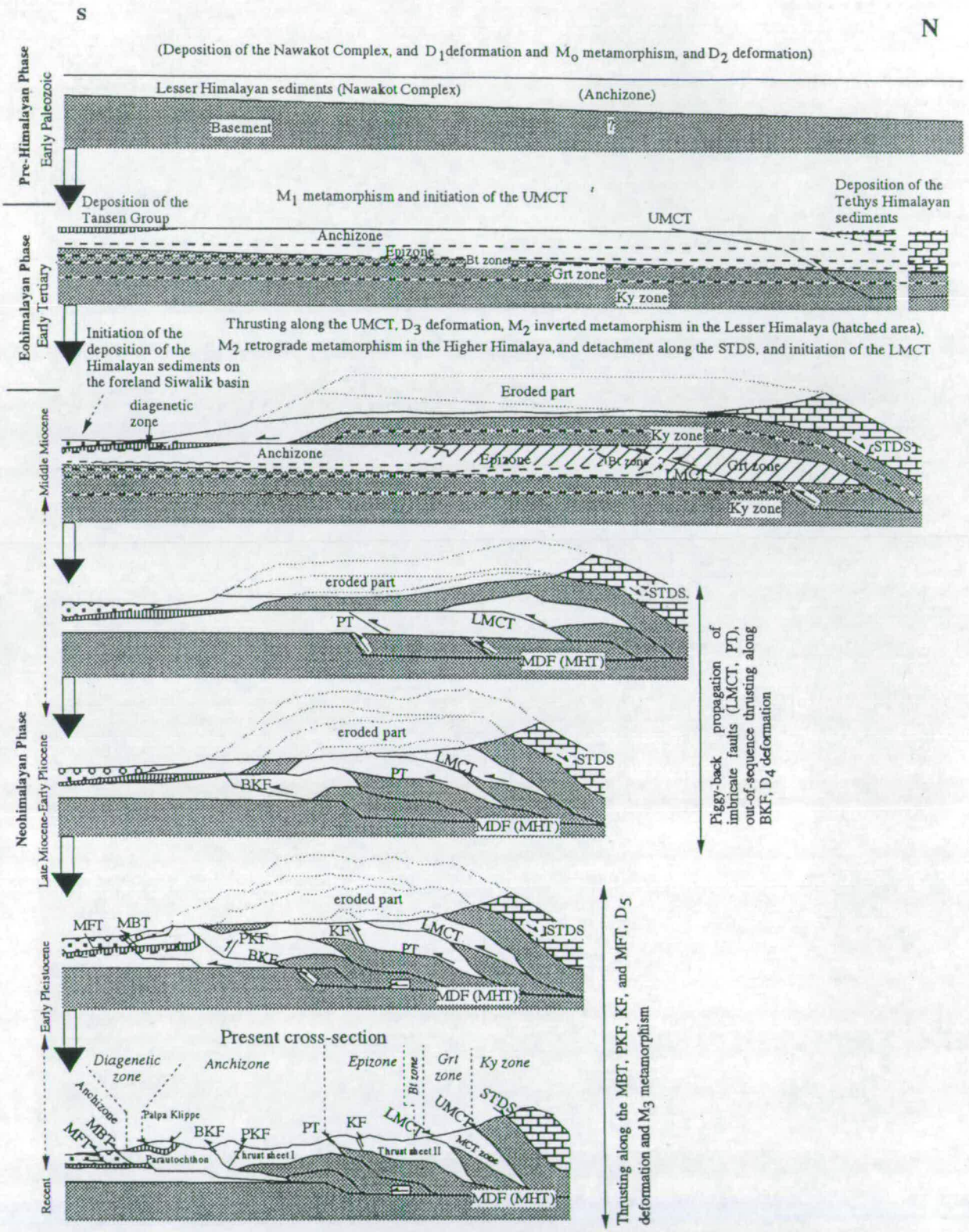


Figure 2.9. Proposed tectono-metamorphic evolution of the Lesser Himalaya in central Nepal, from Paudel & Arita (2000). Bt. - biotite, Grt. - garnet, Ky. - kyanite. UMCT - Upper Main Central Thrust, LMCT - Lower Main Central Thrust, STDS - South Tibetan Detachment System, MDF - Main Detachment Fault, PT - Phalebas Thrust, BKF - Bari Gad-Kali Gandaki Fault, PKF - Pindi Khola Fault, MBT - Main Boundary Thrust, MFT - Main Frontal Thrust.

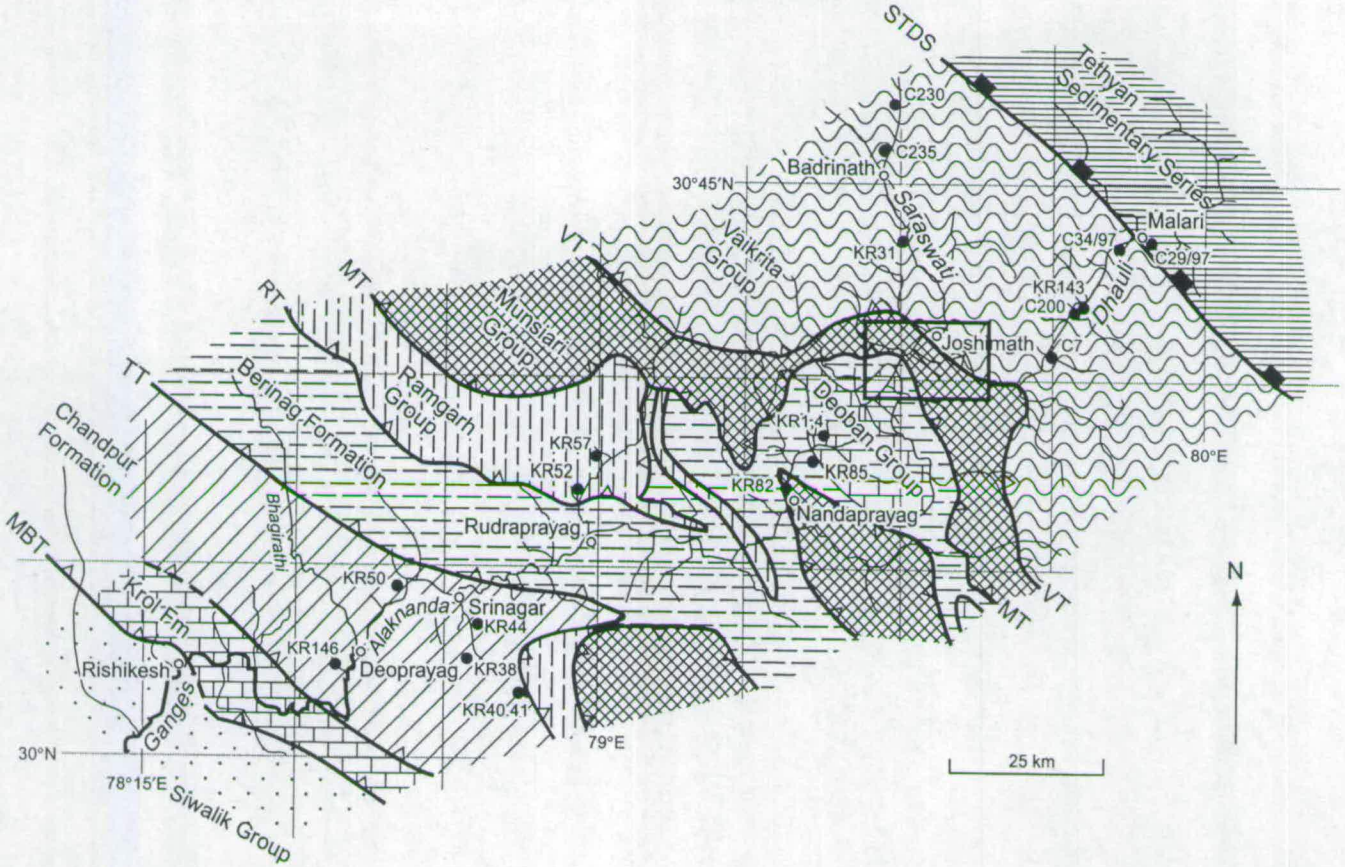


Figure 2.10. Geologic sketch map of the Malari-Rishikesh section of the Garhwal Himalaya, showing different Lesser Himalayan units and separating the Inner and Outer Lesser Himalaya, from Ahmad et al. (2000). STDS - South Tibetan Detachment System, VT - Vaikrita Thrust, MT - Munsiari Thrust, RT - Ramgarh Thrust, TT - Tons Thrust, MBT - Main Boundary Thrust.

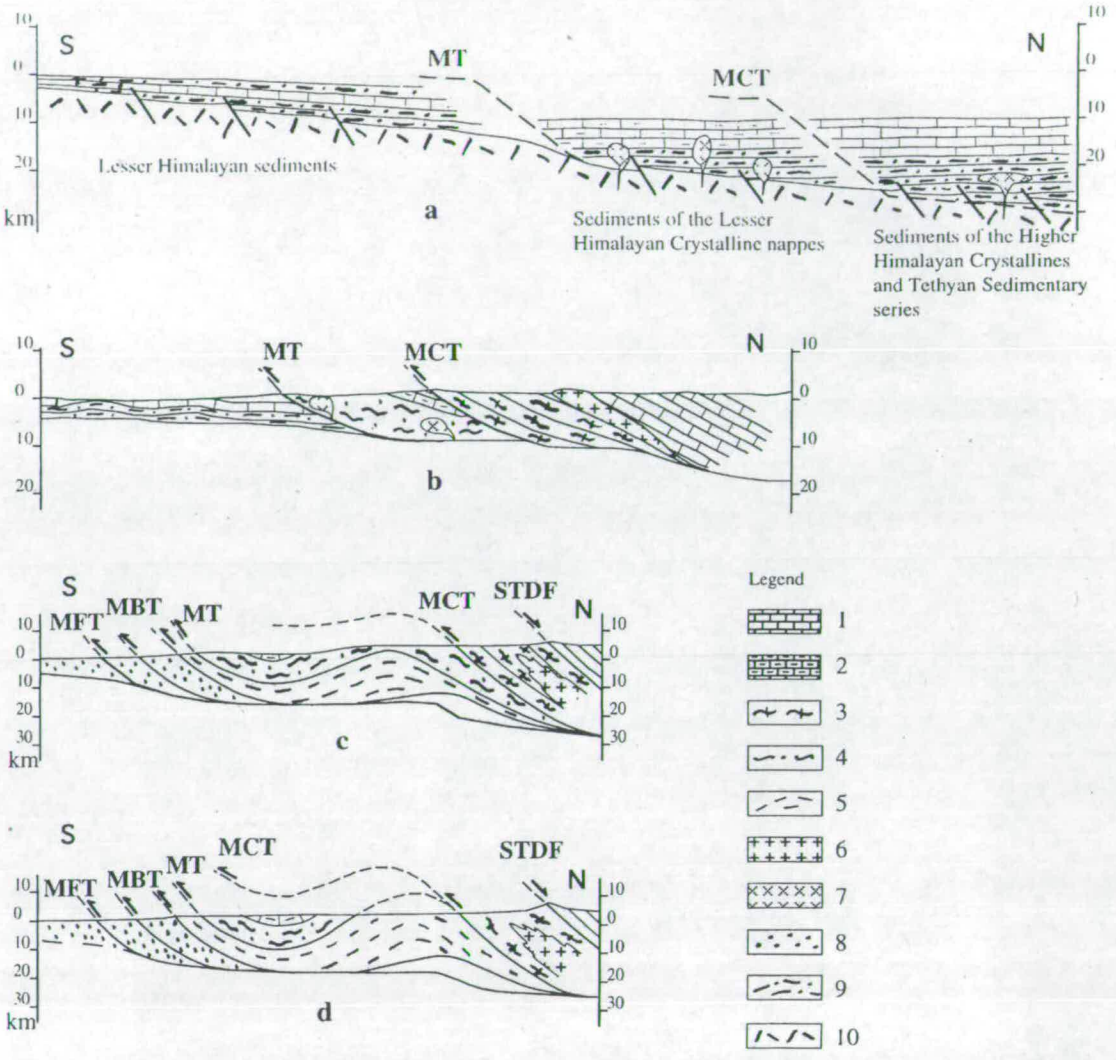


Figure 2.11. Schematic evolution of the Himalayas, from Upreti & Le Fort (1999). **a** - reconstruction of the proto-Main Central Thrust (MCT) and proto-Mahabarat Thrust (MT), **b** - evolution of thrust tectonics along the Main Central Thrust and Mahabarat Thrust, **c** & **d** show two different scenarios for the development of the Lesser Himalayan Crystalline Thrust Sheets, in **c** the Crystalline Thrust Sheets are separate from the Main Central Thrust and represent a different lithotectonic unit, whereas in **d** they have splayed from the Main Central Thrust system and consist of Greater and Tibetan Himalayan lithologies. 1 - Tibetan Himalayan Zone, 2 - Crystalline Thrust Sheet Palaeozoic sedimentary series, 3 - Greater Himalayan Zone, 4 - Crystalline Thrust Sheet metamorphic rocks, 5 - Lesser Himalayan metasediments and sediments, 6 - Tertiary granites, 7 - Cambro-Ordovician granites, 8 - Siwalik sediments, 9 - Pelitic and arenaceous sediments of the Indian continental margin sea, 10 - Indian shield, STDF - South Tibetan Detachment Fault, MBT - Main Boundary Thrust, MFT - Main Frontal Thrust.

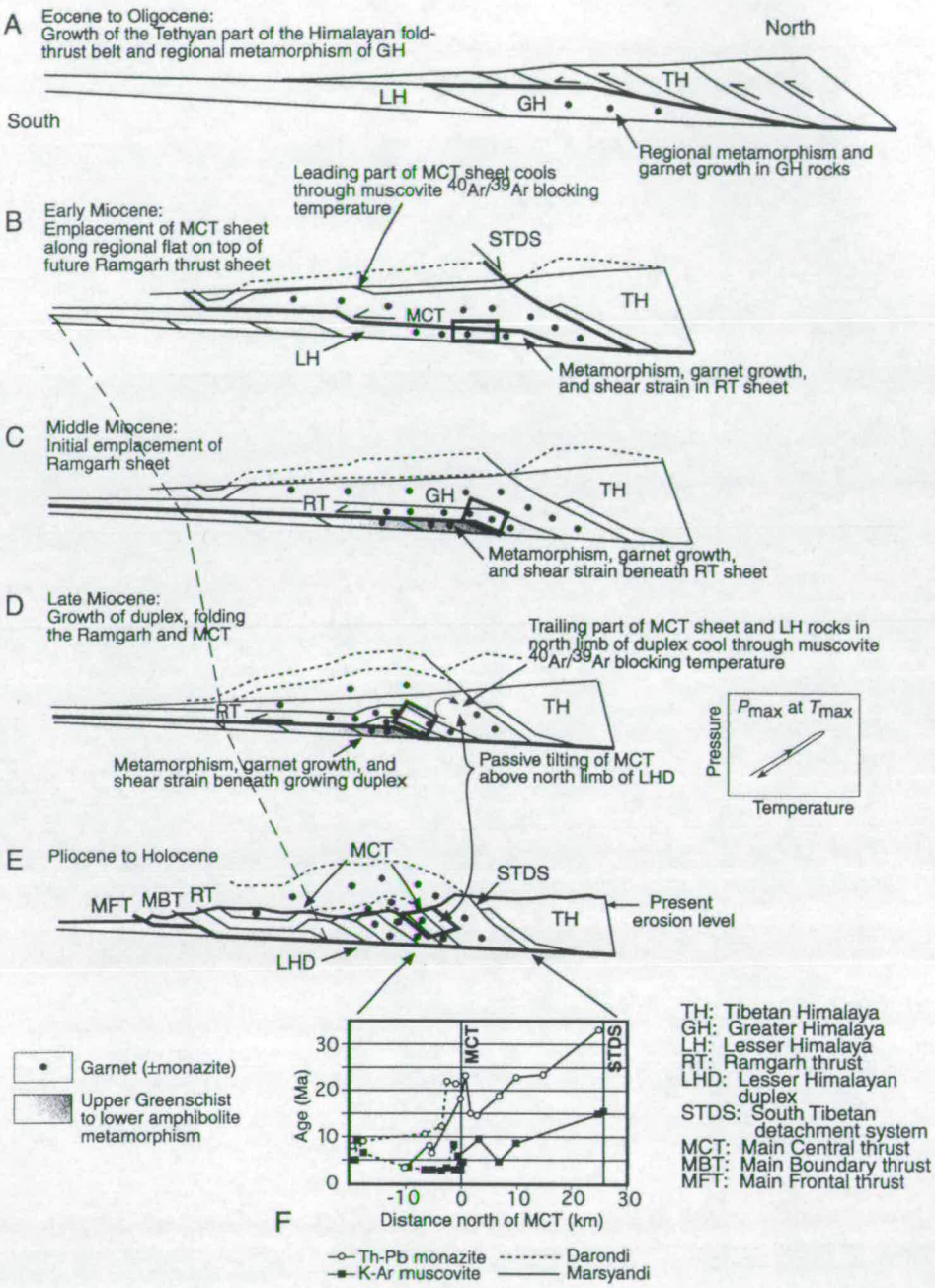


Figure 2.12. Evolution of the Himalayas, from Robinson et al. (2003). Bold lines mark active faults. Polygon highlights part of the Main Central Thrust currently exposed at the surface. Lines of long dashes connecting B-E track the location of the reference point. D: schematic pressure-temperature path for each thrust sheet in duplex. F: Th-Pb monazite and ^{40}Ar-^{39}Ar muscovite ages plotted against distance of samples from trace of Main Central Thrust, from Darondi and Marsyangdi rivers in central Nepal. Arrows indicate approximate distribution of ages relative to the schematic model.



Figure 2.13. Comparison of the stratigraphy of the Himalayan foreland basin between Pakistan and Nepal. Most stratigraphic boundaries have poor age control. Shaded area represents a regional ~ 15-20 Ma unconformity. The Chulung La Formation is only found in Zanskar (northern India) and is not in stratigraphic contact with the Subathu Formation. Nepal references: Sakai, 1983; Kayastha, 1992; DeCelles et al., 1998a, 1998b, 2001. Northern India references: Valdiya, 1980; Najman et al., 1997, 2002, 2004. Northern Pakistan references: Bossart & Ottiger, 1989; Critelli & Garzanti, 1994; Najman et al., 2001, 2002.

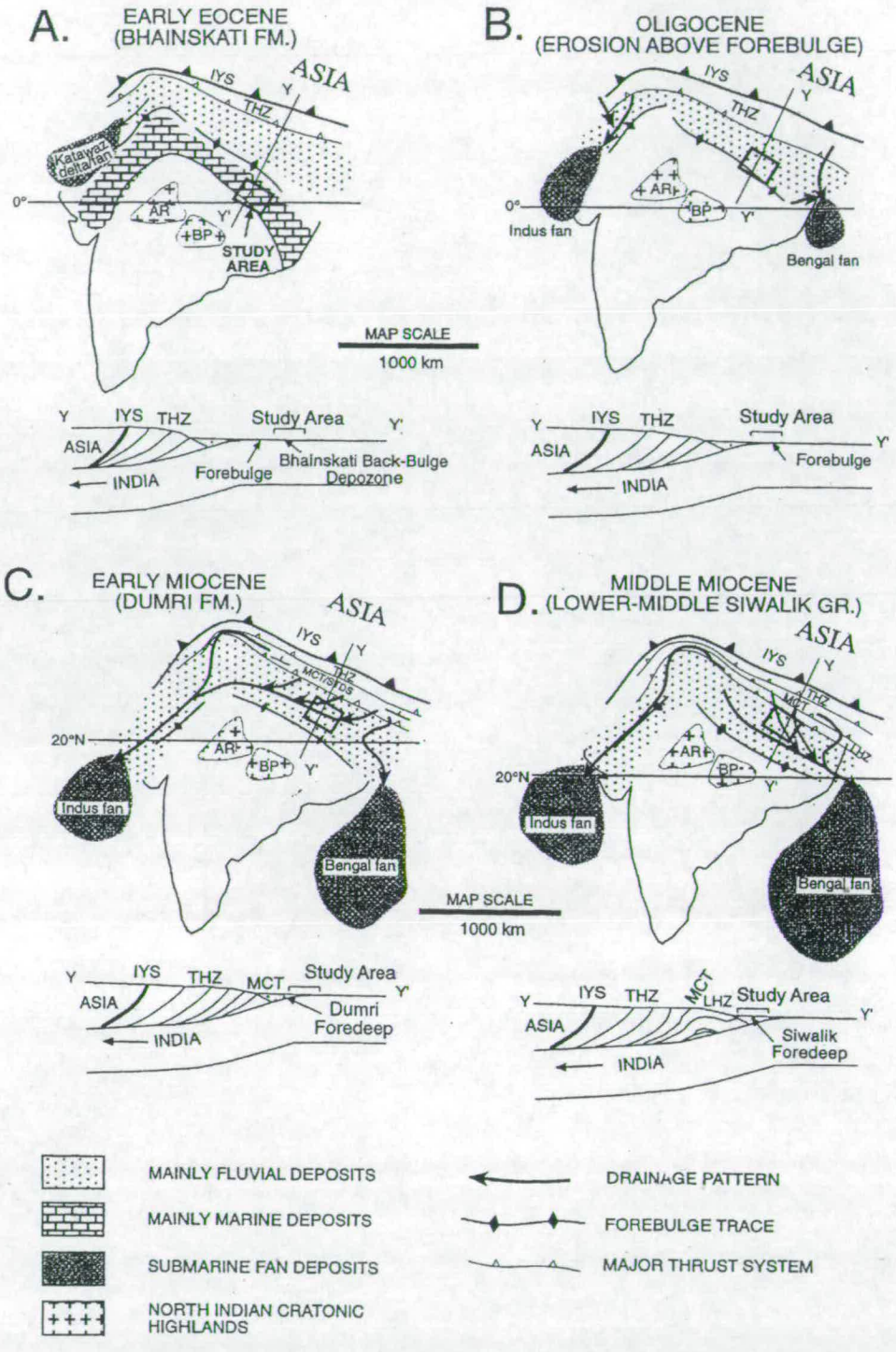


Figure 2.14. Palaeogeographic sketch maps and schematic cross-sections (Y-Y') of the India-Eurasia collision zone during Eocene-Miocene time as the Himalayan foreland basin system developed, from DeCelles et al. (1998b). AR - Aravalli Range, BP - Baghelkhand Plateau, THZ - Tibetan Himalayan Zone, MCT - Main Central Thrust, LHZ - Lesser Himalayan Zone,I YS - Indus-Yarlung Suture Zone.



Plate 2.1. Looking south down the modern Tinau River showing antiformal curve of Siwalik strata in gorge, the Pokhara-Butwal road is on the left.

3. The Himalayan foreland basin and drainage system

"Savour the irony should those orogens most alluring to hard-rock geologists owe their metamorphic muscles to the drumbeat of tiny raindrops." (Hoffman & Grotzinger, 1993)

3.1. Introduction

The modern foreland basin, and the drainage system which feeds it, provide analogues with which to interpret ancient foreland basin sediments and are thus important to consider with any detrital investigation. Using sedimentologic, petrographic, and U-Pb detrital zircon ages from the Middle Eocene to Early Miocene Bhainskati and Dumri Formations in the Lesser Himalaya of Nepal, DeCelles et al. (1998a) propose a foreland basin had developed adjacent to the rising Himalayan Range by Mid-Eocene time. Since then it has been the receiver of enormous volumes of Himalayan detritus and is a dynamic site that is ever impinged upon by the growing fold-thrust belt that feeds it. Today fluvial deposition continues in the foreland basin belt, the site of most Himalayan shortening as the orogen undergoes frontal accretion. Seismic reflection and borehole data from the Potwar Plateau and adjacent areas in northern Pakistan clearly reveal the thin-skinned geometry of thrusting within the foreland (e.g. Seeber et al., 1981; Lillie et al., 1987; Pennock et al., 1989; Ni et al., 1991). During most of the Cenozoic, the rates of migration of the distal pinch-out and of the foreland depocenter suggest such thin-skinned thrusting in the foreland has accommodated ~ 20 % of Indo-Asia convergence (Raiverman et al., 1983; Baker et al., 1988; Bossart & Ottiger, 1989). Current shortening rates of ~ 15-20 mm/yr have been proposed for the foreland basin

and Sub-Himalayan Zone from a variety of indicators (Lyon-Caen & Molnar, 1985; Molnar & Lyon-Caen, 1989; Bilham et al., 1997; DeCelles et al., 1998a, 1998b; Powers et al., 1998).

As folds and thrusts propagate basin-ward within the Sub-Himalayan Zone, earlier foreland basin deposits are shed from the new ridges of uplift and re-deposited again. Over time this produces shifts in the locus of deposition and subsidence, giving rise to the concept of the "migrating foredeep" (Bally et al., 1966). Rivers are commonly diverted during frontal accretion processes, a phenomenon which has a profound effect on the distribution of sediment that enters the foreland basin and thus is relevant to the detrital technique. If river diversion occurred during deposition of the Siwalik Group it is plausible that a resultant change in source area could be erroneously interpreted as a tectonic rather than geomorphological effect. Therefore an appreciation of this process is important before any detrital interpretations are made. Indeed, the field of tectonic geomorphology is becoming increasingly important within the earth sciences (Burbank & Anderson, 2000). Since bedrock rivers are considered to be the fundamental control on mountain belt denudation, the configuration of the drainage network strongly controls the distribution of erosion and consequently exhumation (e.g. Koons, 1994; Stock & Montgomery, 1999). The evolution through time of the foreland basin and contributing drainage network therefore plays a critical role in orogenic evolution. Inspection of the modern system is directly relevant to the detrital technique.

This chapter provides an overview of the Himalayan foreland basin and drainage system. Additionally, simple modelling using DEM data and ArcInfo was carried out to investigate the controls on drainage diversion in southern-central Nepal. DEM's allow the quantification of morphology at scales that are impractical or impossible to measure in the field.

3.2. Provenance limitations

Despite the ongoing success of detrital studies there are inherent limitations when working with detrital mixtures rather than bedrock, especially when considering multiple tributary catchments. Perhaps the most important of these is the difficulty in constraining accurate provenance. It has not yet been possible to precisely model the evolution of drainage systems through time. There will always therefore be uncertainty regarding the source and catchment area of the rivers that deposited the sediment in question. Palaeoflow measurements can help discern the nature of the fluvial system in the foreland basin but possible drainage diversion and reorganisation within the hinterland is an unknown. There is also the potential that a switch in source area associated with drainage reorganisation will be mistakenly interpreted as a tectonic signal in the detrital record. Conversely, some workers have even invoked drainage diversion as the cause of a change in detrital signal where a tectonic explanation would not fit the overall model (e.g. Robinson et al., 2001). Such interpretations are convenient but because of the absence of any direct evidence to indicate such diversion they lack robustness.

3.3. Foreland basin morphology

The Himalayas represent a 2500 km-long arc of mountain ranges stretching between two structural syntaxes associated with the major peaks of Namche Barwa (7782 m) in the east, and Nanga Parbat (8125 m) in the west (Fig. 2.2.). Uplift produced a strong erosional response which has fed foreland and remnant-ocean clastic wedges, deposited in a vast area of > 10^7 km^2 (Garzanti et al., 1996). Today the Indus drainage system alone brings an estimated 300-600 Mt/yr of detritus to the Indian Ocean (Milliman et al., 1984). Overthrusting of the southern margin of Asia, underthrusting of India, and imbrication of slices of Indian crust in the Lesser Himalaya generated a huge crustal load, which has manifested in the largest terrestrial foreland basin on earth. The Himalayan foreland basin is continuous along the full length of the range and arches southward to the Arabian Sea in the west and the Indian Ocean in the east (Fig. 3.1.). Three of the worlds largest rivers traverse it (Brahmaputra, Ganges, and Indus) and are the modern equivalents of a drainage network that for ~ 45 Myr has brought well-mixed detritus from all tectonic zones of the Himalayas into the adjacent foreland basin (DeCelles et al., 1998a). The resultant thick succession of strata (up to 8 km in the proximal foreland) onlaps the northern Indian cratonic shield and records many aspects of Himalayan orogenic evolution (Lyon-Caen & Molnar, 1985). The traditional description of a foreland basin's geometry is that of a "wedge-shaped" basin that deepens toward the hinterland. This applies to the Himalayan foreland basin where the groupings of strata within the succession generally thicken towards the hinterland (Fig. 3.2.).

Foreland basin size is controlled by the rigidity of the flexed crust and on load placement with respect to the edge of the depositional basin and loaded plate. In the central Himalaya, crustal rigidities are estimated to be about 0.7 x 10^{25} N.m which yields predicted widths of > 200 km for the Gangetic basin (Molnar, 1988). Variations in crustal rigidity along-strike and long-lived basement faults have controlled the width and large-scale subsidence distribution of the foreland. The northern foreland basin is also subdivided into sub-basins (100-600 km wide) by basement ridges and spurs (Raiverman et al., 1983). Isopach data define significant sub-basins that indicate the foreland may have been more partitioned in the past (Karunakaram & Ranga Rao, 1979). However, a lack of evidence for truncation against basement highs suggests the depositional surface was maintained above the top of the basement as it is today, despite differential subsidence. Palaeocurrents from Oligocene strata in several sub-basins indicate rivers entered the foreland from the N, NE, and NW (Raiverman et al., 1983; Srivastava & Casshyap, 1983).

Geophysical and borehole data obtained in the Indo-Gangetic Plain indicate that the Siwalik foreland basin sediments overly Archaean metamorphic rocks (Vindhyans) (Karunakaran & Ranga Rao, 1976). Most of the stratigraphic and structural elements present in peninsular India just south of the Indo-Gangetic Plains can be traced below the Siwalik sediments in the plains. The Siwaliks beneath the plains are not tectonically disturbed, except that they show small homoclinal dips to the north. The Siwaliks attain a maximum thickness of ~ 5 km close to the foothills in Nepal and thin away from the Himalayas.

Major deposition is currently taking place on the Indo-Gangetic Plain in the form of fluvial fans that grow from the gorge exits of all the larger rivers. These have areas of 104-105 km^2 but a topographic relief of only ~ 20 m (DeCelles et al., 1998b and references therein). The best-developed fan is the Kosi with a radius of ~ 140 km. There is also the deposition of gravel beds in front of the foothills in the form of a 10-30 km wide piedmont zone called "Bhahar" (Parkash et al., 1980). The 8-10 km wide marshy region south of the Bhahar is termed the Terai in Nepal.

3.3.1. Present drainage configuration

An assessment of the current architecture of Himalayan drainage, especially across the foreland basin, is beneficial before interpreting the provenance and environment of deposition of the ancient sediments because they were most likely deposited under a similar regime.

Himalayan morphology is dictated by longitudinal river systems. These flow from the Southern Tibetan Plateau, carving some of the worlds deepest valleys. In the NW Himalaya the modern Indus River rises in western Tibet (near Mt. Kailas) and flows westward along the Indus-Yarlung Suture Zone for > 600 km before cross-cutting the entire range. It then flows to the south along the mountain front and debauches into the Arabian Sea at the western margin of the Indian subcontinent to feed the Indus Fan, the second largest sediment fan in the world (~ 5 million km^3) (Fig. 1.3.). The modern Indus drainage basin incorporates the Karakoram, Kohistan, and other tectonic units of the suture zone. The Indus also has four major tributaries (including the Chenab and Sutlej rivers) originating in the Himalayas, which flow

transversely and drain the Greater Himalayan Zone. In India, the Ganges River flows to the east along the foreland basin to join the Brahmaputra at the eastern margin of the Indian subcontinent where they enter the Indian Ocean and feed the Bengal Fan, the largest depositional feature on the planet (area: ~ 3 million km^2, maximum thickness: 15 km). The Brahmaputra River in the eastern Himalaya flows eastward for almost 1000 km before cutting across the entire range. It then flows westward for more than 500 km in the Himalayan foreland basin before turning south. The Indus and Bengal Fans represent the distal flysch equivalent of Tertiary to Recent molasse deposited in the foreland basin (Garzanti et al., 1996). Turbidite sedimentation related to the modern Indus Fan started around Early Miocene time (Clift et al., 2001) whilst the Bengal Fan became the main depocenter for Himalayan sediments around Middle-Miocene time (Curray & Moore, 1971, 1974; Davies et al., 1995). The Ganges and Indus rivers account for nearly the entire sediment and water flux across the Himalayan foreland west of the Brahmaputra River. The Ganges-Brahmaputra system, in constrast to the Indus, follows the Greater Himalaya along strike for much of the length of the orogen. The sediment comprising the Bengal Fan is therefore being dominated by Greater Himalayan material (e.g. France-Lanord et al., 1993), whilst the Indus Fan sediment is dominated by tectonic units adjacent to the suture zone (Clift et al., 2000).

According to DeCelles et al. (1998b) the modern Indo-Gangetic Plain is dominated by two types of rivers flowing towards the S or SE:

1. Large rivers (discharge of ~ 10^4 m^3/s) with catchments extending into the interior of the mountain belt.
2. Smaller rivers (discharge of ~ 10^2-10^3 m^3/s) with catchments limited to the frontal part of the mountain belt.

In fact four river systems can be delineated within the foreland: axial trunk rivers, large transverse rivers with hinterland catchments, small transverse rivers with foreland catchments, and rivers sourced on newly created intra-foreland uplifts (Fig. 3.3.). Rivers on the fluvial megafans are highly mobile with anastomosing, braided, and meandering morphologies. This means highly sinuous meandering rivers flow alongside braided or anastomosing rivers over large distances. Shallow ponds and oxbow lakes are also locally abundant. The floodplain receives large amounts of precipitation (1000-1500 mm/yr) and major floods during the monsoon. Monsoon rivers are capable of carrying boulders to the foreland with dimensions of several meters. Water level during the dry season drops over 10 m in the major rivers.

3.3.1.1. Field area

This study is focused on the Gangetic foreland basin, which fronts the eastern 75 % of the Himalayas. The Ganges River follows the shallowly buried crest of the forebulge, whilst the foredeep and wedge-top depozones stretch northward into southern Nepal (Raiverman et al., 1983; Burbank et al., 1996; DeCelles et al., 1998a). The modern Gangetic foreland is dominated by large south-eastwardly (axial) flowing rivers (e.g. the Ganges River, the Ghaghara River, the Yamuna River, the Sapat River) (Fig. 3.3.). These are separated by rapidly changing areas of smaller

sinuous rivers with multiple flow directions. Therefore moving from a distal to proximal location does not mean channel sizes decrease as is the norm, but rather different systems are intersected which could mean a large increase in channel size passing from small meandering channels to a major trunk river. In northern India the modern Ganges and Yamuna rivers flow along the distal margins of the foreland basin and transverse rivers flow several 100 km across the foreland to join them. This drainage configuration strongly contrasts with the modern Indus foreland, where the Indus River flows close to the active fold belt. These two major river systems are separated by the Indus-Ganges drainage divide (Burbank et al., 1996).

As for all but the largest rivers (including the Karnali), outside of the monsoon season there is little evidence for the modern equivalents of the Tinau Khola or Surai Khola rivers (which flow through the Siwalik sections that this thesis focuses on) south of the Siwalik Hills where they are absorbed by the Gangetic Plain. Local ridges of the Churia Range reach a maximum elevation of 1000 m only 3 km north of the plain, thus forming a dramatic topographic barrier. Creation of these ridges has produced a mild diversion in the course of the Tinau River as it crosses the Churia Thrust within the Sub-Himalayan Zone (Fig. 1.5.). The Tinau River is sourced within the southern Lesser Himalaya and is gently meandering with a deranged fluvial pattern, characteristic of a young system. Further west the Surai section cuts the Dundwa Range, following the east-west Mahendra Highway and, in part, the Surai River (Fig. 1.5.). The modern Surai River drains only the Sub-Himalayan Zone. Just to the north the Rapti River is trapped between the Dundwa and Churia Ranges and forms an axial system for over 200 km before breaking south at the town

of Nepalganj in the west where it enters the foreland basin. This type of drainage diversion is characteristic of western Nepal's proximal foreland basin. The present field area thus contains drainage patterns characteristic of areas with active fault-related folding where distinctive features include diversion of pre-existing transverse rivers to an axial course and the development of a series of wind gaps at the loci of antecedent transverse streams (e.g. Jackson et al., 1996; Gupta, 1997; Burbank et al., 1999). The modern Karnali River is one of the Himalayas major fluvial systems. With its source in southern Tibet the Karnali traverses the entire range before entering the foreland basin where it joins the Ganges.

3.4. Himalayan drainage through time

Himalayan drainage studies began early with the antecedent versus consequent debate. Nearly all major Himalayan rivers start north of the High Himalayan peaks in southern Tibet and cut deep gorges through the range. So it was proposed that these rivers had cut back through the Himalayas by headward erosion and captured Tibetan rivers (Burrard & Hayden, 1934). Medlicott (1868) first suggested antecedent drainage, arguing that the rivers were present before uplift of the Himalayan Range and maintained their courses by vigorous down-cutting. Wager (1937) supported the antecedent drainage theory, using the example of the Arun River, which cuts the Himalayas east of Mt. Everest. The Arun cuts a narrow gorge in high-grade crystalline rocks of the Nyonno Ri Range, just north of the High Himalayan peaks. A low pass in soft schist crosses the Nyonno Ri Range slightly east of the Arun gorge. It is likely that a river cutting through by headward erosion would have avoided the more resistant gneisses, so it was inferred that the gorge in

the gneisses must be following a river course antecedent to the uplift of the Nyonno Ri Range. Determining the evolution of river systems is never straightforward however, and it is possible the Nyonno Ri Range uplift may be part of the Quaternary graben structures in Tibet and therefore younger than the main phase of Himalayan uplift. Antecedent drainage across the Nyonno Ri does not prove that the main gorge of the Arun, or other Himalayan rivers, are all antecedent.

The Himalayan longitudinal fluvial-marine depositional system was established soon after collision. The palaeo-Indus in the north, which deposited the Indus molasse, and the palaeo-Ganges in the south, which deposited the Murree molasse, were westward flowing and were established during the Palaeogene (Clift et al., 2000), although there are arguments that place a younger age on the inception of the palaeo-Indus River (Sinclair & Jaffey, 2001). The Palaeogene fluvial system was therefore a mirror image of the modern Ganges-Brahmaputra river system in the eastern Himalaya. However, the area from Waziristan to north of Kabul in Afghanistan experienced transpression and major uplift that outpaced fluvial down-cutting. This caused the abrupt southward diversion of the fluvial system and made the Indian Ocean the new site of sediment accumulation between 21-19 Ma as Indus Fan deposition began (Quyyam et al., 1997). This persisted until closure of the Katawaz Remnant Ocean at the end of Early Miocene time. During Oligo-Miocene times it is also likely that sediment was transported west and east, into the Makran and offshore Sumatra subduction zones respectively (e.g. Moore, 1979; Critelli et al., 1990).

Unlike today in the Indus foreland, where the rivers of the Punjab are tributary to the Indus River, palaeocurrent indicators (Waheed & Wells, 1990) suggest that during Early- and Middle-Miocene times the major fluvial systems flowed orthogonal to each other such that the Potwar system flowed to the south-east (depositing the Chinji Formation in southern Potwar Plateau, Willis, 1993) where it presumably joined the Ganges system (Burbank & Beck, 1991b; Burbank et al., 1996). It seems likely therefore that the Indus-Ganges drainage divide, separating rivers flowing to the Arabian Sea and the Bay of Bengal, was farther west of its present position (Burbank et al., 1996). The comparable scales of sand bodies in the Potwar, Jhelum, and Himachal Pradesh regions suggest that these could be parts of a single large, palaeo-Indus river system that was flowing southward into the Ganges drainage at that time (Burbank et al., 1996). Although showing similar flow directions, the much smaller sandstone thicknesses in Nepal cannot be logical downstream continuations of the main Indo-Gangetic channel system, but must have belonged to a subsidiary tributary system trending sub-parallel to the axial drainage (Burbank et al., 1996). Indeed, no definitive documentation of the continuity of the Indus system with the Ganges has yet been discovered.

Burbank & Beck (1991) purport that the westward-flowing palaeo-Ganges system was replaced by an eastward-flowing system akin to the modern Ganges River during Early- to Middle-Miocene time, associated with continued convergence. They use palaeoflow data to suggest that in the pre-Pliocene Ganges basin axially flowing rivers dominated deposition in the medial and distal foreland basin, a situation that continues today. However, other workers have found no evidence for

such axial flow in ancient Ganges foreland basin sediment (e.g. DeCelles et al., 1998b). It is possible that the ancient Ganges drainage area was larger than that today, extending as far west as the Potwar Plateau in Pakistan (Burbank & Beck, 1991). The age and cause of the Indus-Ganges divide is debated but DeCelles et al. (1998b) use palaeoflow data to suggest it occurred prior to Siwalik deposition as a consequence of the impingement of the Aravali Range of northern India on the foreland basin. Similarly, the Brahmaputra system probably grew at the expense of the palaeo-Indus with westward migration of the drainage divide. Bengal Fan sedimentation commenced thereafter. The fact that the Bengal Fan had prograded far out into the Indian Ocean by the Early Miocene suggests a significant amount of erosion had taken place by that time. Discrimination of the relative contributions from Tibet and the Himalayas to the sedimentary deposits would help to constrain the evolution of the drainage divide with time.

Hinterland tectonic readjustments such as the Miocene extensional movement on the South Tibetan Detachment are likely to have modified regional drainage characteristics. It is possible for example that South Tibetan Detachment extension greatly increased the gradient of the rivers draining southward from the Ganges by lowering the regional base level. If the South Tibetan Detachment also acted to lower the average elevation of the Himalayas, it would have additionally allowed more precipitation to reach the Ganges by reducing the rain-shadow effect.

As a consequence of deformation of the active frontal thrust zone (the Salt Range) at ~ 6 Ma, the northern Pakistan foreland basin became increasingly partitioned, inducing major changes in drainage patterns. Growth of the Salt Range initially

created a large piggyback basin that localised the ancestral Indus River, which was eventually diverted to the SW. In the Potwar Plateau area, it is possible that trunk rivers that had previously flowed eastward into the palaeo-Ganges were deviated to their present course southward to the Indian Ocean (Burbank et al., 1986; Mulder & Burbank, 1993). Today, active uplifts across which the Indus flows appear to exert a strong control on the morphology of the Indus channels. Other major river systems such as the Jhelum River and the Chenab River have been found to be actively migrating in response to either sediment flux variations or current folding south of the Salt Range (Baker et al., 1988).

During compression, rheologic contrasts between foreland basin basement highs and adjacent sedimentary fill have apparently concentrated transverse faulting along the margins of the basement blocks (Talukdar & Sudhakar, 1971). Some of these faults extend into the Lesser Himalayan foothills and have guided the courses of several major rivers as they enter the foreland, including the Chenab, Sutlej, Yamuna, and Ganges (Talukdar & Sudhakar, 1971; Valdiya, 1976). Many modern rivers also enter the foreland either through structural re-entrants or along transverse structures, such as wrench faults (Burbank et al., 1996). Across the foreland, records of initial conglomeratic strata indicate highly diachronous progradation (ranging from > 8 Ma to < 1 Ma) which is influenced by fluvial interaction with local folds and thrusts (Burbank et al., 1996). Axial river systems become evident along nearly the entire northern margin of the foreland during Plio-Pleistocene times (Burbank et al., 1996). Whereas tectonic loading appears to continue to control depositional patterns in the Indus foreland, changes in the position of the axial river and in stratal geometries

suggest erosional unloading during the last 4-5 Ma has become increasingly important adjacent to the Gangetic foreland (Burbank et al., 1996).

3.5. Modelling drainage evolution using ArcInfo

3.5.1. Introduction

The variability of the contributing fluvial network is a primary limitation on the detrital record and becomes more acutely so for increasing numbers of catchments. No previous detrital investigation has made an attempt to assess the potentially important role of drainage evolution with regards to detrital sediment signals beyond a perfunctory acknowledgement of the importance of the process. Although theoretical studies have provided information regarding the relationship between the thermal history of the source and the spread of detrital age data (e.g. Brewer et al., 2003), they have not been linked to a study of the ancient sedimentary record. Combining a detrital investigation with a study of the local controls on drainage diversion is the only way the unknowns involved with using sediment, as opposed to bedrock, will be constrained.

The catalogue of drainage diversions through time discussed above has continued to the present day. This is most obvious and characteristic along the proximal foreland basin in central Nepal (Gupta, 1997) (Fig. 3.3.). The present field area is of particular interest in this regard. Here the Dundwa Range has captured the Rapti River in the west, producing an axially flowing system, whereas in the east the range is cut by a transverse fluvial architecture (Fig. 1.5.). The lithologies in this area consist of poorly cemented sediments and thus it is remarkable that such highly

vulnerable material can divert major trunk streams, which command considerable discharge during the monsoon period. This investigation of the modern system is an attempt to further understand the processes which affect drainage diversion in southern Nepal. As well as providing an interesting geomorphological study, such information is beneficial to the interpretation of detrital data should there be evidence for changes in signatures or sedimentation style.

Studies suggest that the longitudinal stream profile rapidly attains a nearly ideal shape even in the presence of significant tectonism (Hurtrez et al., 1999). This stream profile is the backbone of the erosional landscape. Several orders of magnitude separate the time scales in which tectonic and geomorphologic processes operate thus making a study of their relationship a considerable task. Although in reality whether or not a river is diverted is complicated by a myriad of variables which include changes in uplift rate, heterogeneities in erodibility of the substratum, rates of bedrock weathering, amount of precipitation, small scale structures etc. (e.g. Whipple & Tucker, 1999), it is useful and more manageable to concentrate on one factor which can be modelled to assess its importance. The object of the present work therefore was to ascertain the impact of changes in the spacing of thrusts within the Sub-Himalayan Zone of Nepal on subsequent drainage evolution, a factor that may exert a primary control on river diversion. Looking at a topography map, it appears that the spacing of thrusts and therefore areas of uplift has a direct impact on the potential for a river to cut through the rising ground. Where rivers have retained their transverse course they tend to flow through closely spaced ridges of uplift as opposed to those that have been diverted. With many new thrusts developing in front

of the Himalayas, the current field area is a prime location for researching such a hypothesis.

River diversion in Nepal is a consequence of thrust-cored anticlines producing growing ridges of uplift within the Sub-Himalayan Zone. As successive thrust slices are incorporated into the Sub-Himalayan Zone above the Main Frontal Thrust, multiple ridge uplift redirects fluvial systems, causing them to flow axially around the area of uplift. Composite frontal ridges have caused large-scale diversions of some Himalayan rivers (Gupta, 1997). Similar diversions at positions north of the Main Boundary Thrust suggest that this structure has had much the same effect on past drainage paths across the Himalayan front.

The balance between the mechanics of mountain building and of fluvial down-cutting determines whether rivers are entrained by or cut through orogenic structures. A river must be able to erode the crest of the growing fold at a rate equal to, or greater than, the difference between uplift and aggradation rates in order to maintain a smooth concave profile and to sustain its course across the edge of the developing piggyback basin (Ori & Friend, 1984). River long profiles can therefore be used as an indicator of the regional balance between rock uplift and incision. In order to maintain a pre-thrusting river course or to bevel off newly emergent topography, stream power has to be sufficient to keep pace with the rate of bedrock uplift. If its incision rate is lower than the tectonic uplift, it will be outpaced and reversed by the growing fold (Burbank et al., 1999; Tomkin & Braun, 1999). River entrainment is expected where channel gradient, water discharge and/or flow confinement are low,

or where the sediment load approaches carrying capacity. High sediment loads coupled with low channel gradients are characteristic of the foothills of mountain fronts. Consequently strike-parallel drainage is primarily found on the lee side of the orogenic ridge and in the proximity of structures related to propagation of the mountain front. Streams will be reversed and captured by adjacent ones until their common drainage area, and thus discharge, is large enough to provide sufficient stream power to cut through the growing fold (Tomkin & Braun, 1999). If rivers have the capacity to incise uplifting bedrock, their course may deviate from the structural grain of the orogen, responding to the regional topographic gradient.

As well as diverting pre-existing rivers, the areas of uplift also provide high ground from which new, smaller transverse rivers flow into the foreland basin (Fig. 3.4.). Episodic southward relocation of these basin-margin thrusts has served to define large intermontane basins or "Duns" in the Sub-Himalayan Zone between adjacent anticlines (Parkash et al., 1980 and references therein) (Fig. 3.5.). These Duns are considered a main control on drainage diversion, producing in some cases over 200 km of axial flow. Although deposition continued within the Duns well into the Quarternary, eroding hanging-walls above thrusts created highly variable source areas, and palaeocurrents indicate flow off both the forelimbs and backlimbs of folds, as well as along the structural troughs lying parallel to their crests (Burbank et al., 1996). Rivers have been diverted around the plunging ends of the anticlines or else flow across them through water gaps.

3.5.2. Limitations

Many factors control topographic evolution at a mountain front and the consequent drainage evolution, making an all-inclusive numerical model so far illusive. The physics of river incision is complex and thus one cannot hope to generate a quantitative model for a region where there are many changing variables such as lithology and climate and so studies must be restricted to enlightening particular aspects of the process. The ability to derive quantitative estimates for the link between tectonic and surface processes is also severely limited by the sparse data available to calibrate model parameters that describe erosive efficiency (Howard & Kerby, 1983; Stock & Montgomery, 1999; Snyder et al., 2000; Whipple et al., 2000).

Whipple et al. (2000) highlight that besides the range of plausible erosion law exponents, handling the scale jump from local flow conditions (velocity, shear stress, vorticity) to conditions useful to large scale modelling is a significant challenge. The important shear stress-dependent factors of uplift-rate, rock mass quality, and precipitation may differ significantly in space and time, a significant modelling limitation. Whipple et al. (2000) found that where rocks are massive or joint sets are so widely spaced that plucking is inhibited, some combination of abrasion by bedload, suspended load and cavitation is responsible for bed lowering. Thus factors such as how bedrock is being eroded must be ascertained before any reliable quantification can be achieved.

3.5.3. Previous Work

Hovius (1996) used the Sub-Himalayan Zone of Nepal to show that the spacing of drainage basins can be expressed using a spacing ratio, defined as the ratio of the half-width of the mountain belt to the distance between the outlets of adjacent catchments with headwaters immediately below the main divide, as measured at the base of the mountain front. He demonstrated that spacing ratios between individual catchments show a gamma-type distribution around a median of 2.13 and that this can be used to characterise drainage organisation on a mountain belt scale. This consistency suggests that some of the early formed irregularities in river courses developed in response to individual growing folds or faults are smoothed during drainage expansion and competition. In Nepal, growing structures within the Sub-Himalayan Zone appear to have caused strong drainage diversion and likely capture, such that the spacing ratio is as low as 1.2 (Hovius, 1996).

Hurtrez et al. (1999) established that the Siwalik Hills undergo rapid tectonic uplift of rates of up to 15 mm/yr from the geometric pattern of a fault bend model of fold growth. They observe a correlation between relief and uplift at all length scales of topography shorter than 600 m, which suggests that all orders of streams comprising the drainage network are able to adjust to the tectonic signal. Likewise Burbank & Beck (1991) showed that in the northern Pakistan foreland, uplift has been balanced by erosion for long periods (up to 200 ka). High rates of erosion (1-15 mm/yr) of fluvial strata persisted over these intervals. From mass balance calculations Hurtrez et al. (1999) estimate the average elevation is only 10 % of the surface uplift, suggesting that a dynamic equilibrium has been reached quite rapidly. They suggest

high diffusion coefficients (order of 10 m^2/yr) may be obtained by either a very efficient linear diffusion or by landsliding. Both of which may be active given the nature of the unconsolidated substratum and favourable climatic conditions. Other studies have concluded that bedrock landsliding is the most important hillslope process in operation and is required for a growing ridge to attain topographic steady-state (Hovius et al., 1997; Densmore et al., 1998; Champel et al., 2002).

The ideas of rock resistance, discharge and slope were first incorporated into a stream power law for bedrock incision by Howard & Kirby (1983), who argued that incision should be proportional to the shear stress exerted by the dominant discharge. They developed a stream power erosion law to explain the detachment-limited rate of bedrock channel erosion:

$$\varepsilon = KA^mS^n \quad (1)$$

where ε is the detachment-limited rate of bedrock channel erosion, m and n are positive constants that depend on the process of erosion, basin hydrology and channel hydraulic geometry, K is a dimensional coefficient of erosion, S represents the channel gradient, and A represents the upstream contributing area (proxy for discharge). The equation relies on three assumptions – 1) coefficients and exponents are spatially uniform and temporally invariant 2) a discharge can be found which characterises the flow 3) precipitation is sufficiently uniform for A to constitute a suitable proxy for discharge. Howard & Kirby (1983) found this to work in badlands assuming incision rates are linearly proportional to bed shear stress (m=1/3, n=2/3).

They calculated that for a channel whose width increases as the square root of bankfull discharge and in which bedrock incision occurs predominantly during bankfull or larger discharges $0.3 < m < 0.4$. There are multivariate controls on K such as lithology, climate, and sediment load. The m/n ratio is independent of dominant erosion processes, and depends only on the relative rates of increase of discharge with drainage area and of channel width and discharge. The ratio is expected to fall within a narrow range ($0.35 \leq m/n \leq 0.6$). Although the m/n ratio strongly influences the concavity of equilibrium channels, many additional factors can affect profile concavity: disequilibrium conditions, systematic downstream variations in either rock uplift rate or erodibility K, or regression of data that cross the bedrock-alluvial transition. Other bedrock channel erosion laws have been formulated but are less readily cast in terms of the physics of observed erosion processes (Whipple & Tucker, 1999). The undercapacity model of Beaumont et al. (1992) has the advantage of treating transport-limited and detachment-limited behaviour within a single algorithm.

Kirby & Whipple (2001) used two main tributaries of the Bagmati and Bakeya rivers in southern Nepal to calibrate a detachment-limited stream power incision model (Howard et al., 1994), incorporating the work of Lavé & Avouac (2000) on terraces. They found for the Siwalik Hills in Nepal, $m/n = 0.46$, $n = 0.66$ (incision linearly proportional to shear stress), $n = 1$ (incision linearly proportional to unit stream power), and $K = 4.3 \times 10^{-4}\ m^{0.2}/yr$. These values yield estimates of spatially variable erosion rates that mimic expected variations in rock-uplift rate across a fault-bend fold such as those which cause most uplift in the Sub-Himalayan Zone. They report

pronounced river profile concavity variations with respect to uplift rate in the Siwalik Hills.

Champel et al. (2002) used a tectonic-surface processes model to determine that the Dundwa Range in the Sub-Himalayan Zone of Nepal developed by linkage of several component segments. They conclude that as a result of fault segment linkage the observed drainage patterns may be controlled by fault geometry rather than relative rates of tectonics or surface processes. They used the modelling programme CASCADE (Braun & Sambridge, 1997), that includes numerical formulations for fluvial incision and bedrock landsliding, to show that the Duns develop by linkage of two fault segments and are eventually breached when sedimentation within them permits larger axial rivers. A lateral displacement gradient sets up an axial slope behind the growing fold which efficiently diverts all drainage so that the fold itself is shielded from rivers with large incision capacity. With this they attempt to explain the large-scale river deflection observed throughout the Siwalik belt in Nepal. This model does not however explain the development of wind or water gaps on the active structures, because it predicts drainage will be deflected continuously around them. Champel et al. (2002) concur that the relatively constant elevation of the Siwalik fold ridges, independent of the amounts of tectonic uplift and denudation, suggests they have reached topographic steady-state. Van der Beek et al. (2002) applied numerical modelling to the same hills in southern Nepal and purport that the dip of the detachment underlying a thrust-cored ridge of uplift determines the efficiency of thrust uplift in relation to river diversion, and therefore exerts a first-order control on the stream network. Recent analysis of medium-resolution digital topography by

Duncan (1997) also indicates a strong control on the Himalayan frontal topography by active faults. Similar to Champel et al. (2002), Van der Beek et al. (2002) found that for a nonzero detachment dip, the lateral dispacement gradient sets up an axial slope behind the growing fold that diverts drainage so that the fold is shielded from rivers with large incision capacity. This would suggest the fault-segment length, rather than uplift or incision rates, is a first-order control on river diversion. They conclude that the contrasting drainage arrangement between central and western Nepal is mainly controlled by variations in the dip of the under-thrusting Indian plate. Alternative models have stressed the importance of both drainage entrenchment within easily eroded lithologies (Oberlander, 1985; Tucker & Slingerland, 1994) and fluvial aggradation behind the fold (Humphrey & Konrad, 2000).

3.5.4. Methodology

Using a 90 m resolution DEM base we simulated Himalayan rivers throughout the field area in the Sub-Himalayan Zone and foreland basin of southern Nepal (Fig. 3.6.). Stream gradients were plotted and these were then used to assess the impact of variations in stream power on their down-cutting potential in relation to modern-day uplift rates above emerging thrusts in the proximal foreland. The modelling programme ArcInfo was employed to rapidly calculate stream profiles and stream power by using simple algorithms (see Appendix II). The aml's (arc macro language) require the user to manually choose the river which is to be investigated, this involves obtaining accurate coordinates for the source (pour point) and mouth. The following equation (a modification of equation 1) was used to generate a stream power plot for each river of interest:

$$\text{Streampower} = (4.3 \times 10^{-4}) \times (\text{upstream} \times 10^{0.3}) \times (\text{powslope_grid} \times 10^{0.66})$$

Values for the coefficient of erosion and the positive constants m and n were taken from Kirby & Whipple's (2001) work in the same region. Only rivers that extend fully to the crest of the Dundwa Range were included in the analysis.

3.5.5. Results

Figure 3.7. shows normalised river profiles so that at 0 km along the x-axis the plot for each river starts at the crest of the southern-most ridge adjacent to the foreland basin (Dundwa Range). The thinner black line plots represent smaller tributaries, which are actually sourced from the Dundwa ridge and have been generated as a

result of its recent uplift. The two red plots represent larger rivers, which have a more northerly source and one of these is the Tinau River. This plot allows direct comparison between most of the transverse systems in the central Nepal field area. All rivers display a steep profile within ~ 5 km of the crest of the Dundwa Range. Slopes are then seen to almost exponentially decrease with distance south into the foreland basin. By ~ 20 km from the ridge, river profiles are almost flat, perhaps indicating that they have progressed beyond the southerly limit of the main fan accumulation zone. The purpose of this plot is to highlight the striking difference between the smaller rivers and the two larger rivers. It is clear that the larger rivers maintain a steeper profile for greater distances into the foreland basin than the smaller tributaries, and eventually lose most of their gradient in a more abrupt fashion.

Figure 3.8. shows the variation of stream power with respect to distance downstream for the Tinau River and a smaller river (river 28) sourced from the Dundwa Range. There is clearly a major difference between the Tinau River and the smaller tributary. Whilst this is the case for all the other smaller rivers in comparison to the two larger ones, restricting the plot to two profiles simplifies it. The polynomial plot for the Tinau River shows far higher stream power values within the first 10 km compared to the smaller river and the plots are seen to cross at two points further downstream at ~ 22 km and ~ 58 km.

3.5.6. Discussion

Our stream power modelling suggests the spacing of ridge uplift within the Sub-Himalayan Zone has a direct impact on subsequent drainage evolution. It appears that should subsequent thrusting be located within ~ 10 km downstream of the previous thrust then larger rivers with higher discharges and sediment load are likely to breach the ridge of uplift and maintain their original course, assuming uplift rates of ~ 15 mm/yr (Lavé & Avouac, 2000). It is more likely that the larger rivers would not be diverted by a ridge of uplift within 22 km of the thrust front. Smaller systems which have come about through previous diversion, however, seem destined to be captured and redirected once again. The reason for this is most likely due to the larger rivers retaining a steeper profile due to the larger alluvial fans that must result from their greater sediment load (this factor may also induce further complications such as the difference between detachment- and transport-limited systems depending on sediment flux). From thrust spacing in the Sub-Himalayan Zone it is likely that any subsequent thrusts will be located within this 20 km zone. The smaller channels that are cut-off behind the new ridge of uplift will most likely collect and produce a new axial system. However, should the new ridge of uplift occur more distally then surprisingly, modelling suggests the smaller rivers are less likely to be captured. This may reflect the smaller channels gradually accumulating more tributaries and therefore actually forming larger rivers downstream at a greater rate than the rivers which start off larger at the range front. Indeed, modern-day maps show this is the case (Fig. 3.4.). Larger rivers do not join adjacent systems until at more distal locations in the foreland basin. This scenario makes sense when you consider that following initial capture, the smaller rivers have a reduced stream power but are

more numerous and closely spaced than those that breached the uplift and therefore have a greater chance of joining downstream. It thus appears that once a drainage network has been captured and an axial system initiated, the increase in tributary streams and therefore spreading of power means that the system is more likely to be further diverted in the future should subsequent thrusting be located within 20 km of the previous ridge of uplift.

The strong drainage pattern contrast between west and east Nepal is joined by a difference in the spacing of ridge uplift, supporting the conclusions of this study. Where more widely spaced thrusting in western Nepal has created deposition in Duns and drainage diversion, much more closely spaced thrusting both around the Duns in western Nepal and more generally in eastern Nepal has not resulted in axial stream development. Therefore, whilst flexural models, section balancing, seismic profiles, and dislocation modelling of geodetic data (Lyon-Caen & Molnar, 1985; Jackson & Bilham, 1994; Jouanne et al., 1999; Larson et al., 1999; Mugnier et al., 1999; Lavé & Avouac, 2000) support Van der Beek et al's. (2002) suggestion that the difference in detachment dip between west and east Nepal has caused the difference in drainage patterns, this study shows that the spacing of ridge uplift and therefore thrusting also has a fundamental control on the potential for diversion.

As rivers leave the Himalayan foothills and enter the foreland basin they immediately lose significant energy through the change in steepness of slope. This occurs over a short distance, which from the modelling appears to be potentially significant with regards to river capture behind future uplift. All along the Nepalese

proximal foreland, there is a continuous curtain of alluvial fans, deposited as a result of the dramatic reduction in gradient where the foothills meet the Gangetic Plain. These serve to maintain a minimal gradient before the river enters the foreland basin proper and may be significant in terms of river power and down-cutting potential.

For this study the model parameters do not need to accurately represent real conditions because the variation in stream profiles give the relative differences between streams assuming the model parameters are equal. Further work would be to run similar models but investigate transport-limited systems (Willgoose et al., 1991) and excess stream power systems (Densmore et al., 1998; Lavé & Avouac, 2001) and more complicated hybrid sediment-flux dependent models such as the undercapacity model (Kooi & Beaumont, 1994) or the Tools model (Sklar & Dietrich, 1998). In the Dundwa Range, the highest erosion is predicted during monsoon times but then rivers will be transport-limited. During the dry season relict blocks from the monsoon may maintain the channels as transport-limited or they may only become transport-limited at the start of the alluvial fans. Therefore the detachment-limited modelling of this study may be an over simplification. The controls on thrust spacing along the foreland would also be interesting to model. Burbank et al. (1996) suggest the thickness of the pre-tectonic hanging-wall will influence the spacing of thrusts (Dixon & Liu, 1992; Marshak & Wilkerson, 1992) because of a tendency for the spacing of folds and faults to be proportionate to the thickness of the "beam" being deformed. Creation of a Dun and the accumulation of sediment within it most likely has a different effect on the location of any future thrusting than in Dun-free regions.

3.6. Conclusion

This small study serves to emphasise the sensitivity of the drainage system in southern Nepal to small-scale changes in thrusting characteristics. It appears that not only the rates and geometry of thrusting, but also the spacing of thrusts can be an important factor in the geomorphological evolution of the proximal Himalayan foreland basin. A minor change in the placement of a thrust could result in river diversion, which would in turn produce a strong detrital signal. Whilst the controls on such processes are complex and difficult to predict they can have a dramatic impact on detrital investigations and thus represent an important area for future research.

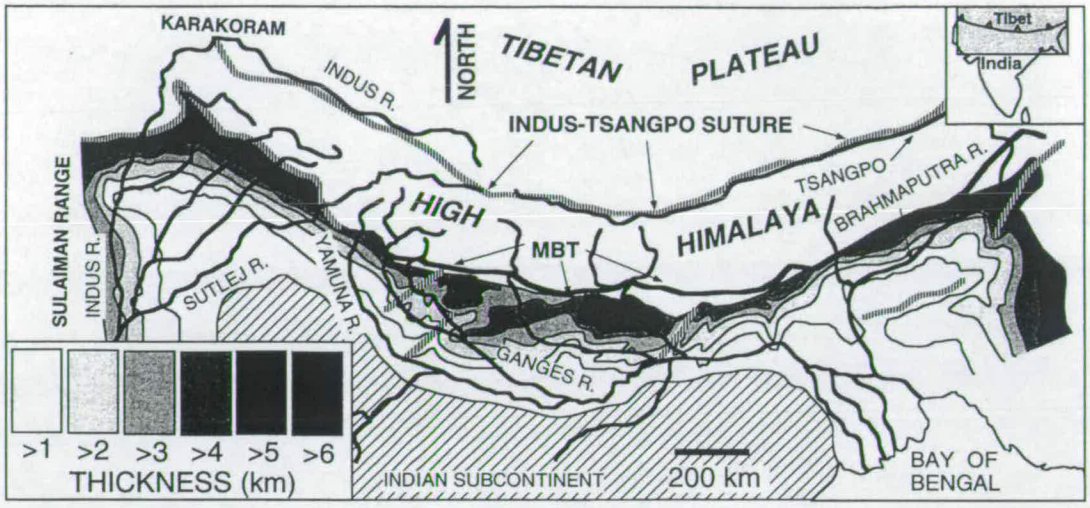


Figure 3.1. Extent of Himalayan foreland basins with sediment thickness indicated, from Burbank et al. (1996). MBT - Main Boundary Thrust.

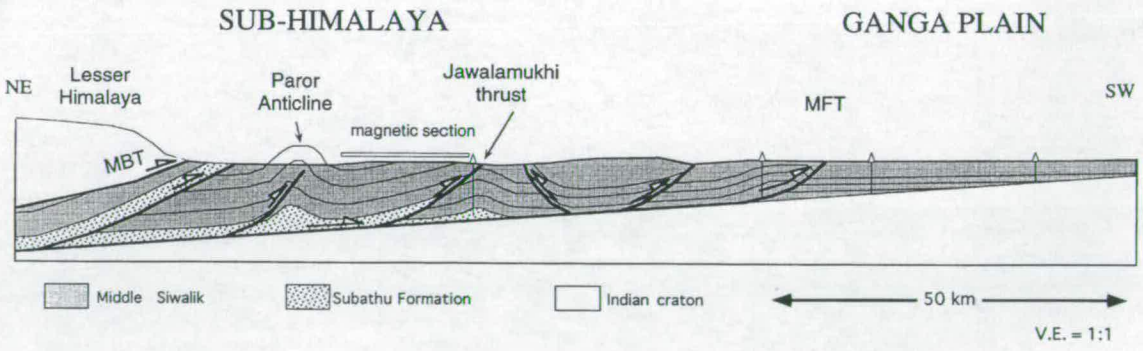


Figure 3.2. Cross-section through the northern Pakistan foreland basin showing wedge of foreland basin sediment, from Burbank et al. (1996). MBT - Main Boundary Thrust, MFT - Main Frontal Thrust.

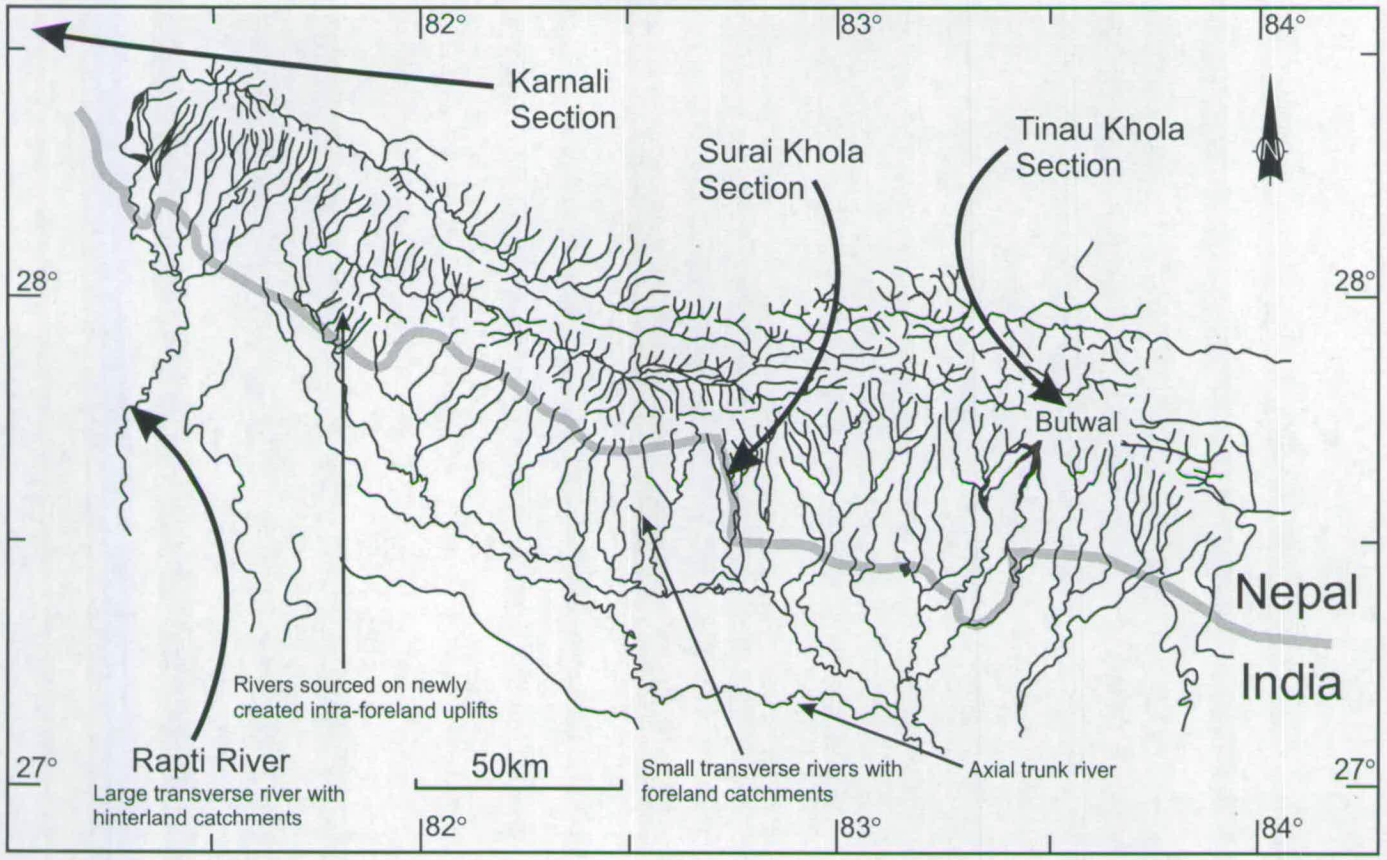


Figure 3.3. Drainage map for part of the Ganges system along the Nepal-India border. The plot highlights the difference in drainage patterns between west and east. The Rapti River flows axially for over 100 km in the west, whereas no such diversion has taken place further east.

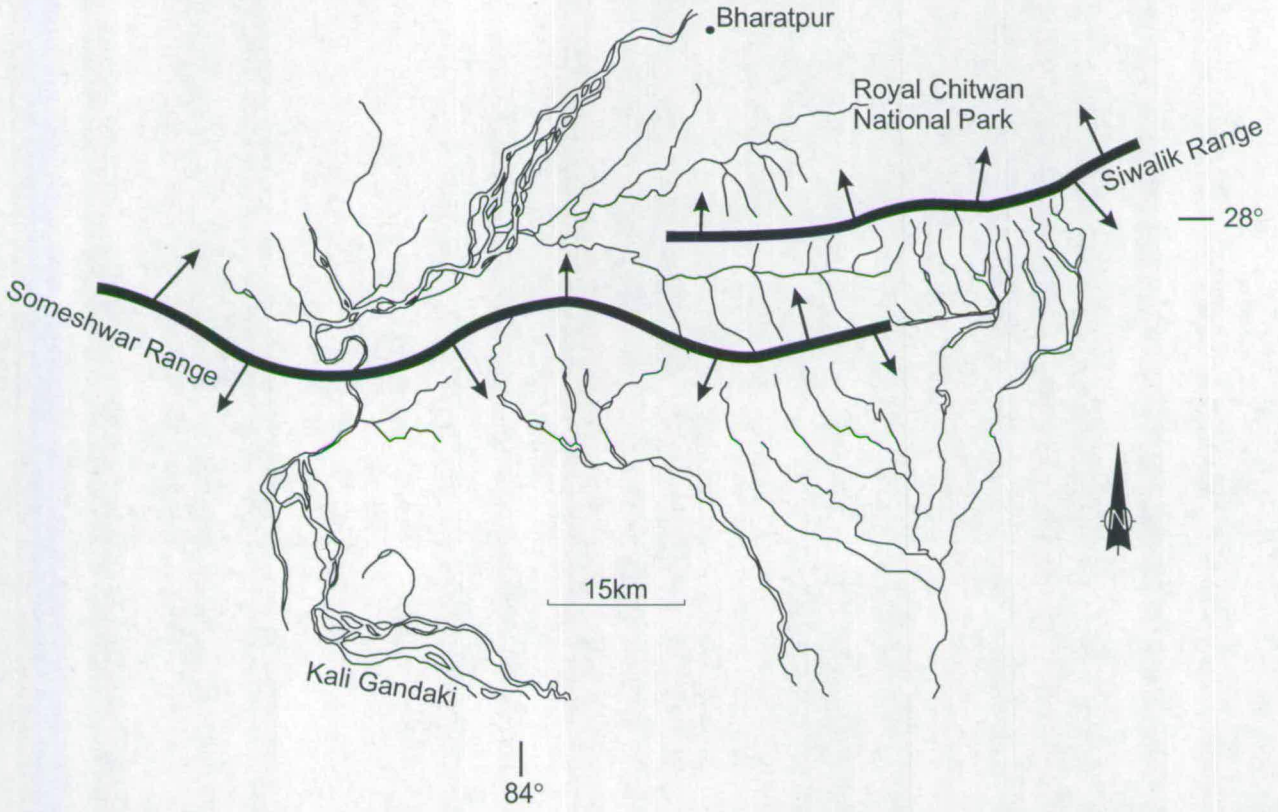


Figure 3.4. Simplified sketch map of drainage architecture for central-southern Nepal, east of the Tinau Khola section. The plot highlights the difference in drainage pattern between the larger Kali Gandaki River as it traverses the foreland basin and those of smaller tributaries that have formed as a result of recent capture behind the growing Siwalik and Someshwar Ridges.

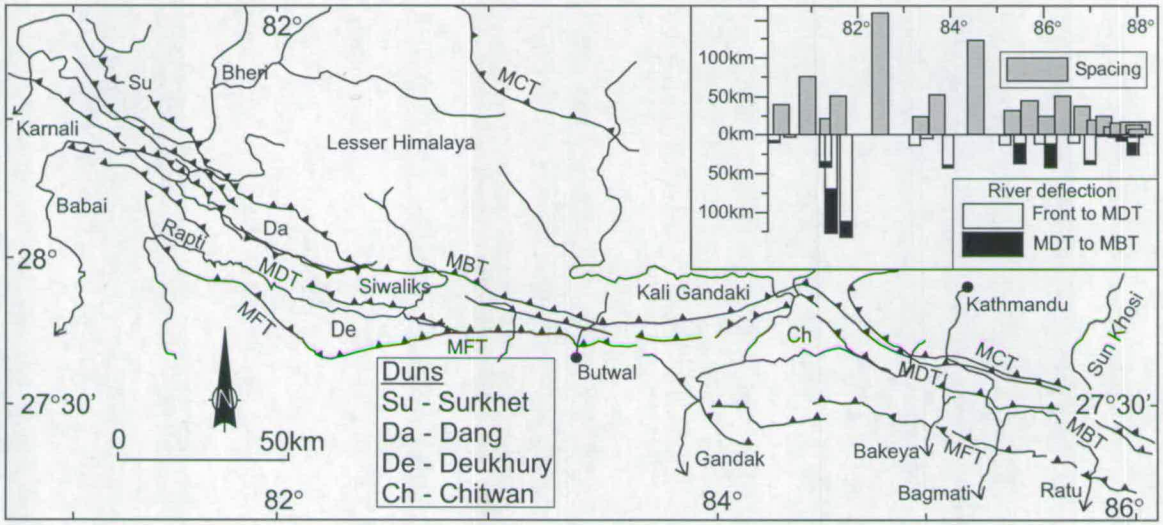


Figure 3.5. Simplified structural and drainage map of the Nepal Himalaya, showing position of Duns, from Van der Beek et al. (2002). MCT - Main Central Thrust, MBT - Main Boundary Thrust, MDT - Main Dun Thrust, MFT - Main Frontal Thrust. Inset plot shows river spacing (upward y-axis) and diversion (downward y-axis: white - at Main Frontal Thrust, black - at Main Dun Thrust) for streams traversing the Siwaliks, as a function of longitude.

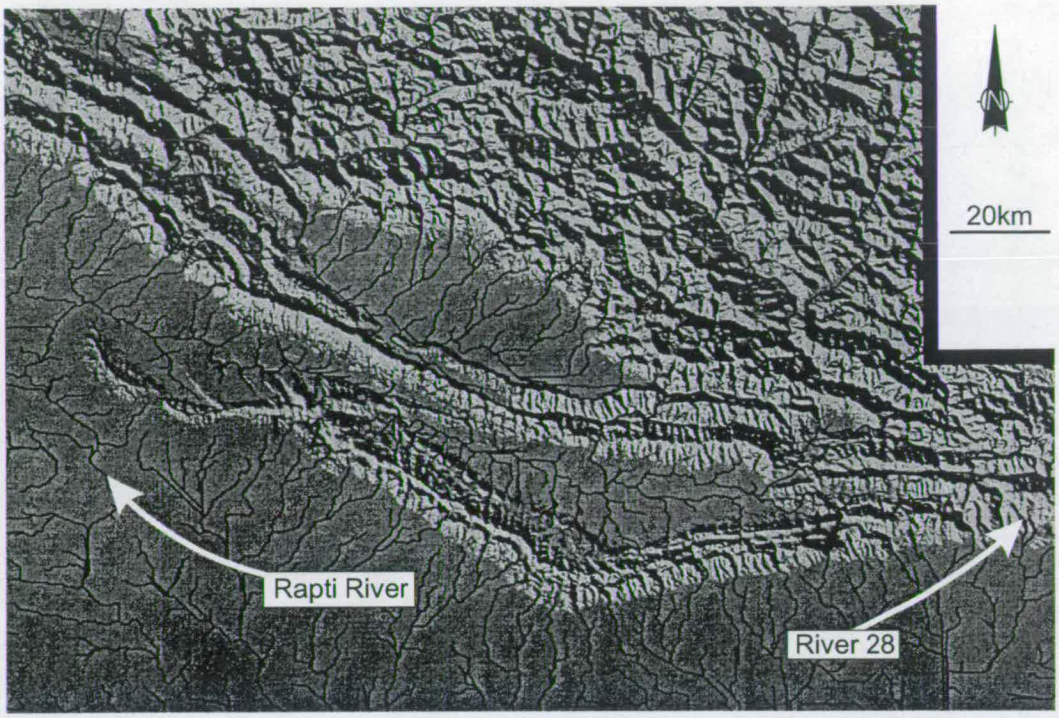


Figure 3.6. DEM image of the Deukhury Dun in south-central Nepal which has diverted the Rapti River axially for over 100 km. The Dun is located between the Surai Khola and Karnali Siwalik sections. River 28 refers to the river which is plotted in figures 3.7. & 3.8.

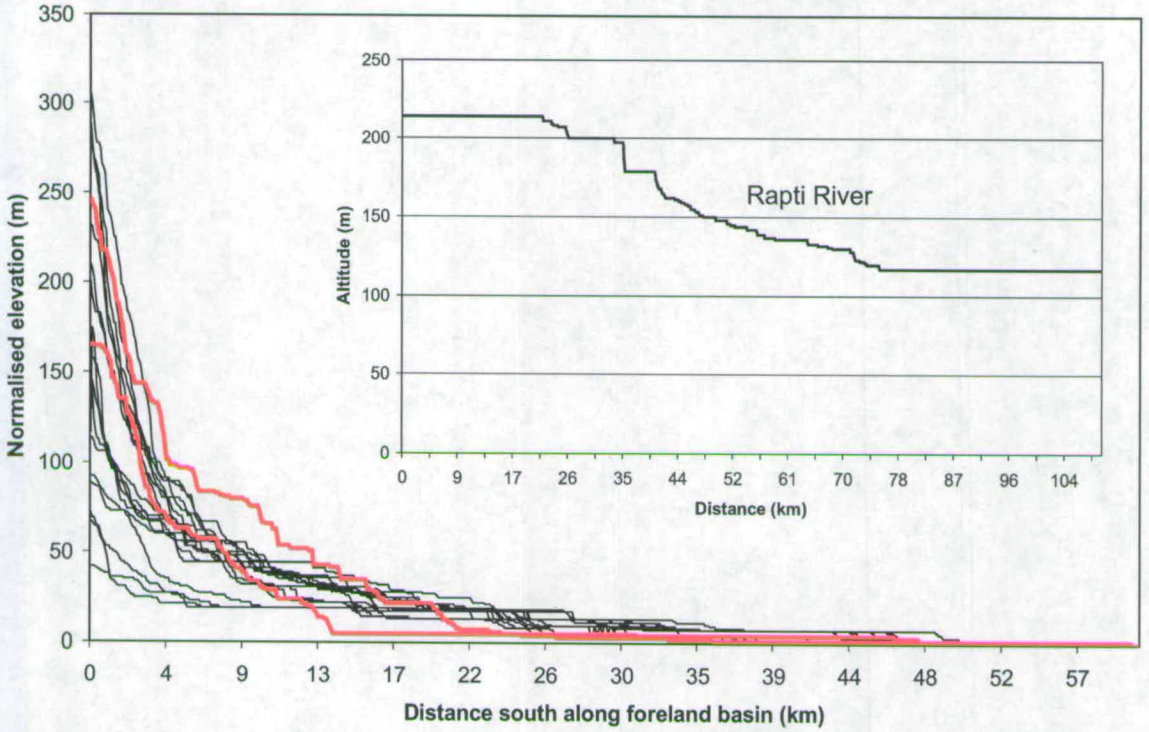


Figure 3.7. Normalised river profiles with artificial altitudes. Thin lines depict rivers that are sourced from the south face of the Dundwa Range, whereas the thicker lines represent larger systems which cut through the Dundwa Range. Distance is in a southwards direction away from the thrust front and along the foreland basin. The Rapti River profile is shown as a separate plot, which begins within the Deukhury Dun. Note that the other rivers flow along the same altitude in the foreland basin as the Rapti River when plotted normally. The Rapti however does not show such a dramatic break in slope because it has breached the Dundwa Range more thoroughly.

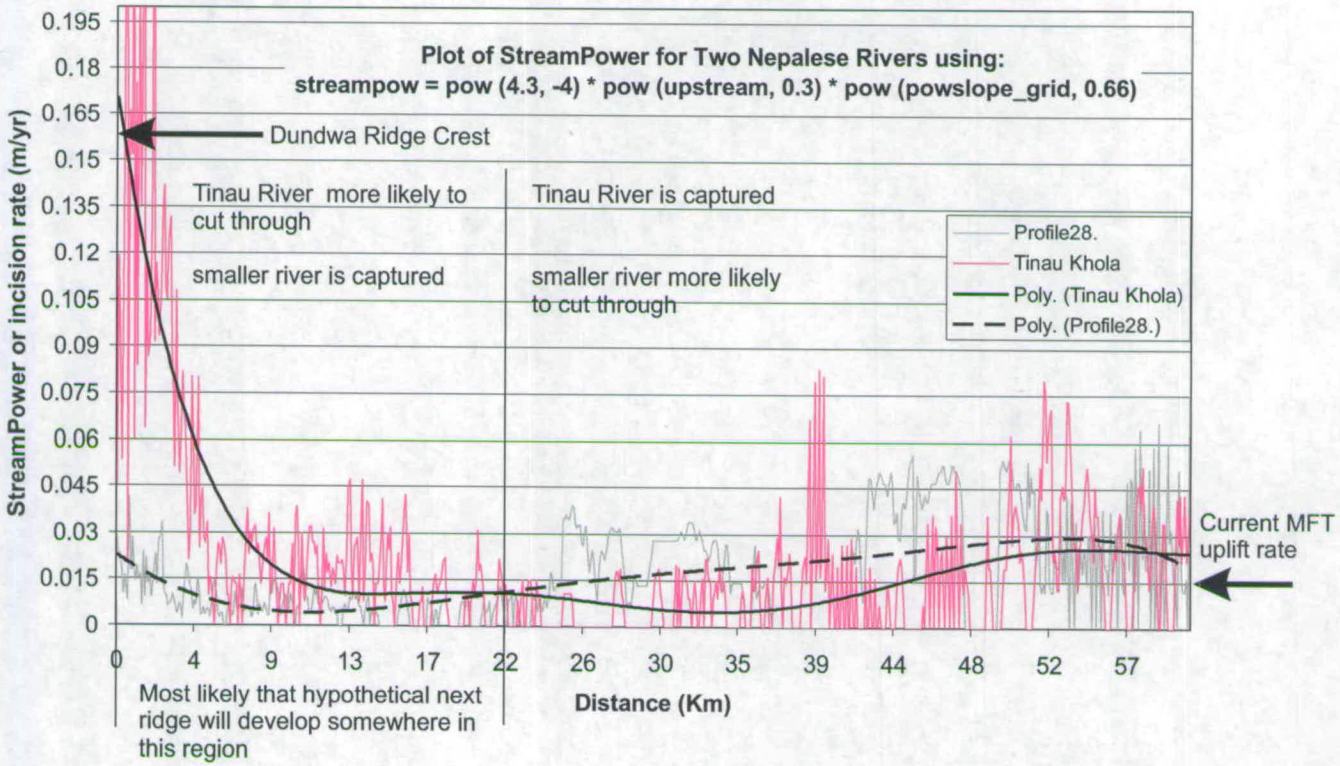


Figure 3.8. The variation in stream power or incision rate in relation to distance south along the foreland basin for the Tinau River and a smaller river sourced from the Dundwa Range. The black lines are highly smoothed plots for the respective rivers. The current MFT (Main Frontal Thrust) uplift rate is taken from Lave & Avouac (2000).

4. Sedimentology

4.1. Introduction

Although the sections comprising this thesis are famed for their exposure and continuity in Nepal and have thus been well studied, the logging undertaken as part of this research is the most detailed to date. This chapter explains the facies characteristics and palaeoflow data that were recorded along each section on a cm-scale. The data obtained allows analysis of sedimentation rates during deposition and an appreciation of the evolution of facies and palaeoflow directions up-section. Such information is relevant to any detrital investigation in terms of the nature of the fluvial systems that deposited the rocks under analysis, their provenance, and the environment of deposition that evolved during hinterland reorganisation. Indeed, fluvial deposits are sensitive indicators of allogenic processes. Together, the separate molasse deposits that comprise the Himalayan detrital record and the Indus and Bengal Fans document the temporal and spatial relationship of the Himalayan fluvial-marine depositional system from Eocene to Recent.

4.1.1. Siwalik Group subdivisions

The Siwalik Group has traditionally been informally divided, on the basis of facies characteristics and heavy mineral trends, into Lower, Middle, and Upper sub-groups (e.g. Sahni & Mathur, 1964; Quade et al., 1995). This three-fold division reflects obvious changes in depositional style and palaeoenvironment. However, the scheme is purely lithostratigraphic and cannot be used for detailed chronostratigraphy. Furthermore, these informal boundaries are diachronous between sections and

suggest more abrupt facies changes than were witnessed in Nepal as part of the present study. Consequently, the Siwalik Group is not divided as such in this thesis, and for the same reasons the Surai Khola formations proposed by Corvinus (1988) are not inherited.

4.2. Previous work

The Siwalik Group crops out within the Sub-Himalayan Zone along a continuous belt, 2500 km long, from NW Pakistan to NE India (Fig. 1.1.). The system of rivers from which the Siwaliks were deposited most likely flowed into the Indus and Bengal Fans where they released the remaining sediment load, the depositional periods of the two fans being almost the same (Miocene to Present; Derry & France-Lanord, 1996). A profusion of studies have documented these rocks from the earliest Himalayan investigations to the present day (e.g. Sahni & Mathur, 1964; Parkash et al., 1980; Willis & Behrensmeyer, 1994; Gupta, 1997; Khan et al., 1997; Zaleha, 1997a, 1997b). Most efforts have been focused in the NW Himalaya due to superior exposure. But in recent times, with the expansion of road access and palaeomagnetic work and a need to complete the story across the entire length of the range, more workers have been attracted to eastern outcrops (e.g. Harrison et al., 1993; DeCelles et al., 1998b).

Sahni & Mathur (1964) described the Siwalik Group in NW India as a typical molasse deposit. The molasse consists of a 5-8 km thick Mid-Miocene to Pliocene fluvial succession which thins away from the mountain front (Parkash et al., 1980; Burbank et al., 1996). Siwalik rocks have received significant attention in terms of

sedimentology (e.g. Auden, 1935; Tandon, 1976; Sharma, 1977; Parkash et al., 1980; Burbank et al., 1986, 1988; Johnson et al., 1986; Baker et al., 1988; Burbank et al., 1988b; Burbank & Beck, 1989, 1991; Mulder & Burbank, 1993; Willis, 1993; Harrison et al., 1993; Quade et al., 1995; Burbank et al., 1996; DeCelles et al., 1998b; Nakayama & Ulak, 1999). Generally, these studies show a strong similarity between sections along-strike in terms of facies characteristics and palaeoflow, although there have been debates surrounding the possible transverse versus axial nature of some major trunk rivers. By constructing a detailed biostratigraphy and magnetostratigraphy for the Siwalik Group, Corvinus & Rimal (2001) and other workers enabled the correlation between sections across the mountain range. Combining investigations from Pakistan to Nepal, the Siwaliks can be generalised as a coarsening- and thickening-upwards succession of mudstone, sandstone, and conglomerate.

4.2.1. Modern and ancient fluvial system

Siwalik palaeocurrents generally indicate south to south-easterly or south-westerly flow from Late Miocene to recent times (Parkash et al., 1980 and references therein; Burbank et al., 1996; DeCelles et al., 1998b). These palaeoflow directions suggest the rivers were part of a tributary system oriented more or less transverse to the mountain front as are many of the present Ganges tributaries. A gradual transition from south-easterly to south-westerly flow in an upstream direction towards the Himalayan foothills is a characteristic of the modern day Ganges drainage system and has also been found in the Siwalik Group sediments (Burbank et al., 1996) (Fig. 3.3.). Burbank et al. (1996) record dominant south-easterly palaeoflow in the Surai

Khola section of Nepal but this switched to dominantly south-westerly for the last 4 Myr of deposition. The tendency towards increasingly south-easterly flow in more distal reaches reflects the rough easterly tilt of the basin towards the Bay of Bengal. Burbank et al. (1996) suggest an axial river system developed during Middle Siwalik deposition as a response to Main Boundary Thrust movement and subsidence in the proximal foreland basin. Burbank (1992) suggests that the present transverse drainage is a relatively recent development (post-Pliocene) due to erosional unloading and isostatic rebound. However, the age of significant loading as a result of Main Boundary Thrust movement has yet to be constrained. Indeed, the idea of an axial drainage arrangement conflicts with palaeoflow and lithofacies data collected by DeCelles et al. (1998b) in the Siwalik Group of Nepal, which suggest transverse flow existed since at least Mid-Miocene time. DeCelles et al. (1998b) speculate that the deposits of an axial system may be preserved in older sediments that are not exposed.

There are other indicators of a similarity between the ancient and the modern foreland basin river systems. Parkash et al. (1980) interpret Siwalik deposits in NW India as having been deposited predominantly in the form of large mega-cones, very similar to those forming currently on the Indo-Gangetic Plain. They recognise two coarsening-upward cycles consisting of sandstone-clay alternations in the lower succession, passing gradually into coarse sandstones and/or conglomerates towards the top. In a more recent study DeCelles et al. (1998b) remark on the similarity in morphology between middle to upper Siwalik rivers and the modern transverse tributaries of the Ganges, wherein gravel deposition is restricted to within ~ 20 km of

the topographic front. Further west, the Siwalik strata of the Potwar Plateau in NW Pakistan have been interpreted to represent deposits generated by a large river system, probably the ancestral Indus River (Burbank and Beck, 1991; Mulder & Burbank, 1993; Abbasi & Friend, 2000).

4.2.2. Facies characteristics in Nepal

DeCelles et al. (1998b) divide the Siwalik Group of western Nepal into five general lithofacies types: sandy fluvial channel, gravelly fluvial channel, crevasse splay, paludal floodplain, and palaeosol deposits. Most Siwalik sections can be fully explained by the juxtaposition of these facies in varying sequences. Nakayama & Ulak (1999) describe the Surai Khola section in more detail, distinguishing eight facies types that essentially correlate with those of DeCelles et al. (1998b). Histatomi & Tanaka (1994) also performed facies analyses on the middle to lower part of the Tinau Khola section in Nepal. They note that sedimentation began in a meandering river environment, changed to a predominantly sheet-splay type at 10 Ma and became braided at 7.5 Ma. Similarly, DeCelles et al. (1998b) found that the Siwalik Group of western Nepal records a change from small channels and well-drained floodplains to much larger channels and more poorly drained floodplains from Middle- to Late-Miocene time. They record a variety of river morphologies but highly sinuous rivers seem to have dominated during Early Miocene time whilst anastomosed and braided rivers prevailed during Middle- to Late-Miocene time. DeCelles et al. (1998b) suggest this change in depositional characteristics reflects an increase in rainy season discharge. Indeed, the modern Gangetic floodplain receives large amounts of precipitation (1000-1500 mm/yr) and major floods during the

monsoon. Water level during the dry season drops over 10 m in the major rivers. The middle Siwalik horizons most likely accumulated under a similar monsoonal climatic regime (Quade et al., 1995).

At the top of the Siwalik Group meandering river deposits give way to continuous conglomerate horizons. Parkash et al. (1980) found that the conglomerate thickness is variable and increases in the proximity of large rivers and they mostly reflect the composition of the rocks exposed immediately to the north. Along with recycled Siwalik rocks, they report an abundance of quartzite pebbles in the conglomerates which they suggest have mainly a Lesser Himalayan provenance. These youngest Siwalik strata have commonly been affected by proximal tectonism (Mugnier et al., 1999).

4.2.3. Sedimentation rates

Appel et al. (1991) calculate average acccumulation rates for the Surai Khola section of ~ 0.17 km/Myr. However, a number of workers have noted that sediment accumulation rates, sandstone/siltstone ratios, mean grain size, and the thickness and amalgamation of sandstone bodies all increase after 11 Ma in sections from Pakistan to Nepal (Meigs et al., 1995; Burbank et al., 1996 and references therein) (Fig. 4.1.). In fact, beginning ~ 11 Ma throughout the foreland all sections display an increase in sedimentation. Most commonly rates increased by 35-75 %, with some of the highest Himalayan accumulation rates (~ 1 km/Myr) occurring during this interval (Burbank et al., 1996 and references therein). Willis (1993) calculates that in the Potwar Plateau and Himachal Pradesh, discharges were probably four times greater

or more during this period, similar to those of major transverse rivers flowing across the foreland today. In the lower Indus basin a transition from marine to fluvial deposition occurred at ~ 11 Ma (Khan et al., 1988). Across the Potwar Plateau, the Jhelum re-entrant, Himachal Pradesh, and western Nepal there was an abrupt upward coarsening at ~ 11 Ma such that channel sandstones comprise ~ 70 % of these successions (Burbank et al., 1996). Additionally, in the northern Indian Ocean deep-sea sediments record an abrupt increase in mass accumulation rate between ~ 11-6 Ma (Rea, 1992).

The reason for this ubiquitous switch in depositional characteristics at ~ 11 Ma has not been resolved. DeCelles et al. (1998b), who record an increase in channel size within the Siwaliks of Nepal at ~ 10.8 Ma, interpret the change (using petrography data) as a response to increased rainy season discharge along with erosion of the Lesser Himalayan Crystalline Thrust Sheets and the growing Lesser Himalayan Duplex. A similar climatic change is indicated by oxygen isotopic data from bivalve shells and mammal teeth (Dettman et al., 2001). Other workers, however, favour the idea that the inception of the Main Boundary Thrust at this time resulted in increased erosion rates and foreland basin subsidence (Meigs et al., 1995; Burbank et al., 1996).

4.3. Magnetostratigraphy problems

This study relies on the magnetostratigraphic age calibration of the Tinau Khola and Surai Khola sections by Ojha (personal communication, 2002) and that of Gautam & Fujiwara (2002) for the Karnali section. An issue that is important to address is the variability between the data of Ojha (personal communication, 2002) and previous work conducted by Appel et al (1991) along the Surai Khola section and Gautam & Appel (1994) along the Tinau Khola section (Fig. 4.2.). The respective authors explain that the differences (which amount to variations of up to 2 Myr in the age of samples from the same stratigraphic height) are due to the type of sample upon which the palaeomagnetism was determined. The Appel et al. (1991) study exclusively sampled sandstones whilst Ojha (personal communication, 2002) exclusively sampled laminated siltstones. The discrepancy between these two data sets (mostly < 1 Myr) does not, however, have a significant effect on the final interpretations of this study because ages for the crucial 12-10 Ma period show a good correlation. There is also strong evidence to suggest finer-grained sediment provides more reliable magnetic age data, based on the often greater abundance of single magnetic domain particles (Butler, 1992). Thus this study uses the data of Ojha (personal communication, 2002).

4.3.1. General sources of error

The Siwalik Group in Nepal contains only sparse fossils, hence it is not possible to use biostratigraphy for age calibration with any accuracy. Magnetostratigraphy has therefore proved an essential tool for determining the age of Siwalik Group sediments in Nepal (e.g. Appel et al., 1991; Harrison et al., 1993; Gautam & Appel,

1994; Roesler et al., 1997; Ojha et al., 2000; Gautam & Fujiwara, 2002). Additionally, radiometric dating of ash horizons has proved useful for calibrating the magnetostragigraphic record. The allignment of detrital magnetic particles by the ambient magnetic field that may occur in sediment during deposition gives rise to the detrital remnant magnetisation (DRM). In the geological time scale the study of the geomagnetic field requires some model for use in analysing palaeomagnetic results so that global comparisons are possible. The model used is termed the geocentric axial dipole field (GAD). Measurement of the palaeomagnetic pole, which should have the same value at any locality, allows the comparison of results from any area. However, this technique is susceptible to a number of uncertainties or variables that can increase the potential error surrounding calculated ages.

Burbank et al. (1996) list five main limitations on the accuracy of palaeomagnetic age data:

1) It is possible that the magnetic polarity recorded by a stratum will not be syn-depositional.
2) Numerous magnetozones have been based on single sites which increases the possibility that the calculated polarity does not indicate the polarity at the time of deposition.
3) Preserved strata may contain an incomplete record of magnetic reversals because of erosion or the presence of strata which are unsuitable for sampling.
4) Field measurements of stratigraphic thickness introduces typical uncertainties of ~ 10 %.

5) It is assumed that deposition is fairly constant. If not, correlation with the Magnetic Polarity Time Scale (MPTS) may be ambiguous (Talling & Burbank, 1993).

Although such sources of error naturally reduce the accuracy of the age data for the Siwalik Group, previous work indicates the ages as a whole are reliable. Several studies within the Siwaliks have demonstrated that the magnetic signal revealed through thermal demagnetisation usually was acquired at or very near the time of deposition (Tauxe & Badgley, 1988; Tauxe et al., 1990). From analysis of five sections in Nepal, Roesler et al. (1997) found that, although gaps in the sections and variable demagnetisation behaviour of the haematite-bearing sediments was problematic, double-sampled parts of some sections yielded similar results. Appel et al. (1991) also report that antiparallel mean directions of the normally and reversely polarised samples of the Surai Khola section indicate that the characteristic remnant magnetisation (ChRM) is of primary origin. Indeed, around 97 % of the Surai Khola samples yielded characteristic remanence and associated polarity (Gautam & Roesler, 1999). Appel et al. (1991) show that the frequencies of reversals in the Surai Khola section equals that in the standard polarity time scale. Based on their calculated sedimentation rates, erosion in the order of 100 m would be required for a reversal to have been lost from the section. There is no evidence for the existence of any important sedimentation gaps in either the Karnali, Surai Khola, or Tinau Khola sections. Indeed, despite the usual magnetostratigraphic age problems the present combination of faunal data with magnetostratigraphy and radiometric dates on ashes

permits classification of the Himalayan foreland as probably the best-dated terrestrial foreland basin in the world (Burbank et al., 1996).

4.4. Results

Simplified logs for each section are shown in Figures 4.3. to 4.5. and full detailed logs are given in Appendix III. The overall sedimentology of these sections and interpretations of their environments of deposition compare well with classic Siwalik descriptions along the length of the Himalayas. In general the group can be described as a coarsening- (grainsize: 100 to 400 phi) and thickening-upwards (beds: few cm to > 5 m) succession of mudstone and sandstone with conglomerate at the top. Sandstones are all moderately mature lithic arenites with abundant mica. Conglomerate has been removed by faulting along the Tinau Khola section and is present along the Karnali section but occurs above the level of youngest magnetostratigraphic dating at ~ 5 Ma (Gautam & Fujiwara, 2000) and so is absent from the log. Bedding in all three sections strikes NW-SE with northerly dips of ~ 30-60° except for a ~ 300 m stretch along the Surai Khola section near Dobata village where the beds are overturned. The Siwalik Group is divided into six facies types according to their sedimentary characteristics, dealt with here in turn. These descriptions apply to all three sections. Table 4.1. summarises the facies characteristics and interpretations.

Facies Type	Description	Stratigraphic Occurrence	Interpretation	Re-named
1	Up to 2 m thick lenticular bodies of fine-medium grained mudstone and sandstone, upward fining, trough and planar cross-lamination, ripples	Only in lower part of Siwalik Group	Distal fluvial meandering and anastomosed channel deposits.	Small channel facies
2	2-5 m thick fractured organic-rich horizons, fine grained, no primary bedding, red or grey, common trace fossils, root casts, burrows, calcite and iron nodules	Present throughout Siwalik Group but more common in lower half.	Immature palaeosols	Palaeosol facies
3	Mainly < 1 m thick fine grained stacked sandstone beds, trough and planar cross-lamination, ripple cross-lamination, and climbing-ripple cross-lamination	Mainly lower Siwalik Group	Crevasse splay deposits	Crevasse splay facies
4	< 2 m thick laminated mudstones, highly fissile, leaf fossils	Limited abundance throughout Siwalik Group, mainly at base of sandstone bodies	Deposited from standing water on floodplain	Floodplain facies
5	Up to 6 m thick medium-coarse grained sandstone bodies, stacked beds reach up to 40 m thick, upward fining and thickening, thalweg deposits, trough and planar cross-stratification, flutes, dewatering structures	Dominant facies in middle section of Siwalik Group and continues into upper Siwalik horizons.	Large meandering channel sandstones.	Meandering channel facies
6	Up to 5 m thick coarse grained sandstone lenses and conglomerate beds, strong imbrication, trough cross-stratification	Uppermost Siwalik horizons.	Proximal fluvial fan deposits, from high-energy braided rivers.	Braided channel facies

Table 4.1. Summary of Siwalik Group lithofacies.

4.4.1. Facies type 1.

Facies type 1 occurs exclusively in the lower part of all three Siwalik sections where it dominates and is lost once facies type 5 appears in the section (see below). The facies consists of cm- to m-scale beds (maximum thickness of ~ 2 m) (Plates 4.1. and 4.2.). These beds outcrop as laterally restricted (over a maximum distance of 5 m) and isolated fine-grained (mud and sand) lenticular horizons encased within facies types 2-4 (see below) (Plate 4.3.). There is a rough bundling of upward-fining mud-rich or sand-rich units and sandstone body bases are generally flat to slightly

erosional. "Wings" of sandstone are often present within surrounding mudstones (up to 1 m long). The sandstone bodies commonly contain calcareous nodules and trace fossils and are associated with bioturbated and pigmented mudstones. Larger beds (up to 2 m) often display a thin channel lag, planar lamination and flow indicators towards the top that include ripples, trough cross- and climbing-ripple cross-lamination. Ripple lamination is well preserved in the thinner sandstone beds. Intercalated black or grey mudstones are well laminated and mica-rich. For an example of facies type 1 see the 0-50 m section of the detailed Tinau Khola section log where typical facies type 1 beds are shown at 0 m, 35 m, and 43 m (Appendix III).

4.4.1.1. Facies type 1. interpretation (small channel facies)

Facies type 1 is characterised by small channel sandstones that show a rough bundling of upward-fining mud- or sand-rich units that was most likely caused by lateral channel migration. Along with the fine-grained nature of the sandstone and the high mudstone to sandstone ratio this suggests deposition occurred in a location between larger trunk rivers. A similar scenario exists in the present distal foreland basin whereby small channels redistribute sediment between larger trunk rivers. Due to the similarities between Siwalik sedimentology and the modern foreland basin and the up-section coarsening of sandstone beds, indicative of a distal to proximal setting, the small channel facies was most likely deposited in a distal location. "Wings" of sediment that extend into adjacent mudstone for up to 1 m laterally represent levee-type deposits (Hughes & Lewin, 1982). The presence of facies type 3 (crevasse splay facies) also requires levee development by anastomosed or

meandering rivers (Smith & Smith, 1980). Well-laminated and mica-rich intercalated black or grey mudstones are interpreted to be the products of rapid flood deposition. Finer-grained and thinner (< 2 m) beds with lateral accretion elements indicative of point-bar deposition (Allen, 1970) are interpreted as having been deposited by meandering channel systems. Thicker sandstones which show lateral accretion and are cut by small (10's of cm) channels (chute channels; Levey, 1978) may reflect vertical bar aggradation. Sedimentary structures in these units which include channel lags, planar lamination, and ripples are also indicative of point bar deposition. These sedimentary features are best exposed along the Tinau Khola section. Facies type 1 is therefore interpreted to comprise anastomosed and meandering ribbon channels and is re-named the small channel facies. Due to the size and nature of these beds it is possible they were deposited either from established channels or from heavy rainfall on the plain itself, which resulted in brief channel formation. It thus seems likely that the channels were a product both of major floods on the alluvial plain and longer-term channel migration.

4.4.2. Facies type 2.

Facies type 2 is marked by fine-grained, highly fractured beds (maximum thickness of 10 m, generally 2-5 m thick) above sandstone bodies (Plate 4.4.). Individual beds tend to coarsen upwards. Organic matter is abundant as humic horizons at the top of the beds and pale blue root casts and burrow traces are common. Beds tend to be grey, red or yellow in colour with a bulbous, fractured facade. Blocky, columnar, and prismatic structures are common. There is minor evidence for clay swelling, resulting in the loss of original texture with the production of pseudoanticlines and

desiccation. Mottled colouring is occasionally evident with red, green, brown, ochre and bleached patches. Calcite and iron nodules are commonly abundant, particularly in the lower Siwalik units. These nodules are seen in places to pseudomorph earlier burrows or root traces. The calcite nodules commonly increase in abundance upwards within beds and in rare cases culminate in a continuous laminated limestone-type or caliche layer, the thickest witnessed was ~ 1.5 m along the Surai Khola section. Root traces are preserved either as carbonaceous films where conditions were reducing, or as casts, and are sometimes surrounded by halos of discolouration (commonly pale blue). Occasional trace fossils show linear or spiralling patterns up to several cm long. Trace fossils can also be found in other facies types throughout the sections but they are less abundant. The contact between facies type 2 and underlying sandstones is commonly sharp and the top surface of the sandstone is often bioturbated. The contact with overlying sandstones is also typically abrupt with a convex-down scour surface. Typical examples of facies type 2 beds are shown along the detailed Tinau Khola section log at 13 m and 160 m (Appendix III).

4.4.2.1. Facies type 2. interpretation (palaeosol facies)

Facies type 2 is interpreted as a product of palaeosol deposition due to the blocky and bioturbated nature of the beds, and so is re-named the palaeosol facies (Roeschmann, 1971). The beds appear to have been immature soils with no evidence for pedogenic horizon development and only limited disruption related to root growth or bioturbation. Limited bed thickness suggests these are typical "alluvial soils", formed on temporarily exposed surfaces in an area of active aggradation so that there

was not enough time for prolonged pedogenesis (Leeder, 1975; Kraus & Aslan, 1993). The humic horizons at the top of the palaeosols would have provided organic acids and aided clay eluviation in the upper horizon thus leaving the coarser grains towards the top of the soil, a possible explanation for the almost ubiquitous reverse grading. Re-precipitation of eluviated material could account for the common abundance of calcite and iron nodules. Trace fossils belong to the Skolithos and Scoyenia Ichnofacies. Limestone-type or caliche layers record arid to sub-humid fluctuating conditions where evaporative loss exceeded the supply of water to the surface (Goudie, 1973). Darker grey colours, more common in higher levels of the sections, suggest more poorly drained conditions than the red or yellow horizons which are more common in lower levels of the sections (Coleman, 1966). Mottled colouring suggests a heterogeneous distribution of pH. Halos of discolouration surrounding some root casts attest to mineral precipitation due to local chemical heterogeneities. Common mineral precipitation, limited organic accumulation, and predominant red oxidation colours are all indicative of a poorly drained floodplain where water was lost through evaporation or transpiration.

4.4.3. Facies type 3.

This facies is less common than types 1 and 2 and mainly found within the lower Siwalik succession where it typically overlies thicker sandstone bodies and reaches a maximum thickness (numerous beds) of up to 5 or 6 m. It is instantly recognisable due to the stacking of fine-grained sandstone beds a few cm to 10's of cm thick which tend to coarsen-upwards (Plate 4.5.). The sharp-based thin lenticular sandstone beds display occasional erosional relief on the bases and are interbedded

with facies types 1,2 and 4. Individual beds variably display parallel lamination, trough and planar cross-lamination, ripple cross-lamination, and climbing-ripple cross-lamination (Singh, 1972) (Plate 4.6.). The top surfaces of this facies are typically bioturbated with evidence for root growth and burrowing. Typical examples of facies type 3 beds are shown along the detailed Tinau Khola section log at 70 m and 230 m (Appendix III).

4.4.3.1. Facies type 3. interpretation (crevasse splay facies)

The distinctive thinly stacked lenticular sandstone beds of facies type 3 with sedimentary structures such as climbing-ripple cross-lamination are indicative of a steady unidirectional flow with an excess sediment supply. Numerous fining- and thinning-upwards beds (maximum bed thickness of 2 m) are indicative of episodic and decelerating flows. Such features are most likely the result of crevasse splays and so these deposits are re-named the crevasse splay facies. The high-energy catastrophic nature of crevasse splays would explain the common occurrence of erosional bases to beds. Facies types 2 and 5 supersede the crevasse splay facies up-section.

4.4.4. Facies type 4.

This facies consists of less than 2 m thick well-laminated mudstones that are typically black or dark grey in colour and contain abundant organic matter (common leaf and bone fossils, coal and lignite seams). Although this facies is of limited abundance, it is commonly found at the base of sandstone bodies from facies types 1 and 5. There are rare 1-10 cm thick coal horizons. This facies often has a fissile shale-like nature in the field and yields many leaf impressions. Typical examples of facies type 4 beds are shown along the detailed Tinau Khola section log at 30 m and 893 m (Appendix III).

4.4.4.1. Facies type 4. interpretation (floodplain facies)

The finely bedded, well-laminated and unoxidised mudstones of facies type 4 indicate these deposits are associated with water-logged conditions. The abundance of leaf fossils creates a picture of a vegetated foreland basin where leaves would be collected in areas of standing water. Lakes would have formed, probably due to compaction of earlier fine-grained sediments and were subsequently infilled by deltas fed from crevasse splays from adjacent channels. Such deposits could also reflect channel abandonment (Williams & Rust, 1969) and chute or neck cut-offs forming oxbow lakes. These units are therefore referred to as the floodplain facies. DeCelles et al. (1998b) concluded that this facies probably formed in poorly drained areas that ultimately were the targets of channel avulsions. Occasionally these deposits are superseded by palaeosols, reflecting emergence and new plant colonisation.

4.4.5. Facies type 5.

Facies type 5 first appears along the Tinau Khola section at ~ 10.9 Ma, along the Surai Khola section at ~ 5 Ma, and along the Karnali section at ~ 9.1 Ma. This facies is characterised by amalgamated (up to 50 m thick sequences of stacked sandstone beds) and laterally accreted sandstone beds that coarsen and thicken upwards. The sandstone beds are typified by an asymmetrical vertical cross-section with occasional quartzite clasts (1-5 cm) occupying the lowest part, high width to depth ratios, and common internal planes at various angles to the bedding plane. There are also intercalated siltstone horizons. The thickest sandstone bodies (> 5 m) tend to be massive. In general the sandstones become increasingly multi-storey and clast-rich up-section. Mudstones are commonly intercalated with the sandstone beds and can contain molluscan fossils locally. Previous workers have found reptilian fossils in this facies along the Surai Khola section and even a molar of Sivapithecus Punjabicus along the Tinau Khola section (Munthe et al., 1983). There are interbedded facies type 4 mudstones but these are thinner (few cm) and less abundant than lower in the section. Mudstone abundance is gradually reduced up-section as the sandstones thicken and become increasingly amalgamated. Soft lignitic material is associated with both the sandstones and the mudstones. The sandstones weather yellow or orange around pockets of the lignitic material. Coal logs are particularly noticeable along the Karnali section and generally become more abundant in higher stratigraphic levels in all three sections.

Some of the coarsest sandstone beds truncate the underlying beds to a depth of several meters. These commonly end with a mudstone horizon a few cm thick. The

sandstones display hierarchies of repetitive bedforms involving mainly planar and trough cross-lamination, ripples, flutes, and soft sediment deformation. Ripple cross-laminated sandstones usually occur towards the tops of amalgamated sandstone units and are finer-grained and more micaceous than underlying sandstones. Mud layers mixing with a sandy matrix to produce flaser bedding and flame structures are a common feature in the middle to upper reaches of the larger sandstone bodies. In extreme cases beds display spectacular convolute bedding, especially common along the Surai Khola section (Plate 4.7.). These beds are also host to frequent soft sediment deformation features. The bases of sandstone-bodies often show load structures when they overlie mudstone horizons. Bedforms are clear in all three sections for this facies type but are particularly well preserved along the Karnali section.

The sandstone bodies are tabular, fine upwards, and have "wings" of sediment extending into adjacent fines over distances of up to 5 m. The "wings" are mainly fine-grained with ripple cross-lamination and are often disturbed by bioturbation along the upper surface. Where sandstone beds reveal sigmoidal internal dipping planes the palaeocurrents tend to trend roughly normal to the trend of the inclined surfaces. The internal dipping surfaces tend to be increasingly well defined towards the top of sandstone-bodies. The upper sections of these horizons are characterised by burrows and root casts. Vertical accretion of laminated sands and muds infilling channels was also recognised. Parallel laminated sandstones usually reveal a parting lineation on bedding surfaces. Epsilon cross-bedding was also recognised in the larger sandstone bodies where the dip azimuth is roughly orthogonal to palaeoflow

derived from smaller structures (Allen, 1963). Typical examples of facies type 5 beds are shown along the detailed Tinau Khola section log at 425 m, 525 m, and 620 m (Appendix III).

4.4.5.1. Facies type 5. interpretation (meandering channel facies)

The common "wings" of sediment extending into adjacent mudstone that occur in the large sandstone beds of this facies with ripple cross-lamination and bioturbation are interpreted as levee deposits (Allen, 1964; Hughes & Lewin, 1982). Also, where palaeocurrents trend roughly normal to the trend of the sigmoidal inclined surfaces within beds and trough cross-bedding is seen in the lower parts, this is indicative of point bar development (Allen, 1970; Bridge & Jarvis, 1982). The upper parts of the point bar beds often contain darker organic-rich horizons as is expected with these deposits (Bridge et al., 1995). The lack of accretion surfaces in the lower parts of some units may record a base-flow discharge that prevented fines accumulating in the deeper parts of the channel. From this evidence the sandstones of facies type 5 are interpreted to have been deposited by a meandering system and so this facies is referred to as the meandering channel facies.

The thickest (~ 5 m) sandstone bodies are massive and most likely reflect rapid deposition from suspension during floods. The up-section increase in clasts and clast size (0.5-15 cm) shows how the rivers gradually became mixed-load systems as the site of deposition approached the thrust front. The mixed-load channels are more asymmetric in outcrop with more noticeable thalweg deposits (Geldof & de Vriend, 1983). Some intercalated siltstone horizons are interpreted as the tops of mid-

channel islands. The occasional combination of ripple lamination and planar lamination may reflect rapid fluctuations in discharge. The high width to depth ratio of these sandstones and common lateral accretion elements most likely reflects heavy loads of suspended sediment and highly erodible banks. Ripple cross-laminated sandstones usually occur towards the tops of channel units and are finer-grained and more micaceous than underlying sandstones, deposited in weak currents with high rates of bed aggradation. Both convolute bedding and soft sediment deformation structures suggest rapid sedimentation.

4.4.6. Facies type 6.

Facies type 6 first appears along the Surai Khola section at ~ 3.6 Ma and in the Karnali section after 5 Ma but has been removed from the Tinau Khola section by faulting. This facies gradually supersedes facies type 5 up-section, forming the uppermost parts of the Siwalik sections, and is marked by the appearance of conglomerates at the top of the Siwalik succession. The conglomerates are dominated by abundant rounded or sub-rounded boulder clasts (with dimensions of tens of centimetres to a meter) which show a strong imbrication. These clasts are embedded in an orange-red clayey or sandy matrix and extensive clast counting (n = 1684 from 17 beds) reveals that they are dominated by quartzite lithologies (Fig. 4.6.). Most beds were divided into lower and upper horizons for clast counting but there is no significant difference either between horizons or individual beds. Beds are generally well sorted and clast-supported (orthoconglomerates) but are occasionally matrix-supported (paraconglomerates). The conglomerates also display occasional clast-free sandstone and mudstone lenses (several centimetres to 5 m

thick) (Plate 4.8.). Plant debris is generally much less abundant in these beds than lower down the successions although thin horizons of facies type 2 contain organics.

The sandstones are typically multi-storey (5-25 m thick units of several beds) and lenticular, with erosion surfaces and occasional trough cross-bedding with graded cross-sets (few cm thick). However, due to the ubiquitous coarse-grained, clast-supported nature of the conglomerates and the large average clast size, sedimentary structures are generally difficult to discern. Beds variably contain ripples and trough-cross bedding and often outcrop in long, continuous cross-bedded sand bodies with internally dipping planes. Clasts in these units increase in size up-section whilst the surfaces of sandstone bodies are often cut by numerous fine-grained channel sandstones 10's of cm in size. A typical example of facies type 6 is shown along the detailed Surai Khola section log at 3490 m (Appendix III).

4.4.6.1. Facies type 6. interpretation (braided channel facies)

Although this facies occurs solely in the upper-most parts of the three sections analysed, it has been observed at lower stratigraphic levels in other sections. The juxtaposition of lens-shaped conglomerate and sandstone channels and common lateral accretion marked by internally dipping planes with large-scale (10's of cm) cross-sets (which likely reflect channel bars; Bridge, 1993) suggests deposition from a high energy braided system (Ore, 1963; Williams & Rust, 1969; Smith, 1970). This facies is therefore re-named the braided channel facies. Large clasts suggest the channels were deposited in a proximal location, as is the norm for braided rivers. The conglomerates were therefore most likely deposited in a proximal fluvial fan

environment, characterised by the migration of a permanent or intermittent channel. This would have undergone random channel shifting through crevassing and bar development. The clast-free sandstone and mudstone lenses (several centimetres to 5 m thick) presumably reflect discharge fluctuations and settling of finer material following channel abandonment (Steel, 1974). Parkash et al. (1980) also recognised clast-free horizons in the conglomerates of NW India. Bar deposits are typically multi-storey, composed of ripples, dunes, and trough-cross bedding and often outcrop in long, continuous cross-bedded sand bodies. Bar clasts tend to show a downstream reduction in size (< 1m to a few cm), eventually resulting in a sharp contrast with the coarse clasts of the adjacent channel floor over which they have advanced. At the upstream end the bars slope gently into the adjacent channel with no change in slope or clast size. Evidence for brief bar emergence was also seen whereby finer suspended sediment has filled-in the pore spaces of the coarser bar gravel. The classic downstream bar evolution outlined by Boothroyd (1972) can be witnessed where bars with boulder-sized clasts pass progressively downstream into pebbly longitudinal braid bars and then into sandy bedforms. Bar surfaces are often cut by numerous erosional channels, most likely formed during falling stage. Bank-attached bars are a feature peculiar to the lowermost conglomerate units. These are witnessed by chute dissection of lateral-accretion units and are commonly exposed adjacent to small (< 1 m) channel sections.

4.5. Palaeoflow

A total of 2440 palaeocurrent directions were measured, making this the most comprehensive data set for each section (Table 4.2.). These were extracted from trough- and planar-cross lamination whenever witnessed and azimuths were also taken from flutes, ripples, climbing-ripples, channels, imbrication, parting lineation, grooves and tool marks. Wherever possible trough axes were measured directly but 3-D exposures of cross-beds are rare. Few measurements were taken of the Surai Khola imbricated conglomerates due to the uniformity of their flow direction, which is very well exposed. For bidirectional data flow is assumed to have been away from the mountain belt, this is supported by unidirectional data from the same beds in most cases. For some beds both limbs from trough cross-sets were measured and combined later on a stereonet to deduce the axis orientation. All measurements were restored to the palaeohorizontal.

Measurements reveal consistent transverse (south-westerly to south-easterly) flow for each section (Figs. 4.3. to 4.5.). Although present, all three sections lack evidence for sustained axial flow (towards WNW or ESE), a characteristic of modern-day Sub-Himalayan Zone drainage in Nepal. The smaller channels in the lower Siwalik sections generally record more scattered flow directions. The mean directions for each section vary only by 20 degrees, showing a consistency of palaeoflow direction between sections.

The full logs give a detailed presentation of how the mean palaeoflow directions vary from bed to bed (Appendix III). Different palaeoflow indicators tend to show the

same flow direction within individual beds, which adds reliability to the data. Flow directions often switch from bed to bed, resulting in a bimodal dataset in some cases. Although the spread of directions is quite high, palaeocurrent directions in individual upward-fining successions show dispersion within 90 degrees and are generally within 20 degrees. The high spread revealed for 150 m intervals in Figures 4.3. to 4.5. partly reflects the large number of flow indicators that were used.

Statistic	Karnali	Surai Khola	Tinau Khola
No. of measurements	498	796	1188
Mean azimuth	182	163	177
Mode azimuth	190	200	140
Standard deviation	12	41	53
Range	79	220	342

Table 4.2. Palaeoflow data statistics.

The large palaeoflow data set suggests the rivers which deposited the Siwalik Group were mostly transverse and therefore generally reflect the drainage configuration of the modern proximal to medial Gangetic Plain. This is ideal as transverse flow enhances both the utility and reliability of the detrital record because the rivers are providing sediment that has been eroded parallel to the tectonic gradient. These results accord well with the findings of other studies on Siwalik rocks across the foreland basin. Furthermore, flow directions for the Surai Khola section determined by this study broadly correlate with those of previous workers along the same section (Burbank et al., 1996; DeCelles et al., 1998b). DeCelles et al. (1998b) found a mean flow direction of 208° for the Surai Khola section as opposed to the strong south-easterly component reported here, but their data was extracted from only 124 measurements, taken on six beds, as opposed to 796 measurements along the entire

section in this study (Table 4.2.). Other authors have also found a complete lack of evidence for sustained axial flow within the Siwalik Group of Nepal (Hisatomi & Tanaka, 1994). Palaeocurrent measurements (n = 500) from the older Dumri Formation in Nepal also indicate that rivers flowed transverse to the range (DeCelles et al., 1998b). Any evidence for axial flow in the three sections studied is minor and restricted to individual beds, most likely reflecting channel readjustments rather than major switches in drainage architecture. Indeed, many Himalayan rivers likely underwent frequent avulsion (Wells & Dore, 1987). Distal facies with smaller channels (small channel facies) generally record more scattered flow directions, suggesting that the lateral and downstream development of channels was weak. In contrast, the consistency of palaeoflow in the meandering channel facies (middle to top of Siwalik sections), particularly in the Karnali section, implies these channels were stable through time. It is likely that in part the palaeoflow data appears more uniform for the Karnali than the other two sections because Karnali measurements were limited to larger channels and fewer flow indicators. Palaeoflow can appear bimodal over several beds, especially for the Tinau Khola section, which suggests rivers were migratory and changeable over short time scales. Flow directions become more transverse along the Surai Khola section above ~ 2550 m. This is not evident in the other two sections because the uppermost Siwalik units are missing from the logs. Likewise on the modern Gangetic Plain, rivers entering the foreland are initially transverse but become increasingly axial away from the thrust front. The consistency in flow direction between all three sections suggests the regional foreland basin drainage pattern did not undergo major reorganisation during Siwalik deposition.

4.6. Facies models

Up-section facies evolution, combined with the palaeoflow data, suggests the rivers that deposited the Siwalik Group in Nepal were fed from large fluvial fans similar to those dominating the modern proximal foreland basin (Fig. 4.7). Furthermore, sandstone ratio and the abundance of bar deposits increase upsection, indicating a change from a distal to a more proximal setting. This facies evolution records the encroachment of the frontal fold-thrust belt on the proximal foreland basin. A general lack of reactivation surfaces (significant erosion of previous beds with sudden facies changes) suggests the Siwalik Group sandstones were deposited by continuous sedimentation apart from frequent hiatuses, marked by palaeosol development.

The predominance of bioturbated, pigmented mudstone, the presence of calcareous nodules and trace fossils, and the association with facies types 1-4 suggest the units that comprise the lowermost Siwalik succession were deposited amongst extensive floodplain deposits that were exposed for considerable time at the surface. An abundance of mudstone indicates that flooding and long periods of standing water characterised the environment of deposition. The lower Siwalik fluvial regime was low energy where argillaceous sediment was laid down in quiet rivers and in swampy floodplain environments. This environment is also indicated by the pollen record of the Surai Khola section (Corvinus & Rimal, 2001), which points to the predominance of aquatic plants in a fresh-water habitat. Small rivers had relatively high sinuosities with a sandy bedload. They were the product of radical reduction in discharge whilst the surrounding floodplain dried-up. Heavy loads of suspended sediment during

these times and highly erodible banks would have produced high width to depth ratios. The abundance of oxidised, calcareous palaeosols also suggests the distal floodplain was relatively stable and well drained but subject to occasional flooding (Coleman, 1966). Mottling indicates episodically saturated environments. In comparison with coeval strata in Pakistan, the palaeosol facies in Nepal is considerably less oxidised and pedogenically altered (Willis & Behrensmeyer, 1994; Khan et al., 1997). Present climatic gradients would produce similar soil contrasts between the arid region of the northern Pakistan foreland and the monsoon-dominated Nepal foreland.

Meandering channels dominate the middle section of the Siwalik Group but are joined by increasingly braided types up-section. The distribution of proximal braided river facies and distal meandering and anastomosed facies in the three Siwalik sections studied is the same as that witnessed in most alluvial basins around the world, such as the alluvial fan systems of Death Valley, California. Although the evolutionary stages for each section are the same, the timing can differ moderately. Most channel shifting and bar accretion would have taken place during monsoonal floods when the rivers became transitional to mixed-load systems. As Coleman (1969) reported for the Brahmaputra River, the whole belt shifts suddenly by avulsion, generally over distances of tens of kilometres on a frequency of a few hundred years, apparently associated with major floods. It also shifts gradually due to tectonic tilting. On a shorter time scale, individual channels within divided reaches shift rapidly, generally through lateral migration. The unstable braided

channels would have been characterised by abundant sediment supply and variable discharge rates.

On the basis of sandstone body thickness, channels ranged up to a few meters deep. DeCelles et al. (1998b) concluded that the channel deposits of the western Nepal sections (including Surai Khola) are comparable to those documented by Willis (1993) in northern Pakistan, which indicate channel-belt discharges in the range of 10^3-10^4 m^3/s. Therefore at bankfull stage, the larger Siwalik channels must have had similar discharges to the present large channels that drain the thrust belt. The Tinau Khola section is noticeably sandier than the other two sections, probably reflecting further progradation of the alluvial fan system out into the foreland basin in the east. The apparently more proximal nature of the Tinau Khola section could also reflect the location of thrusting which has exposed the succession, but since all three sections have been exposed above the youngest Himalayan structure (Main Frontal Thrust) and are roughly at the same structural position along strike this explanation is unlikely.

It is likely the overall coarsening- and thickening-upwards trend reflects increasingly proximal deposition. Although DeCelles et al. (1998b) attribute the up-section facies evolution to increased rainy season dishcarge at ~ 11 Ma, the change is diachronous between sections and therefore does not seem to reflect a regional climate change which would have affected all sections at the same time. Detailed sedimentology reveals a close similarity between the rivers that deposited the Siwalik Group in Nepal and the modern Gangetic plain, eliminating the need to invoke climate change.

It is possible though that such climate change may have been responsible for the increased sedimentation rates between 11-9 Ma across the foreland basin. Dettman et al. (2001) used isotopic data from bivalve shells and mammal teeth to show an intensification of the Asian monsoon at ~ 11 Ma. However, whilst dramatic climate change at ~ 7-8 Ma (there is still much debate surrounding the timing and nature of climate change) has been purported by many workers (e.g. Harrison et al., 1993; Quade et al., 1995, 1997; Konomatsu, 1997; Tanaka, 1997), there is no obvious response in the Siwalik record of the three sections studied. Similarly, Burbank et al. (1996) note that the inferred monsoon intensification at ~ 7-8 Ma does not appear to have led to an increased detrital sediment flux to the foreland. Burbank et al. (1993) suggested decreasing erosion rates since ~ 8 Ma immediately following monsoon strengthening reflects slope stabilisation by increased vegetation and retreat of mountain glaciers. However, measured erosion rates in the modern Himalaya are faster in regions where the monsoon is heavier (Galy & France-Lanord, 2001). In addition, during the last glacial stage erosion rates in the Ganges delta were higher when the monsoon was stronger (Goodbred & Kuehl, 1999). The relationship between monsoon strength and orogenic erosion is therefore poorly understood.

4.7. Provenance

The interpretation of detrital data relies heavily on the ability to reconstruct the extent of the catchment that was the source-region for the depositional site. Having some control on the source areas for the sediment in question is of crucial importance to the detrital method otherwise tectonic inferences cannot be assigned to a particular area. However, this is complicated by the fact that the Himalayas of western Nepal have experienced a minimum of ~ 556-623 km of post-collision shortening (DeCelles et al., 1998b). Tectonic activity to this degree is likely to have caused major drainage reorganisations during the evolution of the orogen. Given the complex geometry and largely unknown temporal evolution of Himalayan drainages, definition of pre-Pleistocene catchments remains fraught with uncertainties (Seeber & Gornitz, 1983).

The Indus-Gangese drainage divide had probably developed prior to the start of Siwalik deposition (pre-16 Ma) due to diversion around the Aravalli Range of India as it approached the fold-thrust belt (DeCelles et al., 1998a). Combining this with palaeoflow data, we can confine potential provenance areas for the three sections analysed to within the Ganges drainage basin. This means the Siwalik sediment of central-western Nepal could have been derived from a region incorporating NW India to Central Nepal. The basic palaeogeographic setting of the system can be considered in terms of the progressive distal to proximal trend of foreland basin sediments relative to their thrust front. Cross-section balancing, fluvial terraces, and GPS data show that the mean Quaternary shortening rate in the Sub-Himalayan belt is ~ 21 mm/yr (Champel et al., 2002). Assuming a Main Frontal Thrust shortening

rate of 21 mm/yr during Siwalik deposition (DeCelles et al., 1998a; Lavé & Avouac, 2000; Mugnier et al., 2004), the base of our three sections (at 12-16 Ma) would have been deposited at a location between ~ 250-330 km from the thrust front at that time. A point this distance from the modern thrust-front in central Nepal is likely to be fed by a river which is sourced in NW India. Even assuming a nearly constant N-S palaeocurrent direction for the Karnali section, if we take into account the mean trend of the Himalayan belt in the area (N120°) and a basin of 300 km between the studied section and the Himalayan front at 16 Ma, a minimum eastward migration of the provenance area of 300km.tan 30° (i.e. 150 km) would be expected. Because the rivers of the Ganges system generally flow from the NW to the SE it is likely that sediment more proximal to the mountain belt will be sourced from an area further to the east in the hinterland. Easterly migration of the provenance area for increasingly proximal sediment is a likely scenario in the modern foreland basin and may also be the case for Late Miocene-Pliocene time (Fig. 4.8.). Palaeoflow indicators suggest most sediment had a northern (Nepal) source area that varied little during deposition.

4.8. Sedimentation rates

Using the detailed logging and magnetostratigraphic ages, calculated mean sedimentation rates are 0.3, 0.37, and 0.37 mm/yr for the Tinau Khola, Surai Khola, and Karnali sections respectively. This is in close agreement with Gautam & Roesler (1999) who calculate average sedimentation rates of 0.35 and 0.32 mm/yr for the Surai Khola and Tinau Khola sections respectively, based on the magnetic polarity time scale of Cande & Kent (1995). Given the coarse-grained nature of the upper parts of the sections and the absence of thick intervals of fine-grained strata, compacted sediment accumulation rates are likely to underestimate true accumulation rates only moderately.

The spreading of magnetostratigraphic ages reveals an increase in sedimentation rates of ~ 400 % for the Tinau Khola section and > 200 % for the Karnali section between ~ 11-9 Ma (Fig. 4.9.). This coincides with an increase in maximum sandstone thickness and the ratio of sandstone to mudstone. Such a change is not so obvious along the Surai Khola section (although bed thickness increases during this period), possibly because the 11-9 Ma interval is recorded by a higher percentage of floodpain fines along this section. Instead, there is a marked increase in sedimentation rate for the Surai Khola at 6 Ma. As noted in section 4.2.3., an ~ 11-9 Ma increase in sediment accumulation rate has been witnessed along the entire length of the Siwalik belt (Burbank et al., 1996; DeCelles et al., 1998b; Gautam & Rosler, 1999; Ojha et al., 2000) and in deep-sea sediments of the Indian Ocean (Hovan & Rea, 1992). There is also an increase in the ratio of channel sandstones to floodplain mudstones throughout this period. An increase in the abundance of

of at least 20-25 km of rock from the Greater Himalaya (Searle et al., 1993). Vance et al. (2003) suggest similar erosion rates have been maintained for at least the last few thousand years and that much Himalayan exhumation is now balanced by erosion.

Using these estimates for Himalayan erosion rates it seems likely that the Siwalik sections analysed by this study (average sedimentation rates of 0.3-0.4 mm/yr) record less than 40 % of the total detritus that was eroded from the growing hinterland. The spreading of sediment over the large area of the foreland basin compared to the catchment size can account for much of this whilst some detritus would have bypassed the foreland basin altogether to be debouched into the Indian Ocean. From a detrital study of Dharamsala and Siwalik molasse in NW India, White et al. (2002) suggest erosion rates of ~ 1.5 mm/yr were maintained for the last 20 Myr and even variable rates of up to 7 mm/year for a duration of 10 Myr whilst the Greater Himalaya were unroofing. This rate then decreased to $\leq$ 0.5 mm/yr following Main Central Thrust-South Tibetan Detachment cessation, resembling sedimentation rates along-strike in Nepal determined by this study for the Siwalik Group.

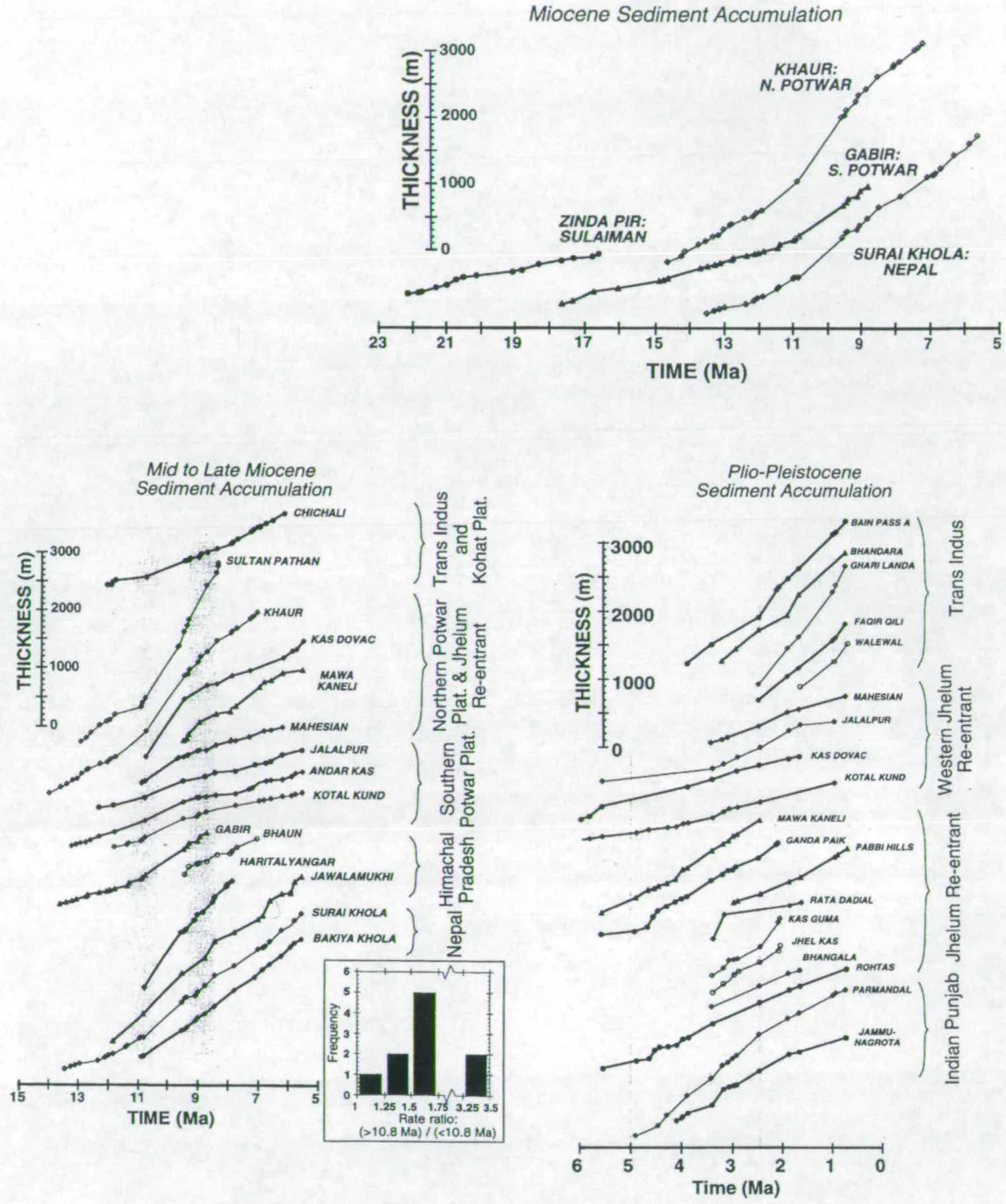


Figure 4.1. Sediment accumulation curves derived from magnetostratigraphy data for sections through molasse basins throughout the Himalayas, from Burbank et al. (1996). The slope of the curve is proportional to accumulation rate.

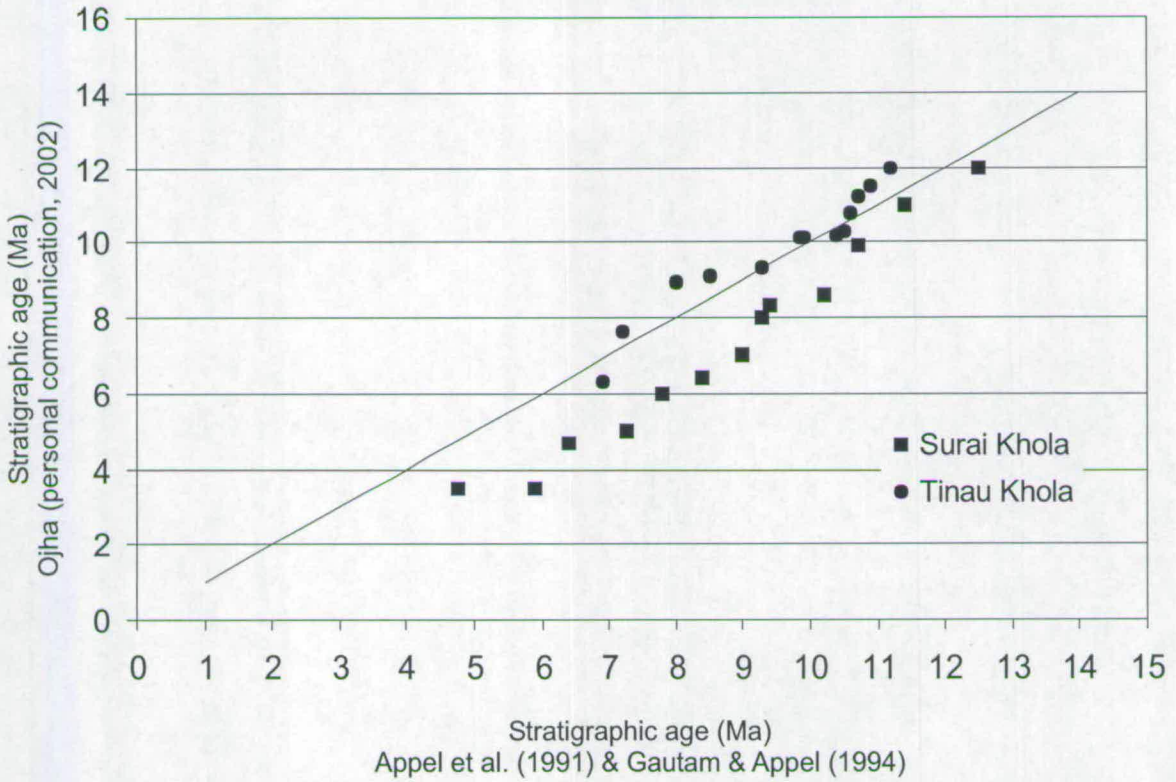


Figure 4.2. Comparison of palaeomagnetic ages for Ojha et al. (personal communication, 2002) versus Appel et al. (1991) / Gautam & Appel (1994) for the Tinau Khola and Surai Khola sections. Ages are based on the geomagnetic timescale of Cande & Kent (1995), the Appel et al. (1991) and Gautam & Appel (1994) ages were taken from Gautam & Roesler (1999). Thin line is the 1:1 line.

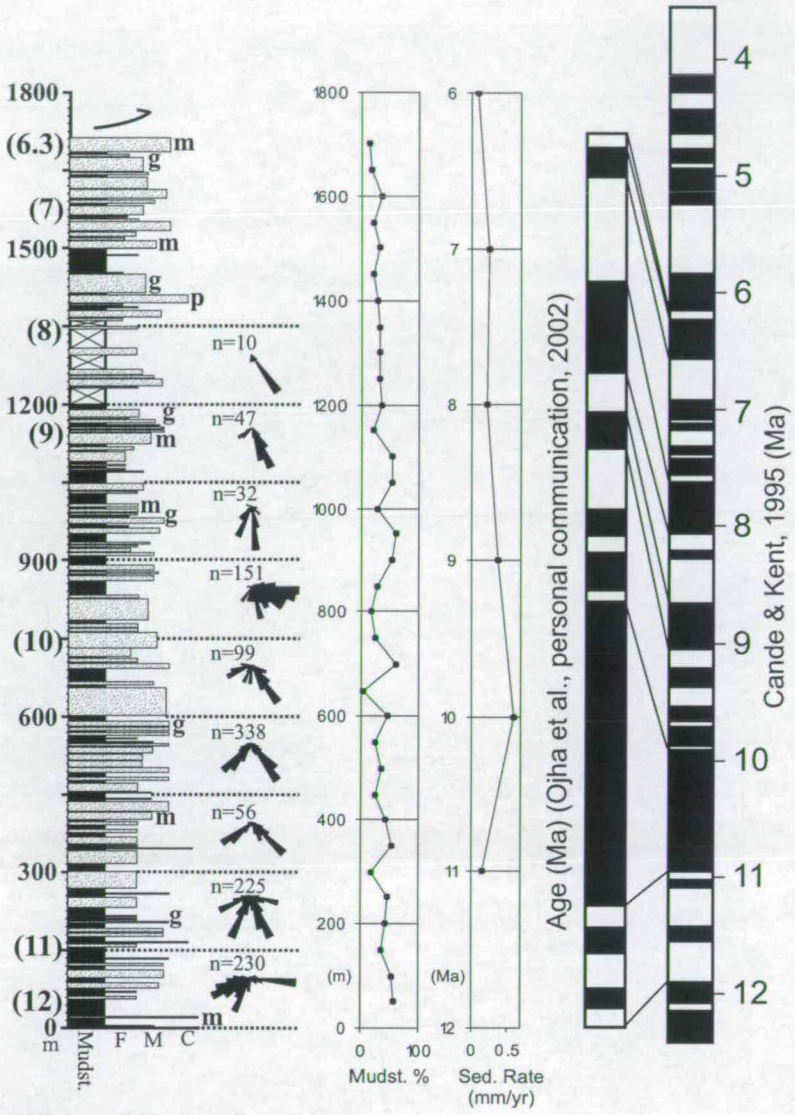


Figure 4.3. Tinau Khola section simplified log. Numbers in brackets indicate stratigraphic age based on the magnetostratigraphy log on the right. Palaeoflow rosettes display data for 150 m intervals. m - location of samples for ^{40}Ar-^{39}Ar dating of white mica, g - location of samples for whole rock geochemistry, p - location of samples for petrography. Also shown are the variation in mudstone percentage and sedimentation rate up-section. The age in Ma of the sedimentation rate plot is on a different scale to that of the log.

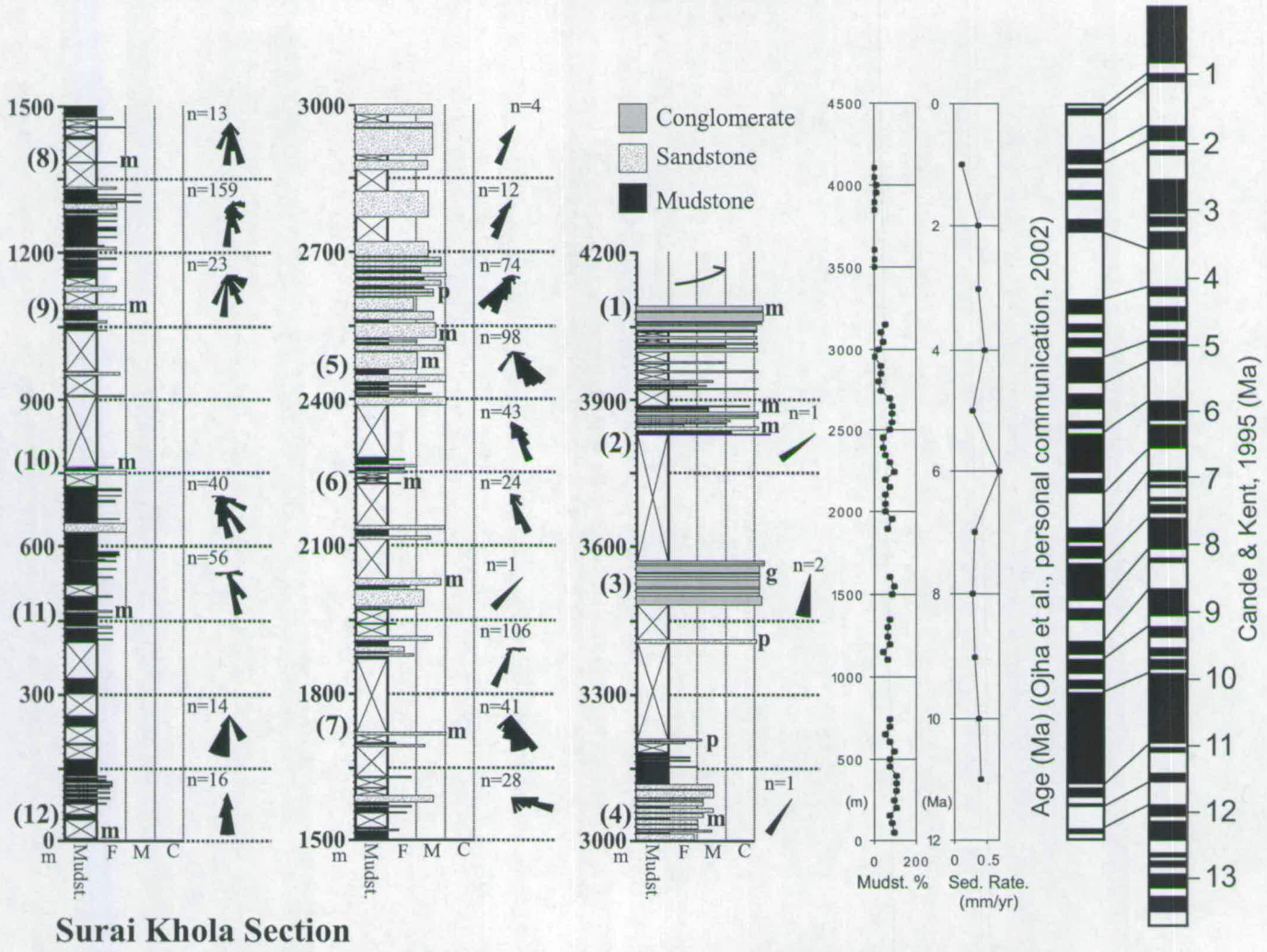
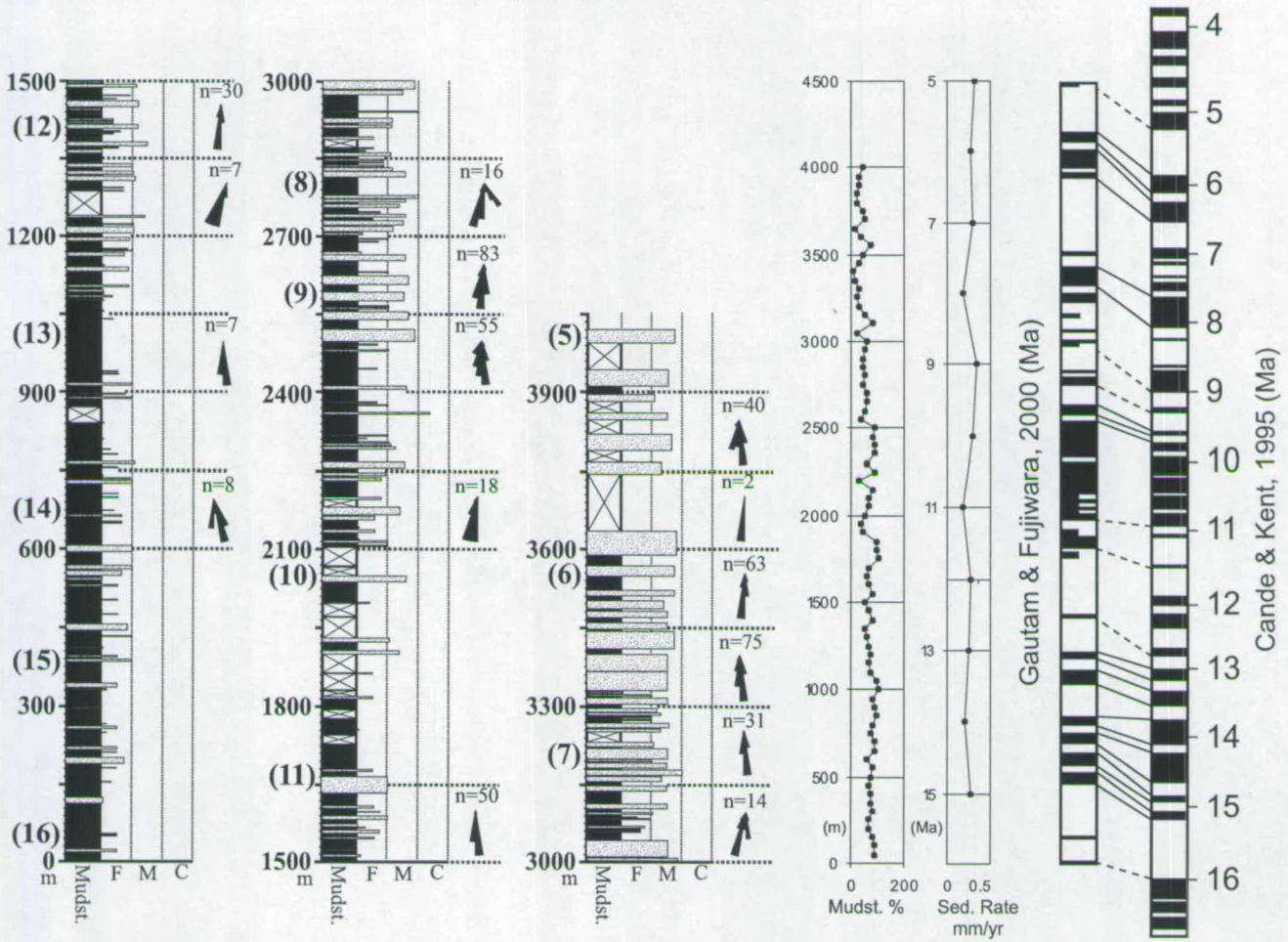


Figure 4.4. Surai Khola section simplified log. Description as for figure 4.3. Gaps in the mudstone percentage plot relate to stretches of no exposure. In some cases these areas were logged if the lithology of the missing units could be identified. The magnetostratigraphy log shows how the sediment ages were derived but is not at the same scale as the log as it is divided into three parts.



Karnali Section

Figure 4.5. Karnali section simplified log. Description as for figures 4.3. & 4.4.

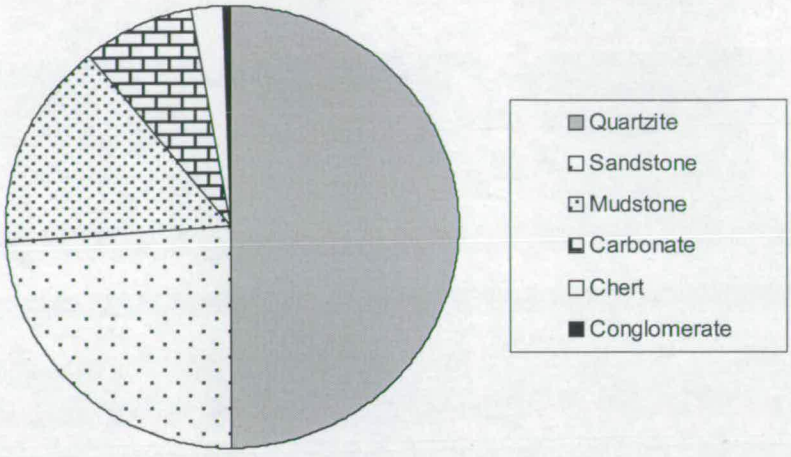


Figure 4.6. Clast count results for the Surai Khola section conglomerates. A total of 1684 clasts were counted from 17 beds.

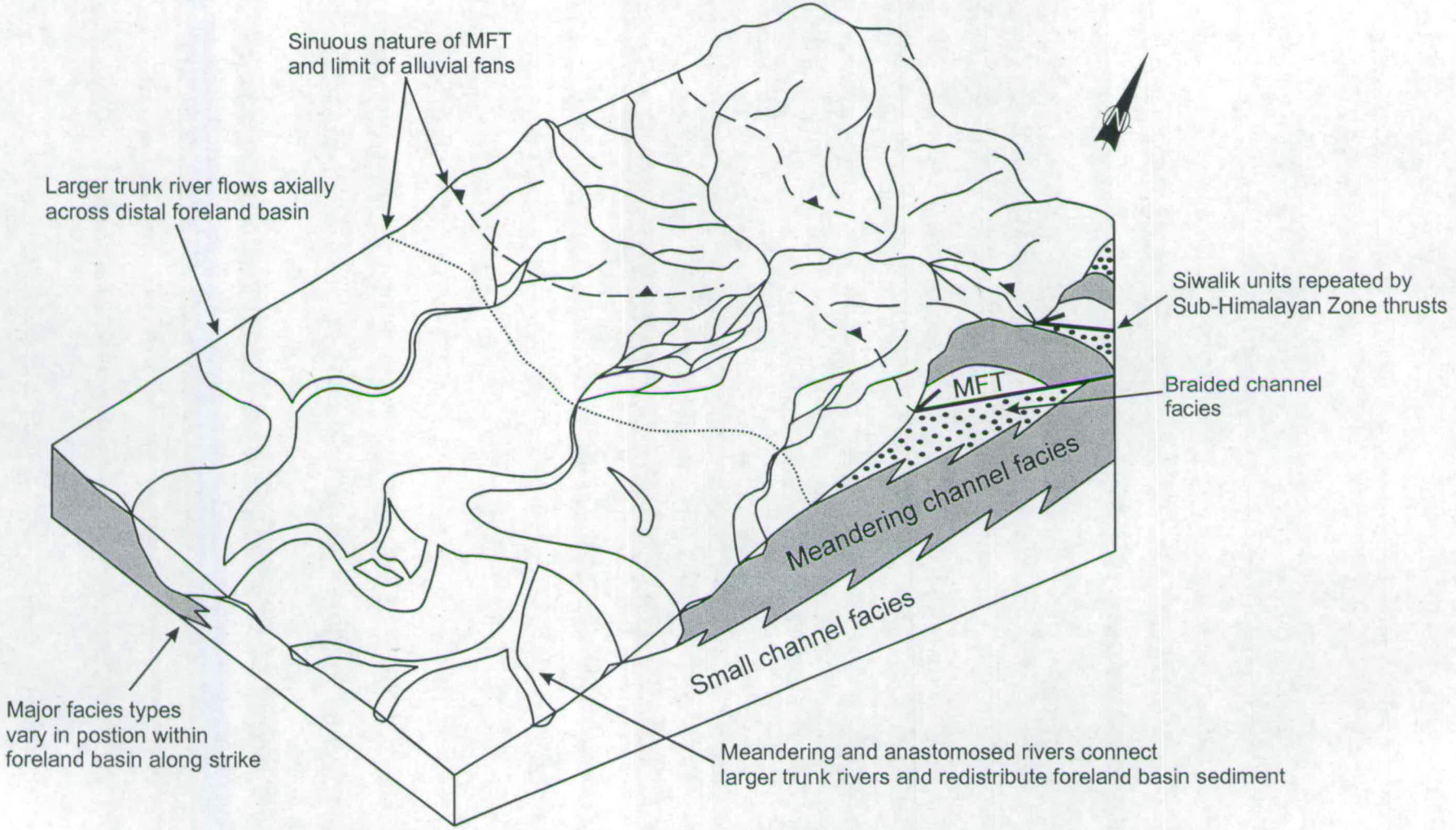


Figure 4.7. Schematic illustration of the interpreted depositional environment of the Siwalik Group in Nepal. MFT - Main Frontal Thrust.

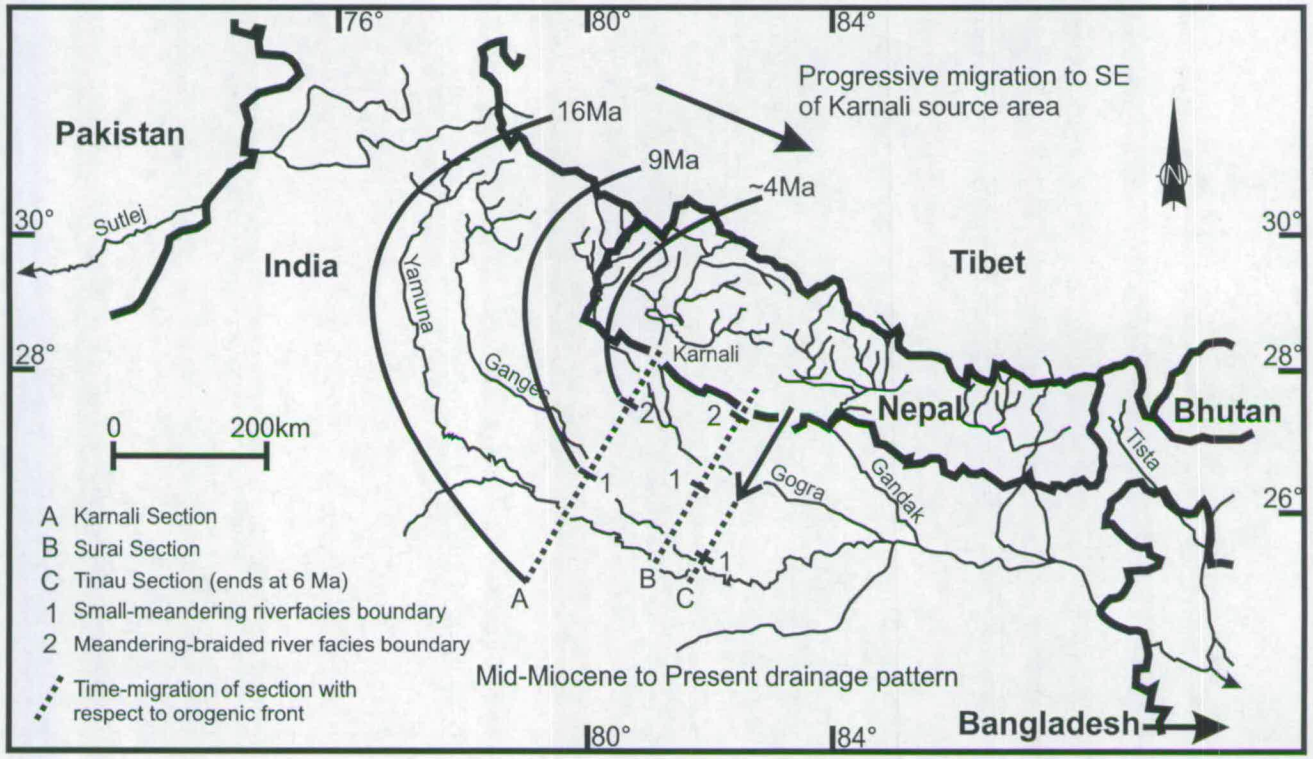


Figure 4.8. Simplified map to show probable easterly migration of the Siwalik source area with time. The Karnali section is used to show how if the zone of deposition approaches the thrust front it will be sourced by rivers with more easterly catchments, 16 Ma represents the base of the section, 9 Ma the small to meandering river facies switch, and 4 Ma the start of conglomerate deposition close to the thrust front.

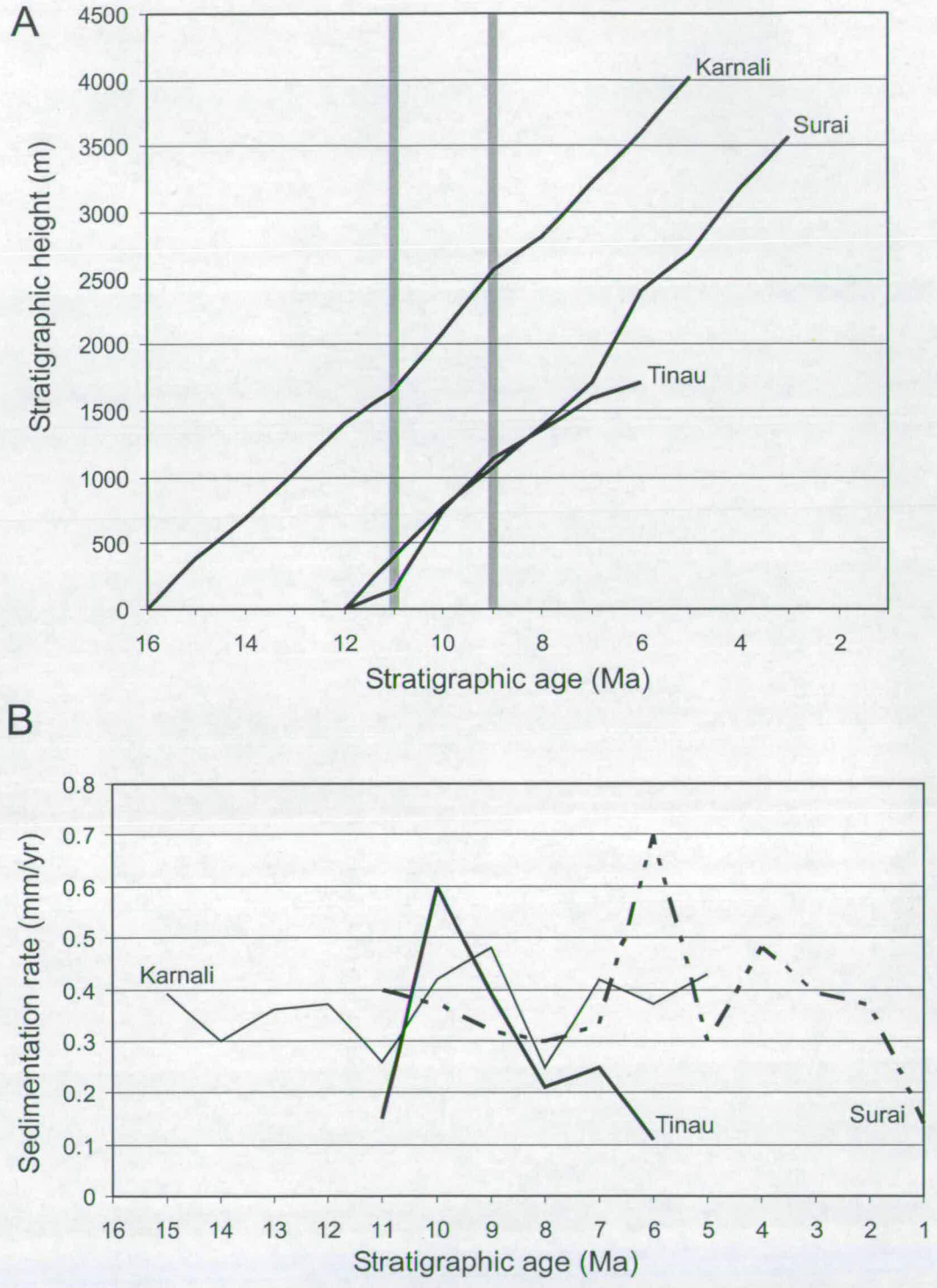


Figure 4.9. A - plot of stratigraphic height versus stratigraphic age for the three Siwalik sections, shaded bands highlight the increase in sediment accumulation between 11 Ma and 9 Ma. **B** - plot of sedimentation rate versus stratigraphic age for the same sections.

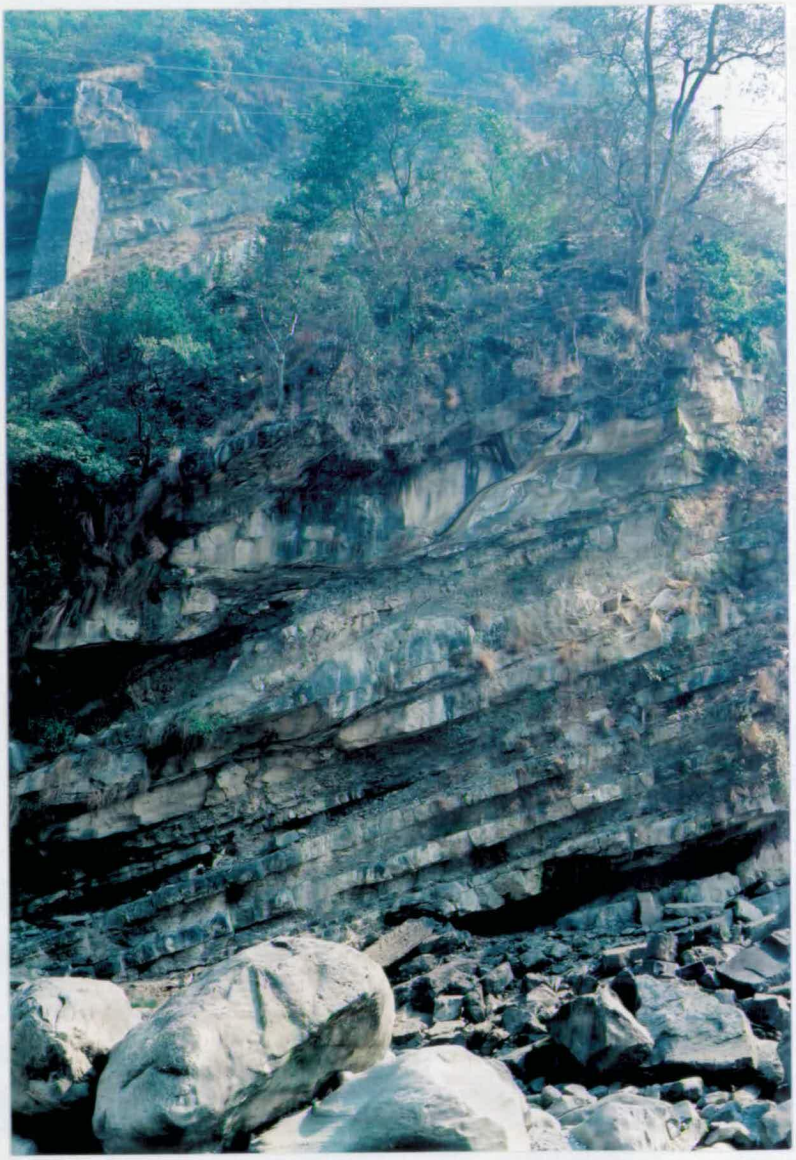


Plate 4.1. Sectional view of the lower Siwalik Group as exposed along the Tinau Khola section, looking roughly east. The thicker sandstone body at the top of the cliff face represents the first evidence for facies type 5 in this section.



Plate 4.2. View of the lower Siwalik Group as exposed along the Surai Khola section, looking roughly NE. The thicker sandstone body on the left which is marked LMB (lower-middle boundary from old threefold Siwalik division) in red paint is the first evidence for facies type 5 in this section.



Plate 4.3. Sectional view looking east along the Tinau Khola section. A lenticular small channel facies sandstone bed cuts into a palaeosol bed beneath, hammer for scale.

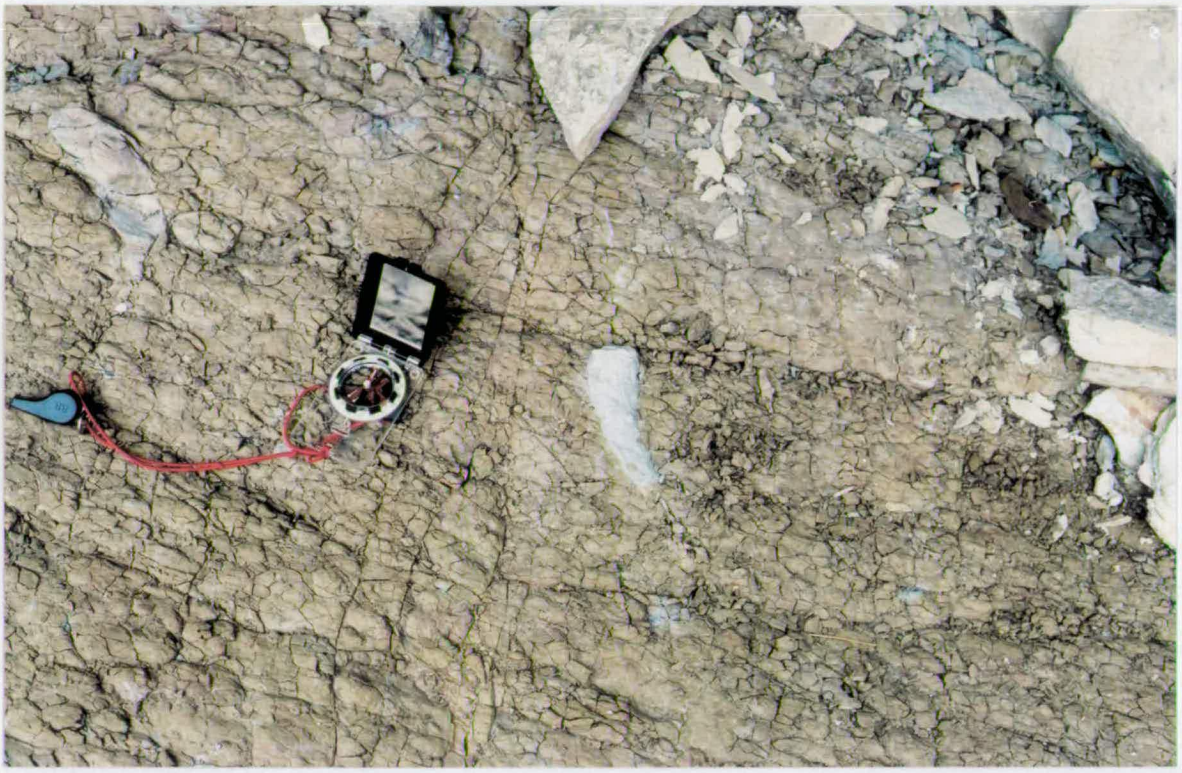


Plate 4.4. Plan view (N to the top) of a typical palaeosol facies bed along the Tinau Khola section showing fractured and oxidised facade and pale blue root cast.



Plate 4.5. Sectional view looking NE of a crevasse splay facies sequence along the Tinau Khola section, hammer for scale. The thin beds coarsen and thicken upwards and are superseded by small channel facies and palaeosol facies beds above.



Plate 4.6. Sectional view looking roughly west along the Tinau Khola section, showing evidence for climbing-ripple cross-lamination within a crevasse splay facies sequence.



Plate 4.7. Sectional view looking roughly east at the base of a meandering channel facies sandstone bed along the Surai Khola section, showing dramatic convolute bedding and water escape structures.

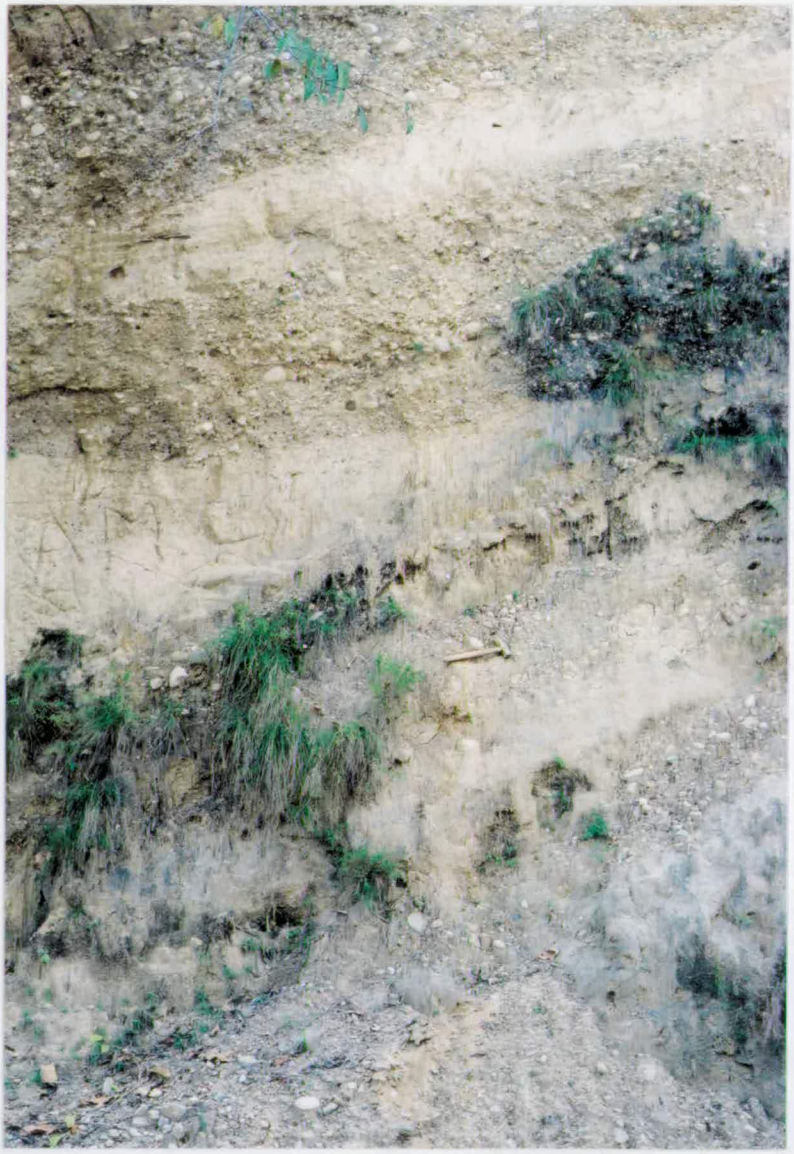


Plate 4.8. Sectional view looking roughly west along the Surai Khola section, showing a typical braided channel facies outcrop with lenses of conglomerate and sandstone, hammer for scale.

5. Petrography and heavy minerals

5.1. Introduction

All orogens exhibit a regional lithological variability. This is particularly evident in the Himalayas where six lithotectonic zones have been juxtaposed by major NW-SE trending structures. Compositional heterogeneities can be exploited for the purpose of determining the provenance of a foreland basin succession by employing petrography and heavy mineral analysis. The greater the degree of hinterland variability, the greater the likelihood of accurate provenance determination. Additionally, if sediment composition is indeed indicative of source area, the up-section change in mollasse composition provides information about the exhumation and erosion of different orogenic source areas through time. This chapter details the results of petrography and heavy mineral analysis for the three Siwalik sections under investigation.

5.2. Limitations

The common inability of sandstone petrography to definitively pinpoint provenance has been highlighted from the earliest studies (e.g. Rapson, 1965). Petrography is less effective if the detrital components under investigation are too cosmopolitan to be of more than general use in tectonic interpretations. Indeed, hinterland erosion has a tendency to produce homogenous quartz-rich detritus and differential weathering can further complicate petrographic data by artificially enhancing the abundance of more durable minerals. There is also the possibility that dense high-grade minerals may not survive long transport distances to the foreland basin.

5.3. Previous work

The value of petrography as a detrital technique began to be recognised when Dickinson & Valloni (1980) related changes in sandstone mineralogy to variations in tectonic setting. Dickinson (1985) then demonstrated that quantitative sandstone detrital modes based on point counts of thin sections could be used to determine provenance. He formulated a number of "fields" which characterise tectonic setting depending on detrital mineral modes. These pioneering studies opened the doors to an area of research that has become pivotal to the success of the detrital technique.

A large amount of petrographic and heavy mineral studies have been conducted on Himalayan molasse deposits. These have driven progress in areas of research that include the timing of collision, to the specifics of hinterland tectonic and drainage evolution throughout development of the orogen.

5.3.1. Timing of India-Eurasia collision

Evidence for the timing of Himalayan collision comes from two main sources. The first is based on reconstructions of past positions of the Indian continent by its relation to the opening history of the Indian Ocean, recorded by magnetic reversal patterns on the sea floor (e.g. Klootwijk et al., 1992). These records show that a wobble in India's motion was followed at 45 Ma by a marked deceleration (11 cm/yr to 4.5 cm/yr) thought to represent collision. The second is based on the stratigraphic record preserved within the orogen, in particular the transition from marine to continental deposition (e.g. Rowley, 1996). Whilst the examples below from the foreland basin serve to illustrate the utility of petrography and heavy mineral data in

assessing the timing of Himalayan collision, other techniques such as geochemistry and isotopic dating have contributed to the debate.

The encroachment of India on Eurasia and the closure of the Tethys Ocean was marked by the sudden arrival of volcanic and ophiolitic detritus on the passive continental margin of the Indian plate (Garzanti et al., 1996). Petrography constrains the timing of collision by providing evidence of the first time Asian detritus is found on the Indian margin and the first time there is evidence of mixed Indian and Asian detritus. Petrographic evidence throughout the Himalayas shows that the onset of collision is marked by a drastic composition change in latest Palaeocene time. South of the suture zone, shallow-marine sediments were overlain by deltaic red beds (e.g. Chulung La Formation in Zanskar) on the back of initial thrust sheets and within subsiding foreland basins such as the Murree Supergroup or the Palaeogene Khojak Formation of the Katawaz Basin, both in northern Pakistan (Garzanti et al., 1987; Bossart & Ottiger, 1989; Gaetani & Garzanti, 1991; Critelli & Garzanti, 1994; Beck et al., 1995). Similar to the Murrees, the lithic grains and heavy mineral suites of the Dharamsala sediments in NW India indicate northern derivation from low- and medium-grade metamorphic rocks and locally from high-grade rocks in the pre-Miocene Himalaya (Raiverman et al., 1983; Najman et al., 1993; Critelli & Garzanti, 1994). These new deposits coincided with a dramatic change in mollasse compositions from quartzarenite (e.g. Lower Patala Formation) to quartzolithic (e.g. Upper Patala and Balakot Formations) or feldspatholithic (e.g. Chulung La Formation) that took place on the passive continental margin of India. Whereas quartzose sandstones were derived from the Indian continental block to the south,

lithic sandstones indicate provenance from the Kohistan-Ladakh suture zone in the north (Garzanti et al., 1996). The coeval shallow-marine Kong Formation (Middle Early Eocene; Baud et al., 1985) within the Tibetan Himalayan Zone contains volcaniclastic silt. This unit is directly overlain by the Spontang ophiolitic allochthon (Garzanti et al., 1996). Petrography shows that at the same time volcanic, ophiolitic, and metasedimentary detritus was rapidly accumulated in subsiding piggy-back and foreland basins (Garzanti et al., 1996).

Major compositional differences between the earliest clastic units of the Himalayas have led to a debate surrounding the possibility of a diachronous collision (Uddin & Lundberg, 1998; Najman & Garzanti, 2000; DeCelles et al., 1994). Uddin & Lundberg (1998) analysed the petrography of Bengal basin sediments in Bangladesh. They document for the first time the contrasts in orogenic history recorded in the Bengal basin and western Himalayan foreland basins. Sands in the Bengal basin are generally more quartzose and less lithic than those from the western Himalayan foreland basins, and pre-Miocene strata in the Bengal system show little or no evidence of orogenic activity. In contrast, Najman & Garzanti (2000) found that Oligocene-Miocene sediments of the Dagshai and Kasauli Formations in NW India consist mainly of metapelitic detritus whereby the Dagshai records the first appearance of Himalayan metamorphic detritus during Late Oligocene and metamorphic grade increased from then on. Both authors conclude this west to east petrographic variation is at least in part due to a west to east progression of the Himalayan collision.

5.3.2. Himalayan evolution

Himalayan detritus shows a general evolution of petrography whereby increasingly younger deposits trend towards the "ideal arkose" composition, which reflects deepening of erosion into the growing orogen (Garzanti et al., 1996) (Fig. 5.1.). Petrography studies of Murree sandstones from the Kashmir-Hazara Syntaxis indicate primary derivation from low-grade metasedimentary rocks with minor volcanic, sedimentary, and ophiolitic sources (Critelli & Garzanti, 1994). An absence of high-grade metamorphic material means the Murree could not have been derived from the metamorphosed Greater Himalaya and therefore uplift in the emergent Himalaya was insufficient to expose high-grade rocks to erosion. This is surprising considering Eocene ages for peak metamorphism in many areas of the Himalayas and given the Eocene ages for cooling below ~ 200°C from fission-track ages (Zeitler, 1985). During deposition of the Murree Supergroup from early Oligocene (Najman et al., 2001) to early Miocene time the proportion of detrital feldspars and metamorphic detritus increased only slightly, suggesting limited dissection of the proto-Himalayan belt and erosion to deeper metamorphic levels during earliest Miocene time. At the same time, Chulung La deltaic red beds were deposited in a thrust-top basin south of the suture zone and contain abundant volcanic detritus suggesting arc-trench provenance (Critelli & Garzanti, 1994).

The petrography of the Latest Palaeocene-Middle Eocene Subathu Formation of NW India is dominated by suture zone material (Najman & Garzanti, 2000). Suture zone derivation was drastically reduced by the time the Daghshai Formation was deposited in NW India (post-Middle Oligocene time). Along with the first appearance of

Himalayan detritus, this indicates the embryonic thrust belt had attained significant elevation (Najman & Garzanti, 2000). Indeed, all foreland basin sediments of Lower Oligocene age or younger (after Subathu Formation deposition) were dominated by Greater Himalayan Zone sources (Najman et al., 2000). This includes the Dumri Formation in Nepal, which was derived from Greater and Tibetan Himalayan source areas (DeCelles et al., 1998b). A quartz-phyllite-plagioclase association is characteristic of the Dumri Formation and heavy minerals include Hornblende + Zircon + Epidote + Chlorite + Tourmaline which is similar to equivalent lithologies in NW India (Najman et al., 1993; DeCelles et al., 1998a). According to DeCelles et al. (1998a), following Dumri deposition the deformation front of the fold-thrust belt migrated southward into the Crystalline Thrust Sheets of the Lesser Himalaya and eventually into Lesser Himalayan metasedimentary rocks during Siwalik deposition.

The Kasauli Formation unconformably overlies the Dagshai Formation in NW India and contains garnet compositions that reflect derivation from medium-grade to amphibolite facies metamorphic rocks (Najman & Garzanti, 2000). The influx of higher-grade metamorphic lithic grains during Early Neogene time in the Kasauli Formation coincides with bedrock estimates for rapid Main Central Thrust-South Tibetan Detachment displacement and supports suggestions that Greater Himalayan Zone rocks were rapidly unroofing at this time, producing a sharp increase in denudation rates (Harrison et al., 1992, 1993). Following Kasauli deposition the lower part of the Siwalik Group began to be deposited from northern Pakistan to Nepal (Tandon, 1976; Parkash et al., 1980; Johnson et al., 1985; Burbank & Beck, 1991).

White et al. (2002) worked on the Oligocene-Early Miocene Dharamsala or Murree Group in Himachal Pradesh (outcrops NW along-strike of the Dagshai and Kasauli Formations) and their study includes the lower most Siwalik Group, spanning 21-12.5 Ma. They found that the Lower Dharamsala sandstones contain abundant low- to medium-grade metasedimentary clasts and garnet along with micas and other heavy minerals. White et al. (2002) conclude that the source of the Lower Dharamsala comprised low- to medium-grade mica-schists with a minor sedimentary and volcanic source. By contrast the Upper Dharamsala was found to be dominated by sedimentary and low-grade material with a significant dolostone component, whilst the amount of micas decreased from the Lower Dharamsala. They found that the base of the Siwalik Group contains more quartz than the Dharamsala but at the expense of metamorphic lithics and carbonate rock fragments and that heavy minerals indicate a medium-grade metamorphic source for the Siwalik Group. White et al. (2002) interpret the Lower Dharamsala sediments to have been derived predominantly from the metamorphosed Greater Himalaya whereas the Upper Dharamsala to have been derived from the Chamba Nappe (Haimantas, protolith of the Greater Himalaya) or an equivalent which is a low-grade tectonostratigraphic cover of the Greater Himalaya. The authors suggest any Lesser Himalayan input was minor for all parts of the succession studied. They interpret the provenance change between Lower and Upper Dharamsala deposition at 17 Ma to reflect a reorganisation of the orogenic wedge with cessation of South Tibetan Detachment extension and propagation of thrusting south from the Main Central Thrust. The petrography of this study does not suggest significant down-cutting into deeper levels of the Greater Himalaya through time. In fact, the difference between the

metamorphic grade White et al. (2002) record in the Dharamsala Group (maximum staurolite- to garnet-grade) and the present day kyanite- and sillimanite-grade of much of the exposed Greater Himalaya in NW India is consistent with the limited (10-15 km) exhumation of the Greater Himalaya between 17 Ma and the present indicated by pressure and temperature constraints from hinterland bedrock (e.g. Searle et al., 1999).

Najman et al. (2003) worked on the 18-14 Ma Kamlial Formation in the Potwar Plateau, Pakistan. These quartz-poor lithofeldspathic sandstones lie above the Murree Formation and from petrography the authors infer a dominant magmatic arc provenance, completely unlike the more common recycled orogen foreland basin deposits (Fig. 5.2.). There was also a subordinate contribution from a rapidly exhuming source, most likely the Nanga Parbat Haramosh Massif. The switch to a magmatic arc source rather than the more southerly thrust stack source of the Murree Formation is interpreted to reflect a diversion of the palaeo-Indus River to its present position, which crosses the Kohistan arc and Himalayas to debouch into the foreland.

Many studies have addressed the framework composition of Siwalik sandstones and the accessory mineral assemblages (e.g. Krynine, 1937; Chaudhri, 1971; 1972; Tandon, 1976; Parkash et al., 1980; White et al., 2002). A pronounced enrichment of medium- to high-grade metamorphic detritus, feldspar, and accessory minerals in the Siwalik Group records deeper erosion into the Greater Himalaya due to exhumation above the Main Central Thrust (Garzanti et al., 1996) (Fig. 5.3.). The first Siwalik units are marked by the appearance of staurolite and epidote, which normally persist

throughout the sequence. During Siwalik deposition the abundance of detrital feldspar increased and an increasingly higher-grade suite of heavy minerals was derived from continued Greater Himalayan unroofing. Beginning ~ 12-11 Ma, Siwalik sandstones record a sharp increase in coarse K-feldspar (DeCelles et al., 1998b). DeCelles et al. (2001) propose that this was derived from the Dadeldhura granite (part of the Dadeldhura Crystalline Thrust Sheet). If correct this places an age constraint on the emplacement of the Crystalline Thrust Sheets and development of the Lesser Himalayan Duplex. A concomitant influx of metacarbonate lithic grains and Palaeoproterozoic zircons (> 1.7 Ga) were most likely derived from the Lesser Himalaya (DeCelles et al., 1998a). Critelli & Ingersoll (1994) analysed Siwalik sandstone petrography from the Potwar Plateau, NW Pakistan. These are composed of low- to medium-grade metamorphic and sedimentary detritus with subordinate ophiolitic and volcanic detritus of probable suture zone and Greater Himalayan Zone origin. They interpret the siliciclastic grains to be derived from the Tibetan and Lesser Himalayan Zones. Critelli & Ingersoll (1994) found the Nepal Siwalik Group (Surai Khola and Bakiya Khola sections) to be more quartzose than the Pakistan equivalents which are more feldspathic, and that the hornblende content increases up-section. In fact at 11 Ma in Pakistan the heavy mineral assemblage changed abruptly whereby the abundance of blue-green hornblende increased threefold (Cerveny et al., 1989; Mulder, 1991). Apart from a greater abundance of accessory minerals, Critelli & Ingersoll (1994) found that modern sands from various rivers in Nepal are similar in composition to the Siwalik sections. Since Pleistocene times when the Siwalik Group began accreting in the Sub-Himalayan Zone, greater

volumes of polycyclic grains have been carried to the foreland basin (Parkash et al., 1980).

5.4. Methodology

Three hundred points by the Gazzi-Dickinson point-counting method (Ingersoll et al., 1984; Zuffa, 1985), and 200-250 transparent heavy minerals by the "ribbon-counting" or "Flett" methods (Manage & Maurer, 1992), were counted on samples from each section at 1 Myr intervals. Modern sand samples from the Tinau, Surai, and Karnali rivers were also analysed to provide an actualistic reference. Heavy minerals were concentrated with sodium metatungstate (density 2.9 g/cm^3), using the 63 to 250-micron size fraction treated with oxalic and acetic acid to eliminate iron oxides, and carbonates respectively (Parfenoff et al., 1970). Metamorphic lithic grains were classified according to both composition and metamorphic grade, mainly inferred from degree of recrystallisation of mica flakes (Garzanti & Vezzoli, 2003). Confidence intervals for the mean were calculated according to the Weltje (2002) methods, devised specifically for unit-sum constrained data (Aitchison, 1986). Grain-size control was minimised by using only the fine sand fraction for all studied samples. All petrographic work was conducted at the Milano-Bicocca University, Italy.

5.5. Results

All petrographic and heavy mineral raw data and key are given in the petrography data files on the CD at the back of the thesis. Selected petrographic modes and heavy mineral trends are displayed as ternary plots in Figure 5.4. and in relation to stratigraphic age in Figure 5.5. Sandstone samples from all three sections are quartzolithic and plot within the "recycled orogen" field of Dickinson (1985) (Fig. 5.4.). Average composition for the three sections is relatively monotonous (Tinau Khola section: Q 58 F 6 Lv 1 Ls 18 Lm 26; Surai Khola section: Q 51 F 6 Lv 0 Ls 42 Lm 25; Karnali section: Q 59 F 8 Lv 1 Ls 30 Lm 21). There are no significant differences in bulk petrography between the three sections, a similarity which extends to the modern sediment (Tinau River: Q 57 F 5 Lv 1 Ls 43 Lm 21; Surai River: Q 63 F 3 Lv 1 Ls 66 Lm 11; Karnali River: Q 64 F 13 Lv 1 Ls 46 Lm 13) and coeval Siwalik sections of Nepal along strike (e.g. DeCelles et al., 1998a). The sandstones are characterised by large amounts of sedimentary to low-grade metasedimentary lithic grains and minor medium- and high-grade metamorphic material. Lithic grains include common sedimentary (dolostone, limestone, shale, sandstone) and mainly very low- to medium-rank metasedimentary types. The Karnali section has a lower metamorphic grade on average compared to the Tinau Khola and Surai Khola sections (Tinau Khola metamorphic index (MI): 210-252, Surai Khola MI: 166-212, Karnali MI: 153-186) (Fig. 5.5.). There are high quartz/feldspar ratios and low plagioclase/feldspar ratios throughout the succession. Quartz grains are dominantly monocrystalline with subordinate polycrystalline types. In the Karnali section the proportion of dolostone increases at 12 Ma. Detrital micas are minor (usually < 10 % of detrital grains) but are most abundant in the Tinau

Khola section (up to 22 % of detrital grains) (Fig. 5.5.). Authigenic calcite occurs in many samples (≤ 25 % of the rock), but it does not show significant correlation with the abundance of specific types of detrital grains. Quartz cements are more common in the upper part of the Tinau Khola section (7-12 %).

Heavy mineral suites constitute mostly 1 % or less of detrital grains, and ferromagnesian silicates are rare or lacking. The heavy minerals are dominated by garnet (12-73 % of heavy transparent minerals) and ultrastables (zircon, tourmaline, rutile; 9-86 % of heavy transparent minerals), along with minor chloritoid, epidote, staurolite, kyanite and sillimanite. Kyanite and sillimanite are most common in the Surai Khola section. There are also trace amounts of sphene, apatite, brookite, and zoisite. Tourmaline dominates the ultrastables. As with the bulk petrography, the average heavy mineral composition of the Siwalik Group (Tinau Khola section: ZTR 51 LgM 7 Gt 39 HgM 2; Surai Khola section: ZTR 31 LgM 11 Gt 40 HgM 16; Karnali section: ZTR 43 LgM 10 Gt 37 HgM 4) are again reflected in the modern sand assemblages (Tinau River: ZTR 34 LgM 7 Gt 51 HgM 6; Surai River: ZTR 16 LgM 15 Gt 43 HgM 23; Karnali River: ZTR 7 LgM 16 Gt 27 HgM 2). Commonly rounded ultrastable grains are more abundant in the Tinau Khola and Karnali sections. Combined with low heavy mineral concentrations, this indicates a greater influence of recycling with respect to sandstones of the Surai Khola section.

Whilst the heavy mineral suites generally show a gradual evolution between ~ 10 Ma and the present, the proportion of low-grade heavy minerals (epidote, zoisite, chloritoid) increases slightly at 12 Ma in the Tinau Khola section and significantly in

all sections by 8 Ma (Fig. 5.5.). In the Tinau Khola section ultrastables and garnet are replaced by garnet-dominated assemblages at 8.9 Ma followed by the appearance of staurolite, minor kyanite and epidote-group minerals at 7.5 Ma. In the Surai Khola section ultrastables with minor garnet and staurolite at 8.6 Ma are replaced by garnet-dominated assemblages with staurolite and minor kyanite at 8 Ma, kyanite becomes common and sillimanite appears at 7 Ma along with epidote-group minerals. In the Karnali section ultrastables and garnet dominate from 16-12 Ma with staurolite appearing at 9 Ma and kyanite becoming common at 6.9 Ma. The heavy mineral transition from minor staurolite to common kyanite between 8-7 Ma coincides with high feldspar abundance during the same period in all three sections and high garnet abundance in the Surai Khola section (Fig. 5.5.). The Tinau Khola and Surai Khola sections also record a slight increase in metamorphic index (MI) during this interval.

5.5.1. Modern rivers

The Tinau Khola and Surai Khola sections show similar petrographic characteristics to the modern river sand. The Karnali section is, however, distinctly lower in metamorphic grade on average (MI: 177) than the modern Karnali River sand (MI: 294). For all three sections the modern river sands have different heavy mineral contents compared to the sediment of the sections, showing a sharp increase in blue-green hornblende and diopside. Sand from the modern Tinau River at the mountain front (Q 57 F 5 Lv 1 Ls 43 Lm 21) is very different from that collected just north of the Main Boundary Thrust (Q 25 F 0 Lv 0 Ls 28 Lm 54) (Fig. 5.6.). The Tinau River at the mountain front yielded higher amounts of quartz, zircon, and garnet but lower

amounts of epidote, whilst the small amounts of kyanite and staurolite are not present in the sample taken north of the Main Boundary Thrust.

5.6. Discussion

The composition of Siwalik sandstones remains relatively constant through time, and is remarkably similar to modern river sands. The bulk of the detritus is very low-grade (anchimetamorphic) and therefore chiefly shallow structural levels of the orogen were being eroded during deposition of all three sections, perhaps from more frontal parts of the thrust belt (e.g. Lesser Himalaya), with deeper levels (e.g. Greater Himalaya) exposed further upstream but representing only a very minor part of the total detritus. Petrographic modes therefore suggest that sedimentary to low-grade metamorphic detritus dominated the supply of sediment to the foreland basin (~ 90 %) throughout deposition of the Tinau Khola, Surai Khola, and Karnali sections. The low-grade/sedimentary source could be the Lesser Himalayan Zone and/or the low-grade teconostratigraphic covers of the Greater Himalaya such as those that outcrop today as the Haimantas in Kashmir or the Sanctuary Formation in Nepal. It is likely that in the Miocene there were still large patches of very low to low-grade tectonostratigraphic covers of the Greater Himalayan Zone. Tibetan Himalayan derivation is also possible but less likely because few big rivers today have headwaters as far north as the Tibetan Himalaya, and these carry much more high-grade metamorphic detritus than documented in the Nepal Siwalik Group. The marked increase in dolostone abundance after 12 Ma is indicative of a Lesser Himalayan provenance (Lesser Himalaya is rich in PreCambrian dolostones). Indeed, dolostone grains of probable Lesser Himalayan origin are present throughout

all three sections and increase in abundance up-section. This could indicate that the Lesser Himalaya were eroding as early as 17 Ma and became progressively exposed in the source area from then on. However, the petrography alone does not provide sufficient clarity to allow robust provenance control. For example, the definition of the Lesser Himalaya is somewhat vague. The Lesser Himalaya today is a composite terrane and the Miocene Lesser Himalaya is very poorly understood.

The increase in feldspar and garnet abundance in the Siwalik Group between 9 and 6 Ma hints at an increasing contribution from the Greater Himalaya. This probably reflects a deepening of the erosion level into high-grade Greater Himalayan rocks as recorded by the heavy mineral trends. The evolution of heavy mineral suites from staurolite to dominantly kyanite between 8-7 Ma and increase in metamorphic index in all three sections indicates erosion of amphibolite-facies metasediments in the drainage basin during this period. In Nepal, the Dumri Formation molasse (~ 20-15 Ma) lacks both high-grade minerals and medium- to high-grade lithic material (DeCelles et al., 1998b) and thus our data from the Siwalik succession record the time when the highest-grade rocks first became exposed. DeCelles et al. (1998a) found kyanite and sillimanite from the Khutia Khola section in far western Nepal at ~ 11 Ma, indicating some variation along strike. It therefore seems that whilst sedimentary and greenschist facies rocks dominated the source area during initial Siwalik sedimentation, amphibolite facies source rocks were unroofed by 8 Ma (garnet, staurolite, minor kyanite) and have been widely exposed since at least 6 Ma (garnet, kyanite, minor sillimanite).

Although the heavy mineral suites depict an apparent gradual unroofing trend it is important to note that an up-section decrease in diagenetic dissolution can mimic unroofing trends (Morton, 1985). The superposition of these two effects hampers a straightforward reconstruction of tectonic or erosional histories from heavy mineral suites. The virtual absence of amphiboles and pyroxenes and the low abundance of heavy minerals and ferromagnesian silicates is indicative of pronounced diagenetic dissolution of mafic minerals in Nepal. However, the modern river sands are characterised by these same features and in the only sandstone sample where a few hornblende grains are present they do not show sawtooth edges (indicative of incipient dissolution).

Because there is no significant correlation with the abundance of authigenic calcite to specific types of detrital grains, evidence for selective mineral replacement is lacking. The abundance of labile sedimentary and metamorphic lithic fragments also indicates that the detrital modes have not been significantly affected by mechanical abrasion or chemical weathering. Recycling of older sandstones is indicated by the occurrence of rounded quartz grains, locally showing abraded overgrowths. The more abundant and more commonly rounded ultrastable grains in the Tinau Khola section, along with lower heavy mineral concentrations, indicates a greater influence of recycling with respect to the sandstones of the other two sections.

5.6.1. Modern Rivers

Bulk petrography and heavy mineral composition of the modern rivers reflects the ancient sediment and most likely is a result of recycling of the exposed sections. The modern Surai River drains only the Siwalik Group whilst the modern Tinau River catchment does not extend far north of the Main Boundary Thrust. The modern Karnali River however does have a significant drainage area beyond the Siwalik Group, a difference which is reflected in a moderately different petrography. Sand from the modern Tinau River taken just above the Main Boundary Thrust (north of the Siwalik section) is totally different from the modern Tinau at the mountain front (base of the Siwalik section). Because the latter is petrographically very similar to the Siwalik section it most likely carries mainly detritus recycled from the Siwaliks. The sample taken from above the Main Boundary Thrust was derived entirely from the Lesser Himalayan Zone, reflected in the lack of high-grade metamorphic minerals and abundance of epidote. This also implies that the river which deposited the Tinau Khola section drained quite different rock units to the modern Tinau River. The ancient river may either have extended further north into the Crystalline Thrust Sheets or Greater Himalayan Zone or have drained the same area as it does today but it consisted of rock types that have subsequently been removed (it is likely the Crystalline Thrust Sheets were once more extensive). In the modern Karnali River the higher metamorphic grade of lithic grains and increase in hornblende and diopside compared to the entire Karnali Siwalik section also indicate a change in catchment area.

5.6.2. Comparison with Siwalik sediments along-strike

Siwalik sandstones in northern Pakistan have typically low quartz/feldspar ratios (Abbasi & Friend, 1989; Critelli & Ingersoll, 1994; Pivnik & Wells, 1996), probably because of a significant contribution from plutonic rocks of the Ladakh-Kohistan arcs and/or the Karakoram Range. In the classic Jawalamukhi section of northern India, quartzolithic compositions in the lower part (13-11.7 Ma) are sharply replaced by lithic compositions upwards (11.5-7 Ma; Najman et al., 2004). Quartzolithic compositions that compare with those in this study are widespread in Nepal (Critelli & Ingersoll, 1994; DeCelles et al., 1998b).

As far as dense minerals are concerned, a general trend from dominant ultrastables, garnet, and minor staurolite in the lower Siwalik beds, to increasing garnet associated with kyanite and then with sillimanite upwards has long been recognised (Chaudhri, 1972). In the Dharamsala/Jawalamukhi section, staurolite appears at 20.3 Ma, kyanite at 13.8 Ma (Dharamsala) to 12.2 Ma (Jawalamukhi), and sillimanite at 7.7 Ma. The data may be interpreted as indicating significantly later exhumation of amphibolite facies rocks in Nepal than in the northwestern Himalaya. However, given the scarce information available this interpretation remains tentative. If exhumation was diachronous there is more than one potential cause. In particular, the relationships between denudation and climatic changes are poorly understood, and palaeodrainage patterns are virtually unknown, factors that can greatly impact exhumation. In general the petrography and heavy mineral characteristics of the Nepal sections are more homogenous than sections further west, which may reflect

climatic differences. Nepal is wetter than the western Himalayas so the more unstable grains may have a greater chance of being removed by weathering.

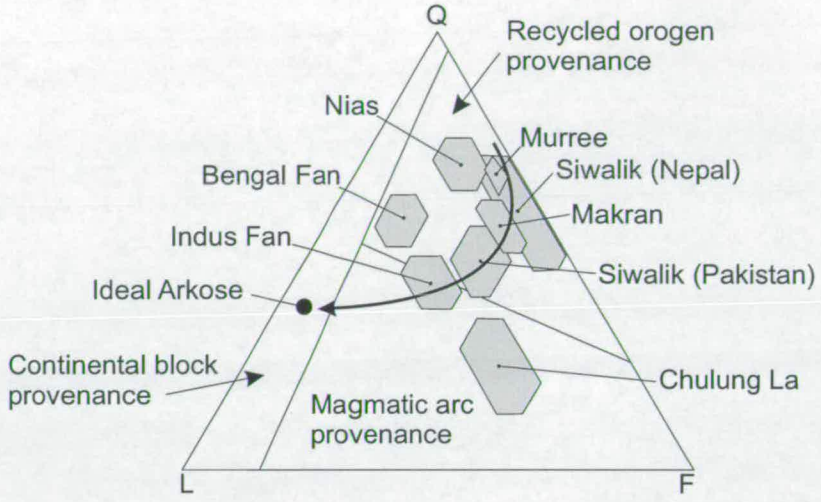


Figure 5.1. Triplot showing the relative proportions of quartz (Q), feldspar (F), and total lithics (L) for various Himalayan molasse and flysch deposits, adapted from Garzanti et al. (1996). There is a distinct compositional shift towards ideal arkose compositions for younger detritus, reflecting deepening erosion into continental crust.

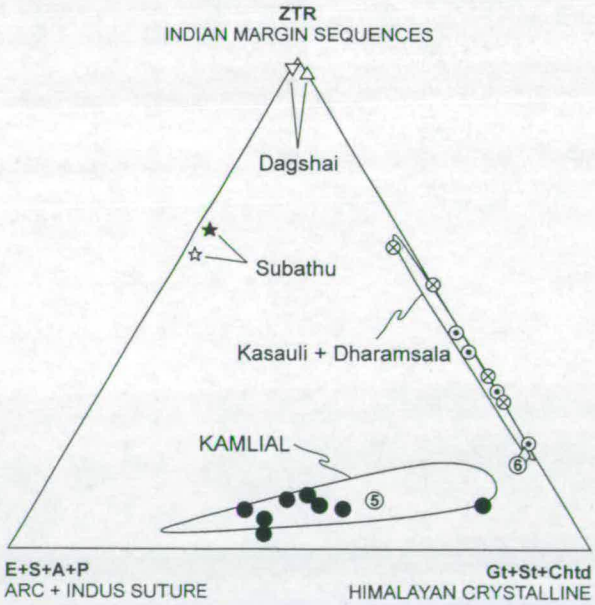


Figure 5.2. Triplot showing the proportions of various heavy minerals in Tertiary Himalayan molasse deposits, from Najman et al. (2003). ZTR - zircon + tourmaline + rutile, E - epidote, S - spinel, A - amphibole, P - pyroxene, Gt - garnet, St - staurolite, Chtd - chloritoid. 99 % confidence intervals are shown.

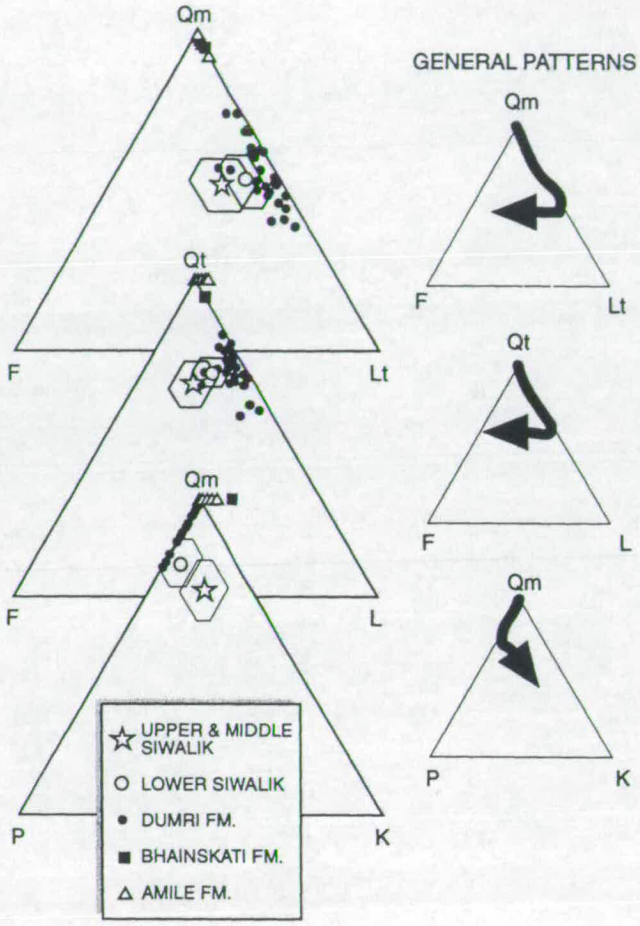


Figure 5.3. Triplots showing the compositions of Amile, Bhainskati, Dumri, and Siwalik sandstone samples from Nepal, from DeCelles et al. (1998b). Qm - monocrystalline quartz, F - total feldspar, Lt - total lithic fragments, Qt - total quartzose grains, L - non-quartzose lithic fragments, P - plagioclase.

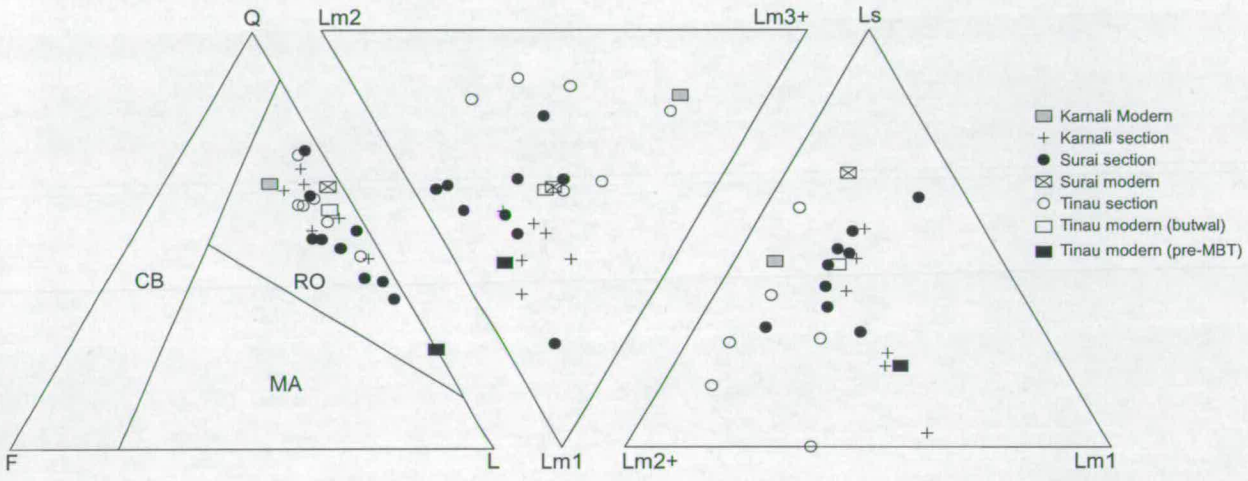


Figure 5.4. Petrography ternary plots for the three Siwalik sections under investigation. Q - quartz, F - feldspars, L - total lithics, Lm1 - slate to metasandstone grains, Lm2 - phyllite to quartz/sericite grains, Lm2+ - Lm2+Lm3+Lm4+Lm5 (low to very high rank metamorphic lithics with strong cleavage or schistosity), Lm3+ - Lm3+Lm4+Lm5 (medium to very high rank, metamorphic lithics with small to large muscovite lamellae), Ls - sedimentary lithics, RO - recycled orogen, MA - magmatic arc, CB - continental block (fields from Dickinson, 1985).

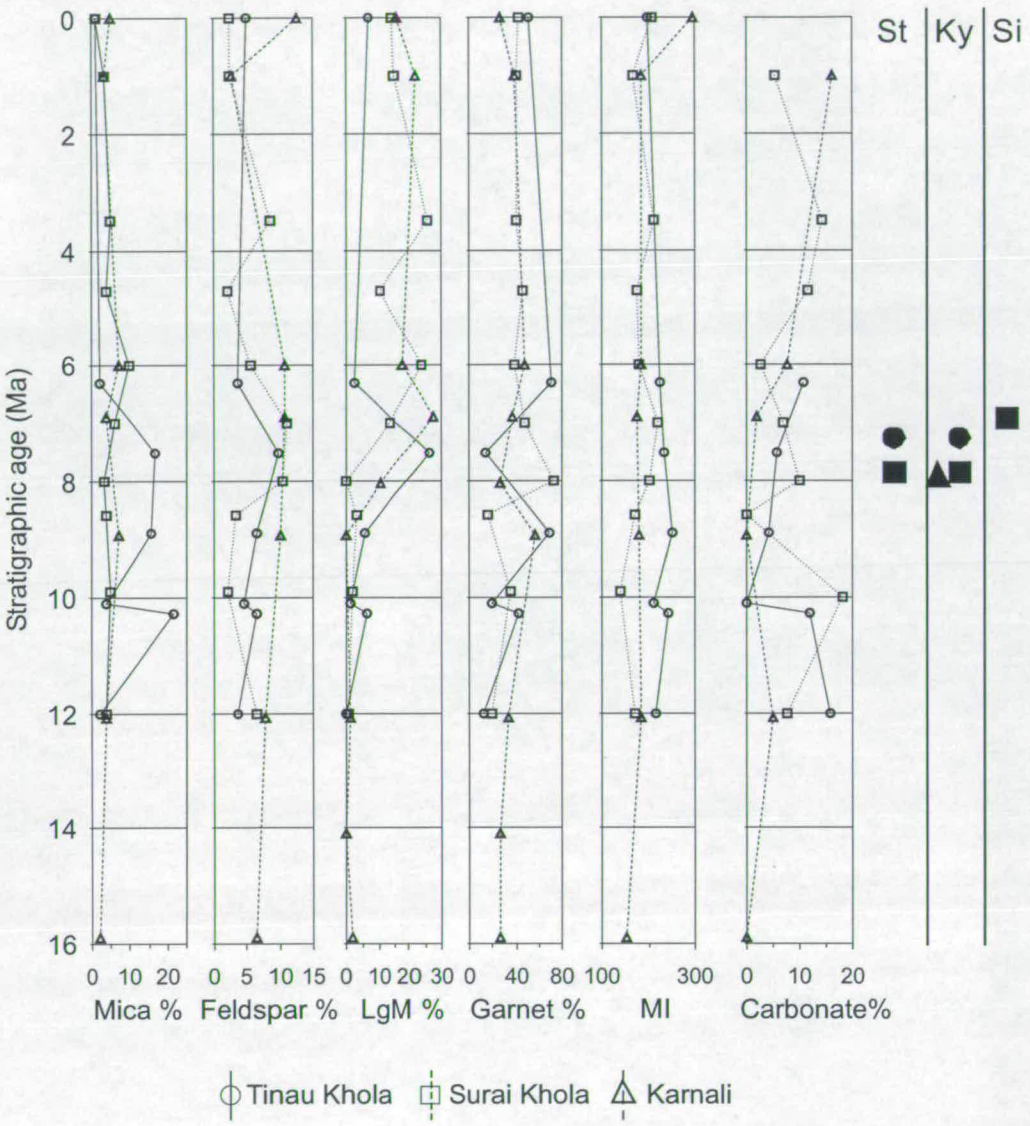


Figure 5.5. Variation in petrography with respect to stratigraphic age for the three Siwalik sections under investigation, plotted as percentage of detrital component (for example 10 % garnet = 20 grains counted from 200 transparent heavy mineral grains). The plot on the right shows when metamorphic index minerals first appear in the section. LgM - low-grade metamorphic lithics, MI - metamorphic index (see petrography data file on cd for explanation), St - staurolite, Ky - kyanite, Si - sillimanite.

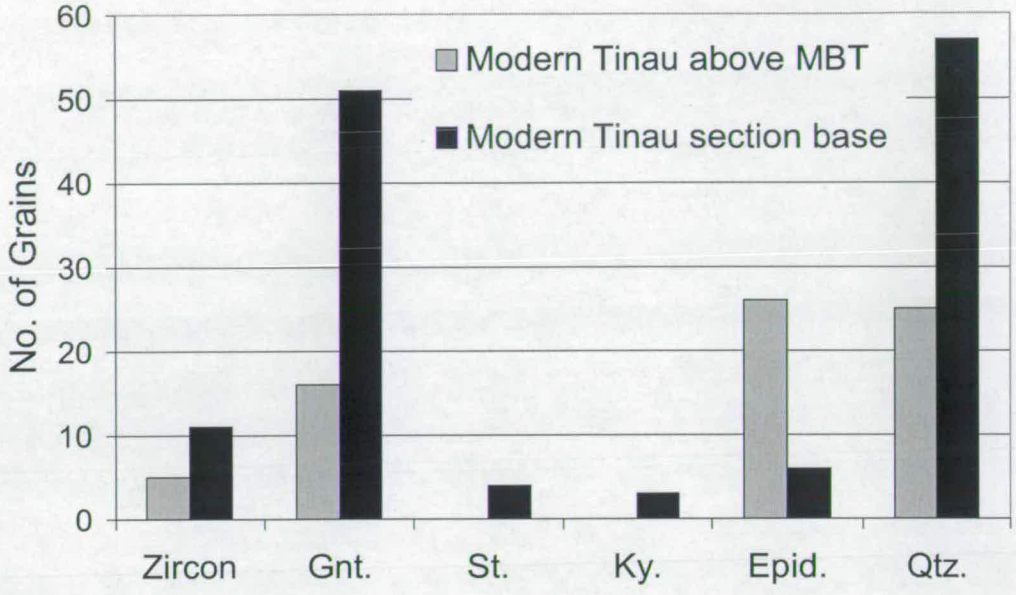


Figure 5.6. Comparison between the heavy mineral content of the modern Tinau River as sampled just above the Main Boundary Thrust (MBT) and at the start of the Siwalik section where the river enters the foreland basin. Number of grains plotted as percentage of detrital component. Gnt. - garnet, St. - staurolite, Ky. - kyanite, Epid. - epidote, Qtz. - quartz.

6. Geochemistry

6.1. Introduction

Detrital geochemistry is often influenced by source-rock composition and is therefore indicative of provenance (Wronkiewicz & Condie, 1987). The variation of detrital geochemistry with time can be linked to the erosional and unroofing history of the hinterland as controlled by the kinematic development of the orogen. Because the Himalayas are zoned in terms of characteristic geochemical signatures they are well suited to such an approach (e.g. Ahmad et al., 2000 and references therein; Robinson et al., 2001) (Table 6.1.). In particular, the sharp contrast in ε_{Nd} values between the presently exposed Greater Himalaya (-10 to -18 average) and the Lesser Himalaya (-23 to -26 average) has commonly been used to identify sediment provenance (France-Lanord et al., 1993; Najman et al., 2000; Robinson et al., 2001; Galy & France-Lanord, 2001). This Chapter presents the results of whole-rock Rb-Sr and Sm-Nd geochemical analysis that was carried out on mudstone samples and quartzite clasts from the three Siwalik sections under investigation. Both Nd and Sr isotopic composition are useful in provenance studies. The Sm-Nd isotopic system has been widely used due to its resistance to perturbation by common crustal processes (Harris et al., 1990). This is because rare earth elements (REE's) are relatively insoluble and therefore protected against sedimentary fractionation (Taylor & McLennan, 1985). In contrast, Sr is soluble and shows large differences between minerals that have very different Rb/Sr ratios. Nevertheless, the large difference in $^{87}Sr/^{86}Sr$ between Himalayan lithotectonic zones (particularly the Greater and Lesser

Himalaya) appears to be reflected in the characteristic $^{87}Sr/^{86}Sr$ record of detrital sediment (Galy, 1999; White et al., 2002).

Tectonostratigraphic Zone	$\varepsilon_{Nd}(0)$	$^{87}Sr/^{86}Sr$
Greater Himalayan Zone	-10 to –18	0.73 to 0.84
Greater Himalayan Protolith	-10 to –18	
Dadeldhura Thrust Sheet	-7.6 to -11.8	
Inner Lesser Himalayan Zone	-23 to –28	0.75-5
Outer Lesser Himalayan Zone	-17 to –18	0.75-5
Tibetan Himalayan Zone	-15 to –17	0.7 to 0.75

Table 6.1. Variation in whole-rock Nd-Sr geochemistry signatures for the main Himalayan tectonostratigraphic zones of interest to this study. References: Greater Himalayan Zone: (Ahmad et al., 2000 and references therein; Najman et al., 2000 and references therein); Greater Himalayan Protolith (Richards, 2005); Dadeldhura Thrust Sheet (Robinson et al., 2001); Inner and Outer Lesser Himalayan Zone: (Ahmad et al., 2000 and references therein; Najman et al., 2000 and references therein); Tibetan Himalayan Zone (Derry & France-Lanord, 1996; Najman et al., 2000 and references therein).

6.2. Limitations

Sedimentary mixing can complicate a whole-rock detrital geochemistry study. Unless the geochemical differentiation of the hinterland is clear-cut it is a difficult task to decipher the percentage of a particular source area within the detrital mix. One potential complication of employing detrital geochemisty within the Himalayas is that the Inner and Outer Lesser Himalayan belts have distinct Sr-Nd isotope signatures and the latter overlap with those of the Greater Himalayan Zone (Ahmad

et al., 2000) (Table 6.1.). In Garhwal, NW India, the Outer Lesser Himalayan values are similar to those of the Vaikrita Group of the adjacent Greater Himalaya (ε_{Nd} = -14 to -19) and other Greater Himalayan values from across the Himalayas (Ahmad et al., 2000 and references therein) (Fig. 6.1.). Robinson et al. (2001) found a similar distribution of isotopic signatures for the Lesser Himalaya in Nepal. They found that the lower part of the Lesser Himalaya (the Ranimata Formation) consistently yields the most negative values with a ε_{Nd} range of -25.5 to -21.9, whilst upper Lesser Himalayan samples (Benighat, Syangia, Galyang, and Sangram Formations) yield ε_{Nd} values of -25.3 to -15.9 and so overlap typical Greater Himalayan signatures. Such an overlap can make provenance determination ambiguous. Furthermore, average ε_{Nd} values of -15 to -17 for the Tibetan Himalayan Zone (Derry & France-Lanord, 1996) are very similar to typical Greater Himalayan values.

6.3. Previous Work

6.3.1. Depositional relationships

A poor understanding of the original depositional relationships between Himalayan zones has hindered models of orogenic evolution. Geochemistry has played a major role in evaluating this issue (Myrow et al., 2003). According to isotopic results the Lesser and Greater Himalaya were derived from sedimentary precursors with distinctly different depositional ages and provenance (France-Lanord et al., 1993; Massey, 1994; Parrish & Hodges, 1996; Ahmad et al., 2000). Characteristic whole-rock ε_{Nd} geochemistry values for the Greater Himalayan Zone are -10 to -18. Lesser Himalayan Zone units are thought to represent the proximal, and slightly older,

equivalents of the Tibetan Himalayan Zone (Tethyan) Indian margin deposits (Garzanti, 1999). The Lesser Himalaya yields characteristic whole-rock Nd values of ε_{Nd} = -23 to -26 (Ahmad et al., 2000 and references therein; Robinson et al., 2001) and high $^{87}Sr/^{86}Sr$ ratios (mostly > 0.8) which contrast with those for the Greater Himalaya and reflect their derivation from Archaean rocks of the Indian Craton during the Mid-Proterozoic (Robinson et al., 2001).

6.3.2. Structural mapping

The differences in geochemical signatures between Himalayan tectonostratigraphic zones have been used to distinguish between these zones and therefore define boundary structures in the field when metamorphic or structural evidence is not definitive (e.g. Argles et al., 2003). This ability to differentiate zones is important in areas such as the Main Central Thrust where the location of the thrust is debated due to the lack of a clear structural discontinuity (Arita, 1983; Pecher, 1989; Hodges, 2000; Catlos et al., 2001). Ahmad et al. (2000) illustrate the utility of Nd and Sr isotope systematics in constraining the location of major thrust systems which separate lithologically similar sedimentary sequences. They use this technique to identify the true Main Central Thrust within the Garhwal Himalaya, NW India.

6.3.3. Provenance and tectonic evolution

Using Nd and Sr isotope systematics, Derry & France-Lanord (1996) showed that the Himalayan provenance for Bengal Fan sediments has changed little over the last 17 Myr. The Nd geochemistry of the Bengal Fan is dominated by a strong Greater Himalayan Zone signature of -15 to -17. From geochemistry studies it thus appears that an analogue of the Greater Himalayan Zone was providing detritus to the Bengal Fan by Middle Miocene time and therefore must have begun exhuming by then (France-Lanord et al., 1993).

In more recent times detrital geochemistry research has extended to terrestrial molasse basins. Najman et al. (2000) found that the whole-rock geochemistry of the Subathu Formation in NW India (ε_{Nd}: -9; $^{87}Sr/^{86}Sr$: 0.710-0.715) plots between Tibetan Himalayan Zone and suture zone values, whereas the Dagshai and Kasauli Formations (ε_{Nd}: -12 to -18; $^{87}Sr/^{86}Sr$: 0.755-0.775) are characteristic of the Greater Himalaya or the highest $^{87}Sr/^{86}Sr$ yielding rocks of the Tibetan Himalayan Zone (Fig. 6.2.). They interpret this switch to mark the emergence of the Himalayan metamorphic core, forming a barrier to sediment derived from the northern Tibetan Himalaya and suture zone sources. Petrographic analysis of the same sediment (Chapter 5) reveals a similar evolution. In Nepal, samples from the Bhainskati Formation molasse have ε_{Nd} values of -14.9 to -8.1 whilst Dumri Formation samples yield values in the range -14.5 to -13.1 (DeCelles et al., 2004) (Fig. 6.3.). This increasingly negative up-section trend seen in the Bhainskati and Dumri Formations suggests the source in the Eocene (ε_{Nd}: -8.1) was sediment from the upper part of the

Tibetan Himalayan Zone whilst the Early Miocene values (ε_{Nd}: -14.1) reflect average Greater and Tibetan Himalayan signatures (Najman et al., 2001). Therefore as with the Bengal Fan, foreland basin sediment has been dominated by a Greater Himalayan geochemical signature from the time of Dumri deposition to the present.

Robinson et al. (2001) were the first to conduct Nd isotopic studies in the Sub-Himalayan Zone (Siwalik Group) of Nepal, which they compared to the results of bedrock analysis in the potential source zones. This work further helped to establish the value of Nd isotopes in distinguishing between lithotectonic zones. Their data shows that the Greater and Tibetan Himalayan Zones (ε_{Nd}: -16) dominated the source areas for foreland basin sediments in Nepal during Eocene to Pliocene time. In western Nepal there is a shift to more negative values (ε_{Nd}: -16 to -18) up-section, which they interpret as marking the erosional breaching of the Lesser Himalayan Duplex (Fig. 6.3.). This switch occurs at ~ 10 Ma along the Khutia Khola section in far west Nepal and ~ 11 Ma along the Surai Khola section in central-west Nepal. In a study which yielded similar results for the Karnali section in far west Nepal, Huyghe et al. (2001) argue for the simultaneous inception of several thrusts ahead of the Main Central Thrust at ~ 12 Ma to account for the up-section change in Nd values (Fig. 6.4.). Robinson et al. (2001) propose that the absence of a similar up-section shift in eastern Nepal sections reflects less erosional unroofing in that region. This conclusion is supported by present outcrop patterns whereby far less Lesser Himalayan rocks are exposed in the east. They also found that the Surai Khola section becomes less negative through Middle- to Late-Miocene time, arriving at ε_{Nd}: -15.5 by 4 Ma. Younger units then yield values between -17.7 and -16.4. Likewise

the ε_{Nd} values at Khutia Khola remain steady at -18 through Middle- to Late-Miocene time but revert back to a stronger Greater/Tibetan Himalayan signature of -15 between 5 Ma and 4 Ma. The authors interpret these late shifts to reflect stream capture of Greater Himalayan detritus in the hinterland river system as opposed to a change in tectonic style.

6.3.4. Climate

Whilst there is a growing body of work utilising detrital geochemistry as a provenance tool and indicator of hinterland reorganisation, the geochemistry technique has been most readily applied to study the impact the Himalayas have had on climate and seawater chemistry (e.g. Beck et al., 1995; Konomatsu, 1997). As climate drives changes in erosion rates at ~ 10^4 yr time scales, an interesting feedback takes place between orogenic growth and climate change.

6.3.4.1. Global seawater geochemistry

Since the Cretaceous strontium seawater ratios have increased gradually from ~ 0.7077 to the present value of ~ 0.70924-0.709211 (Elderfield, 1986). The monotonic rise of seawater $^{87}Sr/^{86}Sr$ over the last 40 Myr has been linked by some to erosion of the Himalayas, a source with high $^{87}Sr/^{86}Sr$ ratios (Edmond, 1992; Quade et al., 1997; Najman et al., 2000). Indeed, modern Himalayan rivers have elevated $^{87}Sr/^{86}Sr$ ratios (Edmond, 1992). Workers have debated the relative contributions from potential Himalayan source lithologies (Harris et al., 1998; Singh et al., 1998; Galy & France-Lanord, 1999; Bickle et al., 2001). Tourmaline-bearing leucogranites of the Greater Himalaya have extremely high $^{87}Sr/^{86}Sr$ ratios, as do the gneisses they

intrude and these rocks are thus believed to be an important source of radiogenic strontium (Edmond, 1992). Himalayan carbonates, particularly abundant within the Lesser Himalaya, also have high $^{87}Sr/^{86}Sr$ ratios (Bickle et al., 2001; Quade et al., 2003). Harris et al. (1998) found that the cation geochemistry of the Bhote Kosi River in eastern Nepal is dominated by Ca and Mg ions, suggesting that carbonates are the predominant lithology undergoing dissolution, particularly within the Lesser Himalaya. Quade et al. (2003), in a study along the Seti River in Nepal, found that 36-39 % of strontium comes from Tibetan and Greater Himalayan terranes, 40-53 % from the Lesser Himalaya, and 8-23 % from the Crystalline Thrust Sheets. They found that many modern rivers in Nepal (Seti, Bhote, Kali Gandaki) display large downstream increases in $^{87}Sr/^{86}Sr$ (up to 0.75-0.77) that relate directly to the local presence of metacarbonates, particularly in the Lesser Himalaya. Indeed, Harris et al. (1998) discovered that when the Bhote Kosi traverses the Lesser Himalaya, the $^{87}Sr/^{86}Sr$ ratio of the dissolved load rises sharply to > 0.768. Large drainages that lack these Lesser Himalayan carbonates, such as the Arun River in eastern Nepal, have relatively low $^{87}Sr/^{86}Sr$ ratios (Quade et al., 2003). Modelling has confirmed the significance of the fluxes from rivers draining the Himalayas to the seawater strontium shift (Richter et al., 1992; Galy, 1999; English et al., 2000).

The strontium seawater shift over the last 40 Myr coincides with a transition from low $^{87}Sr/^{86}Sr$ values in the Subathu Formation to high $^{87}Sr/^{86}Sr$ values in the Dagshai Formation foreland basin sediments of NW India (Najman et al., 2000). Petrography (Chapter 5) indicates a change in provenance whereby the Dagshai records the first detritus from the exhuming Greater Himalaya and this may also explain the change

in $^{87}Sr/^{86}Sr$ values. Within the general trend of increasing $^{87}Sr/^{86}Sr$ ratios, shorter perturbations have also been highlighted. There has been a steady rise in $^{87}Sr/^{86}Sr$ ratios since ~ 9 Ma in Siwalik Group sediments (Quade et al., 1997; English et al., 2000) and in the Bengal Fan (Derry & France-Lanord, 1996). The values then fall to modern river standards after ~ 3 Ma (Quade et al., 1997). DeCelles et al. (2001) interpret the rise in Siwalik Group $^{87}Sr/^{86}Sr$ at ~ 9 Ma to suggest Lesser Himalayan erosion from carbonates now exposed in the southern part of the duplex.

Despite the links between the uplift of Himalayan lithologies and the change in seawater chemistry, there is nearly an inverse correlation between mass accumulation rates in the northern Indian Ocean and the $^{87}Sr/^{86}Sr$ records of the Bengal Fan and Siwalk Group sediments (Derry & France-Lanord, 1996; Quade et al., 1997). The cause of the $^{87}Sr/^{86}Sr$ switch therefore appears more complicated than simply an increase in Himalayan sediment flux. Changes in strontium flux as well as $^{87}Sr/^{86}Sr$ ratio must have played important roles in controlling the seawater ratio (DeCelles et al., 1998b). The $^{87}Sr/^{86}Sr$ ratio has been rising rapidly for a long time so it is probable that multiple sources of radiogenic stontium contributed to the long-term trend.

6.4. Methodology

A whole-rock geochemistry data set was obtained from seven mudstone samples from the Tinau Khola section, one conglomerate matrix sample from the Surai Khola section, and a total of six quartzite clasts from all three sections. Whole-rock Sm-Nd and Rb-Sr (mudstone only) isotopic ratios were measured at Cambridge University, England. Mudstones were used because finer samples provide greater accuracy in geochemical studies. Finer grains tend also to have a more accurate source signature, associated with greater mixing and homogeneity. Quartzite pebbles were sampled where possible and are mainly limited to the upper Siwalik units. These were taken to provide data that has not been complicated by sedimentary mixing. Only one conglomerate matrix sample was analysed from the Surai Khola section because previous work had already covered this section in detail (Huyghe et al., 2001; Robinson et al., 2001). Analytical techniques follow Ahmad et al. (2000) using a mixed ^{150}Nd-^{149}Sm spike. The samples were furnace-heated for 8 hours at 900°C to remove organics. HF, HNO^3 and HCL dissolution stages were carried out in Teflon Savillex vials in pressure vessels at 180°C for 8 hours. Sr, Nd and Sm were separated using standard ion-exchange columns (Bickle et al., 1988). During the time of these analyses, the internal Johnson Matthey standard gave $^{143}Nd/^{144}Nd$ = 0.51111 ± 8 (2σ) and $^{145}Nd/^{144}Nd$ = 0.348399 ± 7 (2σ) and the NBS987 Sr standard gave $^{87}Sr/^{86}Sr$ = 0.710259 ± 8 (2σ). Sr, Nd and Sm blanks were less than 0.05% of sample. Goldstein et al's (1984) chondrite normalised $^{143}Nd/^{144}Nd$ value (0.512638) was used for calculating ε_{Nd}. Further notes regarding the whole-rock geochemistry technique are given in Appendix IV.

6.5. Results

Detailed results for all geochemical analyses are given in Tables 6.2. to 6.4.. The ε_{Nd} and Sr values for Siwalik Group mudstones are plotted against stratigraphic age in Figure 6.5. ε_{Nd} values are remarkably constant. All Tinau Khola mudstone samples and one Surai Khola conglomerate matrix sample yielded ε_{Nd} values of ~ -17. Although less pronounced than the trend recognised by Quade et al. (1997), our $^{87}Sr/^{86}Sr$ values for Tinau Khola (mean of 0.739496) show an increase between 12-6 Ma with the highest value occurring after 8 Ma. The $^{87}Sr/^{86}Sr$ values for Tinau Khola and the Surai Khola conglomerate (0.765286) correlate well with those of previous studies and modern rivers in Nepal (Quade et al., 2003). These are very high compared to the global average for rivers of ~ 0.7119 and estimates for the bulk earth today 0.7045-0.7052 (Rollinson, 1993; Quade et al., 1997). Figure 6.6. shows the Siwalik samples plotted against average Nd-Sr isotopic values of major Himalayan source zones, revealing a strong Greater Himalayan affinity. My data for Tinau Khola lie at the overlap of typical Greater and Tibetan Himalayan signatures.

Clasts are a more reliable indicator of provenance than a sample of matrix sediment because of the uncertainties regarding the effect of sedimentary mixing on whole-rock detrital geochemistry. ε_{Nd} values for the clasts were more varied than the mudstone, ranging from -14 to -30 (Table 6.4., Fig. 6.7.).

Sample	Age (Ma)	Strat. Height (m)	$^{143}Nd/^{144}Nd$	$^{142}Nd/^{144}Nd$	$^{145}Nd/^{144}Nd$	$^{148}Nd/^{144}Nd$	$^{150}Nd/^{144}Nd$	Conc. spkwt/smwt	ε_{nd}	Run No.
JMOrange	-	-	0.511110 [8]	1.141886 [11]	0.348399 [7]	0.241560 [33]	0.256432 [58]	189/200		5541
Yv 42D	-	-	0.512334 [10]	1.142063 [13]	0.348420 [7]	0.241815 [43]	0.369274 [66]	29.4467 [184]		5542
TA2	6.2	1675	0.511788 [8]	1.142115 [11]	0.348429 [6]	0.241757 [29]	0.343998 [138]	24.8817 [138]	-16.5	5543
TA2B	7.6	1430	0.511751 [7]	1.142041 [9]	0.348430 [7]	0.241841 [20]	0.380485 [35]	27.149504 [91]	-17.3	5544
TA4	8.4	1193	0.511770 [6]	1.142272 [9]	0.348430 [5]	0.241792 [21]	0.359216 [35]	31.857029 [102]	-16.9	5545
TA7D	9.4	1004	0.511768 [8]	1.142405 [17]	0.348421 [7]	0.241755 [34]	0.340992 [76]	37.449252 [249]	-16.9	5546
TA12	10.1	590	0.511733 [9]	1.141911 [10]	0.34814 [7]	0.241711 [27]	0.320647 [46]	46.459476 [174]	-17.6	5547
TA19	10.8	220	0.511758 [7]	1.143095 [19]	0.348429 [7]	0.241859 [27]	0.393324 [43]	24.924651 [109]	-17.2	5548
TA16	12	5	0.511769 [7]	1.142054 [10]	0.348420 [7]	0.241721 [22]	0.322092 [37]	45.67554 [140]	-16.9	5549
Cong. 2	2.7	3515	0.511776 [7]	1.141941 [10]	0.348440 [7]	0.241864 [23]	0.397507 [35]	24.276240 [85]	-16.8	5550
Blank	-	-	115.382233 [9516]	1.022991 [2349]	0.392981 [1085]	0.0024 [132.6981]	0.487499 [3688]	0.0007516 [42.7784]	750pg	5551

Table 6.2. Whole rock Nd geochemistry results (1σ errors in brackets). TA samples are from the Tinau Khola section, Cong.2 is from the Surai Khola section, Spkwt – spike weight, smwt – sample weight.

Sample	Age (Ma)	Strat. Height (m)	Fil Corr.	Beam	$^{87}Sr/^{86}Sr$ Corr.	$^{87}Sr/^{86}Sr$ Dyn. Av.	$^{87}Sr/^{86}Sr$ HI/AX	$^{87}Sr/^{86}Sr$ AX/LI	Ratios
NBS987	-	-	2.68	~1.5v	0.710259 [8]	0.710257 [8]	0.710249 [10]	0.710255 [10]	189/200
TA2	6.2	1675	2.686	~1.3v	0.748211 [18]	0.748210 [18]	0.748216 [30]	0.748203 [17]	198/200
TA2B	7.6	1430			0.738434 [42]	0.738434 [42]			14/16
TA4	8.4	1193	2.657	~1.1v	0.733790 [12]	0.733788 [12]	0.733784 [13]	0.733793 [14]	93/100
TA7D	9.4	1004	2.672	~1.9v	0.742381 [8]	0.742379 [8]	0.742384 [9]	0.742375 [10]	194/200
TA12	10.1	590			0.740718 [18]	0.740718 [18]			134/140
TA19	10.8	220			0.735873 [13]	0.735873 [13]			56/60
TA16	12	5			0.737067 [17]	0.737067 [17]			171/180
Cong. 2	2.7	3515	2.611	~1.7v	0.765286 [8]	0.765284 [8]	0.765278 [11]	0.765291 [10]	125/132
					84/86Sr	**87/86Sr**	**88/86Sr**	**85/86Sr**	
Blank	-	-			51.459359 [757]	0.689239 [953]	8.033216 [1002]	0.000315 [37.4551]	24/25

Table 6.3. Whole-rock Sr geochemistry results.

Sample/Strat. age	Sm	1s	Nd	1s	Sm/Nd	1s	$^{147}Sm/^{144}Nd$	1s	$^{143}Nd/^{144}Nd$	1s	TMORB (Ma)	1s	ε_{Nd}	1s	$^{87}Sr/^{86}Sr$	1s
TinauPebbles Tinau Khola 7.6 Ma	0.709	0.0023	3.477	0.003	0.2039	0.0007	0.12325	0.00041	0.511650	12	2519	23	-19.3	0.2	0.731847	7
DankPebbles Surai Khola 3.1 Ma	1.314	0.0003	7.069	0.007	0.1859	0.0004	0.11235	0.00022	0.511516	8	2449	13	-21.9	0.2	0.934464	5.5
MSPebbles SaddlePoint Surai Khola 3.9 Ma	1.188	0.0003	7.530	0.008	0.1578	0.0003	0.09536	0.00019	0.511930	6	1571	8	-13.8	0.1	0.721769	6
MSPebbles348 Surai Khola 4.8 Ma	3.479	0.0075	16.094	0.016	0.2162	0.0005	0.13066	0.00031	0.511716	7	2622	16	-18.0	0.1	0.874548	7
K13P Karnali < 5 Ma	1.245	0.0001	6.785	0.007	0.1835	0.0004	0.11090	0.00022	0.511295	6	2738	11	-26.2	0.1	0.759698	5.5
F19Pebbles Karnali 6 Ma	1.194	0.0001	7.409	0.007	0.1612	0.0003	0.09739	0.00019	0.511103	13	2671	17	-29.9	0.3	0.745032	5

Table 6.4. Whole-rock Nd and Sr geochemistry results for quartzite clasts.

6.6. Discussion

ε_{Nd} isotopic values of around -17 for mudstone samples indicate dominant derivation from the Greater Himalaya which now forms the high-grade metamorphic core of the mountain range. Assuming average ε_{Nd} values of -15 for the Greater Himalaya and Greater Himalayan protolith and -25 for the Lesser Himalaya (Table 6.1.), a value of -17 indicates a contribution of ~ 18-20 % from the Lesser Himalayan Zone using equation 3 from Vance et al. (2003) and their calculated erosion rates (note that the large spread of Greater Himalayan and Lesser Himalayan values introduces large uncertainties to this calculation). In fact, at present the Lesser Himalayan Zone contributes between 20-50% of the solid load to rivers that drain the orogen (Galy, 1999). The relatively low abundance of mica and monazite in the Lesser Himalaya (minerals that have a strong control on detrital Nd geochemistry), and high abundance of carbonate which could be lost in solution and can have a diluting effect on REE concentrations, means that the Greater Himalaya would have a tendency to swamp the mixed geochemical signal. Indeed, the Lesser Himalayan Zone has a lower REE abundance than the Greater Himalaya because carbonates comprise approximately 30 % of the lithologies (Robinson et al., 2001). So an equal measure of detritus received from the Lesser and Greater/Tibetan Himalayan sources would be dominated by Nd from the Greater and Tibetan Himalayan Zones. This idea is supported by modern sand from the Trisuli River in central Nepal which drains all three zones and yields an ε_{Nd} value of -17.

Combining our geochemistry data with that of Galy (1999), Huyghe et al. (2001), and Robinson et al. (2001) (Fig. 6.8.) it seems that $^{87}Sr/^{86}Sr$ values are very consistent between all three sections until after 6 Ma where the Surai and Karnali signatures begin to diverge a little, the Surai tending to give significantly higher values. One possible reason for this is that the Surai River may have drained only Lesser Himalayan units at this time whilst the Karnali River contained a more mixed load. The modern drainage arrangement whereby the Surai River drains only the Sub-Himalayan Zone and the Karnali River extends back to the Tibetan Himalaya is a similar situation. I find a subtle increase in $^{87}Sr/^{86}Sr$ from 12 Ma onwards in the Tinau Khola section. This correlates with work by Huyghe et al. (2001) and Robinson et al. (2001) who report increasingly negative ε_{Nd} values for the Surai Khola and Karnali sections after 12 Ma. Such a trend could be interpreted to indicate a steady increase in the proportion of Lesser Himalayan detritus entering the foreland basin during the last 12 Myr. Our evidence for more negative (-18 to -30) Lesser Himalayan ε_{Nd} values in quartzite clasts, back to at least 7.6 Ma in the Tinau Khola section, 6 Ma in the Karnali section, and 4.8 Ma in the Surai Khola section (clasts are lacking in the older parts of these sections) provides further evidence for erosion of the Lesser Himalaya by those times.

The highly negative ε_{Nd} values for samples F19Pebbles (-29.9) (Karnali section, 6 Ma) and K13P (-26.2) (Karnali section, < 5 Ma) suggest these have an Inner Lesser Himalayan provenance as identified by Ahmad et al. (2000). The less negative ε_{Nd} values for samples TinauPebbles (-19.3) (Tinau Khola section, 7.6 Ma) and DankPebbles (-21.9) (Surai Khola section, 3.1 Ma) suggest Outer Lesser Himalayan

derivation. Samples MSPebbles348 (-18) (Surai Khola section, 4.8 Ma) and MSPebblesSaddlePoint (-13.8) (Surai Khola section, 3.9 Ma) have a Greater Himalayan affinity but the likelihood of a Greater Himalayan clast of up to 5 cm in size reaching the foreland basin is dubious, thus these signatures more likely represent a less negative component of the Outer Lesser Himalaya. The clear difference between the mudstone and quartzite clast whole-rock geochemistry has implications for the detrital geochemistry technique in general. Whilst clasts are unlikely to represent as large a source area as finer sediment, they are far more useful as precise constrainers of provenance. Therefore it seems that where possible, clasts should be incorporated into any detrital whole-rock geochemical investigation.

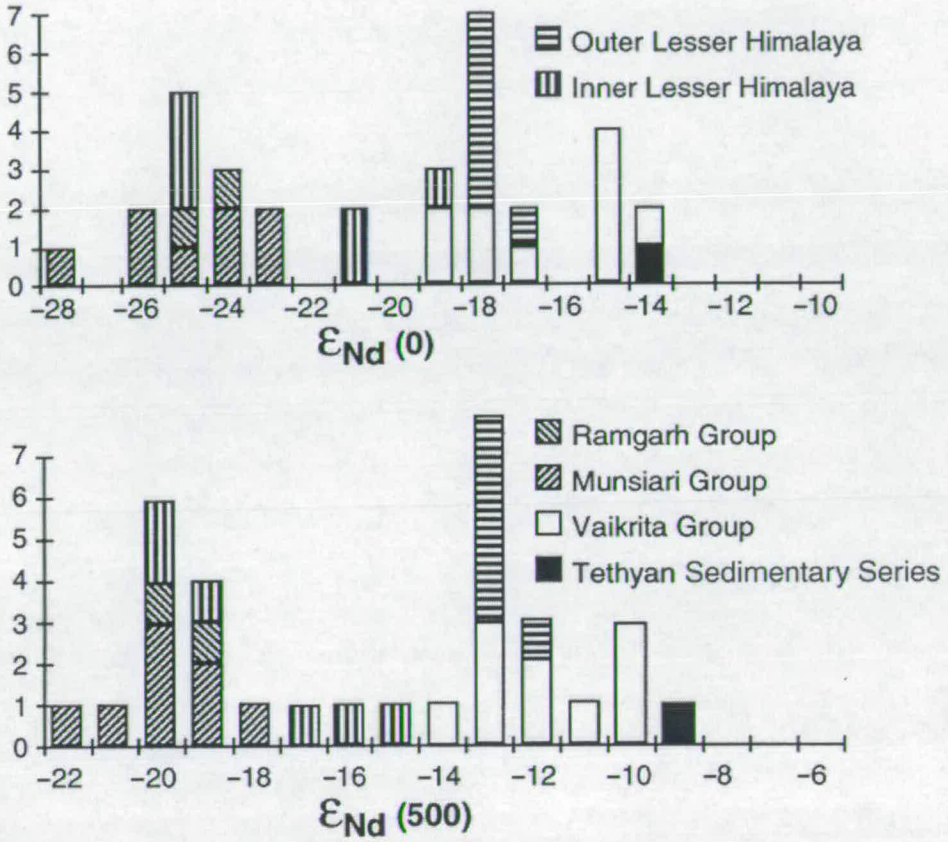


Figure 6.1. ε_{Nd} values for the Outer and Inner Lesser Himalaya and for lithotectonic groups in Garhwal, from Ahmad et al. (2000).

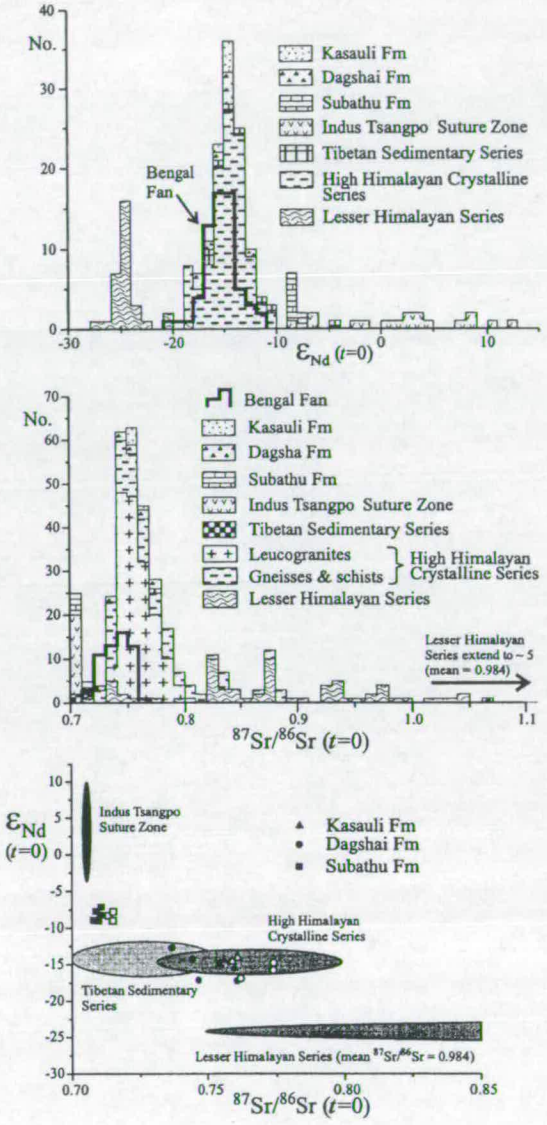


Figure 6.2. Nd and Sr data from molasse deposits in NW India compared to typical values for major Himalayan source zones, from Najman et al. (2000). Ellipses in the bottom plot illustrate 1σ distributions of fields.

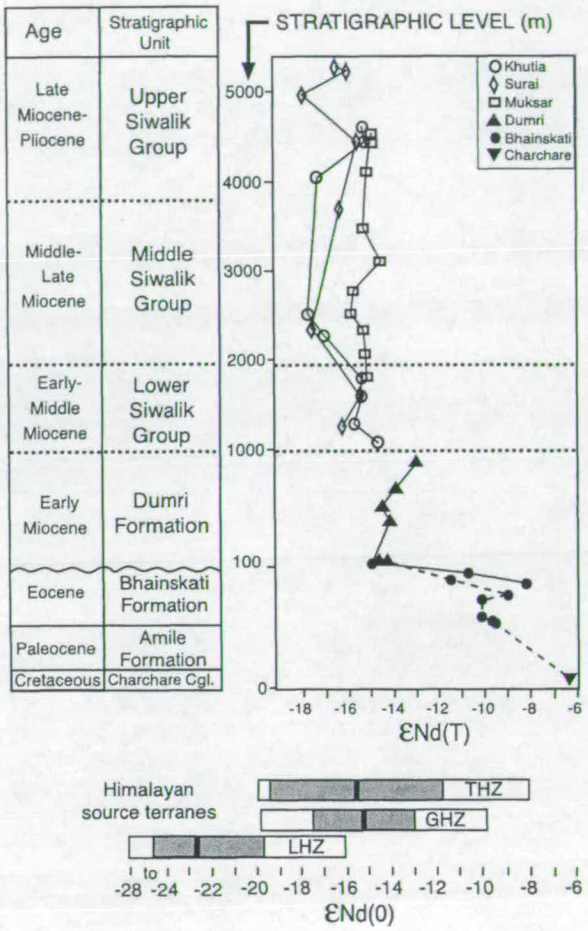
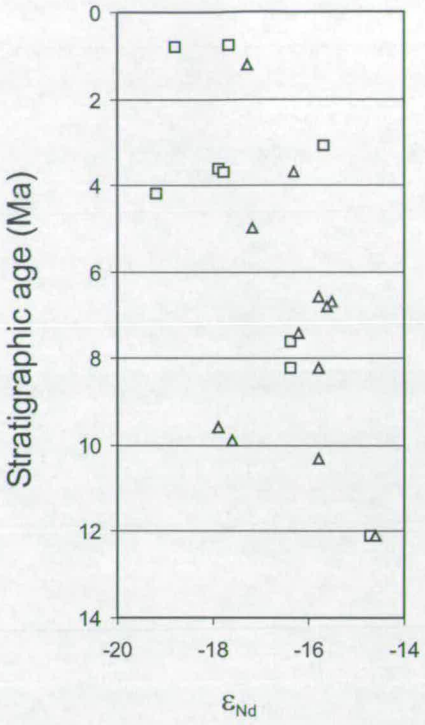


Figure 6.3. ε_{Nd} values for Nepalese molasse deposits versus stratigraphic height, from DeCelles et al. (2004). Most data is from Robinson et al. (2001), dashed line connects data from DeCelles et al. (2004).

Figure 6.4. ε_{Nd} values for the Surai Khola section (squares) and Karnali section (triangles) versus stratigraphic age, from Huyghe et al. (2001).



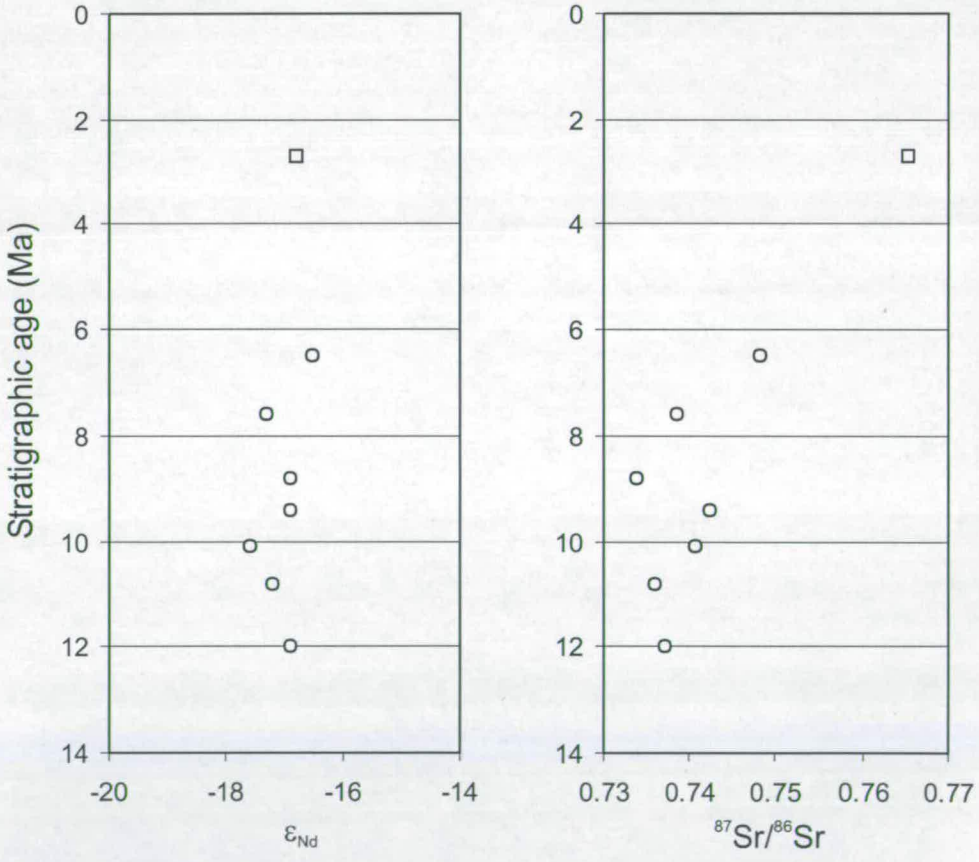


Figure 6.5. ε_{Nd} and $^{87}Sr/^{86}Sr$ values from this study versus stratigraphic age for Tinau Khola section mudstones (circles) and one Surai Khola section conglomerate matrix sample (square).

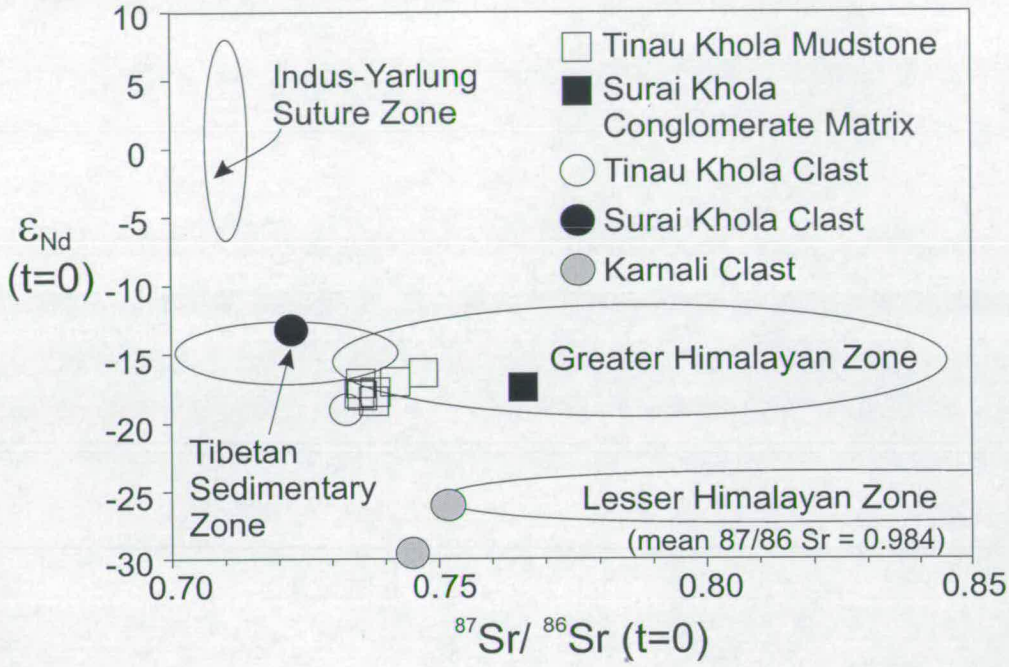


Figure 6.6. Whole-rock Nd-Sr isotopic data from the Tinau Khola section mudstone samples, a single Surai Khola conglomerate matrix sample, and quartzite clasts from all three sections, compared with typical values for major Himalayan tectonic zones. Two Surai Khola clasts with $\varepsilon_{Nd}/^{87}Sr/^{86}Sr$ values of -21.9/0.934 (DankPebbles, Surai Khola section, 3.1 Ma) and -18/0.875 (MSPebbles348, Surai Khola section, 4.8 Ma) fall outside the limits of the plot due to their high $^{87}Sr/^{86}Sr$ values. Modified from White et al. (2002). Ellipses illustrate 1σ distributions of fields, Lesser Himalayan $^{87}Sr/^{86}Sr$ ratios > 2 are excluded from the plot and ε_{Nd} values restricted to the Inner Lesser Himalaya.

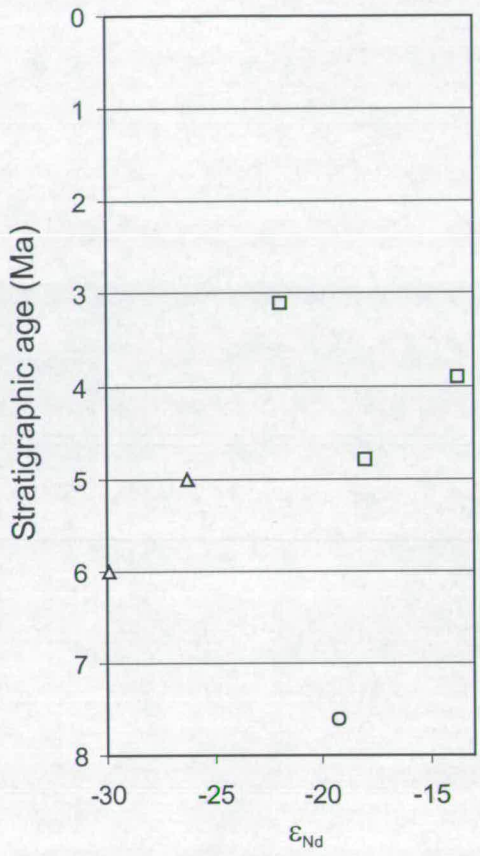


Figure 6.7. ε_{Nd} values for quartzite clasts from the Tinau Khola section (circle), Surai Khola section (squares), and Karnali section (triangles) versus stratigraphic age.

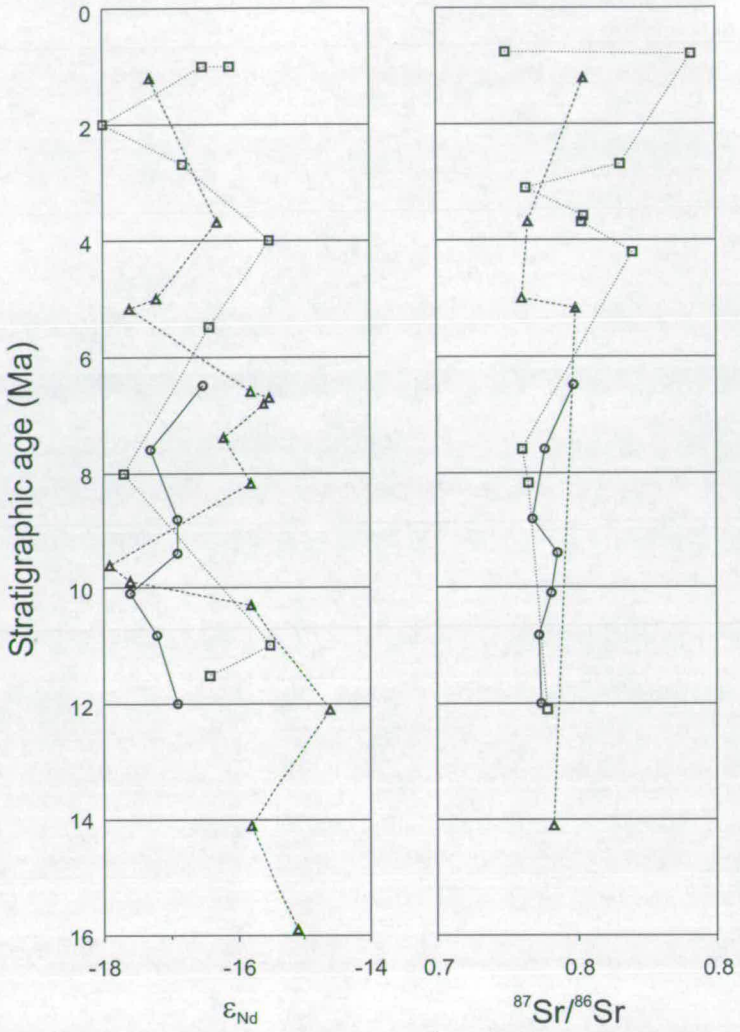


Figure 6.8. Variation in the geochemical signatures found in this study combined with those of other studies with stratigraphic age. Incorporates data from Galy (1999), Huyghe et al. (2001), Robinson et al. (2001) and five unpublished samples from P. Huyghe.

7. ^{40}Ar-^{39}Ar Thermochronology

7.1. Introduction

Detrital mineral thermochronology has been used to investigate the thermal evolution of basins (Brandon & Vance, 1992); source-area characteristics (Krogh & Keppie, 1987; Hurford & Carter, 1991; Garver & Brandon, 1994); stratigraphic age of the host sediment (Najman et al., 1997); and the erosional and tectonic history of orogens (Garver & Brandon, 1994; Bernet et al., 2001). First described by Merrihue & Turner (1966), ^{40}Ar-^{39}Ar dating has become synonymous with the detrital technique. ^{40}Ar-^{39}Ar dating of white mica is an ideal detrital thermochronology method because a single and relatively precise age can be obtained which represents cooling due to exhumation and is not affected by extreme weathering or burial (Najman et al., 1997, 2001). Each mineral within a given isotopic system has a critical temperature at which the mineral cools to stabilise the daughter product (Cliff, 1985). The closure temperature for Ar in white mica is low enough to give a good indication of later stage exhumation, but high enough to avoid resetting wider "normal" burial conditions. The detrital grain age obtained represents the time of cooling through the white mica closure temperature in the source region as long as there has not been any post-burial resetting.

In orogenic terrains isotherms migrate through rocks during exhumation, cooling minerals below their respective closure temperatures. Mineral ages are therefore indicative of exhumation history. Given a relatively undeformed, first-cycle sedimentary sequence, each horizon may preserve the specific time when the white

mica detritus passed through the argon closure temperature in the source region. Even if the sequence is not continuous then the mineral cooling ages give information regarding the exhumation of the source area when compared to the host sediment depositional age. Because the cooling age of rocks in different source areas can be diagnostic, sediment provenance analysis is also an important application of detrital thermochronology, and can be used in conjunction with petrographic and geochemical data (e.g. Hurford and Carter, 1991; Carter, 1999; Gehrels et al. 1999). Detrital ages can also give a maximum age for sedimentation where no other dating method is possible. A further aspect of detrital thermochronology in provenance analysis is its application in landscape evolution studies. Provenance information can be used to trace pathways of sediment transport (Cawood and Nemchin, 2001), and detect positions of drainage divides relative to distinct tectonic units (Von Eynatten et al., 1999; Spiegel et al., 2001; Von Eynatten and Wijbrans, 2003). Such information can be invaluable in reconstructing the dynamic evolution of orogens through time. Furthermore, this information can help the reconstruction of palaeocurrent directions and identify marine connections, which in turn have implications on palaeoecology and climatic evolution.

One advantage of ^{40}Ar-^{39}Ar dating over the traditional K-Ar method is that it allows the step-heating technique. Complex polymetamorphic histories often result in the occurrence of an excess argon component in the mineral grain or in radiogenic argon loss. Both processes induce incorrect age determination. If ^{40}Ar-^{39}Ar ages give a flat plateau from step-heating ages, this indicates the sample was a closed system for both Ar and K since it last cooled. The lowest temperature steps are those most

likely to be affected by alteration and therefore if all steps are similar, giving a flat plateau, little alteration has taken place. A further advantage of step heating is that the plateau age is the most reliable age for the mineral grain.

Like the K-Ar dating technique, the ^{40}Ar-^{39}Ar method is principally based on the decay of ^{40}K to ^{40}Ar but ^{40}K is measured in an indirect way. K-bearing minerals, such as K-feldspars, amphiboles, or white mica, are irradiated with fast neutrons in a nuclear reactor. Irradiation causes the formation of ^{39}Ar by a neutron capture/proton emission reaction. ^{39}Ar can be used as a measure for ^{39}K, and, since the $^{39/40}K$ ratio is constant in the crust, also as a measure for ^{40}K (McDougall & Harrison, 1988). The ^{40}Ar-^{39}Ar method has the advantage over K-Ar dating in that K and Ar are determined on the same sample and that only measurements of Ar isotope ratios, instead of absolute concentrations, are required. Therefore, this method can be used to date relatively small samples. The most commonly used mineral in ^{40}Ar-^{39}Ar studies of detrital grains is white mica (e.g., Najman et al., 2001; Von Eynatten & Wijbrans, 2003). White mica ($K_2Al_4[Si_6Al_2O_{20}](OH,F)_4$) occurs in a wide variety of geological environments, over a wide metamorphic range, and within intermediate to acid igneous rocks. It is also a common constituent of pegmatites associated with granites and granodiorites (Deer et al., 1992).

Detrital ages are bound to provide a more complete sampling of the source area than can be attained from isolated bedrock cooling ages that are then extrapolated to a wider region. Although detailed studies on individual bedrock samples can provide a rich cooling history, such studies commonly provide data on a few discrete points in

a landscape and are restricted to existing outcrop or boreholes. This means that very few rocks presently exposed will contain information about exhumation during a specific period. Additionally, thermochronology on bedrock is limited by the fact that only a narrow depth range within the lithosphere has a temperature distribution appropriate to the dating technique used. In contrast, a handful of sand can contain thousands of grains extracted from throughout the catchment region of the source river, including areas with glaciation or extreme relief, conditions which thwart direct bedrock sampling. Thermochronologic studies of detrital samples can therefore potentially encapsulate the full spectrum of bedrock cooling ages in a catchment (Brandon & Vance, 1992; Garver et al., 1999).

7.2. The lag-time concept

^{40}Ar-^{39}Ar dating of muscovite yields ages that reflect the time at which a particular grain cooled below its closure temperature, ~ 350-420°C in the case of muscovite depending on crystal size, cooling rate and the kind of white mica (phengite, muscovite etc.) used (Dodson, 1973; 1979; McDougall and Harrison, 1988; Von Eynatten and Wijbrans, 2003). The time difference between the mineral cooling age and the depositional age of the host sediment is commonly termed the lag-time (e.g. Garver et al., 1999). The lag-time is thus a measure of the relative exhumation rate in the source area prior to deposition of the mineral analysed, integrating the mineral closure temperature over the time needed for exhumation of the mineral to the surface, to the time of erosion, transportation and deposition. Exhumation rate is thus expressed as:

$$\varepsilon_m = [(Tc-Ts)/G] / \Delta T$$

where ε_m = exhumation rate (modal value of the range of rates calculated), Tc = mineral closure temperature, Ts = mineral surface temperature, G = geothermal gradient at the time of mineral blocking, and ΔT = lag-time. Thus the muscovite lag-time portrays the relative exhumation rate, whilst the range of ages obtained is a function of the duration of the exhumation event. Modelling the thermal structure of the crust at the time of uplift then allows the quantification of exhumation rates from the lag-time data (Fig. 7.1.). Deriving lag-times for minerals throughout a foreland basin succession therefore enables an assessment of the exhumation history of the hinterland throughout the time of sedimentation. Exhumation rates are not necessarily the same as erosion rates because crust may be exhumed by extension as well as erosion (Vance et al., 2003). Mineral ages may not also simply reflect the rise of a rock towards the surface but could reflect a relaxation of the geothermal gradient together with normal erosion. Therefore uplift rates are apparent rather than real and the term exhumation rate is more accurate.

7.3. Limitations

Detrital thermochronology limitations are associated with obtaining a representative range of ages and modelling constaints, and technical aspects associated with radioactive decay, laboratory measurement of isotopes, and data interpretation. Along with the factors listed below, determination of an accurate age for the host sediment is a separate limitation to obtaining reliable lag-times (see Chapter 4 for magnetostratigraphy limitations).

Detrital thermochronology relies on a number of fundamental assumptions. It is assumed that the mineral age has been preserved after weathering, transportation and deposition. The technique is only possible if the mineral has not been altered or reset above its closure temperature since burial. Testing that this has not occurred (by using techniques such as step heating, illite crystallinity, and electron microprobe analysis of the mineral) is critical. Specific requirements should be satisfied when using detrital minerals in an exhumation study. These are sufficient age precision; preservation of the cooling age after weathering, transportation, and deposition; adequate sedimentary mixing to provide a basin-wide representation; and rapid transport times to minimise sediment storage.

7.3.1. Transport times

The time for erosion and transport is regarded as geologically instantaneous compared to the time needed for exhumation. If some delay had occurred however, due to ponding behind an emergent thrust for example, the calculated lag-times would underestimate hinterland exhumation rates. Therefore, short lag-times can always be interpreted as rapid exhumation whereas long lag-times need not mean slow exhumation.

7.3.2. Number of grains

It is assumed that there has been adequate sedimentary mixing for a detrital sample to be able to capture values represented in the basin. A minimum of ~ 50 grains should be dated to try and ensure the fullest range of values are captured (Brewer et al., 2003). In fact Brewer et al. (2003) calculate that ~ 60+ grains for a simple one basin source area and ~ 90+ grains for a more complex 2-basin source area are needed to achieve a mismatch between calculated ages and the age range of the catchment of ≤ 15 % at the 95 % confidence level. This uncertainty in capturing all ages and the possibility of a delay in transport time means the youngest mineral cooling age obtained from a detrital sample batch can only be used to interpret a minimum exhumation rate because of the possibility that younger grains have been missed in the sampling.

Although detrital thermochronologic ages are a direct product of cooling and erosion in the source area, the frequency distribution of ages also reflects the topography, mineral distribution, and geomorphology of the contributing catchment (Brewer et al., 2003). It has not yet been possible to model such complexities with any accuracy. Several thermochronology studies have shown that, for any given erosion rate, topographic relief will produce a spectrum of ages and deflect isotherms (e.g. Henry et al., 1997; Stuwe & Hintermuller, 2000). Figure 7.2. shows histograms of theoretical detrital white mica ages depending on exhumation rate and duration. Brewer et al. (2003) show that hypsometry defines the shape of the detrital age frequency range. This natural variability commonly introduces incalculable complexity into the interpretation of detrital ages derived from the stratigraphic

record because past hinterland relief is unknown. Increasing relief causes greater deflection of isotherms from their original horizontal orientation and as erosion rates increase, all isotherms move closer to the surface (causing maximum deflection of the lowest temperature isotherms). This process does not have a significant effect on the ~ 350°C white mica isotherm however (Brewer et al., 2003). Stock & Montgomery (1996) used the cooling age signal in basins to constrain palaeotopography. They found that a sample of 40 grains is required to provide a 90 % probability of capturing 90 % of the relief of a basin. Detrital cooling age frequencies will also be weighted towards lithologies that supply more thermochronometer per unit area if the source area comprises numerous contrasting rock units. Differential erosion rates across a catchment (a likely scenario) represent another potential source of error, biasing the number of grains collected from different provenance areas.

7.3.3. Interpretation of ages

The inability to determine whether a sample accurately represents the range of white mica ages in a catchment presents a limitation on the detrital thermochronology technique in terms of which mineral cooling age to use for determining a lag-time. In some cases a sample may yield a large group of similar ages but also one very young grain age. The single young grain would provide a short lag-time but is not representative of the sample and may be anomalous. Taking an average age is also unsatisfactory due to the range of ages normally obtained and the fact that information regarding exhumation rates depends on the shortest lag-times. Therefore in this study we quote both the youngest single grain ages and the youngest peak

ages from a cumulative probability plot of the entire population (e.g. Fig. 7.8.). The cumulative probability plot statistically weighs all grain ages in terms of their abundance and error. All interpretations are based on the youngest peak age data because these are statistically more robust.

7.3.4. Types of white mica

The paragenesis of white mica is such that different metamorphic conditions will result in white micas with distinct chemistry and therefore radiogenic isotope retentivity. The name phengite is used to describe white micas in which the Si:Al ratio is greater than 3:1 and in which an increase of Si is accompanied by substitution of Mg or Fe^{2+} for Al in octahedral sites. Phengitic white mica ($K_2[Al_3(Fe,Mg)][Si_7Al,O_{20}](OH,F)_4$) is formed in pelitic sediments by replacing illite during epizone metamorphism (Yardley, 1989). Phengite is commonly formed during low-grade regional metamorphism and high-pressure metamorphism of pelites, whereas muscovite is common in higher grades (garnet to sillimanite). It is possible to distinguish between the two types but for our purposes this is not necessary and the presence of high-pressure rocks in the source area is unknown. If a source area comprised a mixture of phengite and muscovite that could not be differentiated, the difference in closure temperature for Ar between the two types would greatly increase the potential error for calculation of exhumation rates because this is controlled by closure temperature. Phengite is however unlikely to be abundant in the source area for the Siwalik Group of Nepal and so would not be hazardous to the determination of exhumation rates in this study.

7.3.5. Geothermal gradient

The depth to the white mica blocking temperature is estimated by making assumptions about the minerals closure temperature and the thermal structure of the crust. Any exhumation calculations therefore require an estimate of the evolving geotherm. This perhaps provides the greatest potential for error in the thermochronology method. Nevertheless, the time between exhumation initiation and the geotherm attaining an equilibrium depth is short. As exhumation rate increases this response time decreases and consequently so does the accuracy of the technique.

The geothermal gradient at the time of exhumation is assumed to be predictable and amenable to modelling. Most studies assume a vertical rock trajectory towards the surface, with erosion occurring perpendicular to that path. Indeed, the main consequence of denudation by erosion is to enhance heat advection, resulting in a steeper near-surface geothermal gradient. Therefore assuming a constant geothermal gradient may result in overestimating exhumation rates (Moore & England, 2001). More complex processes involving lateral advection due to horizontal shortening are also difficult to model (Batt & Brandon, 2002; Willett & Brandon, 2002). Equilibrium thermal structure and isothermal geometry are further assumptions. Unfortunately, high denudation, high local relief, or underthrusting of colder rocks can strongly affect or even temporarily reverse the normal geothermal gradient and greatly complicate data interpretation. These issues are particularly applicable to the Himalayas where erosion occurs at least in part as rocks are uplifted along structural ramps. Such rocks can have a complex thermal history. Cooling by the under-

thrusting slab, accretion of under-thrust material to the hanging wall, shear heating, and time can all affect the thermal structure and resulting cooling history.

In this study we employ the modelling work of White (2001) to determine the evolution of the Himalayan geotherm. White (2001) used an analytical solution for the combined advective and conductive 1D transport of heat and matter (Bickle & McKenzie, 1987), ignoring heat generation by radioactive decay and chemical reactions. The model also ignores the effects of topography and relief and assumes vertical particle trajectories at constant velocity. White (2001) approximated the exhumation history of the Himalayan crust using equations 18 and 24 from Bickle & McKenzie (1987) (Fig. 7.3.). Our modelled crust is 35 km thick and 700°C at the base giving a geothermal gradient of 20°C/km (sympathetic to peak M1 metamorphic conditions). In most mountain belts movement of rock occurs from the mid to lower crust to the surface along decollements, therefore depths of 35 km are appropriate. This is a reasonable approximation for the thermal structure of overthrust crust 10-20 Myr after thickening in which temperatures increase to 650-750°C over the top ~ 35 km and then exhibit smaller increases over the lower part of the crust partly due to its lower time constant and partly because maximum temperatures are probably buffered by melting (e.g. Spear, 1989). White (2001) incorporated the relaxation of the thermal gradient over time as exhumation rates decrease in a second model.

7.3.6. Closure temperature

Mechanisms other than temperature can affect the retentivity of radiogenic isotopes within a mineral (Dodson, 1973; Jenkin, 1997). For example, fluid migration (can enhance diffusion and promote re-crystallisation) and deformation (faulting enhances fluid flow and damage to the crystal lattice can promote isotope mobility) within a rock can play a dominant role in isotope behaviour (Villa, 1997). Additionally, if a white mica is formed or re-crystallised below its closure temperature, the age will reflect the time of crystallisation, not the time the white mica reached its closure temperature. Also, the closure temperature can be affected by grain size, composition, inherited radiogenic ^{40}Ar, and the rate of cooling through the closure interval (Dodson, 1973). In this study we assume the closure temperature for white mica is 400°C which ignores the effects of cooling rate and grain size.

7.4. Previous work

7.4.1. Exhumation studies

The pioneering detrital thermochronology study in the Himalayas was undertaken by Cerveny et al. (1988) in the Potwar area of northern Pakistan using fission-track dating of detrital zircons. Their data show that throughout the 18 Myr record, depositional ages and the youngest mineral cooling ages differed by less than 3 Myr. Thus rapid bedrock uplift and erosion must have been sustained at various sites within the Indus catchment throughout the Neogene. Based on ^{40}Ar-^{39}Ar dating, subsequent studies have demonstrated a similar coincidence of cooling and depositional ages (Copeland & Harrison, 1990; Harrison et al., 1993). It therefore

seems apparent that bedrock uplift rates, cooling, and denudation at rates similar to those today at Nanga Parbat (> 3 mm/yr; Zeitler, 1985) have been present in the Himalayas throughout the Neogene. This data has been used as evidence for accelerated Early Miocene Himalayan uplift to account for such rapid rates of exhumation by the start of the Neogene (Harrison et al., 1992).

A commonly cited detrital ^{40}Ar-^{39}Ar study within the Himalayas is that by Copeland & Harrison (1990) who applied the technique to single K-feldspars (n = 68) and muscovites (n = 49) from the Bengal Fan (Fig. 7.4.). This provided a stratigraphic link between the Bengal Fan and tectonic events in the source area. Host sediment depositional age is a vital requirement with any detrital investigation and in the case of the Bengal Fan sediments (18-0 Ma) this was achieved using the palaeontological record (e.g. Gartner, 1990; Cochran, 1990). Copeland & Harrison (1990) recorded a zero-aged lag-time at every stratigraphic level and concluded that throughout the Neogene some part of the orogen was undergoing rapid exhumation and erosion (1-10 mm/yr). The same conclusion was derived from fission-track dating of detrital apatites from the Bengal Fan which indicate minimum orogen-wide average erosion rates of 0.5 to 1.5 mm/yr during the last 18 Ma (Corrigan & Crowley, 1990). Copeland & Harrison (1990) suggested very rapid uplift (> 5 mm/yr) was distributed in brief pulses over different parts of the mountain belt from the Miocene onwards. However, they also record a small population of negative lag-times (where the mineral cooling age is younger than its age of sedimentation), which is problematic and may reflect diagenesis. Although clearly derived from the Greater Himalaya, the authors were unable to identify a more exact provenance for the youngest grains

because of the lack of such cooling ages found by bedrock studies. This is one example of the value of combining detrital thermochronology with other provenance techniques such as petrography and geochemistry. The Bengal Fan receives sediment from a large part of the Himalayas and because of this any tectonic inferences drawn by the detrital work of Copeland & Harrison (1990) cannot be tied to specific source locations. More recent detrital studies have therefore been carried-out on sediments closer to the mountain belt. These provide a clearer picture of orogenic evolution because a more restricted drainage area limits the extent of the potential source zone.

Harrison et al. (1993) investigated two terrestrial molasse deposits using ^{40}Ar-^{39}Ar dating of detrital K-feldspars. For the Bakiya Khola section foreland basin sediments in south-central Nepal (10.8-4.9 Ma depositional age), east of the present field area, the minimum lag-time throughout deposition was ~ 3 Myr. This suggests relatively rapid exhumation of the source area during that time. In a related study Burner (1995) undertook ^{40}Ar-^{39}Ar dating of K-feldspar grains and calculated average exhumation rates of 2.1 and 1.1 mm/yr for the Bakiya Khola section and Surai Khola section further west. The Bakiya Khola ages ranged mainly between 21-7 Ma, however, only 26 % of the Surai Khola ages were younger than 21 Ma. Burner (1995) found that the average difference between the minimum mineral age and stratigraphic age is 10.5 and 12.6 Ma for the Bakiya Khola and Surai Khola sections respectively. The fastest exhumation rates recorded by the Surai Khola section occurred between 5-6 Ma (4-5 Myr lag-time). The Bakiya Khola section showed 1-2 Myr lag-times between 8-9 Ma and again at 5-6 Ma. Fission-track ages from detrital

zircons in the Siwalik sandstones of northern Pakistan and India also suggest rapid uplift of the Himalayas over the past ~ 20 Ma (Zeitler et al., 1986). White et al. (2002) found no evidence for equally short lag-times between 17 Ma and 12 Ma from ^{40}Ar-^{39}Ar dating of white mica belonging to the Upper Dharamsala and Lower Siwalik units of NW India (Fig. 7.5.). They did however find evidence for rapid exhumation (1-3 Myr lag-times) within the Lower Dharamsala Member (21-17 Ma depositional age), which was deposited during sillimanite-grade metamorphism and Main Central Thrust movement. White et al. (2002) used thermal modelling to show that their mica age distribution could relate to high exhumation rates of up to 5 mm/yr prior to Lower Dharamsala deposition followed by rates of 1 mm/yr from 20 Ma onwards, broadly consistent with Greater Himalayan bedrock data. On the contrary, ^{40}Ar-^{39}Ar K-feldspar ages from a clast of the Kailas conglomerate in Tibet indicate a change from slow to very rapid cooling at ~ 19 Ma (Harrison et al., 1993). The different conclusions of these studies highlights the value of conducting numerous local detrital investigations along the length of a mountain belt to substantiate records for periods of regional activity and also allow a greater appreciation of tectonic diachroneities.

7.4.1.1. Modern Rivers

As with ancient sediment, modern river sand contains a thermochronological record of orogenic evolution. Bertrand et al. (2001) obtained ^{40}Ar-^{39}Ar ages of detrital muscovites from the sands of modern rivers in central and western Nepal. They found a subtle correlation between grain size and mineral age, suggesting the coarser material yields younger ages. The Karnali River gave a mode of 18 Ma and a mean of 16 Ma from 210 grains whilst the Narayani River gave 9.5 Ma and 10.5 Ma respectively. Similar to previous studies they found no micas younger than 4 Ma, indicating that the source area has not undergone rapid exhumation in the last few million years. The authors suggest no region in central Nepal has experienced sustained rates of erosion greater than approximately 6 mm/yr during the last 2-3 Myr. During the past few Myr, it thus appears that only the syntaxes of the Himalayas have undergone rapid erosion. Brewer et al. (2003) performed ^{40}Ar-^{39}Ar dating on muscovites from the Marsyandi and Dordi rivers in central Nepal. Grains from the upper Marsyandi gave an age range of 11.2 ± 1.4 to 18.7 ± 1.3 Ma with a sharp peak at ~ 17 Ma and a younger tail from 10-14 Ma (n = 35). The Dordi ages ranged from 2.6 ± 1.2 to 12.7 ± 0.5 Ma (n = 39). Using a thermal model they calculate erosion rates of 0.95 km/Myr for the upper Marsyandi and 2.15 km/Myr for the Dordi basin.

7.4.2. Other uses of detrital ^{40}Ar-^{39}Ar ages

Not all of the Himalayan tectonic zones have reached temperatures sufficient to crystallise, re-crystallise or reset micas within the bedrock. Although detrital grains with pre-Himalayan signatures cannot quantify exhumation rates, they can be

important in distinguishing provenance between tectonic zones. For example, Lesser Himalayan lithologies largely retain pre-Himalayan cooling ages (with minor garnet grade exceptions such as in Sutlej), and are therefore distinguishable from the Greater Himalaya by mineral age alone. Using this approach, Najman et al. (1997) found that white mica from the Dagshai Formation in NW India yields Himalayan ages, and they used this to show that the Greater Himalayan thrust stack had began unroofing by the start of deposition.

The variation in mineral age data and exhumation rates provides information regarding the possible steady-state of an orogen. Where the youngest white mica ages decrease in proportion to the host sediment stratigraphic age (giving a constant lag-time) this is indicative of an exhumational steady-state (Willett & Brandon, 2002). Brewer et al. (2003) predict that for muscovite, deformation and erosion must remain steady for 5 Ma or more before a thermal steady-state can be approached. Bernet et al. (2001) utilised downstream changes in detrital age populations to examine the mixing of source areas with different cooling ages. They used the difference between the mineral cooling ages and the depositional ages to test for the presence of thermal steady-state.

Other significant work using ^{40}Ar-^{39}Ar detrital ages has been within otherwise non-datable sedimentary rocks of the Himalayan foreland, to provide a maximum depositional age. Using this technique Najman et al. (1997, 2001) constrained the age of foredeep deposits in NW India and Pakistan. ^{40}Ar-^{39}Ar dating of single white micas has provided maximum depositional ages of < 28 Ma and < 25 Ma for the

Dagshai Formation at two localities and < 28 Ma and < 22 Ma for the Kasauli Formation (Najman et al., 1997). These ages suggest the start of substantial exhumation and erosion from the rising Himalayas was occurring by ~ 28 Ma in NW India.

7.5. Methodology

Single grains of white mica (150 to > 425 μm) were handpicked from 36 sandstone samples and collected in Al foil pots. Sixteen single grains from four different samples were analysed using the step-heating technique to test for potential alteration. Nearly 1400 single grains where analysed by total fusion. The foil pots were irradiated at the in-core, dummy fuel element facility at the 1 MW TRIGA, Oregon State University. 21 samples were irradiated for seven hours (J = ~ 0.001) and 15 samples were irradiated for 12 hours (J = ~ 0.003). Standards were placed throughout the sample vial for calculating the irradiation flux parameter (J) value: J = $e^{\lambda t}$-1 / (^{40}Ar-^{39}Ar). The J value depends on sample location in the reactor and was monitored with either the Taylor Creek rhyolite (TCR-2a) at 27.92 Ma or the Fish Canyon tuff sanidine (FC-1) at 27.61 Ma, which were dispersed amongst the foil pots sent for irradiation. We used sanidine standards (cross-calibrated with biotite) since they are easy to clean from the machine after running. Analytical techniques and plateau age calculations follow White et al. (2002) except that samples were degassed. Errors are quoted at the 2σ level of analytical precision. Analysis was conducted at the Scottish Universities Environmental Research Centre (SUERC). All Karnali section samples were analysed at MIT whilst samples K1 to K4 were

also analysed at SUERC. Additional ^{40}Ar-^{39}Ar technique notes are given in Appendix V.

7.6. Results

The full laser fusion and step-heating ^{40}Ar-^{39}Ar data set is given in the cd at the back of the thesis. Step-heating of 16 of the larger Surai Khola white micas (not carried-out for the Tinau Khola and Karnali sections) yielded plateau ages that range from 14.8 ± 0.16 Ma to 20.08 ± 0.13 Ma (Table 7.1.). The ages are concordant within 95 % confidence intervals (MSWD < 2.5). Flat age plateaus indicate that the Siwalik white micas were closed for both Ar and K since initial cooling, reducing the possibility for alteration. For step-heating data, lower ages at low temperature steps are indicative of partial radiogenic ^{40}Ar loss, caused by heating or deformation whilst the converse is evidence for ^{39}Ar loss associated with recoil of the ^{39}K nucleus arising from emission of a proton during the (n,p) nuclear reaction. There is no evidence for either of these processes having affected the white micas studied because step-heating ages are consistent between temperature increments. The ages can therefore be interpreted as geologically meaningful. Although time and cost factors meant most ages were determined by total fusion, the validity of the total fusion age data is supported by the step-heating results.

Sample	Strat. age (Ma)	Plateau age (Ma)		error	MSWD
SKA14	1	15.89	±	0.12	1.92
SKA14	1	15.84	±	0.24	0.84
SKA14	1	14.80	±	0.16	1.10
SKA14	1	16.14	±	0.20	1.52
SKA14	1	15.48	±	0.01	0.79
SK2760	5	16.81	±	0.18	2.16
SK2760	5	15.15	±	0.20	2.03
SK2760	5	14.97	±	0.17	1.25
SK2760	5	20.08	±	0.13	1.11
SK2760	5	15.07	±	0.11	1.25
SK1780	7	17.15	±	0.29	1.80
SK1780	7	17.90	±	0.43	0.63
SK1780	7	16.50	±	0.32	0.33
SK1780	7	17.13	±	0.18	0.55
SK1448	7.8	18.29	±	0.15	0.44
SK1448	7.8	16.04	±	0.17	0.22

Table 7.1. Step-heating results for Surai Khola detrital white micas.

Figure 7.6. shows the total fusion ages plotted against stratigraphic age. Figure 7.7. shows the variation of lag-time with stratigraphic age for the youngest mica and youngest peak age from a cumulative probability plot. Some mica ages from the Karnali section give errors of up to 4 Myr and two micas plot below the 1:1 line (probably due to alteration), good reasons to refer to the youngest peak ages rather than single grain age data. Typical errors are in the range of 0.2 to 1 Myr (2σ) for SUERC ages and 0.5 to 5 Myr for MIT ages (2σ). Lag-times generally increase up-section.

Cumulative probability plots of the post-collision ages (< 50 Ma, > 95 % of detrital grains) reveal Gaussian age distributions with a total combined mode of 16.8 Ma (Fig. 7.8.). Spiked frequency plots are partly due to ages with low errors, whereas wide tails are caused by ages with large associated errors. The highest age frequency

generally falls between 20-15 Ma. The youngest micas tend to be in lowest abundance (53 grains aged 14-15 Ma, 34 grains aged 13-14 Ma, nine grains aged 12-13 Ma, three grains aged 11-12 Ma, and three grains (two with high errors) aged 10-11 Ma). Pre-Himalayan ages span back to 1200 Ma, reflecting thermal histories prior to India-Asia collision, and are more abundant in sediment deposited at 12 Ma and older.

7.6.1. Tinau Khola section

From six samples, almost 90 % of Tinau Khola white micas (n=233) gave Himalayan ages (< 50 Ma). White mica ages range from 14.43 Ma to 1586.8 Ma. 51% of ages lie between 17 Ma and 23 Ma (period of Main Central Thrust movement), and the cumulative probability plot gives a total mode of 17.8 Ma. Less than 2 % of ages are Pre-Cambrian. There are no white mica ages that are younger than the stratigraphic age. Errors are very low with almost 90 % of grains yielding an error of less than 2 Myr and over 70 % give errors of less than 1 Myr (2 σ). The largest error of 20.2 Myr (2 σ) is for the oldest grain. White micas from the base of the section at 12 Ma give lag-times of 4.4/8.5 Myr (youngest mica age/youngest peak age), which relate to approximate exhumation rates of 2.3/1.5 mm/yr using 1D thermal modelling (White, 2001). The section then has minimum lag-times of 5-5.7/5.4-5.8 Myr between 9-10 Ma giving 2-2.1/2 mm/yr exhumation rates. Lag-times then gradually increase up-section and show a maximum of 8.34/8.6 Myr for 6.3 Ma sediment at the top (1.5/1.5 mm/yr exhumation rates).

7.6.2. Surai Khola section

From 15 samples, 99 % of Surai Khola white micas (n=664) gave Himalayan ages (< 50 Ma). White mica ages range from 10.76 Ma to 370.4 Ma. 52 % of ages lie between 17 Ma and 23 Ma and the cumulative probability plot gives a total mode of 16.8 Ma. Over 70 % of grains give errors of less than 1 Myr (2 σ). White micas from the base of the section at 12 Ma give lag-times of 4.44/6.4 Myr (youngest mica age/youngest peak age), which relate to approximate exhumation rates of 2.3/1.8 mm/yr. Lag-times are still relatively short for 10 Ma sediment (1.44/4.7 Myr), giving exhumation rates of 4.3/2.2 mm/yr. Lag-times then increase significantly to 13.8 Myr by 1 Ma at the top of the section (1.1/1.1 mm/yr exhumation rates).

7.6.3. Karnali section

From ten samples 88 % of Karnali white micas (n=478) gave Himalayan ages (< 50 Ma). White mica ages range from 10.33 Ma to 1704 Ma. 27 % of ages lie between 17 Ma and 23 Ma and the cumulative probability plot gives a total mode of 16.8 Ma. Errors for the Karnali ages are different depending on where the white micas were analysed. 69 % of the SUERC ages give errors of less than 1 Myr (2 σ) whilst only 40 % of the MIT ages give errors of less than 1 Myr (2 σ). It is important to note that the MIT analyses (n=309) gave younger white mica ages but higher errors. This difference most likely reflects machine sensitivity at the time and highlights the difficulty of achieving a similar level of ^{40}Ar-^{39}Ar age accuracy between laboratories. Combining the two sets of analyses, white micas at the base of the section at 16 Ma give the shortest lag-times of 0.9/3.6 Myr (youngest mica age/youngest peak age),

which relate to approximate exhumation rates of 5.4/2.6 mm/yr. Lag-times are 3.4/7.9 Myr for sediment at 12 Ma (2.7/1.6 mm/yr exhumation rates) and 4/4.5 Myr for sediment at 10.85 Ma (2.4/2.3 mm/yr exhumation rates). Lag-times then gradually increase up-section until reaching 12.5/12.7 Myr for sediment at 1 Ma (1.1/1.1 mm/yr exhumation rates).

7.7. Discussion

The metamorphosed Greater Himalaya must have been the main source for the post-collision aged (< 50 Ma) white micas, which dominate the three sections studied. White micas in the Lesser Himalaya are not as abundant and finer-grained. Older pre-collision aged micas could have been derived from a Lesser Himalayan, Tibetan Himalayan, or Greater Himalayan protolith source area but the absence of a distinct age group and the low abundance of these grains restrict their use as a provenance indicator. The cumulative probability plots do not show major differences between samples except a significantly older age population for the oldest Karnali samples and as such suggest the crust of the respective source areas was similar and underwent the same exhumation history.

The grain-size range we were able to analyse was limited by machine accuracy, thus biasing our picking towards larger grains. Where smaller grains (< 250 μm) had to be analysed they tended to yield older ages on average (Fig. 7.9.), leading in some cases to re-sampling in order to obtain larger grains. This could explain the appearance of older grains in older, finer sediment. However, because this apparent

grain-size bias means we simply risk missing some older ages it has no effect on the minimum lag-time and therefore on our interpretations.

In northern India, White et al. (2002) documented essentially zero-aged lag-times from micas in foreland basin sediments aged 20-17 Ma, indicating extremely rapid exhumation. Using simple one-dimensional thermal modelling, which allows for advective modification of the geotherm, they calculated exhumation rates of up to 5 mm/yr for the Greater Himalaya at 20 Ma, subsequently slowing to 1mm/yr. The present study shows no evidence of such rapid exhumation. Our shortest lag-time of 3.6 Myr (from youngest peak age) at 16 Ma equates to an approximate exhumation rate of 2.6mm/yr for the Greater Himalaya (Fig. 7.7.), using the same one-dimensional thermal modelling as described in White (2001). After ~ 10 Ma there are no lag-times shorter than 5 Myr (lag-time of 4.7 Myr at 10 Ma, corresponds to an approximate exhumation rate of 2.2 mm/yr) and subsequent exhumation was slower with a mean of 1.5 mm/yr.

A white mica age mode of 16.8 Ma indicates the period of most rapid Greater Himalayan unroofing, whereby maximum erosion is associated with maximum exhumation. This correlates well with isotope data from the hinterland (Hodges, 2000). The skewed cumulative probability age distributions with the mode close to the minimum age and a tail towards the maximum age is indicative of a terrain subject to variable exhumation rates, with maximum erosion from areas experiencing maximum exhumation (Garver et al., 2000). The trend of decreasing youngest peak ages up-section is indicative of continued exhumation into deeper levels of the

Greater Himalaya throughout the period under study. Increasing lag-times throughout the period of time studied indicates that exhumation of the Greater Himalaya was slowing down. The fact that there are no micas younger than 10-12 Ma, no lag-times less than 5 Myr after 10 Ma, and there is a change of provenance at ~ 12 Ma, indicates that this period represents the time of transference of exhumation south of the Greater Himalaya.

There is no evidence from the three Nepal sections to indicate late-stage (post-10 Ma) reactivation of the Main Central Thrust as purported by many workers (e.g. Harrison et al., 1997; Catlos et al., 2002) (Fig. 2.2.). However, it is possible that young ages were missed by the sampling process due to being volumetrically insignificant. Brewer et al. (2003) found very young ages in modern river sands but these were sampled close to the Main Central Thrust, not the foreland. It is conceivable that these young ages would become highly diluted by the time the river had passed through to the Gangetic Plain. Therefore, the lack of post-10 Ma mica ages within the Siwalik sediment does not negate the possibility of late-stage Main Central Thrust reactivation.

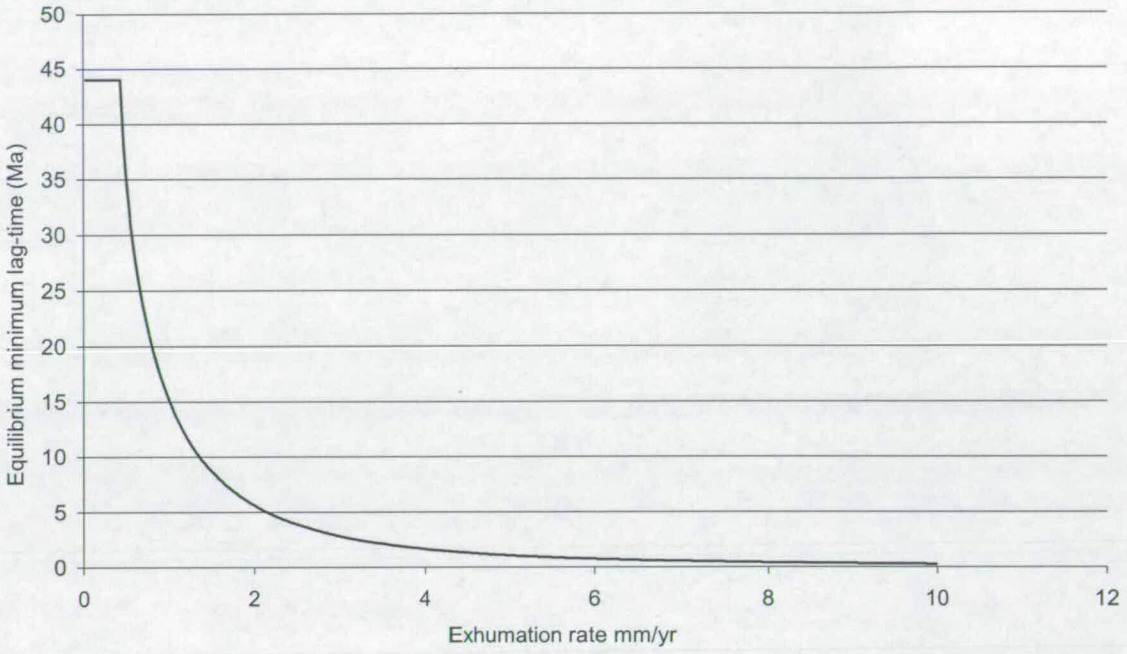


Figure 7.1. Equilibrium lag-time for a range of exhumation rates, based on a geothermal gradient of 20°C/km and a white mica closure temperature of 400°C.

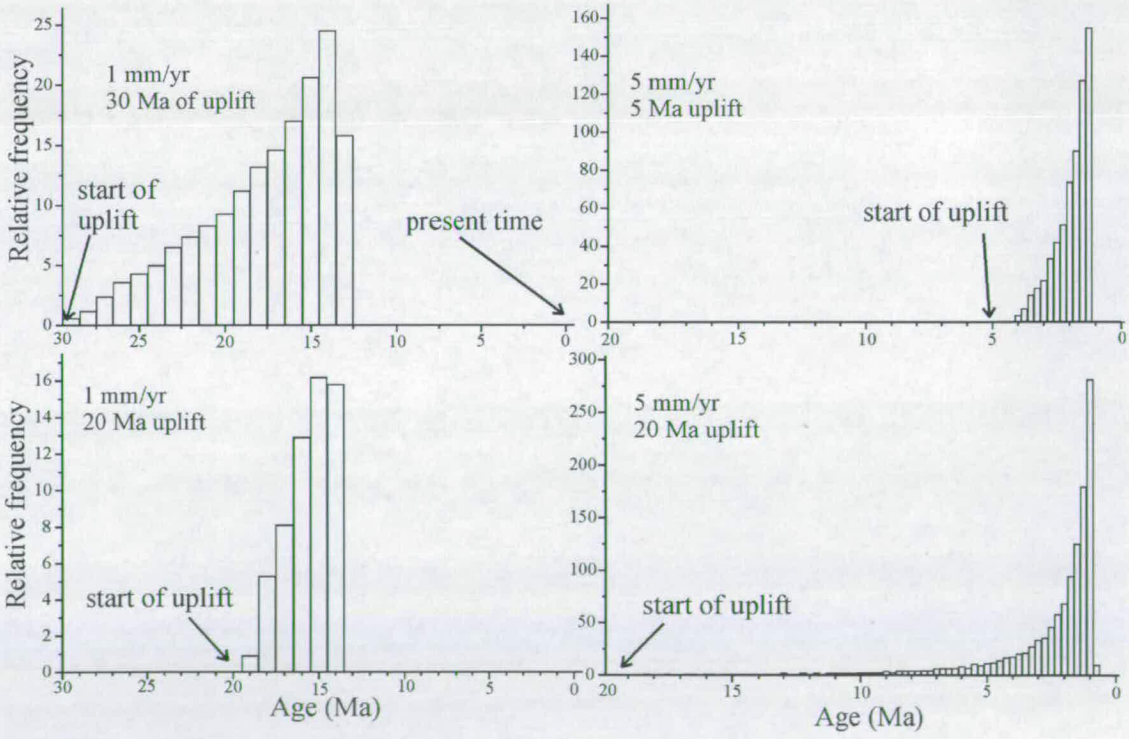


Figure 7.2. Modelled histograms of detrital white mica ages eroded from a catchment with variable exhumation rates after a fixed period of exhumation, from White (2001).

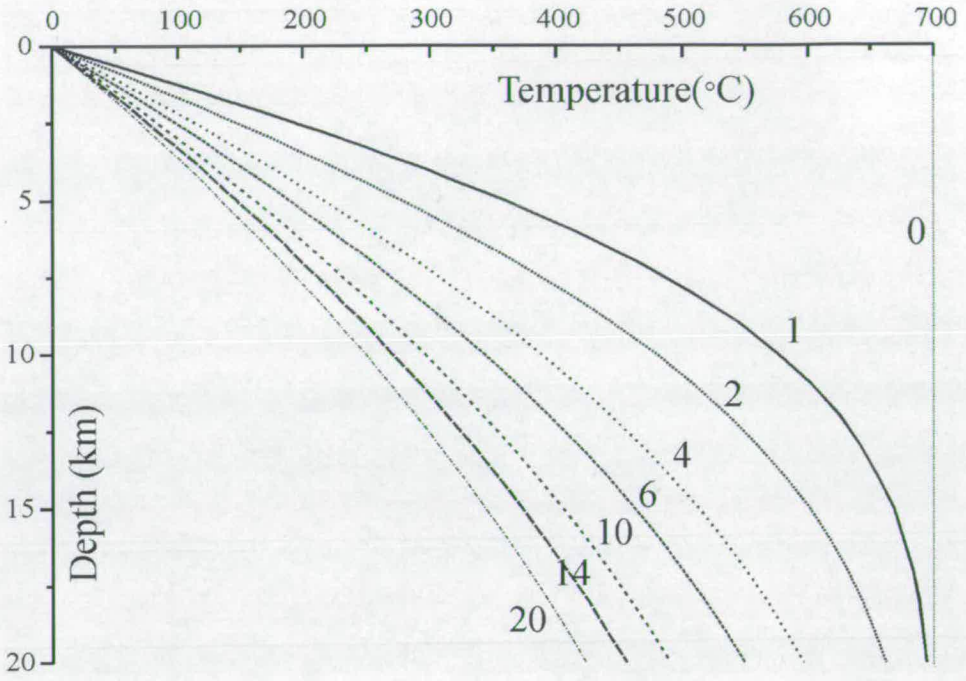


Figure 7.3. Geotherms for a cooling slab through time, from White (2001). Numbers refer to time in Myr's.

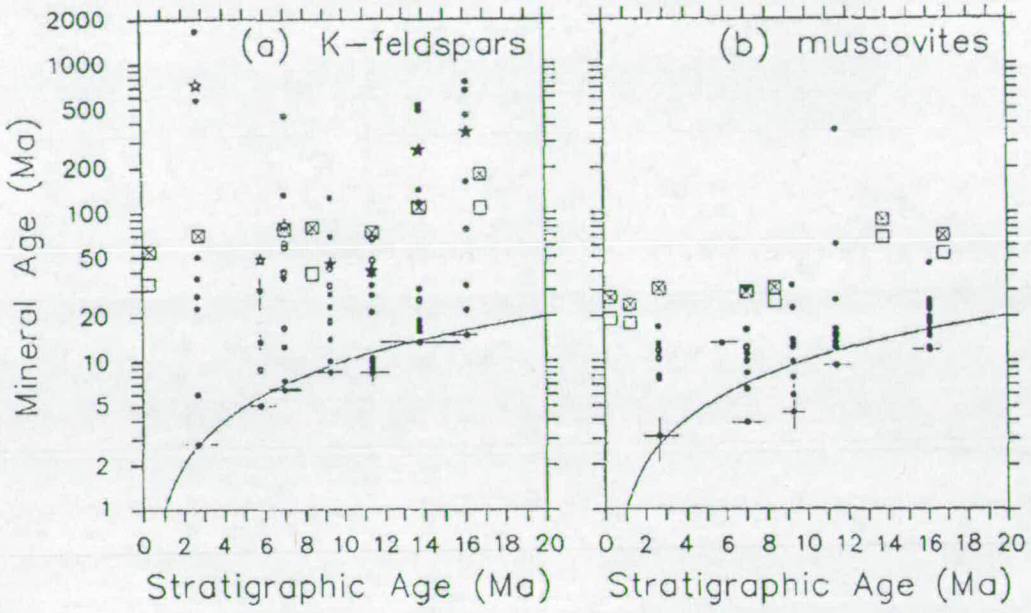


Figure 7.4. Mineral age versus host sediment depositional age plot for samples from the Bengal Fan, from Copeland & Harrison (1990). Circles represent minimum age on age spectrum or total fusion age where only one step was performed. Open squares represent minimum ages on age spectra from multigrain separates. Squares with X are total fusion ages of multigrain separates. Stars represent weighted average of single-crystal analyses from one stratigraphic interval. Curved line represents 1:1 line where mineral age equals host sediment age.

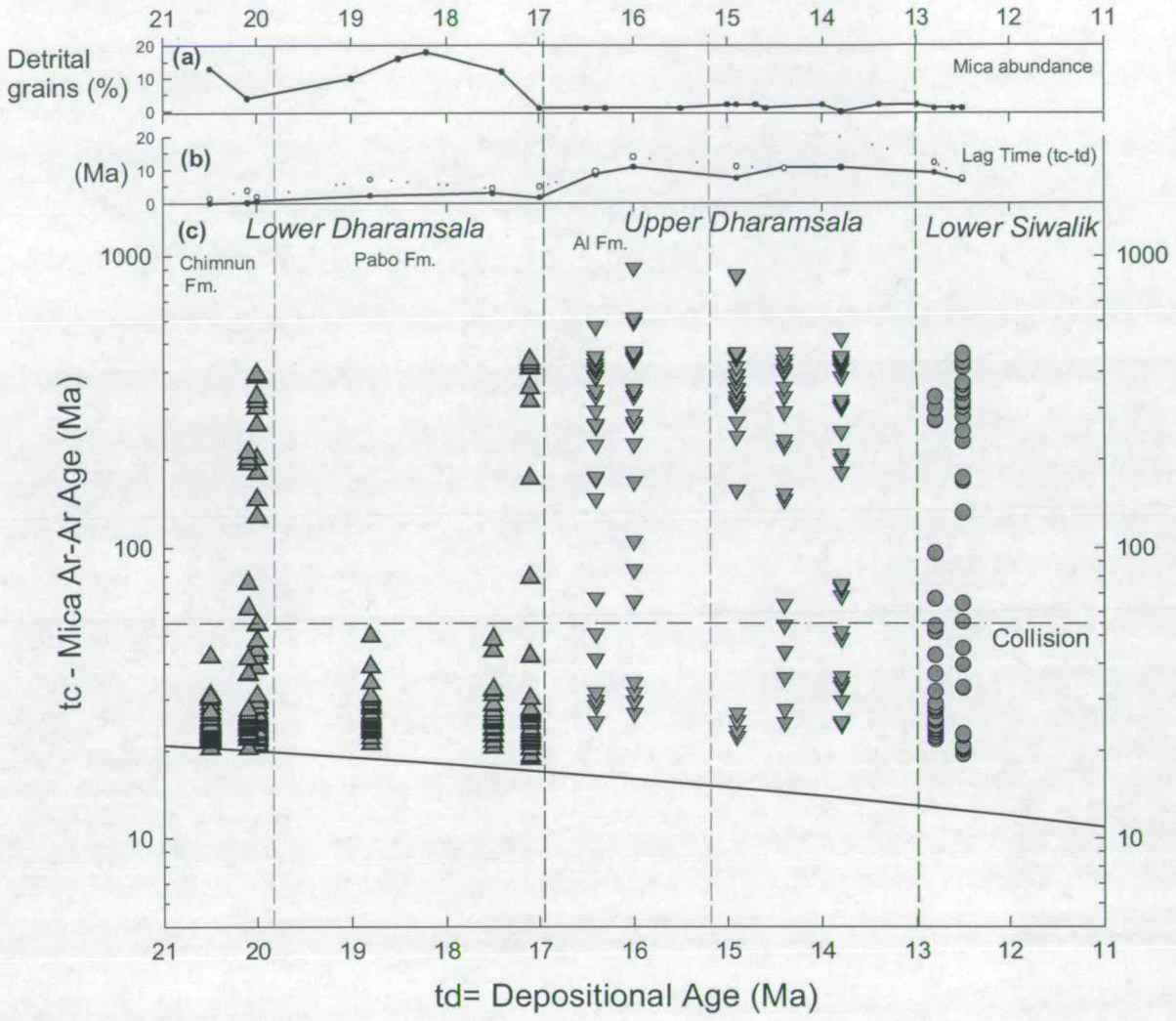


Figure 7.5. White mica ages versus depositional age of host sediment from the Dharamsala and Lower Siwalik succession in NW India, from White (2001). Also shown are the change in lag-times and mica abundance with depositional age.

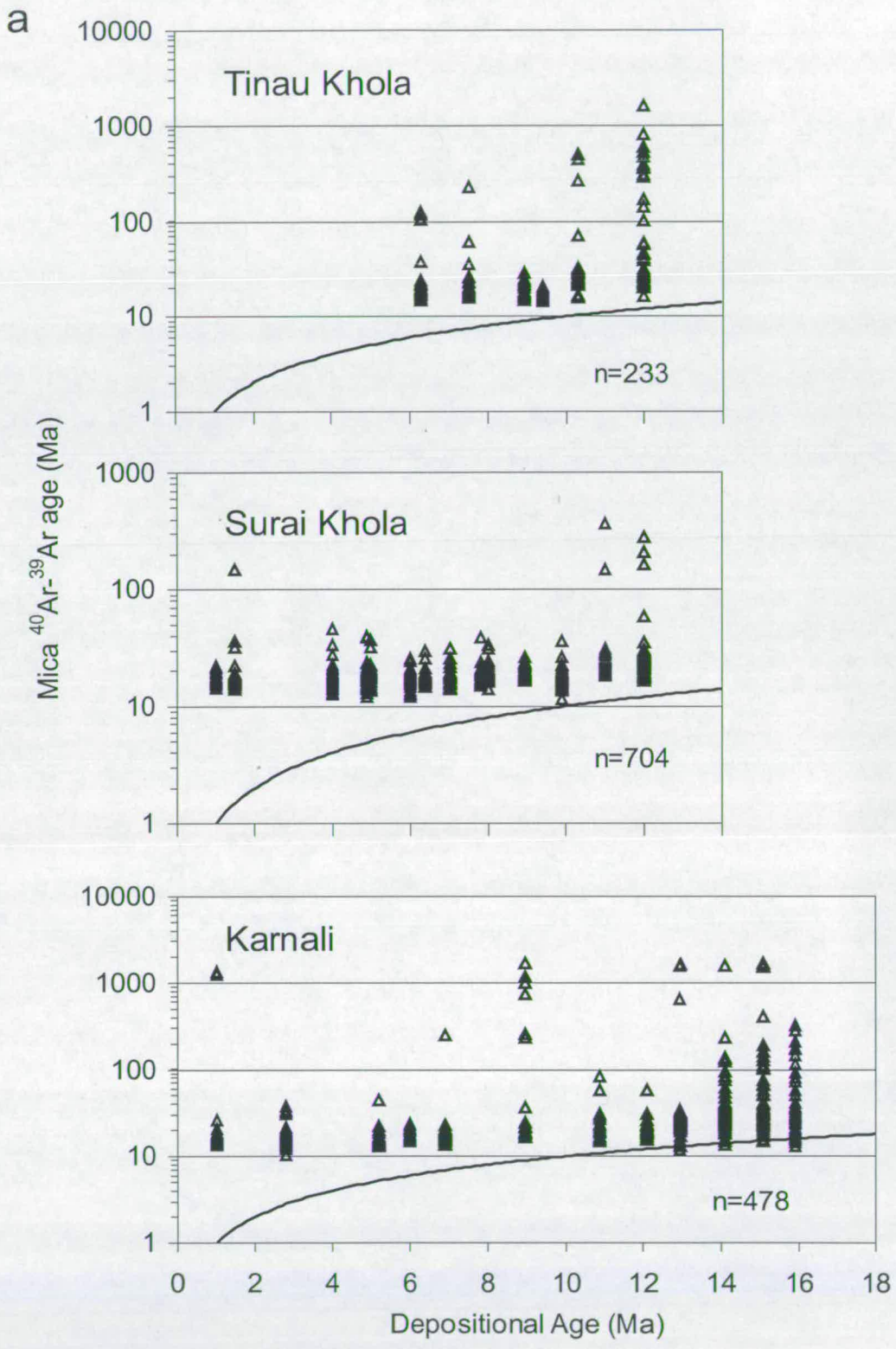


Figure 7.6.a Caption on next page.

Figure 7.6.a Semi-log plot of detrital white mica cooling ages versus the stratigraphic age of the host sediment for the three sections from this study. Curved line represents zero-age lag-times where mica age equals sedimentary age and so mica ages should lie above this line. Two white micas for the 16 Ma Karnali sample plot below the 1:1 line and are not within error of a zero-age lag-time. This could be due to some kind of alteration but they are only 2 in a data set of 1415 white micas. The modal age for the Tinau Khola section is 17.8 Ma and for the Surai Khola and Karnali sections is 16.8 Ma.

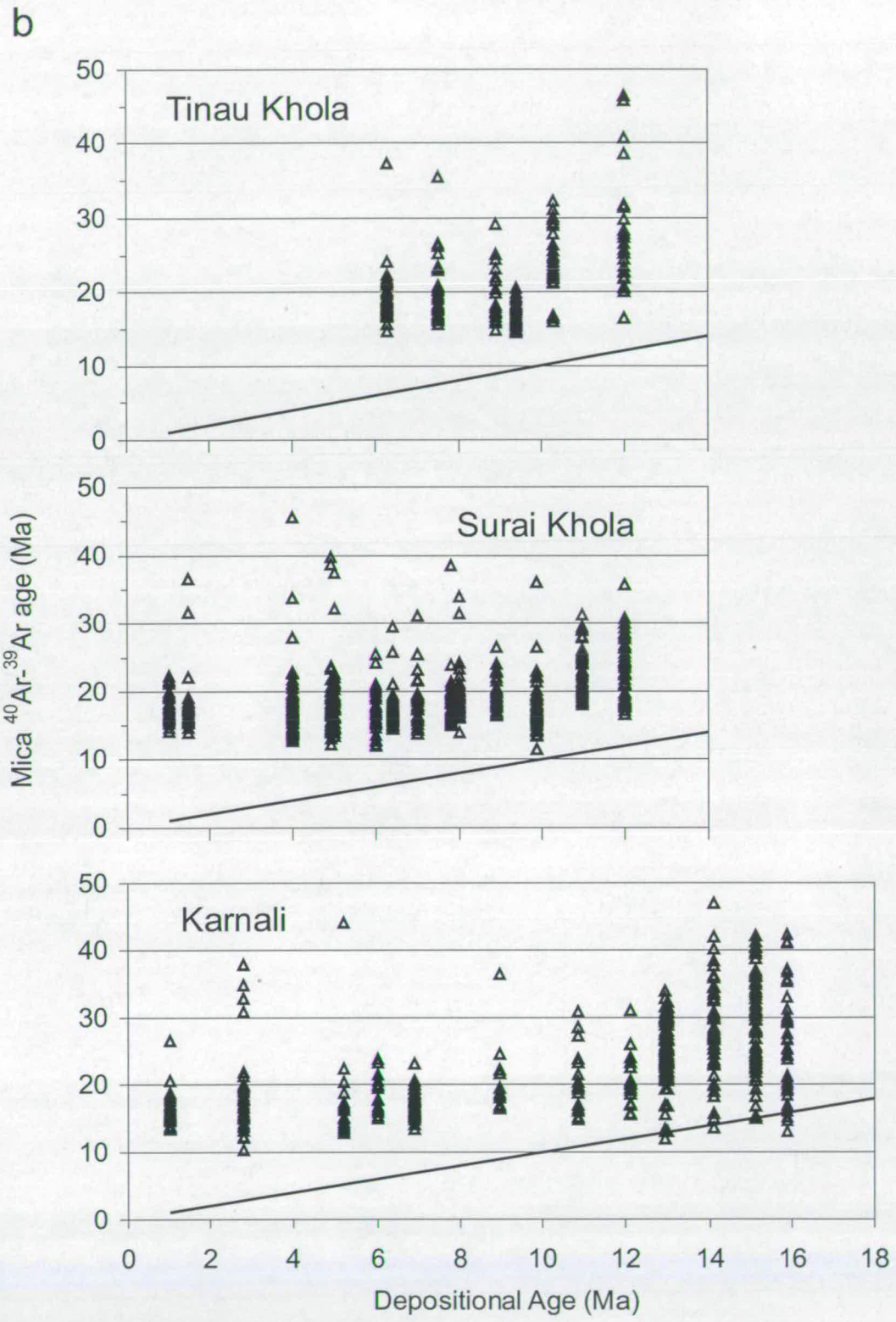


Figure 7.6.b The same plots but this time only for Himalayan aged white micas and not logarithmic to give greater clarity.

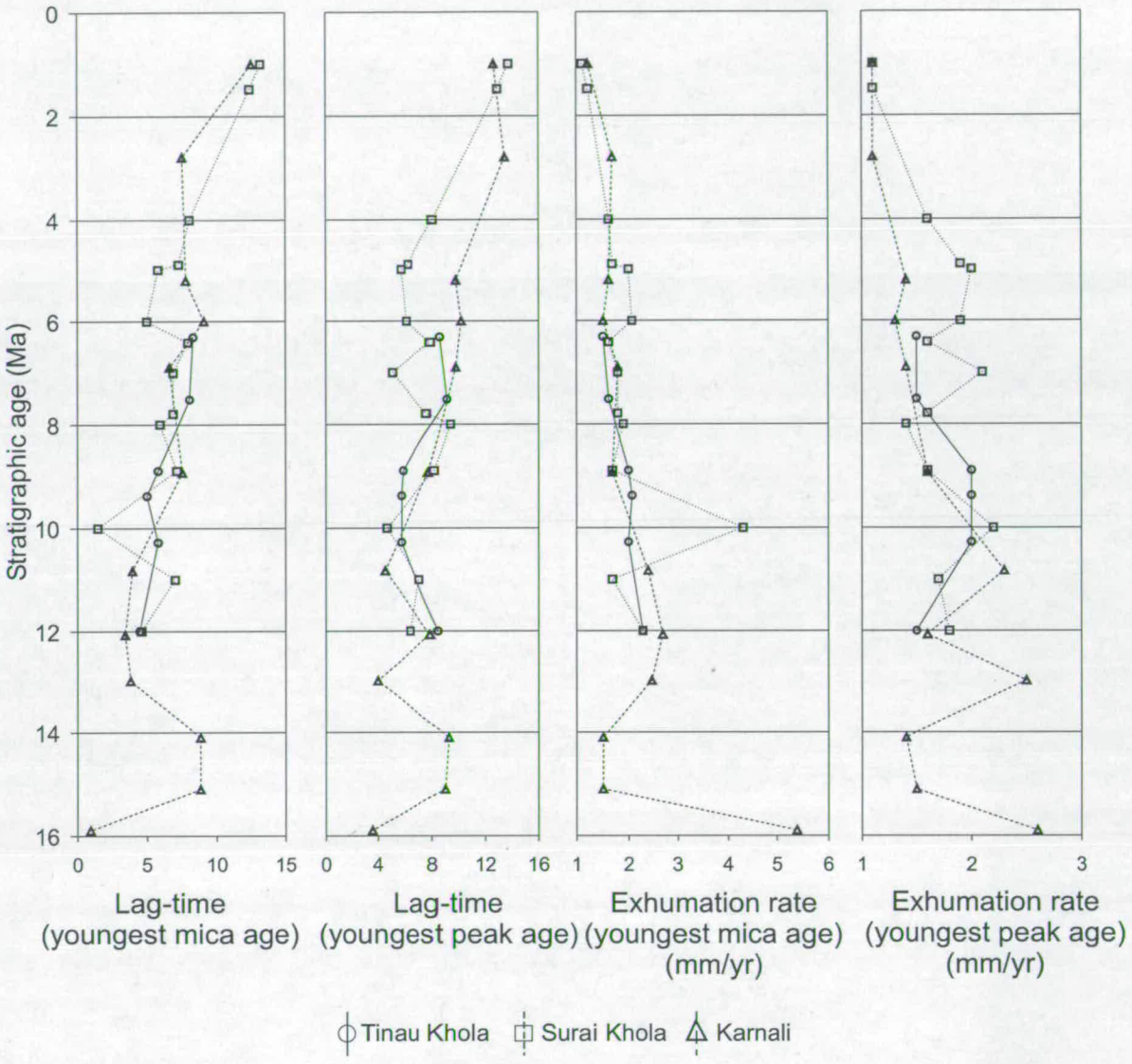


Figure 7.7. The variation in lag-times and exhumation rates for the three Siwalik sections of this study with respect to depositional age. Calculations for both youngest white mica and peak ages are shown but peak age data is used for all interpretations. The youngest Karnali single grain ages that were dated at SUERC were used to calculate lag-time for the 16-12 Ma sediment due to the large errors associated with the younger ages that were run at MIT.

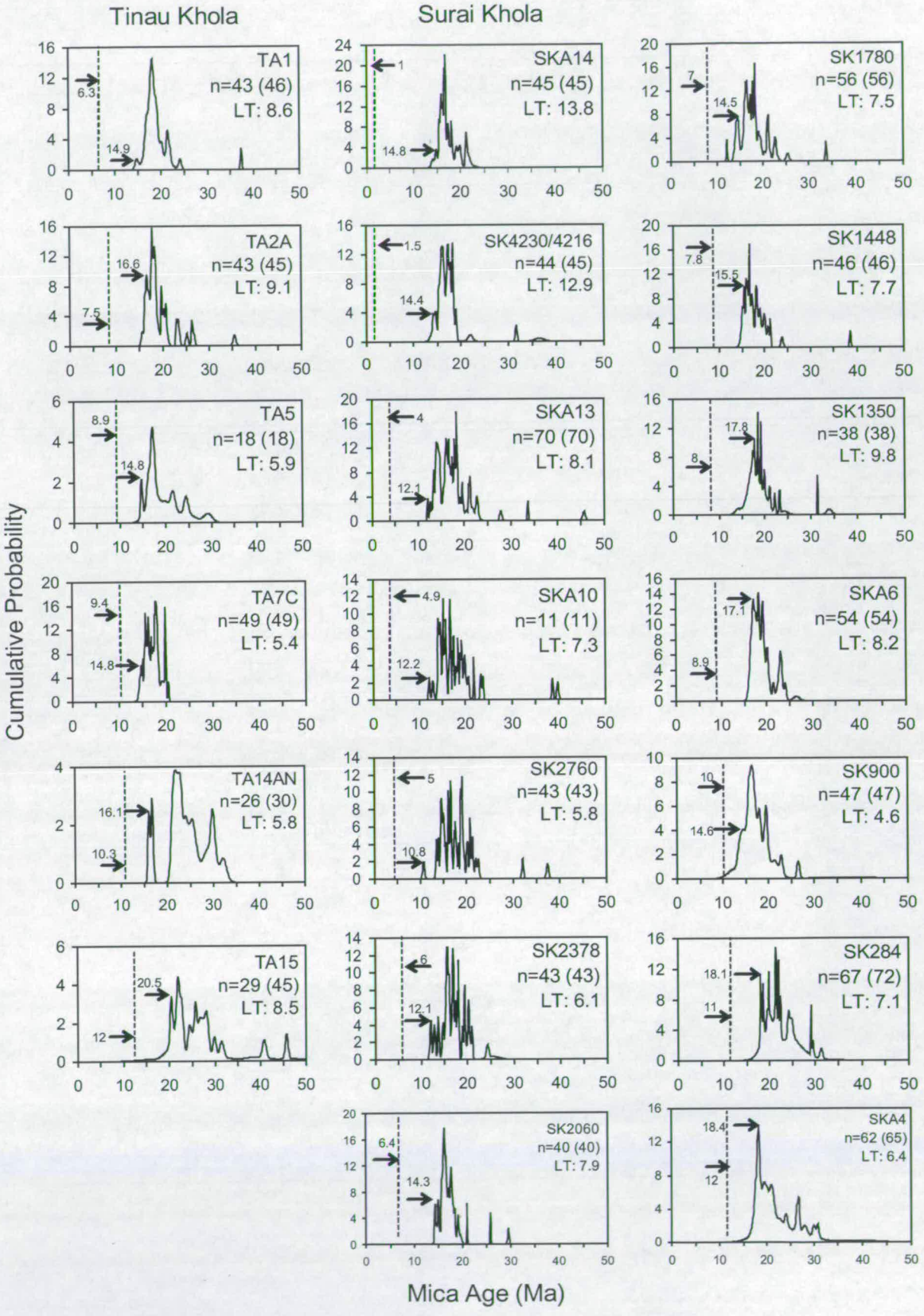


Figure 7.8. Caption on next page.

Figure 7.8. Cumulative probability plots of detrital white mica ages, continued on next page. The dashed line shows the host sediment depositional age, also indicated by arrow (in Myr). Arrow also indicates the age (in Ma) of the chosen youngest peak for determining lag-time. Sample age increases from top to bottom. For sample numbers TA = Tinau Khola, SK = Surai Khola, K = Karnali, n = number of dated grains younger than 50 Ma, (n) = total number of dated grains, LT = lag-time for youngest peak age.

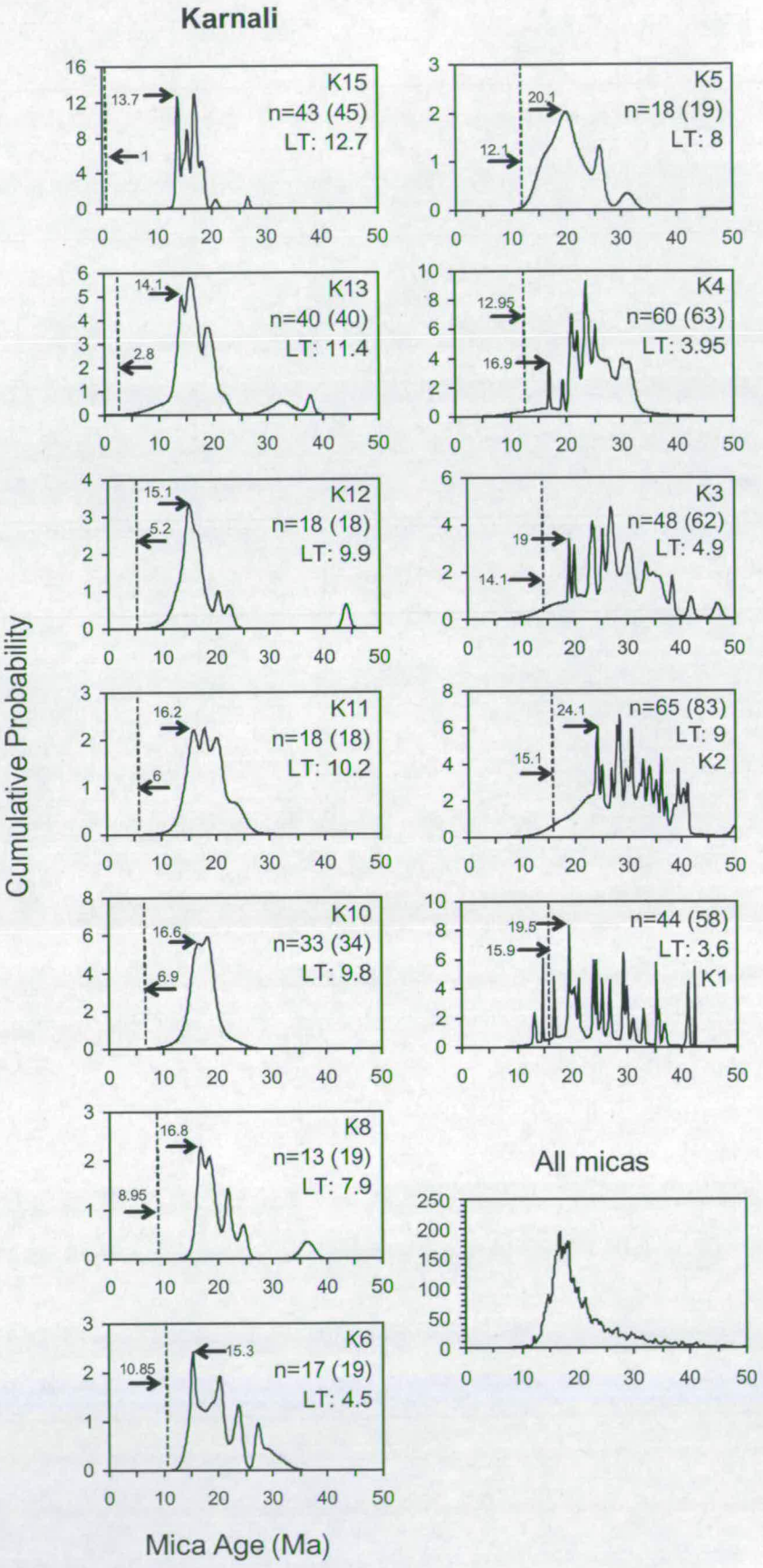


Figure 7.8. continued.

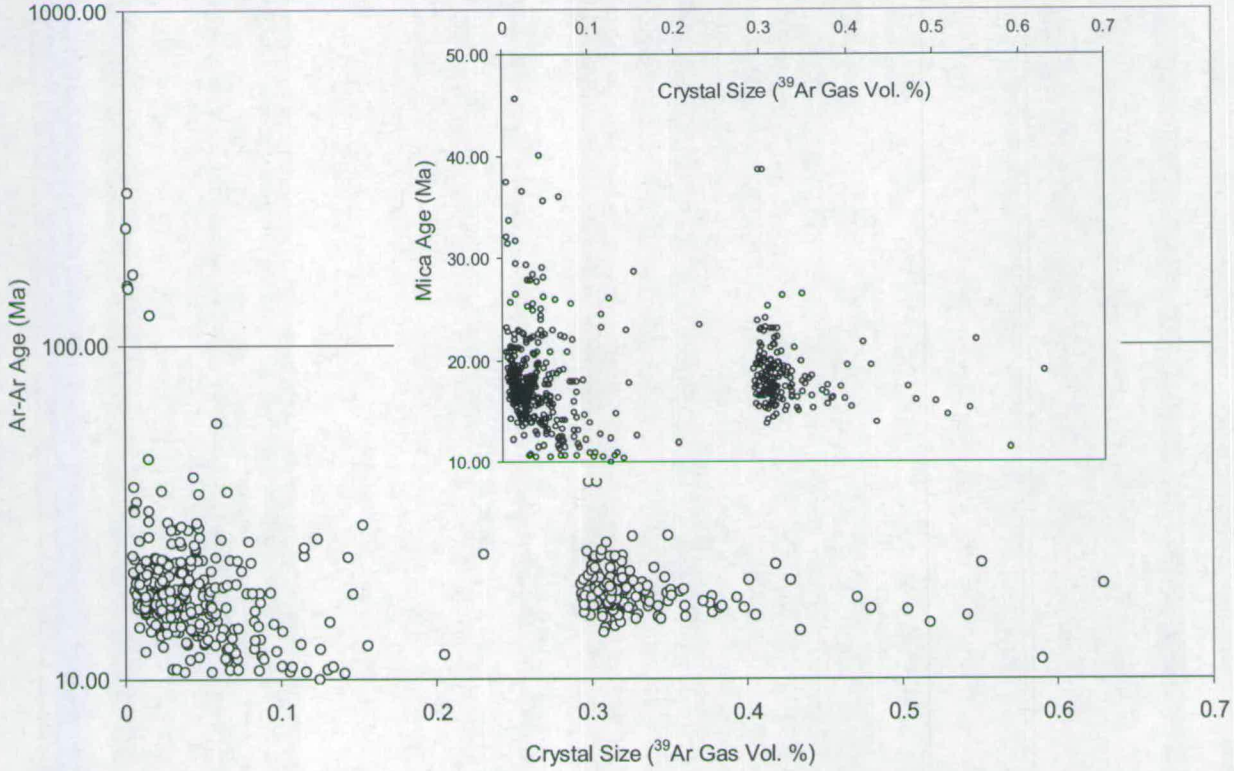


Figure 7.9. Semi-log plot of white mica ^{40}Ar-^{39}Ar age versus the size of the white mica grain (using ^{39}Ar gas volume % as a proxy). Inset plot shows same data but is not logarithmic and restricted to Himalayan aged white micas.

8. Fission-track dating

8.1. Introduction

The first descriptions of mineral dating using fission-track techniques date back to the 1960's (Wagner & Van den Haute, 1992). The technique is used across a diverse range of geodynamic settings to record rock cooling in response to exhumation. Fission-track analysis has been widely applied to Himalayan studies to constrain bedrock or sediment source cooling histories (Zeitler, 1985; Cerveny et al., 1988, 1989; Carpena & Rutkiewicz, 1989; Zeitler et al., 1989; Foster et al., 1994; Arita & Ganzawa, 1997; Searle et al., 1997; Jain et al., 2000; Stuewe & Foster, 2001; Schlup et al., 2003).

In an attempt to constrain the history of Main Boundary Thrust movement, samples from the Main Boundary Thrust sheet were taken for apatite and zircon fission-track dating. This work was designed to complement the detrital study and therefore samples were taken, as far as possible, to the north of the Siwalik sections under investigation (Fig. 8.1.). Samples were extracted at two locations immediately above the Main Boundary Thrust within the Lesser Himalayan Zone. However, this was not possible for the Karnali area in far western Nepal for reasons of safety. The samples were taken from sedimentary units within the Kerabari Limestone Formation, estimated to be Lower Ordovician in age (Sakai, 1983). There are very few published fission-track studies of the Main Boundary Thrust and none of these include zircon ages. Three apatite fission-track dates from structures at the leading edge of the Main Boundary Thrust in the Kohat region of NW Pakistan indicate rapid

cooling between 8 Ma and 10 Ma followed bedrock uplift and erosion along the Main Boundary Thrust sheet that began an estimated ~ 1-2 Ma earlier (Meigs et al., 1995). With such a dearth of research in this area there is the chance to break new ground even with a small-scale investigation.

8.2. Limitations

A measured fission-track age may directly record the time of cooling or may relate to a more complex cooling history in which case the age has little direct meaning. In order to understand the significance of a fission-track age, track lengths are measured. All newly formed tracks have the same initial length. Exposure to elevated temperatures and time results in progressive shortening of tracks or, if the temperatures are high enough, causes the track to completely fade away, a process known as annealing. Annealing may be partial, the result of track shortening at low temperatures, or complete where tracks disappear at high temperatures. Tracks form continuously throughout a samples history. In a situation where a sample is cooling from depth and high temperature the earliest formed tracks are exposed to the highest temperatures and will therefore vanish. Later tracks encounter progressively lower temperatures and thus shorten by decreasing amounts as the sample cools further. By measuring the distribution of track lengths in a sample it is possible to identify whether a sample age has direct meaning, the result of rapid cooling through the partial annealing zone (~ 110-60°C in apatite and ~ 200-320°C in zircon, the precise temperatures depending on sample composition and duration of heating), or a more protracted cooling history in which case the measured age is simply an apparent age.

The annealing phenomenon means that track length statistics are important for interpreting the rates of cooling. For apatite, annealing models provide a quantitative description of the time-temperature combinations to cause track annealing (e.g. Laslett et al., 1987; Ketcham et al., 1999). These models enable a samples measured age and track length distribution to be used to reconstruct its cooling history through the partial annealing zone (i.e. through 110-60°C). Unfortunately, the annealing kinetics of fission-tracks in zircon are less well known. Whilst annealing models for zircon exist (e.g. Tagami et al., 1998), a complicating factor has been the recognition that annealing temperatures may shift if the zircons have accumulated sufficient radiation damage, caused principally by alpha-decay. Radiation damage effects can lower the partial annealing zone from ~ 200-320°C down to ~ 170-250°C, although these temperatures are not robustly defined. Nevertheless, only very old zircon grains and/or grains with high amounts of uranium and thorium will accumulate significant amounts of alpha-decay radiation damage to lower the zircon fission-track annealing zone temperatures.

Mineral composition has an important control on the rate of annealing in apatite, particularly the relative proportions of Cl, F, and OH (Gallagher et al., 1998), and there are multicompositional annealing models that describe this (e.g. Ketcham et al., 1999). Compositional control on annealing appears not to be important in zircon. One of the problems inherent in fission-track annealing models is that they are based on laboratory time-scale annealing experiments extrapolated over geological time-scales. However, these extrapolations are consistent with observations of annealing in natural samples that have had well-constrained long-term thermal histories. Both

apatite and zircon annealing models have been validated against borehole samples from sedimentary basins where the burial and heat flow history are known (e.g. Green et al., 1989; Tagami et al, 1996).

8.3. Methodology

Concentrates of apatite and zircon were made using conventional magnetic and heavy liquid separation techniques. Apatite and zircon mounting, polishing, and etching followed standard procedures of the London Fission Track Research Group (apatite etching with 5N HNO3 at 20°C for 20 seconds, and zircon etching, using multiple mounts, with KOH-NaOH at 225 ± 5°C for between 12-48 hours). Mounts were irradiated with muscovite external detectors and dosimeter glass CN-5 for apatite, and CN-2 for zircon (to monitor neutron fluence) at the well-thermalised (Cd for Au > 200) thermal neutron facility of the Hifar reactor, Lucas Heights, Australia. Track densities were measured using a Zeiss axioplan optical microscope at 1250x magnification with dry objective for apatite and an oil objective for zircon. Ages (± 1σ) were calibrated by the zeta method (Hurford & Green, 1983), using a zeta factor of 338 ± 5 for apatite, and of 127 ± 5 for zircon determined by multiple analyses of apatite and zircon standards following the IUGS recommendations (Hurford, 1990). Analyses were by the external detector method using 0.5 for the $4\pi/2\pi$ geometry correction factor. Only crystals with prismatic sections parallel to c-crystallographic axis were analysed. Ages were calculated using ζ_{CN5} = 339 ± 5 calibrated by > 33 analyses of IUGS apatite age standards. All analyses were conducted at University College London (UCL), England. Further fission-track technique notes are given in Appendix VI.

8.4. Results

All fission-track data is presented in Table 8.1. Four samples yielded apatites suitable for analysis, three samples yielded zircon, and a total of 159 grains were analysed. Figure 8.2. shows two zircon grains from the sample set with clear well developed fission-tracks. Figure 8.3. shows fission-track ages plotted against partial annealing zone temperatures. Of the three zircon-yielding samples two were from the western sample location on the road to Sandhikarka. The zircons reveal a dominant 18-20 Ma age component (Fig. 8.4.) that is significantly younger than the sediment depositional age. However, the presence of grains substantially older (up to ~ 750 Ma) than depositional age indicates partial resetting, otherwise all grains would have been reset by the 18-20 Ma event. There is no major difference in the zircon age modes between the two sample localities except that the eastern Palpa 4 sample yielded a slightly higher proportion of older grains (all ~ 270 Ma). The apatite fission-track ages show more variation compared to the zircons, ranging from 8.4 ± 2.9 Ma to 14.5 ± 1 Ma in the east and 6.4 ± 1.4 Ma to 11.5 ± 2.0 Ma in the west, from a total of 44 grains. This variation in ages may relate in part to the relatively few grains (< 10), and thus spontaneous tracks, that were analysed in each sample. In sample LH54, 22 grains were counted and therefore this sample is considered to give the most statistically reliable age.

Sample	n	ρ_d	N_d	ρ_s	n_s	ρ_i	n_i	χ^2	RE%	Central Age (Ma)	Age components (samples with mixed grain ages)	Zircon track lengths
2. Palpa 4 (AFT)	5	1.123	6228	0.083	23	1.778	493	<1	49.1	8.4±2.9		
7. Palpa 4 (ZFT)	39	0.355	2437	4.574	3322	2.801	2034	<1	76.3	30.2±3.8	20.2±0.9 (28 grains) 270±30 Ma (7 grains)	10.90 μm for the 20.2 Ma age mode, n = 23 and 9.59 μm for the 270 Ma mode, n = 14
4. LH54 (AFT)	22	1.123	6228	0.188	258	2.470	3376	60	1.5	14.5±1		
3. Sandy 8 (AFT)	9	1.123	6228	0.136	34	2.236	561	50	0.3	11.5±2.0		
5. Sandy 8 (ZFT)	30	0.358	2437	2.99	1634	2.933	1666	0	46.1	19.3±1.8	17.9±0.9 Ma (30 grains) 757±257 Ma (1 grain)	11.47 ± 0.18 µm (s.d. = 1.14 μm) from 17.9 Ma age mode,n = 39
1. Sandy 6 (AFT)	8	1.123	6228	0.089	30	2.763	923	<1	30.2	6.4±1.4		
6. Sandy 6 (ZFT)	46	0.357	2437	2.552	2472	2.825	2737	<1	39.7	20.6±1.4	18.3±0.9 Ma (41 grains) 46.2±5.5 Ma (4 grains) 279±92 Ma (1 grain)	11.23 μm for the 18.3 Ma age mode, n = 58

Table 8.1. Caption on next page.

Table 8.1. Apatite and zircon fission-track results. Numbers in bold refer to Figure 8.3. AFT – Apatite fission-track, ZFT – zircon fission-track, n – number of grains. (i). Track densities ($\rho_{d,s,i}$) are ($x10^{6}$ tr cm^{-2}) with numbers of tracks counted ($N_{d,s,i}$) shown in brackets; Zeiss Axioplan microscope, 1250x total magnification; 100x dry objective; (ii). analyses by external detector method using 0.5 for the $4\pi/2\pi$ geometry correction factor; only crystals with prismatic sections parallel to c-crystallographic axis analysed; (iii). irradiation at the well-thermalised (Cd for Au > 200) thermal neutron facility of the Hifar reactor, Lucas Heights, Australia using dosimeter glass CN-5 to monitor neutron fluence; (iv). ages calculated using ζ_{CN5} =339±5 calibrated by >33 analyses of IUGS apatite age standards; (v). $P\chi^2$ is probability for obtaining χ^2 value for ν degrees of freedom, where ν = no. crystals - 1; (vi). central age is a modal age, weighted for different precisions of individual crystals.

In order to constrain whether the youngest age mode at 17.9±0.9 Ma detected in the zircons records a distinct event or slow cooling history, zircon track lengths were measured. For zircon, mean track lengths of ~ 11 μm indicate the time of rapid cooling. Sample Sandy 8 gave a mean track length of 11.47 ± 0.18 μm (1σ = 1.14 μm) for the 18 Ma age mode based on 39 measurements. Sample Sandy 6 gave a mean track length of 11.23 μm for the 18 Ma mode based on 58 measurements. Sample Palpa 4 give a mean track length of 10.90 μm for the 20 Ma mode based on 23 measurements and 9.59 μm for the older mode based on 14 measurements. Thus no short tracks were found in the youngest age modes at 18 Ma. No meaningful track length data were obtainable for the

apatites because of the low track densities and therefore the significance of the reported apatite ages is ambiguous.

8.5. Discussion

Although a small data set, the zircon ages between 18-20 Ma are statistically robust (forming a large proportion of the population and with low errors) and could indicate rapid cooling at that time (from track length data). Because of the independent geological constraints, i.e. an Ordovician depositional age, we must assume the zircon age populations represent some form of total and/or partial resetting rather than a provenance signature. The older zircon ages require total or partial resetting (temps > 300°C) at some time prior to the Permian. After this, in order to retain old ages the sample must have remained at low temperatures (i.e. < 250°). The presence of a young age mode in the same sample with long track lengths requires rapid cooling around 20 Ma from total annealing temperatures. There are two possible explanations that can reconcile the coexistence of a young totally reset age mode and a partially reset older age mode in the same sample. For both explanations the youngest age mode represents zircons that had high levels of radiation damage that lowered the partial annealing zone to ~ 170-250°C. Scenario 1 requires long-term residence at temperatures between 200-250°C, sufficiently low enough to allow track accumulation throughout the Mesozoic and early Tertiary in low radiation damage grains but high enough to prevent track accumulation in high radiation damage grains. At 20 Ma the samples cooled from these temperatures, the event recorded by the high radiation damage grains. Scenario 2

requires long-term residence at temperatures below 200°C then a reheating event to temperatures ~170-250°C sufficient only to reset the high radiation damage grains. Subsequent cooling occurred at 20 Ma. Common to both scenarios is a requirement for a cooling event at 18-20 Ma.

The mixed zircon ages revealed in the scatter plots suggest partial resetting at temperatures of ~ 170-250°C depending on the level of zircon metamictisation (crystal lattice destruction) due to alpha-recoil damage at the time of heating. The reason for this is that uranium concentrations are fairly similar in both age groups (the abundance of induced tracks from irradiation allows an estimation of the uranium parent concentration of the mineral grain), which means there would have to be different zircon ages prior to deposition, a likely situation. It is therefore conceivable that alpha-recoil damage has lowered the effective closure temperature for most grains (younger ages) and therefore the zircon data do not necessarily record significant cooling. Unfortunately there is no way of detecting whether the zircons have been affected by alpha-recoil damage. Nevertheless, the scale of cooling was not large (~ 100°C), as can be seen by the fact that temperatures did not drop enough to be recorded by the apatites at the same time as the zircons.

Track length data support the proposal that the 20 Ma ages record the time of rapid cooling through the zircon partial annealing zone temperatures. It is important to note however, that with a comparatively small sample set any interpretations remain tentative. Additionally, technical difficulties relating to anisotropic etching and the

effects of alpha-recoil damage in zircon mean that interpretation of experimental data is not straightforward. These data are consistent with rapid cooling, but if alpha-recoil damage lowered the closure temperature this apparent rapid cooling might actually only have involved a modest drop in temperatures, perhaps from 200-250°C down to below 170-180°C. If this were the case then there would be less need to invoke tectonics as a cooling mechanism. If the crustal position of the grains was at the cusp of temperatures that reset zircon, only a small change of temperature would have been required to bring them out of that zone, giving long tracks. Nevertheless, the data record a cooling event at ~ 20 Ma, regardless of its magnitude.

The apatite ages record a later cooling episode between ~ 15-5 Ma. The large spread of ages could reflect compositional variation or local differences in erosion and topography, and are not supported by good statistics. The young ages indicate fairly rapid cooling through 80 ± 20°C to near surface temperatures in 6-8 Myr. Using the most reliable sample (LH54) it took ~ 6-8 Myr to cool between apatite and zircon resetting temperatures (~ 180°C to < 100°C). Fission-track ages therefore indicate an average cooling rate of ~ 8-15°C/Ma. My fission-track ages are similar along-strike, suggesting this cooling history applies to the Main Boundary Thrust over considerable distances in Nepal and it is a single continuous thrust sheet, a fault which has a debated lateral diachroneity and decompartmentalisation.

If the Main Boundary Thrust was active at 18-20 Ma this has important implications for Himalayan kinematics and suggests the Main Boundary Thrust may have been

synchronous with more hinterland-ward structures including the Main Central Thrust, a scenario that has been entertained on a structural basis by previous workers (e.g. Wobus et al., 2003). However, even ignoring the likelihood of alpha-recoil damage, the cooling event indicated by our zircon fission-track ages is limited due to the younger apatite ages. It is therefore proposed that the zircon fission-track ages reflect partial annealing during minor cooling and the main phase of Main Boundary Thrust movement occurred at a later time, probably ~ 11 Ma as indicated by petrographic changes (Chapter 5) and the increase in Siwalik sedimentation rates that I record at that time (Chapter 4). This is in agreement with the inception age proposed by previous workers who attribute an increase in foreland subsidence and hinterland denudation at this time to uplift and generation of a new thrust load above the Main Boundary Thrust (e.g. Meigs et al., 1995; Burbank et al., 1996).

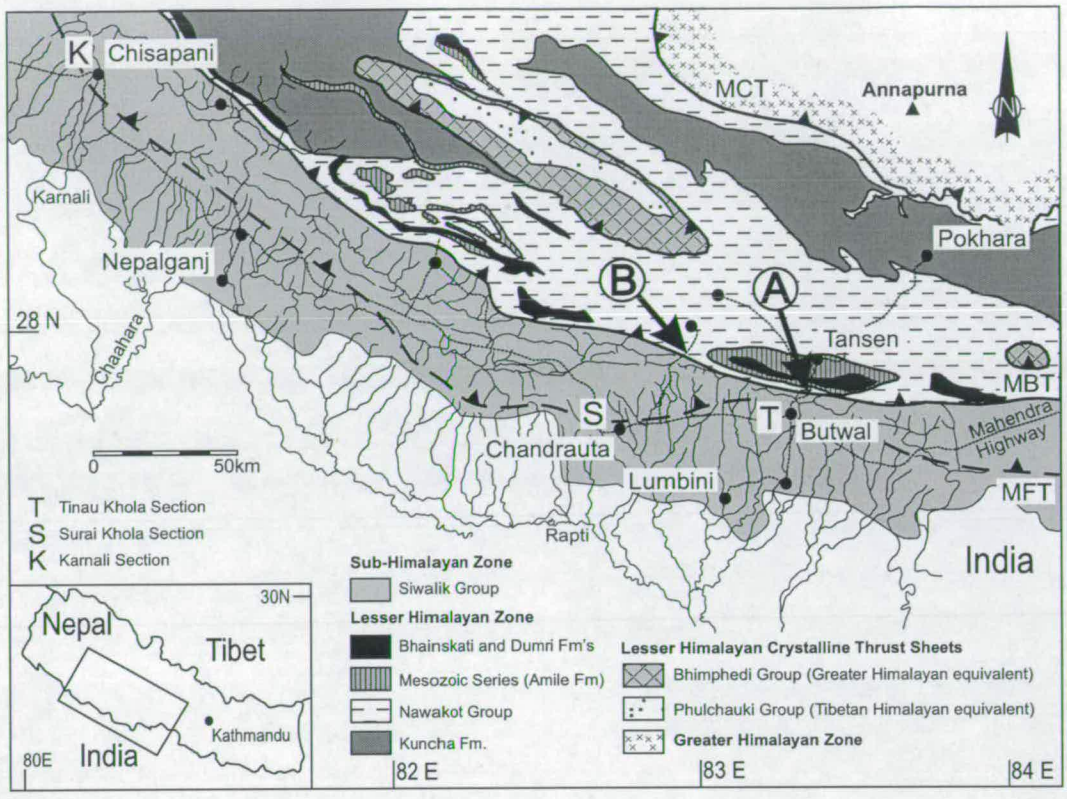


Figure 8.1. Geological map of SW Nepal, inset shows map location. Locations of the three sections under investigation are highlighted. A and B show locations of fission-track samples above the Main Boundary Thrust. MCT - Main Central Thrust, MBT - Main Boundary Thrust, MFT - Main Frontal Thrust. Modified from Amatya & Jnawali (1994).

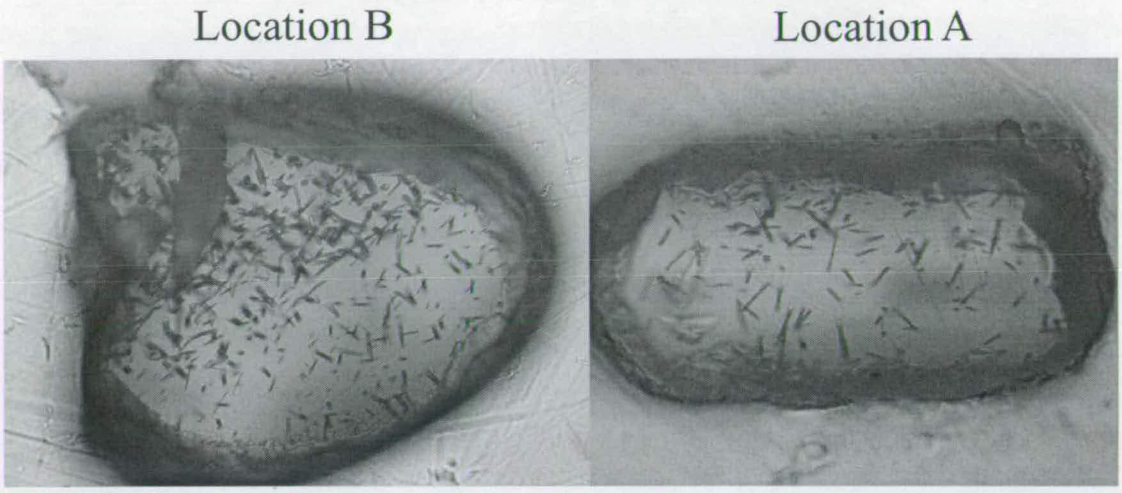


Figure 8.2. The zircon grain on the left is from sample Sandy 6 and is approximately 150x100μm, the photo shows clear confined tracks. The zircon grain on the right is from sample Palpa 4 and is approximately 120x70μm.

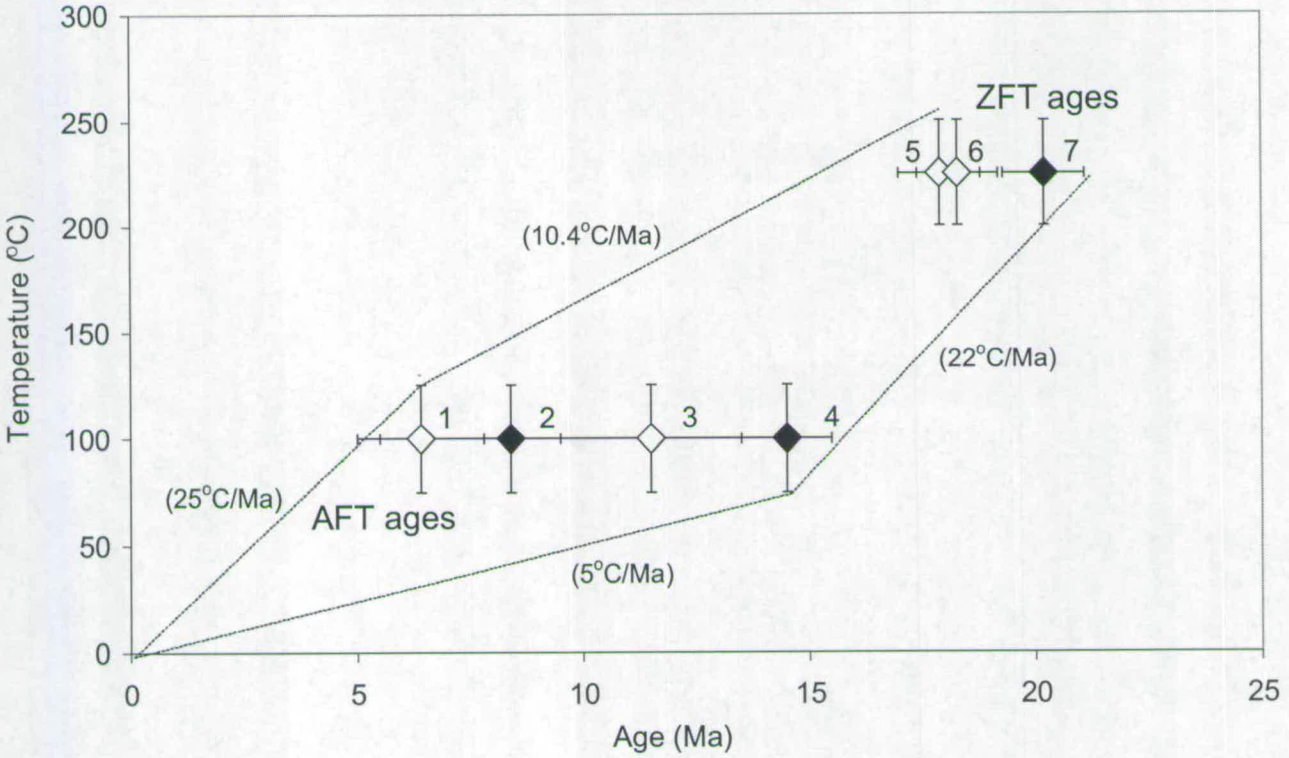


Figure 8.3. Temperature-time plot for the apatite and zircon fission-track data. The white diamonds represent sample location B, the black diamonds sample location A (from figure 8.2.). The numbers refer to the samples in Table 8.1. Dotted lines give rough cooling curves for the Main Boundary Thrust. AFT - apatite fission-track, ZFT - zircon fission-track.

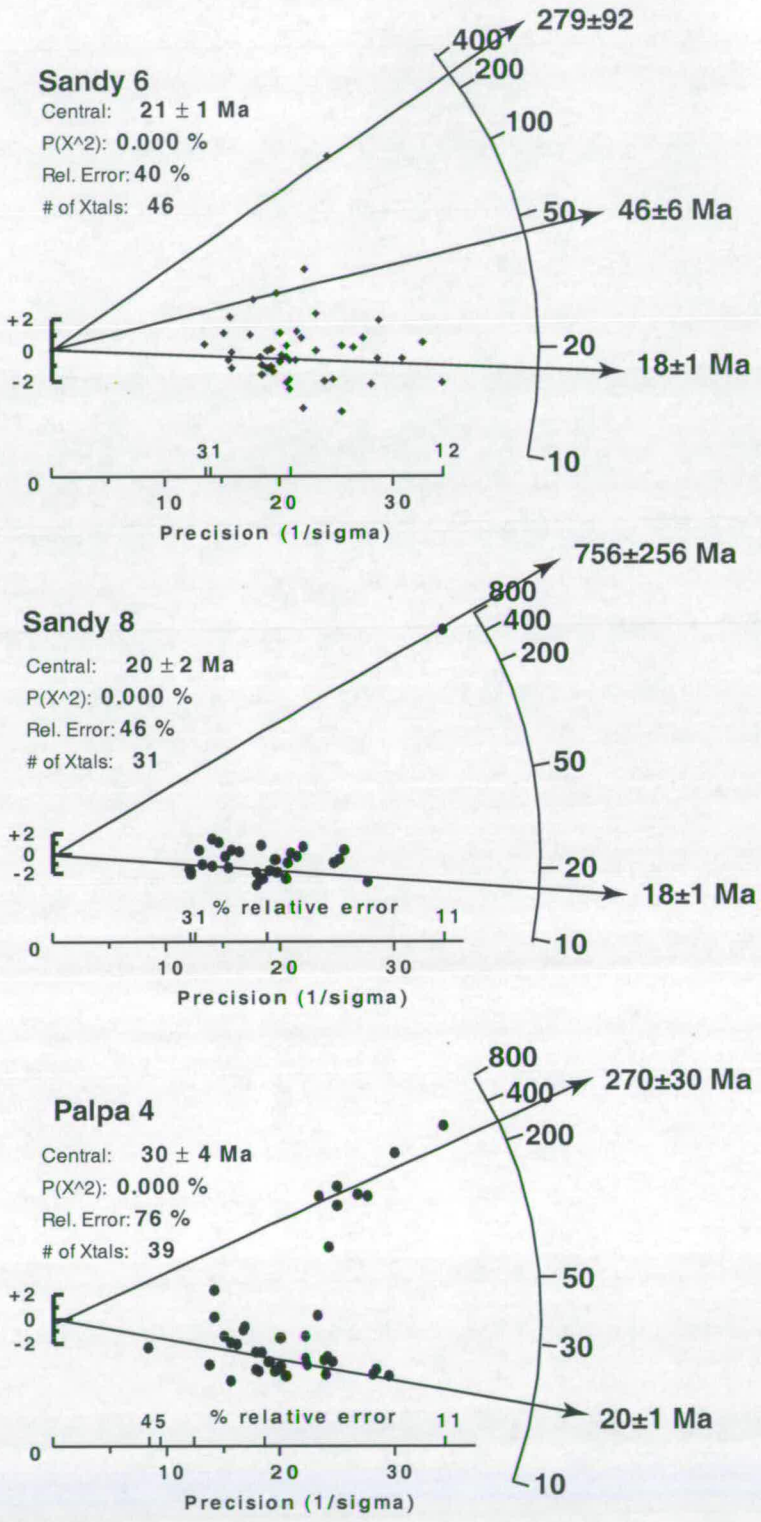


Figure 8.4. Scatter plots of the fission-track data for three zircon samples.

9. Discussion and conclusions

9.1. Introduction

This chapter brings together the results of previous chapters to show how they are related to each other and to construct my final interpretations. The limitation sections in each technique chapter emphasise the importance of combining more than one analytical method when employing the detrital approach due to the greater amount of unknowns involved with using a mixed sediment rather than bedrock. The recognition and tackling of these uncertainties has made the technique increasingly accurate and uncertainties will continue to be lessened and perhaps eliminated as new detrital methods are developed. Since multi-technique detrital studies have been hitherto uncommon, this chapter will hopefully reveal the utility of such an approach. For simplicity the discussion is divided into provenance, tectonic evolution, and drainage evolution sections. The conclusion will then summarise the data in a new model for the Neogene tectonic evolution of the central Himalayas.

9.1.1. Provenance of the Siwalik Group

As discussed in section 4.5.3., I can restrict the provenance of the Tinau Khola, Surai Khola, and Karnali sections to the Gangetic drainage basin. Therefore my findings are applicable to the central Himalayas from NW India to central Nepal.

On initial inspection the petrography and geochemistry results seem to be conflicting. Sandstone petrographic modes suggest that sedimentary to low-grade

metamorphic detritus dominated the supply of sediment to the foreland basin (~ 90 %) throughout deposition of all three Siwalik sections. However, consistent ε_{Nd} isotopic values of around -17 for mudstone samples indicate derivation from the Greater Himalaya, which now forms the high-grade metamorphic core of the mountain range. Because a dominant Greater Himalayan source does not explain the low-grade petrography, the most likely provenance is from the low-grade Greater Himalayan protolith units or tectonostratigraphic covers, which yield similar geochemical signatures (Table 6.1.). It is increasingly likely further back in time that there were large areas of sedimentary and low-grade Greater Himalayan protolith material which now exist as scattered outcrops such as the variously named Haimantas, Kade Formation, or Chamba sequence in NW India (Pognante et al., 1990; Thakur, 1998; Walker et al., 1999) or the Sanctuary Formation of Nepal (Colchen et al., 1986). The homogeneity of the petrography and Nd geochemistry signatures throughout the sections suggests this Greater Himalayan sedimentary cover remained a major source area throughout Siwalik deposition. Similarly, a Haimantas source area was invoked by White et al. (2002) to explain low-grade metasedimentary detritus with Greater Himalayan geochemistry in post-17 Ma foreland basin sediments of the Dharamsala Group, NW India.

It is unlikely that the combined petrographic and geochemical data can be explained by invoking different provenances for the two size fractions since geochemical analysis of Surai Khola and Karnali sandstones by Huyghe et al. (2001) yielded similar results to the present mudstone study, indicating that mudstone signals can be used to characterise the entire sediment influx. If most detritus was sourced from the

Outer Lesser Himalaya (with a Nd signature similar to the Greater Himalayan Zone, Table 6.1.) a similar detrital signal would be produced. But the Outer Lesser Himalaya represents a relatively small portion of the potential source zone. Furthermore, the sedimentary and low-grade detritus that fed the foreland basin was accompanied by subordinate medium- to high-grade lithics and heavy minerals and abundant Himalayan-aged white micas, all characteristic of the Greater Himalaya. The catchment area of the rivers which delivered Siwalik sediment must have therefore stretched north of the Outer Lesser Himalayan Zone.

The metamorphosed Greater Himalaya must have been the main source for the post-collision aged (< 50 Ma) white micas. Most white micas from the Greater Himalaya give Tertiary ^{40}Ar-^{39}Ar ages (Guillot et al., 1994; Coleman & Hodges, 1998; Searle et al., 1999), therefore older pre-collision aged micas in the Siwalik Group could have been derived from a Lesser Himalayan, Tibetan Himalayan, or Greater Himalayan protolith source area. However, the absence of a distinct age group and the low abundance of these older grains restrict their use as a provenance indicator. Relatively low $^{87}Sr/^{86}Sr$ values in Siwalik mudstones (in terms of Himalayan tectonic zones) may also indicate a Tibetan Himalayan Zone source. My data therefore suggest that during Siwalik deposition sediment was mostly derived from Greater Himalayan low-grade protoliths whilst limited exposure of the emerging high-grade metamorphic rocks contributed the younger micas (the metamorphosed Greater Himalaya has a higher mica abundance than the protolith) and heavy minerals.

The proportion of sedimentary detritus versus metamorphic detritus increases at 12 Ma in the Karnali section, as does the amount of carbonate material, both typical of the Lesser Himalaya (Fig. 9.1.j). There is also a subtle increase in $^{87}Sr/^{86}Sr$ from 12 Ma onwards, whilst Huyghe et al. (2001) and Robinson et al. (2001) report increasingly negative ε_{Nd} values for the Surai Khola and Karnali sections after 12 Ma. These up-section changes all point to the first erosion of Lesser Himalayan units from ~ 12 Ma. Our evidence for more negative (-18 to -30) Lesser Himalayan ε_{Nd} values in quartzite clasts, back to 7.6 Ma in the Tinau Khola section, 6 Ma in the Karnali section, and 4.8 Ma in the Surai Khola section provides further evidence for erosion of the Lesser Himalaya by those times. The combination of these up-section changes points to a gradually increasing contribution from the Lesser Himalaya after 12 Ma, a scenario that conforms with current tectonic evolutionary models in which the Lesser Himalayan duplex is exposed from ~ 12 Ma (e.g. DeCelles et al., 2001; Robinson et al., 2003).

It is possible that the increase in seawater $^{87}Sr/^{86}Sr$ ratios over the last 40 Myr is a direct consequence of erosion of the Himalayan orogen (Quade et al., 1997). The significant acceleration of this trend over the last ~ 12 Myr (Richter et al., 1992) may therefore be a response to the exhumation of meta-carbonate Lesser Himalayan rocks as indicated by this study. The lack of a concomitant switch to a greater proportion of Lesser Himalayan-type old white mica grains in the Siwalik Group is probably the result of the mineral's relatively low abundance in Lesser Himalayan sediments. The smaller grain size of the older white mica grains would also have meant they were less likely to have been picked for analysis due to limitations on machine accuracy.

The combination of increasing feldspar and garnet between 9 and 6 Ma in all three sections hints at an increasing contribution from the Greater Himalaya. This probably reflects a deepening of the erosion level into high-grade Greater Himalayan rocks as recorded by heavy mineral trends (Fig. 9.1.m). The evolution of heavy mineral suites from staurolite to dominantly kyanite between 8-7 Ma and increase in metamorphic index in all three sections indicates erosion of amphibolite-facies metasediments in the drainage basin during this period. Decreasing youngest white mica peak ages throughout this period also indicate continued exhumation into deeper levels of the Greater Himalaya.

9.1.2. Exhumation of Siwalik Group source area

A total of 1415 grains of white mica from the three Siwalik sections studied give a good age mode of 16.8 Ma. This indicates the time of greatest exhumation of the Greater Himalayan source area. Each section gives roughly the same age mode, therefore the main phase of exhumation was synchronous along-strike for the central Himalayas. From comparison with petrography data, it is apparent that a lag-time of several million years separates this large-scale exhumation and the start of significant influx of Greater Himalayan detritus to the foreland basin.

Using simple 1D thermal modelling (White, 2001), our shortest white mica lag-time for 16 Ma sediment of 3.6 Myr equates to an exhumation rate of ~ 2.6 mm/yr. This is the fastest exhumation rate (shortest lag-time documented) in the time range under study, and correlates with the ^{40}Ar-^{39}Ar age mode of 16.8 Ma. Exhumation remains

relatively rapid (up to ~ 2.2 mm/yr) until 10 Ma in all three sections (Fig. 9.1.d). Since most low-temperature thermochronometers either yield similar ages to the white mica of this study or much younger ages (Fig. 2.4.), its likely the rapid exhumation recorded by this study ceased at ~ 10 Ma and was followed by more gradual rates. The slowing of Greater Himalayan exhumation after 10 Ma coincides with the petrography and geochemical changes between 12-10 Ma which indicate emergence of the Lesser Himalaya. If initial Lesser Himalayan exhumation was indeed dictated by the Lesser Himalayan Duplex, then the ^{40}Ar-^{39}Ar data and petrography and geochemistry data again seem to support one another. If the 12-10 Ma period marked the cessation of rapid exhumation between the Main Central Thrust-South Tibetan Detachment system and subsequent strain accommodation within the Lesser Himalayan Duplex (following the models of DeCelles et al., 2001 and Robinson et al., 2003), the white mica age data would show an increase in lag-times shortly thereafter and there would be the first signs of Lesser Himalayan unroofing within the Siwalik Group. The fact that there are no micas younger than 10-12 Ma, no lag-times less than 5 Myr after 10 Ma, and there is a change of provenance at ~ 12 Ma with more low-grade and carbonate material indicates that this period represents the time of transference of exhumation south of the Greater Himalaya. The combination of our ^{40}Ar-^{39}Ar white mica ages, petrography, and geochemistry data therefore suggest the 12-10 Ma period represents a time of major change in the dynamics of the Himalayan orogen with reorganisation of the wedge.

Comparison with the detrital work of White et al. (2002) in NW India indicates some diachroneity in exhumation along-strike. For example, White et al. (2002) purport

that a similar change in orogenic dynamics as that indicated by this study occurred as early as 17 Ma in NW India, compared to 10-12 Ma in this study. Furthermore, White et al. (2002) document metamorphosed Greater Himalayan detritus in the Indian foreland basin between 20-17 Ma, whereas the current work suggests such detritus only appears in the foreland basin of Nepal within the last 10 Myr. Indeed, due to inevitable irregularities in the pre-collisional margins of India and Asia, possible collisional obliquity and variable rotation of India with respect to Asia during the Cenozoic, it is likely that collision was not synchronous across the entire collision zone (Searle et al., 1987; Dewey et al., 1989).

Whilst zircon fission-track data may provide evidence for movement along the Main Boundary Thrust as early as 20 Ma, the evidence for partial annealing, poor statistics, and problems with explaining such an early Main Boundary Thrust negate any robust conclusions based on this work. The relatively old apatite fission-track ages indicate possible movement from 14.5 Ma but are also hampered by poor statistics. Whilst some authors have invoked the increase in sedimentation rates throughout the foreland basin and elsewhere as evidence for Main Boundary Thrust movement as early as 11 Ma, this change in sediment flux is more likely a result of the inception of the Lesser Himalayan Duplex at that time which would have generated a large fresh area of uplift to be eroded and perhaps increased flexure of the foreland basin due to the redistribution of hinterland load. Whilst initiation of the Main Boundary Thrust may have taken place as early as 20 Ma, it is more likely the structure is much less ancient with movement perhaps only within the last 5 Myr (e.g. DeCelles et al., 1998a, 2001).

We find no evidence for late-stage (post-10 Ma) reactivation of the Main Central Thrust as purported by many workers (e.g. Harrison et al., 1997; Catlos et al., 2002, Fig. 2.2.). However, it is possible that these younger ages were missed by the sampling process due to being volumetrically insignificant. Brewer et al. (2003) found very young ages in modern river sands (Fig. 2.2.) but these were sampled close to the Main Central Thrust, not the foreland. It is conceivable that these young micas would become highly diluted by the time the river has passed through to the Gangetic Plain. Therefore, the lack of post-10 Ma mica ages within the Siwalik sediment does not thwart the possibility of late-stage Main Central Thrust reactivation.

During steady-state exhumation rocks are expected to cool gradually, resulting in a straight-line cooling curve. We have some evidence for this along the Surai Khola section between 8 and 4 Ma (exhumation rates of ~ 1.6-1.9 mm/yr) and also the Karnali section between 8 and 2.8 Ma, most evident from the youngest single grain age data (exhumation rates of ~ 1.4-1.6 mm/yr) (Fig. 9.1.d). After this period of apparent exhumational steady-state lag-times increase once again up to 12-14 Myr by 1 Ma. However, due to the limited size of the data set the potential evidence for exhumational steady-state remains an observation rather than a conclusion.

9.1.3. Drainage evolution

Whilst the field area in southern central Nepal is characterised by axial drainage within the Sub-Himalayan Zone (perhaps related in part to the spacing of thrust-cored anticlines) the three Siwalik sections reveal no evidence for sustained axial flow. This suggests that the portion of foreland basin in Nepal under study was dominated by transverse rivers during the Neogene and the drainage architecture was consistent for hundreds of kilometres along-strike. The largest change in drainage characteristics is contemporaneous with the main change in hinterland exhumation rates and provenance. This elegantly reveals the direct link between tectonics and geomorphology. With growth of the Lesser Himalayan Duplex, the sedimentary response was that rivers became larger with a greater sediment load and bankfull discharge. These rivers deposited significant fluvial fan deposits whereby proximal fan facies are represented by the uppermost Siwalik conglomerates (braided channel facies). Additionally, it is possible that intensification of the Asian monsoon beginning ~ 11 Ma also contributed to the sedimentological shift (Dettman et al., 2001), although the timing and nature of the climate change, indicated by various workers, is much debated (Burbank et al., 1993; Harrison et al., 1993; Beck et al., 1995; Quade et al., 1995, 1997; Tanaka, 1997). Indeed, the carbon isotope shift recognised in Siwalik paleosols does not coincide with any sedimentological transition (Quade et al., 1995).

9.2. Conclusions - Neogene evolution of the Himalayas

Following initiation of the Main Central Thrust-South Tibetan Detachment system at ~ 23 Ma (Hubbard & Harrison, 1989; Hodges et al., 1996), maximum exhumation rates of the Greater Himalayan Zone continued until 16 Ma, based on lag-times in the Karnali section (Fig. 9.2.a). Exhumation then slowed slightly but remained relatively rapid (~ 2 mm/yr) until 10 Ma. From 12 Ma and by 10 Ma the orogen (at least in the central Himalaya) underwent a dramatic reorganisation whereby the locus of strain accommodation switched from the Main Central Thrust to structures within the Lesser Himalayan Duplex. During this southward growth of the orogenic wedge and accretion of new structures, the rocks of the Lesser Himalayan Zone were exposed within the hinterland for the first time. The change in orogen dynamics between 12 and 10 Ma initiated the generation of a new area of uplift from which fresh detritus was eroded (Fig. 9.2.b). It is likely that the combination of increased sediment flux and foreland subsidence due to the redistribution of tectonic load resulted in a rapid increase in sedimentation rates throughout the Himalayan depositional arena. The change in depositional characteristics may also in part relate to intensification of the Asian monsoon at ~ 11 Ma as indicated by oxygen isotopic data from bivalve shells and mammal teeth (Dettman et al., 2001), but the timing of such intensification is much debated. Throughout the Neogene, Greater Himalayan protolith material contributed to the majority of foreland-bound sediment, whilst exposure of the metamorphosed Greater Himalaya gradually increased from limited outcrops prior to 10 Ma to continuous outcrop at the present. From 10 Ma to the present, exhumation slowed steadily and deeper levels of the Greater Himalaya were gradually exposed (Fig. 9.2.c).

Our conclusions are supported by consistent data from all three sections, suggesting a lateral continuity in tectonic evolution for the central Himalayas and the absence of processes that hinder the use of the detrital technique to document hinterland tectonics, such as sediment ponding and drainage diversion. This work emphasises the utility of combining both a range of procedures and more than one time-equivalent sedimentary section when employing the detrital approach.

9.3. Further work

Using detrital records to infer tectonic-geomorphologic evolution of the Himalayas is an emerging discipline. Future studies would do well to combine a number of detrital techniques and incorporate more than one contemporaneous sedimentary deposit; detailed sedimentology is also important. More research is required in the eastern Himalayas where exposure is limited and there is still much to be done as far as age calibrating all possible molasse deposits. ^{40}Ar-^{39}Ar dating of white mica has proved a useful detrital technique and this could be combined with lower temperature thermochronology such as fission-track dating which would give a better picture of the continuation of exhumation to shallower crustal levels. With regards to detrital geochemistry, studies should incorporate clasts as well as matrix sediment into the analysis to aid provenance determination. More generally, a better picture of the variation in geochemical signatures throughout the potential Himalayan source zones would be helpful. The difficulty in tracking drainage evolution through time remains a fundamental limitation to the detrital method. Ideally all detrital investigations would incorporate a geomorphological study but as a minimum they should include detailed sedimentology so that any links between the tectonic and the geomorphologic may be recognised.

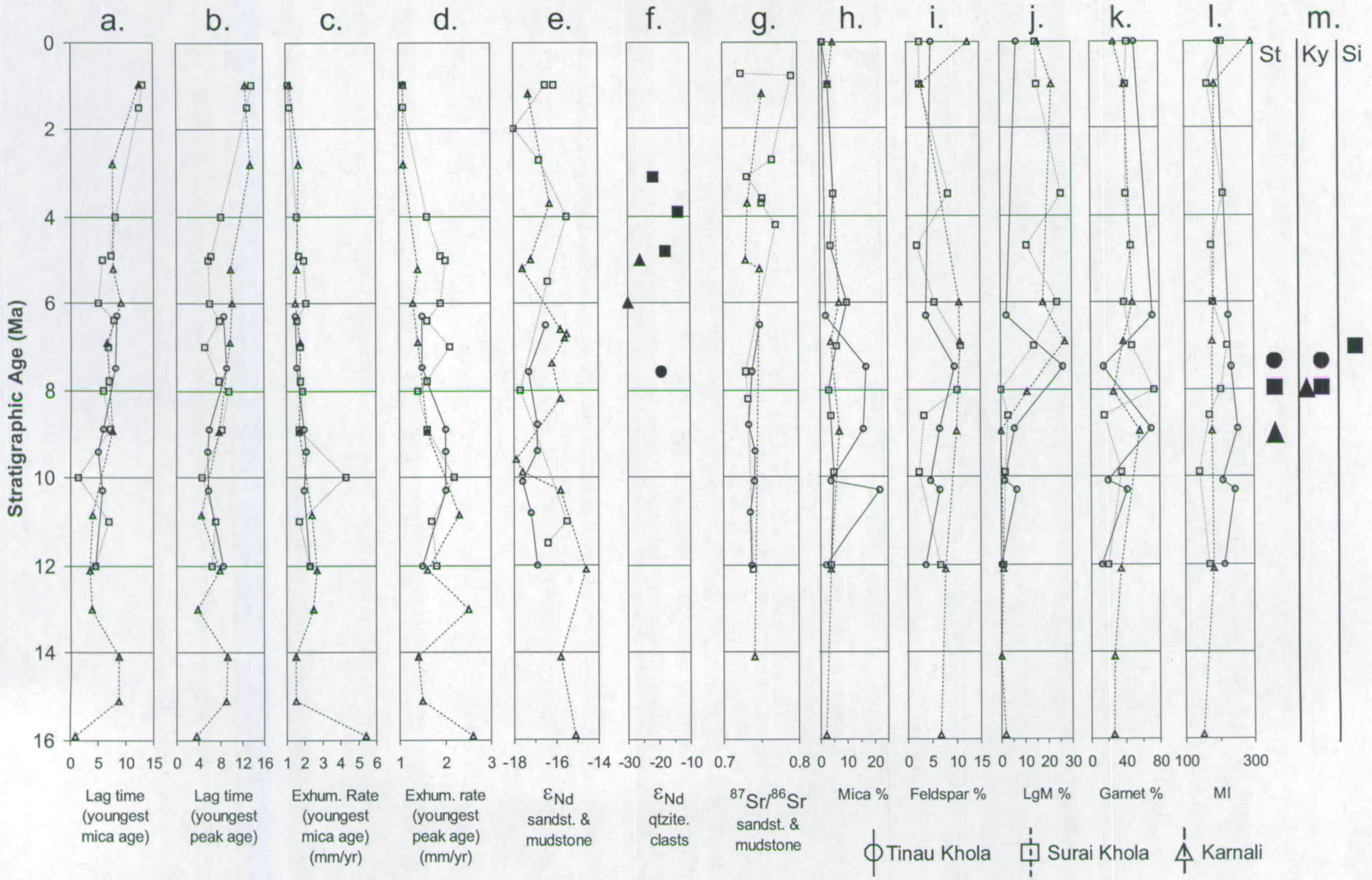


Figure 9.1. Caption on next page.

Figure 9.1. Variation in detrital signatures with respect to stratigraphic age. Circles and solid lines = Tinau Khola section, squares and small dashed lines = Surai Khola section, triangles and long dashed lines = Karnali section. **a.** and **b.** show how the lag-time varies depending on whether the youngest single grain age or the youngest peak age is used for the calculation. The youngest Karnali section single grain ages that were dated at SUERC were used to calculate lag-time for the 16-12 Ma sediment due to the large errors associated with the younger ages that were run at MIT. **c.** and **d.** show how exhumation rate (using the one dimensional model of White (2001)) varies for single grain age and youngest peak age data. **e.** includes data from Huyghe et al. (2001), Robinson et al. (2001), and three unpublished samples from P. Huyghe. **f.** gives ε_{Nd} values for individual quartzite pebbles which are not affected by sedimentary mixing complications. **g.** includes data from Galy (1999), Huyghe et al. (2001), and two unpublished samples from P. Huyghe. **h.** to **k.** show petrographic data plotted as a percentage of the detrital component, LgM = low-grade heavy minerals (epidote, zoisite, chloritoid). **L.** displays MI or metamorphic index data, see petrography data file on cd for explanation of MI. **m.** indicates when metamorphic index minerals first appear in the section.

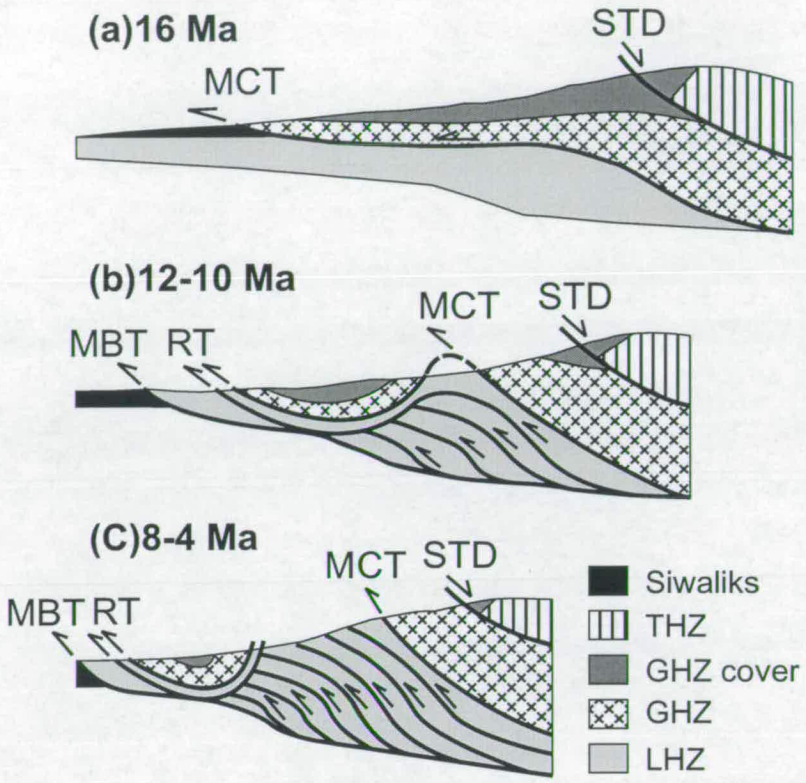


Figure 9.2. Schematic cross-sections through the central Himalayas to show orogenic evolution during Siwalik deposition. STD - South Tibetan Detachment, MCT - Main Central Thrust, RT - Ramgarh Thrust, MBT - Main Boundary Thrust, THZ - Tibetan Himalayan Zone, GHZ - Greater Himalayan Zone, LHZ - Lesser Himalayan Zone.

Acknowledgements

This thesis is dedicated to my parents for putting me through uni.

My gratitude is without measure for the help and encouragement given by my three supervisors, Dr's Yani Najman, Hugh Sinclair, and Malcolm Pringle.

Much help was also received from various other parties in both the field and lab environments – Jean-Louis Mugnier, Pascale Huyghe, Peter van der Beek, Mike Bickle, Hazel Chapman, Andy Carter, Eduardo Garzanti, Sergio Andò, Mike Searle, Peter DeCelles, Stuart Jamieson, Jim Imlach, Dan Barfod, Ajay Sitaula, Danny, and Tank Ojha.

Bibliography

Abbasi, I.A., & Friend, P.F., 2000, Exotic conglomerates of the Neogene Siwalik succession and their implications for the tectonic and topographic evolution of the western Himalaya, *in* Khan, M.A., Treloar, P.J., Searle, M.P., & Jan, M.Q., eds., Tectonics of the Nanga Parbat syntaxis and the western Himalaya: Geological Society Special Publication, v. 170, p. 455-466.

Ahmad, T., Harris, N., Bickle, M., Chapman, H., Bunbury, J., & Prince, C., 2000, Isotopic constraints on the structural relationships between the Lesser Himalayan Series and the High Himalayan Crystalline Series, Garhwal Himalaya: Geological Society of America Bulletin, v. 112, p. 467-477.

Aitchison, J.C., 1986, Stratigraphy, sedimentology and tectonic evolution of the Shimanto Terrane, Southwest Japan: Chikyu Kagaku = Earth Science, v. 40, p. 337-363.

Allen, J.R.L., 1963, The classification of cross-stratified units, with notes on their origin: Sedimentology, v. 2, p. 93-114.

Allen, J.R.L., 1964, Studies in fluviatile sedimentation: sex cyclothems from the Lower Old Red Sandstone, Anglo-Welsh Basin: Sedimentology, v. 3, p. 163-198.

Allen, J.R.L., 1970, A quantitative model of grain size and sedimentary structures in lateral deposits: Geology, v. 7, p. 129-146.

Allen, P.A., Homewood, P., & Williams, G.D., 1986, Foreland basins: an introduction, *in* Allen, P.A., and Homewood, P., eds., Foreland basins: Oxford, Blackwell, p. 3-12.

Allen, P.A., Crampton, S.L., & Sinclair, H.D., 1991, The inception and early evolution of the North Alpine foreland basin, Switzerland: Basin Research, v. 3, p. 143-163.

Alsdorf, D., & Nelson, D., 1999, Tibetan satellite magnetic low; evidence for widespread melt in the Tibetan crust?: Geology, v. 27, p. 943-946.

Amano, K., & Taira, A., 1992, Two-phase uplift of higher Himalayas since 17 Ma: Geology, v. 20, p. 391-394.

Amatya, K., & Jnawali, B., 1994, Geological map of Nepal, DMG / ICIMOD / DCG / UNEP, scale 1:1,000,000.

Appel, E., Roesler, W., & Corvinus, G., 1991, Magnetostratigraphy of the Miocene-Pleistocene Surai Khola Siwaliks in West Nepal: Geophysical Journal International, v. 105, p. 191-198.

Argles, T., Foster, G., Whittington, A., Harris, N., & George, M., 2003, Isotope studies reveal a complete Himalayan section in the Nanga Parbat syntaxis: Geology, v. 31, p. 1109-1112.

Arita, K., 1983, Origin of the inverted metamorphism of the Lower Himalayas, central Nepal: Tectonophysics, v. 95, p. 43-60.

Arita, K., Sharma, T., & Fujii, Y., 1984, Geology and structure of the Jajarkot-Piuthan area, central Nepal: Journal of Nepal Geological Society, v. 4, p. 5-27.

Arita, K., & Ganzawa, Y., 1997, Thrust tectonics and uplift process of the Nepal Himalaya revealed from fission-track ages: Journal of Geography, v. 106, p. 156-167.

Arita, K., & Paudel, L.P., 1997, Thrust tectonics in central Nepal and its significance on the Himalayan Uplift: Journal of Nepal Geological Society, v. 16, p. 38-39.

Arita, K., Dallmeyer, R.D., & Takasu, A., 1997, Tectonothermal evolution of the Lesser Himalaya, Nepal: constraints from $^{40}Ar/^{39}Ar$ ages from the Kathmandu Nappe: The Island Arc, v. 6, p. 372-385.

Auden, J.B., 1935, Traverses in the Himalaya: Records of the Geological Survey of India, Calcutta, v. 69.

Awasthi, N., & Prasad, M., 1989, Siwalik plant fossils from Surai Khola area, western Nepal: The Palaeobotanist, v. 38, p. 298-318.

Baker, D.M., Lillie, R.J., Yeats, R.S., Johnson, G.D., Yousuf, M., & Zamin, A.S.H., 1988, Development of the Himalayan frontal thrust zone; Salt Range, Pakistan: Geology, v. 16, p. 3-7.

Bally, A.W., Gordy, P.L., & Stewart, G.A., 1966, Structure, seismic data, and orogenic evolution of southern Canadian Rocky Mountains: Bulletin of Canadian Petroleum Geology, v. 14, p. 337-381.

Baranowski, J., Armbruster, J., Seeber, L., & Molnar, P., 1984, Focal depths and fault plane solutions of earthquakes and active tectonics of the Himalaya: Journal of Geophysical Research B, Solid Earth and Planets, v. 89, p. 6918-6928.

Barry, J.C., Johnson, N.M., Raza, S.M., & Jacobs, L.L., 1985, Neogene mammalian faunal change in southern Asia; correlations with climatic, tectonic, and eustatic events: Geology, v. 13, p. 637-640.

Bashyal, R.P., 1986, Geology of Lesser Himalaya, far western Nepal: Sciences de la Terre, Memoire, v. 47, p. 31-42.

Batt, G.E., & Brandon, M.T., 2002, Lateral thinking; 2-D interpretation of thermochronology in convergent orogenic settings: Tectonophysics, v. 349, p. 185-201.

Baud, A., Garzanti, E., & Mascle, G., 1985, Latest marine sediments (early Paleogene), geological events and nappe structure in central Zanskar area (NW Himalaya): Leicester, I Himalayan Workshop, Abstracts.

Beaumont, C., Fullsack, P., & Hamilton, J., 1992, Erosional control of active compressional orogens, *in* McClay, K.R., ed., Thrust tectonics: London, Chapman and Hall, p. 1-18.

Beaumont, C., Jamieson, R.A., Nguyen, M.H., & Lee, B., 2001, Himalayan tectonics explained by extrusion of a low-viscosity crustal channel coupled to focused surface denudation: Nature, v. 414, p. 738-742.

Beck, R.A., Burbank, D.W., Sercombe, W.J., Olson, T.L., & Khan, A.M., 1995, Organic carbon exhumation and global warming during the early Himalayan collision: Geology, v. 23, p. 387-390.

Bernet, M., Brandon, M.T., & Garver, J.I., 2001, Exhuming the Alps through time; clues from detrital fission-track ages: Earth system processes; programmes with abstracts, p. 83.

Bernet, M., & Spiegel, C., 2004, Detrital thermochronology; provenance analysis, exhumation, and landscape evolution of mountain belts: Geological Society of America Special Paper, p. 378.

Bertrand, G., Copeland, P., & France-Lanord, C., 2001, (super 40) Ar/ (super 39) Ar dating of detrital muscovites from modern rivers of Nepal: Earth system processes; prgrammes with abstracts, p. 81.

Beyssac, O., Bollinger, L., Avouac, J.-P., & Goffé, B., 2004, Thermal metamorphism in the Lesser Himalaya of Nepal determined from Raman spectroscopy of carbonaceous material: Earth and Planetary Science Letters, v. 225, p. 233-241.

Bickle, M.J., & McKenzie, D., 1987, The transport of heat and matter by fluids during metamorphism: Contributions to Mineralogy and Petrology, v. 95, p. 384-392.

Bickle, M.J., Wickham, S.M., Chapman, H.J., & Taylor, H.P.Jr., 1988, A strontium, neodymium and oxygen isotope study of hydrothermal metamorphism and crustal anatexis in the Trois Seigneurs Massif, Pyrenees, France: Contributions to Mineralogy and Petrology, v. 100, p. 399-417.

Bickle, M.J., Harris, N., Bunbury, J.M., Chapman, H.J., Fairchild, I.J., & Ahmad, T., 2001, Controls on the (super 87) Sr/ (super 86) Sr ratio of carbonates in the Garhwal Himalaya, headwaters of the Ganges: Journal of Geology, v. 109, p. 737-753.

Bilham, R., Larson, K.M., Freymueller, J.T., Jouanne, F., Le Fort, P., Leturmy, P., Mugnier, J.L., Gamond, J.F., Glot, J.P., Martinod, J., Chaudry, N.L., Chitrakar, G.R., Gautam, U.P., Koirala, B.P., Pandey, M.R., Ranabhat, R., Sapkota, S.N., Shrestha, P.L., Thakuri, M.C., Timilsina, U.R., Tiwari, D.R., Vidal, G., Vigny, C., Galy, A., & de Voogd, B., 1997, GPS measurements of present-day convergence across the Nepal Himalaya: Nature, v. 386, p. 61-64.

Boothroyd, J.C., 1972, Coarse-grained sedimentation on a braided outwash fan, northeast Gulf of Alaska: Technical Report – Coastal Research Division, University of South Carolina, p. 127.

Bordet, P., Colchen, M., & Le Fort, P., 1975, Geological studies in the Nyi-Shang region of the Nepalese Himalayas: Paris, CNRS, p. 138.

Bossart, P., & Ottiger, R., 1989, Rocks of the Murree Formation in northern Pakistan; indicators of a descending foreland basin of late Paleocene to middle Eocene age: Eclogae Geologicae Helvetiae, v. 82, p. 133-165.

Brandon, M.T., & Vance, J.A., 1992, Tectonic evolution of the Cenozoic Olympic subduction complex, Washington State, as deduced from fission track ages for detrital zircons: American Journal of Science, v. 292, p. 565-636.

Brasier, M.D., & Singh, P., 1987, Microfossils and Precambrian-Cambrian boundary stratigraphy at Maldeota, Lesser Himalaya: Geological Magazine, v. 124, p. 323-345.

Braun, J., & Sambridge, M., 1997, Modelling landscape evolution on geological time scales; a new method based on irregular spatial discretization: Basin Research, v. 9, p. 27-52.

Brewer, I.D., Burbank, D.W., & Hodges, K.V., 2003, Modelling detrital cooling-age populations; insights from two Himalayan catchments: Basin Research, v. 15, p. 305-320.

Bridge, J.S., & Leeder, M.R., 1979, A simulation model of alluvial stratigraphy: Sedimentology, v. 26, p. 617-644.

Bridge, J.S., & Jarvis, J., 1982, The dynamics of a river bend; a study in flow and sedimentary processes: Sedimentology, v. 29, p. 499-541.

Bridge, J.S., 1993, The interaction between channel geometry, water flow, sediment transport and deposition in braided rivers, *in* Best, J.L., & Bristow, C.S., eds., Braided Rivers: Geological Society of London Special Publication, v. 75, p. 13-71.

Bridge, J.S., et al., 1995, Ground-penetrating radar and coring used to study the large-scale structure of point-bar deposits in three dimensions: Sedimentology, v. 42, p. 839-852.

Brookfield, M.E., 1993, The Himalayan passive margin from Precambrian to Cretaceous times: Sedimentary Geology, v. 84, p. 1-35.

Brown, L.D., Zhao, W., Nelson, K.D., Hauck, M., Alsdorf, D., Ross, A., Cogan, M., Clark, M., Liu, X., & Che, J., 1996, Bright spots, structure, and magmatism in southern Tibet from INDEPTH seismic reflection profiling: Science, v. 274, p. 1688-1690.

Brun, J-P., Burg, J-P., & Chen, G.M., 1985, Strain trajectories above the Main Central Thrust (Himalaya) in southern Tibet: Nature, v. 313, p. 388-390.

Brunel, M., & Kienast, J-R., 1986, Petrologic and structural study of ductile Himalayan thrust faulting across the Everest-Makalu area, eastern Nepal: Canadian Journal of Earth Sciences, v. 23, p. 1117-1137.

Burbank, D.W., & Johnson, G.D., 1983, The late Cenozoic chronologic and stratigraphic development of the Kashmir intermontane basin, northwest Himalaya: Palaeogeography, Palaeoclimatology, Palaeoecology, v. 43, p. 205-235.

Burbank, D.W., Raynolds, R.G.H., & Johnson, G.D., 1986, Late Cenozoic tectonics and sedimentation in the north-western Himalayan Foredeep; II, Eastern limb of the Northwest Syntaxis and regional synthesis, *in* Allen, P.A., & Homewood, P., eds., Foreland basins: Special Publication of the International Association of Sedimentologists, London, Blackwell, v. 8, p. 293-306.

Burbank, D.W., Beck, R.A., Raynolds, R.G.H., Hobbs, R., & Tahirkheli, R.A.K., 1988, Thrusting and gravel progradation in foreland basins; a test of post-thrusting gravel dispersal: Geology, v. 16, p. 1143-1146.

Burbank, D.W., Raynolds, R.G.H., & Bouma, A.H., 1988b, Stratigraphic keys to the timing of thrusting in terrestrial foreland basins; applications to the northwestern Himalaya, *in* Burbank, D.W., ed., New perspectives in basin analysis, New York, Springer-Verlag, p. 331-351.

Burbank, D.W., & Beck, R.A., 1989, Early Pliocene uplift of the Salt Range; temporal constraints on thrust wedge development, Northwest Himalaya, Pakistan, *in* Malinconico, L.Jr., & Lillie, R.J., eds., Tectonics of the western Himalayas: Geological Society of America Special Paper, v. 232, p. 113-128.

Burbank, D.W., & Beck, R.A., 1991, Rapid, long-term rates of denudation: Geology, v. 19, p. 1169-1172.

Burbank, D.W., & Beck, R.A., 1991b, Models of aggradation versus progradation in the Himalayan Foreland: Geologische Rundschau, v. 80, p. 623-638.

Burbank, D.W., 1992, Causes of Recent Himalayan uplift deduced from deposited patterns in the Ganges Basin: Nature, v. 357, p. 680-683.

Burbank, D.W., Derry, L.A., & France-Lanord, C., 1993, Reduced Himalayan sediment production 8 Myr ago despite an intensified monsoon: Nature, v. 364, p. 48-50.

Burbank, D.W., Beck, R.A., and Mulder, T., 1996, The Himalayan foreland basin, *in* Yin, A., and Harrison, T.M., eds., The tectonic evolution of Asia: New York, Cambridge University Press, p. 149-188.

Burbank, D.W., McLean, J.K., Bullen, M., Abdrakhmatov, K.Y., & Miller, M.M., 1999, Partitioning of intermontane basins by thrust-related folding, Tien Shan, Kyrgyzstan: Basin Research, v. 11, p. 75-92.

Burbank, D.W., & Anderson, R.S., 2001, Tectonic geomorphology: Berlin, Blackwell Science, p. 274.

Burchfiel, B.C., & Royden, L.H., 1985, North-south extension within the convergent Himalayan region: Geology, v. 13, p. 679-682.

Burchfiel, B.C., Chen, Z., Hodges, K.V., Liu, Y., Roydon, L.H., Deng, C., & Xu, J., 1992, The South Tibetan detachment system, Himalayan Orogen; extension contemporaneous with and parallel to shortening in a collisional mountain belt: Geological Society of America, Special Paper, v. 269, 41 p.

Burchfiel, B.C., Clark, M., Wang, E., Chen, Z., Liu, Y., & Pan, G., 2000, Tectonic framework of the Namche Barwa region, Eastern Himalayan Syntaxis, SE Tibet: Geological Society of America, Abstracts with Programs, v. 32, p. 33.

Burg, J.P., & Chen, G.M., 1984, Tectonics and structural zonation of southern Tibet, China: Nature, v. 311, p. 219-223.

Burg, J.P., Guiraud, M., Chen, G.M., & Li, G.C., 1984, Himalayan metamorphism and deformations in the North Himalayan Belt (southern Tibet, China): Earth and Planetary Science Letters, v. 69, p. 391-400.

Burg, J-P., Nievergelt, P., Oberli, F., Seward, D., Davy, P., Maurin, J-C., Diao, Z., & Meier, M., 1998, The Namche Barwa syntaxis; evidence for exhumation related to compressional crustal folding: Journal of Asian Earth Sciences, v. 16, p. 239-252.

Burner, S.A., 1995, Isotopic preservation of Himalayan/Tibetan uplift, denudation and climatic histories of Siwalik Group sediments, south-central and south-eastern Nepal: Masters thesis, University of California, Los Angeles, p. 137.

Burrard, S.G., & Hayden, H.H., 1934, A sketch of the geography and geology of the Himalaya Mountains and Tibet: (revised by Burrard, S.G., & Herron, A.M.) Calcutta, Government of India Press, p. 359.

Butler, R.F., 1992, Paleomagnetism: magnetic domains to geologic terranes: Boston, Blackwell, p. 319.

Cande, S.C., & Kent, D.V., 1995, Revised calibration of the geomagnetic polarity timescale for the Late Cretaceous and Cenozoic: Journal of Geophysical Research, B, Solid Earth and Planets, v. 100, p. 6093-6095.

Carpena, J., & Rutkiewicz, W., 1989, Fission-track dating of apatites and zircons from the peak of K2 (8611 m), Pakistan: Eclogae Geologicae Helvetiae, v. 82, p. 735-742.

Carter, A., 1999, Constraining relationships between an evolving hinterland and basin sedimentation using a combined approach to U-Pb and fission-track detrital zircon dating: European Union of Geosciences conference abstracts, v. 4, p. 329.

Carter, A., Roques, D., & Bristow, 2000, Dedudation history of onshore central Vietman; constraints on the Cenozoic evolution of the western margin of the South China Sea: Tectonophysics, v. 322, p. 265-277.

Catlos, E.J., Harrison, T.M., Kohn, M.J., Grove, M., Ryerson, F.J., Manning, C.E., & Upreti, B.N., 2001, Geochronologic and thermobarometric constraints on the evolution of the Main Central Thrust, central Nepal Himalaya: Journal of Geophysical Research, B, Solid Earth and Planets, v. 106, p. 16177-16204.

Catlos, E.J., Harrison, T.M., Manning, C.E., Grove, M., Rai, S.M., Hubbard, M.S., & Upreti, B.N., 2002, Records of the evolution of the Himalayan orogen from in situ Th-Pb ion microprobe dating of monazite: Eastern Nepal and western Garhwal: Journal of Asian Earth Sciences, v. 20, p. 459-479.

Cattin, R., & Avouac, J.P., 2000, Modeling mountain building and the seismic cycle in the Himalaya of Nepal: Journal of Geophysical Research B, Solid Earth and Planets, v. 105, p. 13389-13407.

Cawood, P.A., & Nemchin, A.A., 2001, Paleogeographic development of the East Laurentian margin; constraints from U-Pb dating of detrital zircons in the Newfoundland Appalachians: Geological Society of America Bulletin, v. 113, p. 1234-1246.

Cerveny, P.F., Naeser, N.D., Zeitler, P.K., Naeser, C.W., Johnson, N.M., & Bouma, A.H., 1988, History of Uplift and relief of the Himalaya during the past 18 million years; evidence from fission-track ages of detrital zircons from sandstones of the Siwalik Group, *in* Kleinspehn, K.L., & Paola, C., eds., New perspectives in basin analysis: New York, Springer-Verlag, p. 43-61.

Cerveny, P.F., Johnson, N.M., Tahirkheli, R.A.K., & Bonis, N.R., 1989, Tectonic and geomorphic implications of Siwalik Group heavy minerals, Potwar Plateau, Pakistan, *in* Malinconico, L.L.Jr., & Lillie, R.J., eds., Tectonics of the western Himalayas: Geological Society of America Special Paper, v. 232, p. 129-136.

Chamberlain, C.P., Zeitler, P.K., Barnett, D.E., Winslow, D., Poulson, S.R., Leahy, T., & Hammer, J.E., 1995, Active hydrothermal systems during the recent uplift of Nanga Parbat, Pakistan Himalaya: Journal of Geophysical Research B, Solid Earth and Planets, v. 100, p. 439-453.

Champel, B., Van der Beek, P., Mugnier, J-L., & Leturmy, P., 2002, Growth and lateral propagation of fault-related folds in the Siwaliks of western Nepal; rates, mechanisms, and geomorphic signature: Journal of Geophysical Research B, Solid Earth and Planets, v. 107, p. 1-18.

Chen, Z., Liu, Y., Hodges, K.V., Burchfiel, B.C., Royden, L.H., & Deng, C., 1990, The Kangmar Dome; a metamorphic core complex in southern Xizang (Tibet): Science, v. 250, p. 1552-1556.

Chaudhri, R.S., 1971, Petrogenesis of Cenozoic sediments of north-western Himalayas: Geological Magazine, v. 108, p. 43-48.

Chaudhri, R.S., 1972, Heavy minerals from the Siwalik formations of the northwestern Himalayas: Sedimentary Geology, v. 8, p. 77-82.

Chaudhri, R.S., 1975, Sedimentology and genesis of the Cenozoic sediments of northwestern Himalayas (India): Geologische Rundchau, v. 64, p. 958-977.

Cliff, R.A., 1985, Isotopic dating in metamorphic belts: Journal of the Geological Society of London, v. 142, p. 97-110.

Clift, P., & Gaedicke, C., 2000, Stratigraphic development of the Indus Fan in the context of India-Asia collision: AAPG Bulletin, v. 84, p. 1412.

Clift, P., Shimizu, N., Layne, G., Gaedicke, C., Schlueter, H.U., Clark, M., & Amjad, S., 2000, Fifty-five million years of Tibetan evolution recorded in the Indus Fan: Eos Transactions, v. 81, p. 277-281.

Clift, P.D., Shimizu, N., Layne, G.D., & Blusztajn, J., 2001, Tracing patterns of erosion and drainage in the Paleogene Himalaya through ion probe Pb isotope analysis of detrital K-feldspars in the Indus Molasse, India: Earth and Planetary Science Letters, v. 188, p. 475-491.

Clift, P.D., Carter, A., Krol, M., & Kirby, E., 2002, Constraints on India-Eurasia collision in the Arabian Sea region taken from the Indus Group, Ladakh Himalaya, India, *in* Clift, P.D., Kroon, D., Gaedicke, C., & Craig, J., eds., The tectonic and climatic evolution of the Arabian Sea region: Geological Society Special Publications, v. 195, p. 97-116.

Cochran, J.R., 1990, Himalayan uplift, sea level, and the record of Bengal Fan sedimentation at the ODP Leg 116 sites: Proceedings of the Ocean Drilling Program, v. 116, p. 397-414.

Colchen, M., Le Fort, P., & Pecher, A., 1986, Geological research in the Nepal Himalayas, Annapurna, Manaslu, Ganesh Himal; 1:20,000 geological map: Paris, Cent. Natl. Rech. Sci., p. 137.

Coleman, J.M., 1966, Ecological changes in a massive freshwater clay sequence: Trans. Gulf-Cst Ass. Geol. Soc., v. 16, p. 159-174.

Coleman, J.M., 1969, Brahmaputra river; channel processes and sedimentation: Sedimentary Geology, v. 3, p. 131-139.

Coleman, M.E., 1996, Orogen-parallel and orogen-perpendicular extension in the central Nepalese Himalayas: Geological Society of America Bulletin, v. 108, p. 1594-1607.

Coleman, M.E., 1998, U-Pb constraints on Oligocene-Miocene deformation and anatexis within the central Himalaya, Marsyandi Valley, Nepal: American Journal of Science, v. 298, p. 553-571.

Coleman, M.E., & Hodges, K.V., 1998, Contrasting Oligocene and Miocene thermal histories from the hanging wall and footwall of the South Tibetan detachment in the central Himalaya from (super 40) Ar/ (super 39) Ar thermochronology, Marsyandi Valley, central Nepal: Tectonics, v. 17, p. 726-740.

Copeland, P., & Harrison, T.M., 1990, Episodic rapid uplift in the Himalaya revealed by (super 40) Ar/ (super 39) Ar analysis of detrital K-feldspar and muscovite, Bengal Fan: Geology, v. 18, p. 354-357.

Copeland, P., Harrison, T.M., Hodges, K.V., Maruejol, P., Le Fort, P., & Pecher, A., 1991, An early Pliocene thermal disturbance of the Main Central Thrust, central Nepal; implications for Himalayan tectonics: Journal of Geophysical Research, B, Solid Earth and Planets, v. 96, p. 8475-8500.

Copeland, P., LeFort, P., Ray, S.M., & Upreti, B.N., 1996, Cooling history of the Kathmandu crystalline nappe: $^{40}Ar/^{39}Ar$ results: Enriched: 30th International Geological Congress; Astracts, v. 30, p. 197.

Corrigan, J.D., & Crowley, K.D., 1990, Fission-track analysis of detrital apatites from Sites 717 and 718, Leg 116, central Indian Ocean: Proceedings of the Ocean Drilling Program, v. 116, p. 75-92.

Corvinus, G., 1988, The Mio-Plio-Pleistocene litho- and biostratigraphy of the Surai Khola Siwaliks in West Nepal; first results: Sciences de la Terre, v. 306, p. 1471-1477.

Corvinus, G., & Rimal, L. N., 2001, Biostratigraphy and geology of the Neogene Siwalik Group of the Surai Khola and Rato Khola areas in Nepal: Palaeogeography, Palaeoclimatology, Palaeoecology, v. 165, p. 251-279.

Coward, M.P., & Butler, R.H.W., 1985, Thrust tectonics and the deep structure of the Pakistan Himalaya: Geology, v. 13, p. 417-420.

Covey, M., 1986, The evolution of foreland basins to steady state; evidence from the western Taiwan foreland basin, *in* Allen, P.A., & Homewood, P., eds., Foreland basins, Special Publication of the International Association of Sedimentologists: Oxford, Blackwell, v. 8, p. 77-90.

Critelli, S., De Rosa, R., & Platt, J.P., 1990, Sandstone detrital modes in the Makran accretionary wedge, Southwest Pakistan; implications for tectonic setting and long-distance turbidite transportation: Sedimentary Geology, v. 68, p. 241-260.

Critelli, S., & Garzanti, E., 1994, Provenance of the lower Tertiary Murree redbeds (Hazara-Kashmir Syntaxis, Pakistan) and initial rising of the Himalayas: Sedimentary Geology, v. 89, p. 265-284.

Cullers, R.L., Barrett, T., Carlson, R., & Robinson, B., 1987, Rare-earth element and mineralogic changes in Holocene soil and stream sediment; a case study in the Wet Mountains, Colorado, USA: Chemical Geology, v. 63, p. 275-297.

Curray, J.R., & Moore, D.G., 1971, Growth of the Bengal deep-sea fan and denudation in the Himalayas: Geological Society of America Bulletin, v. 82, p. 563-572.

Curray, J.R., & Moore, D.G., 1974, Sedimentary and tectonic processes in the Bengal deep-sea fan and geosyncline, *in* Burk, C.A., & Drake, C.L., eds., The geology of continental margins: New York, Springer-Verlag, p. 617-627.

Dahal, R., Khosla, S.C., & Sah, R.B., 1997, Fresh water ostracods from the Siwalik beds of Tinau Khola section (Butwal area), western Nepal: Journal of Nepal Geological Society, v. 16, p. 55.

Daniel, C.G., Hollister, L.S., Parrish, R.R., & Grujic, D., 2003, Exhumation of the Main Central Thrust from Lower Crustal Depths, Eastern Bhutan Himalaya: Journal of Metamorphic Geology, v. 21, p. 317-334.

Davies, T.A., Kidd, R.B., & Ramsay, A.T.S., 1995, A time-slice approach to the history of Cenozoic sedimentation in the Indian Ocean: Sedimentary Geology, v. 96, p. 157-179.

Debon, F., Le Fort, P., Sheppard, S.M.F., & Sonet, J., 1986, The four plutonic belts of the Transhimalaya-Himalaya; a chemical, mineralogical, isotopic, and chronological synthesis along a Tibet-Nepal section: Journal of Petrology, v. 27, p. 219-250.

DeCelles, P.G., Gehrels, G.E., Quade, J., Ojha, T.P., Kapp, P.A., & Upreti, B.N., 1998a, Neogene foreland basin deposits, erosional unroofing, and the kinematic history of the Himalayan fold-thrust belt, western Nepal: Geological Society of America Bulletin, v. 110, p. 2-21.

DeCelles, P.G., Gehrels, G.E., Quade, J., & Ojha, T.P., 1998b, Eocene-early Miocene foreland basin development and the history of Himalayan thrusting, western and central Nepal: Tectonics, v. 17, p. 741-765.

DeCelles, P.G., Gehrels, G.E., Quade, J., LaReau, B., & Spurlin, M., 2000, Tectonic implications of U-Pb zircon ages of the Himalayan orogenic belt in Nepal: Science, v. 288, p. 497-499.

DeCelles, P.G., Garzione, C.N., Copeland, P., Upreti, B.N., Robinson, D.M., Quade, J., & Ojha, T.P., 2001, Stratigraphy, structure, and tectonic evolution of the Himalayan fold-thrust belt in Western Nepal: Tectonics, v. 20, p. 487-509.

DeCelles, P.G., Gehrels, G.E., Najman, Y., Martin, A.J., Carter, A., & Garzanti, E., 2004, Detrital geochronology and geochemistry of Cretaceous-Early Miocene strata of Nepal: implications for timing and diachroneity of initial Himalayan orogenesis: Earth and Planetary Science Letters, v. 227, p. 313-330.

Deer, W.A., Howie, R.A., & Zussman, J., 1992, An introduction to the rock-forming minerals: Harlow, Longman Scientific Technical, p. 696.

DeMets, C., Gordon, R.G., Argus, D.F., & Stein, S., 1990, Current plate motions: Geophysical Journal International, v. 101, p. 425-478.

DePaolo, D.J., & Wasserburg, G.J., 1976, Nd isotopic variations and petrogenetic models: Geophysical Research Letters, v. 3, p. 249-252.

Densmore, A.L., Ellis, M.A., & Anderson, R.S., 1998, Landsliding and the evolution of normal-fault-bounded mountains: Journal of Geophysical Research B, Solid Earth and Planets, v. 103, p. 15203-15219.

Derry, L.A., & France-Lanord, C., 1996, Neogene Himalayan weathering history and river (super 87) Sr/ (super 86) Sr; impact on the marine Sr record: Earth and Planetary Science Letters, v. 142, p. 59-74.

De Sigoyer, J., Guillot, S., Lardeaux, J-M., & Mascle, G., 1997, Glaucophane-bearing eclogites in the Tso Morari Dome (eastern Ladakh, NW Himalaya): European Journal of Mineralogy, v. 9, p. 1073-1083.

De Sigoyer, J., Chavagnac, V., Blichert-Toft, J., Villa, I.M., Luais, B., Guillot, S., Cosca, M., & Mascle, G., 2000, Dating the Indian continental subduction and collisional thickening in the Northwest Himalaya; multichronology of the Tso Morari eclogites: Geology, v. 28, p. 487-490.

Dettman, D.L., Kohn, M.J., Quade, J., Ryerson, F.J., Ojha, T.P., & Hamidullah, S., 2001: Geology, v. 29, p. 31-34.

Dewey, J.F., Cande, S.C., & Pitman, W.C., 1989, Tectonic evolution of the India/Eurasia collision zone: Eclogae Geologicae Helvetiae, v. 82, p. 717-734.

Dezes, P., 1999, Tectonic and metamorphic evolution of the central Himalayan Domain in Southeast Zanskar (Kashmir, India): Memoires de Geologie Lausanne, v. 32, p. 152.

Dickinson, W.R., Beard, L.S., Brakenridge, G.R., Erjavec, J.L., Ferguson, R.C., Inman, K.F., Knepp, R., Lindberg, F.A., & Ryberg, P.T., 1983, Provenance of North American Phanerozoic sandstones in relation to tectonic setting: Geological Society of America Bulletin, v. 94, p. 222-235.

Dickinson, W.R., 1974, Plate tectonics and sedimentation, Tectonics and sedimentation, Special Publication: Society of Economic Paleontologists and Mineralogists, v. 22, p. 1-27.

Dickinson, W.R., & Valloni, R., 1980, Plate settings and provenance of sands in modern ocean basins: Geology, v. 8, p. 82-86.

Dickinson, W.R., 1985, Interpreting provenance relations from detrital modes of sandstones, *in* Zuffa, G.G., ed., Provenance of arenites: Dordrecht-Boston, D. Reidel Publishing Company, p. 333-361.

Dietrich, V., & Gansser, A., 1981, The leucogranites of the Bhutan Himalaya (crustal anatexis versus mantle melting): Bulletin Suisse de Mineralogie et Petrographie, v. 61, p. 177-202.

Ding, L., Zhong, D., Yin, A., Kapp, P., & Harrison, T.M., 2001, Cenozoic structural and metamorphic evolution of the eastern Himalayan syntaxis (Namche Barwa): Earth and Planetary Science Letters, v. 192, p. 423-438.

Dixon, J.M., & Liu, S., 1992, Centrifuge modelling of the propagation of thrust faults, In McClay, K.R. ed., Thrust tectonics: London, Chapman and Hall, p. 53-69.

Dodson, M.H., 1973, Closure temperature in cooling geochronological and petrological systems: Contributions to Mineralogy and Petrology, v. 40, p. 259-274.

Dodson, M.H., 1979, Theory of cooling ages, *in* Jaeger, E., & Hunziker, J.C., eds., Lectures in isotope geology: Berlin, Springer-Verlag, p. 194-202.

Duncan, C.C., 1997, Tectonics, topography, climate, and erosion; analysis of Himalayan digital elevation data and numerical modelling: PhD, Cornell University, p. 208.

Edmond, J.M., 1992, Himalayan tectonics, weathering processes, and the strontium isotope record in marine limestones: Science, v. 258, p. 1594-1597.

Edwards, R.M., 1995, (super 40) Ar/ (super 39) Ar geochronology of the Main Central Thrust (MCT) region; evidence for late Miocene to Pliocene disturbances along the MCT, Marsyangdi River valley, west-central Nepal Himalaya: Journal of Nepal Geological Society, v. 10, p. 41-46.

Edwards, M.A., & Harrison, T.M., 1997, When did the roof collapse? Late Miocene north-south extension in the high Himalaya revealed by Th-Pb monazite dating of the Khula Kangri Granite: Geology, v. 25, p. 543-546.

Elderfield, H., 1986, Strontium isotope stratigraphy: Palaeogeography, Palaeoclimatology, Palaeoecology, v. 57, p. 71-90.

England, P., & McKenzie, D., 1982, A thin viscous sheet model for continental deformation: Geophysical Journal of the Royal Astronomical Society, v. 70, p. 295-321.

England, P.C., & Houseman, G.A., 1988, The mechanics of the Tibetan Plateau: Philosophical Transactions of the Royal Society of London A, Mathematical and Physical Sciences, v. 326, p. 301-320.

England, P.C., & Houseman, G., 1989, Extension during continental convergence, with application to the Tibetan Plateau: Journal of Geophysical Research B, Solid Earth and Planets, v. 94, p. 17561-17579.

England, P., Le Fort, P., Molnar, P., & Pecher, A., 1992, Heat sources for Tertiary metamorphism and anatexis in the Annapurna-Manaslu region, central Nepal: Journal of Geophysical Research B, Solid Earth and Planets, v. 97, p. 2107-2128.

English, N.B., Quade, J., DeCelles, P.G., & Garzione, C.N., 2000, Geologic control of Sr and major element chemistry in Himalayan rivers, Nepal: Geochimica et Cosmochimica Acta, v. 64, p. 2549-2566.

Ferrara, G., Lombardo, B., & Tonarini, S., 1983, Rb/Sr geochronology of granites and gneisses from the Mount Everest region, Nepal Himalaya: Geologische Rundschau, v. 72, p. 119-136.

Fleet, A.J., 1984, Aqueous and sedimentary geochemistry of the rare earth elements, *in* Henderson, P., ed., Rare earth element geochemistry: Netherlands, Elsevier, v. 2, p. 343-373.

Fleischer, R.L., Price, P.B., & Walker, R.M., 1975, Nuclear tracks in solids; principles and applications: Berkeley, University of California Press, p. 605.

Flynn, L.J. & Jacobs, L.L., 1982, Effects of changing environments on Siwalik rodent faunas of northern Pakistan: Palaeogeography, Palaeoclimatology, Palaeoecology, v. 38, p. 129-138.

Foster, D.A., Gleadow, A.J.W., & Mortimer, G., 1994, Rapid Pliocene exhumation in the Karakoram (Pakistan), revealed by fission-track thermochronology of the K2 gneiss: Geology, v. 22, p. 19-22.

Foster, G., Kinny, P., Vance, D., Prince, C., & Harris, N., 2000, The significance of monazite U-Th-Pb age data in metamorphic assemblages; a combined study of monazite and garnet chronometry: Earth and Planetary Science Letters, v. 181, p. 327-340.

France-Lanord, C., Derry, L., & Michard, A., 1993, Evolution of the Himalaya since Miocene time: isotopic and sedimentological evidence from the Bengal Fan, *in* Treloar, P.J, and Searle, M.P., eds., Himalayan Tectonics: London, Geological Society, p. 603-621.

France-Lanord, C., & Derry, L.A., 1994, delta (super 13) of organic carbon in the Bengal Fan; source evolution and transport of C3 and C4 plant carbon to marine sediments: Geochimica et Cosmochimica Acta, v. 58, p. 4809-4814.

Frank, W., Gansser, A., & Trommsdorff, V., 1977, Geological observations in the Ladakh area (Himalayas); a preliminary report: Bulletin Suisse de Mineralogie et Petrographie, v. 57, p. 89-113.

Frank, W., Grasemann, B., Guntli, P., & Miller, C., 1995, Geological map of the Kishtwar-ChambaKulu region (NW Himalaya India): Jahrbuch Geologischen Bundesanstalt Wien, v. 138, p. 299-308.

Froude, D.O., Ireland, T.R., Kinny, P.D., Williams, I.S., Compston, W., Williams, I.R., & Myers, J.S., Ion microprobe identification of 4,100-4,200-Myr-old terrestrial zircons: Nature, v. 304, p. 616-618.

Fuchs, G., 1977, The geology of the Karnali and Dolpo regions, western Nepal: Jahrbuch der Geologischen Bundesanstalt Wien, v. 120, p. 165-217.

Fuchs, G., 1982, The geology of western Zanskar: Jahrbuch der Geologischen Bundesanstalt Wien, v. 125, p. 1-50.

Fuchs, G., Widder, R.W., & Tuladhar, R., 1988, Contributions to the geology of the Annapurna Range (Manang area, Nepal): Jahrbuch der Geologischen Bundesanstalt Wien, v. 131, p. 593-607.

Gaetani, M., Garzanti, E., & Jadoul, F., 1985, Main structural elements of Zanskar, NW Himalaya (India): Rendiconti della Societa Geologica Italiana, v. 8, p. 3-8.

Gaetani, M., & Garzanti, E., 1991, Multicyclic history of the northern India continental margin (northwestern Himalaya): AAPG Bulletin, v. 75, p. 1427-1446.

Gallagher, K., Brown, R., & Johnson, C., 1998, Fission track analysis and its applications to geological problems: Annual Review of Earth and Planetary Sciences, v. 26, p. 519-572.

Galy, A., France-Lanord, C., & Derry, L.A., 1996, The late Oligocene-early Miocene Himalayan belt; constraints deduced from isotopic compositions of early Miocene turbidites in the Bengal Fan: Tectonophysics, v. 260, p. 109-118.

Galy, A., 1999, Etude géochimique de l'érosion actuelle de la chaîne himalayenne: PhD, Nancy, Institut National Polytechnique de Lorraine, 466 p.

Galy, A., & France-Lanord, C., 1999, Weathering processes in the Ganges-Brahmaputra basin and the riverine alkalinity budget: Chemical Geology, v. 159, p. 31-60.

Galy, A., & France-Lanord, C., 2001, Higher erosion rates in the Himalaya; geochemical constraints on riverine fluxes: Geology, v. 29, p. 23-26.

Gansser, A., 1964, The geology of the Himalayas: London, Wiley, p. 289.

Gansser, A., 1983, Geology of the Bhutan Himalaya: Memoires de la Societe Helvetiques des Sciences Naturelles, v. 96, p. 181.

Gartner, S., 1990, Neogene calcareous nannofossil biostratigraphy, Leg 116 (central Indian Ocean), *in* Stewart, N.J., & Winkler, W.R., eds., Proceedings of the Ocean Drilling Program: Scientific Results, v. 116, p. 165-187.

Garver, J.I., & Brandon, M.T., 1994, Erosional denudation of the British Columbia Coast Ranges as determined from fission-track ages of detrital zircon from the Tofino Basin, Olympic Peninsula, Washington; with Suppl. Data 9432: Geological Society of America Bulletin, v. 106, p. 1398-1412.

Garver, J.I., Brandon, M.T., Roden-Tice, M.K., & Kamp, P.J.J., 1999, Exhumation history of orogenic highlands determined by detrital fission-track thermochronology, *in* Ring, U., Brandon, M.T., Lister, G.S., & Willett, S.D., eds., Exhumation processes; normal faulting, ductile flow and erosion: London, Geological Society Special Publications, p. 283-304.

Garver, J.I., Brandon, M.T., Soloviev, A.V., & Bullen, M.E., 2000, Towards a more complete record of magmatism and exhumation in continental arcs, using detrital fission-track thermochrometry: Physics and Chemistry of the Earth, Part A: Solid Earth and Geodesy, v. 25, p. 565-570.

Garzanti, E., Baud, A., & Mascle, G., 1987, Sedimentary record of the northward flight of India and its collision with Eurasia (Ladakh Himalaya, India): Geodinamica Acta, v. 1, p. 297-312.

Garzanti, E., & Van Haver, T., 1988, The Indus clastics; forearc basin sedimentation in the Ladakh Himalaya (India): Sedimentary Geology, v. 59, p. 237-249.

Garzanti, E., Critelli, S., & Ingersoll, R.V., 1996, Paleogeographic and paleotectonic evolution of the Himalayan Range as reflected by detrital modes of Tertiary sandstones and modern sands (Indus transect, India and Pakistan): Geological Society of America Bulletin, v. 108, p. 631-642.

Garzanti, E., 1999, Stratigraphy and sedimentary history of the Nepal Tethys Himalaya passive margin: Journal of Asian Earth Sciences, v. 17, p. 805-827.

Garzanti, E., & Vezzoli, G., 2003, A classification of metamorphic grains in sands based on their composition and grade: Journal of Sedimentary Research, v. 73, p. 830-837.

Gautam, P., 1989, Magnetic properties of some late Paleozoic to Tertiary sedimentary rocks of Tansen area, Lesser Himalaya, Nepal: Journal of the Faculty of Science, Hokkaido University, Geology and Mineralogy, v. 22, p. 467-487.

Gautam, P., & Appel, E., 1994, Magnetic-polarity stratigraphy of Siwalik Group sediments of Tinau Khola section in west central Nepal, revisited: Geophysical Journal International, v. 117, p. 223-234.

Gautam, P., & Roesler, W., 1999, Depositional chronology and fabric of Siwalik group sediments in Central Nepal from magnetostratigraphy and magnetic anisotropy: Journal of Asian Earth Sciences, v. 17, p. 659-682.

Gautam, P., & Fujiwara, Y., 2000, Magnetic polarity stratigraphy of Siwalik Group sediments of Karnali River section in western Nepal: Geophysical Journal International, v. 142, p. 812-824.

Gehrels, G.E., DeCelles, P.G., Quade, J., Lareau, B.N., & Spurlin, M.S., 1999, Tectonic imnplications of detrital zircon ages from the Himalayan Orogen in Nepal: Geological Society of America, Abstracts with Programs, v. 31, p. 374.

Geldof, H.J., & de Vriend, H.J., 1983, Distribution of main flow velocity in alternating river bends, *in* Collinson, J.D., & Lewin, J., eds., Modern and Ancient Fluvial Systems: Special Publication of the International Association of Sedimentologists, p. 85-95.

Godin, L., Brown, R.L., & Hanmer, S., 1999, High strain zone in the hanging wall of the Annapurna Detachment, central Nepal Himalaya, *in* Macfarlane, A., Sorkhabi, R.B., & Quade, J., eds., Himalaya and Tibet; mountain roots to mountain tops: Boulder, Geological Society of America, p. 199-210.

Godin, L., Parrish, R.R., Brown, R.L., & Hodges, K.V., 2001, Crustal thickening leading to exhumation of the Himalayan metamorphic core of central Nepal; insight from U-Pb geochronology and (super 40) Ar/ (super 39) Ar thermochronology: Tectonics, v. 20, p. 729-747.

Goldstein, S.L., O'Nions, R.K., & Hamilton, P.J., 1984, A Sm-Nd isotopic study of atmospheric dusts and particulates from major river systems: Earth and Planetary Science Letters, v. 70, p. 221-236.

Goodbred, S.L.Jr., & Kuehl, S.A., 1999, Holocene and modern sediment budgets for the Ganges-Brahmaputra river system; evidence for highstand dispersal to flood-plain, shelf, and deep-sea depocenters: Geology, v. 27, p. 559-562.

Goudie, A., 1973, Duricrusts in Tropical and Subtropical Landscapes: Oxford, Clarendon Press, p. 174.

Gradstein, F.M., von Rad, U., Gibling, M.R., Jansa, L.F., Kaminski, M.A., Kristiansen, I.L., Ogg, J.G., Roehl, U., Sarti, M., Thurow, J.W., Westermann, G.E.G., & Wiedmann, J., 1992, Stratigraphy and depositional history of the Mesozoic continental margin of central Nepal: Geologisches Jahrbuch. Reihe B: Regionale Geologie Ausland, Stuttgart, Germany, v. 77, p. 141.

Graham, S.A., Dickinson, W.R., & Ingersoll, R.V., 1975, Himalayan-Bengal model for flysch dispersal in the Appalachian-Ouachita system: Geological Society of America Bulletin, v. 86, p. 273-286.

Graham, S.A., Ingersoll, R.V., & Dickinson, W.R., 1976, Common provenance for lithic grains in Carboniferous sandstones from Ouachita Mountains and Black Warrior Basin: Journal of Sedimentary Petrology, v. 46, p. 620-632.

Grasemann, B., & Vannay, J-C., 1999, Flow controlled inverted metamorphism in shear zones: Journal of Structural Geology, v. 21, p. 743-750.

Green, P.F., Duddy, I.R., Laslett, G.M., Hegarty, K.A., Gleadow, A.J.W. & Lovering, J.F., 1989, Thermal annealing of fission tracks in apatite: 4. Quantitative modelling techniques and extension to geological timescales: Chemical Geology, v. 79, p. 155-182.

Grujic, D., Casey, M., Davidson, C., Hollister, L.S., Kuendig, R., Pavlis, T.L., & Schmid, S.M., 1996, Ductile extrusion of the Higher Himalayan Crystalline in Bhutan; evidence from quartz microfabrics: Tectonophysics, v. 260, p. 21-43.

Grujic, D., Hollister, L.S., & Parrish, R.R., 2002, Himalayan metamorphic sequence as an orogenic channel; insight from Bhutan: Earth and Planetary Science Letters, v. 198, p. 177-191.

Guillot, S., Pecher, A., & Le Fort, P., 1993, Emplacement of Himalayan leucogranites records Tibetan extrusion: Late orogenic extension in mountain belts; international meeting Documents – BRGM, v. 219, p. 86-87.

Guillot, S., Hodges, K.V., Le Fort, P., & Pecher, A., 1994, New constraints on the age of the Manaslu Leucogranite; evidence for episodic tectonic denudation in the central Himalayas: Geology, v. 22, p. 559-562.

Guillot, S., Le Fort, P., Pecher, A., Barman, M.R., & Aprahamian, J., 1995, Contact metamorphism and depth of emplacement of the Manaslu Granite (central Nepal); implications for Himalayan orogenesis: Tectonophysics, v. 241, p. 99-119.

Guillot, S., 1999, An overview of the metamorphic evolution in central Nepal: Journal of Asian Earth Sciences, v. 17, p. 713-725.

Gupta, S., 1997, Himalayan drainage patterns and the origin of fluvial megafans in the Ganges foreland basin: Geology, v. 25, p. 11-14.

Gurung, D., 1998, Freshwater molluscs from the late Neogene Siwalik Group, Surai Khola, western Nepal: Journal of Nepal Geological Society, v. 17, p. 7-28.

Harris, N., Gass, I.G., & Hawkesworth, C.J., 1990, A geochemical approach to allochthonous terranes; a Pan-African case study: Philosophical Transactions of the Royal Society of London A, Mathematical and Physical Sciences, v. 331, p. 533-548.

Harris, N., Ayres, M., & Massey, J., 1995, Geochemistry of granitic melts produced during the incongruent melting of muscovite; implications for the extraction of Himalayan leucogranite magmas: Journal of Geophysical Research B, Solid Earth and Planets, v. 100, p. 15767-15777.

Harris, N., Bickle, M.J., Chapman, H., Fairchild, I., & Bunbury, J., 1998, The significance of Himalayan rivers for silicate weathering rates; evidence from the Bhote Kosi tributary: Chemical Geology, v. 144, p. 205-220.

Harris, N., Caddick, M., Kosler, J., Goswami, S., Vance, D., & Tindle, A., 2004, The pressure-temperature-time path of migmatites from the Sikkim Himalaya: Journal of Metamorphic Geology, v. 22, p. 249-264.

Harrison, T.M., Copeland, P., Kidd, W.S.F., & Yin, A., 1992, Raising Tibet: Science, v. 255, p. 1663-1670.

Harrison, T.M., Copeland, P., Hall, S.A., Quade, J., Burner, S., Ojha, T.P., & Kidd, W.S.F., 1993, Isotopic preservation of Himalayan/Tibetan uplift, denudation, and climatic histories of two molasses deposits: Journal of Geology, v. 101, p. 157-175.

Harrison, T.M., McKeegan, K.D., & Le Fort, P., 1995, Detection of inherited monazite in the Manaslu leucogranite by (super 208) Pb/ (super 232) Th ion microprobe dating; crystallization age and tectonic implications: Earth and Planetary Science Letters, v. 133, p. 271-282.

Harrison, T.M., Ryerson, F.J., Le Fort, P., Yin, A., Lovera, O.M., & Catlos, E.J., 1997, A late Miocene-Pliocene origin for the central Himalayan inverted metamorphism: Earth and Planetary Science Letters, v. 146, p. E1-E7.

Harrison, T.M., Grove, M., Lovera, O.M., & Catlos, E.J., 1998, A model for the origin of Himalayan anatexis and inverted metamorphism: Journal of Geophysical Research B, Solid Earth and Planets, v. 103, p. 27017-27032.

Harrison, T.M., Grove, M., Lovera, O.M., Catlos, E.J., & D'Andrea, J., 1999, The origin of Himalayan anatexis and inverted metamorphism; models and constraints: Journal of Asian Earth Sciences, v. 17, p. 755-772.

Hauck, M.L., Nelson, K.D., Brown, L.D., Zhao, W., & Ross, A.R., 1998, Crustal structure of the Himalayan orogen at approximately 90° east longitude from Project INDEPTH deep reflection profiles: Tectonics, v. 17, p. 481-500.

Heim, A., & Gansser, A., 1939, Central Himalaya: geological observations of the Swiss expedition 1936, v. 73, p. 245.

Henry, P., Le Pichon, X., & Goffe, B., 1997, Kinematic, thermal and petrological model of the Himalayas; constraints related to metamorphism within the underthrust Indian crust and topographic elevation: Tectonophysics, v. 273, p. 31-56.

Hisatomi, K., & Tanaka, S., 1994, Climatic and environmental changes at 9 Ma and 7.5 Ma in the Churia (Siwalik) Group, west central Nepal: Himalayan Geology, v. 15, p. 161-180.

His Majesty's Government of Nepal, Survey Department map, 1999, Butwal: sheet no. 098-12, 1:25000.

His Majesty's Government of Nepal, Survey Department map, 1999, Bhaluban: sheet no. 2782 04C, 1:25000.

His Majesty's Government of Nepal, Survey Department map, 1999, Karnali Chisapani: sheet no. 2881 06A, 1: 25000.

Hodges, K.V., Parrish, R.R., Housh, T.B., Lux, D.R., Burchfiel, B.C., Royden, L.H., & Chen, Z., 1992, Simultaneous Miocene extension and shortening in the Himalayan Orogen: Science, v. 258, p. 1466-1470.

Hodges, K.V., Hames, W.E., Olszewski, W., Burchfiel, B.C., Royden, L.H., & Chen, Z., 1994, Thermobarometric and (super 40) Ar/ (super 39) Ar geochronologic constraints on Eohimalayan metamorphism in the Dinggye area, southern Tibet: Contributions to Mineralogy and Petrology, v. 117, p. 151-163.

Hodges, K.V., Parrish, R.R., & Searle, M.P., 1996, Tectonic evolution of the central Annapurna Range, Nepalese Himalaya: Tectonics, v. 15, p. 1264-1291.

Hodges, K.V., 2000, Tectonics of the Himalaya and southern Tibet from two perspectives: Geological Society of America Bulletin, v. 112, p. 324-350.

Hodges, K.V., Hurtado, J.M., & Whipple, K.X., 2001, Southward extrusion of Tibetan crust and its effect on Himalayan tectonics: Tectonics, v. 20, p. 799-809.

Hodges, K.V., Schildgen, T., Whipple, K., Wobus, C., & Ruhl, K., 2004, Quaternary deformation, river steepening, and heavy precipitation at the front of the Higher Himalayan ranges: Earth and Planetary Science Letters, v. 220, p. 379-389.

Honegger, K., Dietrich, V., Frank, W., Gansser, A., Thoeni, M., & Trommsdorff, V., 1982, Magmatism and metamorphism in the Ladakh Himalayas (the Indus-Tsangpo suture zone): Earth and Planetary Science Letters, v. 60, p. 253-292.

Hoorn, C., Ojha, T., & Quade, J., 2000, Palynological evidence for vegetation development and climatic change in the sub-Himalayan zone (Neogene, central Nepal): Palaeogeography, Palaeoclimatology, Palaeoecology, v. 163, p. 133-161.

Houseman, G.A., & England, P.C., 1986, Finite strain calculations of continental deformation; 1, Method and general results for convergent zones: Journal of Geophysical Research B, v. 91, p. 3651-3663.

Hovan, S.A., & Rea, D.K., 1992, The Cenozoic record of continental mineral deposition on Broken and Ninetyeast ridges, Indian Ocean; southern African aridity and sediment delivery from the Himalayas: Paleoceanography, v. 7, p. 833-860.

Hovius, N., 1996, Regular spacing of drainage outlets from linear mountain belts: Basin Research, v. 8, p. 29-44.

Hovius, N., Stark, C.P., & Allen, P.A., 1997, Sediment flux from a mountain belt derived by landslide mapping: Geology, v. 25, p. 231-234.

Howard, A.D., & Kerby, G., 1983, Channel changes in badlands: Geological Society of America Bulletin, v. 94, p. 739-752.

Hubbard, M.S., 1989, Thermobarometric constraints on the thermal history of the Main Central thrust zone and Tibetan Slab, eastern Nepal Himalaya: Journal of Metamorphic Geology, v. 7, p. 19-30.

Hubbard, M.S., & Harrison, T.M., 1989, (super 40) Ar/ (super 39) Ar age constraints on deformation and metamorphism in the Main Central Thrust zone and Tibetan Slab, eastern Nepal Himalaya: Tectonics, v. 8, p. 865-880.

Hubbard, M.S., Royden, L., & Hodges, K.V., 1991, Constraints on unroofing rates in the High Himalaya, eastern Nepal: Tectonics, v. 10, p. 287-298.

Hubbard, M., & House, M., 2000, Low temperature dating of high mountain rocks; (U-Th)/He ages from Higher Himalayan samples, eastern Nepal: 15th Himalayan-Karakoram-Tibet workshop, Earth Science Frontiers, v. 7, p. 16-17.

Hughes, D.A., & Lewin, J., 1982, A small-scale flood plain: Sedimentology, v. 29, p. 891-895.

Humphrey, N.F., & Konrad, S.K., 2000, River incision or diversion in response to bedrock uplift: Geology, v. 28, p. 43-46.

Hurford, A.J., & Green, P.F., 1983, The zeta age calibration of fission-track dating: Chemical Geology, v. 41, p. 285-317.

Hurford, A.J., 1990, Standardization of fission track dating calibration; recommendation by the Fission Track Working Group of the I.U.G.S. Subcommission on Geochronology: Chemical Geology, v. 80, p. 171-178.

Hurford, A.J., & Carter, A., 1991, The role of fission track dating in discrimination of provenance, *in* Morton, A.C., Todd, S.P., & Haughton, P.D.W., eds., Developments in sedimentary provenance studies: Geological Society Special Publications, v. 57, p. 67-78.

Hurtado, J.M.Jr., Hodges, K.V., & Whipple, K., 2001, Neotectonics of the Thakkhola Graben and implications for Recent activity on the South Tibetan fault system in the central Nepal Himalaya: Geological Society of America Bulletin, v. 113, p. 222-240.

Hurtrez, J.E., Lucazeau, F., Lave, J., & Avouac, J.P., 1999, Investigations of the relationships between basin morphology, tectonic uplift, and denudation from study of an active fold belt in the Siwalik Hills, central Nepal: Journal of Geophysical Research B, Solid Earth and Planets, v. 104, p. 12779-12796.

Huyghe, P., Galy, A., Mugnier, J.-L., & France-Lanord, C., 2001, Propagation of the thrust system and erosion in the Lesser Himalaya: Geochemical and sedimentological evidence: Geology, v. 29, p. 1007-1010.

Ingersoll, R.V., & Suczek, C.A., 1979, Petrology and provenance of Neogene sand from Nicobar and Bengal fans, DSDP sites 211 and 218: Journal of Sedimentary Petrology, v. 49, p. 1217-1228.

Ingersoll, R.V., Pickle, J.D., Sares, S.W., Bullard, T.F., Ford, R.L., & Grimm, J.P., 1984, The effect of grain size on detrital modes: a test of the Gazzi- Dickinson point-counting method (Holocene, sand, New Mexico, USA): Journal of Sedimentary Petrology, v. 54, p. 103-116.

Ingersoll, R.V., 1988, Tectonics of sedimentary basins: Geological Society of America Bulletin, v. 100, p. 1704-1719.

Jackson, M.E., & Bilham, R., 1994, 1991-1992 GPS measurements across the Nepal Himalaya: Geophysical Research Letters, v. 21, p. 1169-1172.

Jackson, J., Norris, R., & Youngson, J., The structural evolution of active fault and fold systems in central Otago, New Zealand; evidence revealed by drainage patterns: Journal of Structural Geology, v. 18, p. 217-234.

Jadoul, F., Berra, F., & Garzanti, E., 1998, The Tethys Himalayan passive margin from Late Triassic to Early Cretaceous (South Tibet): Journal of Asian Earth Sciences, v. 16, p. 173-194.

Jain, A.K., Kumar, D., Singh, S., Kumar, A., & Lal, N., 2000, Timing, quantification and tectonic modelling of Pliocene-Quaternary movements in the NW Himalaya; evidence from fission track dating: Earth and Planetary Science Letters, v. 179, p. 437-451.

Jaupart, C., & Provost, A., 1985, Heat focussing, granite genesis and inverted metamorphic gradients in continental collision zones: Earth and Planetary Science Letters, v. 73, p. 385-397.

Jenkin, G.R.T., 1997, Do cooling paths derived from mica Rb-Sr data reflect true cooling paths?: Geology, v. 25, p. 907-910.

Johnson, N.M., Opdyke, N.D., Johnson, G.D., Lindsay, E.H., & Tahirkheli, R.A.K., 1982, Magnetic polarity stratigraphy and ages of Siwalik Group rocks of the Potwar Plateau, Pakistan: Palaeogeography, Palaeoclimatology, Palaeoecology, v. 37, p. 17-42.

Johnson, G.D., Zeitler, P., Naeser, C.W., Johnson, N.M., Summers, D.M., Frost, C.D., Opdyke, N.D., & Tahirkheli, R.A.K., 1982b, The occurrence and fission-track ages of late Neogene and Quaternary volcanic sediments, Siwalik Group, northern Pakistan: Palaeogeography, Palaeoclimatology, Palaeoecology, v. 37, p. 63-93.

Johnson, G.D., Opdyke, N.D., Tandon, S.K., & Nanda, A.C., 1983, The magnetic polarity stratigraphy of the Siwalik Group at Haritalyangar (India) and a new last appearance datum for Ramapithecus and Sivapithecus in Asia: Palaeogeography, Palaeoclimatology, Palaeoecology, v. 44, p. 223-249.

Johnson, N.M., Stix, J., Tauxe, L., Cerveny, P.F., & Tahirkheli, R.A.K., 1985, Paleomagnetic chronology, fluvial processes, and tectonic implications of the Siwalik deposits near Chinji village, Pakistan: Journal of Geology, v. 93, p. 27-40.

Johnson, G.D., Raynolds, R.G.H., & Burbank, D.W., 1986, Late Cenozoic tectonics and sedimentation in the north-western Himalayan Foredeep; I, Thrust ramping and associated deformation in the Potwar region, *in* Allen, P.A., & Homewood, P., eds., Foreland basins: Special Publication of the International Association of Sedimentologists, v. 8, p. 273-291.

Johnson, M.R.W., & Oliver, G.J.H., 1990, Precollision and postcollision thermal events in the Himalaya: Geology, v. 18, p. 753-756.

Johnson, M.R.W., Oliver, G.J.H., Parrish, R.R., & Johnson, S.P., 2001, Synthrusting metamorphism, cooling, and erosion of the Himalayan Kathmandu Complex, Nepal: Tectonics, v. 20, p. 394-415.

Johnson, M.R.W., 2003, Insight into the nature of Indian crust underthrusting the Himalaya: Terra Nova, v. 15, p. 46-51.

Johnson, M.R.W., & Harley, S.H., 2003, Kinematic model for the Main Central thrust in Nepal: Comment and Reply: Geology, v. 31, p. 40.

Jouanne, F., Mugnier, J-L., Pandey, M.R., Gamond, J.F., Le Fort, P., Surrurier, L, Vigny, C., & Avouac, J.P., 1999, Oblique convergence in the Himalayas of western Nepal deduced from Preliminary results of GPS measurements: Geophysical Research Letters, v. 26, p. 1933-1936.

Khan, M.J., Opdyke, N.D., & Tahirkheli, R.A.K., 1988, Magnetic stratigraphy of the Siwalik Group, Bhittani, Marwat, and Khasor ranges, northwestern Pakistan and the timing of Neogene tectonics of the Trans Indus: Journal of Geophysical Research B, Solid Earth and Planets, v. 93, p. 11773-11790.

Khan, I.A., Bridge, J.S., Kappelman, J., & Wilson, R., 1997, Evolution of Miocene fluvial environments, eastern Potwar plateau, northern Pakistan: Sedimentology, v. 44, p. 221-251.

Kaneoka, I., & Kono, M., 1981, 40Ar/39Ar dating of Himalayan rocks from the Mount Everest region: Journal of Geophysics, v. 49, p. 207-211.

Karunakaran, C., & Ranga Rao, A., 1979, Status of exploration for hydrocarbons in the Himalayan region – contributions to stratigraphy and structure: Oil and Natural Gas Commission, p. 1-66.

Kayal, J.R., 1996, Precursor seismicity, foreshocks and aftershocks of the Uttarkashi earthquake of October 20, 1991 at Garhwal Himalaya: Tectonophysics, v. 263, p. 339-345.

Kayastha, N.B., 1992, Stratigraphy of the lower Tertiary rocks of Nepal Himalaya: Journal of the Nepal Geological Society, v. 8, p. 21-30.

Ketcham, R.A., Donelick, R.A., & Carlson, W.D, 1999, Variability of apatite fission-track annealing kinetics: III Extrapolation to geological time-scales: American Mineralogist, v. 84, p. 1235-1255.

Kirby, E., & Whipple, K., 2001, Quantifying differential rock-uplift rates via stream profile analysis: Geology, v. 29, p. 415-418.

Klootwijk, C.T., Gee, J.S., Peirce, J.W., Smith, G.M., & McFadden, P.L., 1992, An early India-Asia contact; paleomagnetic constraints from Ninetyeast Ridge, ODP Leg 121; with Suppl. Data 92-15: Geology, v. 20, p. 395-398.

Kohn, M.J., Catlos, E.J., Ryerson, F.J., & Harrison, T.M., 2001, Pressure-temperature-time path discontinuity in the Main Central Thrust zone, central Nepal: Geology, v. 29, p. 571-574.

Konomatsu, M., 1997, Miocene leaf-fossil assemblages of the Churia (Siwalik) Group in Nepal and their paleoclimatic implication: Journal of the Geological Society of Japan, v. 103, p. 265-274.

Konomatsu, M., & Awasthi, N., 1999, Plant fossils from Arung Khola and Binai Khola formations of Churia Group (Siwalik), west central Nepal, and their palaeoecological and phytogeographical significance: The Palaeobotanist, v. 48, p. 163-181.

Kooi, H., & Beaumont, C., 1994, Surface processes model of the effect of tectonic uplift and denudation timescales on large-scale geomorphology: Eos Transactions, v. 75, p. 289.

Koons, P.O., 1994, Three-dimensional critical wedges; tectonics and topography in oblique collisional orogens: Journal of Geophysical Research B, Solid Earth and Planets, v. 99, p. 13301-13315.

Kotila, B.S., & Mathur, P.D., Lower vertebrate fauna from the Upper Siwaliks of Surai Khola, Dang Valley, western Nepal: Journal of the Palaeontological Society of India, v. 42, p. 169-174.

Kraus, M.J., & Aslan, A., 1993, Eocene hydromorphic paleosols: significance for interpreting ancient floodplain processes: Journal of Sedimentary Petrology, v. 63, p. 453-463.

Krogh, T.E., & Keppie, J.D., 1987, Detrital zircon ages indicating a North African provenance for the Goldenville Formation of Nova Scotia: Report – Department of Mines and Energy, Halifax, p. 208.

Kroon, D., Steens, T.N.F., & Troelstra, S.R., 1991, Onset of monsoonal related upwelling in the western Arabian Sea as revealed by planktonic foraminifers: Proceedings of the Ocean Drilling Program, Scientific Results, v. 117, p. 257-263.

Krummenacher, D., Basett, A.M., Kingery, F.A., & Layne, H.F., 1978, Petrology, metamorphism and K/Ar age determinations in eastern Nepal, *in* Saklani, P.S., ed., Tectonic geology of the Himalaya: p. 151-165.

Krynine, P.D., 1937, Petrography and genesis of the Siwalik Series (India): American Journal of Science, v. 204, p. 422-446.

Kutzbach, J.E., Prell, W.L., & Ruddiman, W.F., 1993, Sensitivity of Eurasian climate to surface uplift of the Tibetan Plateau: Journal of Geology, v. 101, p. 177-190.

Lal, R.K., Mukerji, S., & Ackermand, D., 1981, Deformation and Barrovian metamorphism at Takdah, Darjeeling (Eastern Himalaya), *in* Saklani, P.S., ed., Metamorphic tectonites of the Himalaya: Delhi, Today and Tomorrow's, p. 231-278.

Larson, K.M., Buergmann, R., Bilham, R., & Freymueller, J.T., 1999, Kinematics of the India-Eurasia collision zone from GPS measurements: Journal of Geophysical Research B, Solid Earth and Planets, v. 104, p. 1077-1093.

Lavé, J., & Avouac, J.P., 2000, Active folding of fluvial terraces across the Siwaliks Hills, Himalayas of central Nepal: Journal of Geophysical Research B: Solid Earth, v. 105, p. 5735-5770.

Leeder, M.R., 1975, Pedogenic carbonates and flood sediment accretion rates: a quantitative model for alluvial arid-zone lithofacies: Geological Magazine, v. 112, p. 257-270.

Lee, J., Hacker, B., Dinklage, W., Wang, Y., Gans, P., Calvert, A., Wan, J., Chen, W., Blythe, A., & McClelland, W., 1999, Contraction and extension in southern Tibet; structural, petrologic, and thermochronologic constraints from the North Himalayan gneiss domes: Eos Transactions, v. 80, p. 991.

Le Fort, P., 1975, Himalayas; the collided range; present knowledge of the continental arc: American Journal of Science, p. 1-44.

Le Fort, P., Debon, F., & Sonet, J., 1980, The "Lesser Himalayan" cordierite granite belt typology and age of the pluton of Manserah (Pakistan): Proceedings of the International Committee on Geodynamics, v. 13, p. 51-61.

Le Fort, P., 1981, Manaslu leucogranite; a collision signature of the Himalaya, a model for its genesis and emplacement: Journal of Geophysical Research B, Solid Earth and Planets, v. 86, p. 10545-10568.

Le Fort, P., Debon, F., & Sonet, J., 1983, The lower Palaeozoic "Lesser Himalayan" granitic belt; emphasis of the Simchar pluton of central Nepal, *in* Shams, F.A., ed., Granites of Himalayas, Karakoram and Hindu Kush: Punjab University, Pakistan, p. 235-255.

Le Fort, P., 1986, Metamorphism and magmatism during the Himalayan collision, *in* Coward, M.P., & Ries, A.C., eds., Collision tectonics: Geological Society Special Publications, London, v. 19, p. 159-172.

Le Fort, P., Cuney, M., Deniel, C., France-Lanord, C., Sheppard, S.M.F., Upreti, B.N., & Vidal, P., 1987, Crustal generation of the Himalayan leucogranites: Tectonophysics, v. 134, p. 39-57.

Le Fort, P., & France-Lanord, C., 1995, Granites from Mustang and surrounding regions (central Nepal): Journal of Nepal Geological Society, v. 11, p. 53-57.

Levey, R.A., 1978, Bed-form distribution and internal stratification of coarse-grained point bars, Upper Congaree River, S.C., *in* Miall, A.D., ed., Fluvial Sedimentology: Calgary, Mem. Can. Soc. Petrol. Geol., v. 5, p. 105-127.

Lillie, R.J., Johnson, G.D., Yousuf, M., Zamin, A.S.H., & Yeats, R.S., 1987, Structural development within the Himalayan foreland fold-and-thrust belt of Pakistan, *in* Beaumont, C., & Tankard, A., eds., Sedimentary basins and basin-forming mechanisms: Atlantic Geoscience Society Special Publication, v. 5, p. 379-392.

Liu, G., & Einsele, G., 1994, Sedimentary history of the Tethyan basin in the Tibetan Himalayas: Geologische Rundschau, Berlin, Germany, v. 83, p. 32-61.

Lombardo, B., Pertusati, P., Rolfo, F., & Visona, D., 1998, First report of eclogites from the E Himalaya; implications for the Himalayan Orogeny: Momorie di Scienze Geologiche, v. 50, p. 67-68.

Lombardo, B., Rolfo, F., & Compagnoni, R., 2000, Glaucophane and barroisite eclogites from the upper Kaghan Nappe; implications for the metamorphic history of the NW Himalaya, *in* Khan, M.A., Treloar, P.J., Searle, M.P., & Jan, M.Q., eds., Tectonics of the Nanga Parbat syntaxis and the western Himalaya: Geological Society Special Publications, v. 170, p. 411-430.

Lyon-Caen, H., & Molnar, P., 1983, Constraints on the structure of the Himalaya from an analysis of gravity anomalies and a flexural model of the lithosphere: Journal of Geophysical Research B, Solid Earth and Planets, v. 88, p. 8171-8191.

Lyon-Caen, H., & Molnar, P., 1985, Gravity anomalies, flexure of the Indian Plate, and the structure, support and evolution of the Himalaya and Ganga Basin: Tectonics, v. 4, p. 513-538.

Macfarlane, A.M., Hodges, K.V., & Lux, D., 1992, A structural analysis of the Main Central Thrust zone, Langtang National Park, central Nepal Himalaya: Geological Society of America Bulletin, v. 104, p. 1389-1402.

Macfarlane, A.M., 1993, Chronology of tectonic events in the crystalline core of the Himalaya, Langtang National Park, central Nepal: Tectonics, v. 12, p. 1004-1025.

Maluski, H., Matte, P., Brunel, M., & Xiao, X, 1988, Argon 39 - argon 40 dating of metamorphic and plutonic events in the North and High Himalaya belts (southern Tibet, China): Tectonics, v. 7, p. 299-326.

Manage, M.A., & Maurer, H.F.W., 1992, Heavy minerals in colour: London, Chapman & Hall, p. 147.

Marshak, S., & Wilkerson, M.S., 1992, Effect of overburden thickness on thrust belt geometry and development: Tectonics, v. 11, p. 560-566.

Massey, J.A., 1994, Contrasting fluid-deformation-melt histories within the high Himalayan crystallines, Langtang Valley, Nepal: v. 58A, p. 567-568.

McDougall, I., & Harrison, T.M., 1988, Geochronology and thermochronology by the (super 40) Ar/ (super 39) Ar method: Oxford University Press, p. 212.

McDougal, J.W., & Khan, S.H., 1990, Strike-slip faulting in a foreland fold-thrust belt; the Kalabagh Fault and western Salt Range, Pakistan: Tectonics, v. 9, p. 1061-1075.

McElroy, R., Cater, J., Roberts, I., Peckham, A., & Bond, M., 1990, The structure and stratigraphy of SE Zanskar, Ladakh Himalaya: Journal of the Geological Society of London, v. 147, p. 989-997.

McLennan, S.M., 1989, Rare earth elements in sedimentary rocks; influence of provenance and sedimentary processes, *in* Lipin, B.R., & McKay, G.A., eds., Geochemistry and mineralogy of rare earth elements, Reviews in Mineralogy: Mineralogical Society of America, v. 21, p. 169-200.

Medlicott, H.B., 1868, The Alps and the Himalaya, a geological comparison: Quarterly Journal of the Geological Society London, v. 24, p. 34-52.

Meigs, A.J., Burbank, D.W., & Beck, R.A., 1995, Middle-late Miocene (>10 Ma) formation of the Main Boundary Thrust in the western Himalaya: Geology, v. 23, p. 423-426.

Merrihue, C., & Turner, G., 1966, Potassium-argon dating by activation with fast neutrons: Journal of Geophysical Research, v. 71, p. 2852-2859.

Metcalf, R.P., 1993, Pressure, temperature and time constraints on metamorphism across the Main Central thrust zone and high Himalayan slab in the Garhwal Himalaya, *in* Treloar, P.J., and Searle, M.P., eds, Himalayan Tectonics: Geological Society London, Special Publications, v. 74, p. 485-509.

Milliman, J.D., Quraishee, G.S., & Beg, M.A.A., 1984, Sediment discharge from the Indus River to the ocean; past, present and future, *in* Haq, B.U., & Milliman, J.D., eds., Marine geology and oceanography of Arabian Sea and coastal Pakistan: New York, Von Nostrand Reinhold Co., p. 65-70.

Mohan, A., Windley, B.F., & Searle, M.P., 1989, Geothermobaromety and development of inverted metamorphism in the Darjeeling-Sikkim region of the eastern Himalaya: Journal of Metamorphic Geology, v. 7, p. 95-110.

Molnar, P., & Tapponnier, P., 1975, Cenozoic tectonics of Asia; effects of a continental collision: Science, v. 189, p. 419-426.

Molnar, P., & Tapponnier, P., 1978, Active tectonics of Tibet: Journal of Geophysical Research, v. 83, p. 5361-5375.

Molnar, P., 1984, Structure and tectonics of the Himalaya; constraints and implications of geophysical data: Annual Review of Earth and Planetary Sciences, v. 12, p. 489-518.

Molnar, P., 1988, A review of geophysical constraints on the deep structure of the Tibetan Plateau, the Himalaya and the Karakoram, and their tectonic implications, *in* Shackleton, R.M., Dewey, J.F., & Windley, B.F., eds., Tectonic evolution of the Himalayas and Tibet: Philosophical Transactions of the Royal Society of London, Series A: Mathematical and Physical Sciences, v. 326, p. 33-88.

Molnar, P., & Lyon-Caen, H., 1989, Fault plane solutions of earthquakes and active tectonics of the Tibetan Plateau and its margins: Geophysical Journal of the Royal Astronomical Society, v. 99, p. 123-153.

Molnar, P., England, P., & Martinod, J., 1993, Mantle dynamics, uplift of the Tibetan Plateau, and the Indian monsoon: Reviews of Geophysics, v. 31, p. 357-396.

Moore, G.F., 1979, Petrography of subduction zone sandstones from Nias Island, Indonesia: Journal of Sedimentary Petrology, v. 49, p. 71-84.

Moore, M.A., & England, P.C., 2001, On the inference of denudation rates from cooling ages of minerals: Earth and Planetary Science Letters, v. 185, p. 265-284.

Morrison, C.W.K., & Oliver, G.J.H., 1993, A study of illite crystallinity and fluid inclusions in the Kathmandu Klippe and the Main Central Thrust zone, Nepal, *in* Treloar, P.J., & Searle, M.P., eds., Himalayan tectonics: Geological Society Special Publications, v. 74, p. 525-540.

Morton, A., 1985, Heavy minerals in provenance studies, *in* Zuffa, G.G., ed., Provenance of arenites: NATO ASI Series C: Mathematical and Physical Sciences, Dordrecht-Boston, D. Reidel Publishing Company, v. 148, p. 249-277.

Mugnier, J.-L., Mascle, G., & Faucher, T., 1993, Structure of the Siwaliks of western Nepal: an intracontinental accretionary prism: International Geology Review, v. 35, p. 1-16.

Mugnier, J-L., Leturmy, P., Delcaillau, B., & Huyghe, P., 1998, The break-back thrust splay of the Main Dun Thrust (Himalayas of western Nepal): evidence of an intermediate displacement scale between earthquake slip and finite geometry of thrust systems: Journal of Structural Geology, v. 20, p. 857-864.

Mugnier, J.-L., Huyghe, P., Chalaron, E., Vidal, G., Husson, L., Delcaillau, B., Leturmy, P., & Mascle, G., 1999, The Siwaliks of western Nepal I. Geometry and kinematics: Journal of Asian Earth Sciences, v. 17, p. 629-642.

Mugnier, J-L., Huyghe, P., & Gajurel, A.P., 2001, Structural and morphological evidences for displacement pulses along the thrusts of the Siwaliks of western Nepal: Journal of Asian Earth Sciences, v. 19, p. 46.

Mugnier, J.-L., Huyghe, P., Leturmy, P., & Jouanne, F., 2004, Episodicity and rates of thrust sheet motion in Himalaya (Western Nepal), *in* McClay, K.R., ed., Thrust Tectonics and Hydrocarbon Systems: AAPG Memoir, v. 82, p. 91-114.

Mulder, T.J., 1991, Isochronous paleogeographies and stratigraphic evolution of the northwest Himalayan foredeep, 8.5-5 Ma, central and eastern Potwar Plateau, Pakistan: Master's Thesis, University of Southern California, Los Angeles.

Mulder, T.J., & Burbank, D.W., 1993, The impact of incipient uplift on patterns of fluvial deposition; an example from the Salt Range, northwest Himalayan foreland, Pakistan, *in* Marzo, M., & Puigdefabregas, C., eds., Alluvial sedimentation: Special Publication of the International Association of Sedimentologists, v. 17, p. 521-539.

Munthe, J., Dongol, B., Hutchison, J.H., Kean, W.F., Munthe, K., & West, R.M., 1983, New fossil discoveries from the Miocene of Nepal include a hominoid: Nature, v. 303, p. 331-333.

Myrow, P.M., Hughes, N.C., Paulsen, T.S., Williams, I.S., Parcha, S.K., Thompson, K.R., Bowring, S.A., Peng, S.C., & Ahluwalia, A.D., 2003, Integrated tectonostratigraphic analysis of the Himalaya and implications for its tectonic reconstruction: Earth and Planetary Science Letters, v. 212, p. 433-441.

Najman, Y., Clift, P., Johnson, M.R.W., & Robertson, A.H.F., 1993, Early stages of foreland basin evolution in the Lesser Himalaya, N India, *in* Treloar, P. J., & Searle, M. P., eds., Himalayan Tectonics: Geological Society Special Publications, v. 74, p. 541-558.

Najman, Y.M.R., Enkin, R.J., Johnson, M.R.W., Robertson, A.H.F., & Baker, J., 1994, Palaeomagnetic dating of the earliest continental Himalayan foredeep sediments; implications for Himalayan evolution: Earth and Planetary Science Letters, v. 128, p. 713-718.

Najman, Y., Pringle, M.S., Johnson, M.R.W., Robertson, A.H.F., & Wijbrans, J.R., 1997, Laser (super 40) Ar/ (super 39) Ar dating of single detrital muscovite grains from early foreland-basin sedimentary deposits in India; implications for early Himalayan evolution: Geology, v. 25, p. 535-538.

Najman, Y., Bickle, M., & Chapman, H., 2000, Early Himalayan exhumation: constraints from the Indian foreland basin: Terra Nova, v. 12, p. 28-34.

Najman, Y., & Garzanti, E., 2000, Reconstructing early Himalayan tectonic evolution and paleogeography from Tertiary foreland basin sedimentary rocks, northern India, *in* Geissman, J.W., and Glazner, A.F., eds., Special focus on the Himalaya: Boulder, Geological Society of America, p. 435-449.

Najman, Y., Pringle, M., Godin, L., & Oliver, G., 2001, Dating of the oldest continental sediments from the Himalayan foreland basin: Nature, v. 410, p. 194-197.

Najman, Y., Pringle, M., Godin, L., & Oliver, G., 2002, A reinterpretation of the Balakot Formation; implications for the tectonics of the NW Himalaya, Pakistan: Tectonics, v. 21, p. 1-18.

Najman, Y., Eduardo, G., Pringle, M., Bickle, M., Stix, J., & Khan, I., 2003, Early-Middle Miocene paleodrainage and tectonics in the Pakistan Himalaya: Geological Society of America Bulletin, v. 115, p. 1265-1277.

Najman, Y., Johnson, C., White, N.M., & Oliver, G., 2004, Evolution of the Himalayan foreland basin, NW India: Basin Research, v. 16, p. 1-24.

Najman, Y., Carter, A., Oliver, G., & Garzanti, E., 2005, Provenance of Eocene foreland basin sediments, Nepal; constraints to the timing and diachroneity of early Himalayan orogenesis: Geology, v. 33, p. 309-312.

Nakata, T., 1989, Active faults of the Himalaya of India and Nepal, *in* Malinconico, L.L.Jr., & Lillie, R.J., eds., Tectonics of the western Himalayas: Geological Society of America Special Paper, v. 232, p. 243-264.

Nakayama, K., & Ulak, P.D., 1999, Evolution of fluvial style in the Siwalik Group in the foothills of the Nepal Himalaya: Sedimentary Geology, v. 125, p. 205-224.

Nelson, K.D., Zhao, W., Brown, L.D., Kuo, J., Che, J., Liu, X., Klemperer, S.L., Makovsky, Y., Meissner, R., Mechie, J., Kind, R., Wenzel, F., Ni, J., Nabelek, J., Chen, L., Tan, H., Wei, W., Jones, A.G., Booker, J., Unsworth, M., Kidd, W.S.F., Hauck, M., Alsdorf, D., Ross, A., Cogan, M., Wu, C., Sandvol, E.A., & Edwards, M., 1996, Partially molten middle crust beneath southern Tibet; synthesis of Project INDEPTH results: Science, v. 274, p. 1684-1688.

Nesbitt, H.W., MacRae, N.D., & Kronberg, B.I., 1990, Amazon deep-sea fan muds; light REE enriched products of extreme chemical weathering: Earth and Planetary Science Letters, v. 100, p. 118-123.

Ni, J., & York, J.E., 1978, Late Cenozoic tectonics of the Tibetan Plateau: Journal of Geophysical Research, B, Solid Earth and Planets, v. 83, p. 5377-5384.

Ni, J., & Barazangi, M., 1984, Seismotectonics of the Himalayan collision zone; geometry of the underthrusting Indian Plate beneath the Himalaya: Journal of Geophysical Research B, Solid Earth and Planets, v. 89, p. 1147-1163.

Ni, J.F., Ibenbrahim, A., & Roecker, S.W., 1991, Three-dimensional velocity structure and hypocenters of earthquakes beneath the Hazara Arc, Pakistan; geometry of the underthrusting Indian Plate: Journal of Geophysical Research B, Solid Earth and Planets, v. 96, p. 19865-19877.

Oberlander, T.M., 1985, Origin of drainage transverse to structures in orogens: Tectonic geomorphology, Binghamton Symposia in Geomorphology, v. 15, p. 155-182.

Ojha, T.P., Butler, R.F., Quade, J., DeCelles, P.G., Richards, D., & Upreti, B.N., 2000, Magnetic polarity stratigraphy of the Neogene Siwalik Group at Khutia Khola, far western Nepal, *in* Geissman, J.W., and Glazner, A.F., eds., Special focus on the Himalaya: Geological Society of America Bulletin, v. 112, p. 424-434.

Ojha, T.P., Butler, R.F., Quade, J., DeCelles, P.G., & Upreti, B.N., 2001, Magnetic polarity stratigraphy of foreland basin sediments of Nepal Himalaya: Special abstracts issue, 16th Himalaya-Karakoram-Tibet workshop, Journal of Asian Earth Sciences, v. 19, p. 48-49.

Oliver, G.J.H., Johnson, M.R.W., & Fallick, A.E., 1995, Age of metamorphism in the Lesser Himalaya and the Main Central Thrust Zone, Garhwal India; results of illite crystallinity, (super 40) Ar- (super 39) Ar fusion and K-Ar studies: Geological Magazine, v. 132, p. 139-149.

Ore, H.T., 1963, Some criteria for recognition of braided stream deposits: Contr. Geol. Wyoming Uni. Dept. Geol., v. 3, p. 1-14.

Ori, G.G., & Friend, P.F., 1984, Sedimentary basins formed and carried piggyback on active thrust sheets: Geology, v. 12, p. 475-478.

Pandey, M.R., Tandukar, R.P., Avouac, J.P., Lave, J., & Massot, J.P., Interseismic strain accumulation on the Himalayan crustal ramp (Nepal): Geophysical Research Letters, v. 22, p. 751-754.

Parfenoff, A., Pomerol, C., & Tourenq, J., 1970, Mineral grains; methods of study and determination: Paris, Masson et Cie, 574 p.

Parkash, B., Sharma, R.P., & Roy, A.K., 1980, The Siwalik Group (molasse), - sediments shed by collision of continental plates: Sedimentary Geology, v. 25, p. 127-159.

Parrish, R.R., & Hodges, K.V., 1993, Miocene (22+ or -1) Ma metamorphism and two stage thrusting in the Greater Himalayan sequence, Annapurna Sanctuary, Nepal: Geological Society of America, Abstracts with Programs, v. 25, p. 174.

Parrish, R.R., & Hodges, K.V., 1996, Isotopic constraints on the age and provenance of the Lesser and Greater Himalayan sequences, Nepalese Himalaya: Geological Society of America Bulletin, v. 108, p. 904-911.

Paudel, L.P., & Arita, K., 2000, Tectonic and polymetamorphic history of the Lesser Himalaya in central Nepal: Journal of Asian Earth Sciences, v. 18, p. 561-584.

Pearce, J.A., & Cann, J.R., 1971, Ophiolite origin investigated by discriminant analysis using Ti, Zr, and Y: Earth and Planetary Science Letters, v. 12, p. 339-349.

Pearce, J.A., & Cann, J.R., 1973, Tectonic setting of basic volcanic rocks determined using trace element analyses: Earth and Planetary Science Letters, v. 19, p. 290-300.

Pecher, A., & Le Fort, P., 1986, The metamorphism in central Himalaya, its relations with the thrust tectonic: Eos Transactions, v. 67, p. 370-371.

Pecher, A., 1989, The metamorphism in the central Himalaya: Journal of Metamorphic Geology, v. 7, p. 31-41.

Pecher, A., 1991, The contact between the higher Himalaya crystallines and the Tibetan sedimentary series; Miocene large-scale dextral shearing: Tectonics, v. 10, p. 587-598.

Pennock, E.S., Lillie, R.J., Zaman, A.S.H., & Yousaf, M., 1989, Structural interpretation of seismic reflection data from eastern Salt Range and Potwar Plateau, Pakistan: AAPG Bulletin, v. 73, p. 841-857.

Pivnik, D.A., & Wells, N.A., 1996, The transition from Tethys to the Himalaya as recorded in Northwest Pakistan: Geological Society of America Bulletin, v. 108, p. 1295-1313.

Pognante, U., Castelli, D., Benna, P., Genovese, G., Oberli, F., Meier, M., & Tonarini, S., 1990, The crystalline units of the High Himalayas in the Lahul-Zanskar region (Northwest India); metamorphic-tectonic history and geochronology of the collided and imbricated Indian Plate: Geological Magazine, v. 127, p. 101-116.

Pognante, U., & Spencer, D.A., 1991, First report of eclogites from the Himalayan belt, Kaghan Valley (northern Pakistan): European Journal of Mineralogy, v. 3, p. 613-618.

Pognante, U., & Benna, P., 1993, Metamorphic zonation, migmatization and leucogranites along the Everest transect of eastern Nepal and Tibet; record of an exhumation history, *in* Treloar, P.J., & Searle, M.P., eds., Himalayan tectonics: Geological Society Special Publications, v. 74, p. 323-340.

Powell, C.McA., & Conaghan, P.J., 1973, Plate tectonics and the Himalayas: Earth and Planetary Science Letters, v. 20, p. 1-12.

Powers, P.M., Lillie, R.J., & Yeats, R.S., 1998, Structure and shortening of the Kangra and Dehra Dun reentrants, Sub-Himalaya, India: Geological Society of America Bulletin, v. 110, p. 1010-1027.

Prasad, M., & Awasthi, N., 1994, Contribution to the Siwalik flora from Surai Khola Sequence, western Nepal and its palaeoecological and phytogeographical implications: The Palaeobotanist, v. 43, p. 1-42.

Prell, W.L., Niitsuma, N., Emeis, K., Anderson, D., Clemens, S.C., Krissek, L.A., Murray, D.M., Weedon, G.P., Ricken, W., Khalfan, al-T., Ahmed, N., Sulaiman, al-S., Zaher, K., Bloemendal, J., Hayashida, A., Hermelin, J.O.R., Vroon, D., Nigrini, C., Spaulding, S.A., Takayama, T., Pedersen, T.F., Shimmield, G.B., Lo, T.H.H., Barnes, R., Bilak, R.A., Bray, C.J., Busch, W.H., de Menocal, P., Jarrard, R., & Debrabant, P., 1988, Ocean Drilling Program; Milankovitch and monsoons: Nature, v. 331, p. 663-664.

Prell, W.L., & Kutzbach, J.E., 1992, Sensitivity of the Indian monsoon to forcing parameters and implications for its evolution: Nature, v. 360, p. 647-652.

Qayyum, M., Lawrence, R.D., & Niem, A.R., 1997, Discovery of the palaeo-Indus delta-fan complex: Journal of the Geological Society of London, v. 154, p. 753-756.

Qayyum, M., Niem, A.R., & Lawrence, R.D., 2001, Detrital modes and provenance of the Paleogene Khojak Formation in Pakistan: implications for early Himalayan orogeny and unroofing: Geological Society of America Bulletin, v. 113, p. 320-332.

Quade, J., Cerling, T.E., & Bowman, J.R., 1989, Development of Asian monsoon revealed by marked ecological shift during the latest Miocene in northern Pakistan: Nature, v. 342, p. 163-166.

Quade, J., Cater, J.M.L., Ojha, T.P., Adam, J., & Harrison, T.M., 1995, Late Miocene environmental change in Nepal and the northern Indian subcontinent; stable isotopic evidence from Paleosols: Geological Society of America Bulletin, v. 107, p. 1381-1397.

Quade, J., Roe, J., DeCelles, P.G., & Ojha, T.P., 1997, The late Neogene (super 87) Sr/ (super 86) Sr record of lowland Himalayan rivers: Science, v. 276, p. 1828-1831.

Quade, J., English, N., & DeCelles, P.G., 2003, Silicate versus carbonate weathering in the Himalaya; a comparison of the Arun and Seti River watersheds: Chemical Geology, v. 202, p. 275-296.

Rai, S.M., Guillot, S., Le Fort, P., & Upreti, B.N., 1998, Mineral chemistry and tectonothermal evolution of the crystalline sheets in the Kathmandu region, central Nepal; relation to geodynamic context: 13th Himalayan-Karakoram-Tibet workshop, abstract volume, University of Peshawar, v. 31, p. 157-159.

Raiverman, V., Kunte, S.V., & Mukherjea, A., 1983, Basin geometry, Cenozoic sedimentation and hydrocarbon prospects in north western Himalaya and Indo-Gangetic Plains: Petroleum Asia Journal, v. 6, p. 67-92.

Rapson, J.E., 1965, Petrography and derivation of Jurassic-Cretaceous clastic rocks, southern Rocky Mountains, Canada: Bulletin of the American Association of Petroleum Geologists, v. 49, p. 1426-1452.

Ratschbacher, L., Frisch, W., Liu, G., & Chen, C., 1994, Distributed deformation in southern and western Tibet during and after India-Asia collision: Journal of Geophysical Research, v. 99, p. 19917-19945.

Raymo, M.E., & Ruddiman, W.F., 1992, Tectonic forcing of late Cenozoic climate: Nature, v. 359, p. 117-122.

Rea, D.K., 1992, Delivery of Himalayan sediment to the northern Indian Ocean and its relation to global climate, sea level, uplift, and seawater strontium, in The Indian Ocean: A synthesis of results from the Ocean Drilling Program: American Geophysical Union Geophysical Monograph, v. 70, p. 387-402.

Richards, A., 2005, Isotopic mapping of major Himalayan structures: PhD, Milton Keynes, Open University, p. 350.

Richter, F.M., Rowley, D.B., & De Paolo, D.J., 1992, Sr isotope evolution of seawater; the role of tectonics: Earth and Planetary Science Letters, v. 109, p. 11-23.

Robinson, D.M., DeCelles, P.G., Patchett, P.J., & Garzione, C.N., 2001, The kinematic evolution of the Nepalese Himalaya interpreted from Nd isotopes: Earth and Planetary Science Letters, v. 192, p. 507-521.

Robinson, D.M., DeCelles, P.G., Garzione, C.N., Pearson, O.N., Harrison, T.M., & Catlos, E.J., 2003, Kinematic model for the Main Central Thrust in Nepal: Geology, v. 31, p. 359-362.

Roeschmann, G., 1971, Problems concerning investigations of paleosols in older sedimentary rocks, demonstrated by the example of Wurzelboden of the Carboniferous system, *in* Yaalon, D.H., Paleopedology; Origin, Nature and Dating of Paleosols: Jerusalem, International Society of Soil Science and Israel University Press, p. 311-320.

Roesler, W., Metzler, W., & Appel, E., 1997, Neogene magnetic polarity stratigraphy of some fluviatile Siwalik sections, Nepal: Geophysical Journal International, v. 130, p. 89-111.

Roesler, W., & Appel, E., 1998, Fidelity and time resolution of the magnetostratigraphic record in Siwalik sediments; high-resolution study of a complete polarity transition and evidence for cryptochrons in a Miocene fluviatile section: Geophyical Journal International, v. 135, p. 861-875.

Rollinson, H.R., 1993, Using geochemical data; evaluation, presentation, interpretation: Longman Scientific & Technical, UK, p. 352.

Rowley, D.B., 1996, Age of initiation of collision between India and Asia; a review of stratigraphic data: Earth and Planetary Science Letters, v. 145, p. 1-13.

Sah, R.B., 1998, Lithostratigraphy of Nepalese Siwaliks; an appraisal for standardisation: Journal of Nepal Geological Society, v. 18, p. 217-226.

Sahni, M.R., & Mathur, L.P., 1964, Stratigraphy of the Siwalik Group: Proc. 22nd Inter. Geol. Cong. India, pp. 1–24.

Sakai, H., 1983, Geology of the Tansen Group of the Lesser Himalaya in Nepal: Mem. Fac. Sci. Kyushu Univ., v. 25, p. 27-74.

Sakai, H., 1985, Geology of the Kali Gandaki Supergroup of the Lesser Himalayas in Nepal: Memoirs of the Faculty of Science, Kyushu University, Series D: Geology, v. 25, p. 337-397.

Sakai, H., 1989, Rifting of the Gondwanaland and uplifting of the Himalayas recorded in Mesozoic and Tertiary fluvial sediments in the Nepal Himalayas, *in* Taira, A., & Masuda, F., eds., Sedimentary facies in the active plate margin: Terra Sci. Publ. Co., Tokyo, Japan, p. 723-732.

Sarkar, S., 1989, Siwalik pollen succession from Surai Khola of western Nepal and its reflection on palaeoecology: The Palaeobotanist, v. 38, p. 319-324.

Scharer, U., Xu, R., & Allegre, C., 1986, U–(Th) –Pb systematics and ages of Himalayan leucogranites, south Tibet: Earth Planetary Science Letters, v. 77, p. 35–48.

Schelling, D., & Arita, K., 1991, Thrust tectonics, crustal shortening, and the structure of the far-eastern Nepal Himalaya: Tectonics, v. 10, p. 851-862.

Schelling, D., 1992, The tectonostratigraphy and structure of the eastern Nepal Himalaya: Tectonics, v. 11, p. 925-943.

Schlup, M., Carter, A., Cosca, M., & Steck, A., 2003, Exhumation history of eastern Ladakh revealed by (super 40) Ar/ (super 39) Ar and fission-track ages; the Indus River-Tso Morari transect, NW Himalaya: Journal of the Geological Society of London, v. 160, p. 385-399.

Schneider, C., & Masch, L., 1993, The metamorphism of the Tibetan series from the Manang area, Marsyandi Valley, central Nepal, *in* Treloar, P.J., & Searle, M.P., eds., Himalayan tectonics: London, Geological society, p. 357-374.

Schwab, F.L., 1986, Sedimentary "signatures" of foreland basin assemblages; real or counterfeit?, *in* Allen, P.A., & Homewood, P., eds., Foreland basins: Special Publication of the International Association of Sedimentologists, v. 8, p. 395-410.

Searle, M.P., 1983, Stratigraphy, structure and evolution of the Tibetan-Tethys zone in Zanskar and the Indus suture zone in the Ladakh Himalaya: Transactions of the Royal Society of Edinburgh: Earth Sciences, v. 73, p. 205-219.

Searle, M.P., 1986, Structural evolution and sequence of thrusting in the High Himalayan, Tibetan-Tethys and Indus suture zones of Zanskar and Ladakh, western Himalaya: Journal of Structural Geology, v. 8, p. 923-936.

Searle, M.P., Windley, B.F., Coward, M.P., Cooper, D.J.W., Rex, A.J., Rex, D., Tingdong, L., Xuchang, X., Jan, M.Q., Thakur, V.C., & Kumar, S., 1987, The closing of the Tethys and the tectonics of the Himalaya: Geological Society of America Bulletin, v. 98, p. 678-701.

Searle, M.P., Cooper, D.W.J., & Rex, A.J., 1988, Collision tectonics of the Ladakh-Zanskar Himalaya, *in* Shackleton, R.M., Dewey, J.F., & Windley, B.F., Tectonic evolution of the Himalayas and Tibet: Philosophical Transactions of the Royal Society of London, Series A: Mathematical and Physical Sciences, v. 326, p. 117-150.

Searle, M.P., & Rex, A.J., 1989, Thermal model for the Zanskar Himalaya: Journal of Metamorphic Geology, v. 7, p. 127-134.

Searle, M.P., Pickering, K.T., & Cooper, D.J.W., 1990, Restoration and evolution of the intermontane Indus molasses basin, Ladakh Himalaya, India: Tectonophysics, v. 174, p. 301-314.

Searle, M.P. 1991. Geology and Tectonics of the Karakoram Mountains: Chichester, John Wiley and Sons, p. 358.

Searle, M.P., Metcalfe, R.P., Rex, A.J., & Norry, M.J., 1993, Field relations, petrogenesis and emplacement of the Bhagirathi leucogranite, Garhwal Himalaya, *in* Treloar, P.J., & Searle, M.P., eds, Himalayan tectonics: London, Geological Society Special Publications, v. 74, p. 429-444.

Searle, M.P., 1995, The timing of metamorphism, magmatism, and cooling in the Zanskar, Garhwal, and Nepal Himalaya: Journal of Nepal Geological Society, v. 11, p. 103-120.

Searle, M.P., 1996, Cooling history, erosion, exhumation, and kinematics of the Himalaya-Karakoram-Tibet orogenic belt, *in* Yin, A., & Harrison, T.M., eds, The tectonic evolution of Asia: Los Angeles, Cambridge University Press, p. 110-138.

Searle, M.P., Parrish, R.R., Hodges, K.V., Hurford, A., Ayres, M.W., & Whitehouse, M.J., 1997, Shisha Pangma leucogranite, South Tibetan Himalaya; field relations, geochemistry, age, origin, and emplacement: Journal of Geology, v. 105, p. 295-317.

Searle, M.P., 1999, Extensional and compressional faults in the Everest-Lhotse Massif, Khumbu Himalaya, Nepal: Journal of the Geological Society of London, v. 156, p. 227-240.

Searle, M.P., Noble, S.R., Hurford, A.J., & Rex, D.C., 1999, Age of crustal melting, emplacement and exhumation history of the Shivling Leucogranite, Garhwal Himalaya: Geological Magazine, v. 136, p. 513-525.

Searle, M.P., Waters, D.J., Stephenson, B.J., Kohn, M.J., Catlos, E.J., Ryerson, F.J., & Harrison, T.M., 2002, Pressure-temperature-time path discontinuity in the Main Central Thrust Zone, central Nepal; discussion and reply: Geology, v. 30, p. 479-481.

Searle, M.P., & Godin, L., 2003, The South Tibetan detachment and the Manaslu Leucogranite; a structural reinterpretation and restoration of the Annapurna-Manaslu Himalaya, Nepal: Journal of Geology, v. 111, p. 505-523.

Searle, M.P., Simpson, R.L., Law, R.D., Parrish, R.R., & Waters, D.J., 2003, The structural geometry, metamorphic and magmatic evolution of the Everest Massif, High Himalaya of Nepal-South Tibet: Journal of the Geological Society London, v. 160, p. 345-366.

Searle, M.P., & Szulc, A.G., 2005, Channel flow and ductile extrusion of the high Himalayan slab-the Kangchenjunga–Darjeeling profile, Sikkim Himalaya: Journal of Asian Earth Sciences, v. 25, p. 173-185.

Seeber, L., Armbruster, J.G., & Quittmeyer, R.C., 1981, Seismicity and continental subduction in the Himalayan arc, *in* Gupta, H.K., & Delany, F.M., eds., Zagros, Hindu Kush, Himalaya; geodynamic evolution: Geodynamic Series, v. 3, p. 215-242.

Seeber, L., & Gornitz, V., 1983, River profiles along the Himalayan arc as indicators of active tectonics: Tectonophysics, v. 92, p. 335-367.

Sengor, A.M.C., Altiner, D., Cin, A., Ustaomer, T., & Hsu, K.J., 1988, Origin and assembly of the Tethyside orogenic collage at the expense of Gondwanaland, *in* Audley-Charles, M.G., & Hallam, A., eds., Gondwana and Tethys: London, Geological Society Special Publications, v. 37, p. 119-181.

Sharma, C.K., 1977, Geology of Nepal: Kathmandu, Educ. Enterp., p. 164.

Sibson, R.H., 1977, Fault rocks and fault mechanisms: Journal of the Geological Society London, v. 133, p. 191-213.

Simpson, R.L., Parrish, R.R., Searle, M.P., & Waters, D.J., 2000, Two episodes of monazite crystallization during metamorphism and crustal melting in the Everest region of the Nepalese Himalaya: Geology, v. 28, p. 403-406.

Sinclair, H.D., Coakley, B.J., Allen, P.A., & Watts, A.B., 1991, Simulation of foreland basin stratigraphy using a diffusion model of mountain belt uplift and erosion; an example from the Central Alps, Switzerland: Tectonics, v. 10, p. 599-620.

Sinclair, H.D., & Jaffey, N., 2001, Sedimentology of the Indus Group, Ladakh, northern India; implications for the timing of initiation of the palaeo-Indus River: Journal of the Geological Society London, v. 158, p. 151-162.

Singh, I.B., 1972, On the bedding in the natural-levee and point bar deposits of the Gomti River, Uttar Pradesh, India: Sedimentary Geology, v. 7, p. 309-317.

Singh, S.K., Trivedi, J.R., Pande, K., Ramesh, R., & Krishnaswami, S., 1998, Chemical and strontium, oxygen, and carbon isotopic compositions of carbonates from the Lesser Himalaya; implications to the strontium isotope composition of the source waters of the Ganga, Ghaghara, and the Indus rivers: Geochimica et Cosmochimica Acta, v. 62, p. 743-755.

Singh, S.K., Trivedi, J.R., & Krishnaswami, S., 1999, Re-Os isotope systematics in black shales from the Lesser Himalaya; their chronology and role in the (super 187) Os/ (super 188) Os evolution of seawater: Geochimica et Cosmochimica Acta, v. 63, p. 2381-2392.

Sklar, L., & Dietrich, W.E., 1998, River longitudinal profiles and bedrock incision models; stream power and the influence of sediment supply: Geophysical Monograph, v. 107, p. 237-260.

Smith, N.D., 1970, The braided stream depositional environment: Comparison of the Platte River with some Silurian clastic rocks, North-Central Appalachians: Geological Society of America Bulletin, v. 82, p. 3407-3420.

Smith, D.G., & Smith, N.D., 1980, Sedimentation in anastomosed river systems: examples from alluvial valleys near Banff, Alberta: Journal of Sedimentary Petrology, v. 50, p. 157-164.

Smith, D.G., 1983, Anastomosed river deposits: modern examples from Western Canada, *in* Collinson, J.D., & Lewin, J., eds., Modern and Ancient Fluvial Systems: Special Publication of the International Asociation of Sedimentologists, v. 6, p. 155-168.

Spear, F.S., 1989, Relative thermobarometry and metamorphic P-T paths, *in* Daly, J.S., Cliff, R.A., & Yardley, B.W.D., eds., Evolution of metamorphic belts; proceedings of the 1987 joint meeting of the Metamorphic Studies Group and IGCP project 235: Geological Society Special Publications, v. 43, p. 63-81.

Spiegel, C., Kuhlemann, J., Dunkl, I., & Frisch, W., 2001, Oligo-Miocene denudation of the Central Alps; evidence from the foreland basins: Earth system processes; programmes with abstracts, p. 85-86.

Spring, L., Bussy, F., Vannay, J.C., Hunon, S., & Cosca, M.A., 1993, Early Permian granitic dykes of alkaline affinity in the Indian High Himalaya of upper Lahul and SE Zanskar; geochemical characterization and geotectonic implications, *in* Treloar, P.J., & Searle, M.P., Himalayan Tectonics: London, Geological Society Special Publications, v. 74, p. 251-264.

Snyder, N.P., Whipple, K.X., Tucker, G.E., & Merritts, D.J., 2000, Landscape response to tectonic forcing; digital elevation model analysis of stream profiles in the Mendocino triple junction region, Northern California: Geological Society of America Bulletin, v. 112, p. 1250-1263.

Srivastava, V.K., & Casshyap, S.M., 1983, Evolution of the pre-Siwalik Tertiary basin of Himachal Himalaya: Journal of the Geological Society of India, v. 24, p. 134-147.

Srivastava, P., & Mitra, G., 1994, Thrust geometries and deep structure of the outer and lesser Himalaya, Kumaun and Garhwal (India): Implications for evolution of the Himalayan fold-thrust belt: Tectonics, v. 13, p. 89-109.

Steck, A., Epard, J-L., Vannay, J-C., Hunziker, J., Girard, M., Morard, A., & Robyr, M., 1998, Geological transect across the Tso Morari and Spiti areas; the nappe structures of the Tethys Himalaya: Eclogae Geologicae Helvetiae, v. 91, p. 103-122.

Steel, R.J., 1974, New Red Sandstone floodplain and piedmont sedimentation in the Hebridean Province: Journal of Sedimentary Petrology, v. 44, p. 336-357.

Stephenson, B.J., Searle, M.P., Waters, D.J., & Rex, D.C., 2000, Structure of the Main Central Thrust zone and extrusion of the High Himalayan deep crustal wedge, Kishtwar–Zanskar Himalaya: Journal of the Geological Society London, v. 158, p. 637-652.

Stock, J.D., & Montgomery, D.R., 1996, Estimating palaeorelief from detrital mineral age ranges: Basin Research, v. 8, p. 317-327.

Stock, J.D., & Montgomery, D.R., 1999, Geologic constraints on bedrock river incision using the stream power law: Journal of Geophysical Research B, Solid Earth and Planets, v. 104, p. 4983-4993.

Stocklin, J., 1980, Geology of Nepal and its regional frame: Journal of the Geological Society London, v. 137, pp. 1-34.

Stutz, E., & Steck, A., 1986, The western end of the Tso Morari crystalline complex (Upper Himalayas; southern Ladakh, India); subdivision and tectonics of the nappe: Eclogae Geologicae Helvetiae, v. 79, p. 253-269.

Stuewe, K., & Hintermuller, M., 2000, Topography and isotherms revisited: The influence of laterally migrating drainage divides: Earth and Planetary Science Letters, v. 184, p. 287-303.

Stuewe, K., & Foster, D., 2001, (super 40) Ar/ (super 39) Ar, pressure, temperature and fission track constraints on the age and nature of metamorphism around the main central thrust in the eastern Bhutan Himalaya: Journal of Asian Earth Sciences, v. 19, p. 85-95.

Suczek, C.A., & Ingersoll, R.V., 1985, Petrology and provenance of Cenozoic sand from the Indus Cone and the Arabian Basin, DSDP sites 221, 222, and 224: Journal of Sedimentary Petrology, v. 55, p. 340-346.

Suppe, J., 1983, Geometry and kinematics of fault-bend folding: American Journal of Science, v. 283, p. 684-721.

Sverdrup, K.A., Cronin, V.S., & Schurter, G.J., Investigation of late Cenozoic-Recent structural activity near Nanga Parbat-Haramosh Massif, Northwest Himalaya: Geological Society of America, Abstracts with Programs, v. 25, p. 122-123.

Tagami, T., Carter, A. & Hurford, A.J., 1996, Natural long-term annealing of the zircon fission-track system in Vienna Basin deep borehole samples: constraints upon the partial annealing zone and closure temperature: Chemical Geology, v. 130, p. 147-157.

Tagami, T., Galbraith, R. F., Yamada, G. M. & Laslett, G. M., 1998, Revised annealing kinetics of Fission-tracks in zircon and geological implications, *in* Van den Haute, P. & De Corte, F., eds., Advances in Fission-track Geochronology: Amsterdam, Kluwer Academic Press, p. 99-112.

Talling, P.J., & Burbank, D.W., 1993, Assessment of uncertainties in magnetostratigraphic dating of sedimentary strata, *in* Aissaoui, D.M., McNeill, D.F., & Hurley, N.F., eds., Applications of paleomagnetism to sedimentary geology: Society of Economic Paleontologists and Mineralogists Special Publication, v. 49, p. 59-69.

Talukdar, S.N., & Sudhakar, R., 1971, Structure of the southern edge of the Himalaya of North India: Geol. Surv. India Misc. Pub., v. 15, p. 185-93.

Tamrakar, N.K., 2000, Clast morphology of the Siwalik conglomerates from the Dhan Khola Formation, Surai Khola area, mid-western Nepal: Journal of Nepal Geological Society, v. 21, p. 109-122.

Tanaka, S., 1997, Uplift of the Himalaya and climatic change at 10 Ma; evidence from records of carbon stable isotopes and fluvial sediments in the Churia Group, central Nepal: Journal of the Geological Society of Japan, v. 103, p. 253-264.

Tandon, S.K., 1976, Siwalik sedimentation in a part of the Kumaun Himalaya, India: Sedimentary Geology, v. 16, p. 131-154.

Tapponnier, P., & Molnar, P., 1975, Major strike-slip faulting in China; its significance for Asian tectonics: Abstracts with Programs – Geological Society of America, v. 7, p. 425-426.

Tapponnier, P., Arnaud, N., Wittlinger, G., Jingsui, Y., Zhigin, X., Roger, F., & Meyer, B., 2001, Oblique stepwise rise and growth of the tibet plateau: Science, v. 294, p. 1671-1677.

Tauxe, L., & Badgley, C., 1988, Stratigraphy and remanence acquisition of a palaeomagnetic reversal in alluvial Siwalik rocks of Pakistan: Sedimentology, v. 35, p. 697-715.

Tauxe, L., 1990, Use of anisotropy to determine the origin of characteristic remanence in the Siwalik red beds of northern Pakistan: Journal of Geophysical Research B, Solid Earth and Planets, v. 95, p. 4391-4404.

Taylor, S.R., & McLennan, S.M., 1985, The Continental Crust: its Composition and Evolution. An Examination of the Geochemical Record Preserved in Sedimentary Rocks: Oxford, Blackwell, p. 312.

Thakur, V.C., 1980, Tectonics of the Central Crystallines of western Himalaya: Tectonophysics, v. 62, p. 141-154.

Thakur, V.C., 1987, Development of major structures across the northwestern Himalaya, India: Tectonophysics, v. 135, p. 1-13.

Thakur, V.C., 1998, Structure of the Chamba Nappe and position of the Main Central Thrust in Kashmir Himalaya: Journal of Asian Earth Sciences, v. 16, p. 269-282.

Tonarini, S., Villa, I.M., Oberli, F., Meier, M., Spender, D.A., Pognante, U., & Ramsay, J.G., 1993, Eocene age of eclogite metamorphism in Pakistan Himalaya; implications for India-Eurasia collision: Terra Nova, v. 5, p. 13-20.

Tomkin, J.H., & Braun, J., 1999, Simple models of drainage reorganisation on a tectonically active ridge system: New Zealand Journal of Geology and Geophysics, v. 42, p. 1-10.

Tonarini, S., Villa, I.M., Oberli, F., Meier, M., Spencer, D.A., Pognante, U., & Ramsay, J.G., 1993, Eocene age of eclogite metamorphism in Pakistan Himalaya; implications for India-Eurasia collision: Terra Nova, v. 5, p. 13-20.

Treloar, P.J., & Rex, D.C., 1990, Cooling and uplift histories of the crystalline thrust stack of the Indian Plate internal zones west of Nanga Parbat, Pakistan Himalaya: Tectonophysics, v.180, p. 323-349.

Treloar, P.J., Pottis, G.J., Wheeler, J., & Rex, D.C., 1991, Structural evolution and asymmetric uplift of the Nanga Parbat Syntaxis, Pakistan Himalaya: International Journal of Earth Sciences, v. 80, p. 411-428.

Treloar, P.J., Coward, M.P., Chambers, A.F., Izatt, C.N., & Jackson, K.C., 1992, Thrust geometries, interferences and rotations in the Northwest Himalaya, *in* McClay, K.R., ed., Thrust Tectonics: London, Chapman and Hall, p. 325-342.

Treloar, P.J., Rex, D.C., Guise, P.G., Wheeler, J., Hurford, A.J., & Carter, A., 2000, Geochronological constraints on the evolution of the Nanga Parbat syntaxis, Pakistan Himalaya, *in* Khan, M.A., Treloar, P.J., Searle, M.P., & Jan, M.Q., eds, Tectonics of the Nanga Parbat syntaxis and the western Himalaya: Geological Society Special Publications, v. 170, p. 137-162.

Trivedi, J.R., Gopalan, K., & Valdiya, K.S., 1984, Rb-Sr ages of granitic rocks within the Lesser Himalayan nappes, Kumaun, India: Journal of the Geological Society of India, v. 25, p. 641-654.

Tucker, G.E., & Slingerland, R.L., 1994, Erosional dynamics, flexural isostasy, and long-lived escarpments; a numerical modelling study: Journal of Geophysical Research B, Solid Earth and Planets, v. 99, p. 12229-12243.

Turcotte, D.L., & Schubert, G., 1982, Geodynamics; applications of continuum physics to geological problems: New York, John Wiley & Sons, p. 450.

Uddin, A., & Lundberg, N., 1998, Cenozoic history of the Himalayan-Bengal system; sand composition in the Bengal Basin, Bangladesh: Geological Society of America Bulletin, v. 110, p. 497-511.

Upreti, B.N., 1996, Stratigraphy of the western Nepal Lesser Himalaya; a synthesis: Journal of Nepal Geological Society, v. 13, p. 11-28.

Upreti, B.N., 1999, An overview of the stratigraphy and tectonics of the Nepal Himalaya: Journal of Asian Earth Sciences, v. 17, p. 577-606.

Upreti, B.N., & Le Fort, P., 1999, Lesser Himalayan crystalline nappes of Nepal; problems of their origin, *in* Macfarlane, A., Sorkhabi, R.B., & Quade, J., eds., Himalaya and Tibet; mountain roots to mountain tops: Boulder, Geological Society of America, p. 225-238.

Ulak, P.D., & Nakayama, K., 2001, Neogene fluvial systems in the Siwalik Group along the Tinau Khola section, west central Nepal Himalaya: Journal of Nepal Geological Society, v. 25, p. 111-122.

Valdiya, K.S., 1976, Himalayan transverse faults and folds and their parallelism with subsurface structures of North Indian plains: Tectonophysics, v. 32, p. 353-386.

Valdiya, K.S., 1980, Geology of Kumaun Lesser Himalaya: Dehradun, Wadia Institute of Himalayan Geology, p. 291.

Valdiya, K.S., 1992, The main boundary thrust zone of the Himalaya, India: Annales Tectonicae, v. 6, p. 54-84.

Valdiya, K.S., 1995, Proterozoic sedimentation and Pan-African geodynamic development in the Himalaya: Precambrian Research, v. 74, p. 35-55.

Vance, D., & Harris, N., 1999, Timing of prograde metamorphism in the Zanskar Himalaya: Geology, v. 27, p. 395-398.

Vance, D., Bickle, M., Ivy-Ochs, S., & Kubik, P.W., 2003, Erosion and exhumation in the Himalaya from cosmogenic isotope inventories of river sediments: Earth and Planetary Science Letters, v. 206, p. 273-288.

Van der Beek, P., Champel, B., & Mugnier, J-L., 2002, Control of detachment dip on drainage development in regions of active fault-propagation folding: Geology, v. 30, p. 471-474.

Van Haver, T., 1984, Etude stratigraphique, sedimentologique et structurale d'un bassin d'avent arc: exemple du bassin de l'Indus, Ladakh, Himalaya: PhD, University of Grenoble, p. 204.

Vannay, J.C., & Hodges, K.V., 1996, Tectonometamorphic evolution of the Himalayan metamorphic core between the Annapurna and Dhaulagiri, central Nepal: Journal of Metamorphic Geology, v. 14, p. 635-656.

Villa, I.M., 1997, Direct determination of (super 39) Ar recoil distance: Geochimica et Cosmochimica Acta, v. 61, p. 689-691.

Von Eynatten, H., Schlunegger, F., Gaupp, R., & Wijbrans, J.R., 1999, Exhumation of the Central Alps; evidence from (super 40) Ar/ (super 39) Ar laserprobe dating of detrital white micas from the Swiss Molasse Basin: Terra Nova, v. 11, p. 284-289.

Von Eynatten, H., & Wijbrans, J.R., 2003, Precise tracing of exhumation and provenance using (super 40) Ar/ (super 39) Ar geochronology of detrital white mica; the example of the Central Alps, *in* McCann, T., & Saintot, A., eds., Tracing tectonic deformation using the sediment record: Geological Society Special Publications, v. 208, p. 289-305.

Wadia, D.N., 1931, The syntaxis of the northwest Himalaya: its rocks, tectonics and orogeny: Records of the Geological Survey of India, v. 65, p. 189-220.

Wager, L.R., 1937, The Arun river drainage pattern and the rise of the Himalaya: Geographical Journal, v. 89, p. 239-250.

Wagner, M., Altherr, R., & Van den Haute, P., 1992, Apatite fission-track analysis of Kenyan basement rocks; constraints on the thermotectonic evolution of the Kenya Dome; a reconnaissance study: Tectonophysics, v. 204, p. 93-110.

Waheed, A., & Wells, N.A., 1990, Changes in paleocurrents during the development of an obliquely convergent plate boundary (Sulaiman fold-belt, southwestern Himalayas, west-central Pakistan): Sedimentary Geology, v. 67, p. 237-261.

Walker, J.D., Martin, M.W., Bowring, S.A., Searle, M.P., Waters, D.J., & Hodges, K.V., 1999, Metamorphism, melting, and extension; age constraints from the High Himalayan slab of Southeast Zanskar and Northwest Lahaul: Journal of Geology, v. 107, p. 473-495.

Wei, W., Chen, L., Tan, H., Deng, M., Hu, J., Jin, S., Dong, H., & Qiang, J., 1997, MT sounding on the Tibetan Plateau; electrical structure of crust and mantle along the Yadong-Bamucuo profile: Geoscience, v. 11, p. 366-374.

Welje, G.J., 2002, Quantitative analysis of detrital modes; statistically rigorous confidence regions in ternary diagrams and their use in sedimentary petrology: Earth-Science Reviews, v. 57, p. 211-253.

Wells, N.A., & Dore, J.A., 1987, Shifting of the Kosi River, northern India: Geology, v. 15, p. 204-207.

Wesnousky, S.G., Kumar, S., Mohindra, R., & Thakur, V.C., 1999, Uplift and convergence along the Himalayan frontal thrust of India: Tectonics, v. 18, p. 967-976.

Whipple, K.X., & Tucker, G.E., 1999, Dynamics of the stream-power river incision model; implications for height limits of mountain ranges, landscape response timescales, and research needs: Journal of Geophysical Research B, Solid Earth and Planets, v. 104, p. 17661-17674.

Whipple, K.X., Hancock, G.S., & Anderson, R.S., 2000, River incision into bedrock; mechanics and relative efficacy of plucking, abrasion, and cavitation: Geological Society of America Bulletin, v. 112, p. 490-503.

White, N.M., 2001, The Early to Middle Miocene exhumation history of the Himalayas, NW India: PhD, University of Cambridge.

White, N.M., Pringle, M., Garzanti, E., Bickle, M, Najman, Y., Chapman, H., & Friend, P., 2002, Constraints on the exhumation and erosion of the High Himalayan Slab, NW India, from foreland basin deposits: Earth and Planetary Science Letters, v. 195, p. 29-44.

Willems, H., Zhou, Z., Zhang, B., & Graefe, K.U., 1996, Stratigraphy of the Upper Cretaceous and lower Tertiary strata in the Tethyan Himalayas of Tibet (Tingri area, China): Geologische Rundschau, Berlin, Germany, v. 85, p. 723-754.

Willett, S.D., & Brandon, M.T., 2002, On steady states in mountain belts: Geology, v. 30, p. 175-178.

Willgoose, G., Bras, R.L., & Rodriguez-Iturbe, I., 1991, A coupled channel network growth and hillslope evolution model; 1, Theory: Water Resources Research, v. 27, p. 1671-1684.

Williams, P.F., & Rust, B.R., 1969, Sedimentology of a braided river: Journal of Sedimentary Petrology, v. 39, p. 649-679.

Willis, B., 1993, Evolution of Miocene fluvial systems in the Himalayan foredeep through a two kilometer-thick succession in northern Pakistan: Sedimentary Geology, v. 88, p. 77-121.

Willis, B.J., & Behrensmeyer, A.K., 1994, Architecture of Miocene overbank deposits in northern Pakistan: Journal of Sedimentary Research, v. 64, p. 60-67.

Wobus, C.W., Hodges, K.V., & Whipple, K.X., 2003, Has focused denudation sustained active thrusting at the Himalayan topographic front?: Geology, v. 31, p. 861-864.

Wronkiewicz, D.J., & Condie, K.C., 1987, Geochemistry of Archean shales from the Witwatersrand Supergroup, South Africa; source-area weathering and provenance: Geochimica et Cosmochimica Acta, v. 51, p. 2401-2416.

Wu, Changde, Nelson, K.D., Wortman, G., Samson, S.D., Yue, Y., Li, J., Kidd, W.S.F., & Edwards, M.A., 1998, Yadong cross structure and South Tibetan detachment in the east central Himalaya (89 degrees -90 degrees E): Tectonics, v. 17, p. 28-45.

Wyss, M., Hermann, J., & Steck, A., 1999, Structural and metamorphic evolution of the northern Himachal Himalaya, NW India; (Spiti-eastern Lahul-Parvati Valley traverse): Eclogae Geologicae Helvetiae, v. 92, p. 3-44.

Yardley, B.W.D., 1989, An introduction to metamorphic petrology: New York, Longman Earth Science Series, Harlow/Wiley, p. 248.

Yeats, R.S., & Lillie, R.J., 1991, Contemporary tectonics of the Himalayan frontal fault system; folds, blind thrusts and the 1905 Kangra earthquake: Journal of Structural Geology, v. 13, p. 215-225.

Yeats, R.S., Nakata, T., Farah, A., Fort, M., Mirza, M.A., Pandey, M.R., & Stein, R.S., 1992, The Himalayan frontal fault system: Annales Tectonicae, v. 6, p. 85-98.

Ye, H., Yeh, H., Zhang, W., Yu, Z., & Xiu, Q., 1999, Seismicity and recent crustal movement in the Himalayas: Seismology and Geology, v. 3, p. 9-21.

Zaleha, M., 1997a, Intra- and extra-basinal controls on fluvial deposition in the Miocene Indo-Gangetic foreland basin, northern Pakistan: Sedimentology, v. 44, p. 369-390.

Zaleha, M., 1997b, Fluvial and lacustrine palaeoenvironments of the Miocene Siwalik Group, Khaur area, northern Pakistan: Sedimentology, v. 44, p. 349-368.

Zeitler, P.K., Johnson, N.M., Naeser, C.W., & Tahirkheli, R.A.K., 1982, Fission-track evidence for Quaternary uplift of the Nanga Parbat region, Pakistan: Nature, v. 298, p. 255-257.

Zeitler, P.K., 1985, Cooling history of the NW Himalaya, Pakistan: Tectonics, v. 4, p. 127-151.

Zeitler, P.K., Johnson, N.M., Briggs, N.D., & Naeser, C.W., 1986, Uplift history of the NW Himalaya as recorded by fission-track ages on detrital Siwalik zircons: Proceedings of the symposium on Mesozoic and Cenozoic geology in connection of the 60th anniversary of the Geological Society of China, p. 481-494.

Zeitler, P.K., Sutter, J.F., Williams, I.S., Zartman, R.E., & Tahirkheli, R.A.K., 1989, Geochronology and temperature history of the Nanga Parbat-Haramosh Massif, Pakistan, *in* Malinconico, L.L.Jr., & Lillie, R.J., eds., Tectonics of the western Himalayas: Geological Society of America Special Paper, v. 232, p. 1-22.

Zeitler, P.K., Chamberlain, C.P., & Smith, H.A., 1993, Synchronous anatexis, metamorphism, and rapid denudation at Nanga Parbat (Pakistan Himalaya): Geology, v. 21, p. 347-350.

Zhao, W.L., Nelson, K.D., & Team, P.I., 1993, Deep seismic reflection evidence for continental underthrusting beneath southern Tibet: Nature, v. 366, p. 557-559.

Zhang, H., Harris, N., Parrish, R., Kelley, S., Zhang, L., Rogers, N., Argles, T., & King, J., 2004, Causes and consequences of protracted melting of the mid-crust exposed in the North Himalayan antiform: Earth and Planetary Science Letters, v. 228, p. 195-212.

Zuffa, G.G., 1985, Provenance of arenites: Dordrecht-Boston, D. Reidel Publishing Company, p. 408.

Appendix

I Sample Lists

Karnali section

Sample	Strat. Height (m)	Strat. Age (Ma)	Lithology		Long			Lat		Locality	Technique
K1	2	15.9	SST	81°	17'	09"	28°	39'	01"	Section base, first exposure N of Chisapani	A,C
K1M	0	15.9	MUDST	81°	17'	09"	28°	39'	01"	5m below K1 bed	B
K2	385	15.1	SST	81°	17'	15"	28°	39'	14"	S gauging station, A42	A
K3	683	14.1	SST	81°	17'	13"	28°	39'	26"	East bank, N of river gauging station	C
K3M	685	14.1	MUDST	81°	17'	13"	28°	39'	26"	Above K3 bed	B
K4	1040	13	SST	81°	17'	14"	28°	39'	38"	Right bank, A132	A
K5	1403	12.1	SST	81°	17'	09"	28°	39'	52"	East bank	A
K5M	1394	12.1	MUDST	81°	17'	09"	28°	39'	52"	Below K5 bed	B
K6	1665	10.9	SST	81°	17'	07"	28°	40'	04"	Right bank, B48	A
K7	2080	9.9	SST	81°	17'	20"	28°	40'	20"	On road, N gully, C29	A
K7M	2103	9.9	MUDST	81°	17'	20"	28°	40'	20"	West bank, opposite fishermans teahouse	B
K8	2560	8.95	SST	81°	17'	04"	28°	40'	41"	West bank, thick SST bed	A
K9	2810	8.05	SST	81°	17'	01"	28°	40'	58"	22m thick SST bed, D69	A
K9M	2812	8.05	MUDST	81°	17'	01"	28°	40'	58"	West bank	B
K10	3225	6.9	SST	81°	16'	54"	28°	41'	17"	West bank	A
K11	3590	6	SST	81°	16'	52"	28°	41'	40"	West bank, upsection from rapids	A
F19Pebbles	3590	6	Clasts	81°	16'	52"	28°	41'	40"	West bank	B
K12	4026	5.2	SST	81°	16'	08"	28°	42'	07"	West bank, top of dated section, G29	A
K12M	4021	5.2	MUDST	81°	16'	08"	28°	42'	07"	West bank, top of dated section, G29	B
K13P	?	?	Clasts	81°	16'	28"	28°	43'	11"	East bank, Karnali bridge ~2 km N of section	B
K13	?	~2.8	SST	81°	16'	28"	28°	43'	11"	East bank, Karnali bridge	A

K14	?	~1	SST	81°	16'	14"	28°	42'	38"	~1km N of section	A
K15	?	<1	SST	81°	15'	26"	28°	44'	17"	West bank, 300 m S of Bheri River confluence	A
Karnali Sand	n/a	Modern	Sand	81°	17'	13"	28°	39'	26"	As for sample K3	A
Karnali Mud	n/a	Modern	Mud	81°	17'	13"	28°	39'	26"	As for sample K3	B
KSandBheri	n/a	Modern	Sand	81°	15'	39"	28°	44'	34"	Above Bheri confluence	B

A = Petrography, B = Geochemistry, C = Ar-Ar dating

Where two sample names are given this indicates resampling at same locality during second field season.

Surai Khola section

Sample	Strat. Height (m)	Strat. Age (Ma)	Lithology		Long			Lat		Locality	Technique
SKA4	0	12	SST	82°	50'	35"	27°	44'	54"	Base of section, beneath white bridge at bend in road	A,C
SKA4N	45	12	SST							Next available outcrop	C
SK284/SK284N	465	11	SST	82°	50'	86"	27°	45'	07"	Opposite Paira Khola sign	C
SK900/SK900N	760	9.9	SST	82°	50'	95"	27°	45'	33"	Above Jungli Khola, lots of drill holes in outcrop	A,C
SKA6	1085	8.9	SST	82°	50'	47"	27°	45'	22"	100 m upsection from Jungli Khola	A,C
SK1350	1384	8	SST							Go past Chor Khola / village and around long bend in road	A,C
SK1448	1465	7.8	SST								C
SK1780	1720	7	SST							Amongst lots of no exposure	A,C
SK2060	2030	6.4	SST	82°	50'	24"	27°	45'	48"		C
SK2378	2224	6	SST							Amongst lots of no exposure	A,C
SK2760	2525	5	SST							100 m past Kaila Khola	C
SKA10	2575	4.9	SST	82°	50'	40"	27°	46'	11"	Just before Surai Khola bridge	A,C
MSPebbles348	2622	4.8	Clasts	82°	50'	06"	27°	46'	15"		B
SKA13/SKA13N	3050	4	SST	82°	50'	22"	27°	46'	62"	Tintre Khola	A,C
MSPebbles SaddlePoint	3200	3.9	Clasts	82°	49'	05"	27°	46'	39"	Saddle Point	B
DANKPebbles	3405	3.1	Clasts	82°	48'	18"	27°	46'	54"	Just after Dan Khola bridge	B
Cong.2	3515	2.7	Cong.Matrix	82°	48'	15"	27°	47'	06"	After small shrine	B
SK4216	3925	1.5	SST							100 m upsection from Dan Khola village, past small bridge	C
SK4230	3940	1.5	SST								C
SKA14	4090	1	SST							Top of section, milestone 677	A,C
Surai Sand	n/a	Modern	Sand	82°	50'	21"	27°	44'	34"	W of road before start of incline through Dundwa Range	A

Tinau Khola section

Sample	Strat. Height (m)	Strat. Age (Ma)	Lithology		Long			Lat		Locality	Technique
TA15/TA15AN	0	12	SST	83°	27'	56"	27°	43'	12"	Base of section, just N of anticline (visible along river)	A,C
TA16	5	12	MUDST	83°	28'	17"	27°	43'	21"		B
TA19	220	10.8	MUDST								B
TA14AN	398	10.3	SST	83°	28'	09"	27°	43'	29"	150 m south of suspension bridge	A,C
TA12alpha	495	10.1	SST	83°	28'	26"	27°	43'	76"	50 m downsection from Hindu Temple	A
TA12	590	10.1	MUDST							Bend in road upsection from Hindu Temple	B
TA7D	1004	9.4	MUDST	83°	27'	98"	27°	44'	33"		B
TA7C	1005	9.4	SST							50 m upsection from "Pokhara 150 km" sign	C
TA5	1180	8.9	SST	83°	27'	51"	27°	44'	24"	Tributary confluence	A,C
TA4	1193	8.9	MUDST								B
TinauPebbles	1412	7.6	Clasts								B
TA2B	1430	7.6	MUDST							Landslide	B
TA2A	1500	7.5	SST								A,C
TA2	1675	6.4	MUDST								B
TA1	1710	6.3	SST							Top of section at Dhoban village	A,C
TinauSand	n/a	Modern	Sand	83°	27'	47"	27°	41'	59"	Where Tinau river flows through Butwal	A
TinauMud	n/a	Modern	Mud	83°	28'	09"	27°	43'	29"	Same as TinauSand	B
Dumre Mud	n/a	Modern	Mud	83°	31'	56"	27°	47'	44"	Tinau river immediately north of MBT	A

A = Petrography, B = Geochemistry, C = Ar-Ar dating

Where two sample names are given this indicates resampling at same locality during second field season.

Fission-track samples

Sample	Strat. Age (Ma)	Lithology		Long			Lat		Locality	Technique
Palpa4	L. Ordovician (?)	SST	83°	31'	41"	27°	46'	02"	Along Butwal-Pokhara road, just N of MBT	AFT,ZFT
LHS4	L. Ordovician (?)	SST	83°	32'	47"	27°	47'	42"	Along Butwal-Pokhara road, milestone: Butwal (19 km)	AFT
Sandy8	L. Ordovician (?)	SST	83°	06'	11"	27°	51'	47"	N of Thada village on road to Sandikharka	AFT,ZFT
Sandy6	L. Ordovician (?)	SST	83°	06'	58"	27°	52'	09"	S of Narapani, N of Thada on road to Sandikharka	AFT,ZFT

```
/* This aml produces river profiles from DEM data
&ty *** Welcome to szulcprofile.aml ***
&ty
&ty
&ty - for the production of river profiles using arc
&ty
&sv sourcex = [response 'enter source cell x coords']
&sv sourcey = [response 'enter source cell y coords']
&sv pourx = [response 'enter pour cell x coords']
&sv poury = [response 'enter pour cell y coords']
&if [exists source_cover -cover] &then kill source_cover
&if [exists pour_cover -cover] &then kill pour_cover
generate source_cover
points
1, %sourcex%, %sourcey%
end
quit
generate pour_cover
points
2, %pourx%, %poury%
end
quit
&ty ****************************************
&if [exists source_grid -grid] &then kill source_grid
&if [exists pour_grid -grid] &then kill pour_grid
pointgrid source_cover source_grid
86.957
y
nodata
pointgrid pour_cover pour_grid
86.957
y
nodata
&if [exists cost_dist -grid] &then kill cost_dist
&if [exists costbacklink -grid] &then kill costbacklink
grid
cost_dist = costdistance (pour_grid, network_gridx, costbacklink)
&if [exists profile_grid -grid] &then kill profile_grid
profile_grid = costpath (source_grid, pour_grid, costbacklink, bycell)
q
rm profile.txt
grid
profile.txt = sample (profile_grid, fnepal_dem)
&ty
&ty
q
&ty Profiling complete, profile.txt ready for excel manipulation
&return
```

```
/* This aml produces streampower plots from DEM data
&ty *** Welcome to szulcstreampower.aml ***
&ty
&ty
&ty - for the production of streampower plots using arc
&ty
&sv sourcex = [response 'enter source cell x coords']
&sv sourcey = [response 'enter source cell y coords']
&sv pourx = [response 'enter pour cell x coords']
&sv poury = [response 'enter pour cell y coords']
&if [exists source_cover –cover] &then kill source_cover
&if [exists pour_cover –cover] &then kill pour_cover
generate source_cover
points
1, %sourcex%, %sourcey%
end
quit
generate pour_cover
points
2, %pourx%, %poury%
end
quit
&ty **********************************
&if [exists source_grid –grid] &then kill source_grid
&if [exists pour_grid –grid] &then kill pour_grid
pointgrid source_cover source_grid
86.957
y
nodata
pointgrid pour_cover pour_grid
86.957
y
nodata
&if [exists cost_dist –grid] &then kill cost_dist
&if [exists costbacklink –grid] &then kill costbacklink
grid
cost_dist = costdistance (pour_grid, network_gridx, costbacklink)
&if [exists profile_grid –grid] &then kill profile_grid
profile_grid = costpath (source_grid, pour_grid, costbacklink, bycell)
q
rm profile.txt
grid
profile.txt = sample (profile_grid, streampow)
&ty
&ty
q
&ty Profiling complete, profile.txt ready for excel manipulation
&return
```

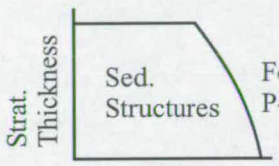
III Detailed logs

Tinau Khola Section Sedimentary Log

Sedimentary Structures

- Bed boundary
- Lamination
- Planar Cross-Stratification
- Trough Cross-Stratification
- Load Structure
- Asymmetric Ripples
- Lateral Accretion
- Erosional Contact
- 40 Strike and Dip of Bed (Dip value)
- Parting Lineation
- Clasts/Imbrication (If P-current is shown)
- Flutes
- C Calcareous
- Channel(s)
- Convolute Bedding
- Dessication Cracks
- No Exposure
- Flaser Bedding
- Bioturbation (Assumed for P-Soils)
- Water Escape Structures
- Oxidised nodule
- Calcareous nodule
- Slump Structures
- Crevasse Splay
- Grooves
- xxx Tool Marks
- Climbing Ripples
- Palaeosol

Log Format



Symbols refer to bed as a whole unless drawn in a specific location. Sandstones, Siltstones and Mudstones are distinguished by grainsize only.

Palaeocurrent Information

- ↔ Palaeoflow, direction unknown (assumed towards foreland)
- → Palaeoflow, direction known
- PCL Planar Cross-Lamination
- TCL Trough Cross-Lamination
- C Channel
- T Tools
- G Grooves
- I Imbrication
- R Ripples
- Flutes
- PL Parting Lineation
- CR Climbing Ripples

Fossils

- Burrows
- Roots
- Bones
- Leaves
- Wood
- Shell
- Molluscs
- Trace Fossils

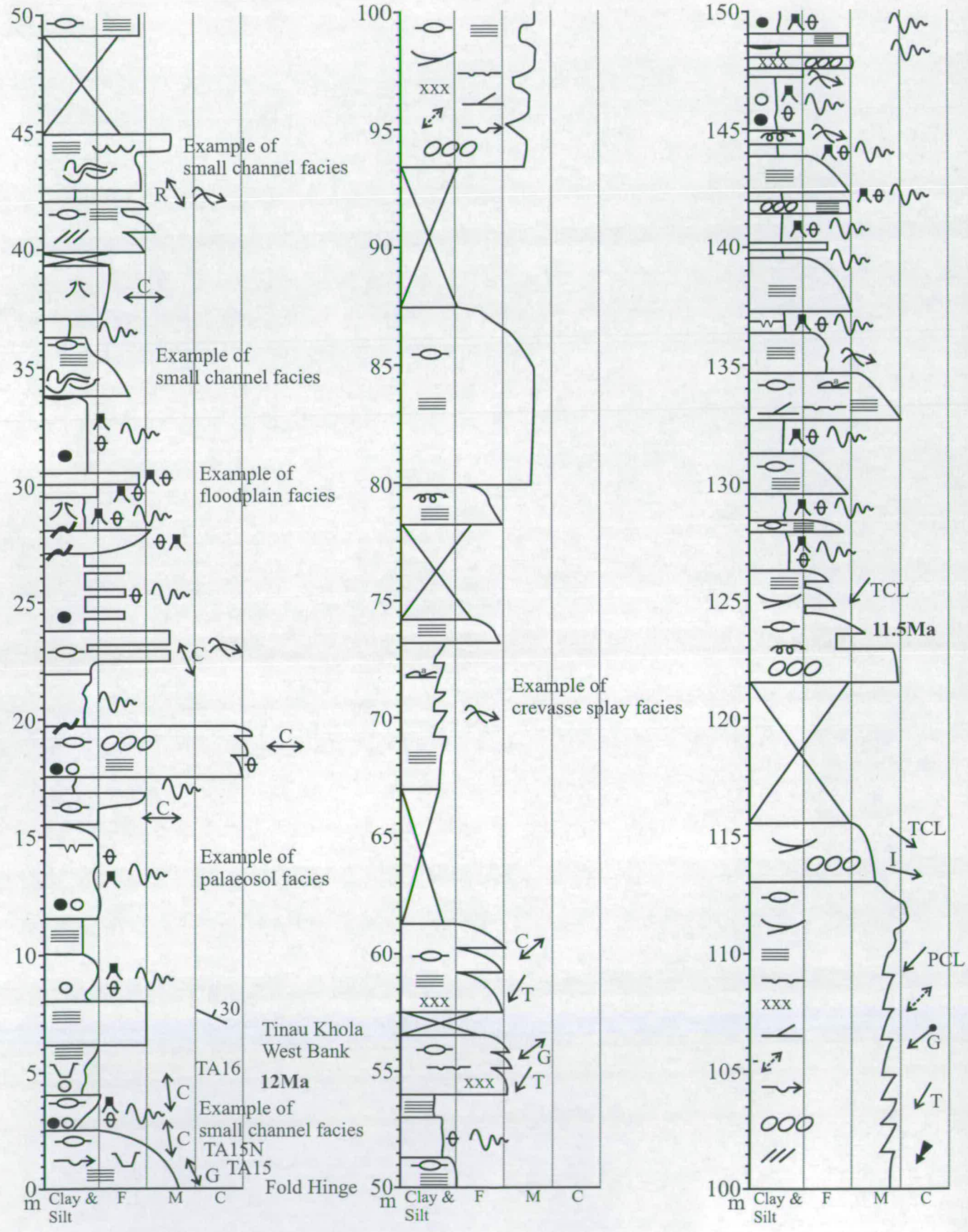
Grainsize (mm)

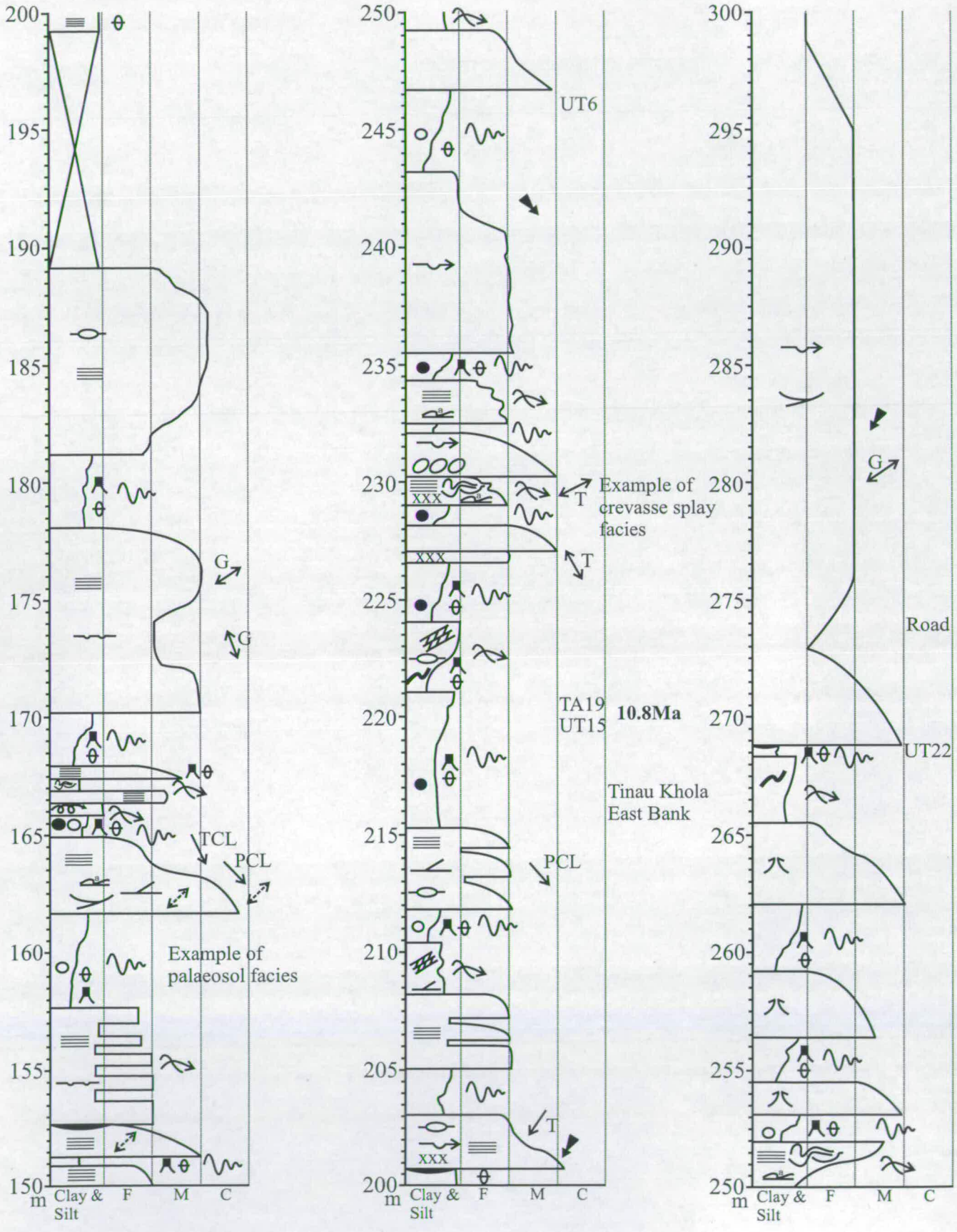
Clay	<0.002
Silt	0.002-0.06
Fine	0.06-0.2
Medium	0.2-0.6
Coarse	0.6-2

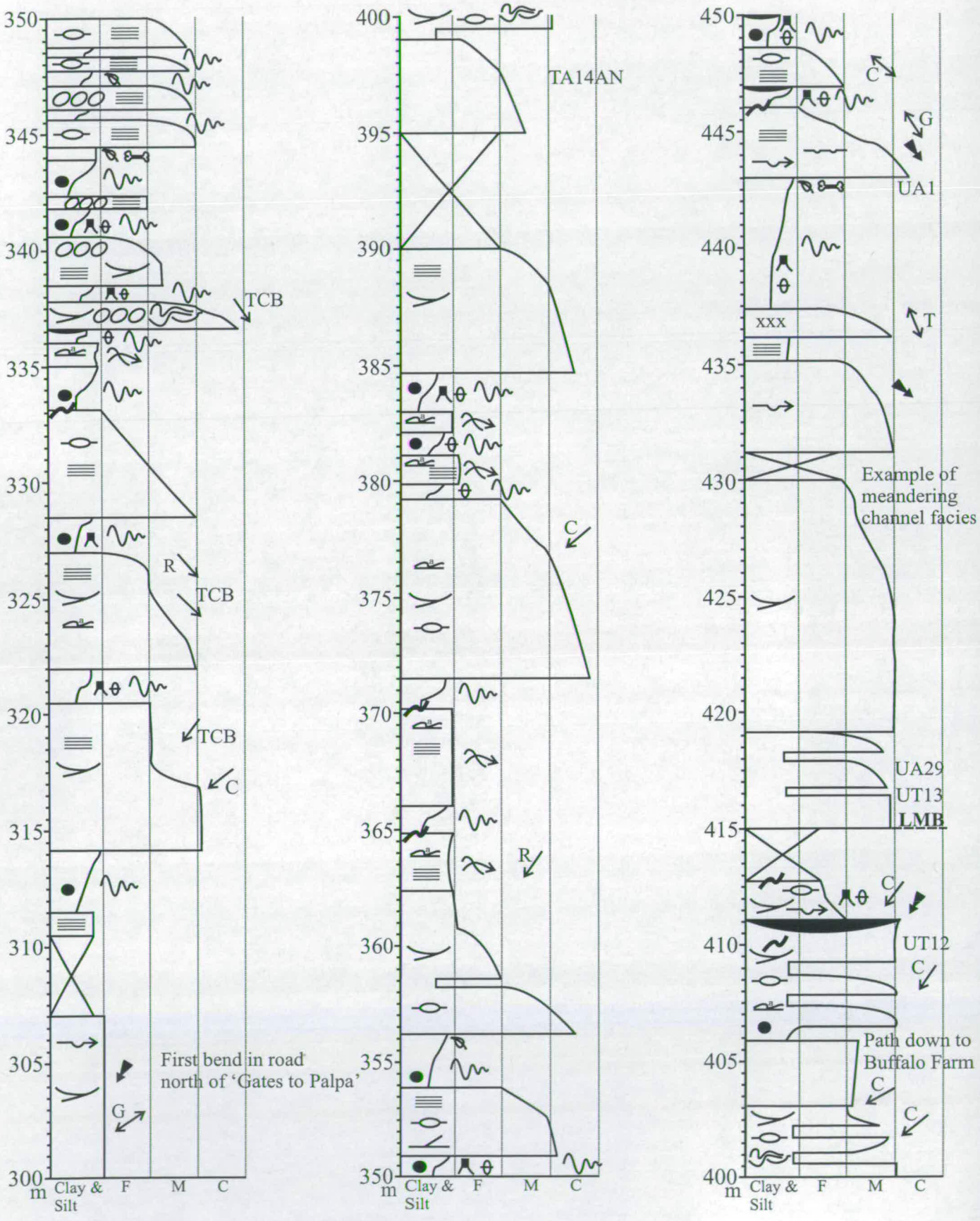
When concerning conglomerates, grainsize refers to the matrix.

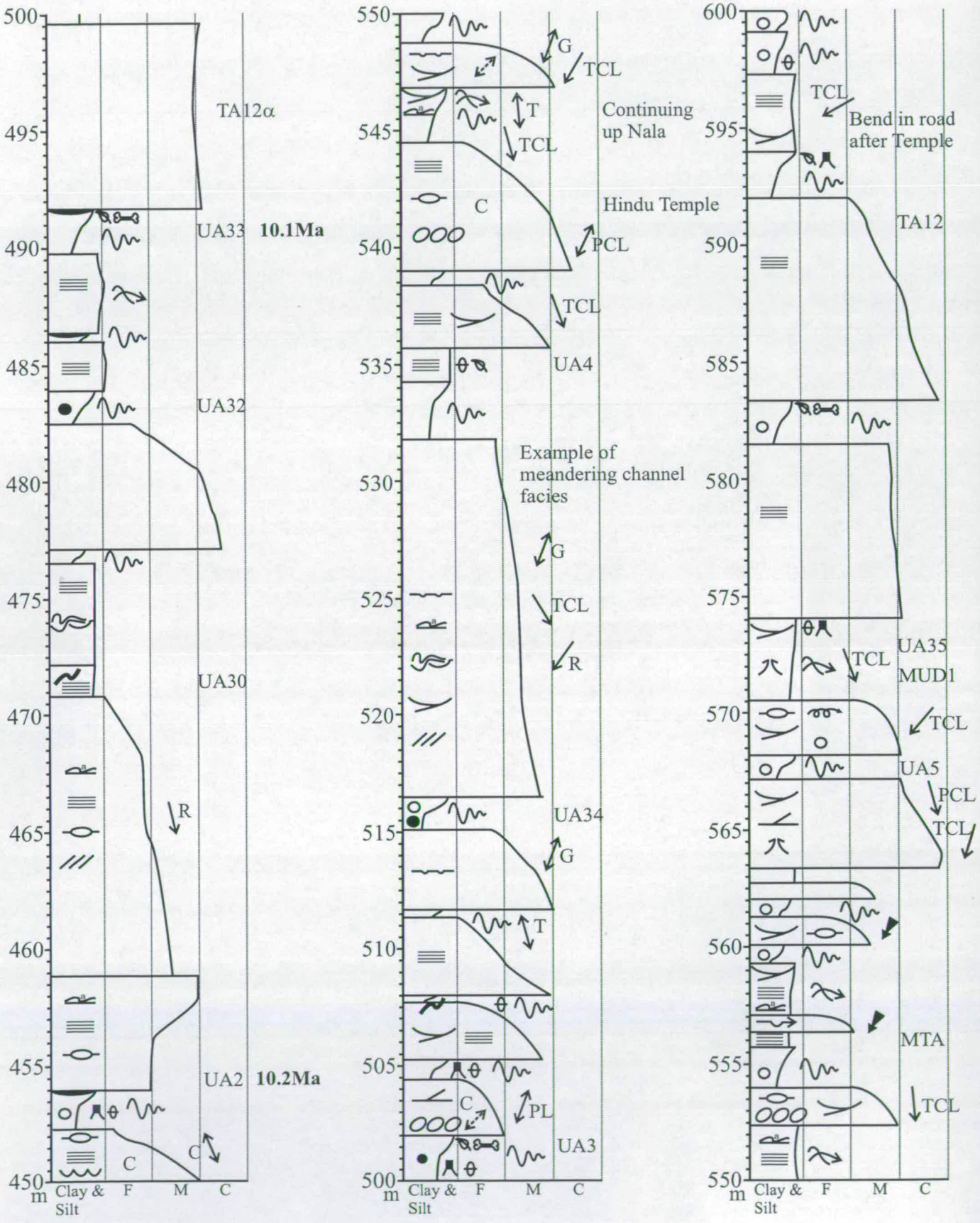
Others

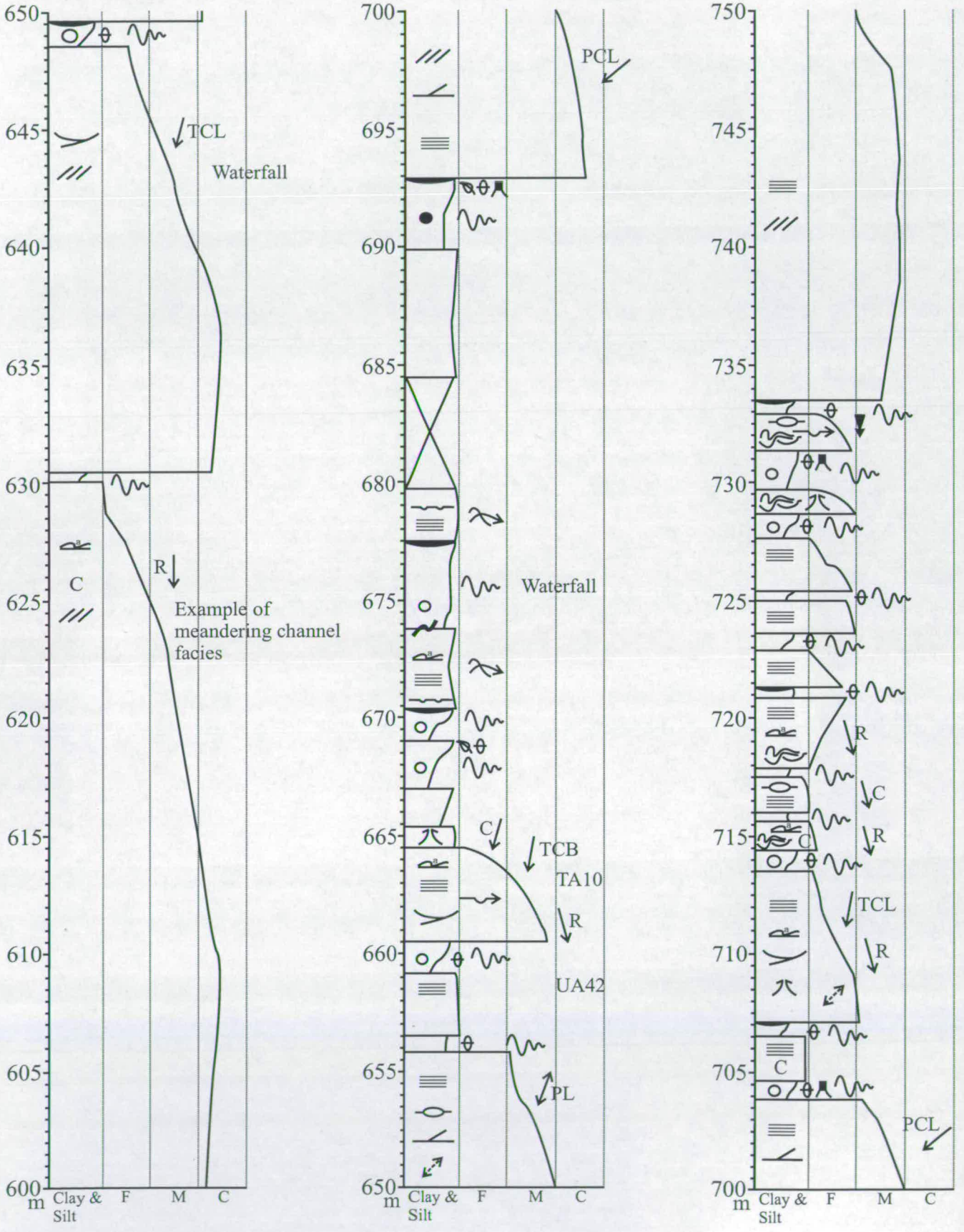
UA	P-Mag. Samples
TA18A	Sample No.
LMB	Lower-Middle Siwalik Boundary
MS2	Middle Siwalik 2 (Pebbly)

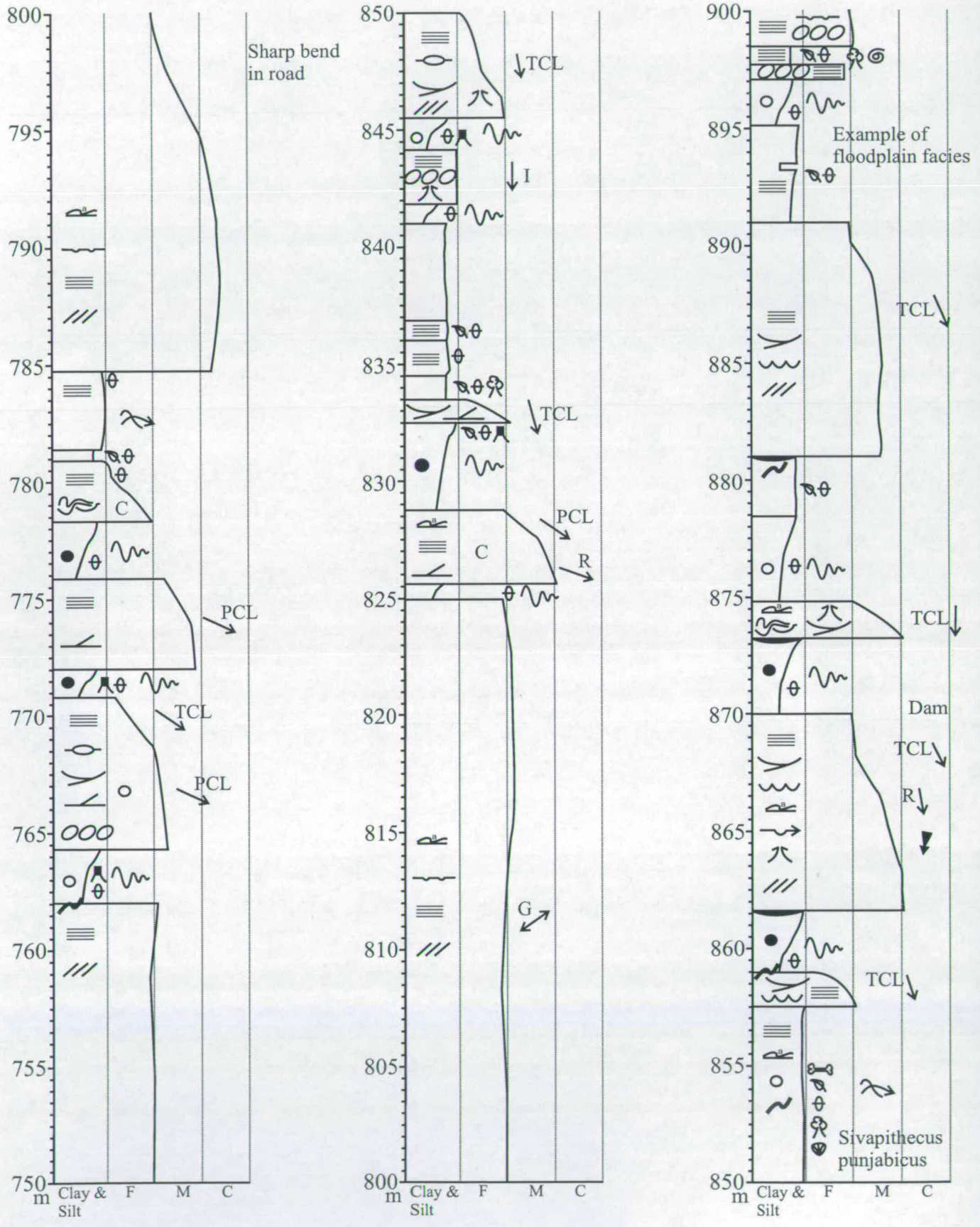

Example of small channel facies
Example of small channel facies
Example of floodplain facies
Example of palaeosol facies
Example of small channel facies
Example of crevasse splay facies
Tinau Khola West Bank
12Ma
TA16
TA15N
TA15
Fold Hinge
11.5Ma
TCL
PCL
Clay & Silt
F
M
C
m

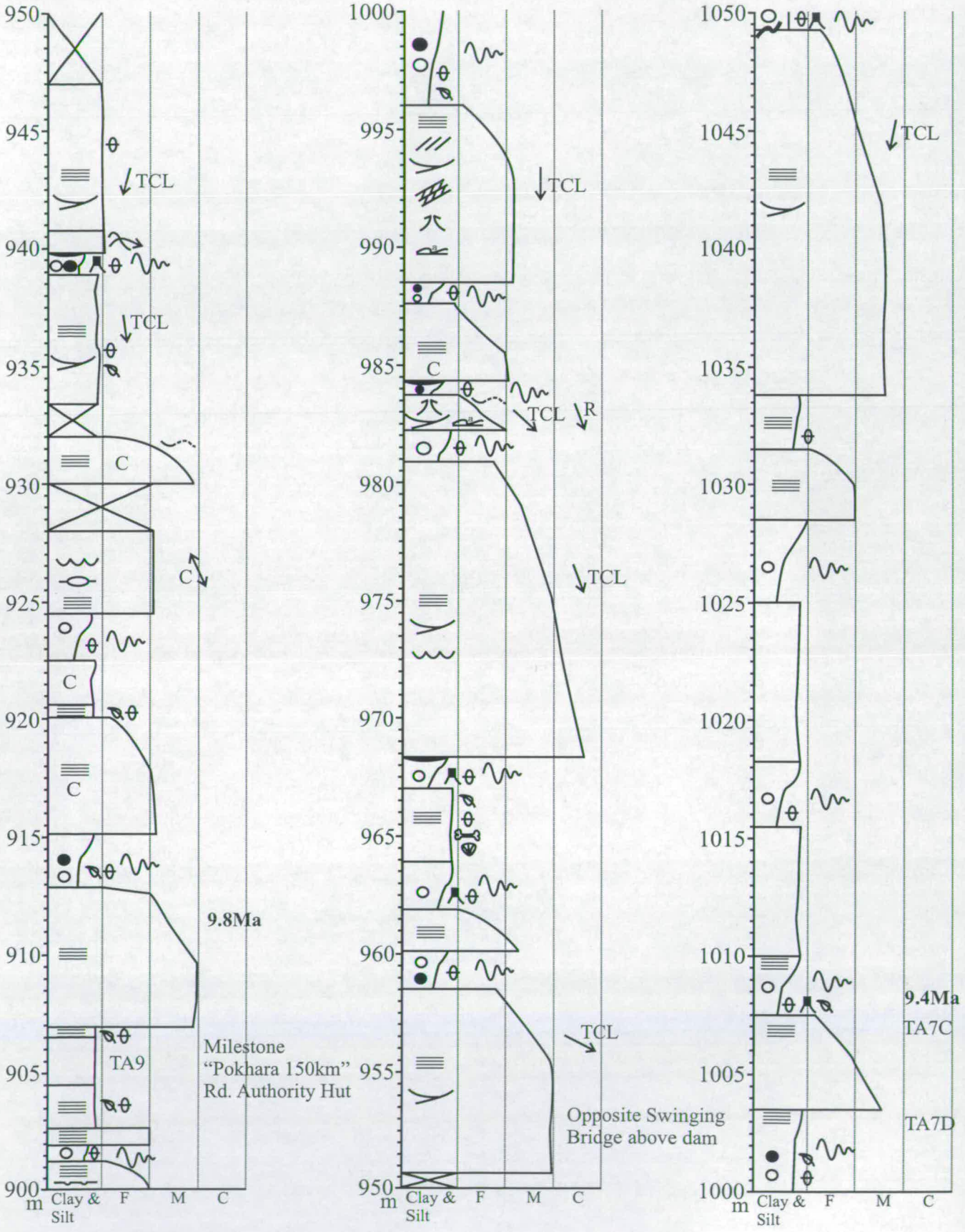

200
195
190
185
180
175
170
165
160
155
150
m
Clay & Silt
F
M
C
G
G
TCL
PCL
Example of palaeosol facies
250
245
240
235
230
225
220
215
210
205
200
UT6
T
Example of crevasse splay facies
T
TA19
UT15
10.8Ma
Tinau Khola East Bank
PCL
T
XXX
300
295
290
285
280
275
270
265
260
255
250
G
Road
UT22

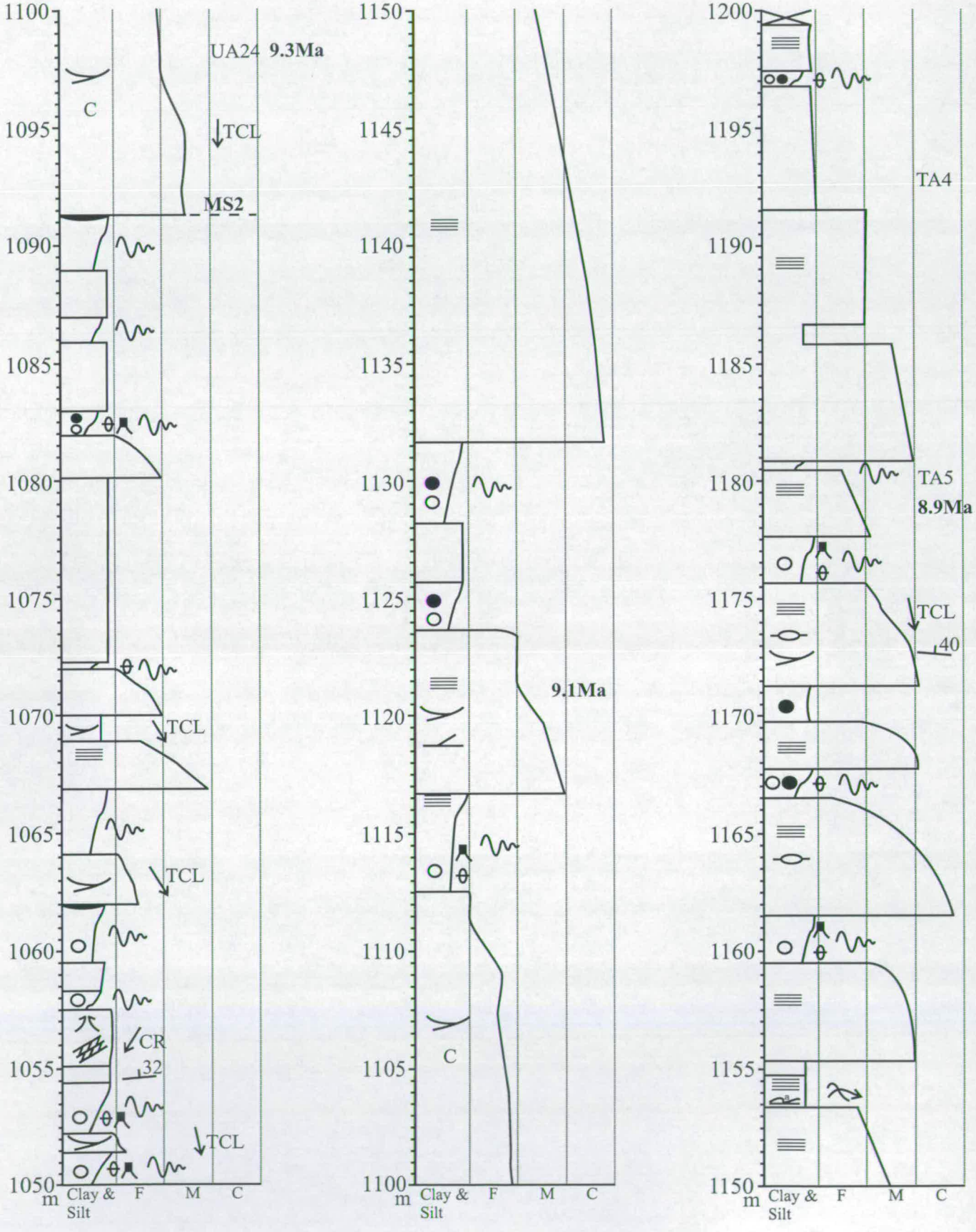

350
345
340
335
330
325
320
315
310
305
300
m
Clay & Silt
F
M
C
TCB
R
TCB
TCB
C
G
First bend in road north of 'Gates to Palpa'
400
395
390
385
380
375
370
365
360
355
350
TA14AN
C
R
450
445
440
435
430
425
420
415
410
405
400
C
G
UA1
xxx
T
Example of meandering channel facies
UA29
UT13
LMB
C
UT12
C
Path down to Buffalo Farm
C
C

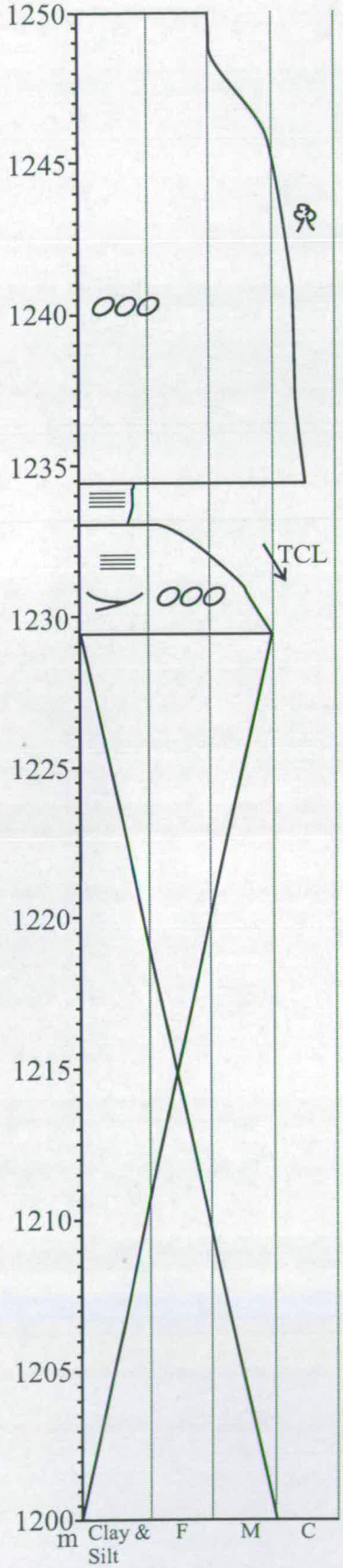

500
495
490
485
480
475
470
465
460
455
450
m
Clay & Silt
F
M
C
TA12α
UA33
10.1Ma
UA32
UA30
R
UA2
10.2Ma
C
C
550
545
540
535
530
525
520
515
510
505
500
G
TCL
T
TCL
C
Continuing up Nala
Hindu Temple
PCL
TCL
UA4
Example of meandering channel facies
G
TCL
R
UA34
G
T
C
PL
UA3
600
595
590
585
580
575
570
565
560
555
550
TCL
Bend in road after Temple
TA12
TCL
UA35
MUD1
TCL
UA5
PCL
TCL
MTA
TCL

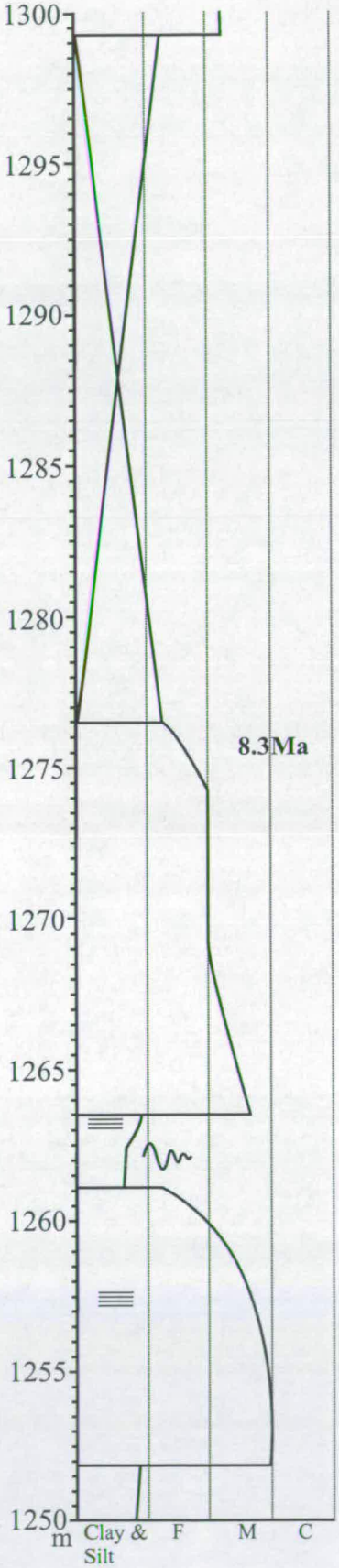

650
645
640
635
630
625
620
615
610
605
600
m
Clay & Silt
F
M
C
TCL
Waterfall
R
C
Example of meandering channel facies
700
695
690
685
680
675
670
665
660
655
650
PCL
Waterfall
C
TCB
TA10
R
UA42
PL
750
745
740
735
730
725
720
715
710
705
700
R
C
R
C
TCL
R
C
PCL

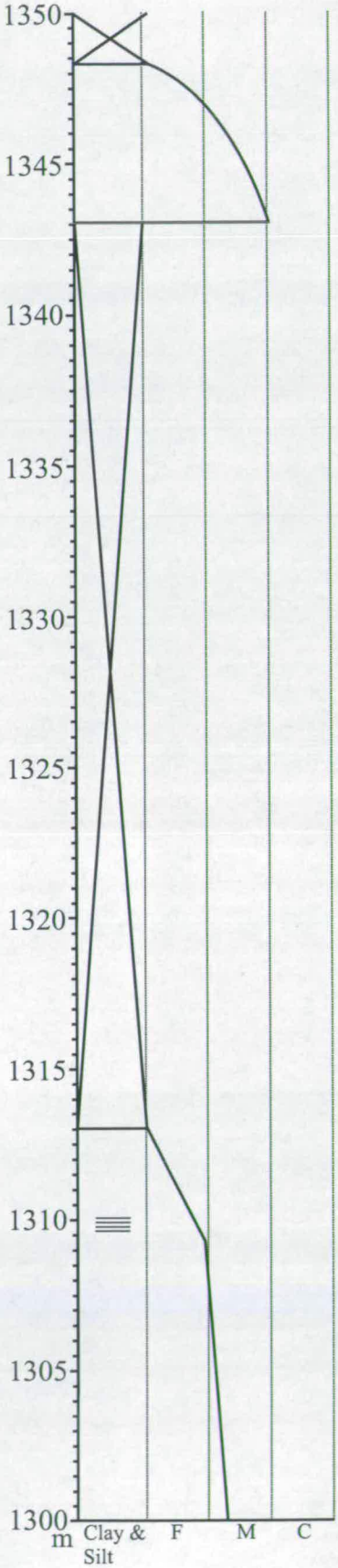

800
795
790
785
780
775
770
765
760
755
750
m
Clay & Silt
F
M
C
Sharp bend in road
C
PCL
TCL
PCL
850
845
840
835
830
825
820
815
810
805
800
TCL
I
TCL
PCL
C
R
G
900
895
890
885
880
875
870
865
860
855
850
Example of floodplain facies
TCL
TCL
Dam
TCL
R
TCL
Sivapithecus punjabicus

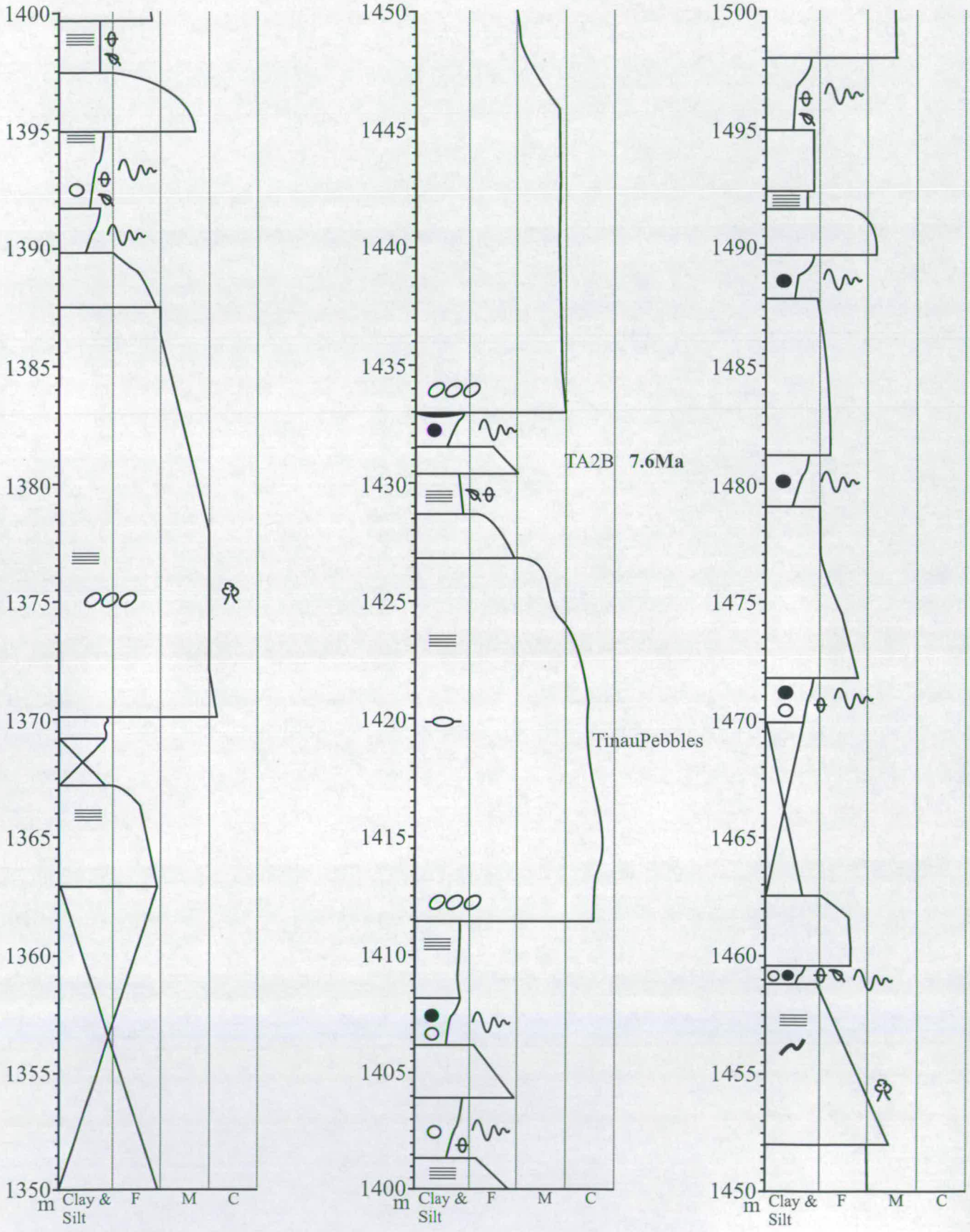

950
945
940
935
930
925
920
915
910
905
900
m
Clay & Silt
F
M
C
TCL
C
9.8Ma
TA9
Milestone
"Pokhara 150km"
Rd. Authority Hut
1000
995
990
985
980
975
970
965
960
955
950
R
Opposite Swinging
Bridge above dam
1050
1045
1040
1035
1030
1025
1020
1015
1010
1005
1000
9.4Ma
TA7C
TA7D

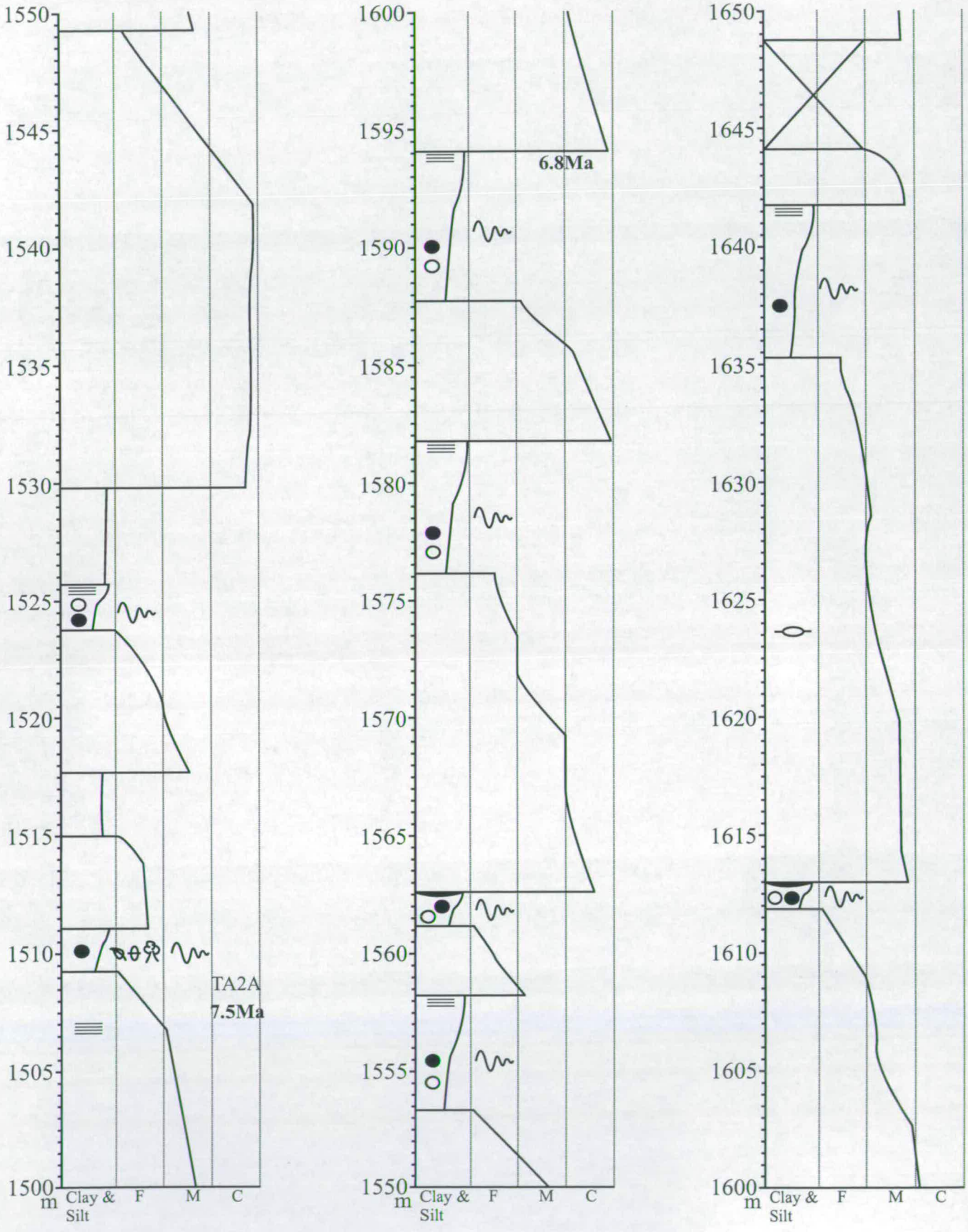

1100
1095
1090
1085
1080
1075
1070
1065
1060
1055
1050
m
Clay &
Silt
F
M
C
UA24 9.3Ma
C
TCL
MS2
TCL
TCL
CR
32
TCL
1150
1145
1140
1135
1130
1125
1120
1115
1110
1105
1100
9.1Ma
C
1200
1195
1190
1185
1180
1175
1170
1165
1160
1155
1150
TA4
TA5
8.9Ma
TCL
40

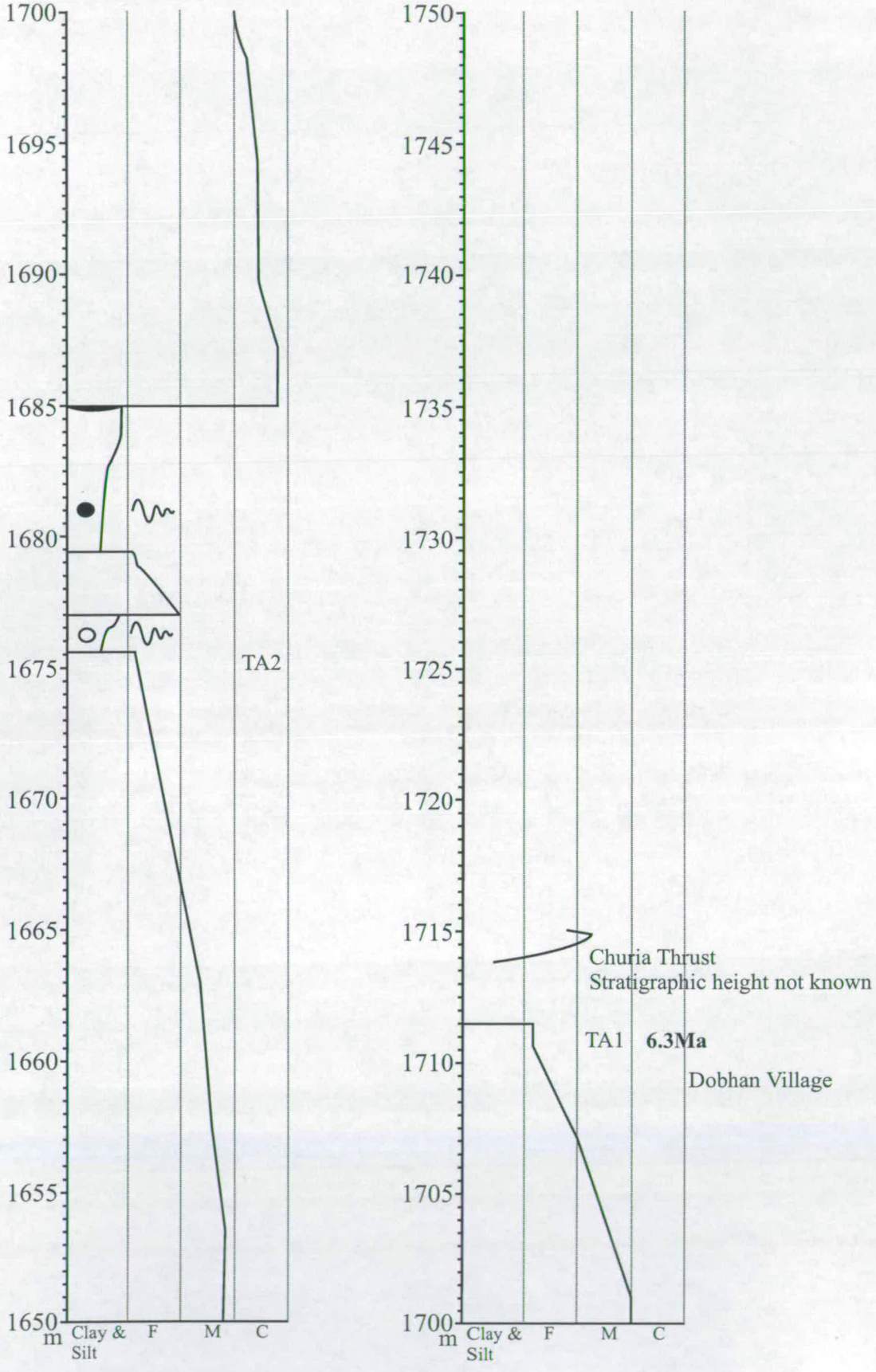

1250
1245
1240
1235
1230
1225
1220
1215
1210
1205
1200
TCL
m
Clay &
Silt
F
M
C


1300
1295
1290
1285
1280
1275
1270
1265
1260
1255
1250
8.3Ma
m
Clay &
Silt
F
M
C


1350
1345
1340
1335
1330
1325
1320
1315
1310
1305
1300
m
Clay &
Silt
F
M
C


1400
1395
1390
1385
1380
1375
1370
1365
1360
1355
1350
m
Clay &
Silt
F
M
C
1450
1445
1440
1435
1430
1425
1420
1415
1410
1405
1400
TA2B 7.6Ma
TinauPebbles
1500
1495
1490
1485
1480
1475
1470
1465
1460
1455
1450


1550
1545
1540
1535
1530
1525
1520
1515
1510
1505
1500
m
Clay &
Silt
F
M
C
TA2A
7.5Ma
1600
1595
1590
1585
1580
1575
1570
1565
1560
1555
1550
6.8Ma
1650
1645
1640
1635
1630
1625
1620
1615
1610
1605
1600

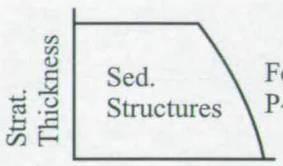

1700
1695
1690
1685
1680
1675
1670
1665
1660
1655
1650
m
Clay & Silt
F
M
C
TA2
1750
1745
1740
1735
1730
1725
1720
1715
1710
1705
1700
m
Clay & Silt
F
M
C
Churia Thrust
Stratigraphic height not known
TA1
6.3Ma
Dobhan Village

Surai Khola Section Sedimentary Log

Sedimentary Structures

- Bed boundary
- Lamination
- Planar Cross-Stratification
- Trough Cross-Stratification
- Load Structure
- Asymmetric Ripples
- Lateral Accretion
- Erosional Contact
- 40 Strike and Dip of Bed (Dip value)
- Parting Lineation
- Clasts/Imbrication (If P-current is shown)
- Flutes
- C Calcareous
- Channel(s)
- Convolute Bedding
- Dessication Cracks
- No Exposure
- Flaser Bedding
- Bioturbation (Assumed for P-Soils)
- Water Escape Structures
- Oxidised nodule
- Calcareous nodule
- Slump Structures
- Crevasse Splay
- Grooves
- xxx Tool Marks
- Climbing Ripples
- Palaeosol

Log Format



Symbols refer to bed as a whole unless drawn in a specific location. Sandstones, Siltstones and Mudstones are distinguished by grainsize only.

Palaeocurrent Information

- ↔ Palaeoflow, direction unknown (assumed towards foreland)
- → Palaeoflow, direction known
- PCL Planar Cross-Lamination
- TCL Trough Cross-Lamination
- C Channel
- T Tools
- G Grooves
- I Imbrication
- R Ripples
- Flutes
- PL Parting Lineation
- CR Climbing Ripples

Fossils

- Burrows
- Roots
- Bones
- Leaves
- Wood
- Shell
- Molluscs
- Trace Fossils

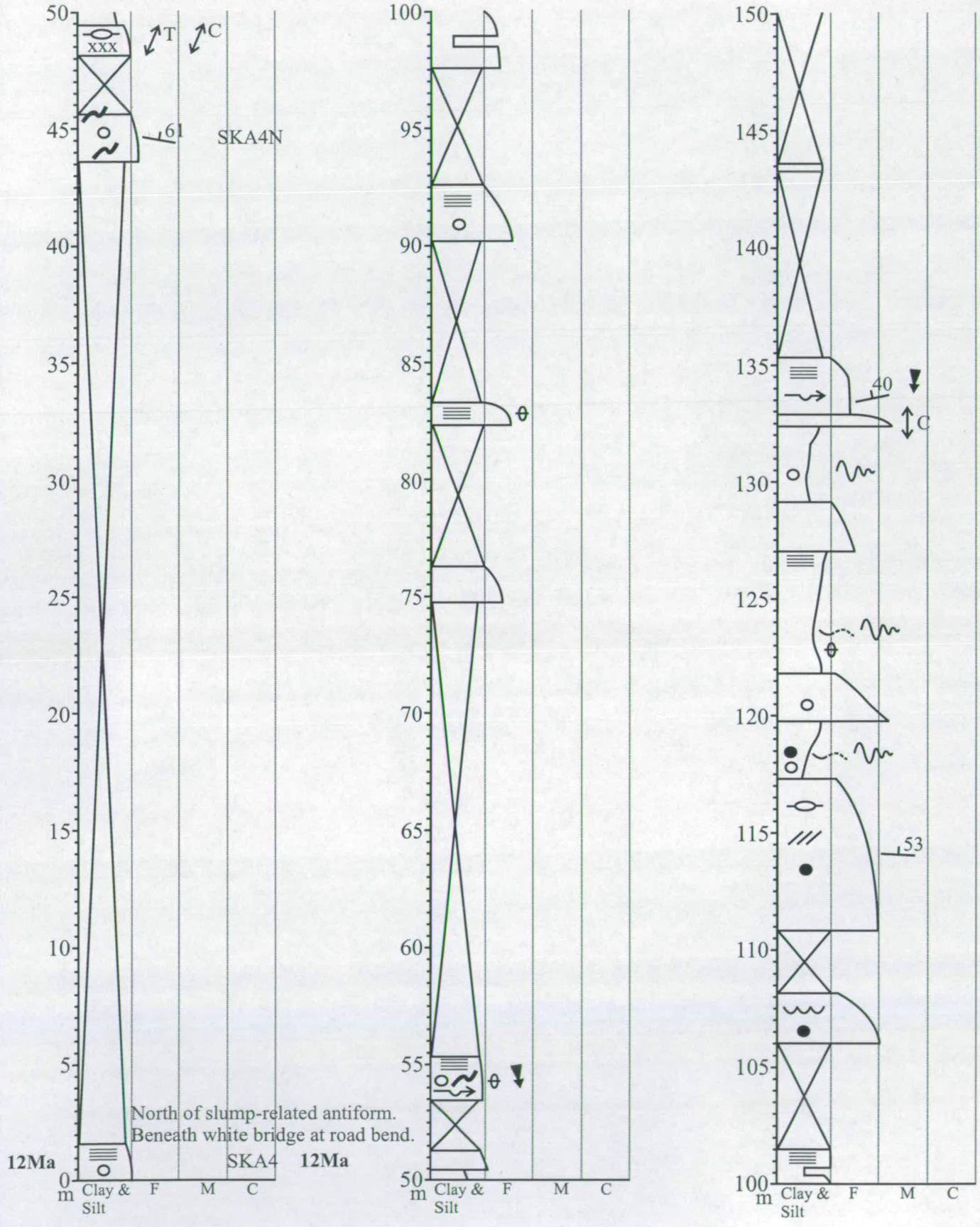
Grainsize (mm)

Clay	<0.002
Silt	0.002-0.06
Fine	0.06-0.2
Medium	0.2-0.6
Coarse	0.6-2

When concerning conglomerates, grainsize refers to the matrix.

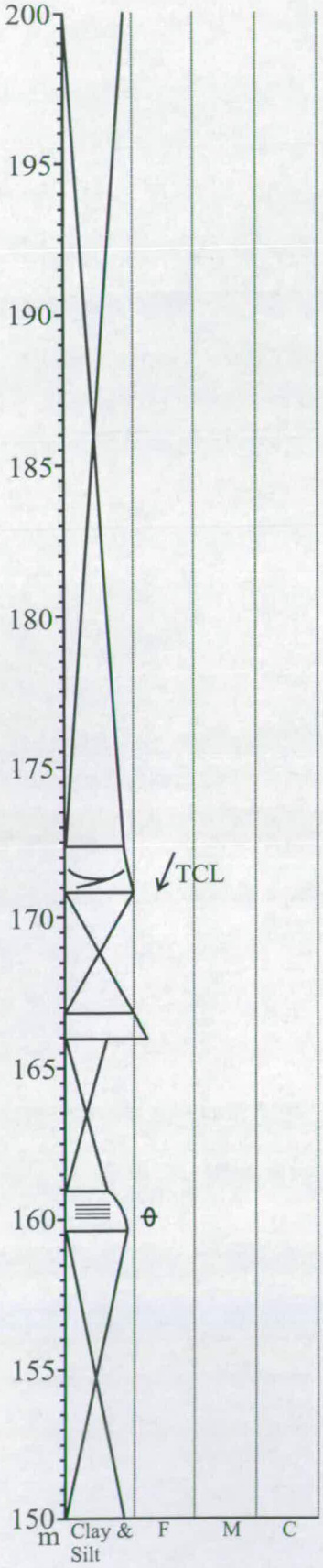
Others

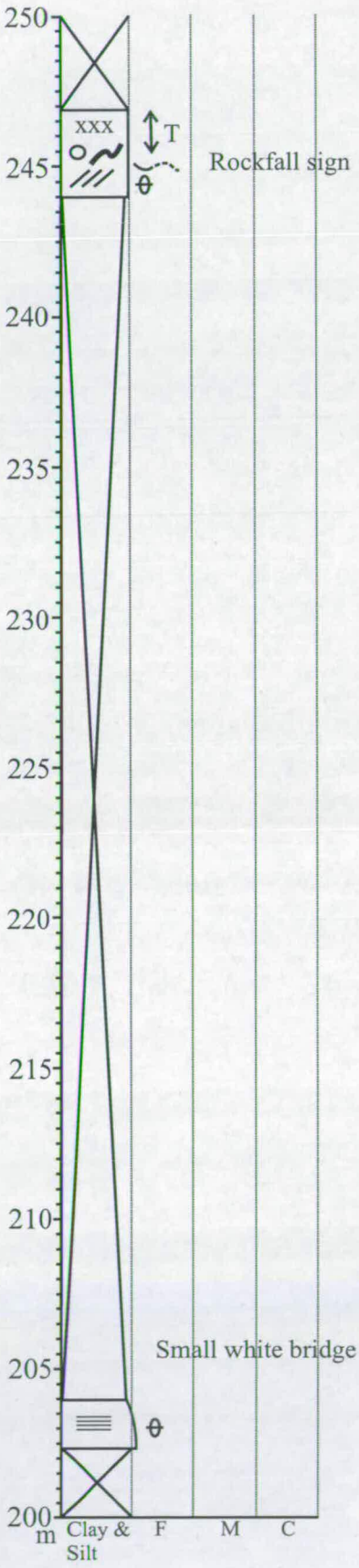
UA	P-Mag. Samples
TA18A	Sample No.
LMB	Lower-Middle Siwalik Boundary
MS2	Middle Siwalik 2 (Pebbly)

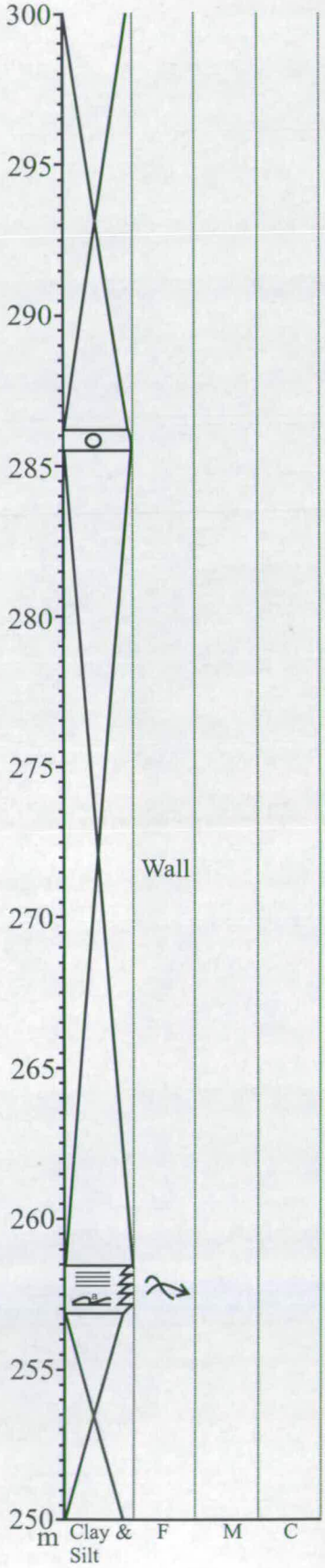


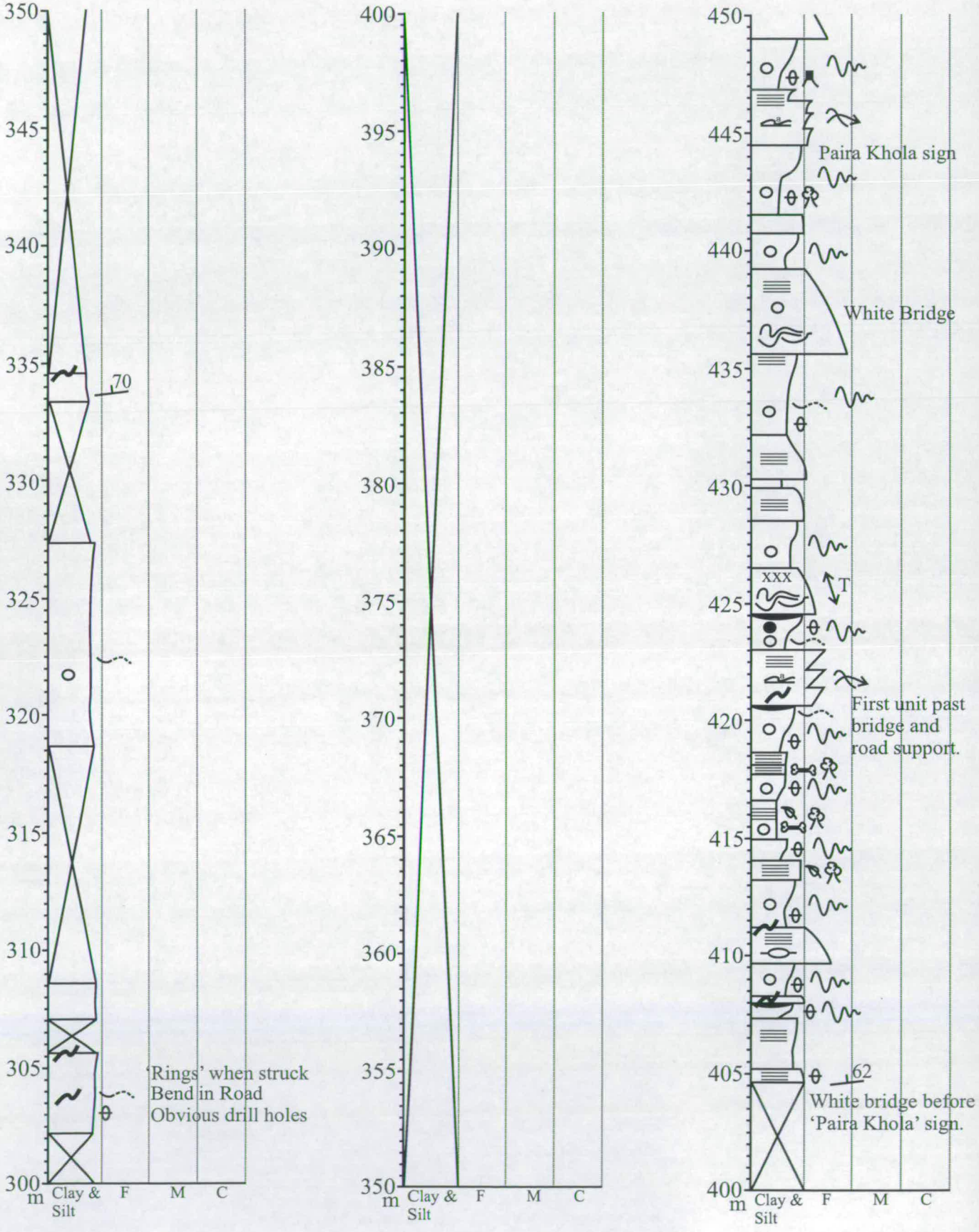
North of slump-related antiform.
Beneath white bridge at road bend.

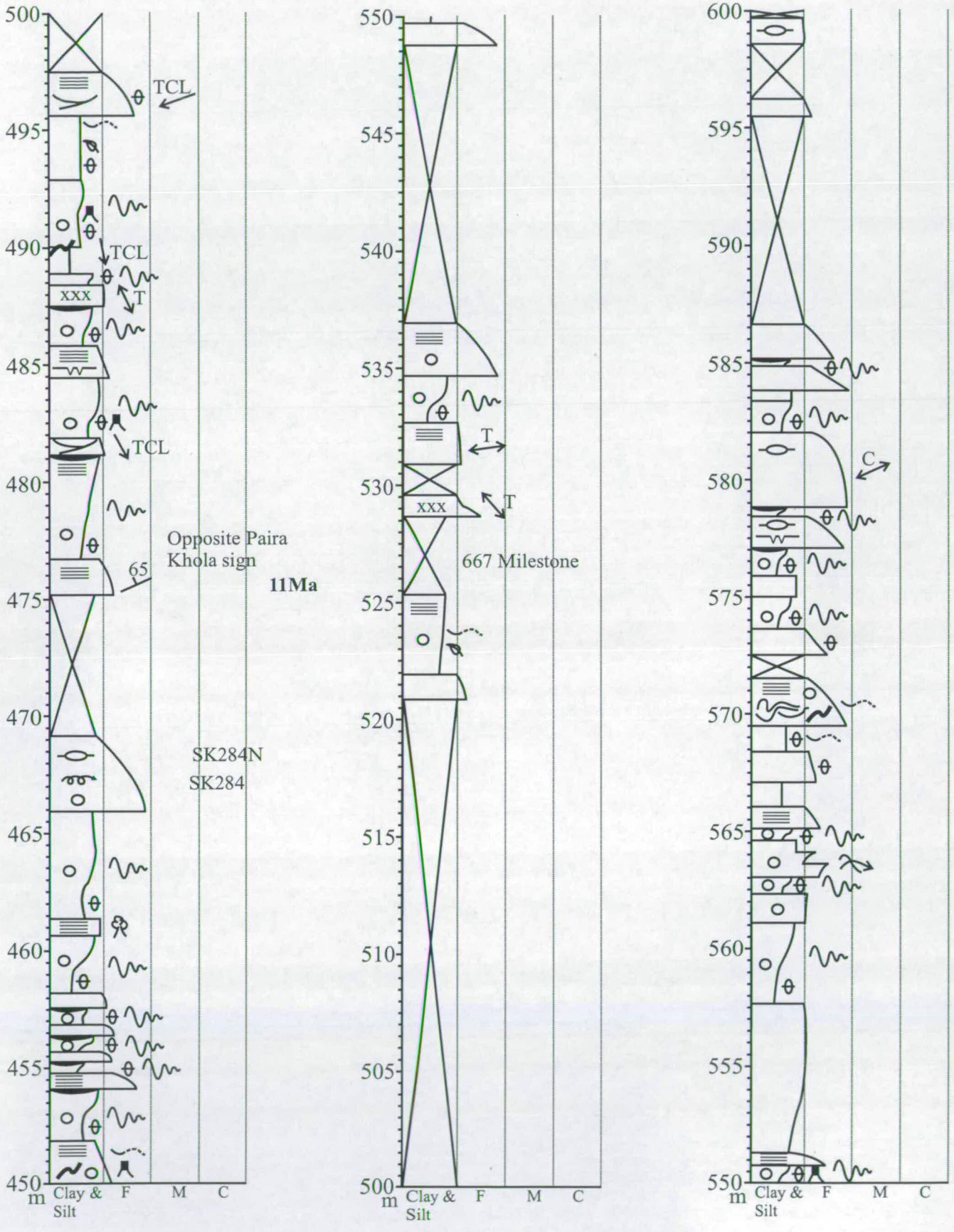
SKA4 **12Ma**

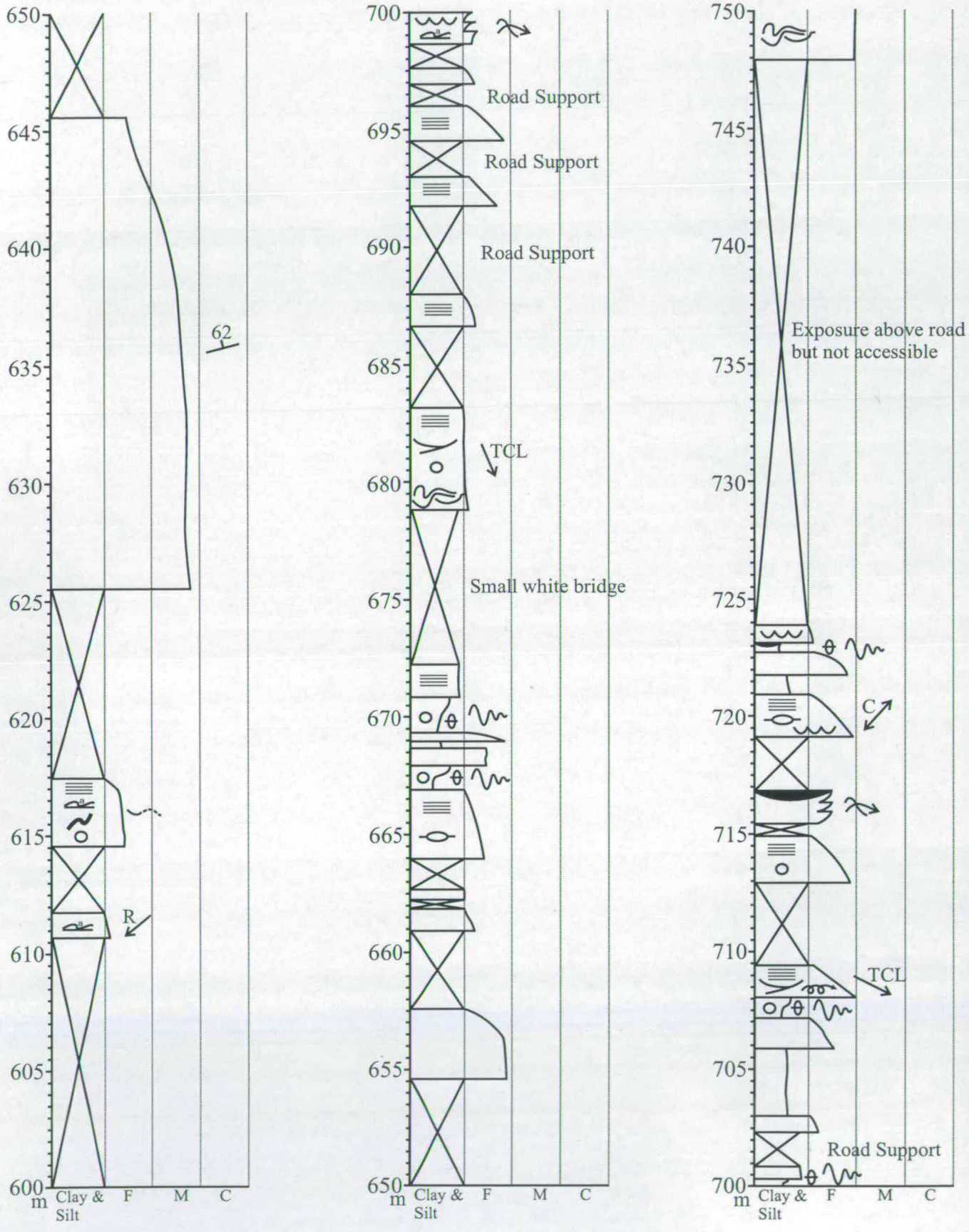

200
195
190
185
180
175
170
165
160
155
150
m
Clay &
Silt
F
M
C
TCL

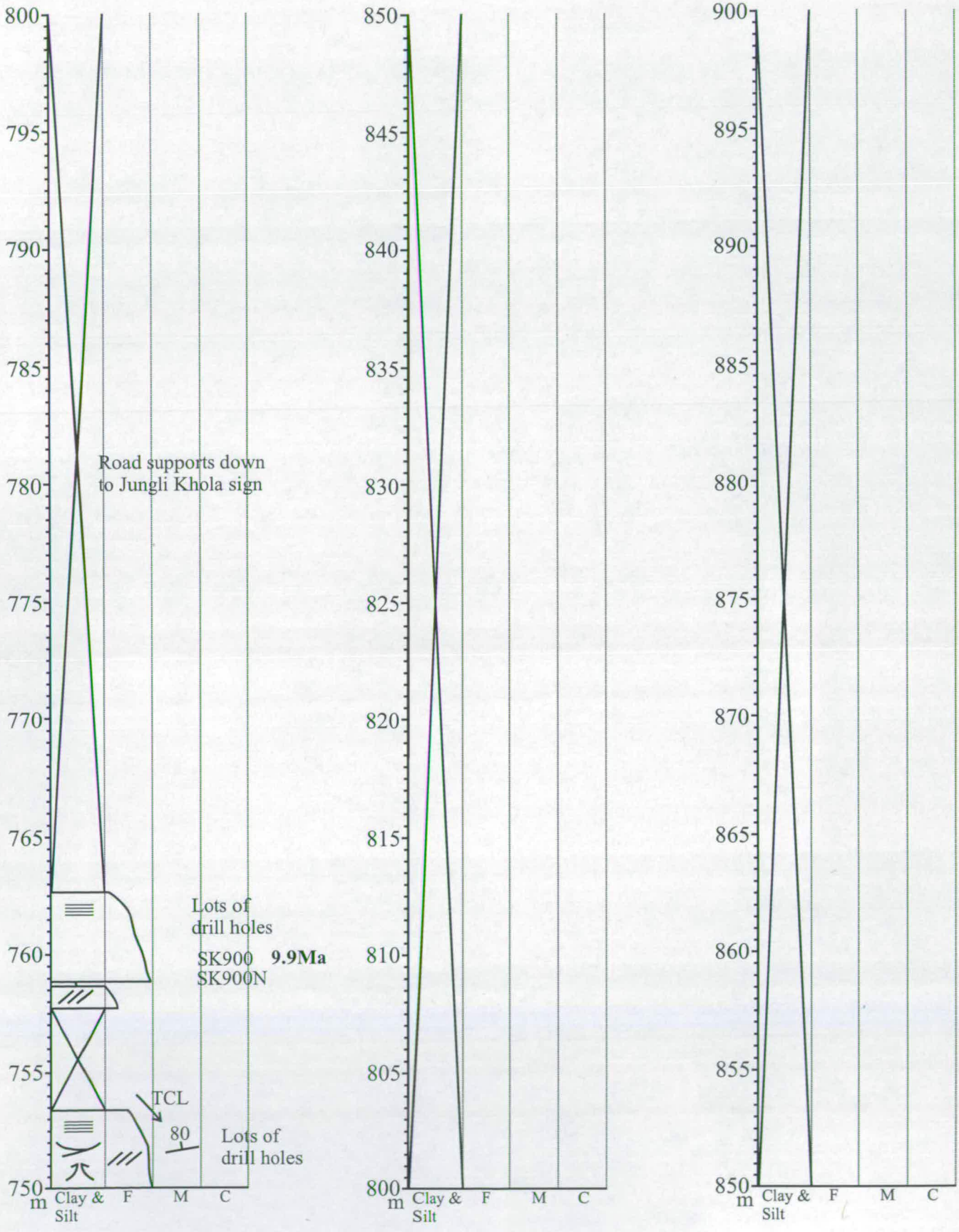

250
245
240
235
230
225
220
215
210
205
200
m
Clay &
Silt
F
M
C
xxx
T
Rockfall sign
Small white bridge

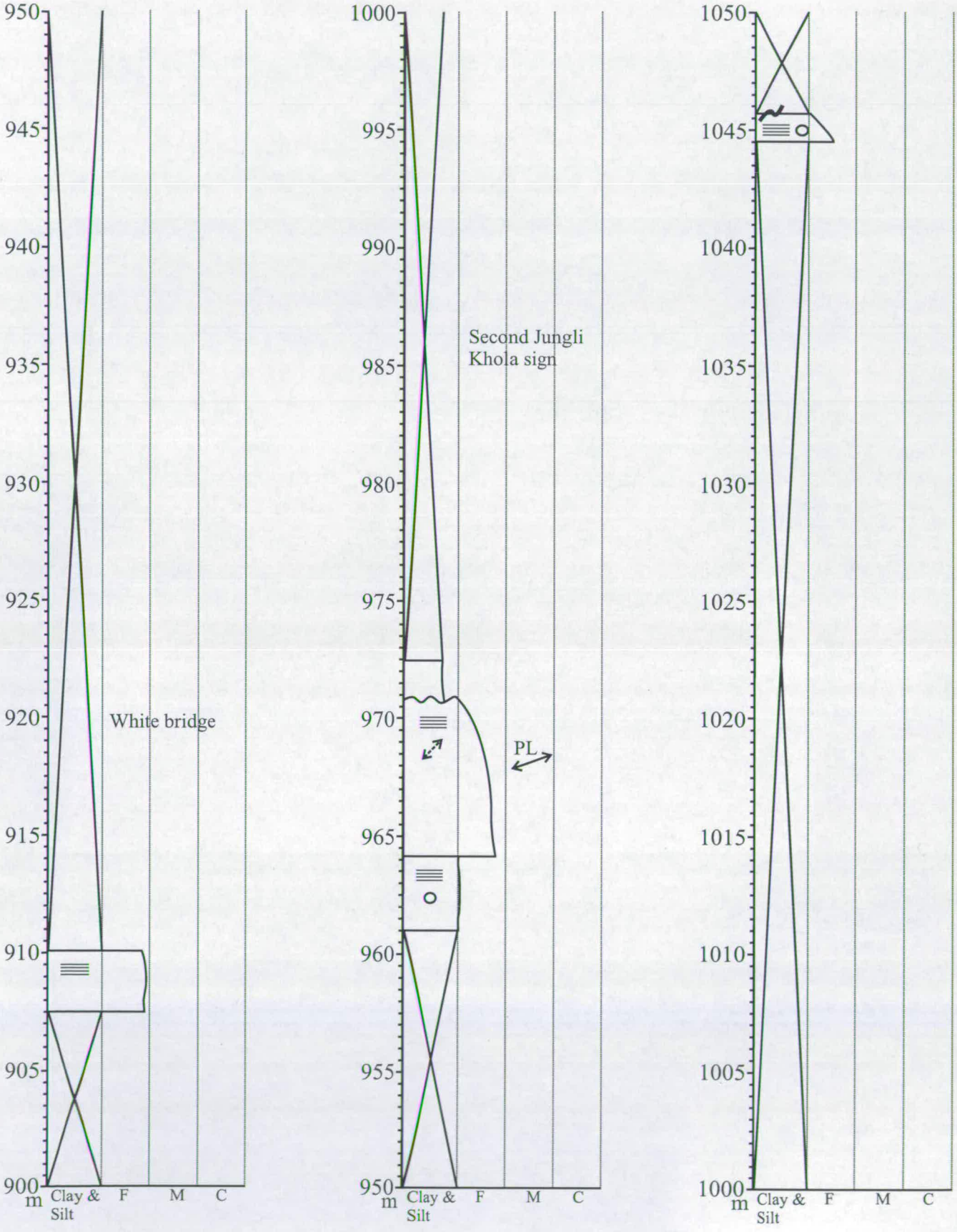

300
295
290
285
280
275
270
265
260
255
250
m
Clay &
Silt
F
M
C
Wall

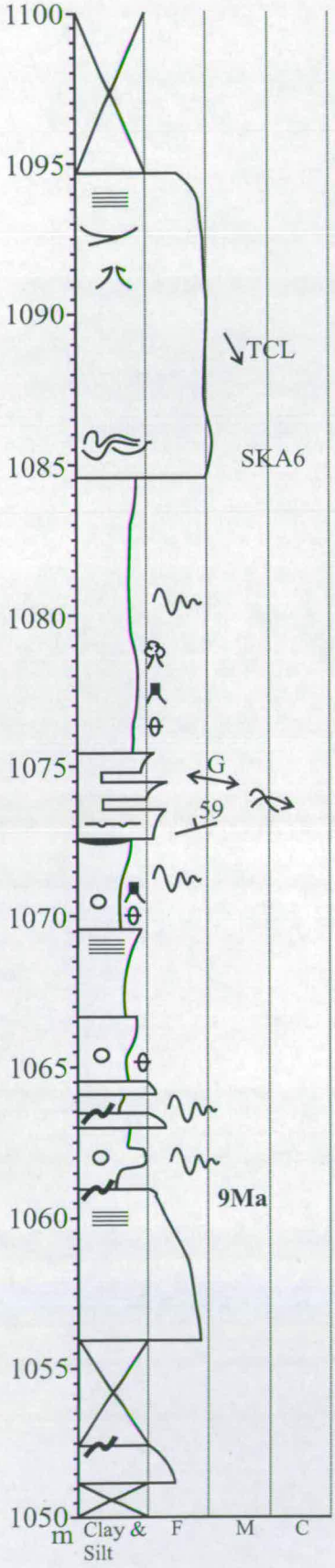

350
345
340
335
330
325
320
315
310
305
300
m
Clay & Silt
F
M
C
70
'Rings' when struck
Bend in Road
Obvious drill holes
400
395
390
385
380
375
370
365
360
355
350
m
Clay & Silt
F
M
C
450
445
440
435
430
425
420
415
410
405
400
m
Clay & Silt
F
M
C
Paira Khola sign
White Bridge
xxx
T
First unit past bridge and road support.
62
White bridge before 'Paira Khola' sign.

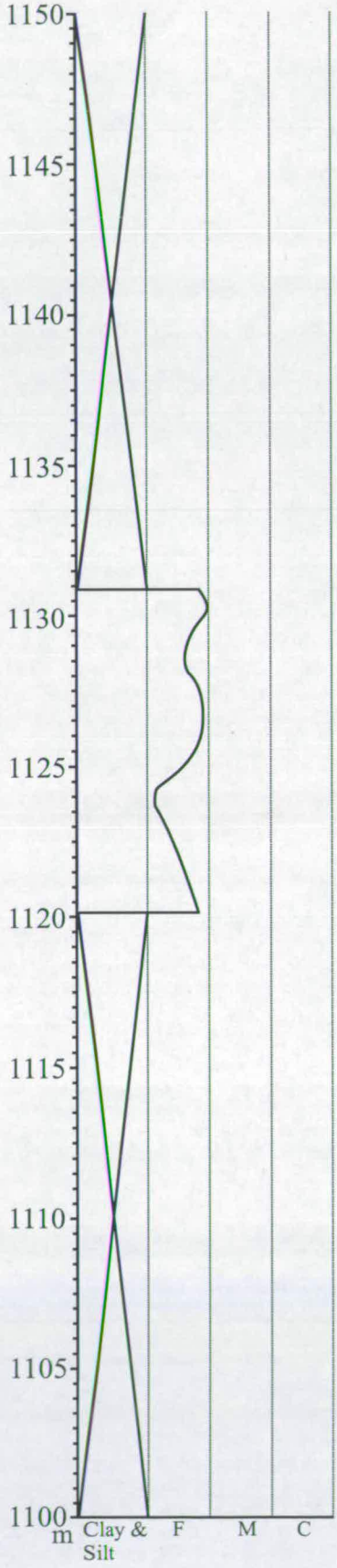

500
495
490
485
480
475
470
465
460
455
450
m
Clay &
Silt
F
M
C
TCL
TCL
XXX
T
TCL
Opposite Paira
Khola sign
65
11Ma
SK284N
SK284
550
545
540
535
530
525
520
515
510
505
500
T
XXX
T
667 Milestone
600
595
590
585
580
575
570
565
560
555
550
C

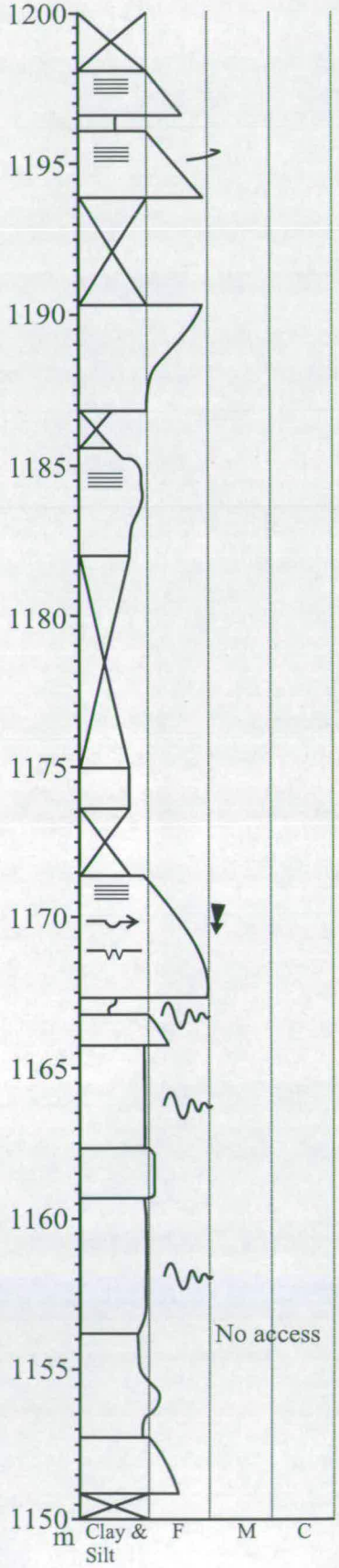

650
645
640
635
630
625
620
615
610
605
600
m
Clay &
Silt
F
M
C
62
R
700
695
690
685
680
675
670
665
660
655
650
Road Support
Road Support
Road Support
TCL
Small white bridge
750
745
740
735
730
725
720
715
710
705
700
Exposure above road
but not accessible
C
TCL
Road Support

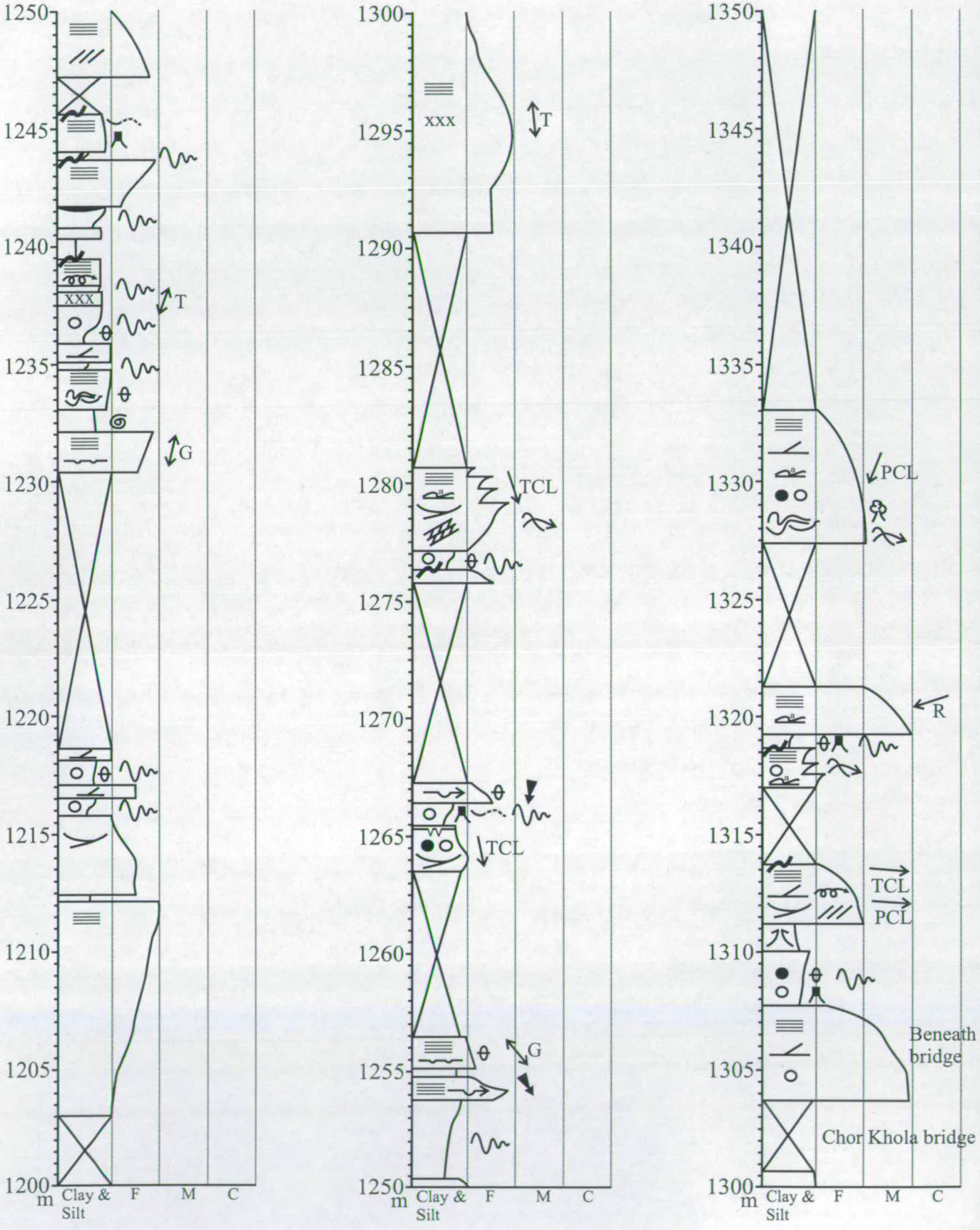

800
795
790
785
780
775
770
765
760
755
750
m
Clay & Silt
F
M
C
Road supports down to Jungli Khola sign
Lots of drill holes
SK900 9.9Ma
SK900N
TCL
80
Lots of drill holes
850
845
840
835
830
825
820
815
810
805
800
900
895
890
885
880
875
870
865
860
855
850

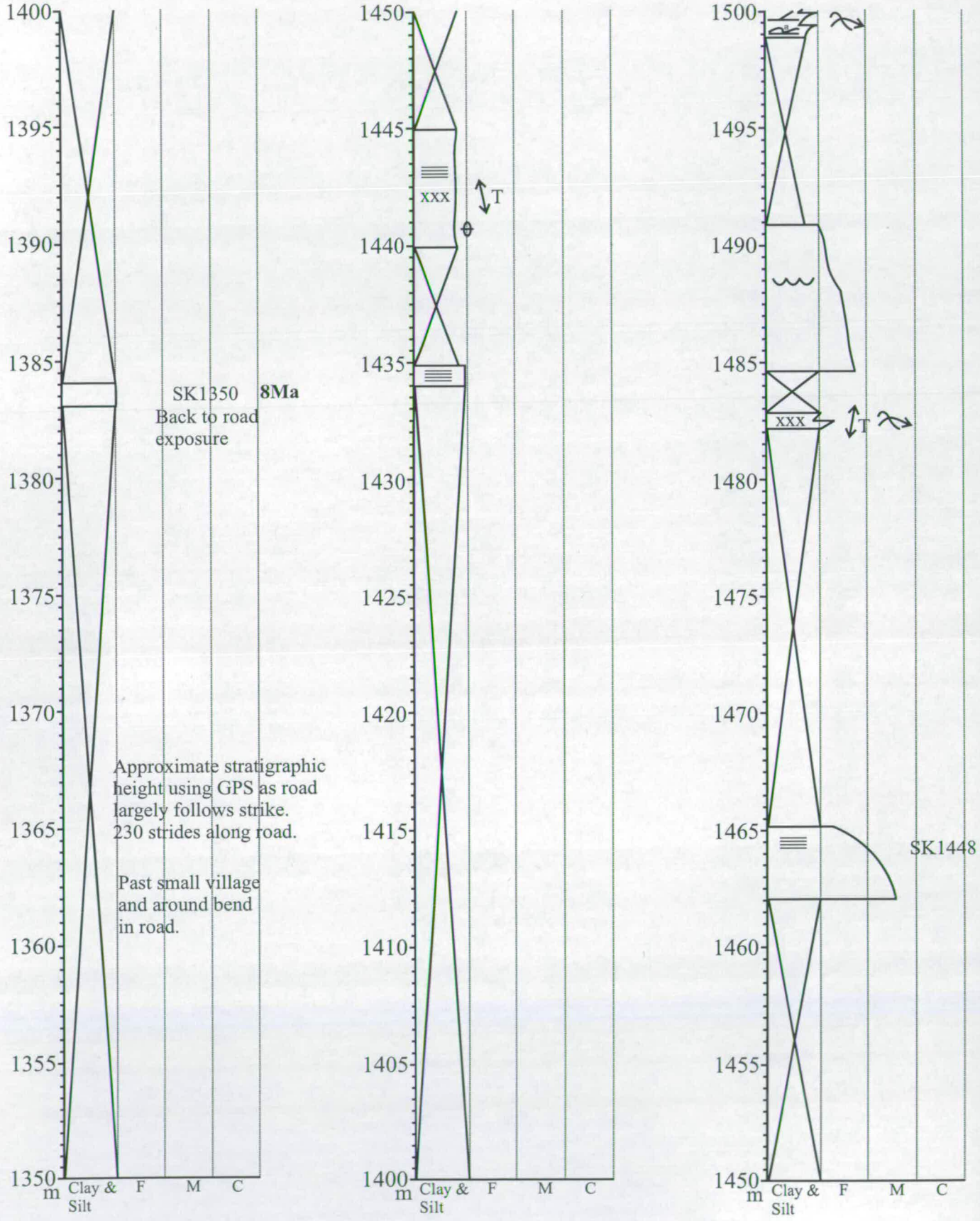

950
945
940
935
930
925
920
915
910
905
900
m
Clay & Silt
F
M
C
White bridge
1000
995
990
985
980
975
970
965
960
955
950
m
Clay & Silt
F
M
C
Second Jungli Khola sign
PL
1050
1045
1040
1035
1030
1025
1020
1015
1010
1005
1000
m
Clay & Silt
F
M
C

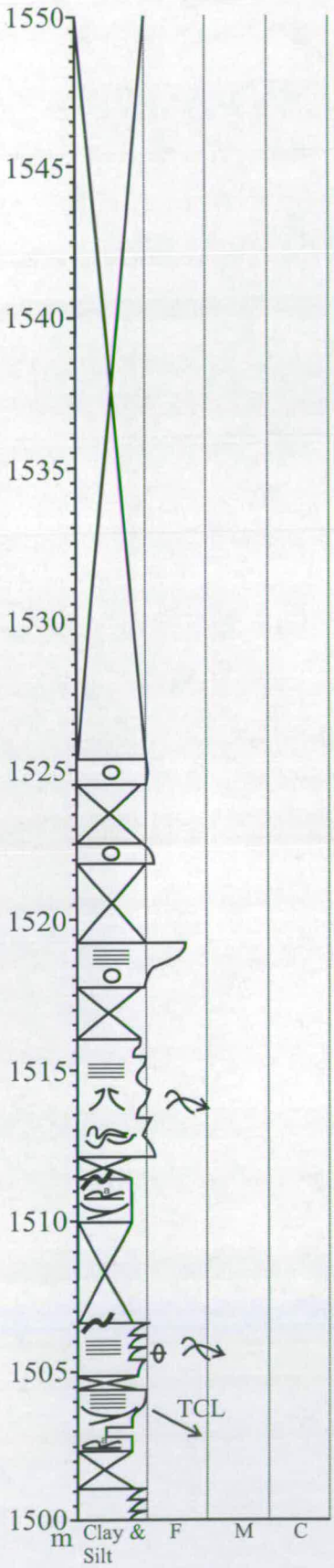

1100
1095
1090
1085
1080
1075
1070
1065
1060
1055
1050
TCL
SKA6
G
59
9Ma
m
Clay &
Silt
F
M
C

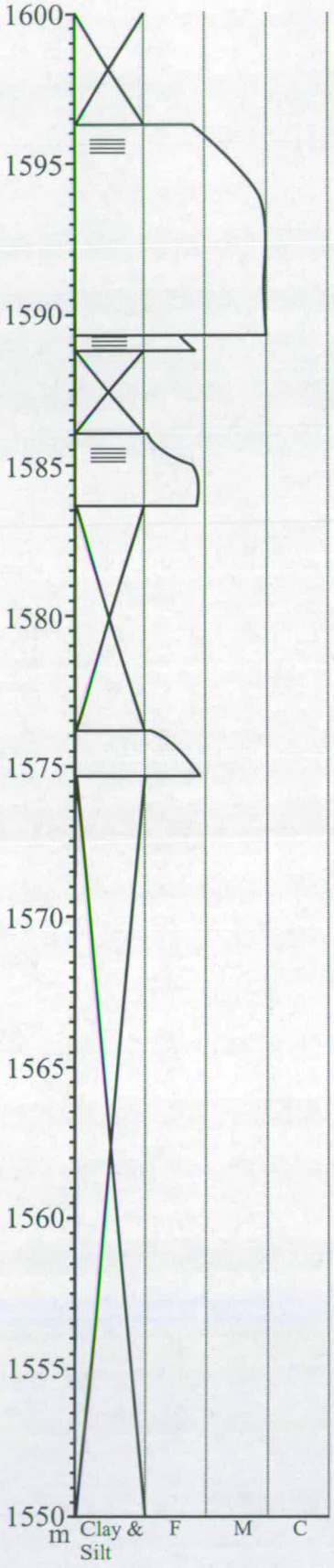

1150
1145
1140
1135
1130
1125
1120
1115
1110
1105
1100
m
Clay &
Silt
F
M
C

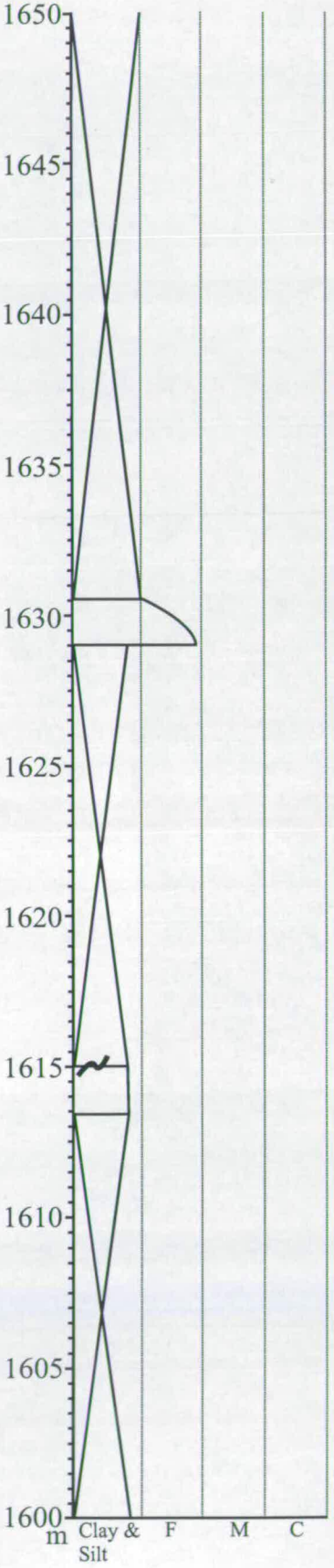

1200
1195
1190
1185
1180
1175
1170
1165
1160
1155
1150
No access
m
Clay &
Silt
F
M
C

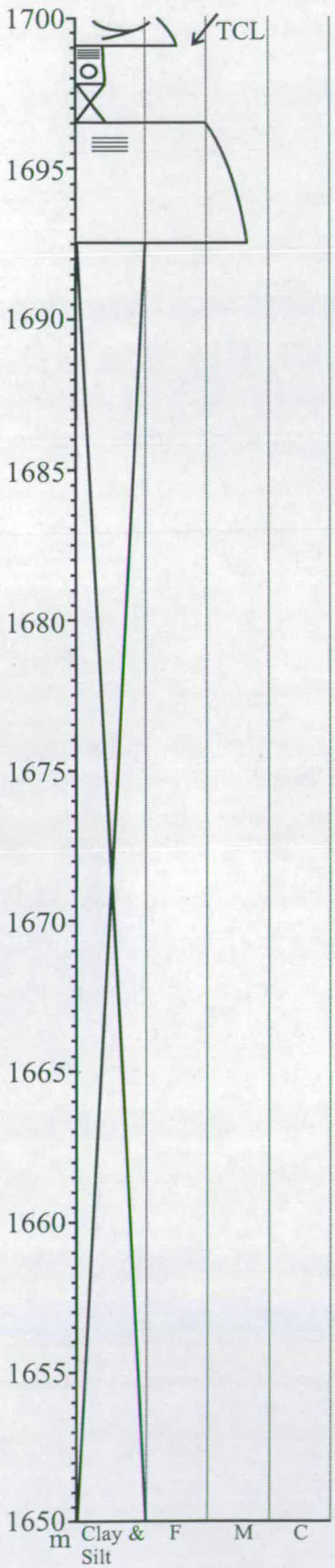

1250
1245
1240
1235
1230
1225
1220
1215
1210
1205
1200
m
Clay &
Silt
F
M
C
xxx
T
G
1300
1295
1290
1285
1280
1275
1270
1265
1260
1255
1250
TCL
1350
1345
1340
1335
1330
1325
1320
1315
1310
1305
1300
PCL
R
Beneath
bridge
Chor Khola bridge

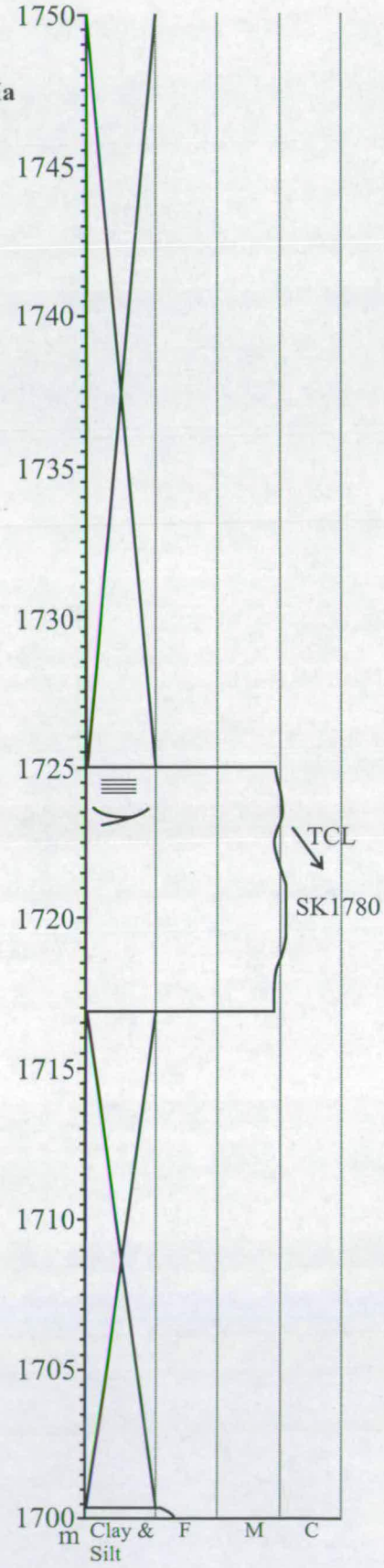

1400
1395
1390
1385
1380
1375
1370
1365
1360
1355
1350
m
Clay & Silt
F
M
C
SK1350 8Ma
Back to road exposure
Approximate stratigraphic height using GPS as road largely follows strike.
230 strides along road.
Past small village and around bend in road.
1450
1445
1440
1435
1430
1425
1420
1415
1410
1405
1400
xxx
T
1500
1495
1490
1485
1480
1475
1470
1465
1460
1455
1450
SK1448

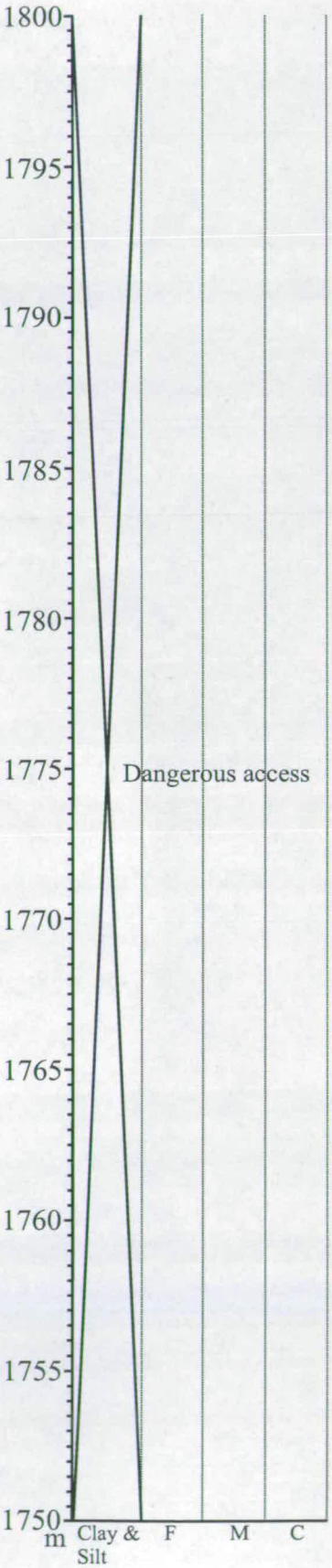

1550
1545
1540
1535
1530
1525
1520
1515
1510
1505
1500
TCL
m
Clay &
Silt
F
M
C

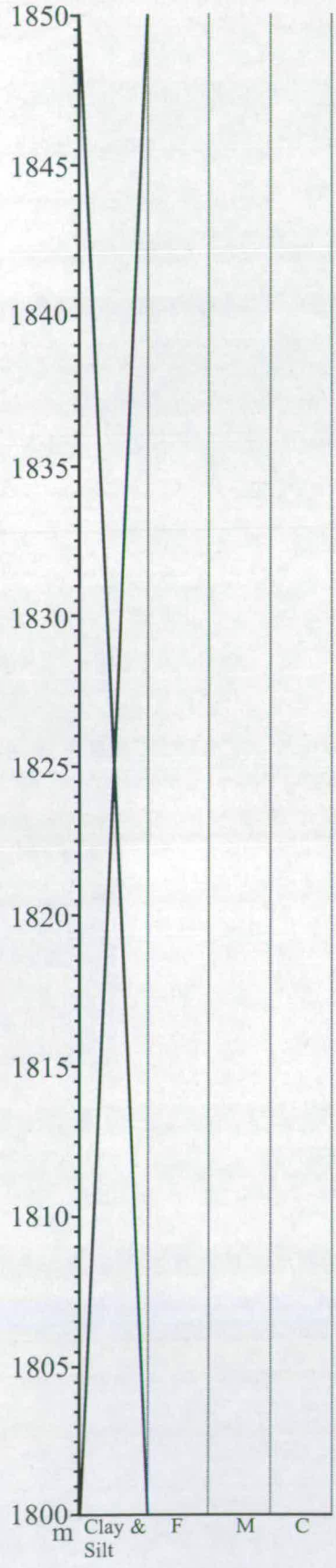

1600
1595
1590
1585
1580
1575
1570
1565
1560
1555
1550
m
Clay &
Silt
F
M
C

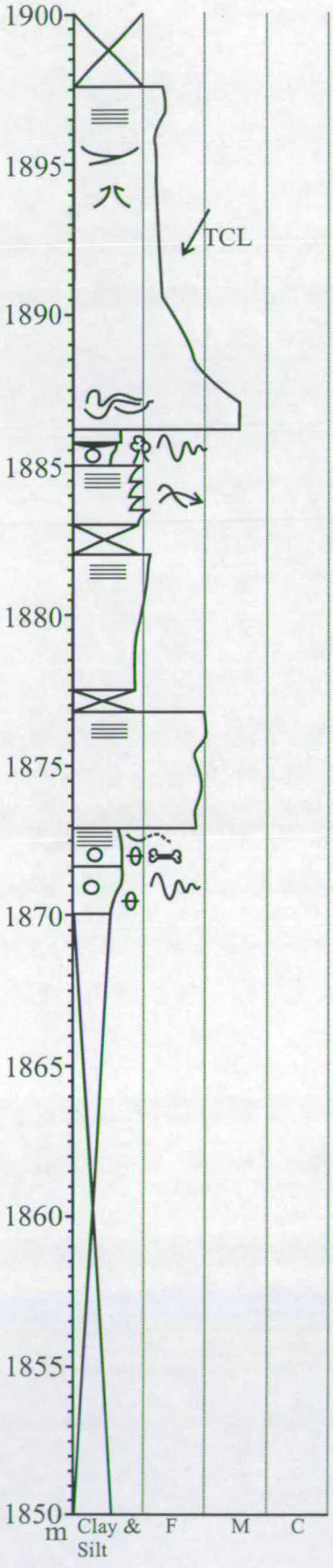

1650
1645
1640
1635
1630
1625
1620
1615
1610
1605
1600
m
Clay &
Silt
F
M
C

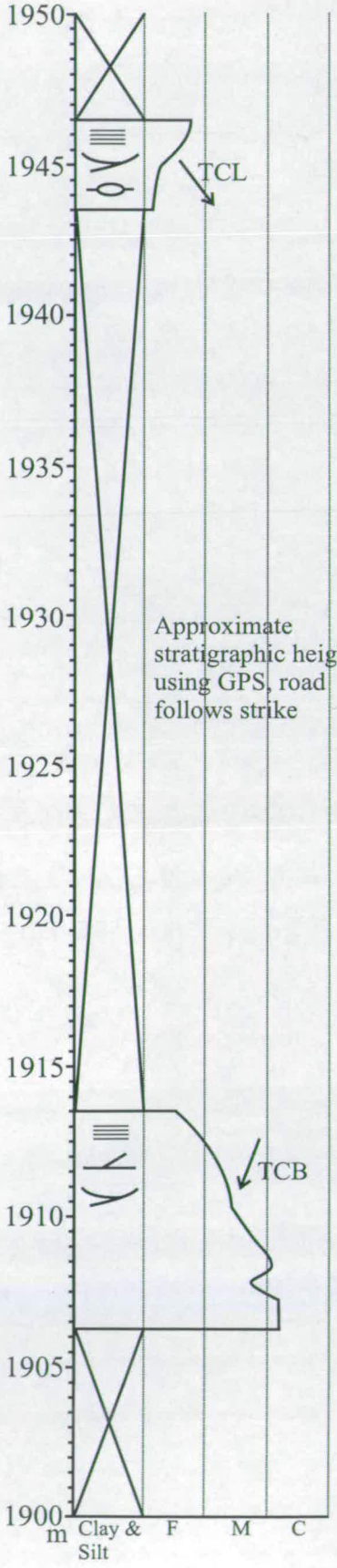

1700
1695
1690
1685
1680
1675
1670
1665
1660
1655
1650
m
TCL
Clay &
Silt
F
M
C

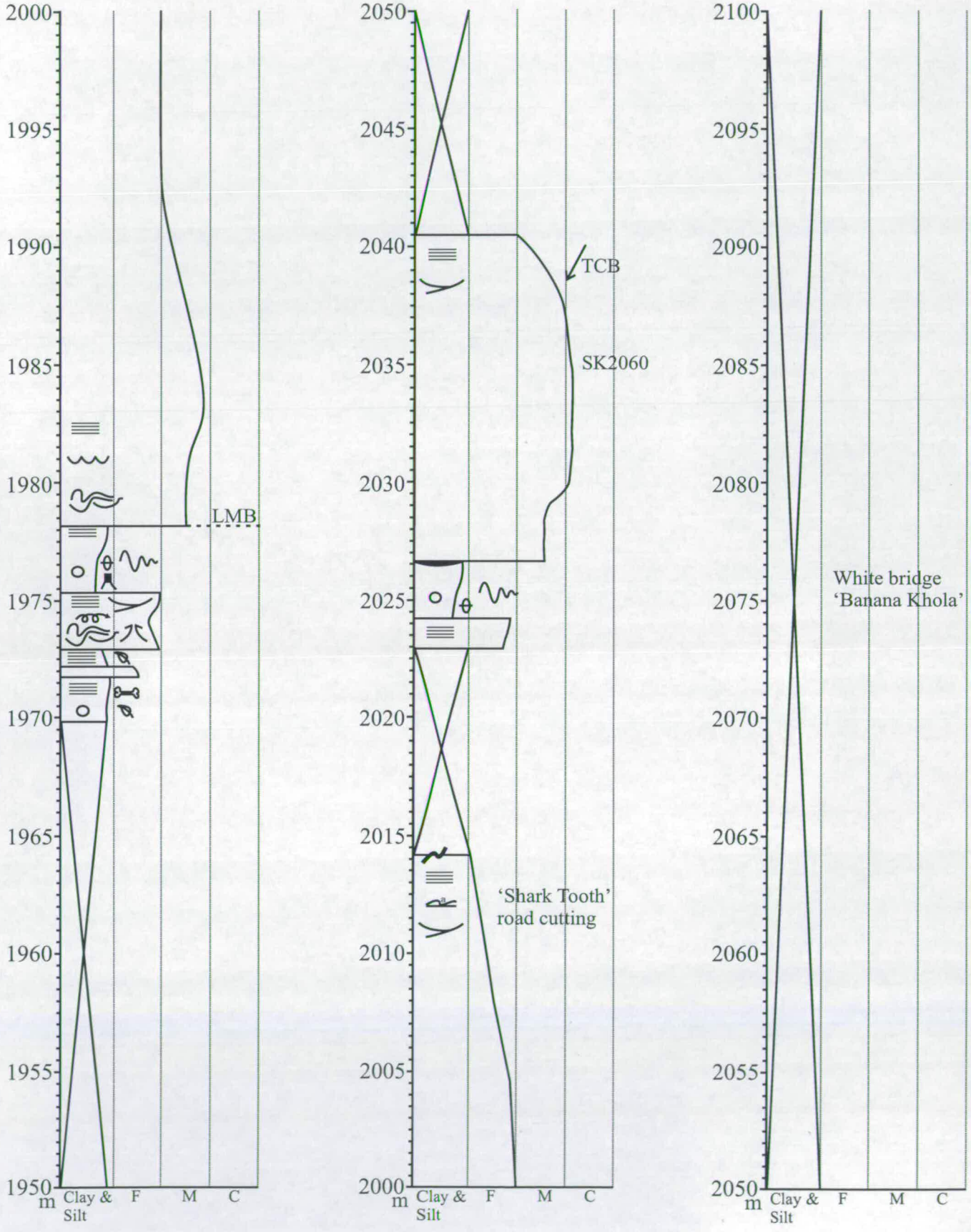

7Ma
1750
1745
1740
1735
1730
1725
1720
1715
1710
1705
1700
m
TCL
SK1780
Clay &
Silt
F
M
C

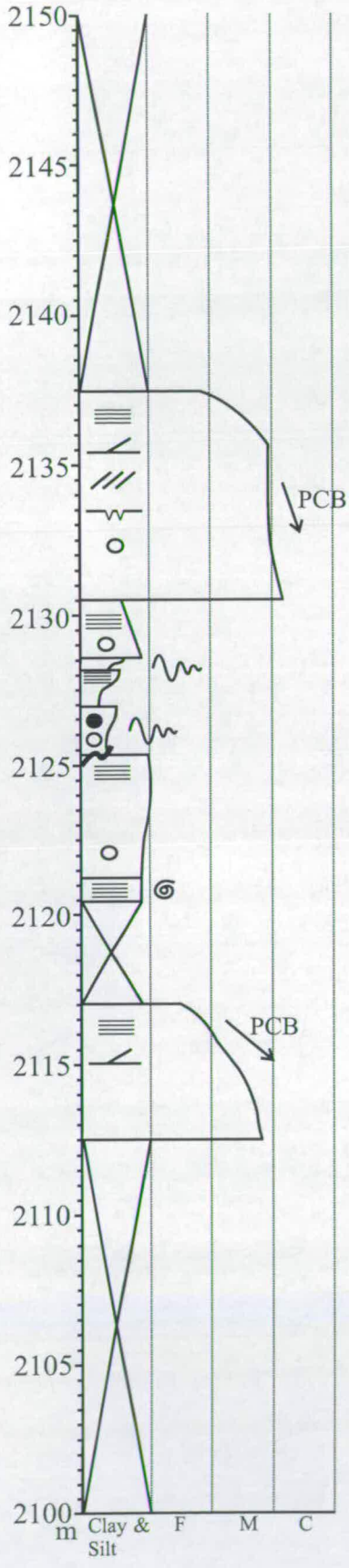

1800
1795
1790
1785
1780
1775
1770
1765
1760
1755
1750
m
Dangerous access
Clay &
Silt
F
M
C

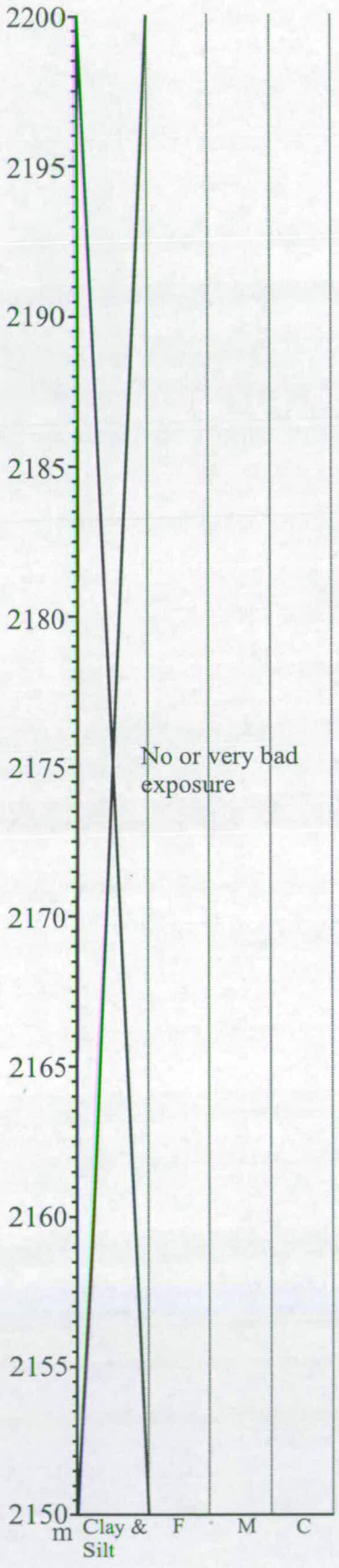

1850
1845
1840
1835
1830
1825
1820
1815
1810
1805
1800
m
Clay &
Silt
F
M
C

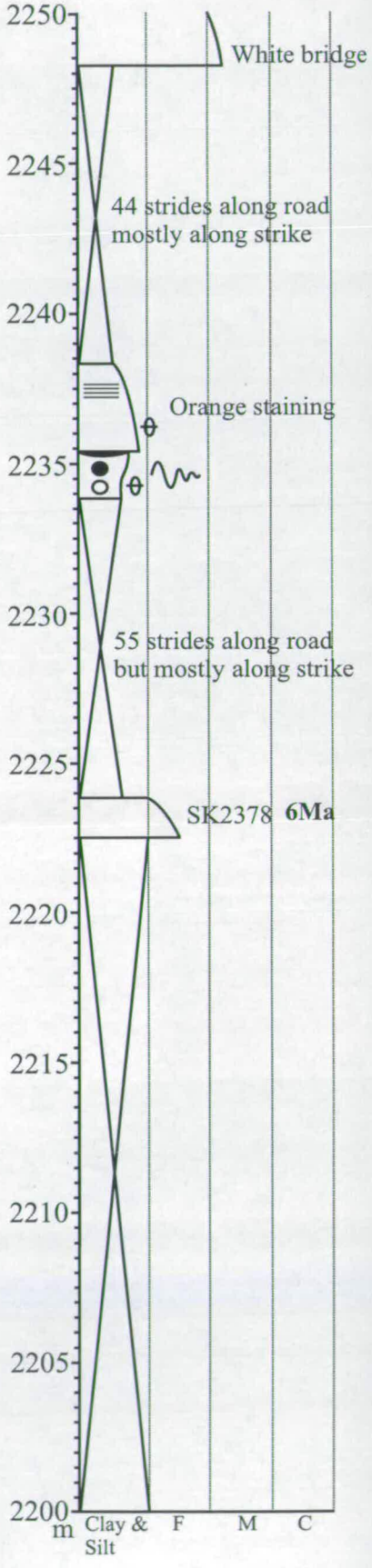

1900
1895
1890
1885
1880
1875
1870
1865
1860
1855
1850
TCL
m
Clay &
Silt
F
M
C

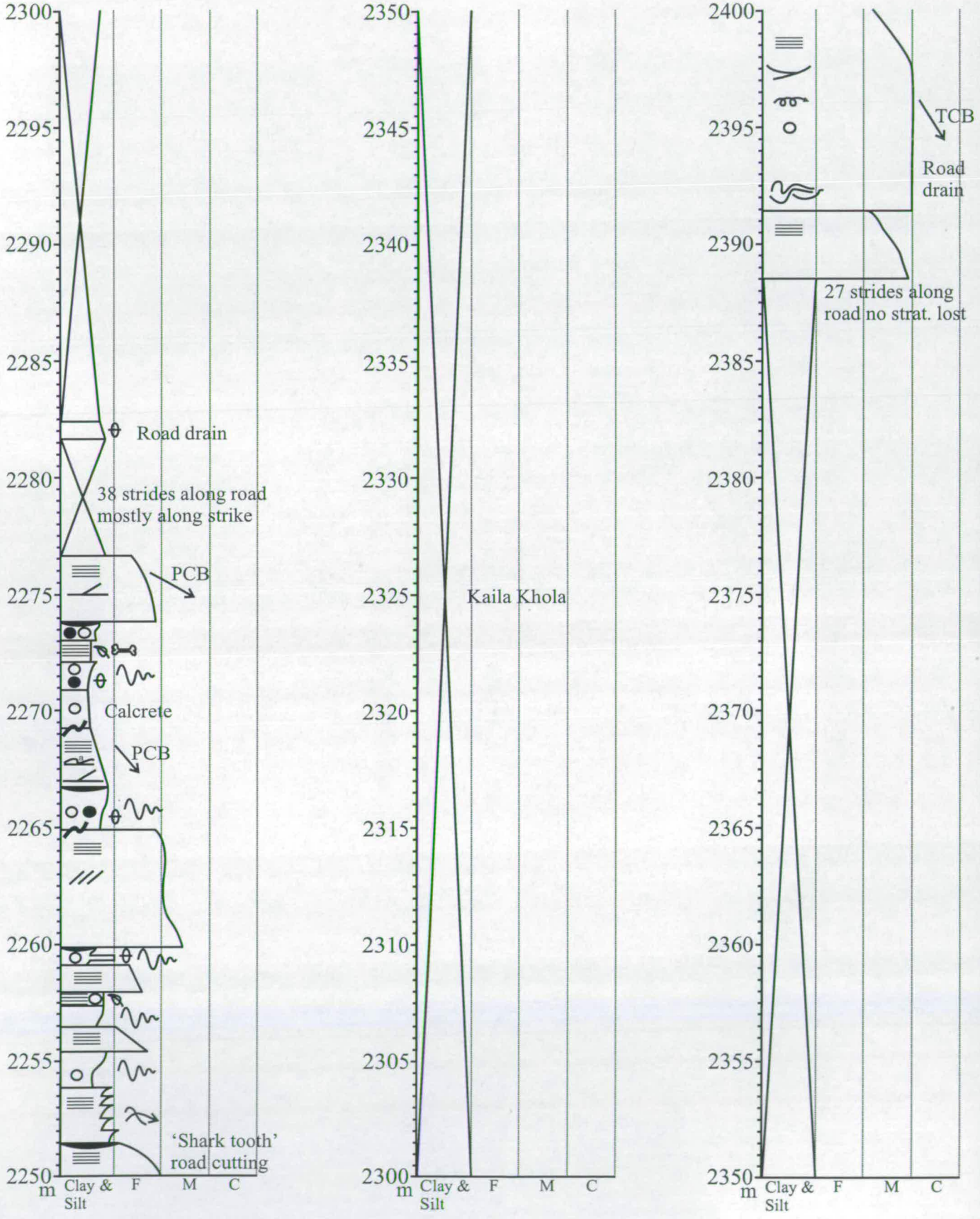

1950
1945
1940
1935
1930
1925
1920
1915
1910
1905
1900
TCL
TCB
Approximate
stratigraphic height
using GPS, road
follows strike
m
Clay &
Silt
F
M
C

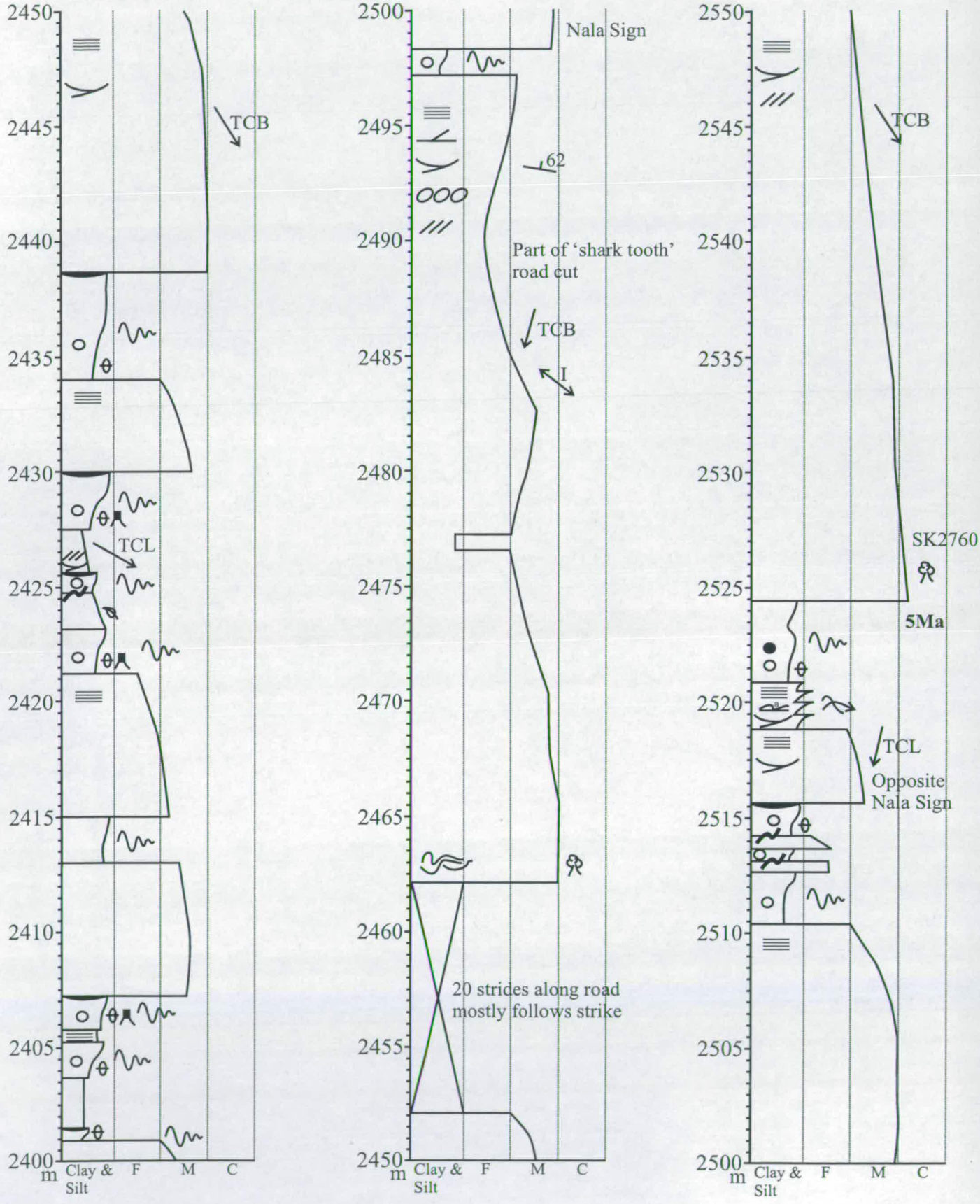

2000
1995
1990
1985
1980
1975
1970
1965
1960
1955
1950
LMB
m
Clay &
Silt
F
M
C
2050
2045
2040
2035
2030
2025
2020
2015
2010
2005
2000
TCB
SK2060
'Shark Tooth'
road cutting
2100
2095
2090
2085
2080
2075
2070
2065
2060
2055
2050
White bridge
'Banana Khola'

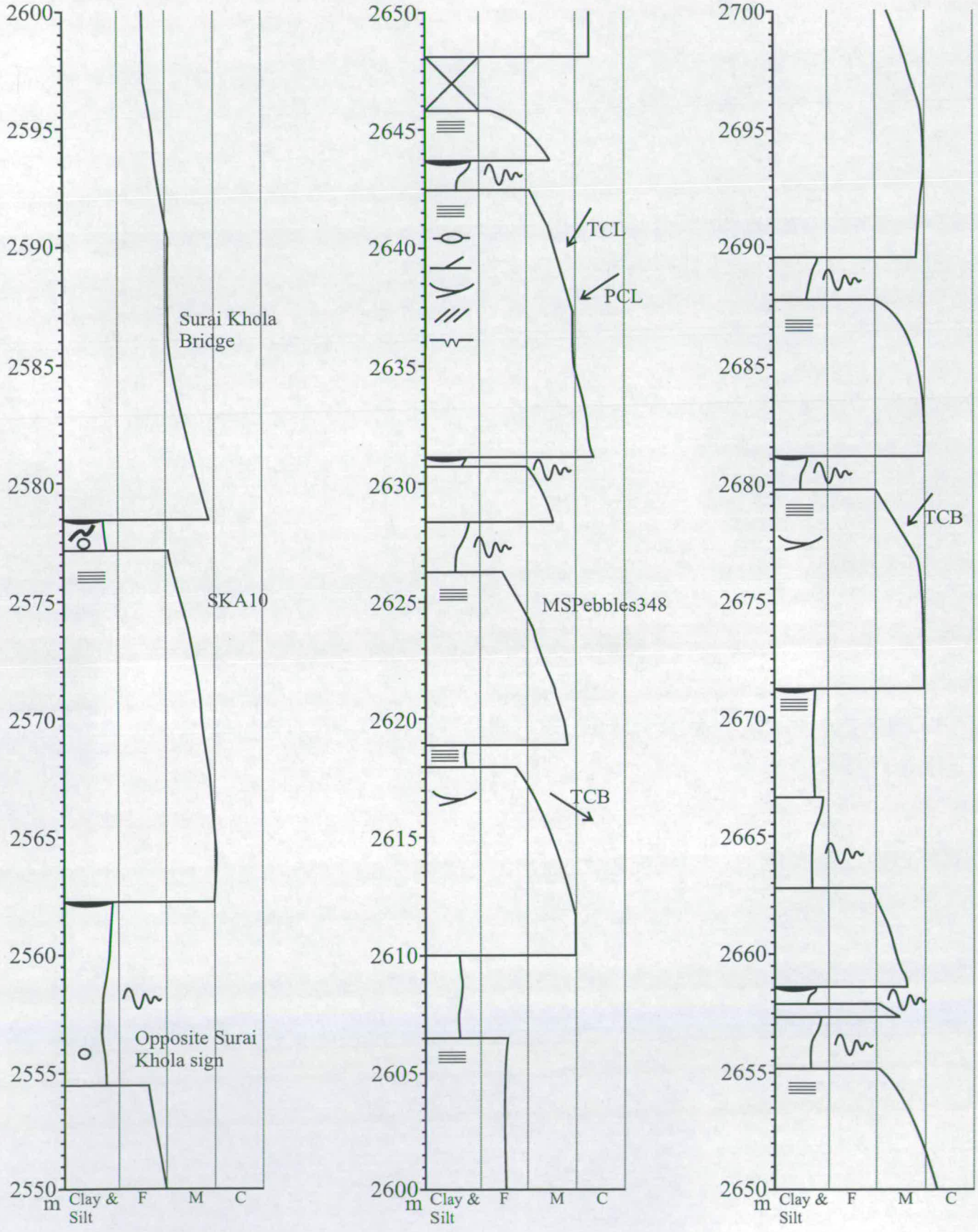

2150
2145
2140
2135
2130
2125
2120
2115
2110
2105
2100
PCB
PCB
m
Clay &
Silt
F
M
C

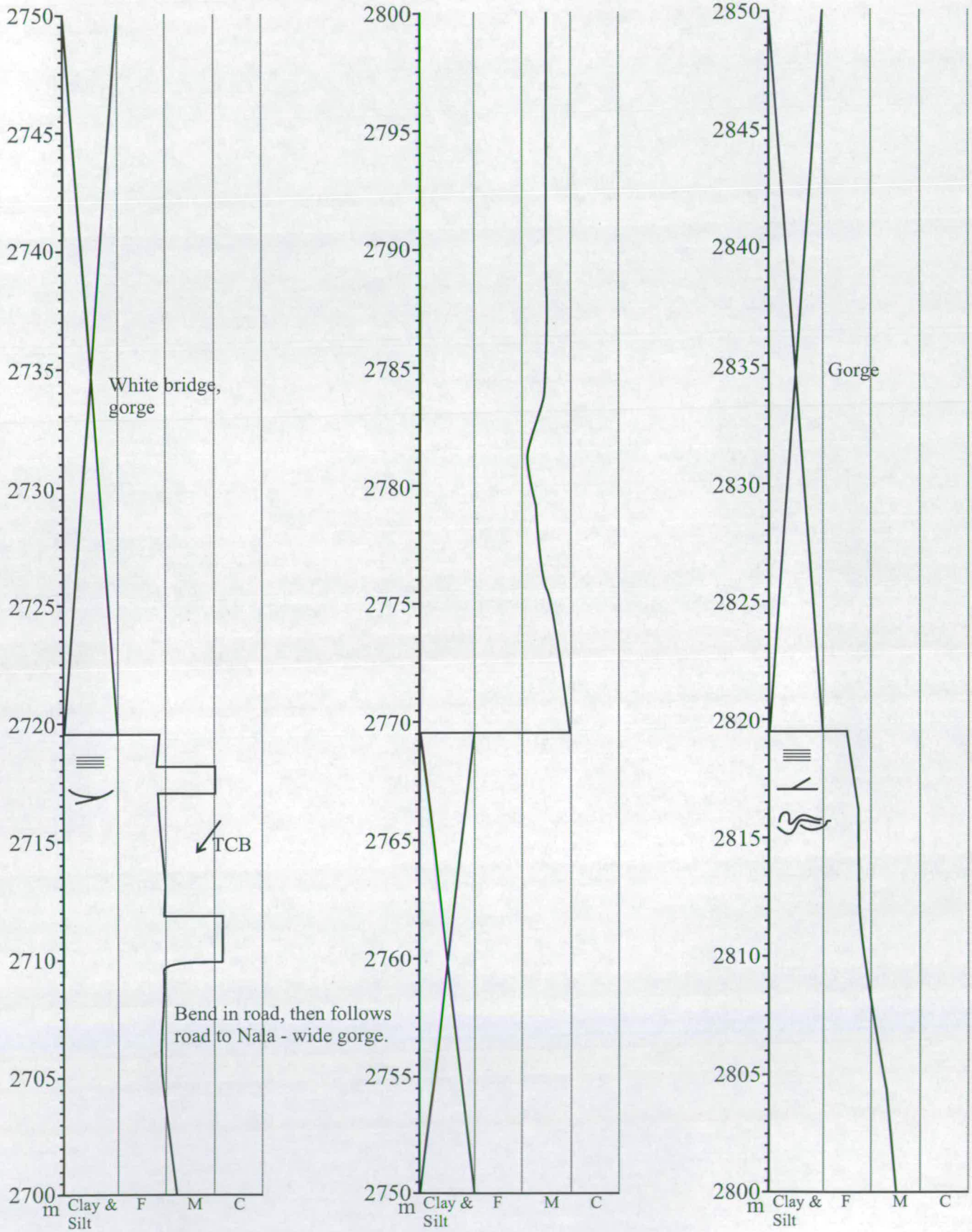

2200
2195
2190
2185
2180
2175
2170
2165
2160
2155
2150
No or very bad
exposure
m
Clay &
Silt
F
M
C

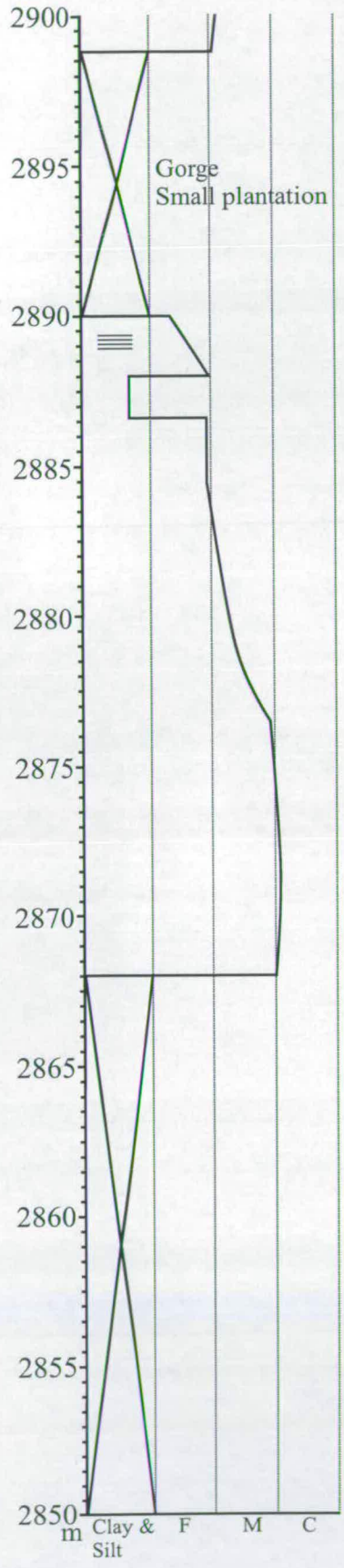

2250
2245
2240
2235
2230
2225
2220
2215
2210
2205
2200
White bridge
44 strides along road
mostly along strike
Orange staining
55 strides along road
but mostly along strike
SK2378 6Ma
m
Clay &
Silt
F
M
C

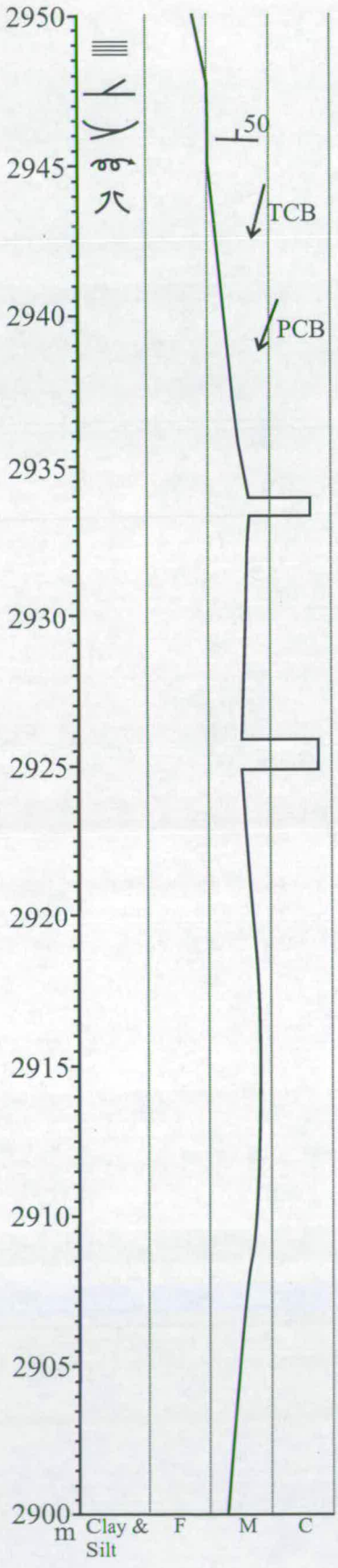

2300
2295
2290
2285
2280
2275
2270
2265
2260
2255
2250
m
Clay & Silt
F
M
C
Road drain
38 strides along road mostly along strike
PCB
Calcrete
PCB
'Shark tooth' road cutting
2350
2345
2340
2335
2330
2325
2320
2315
2310
2305
2300
Kaila Khola
2400
2395
2390
2385
2380
2375
2370
2365
2360
2355
2350
TCB
Road drain
27 strides along road no strat. lost

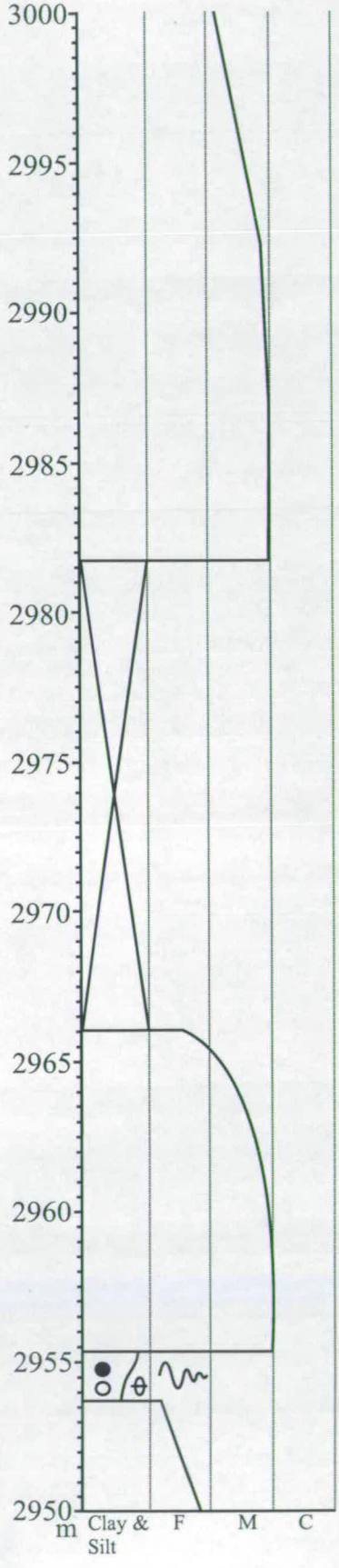

2450
2445
2440
2435
2430
2425
2420
2415
2410
2405
2400
m
Clay &
Silt
F
M
C
TCB
TCL
2500
2495
2490
2485
2480
2475
2470
2465
2460
2455
2450
Nala Sign
62
Part of 'shark tooth'
road cut
TCB
I
20 strides along road
mostly follows strike
2550
2545
2540
2535
2530
2525
2520
2515
2510
2505
2500
TCB
SK2760
5Ma
TCL
Opposite
Nala Sign

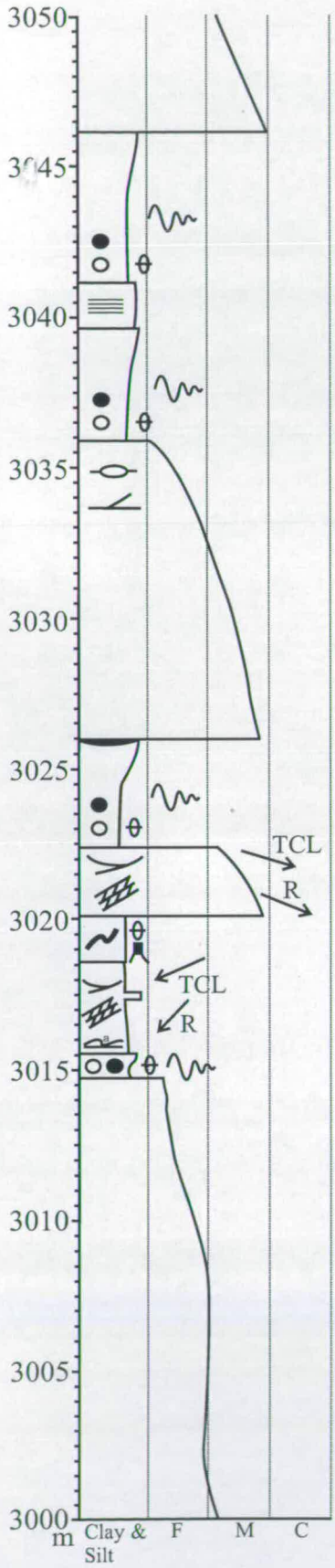

2600
2595
2590
2585
2580
2575
2570
2565
2560
2555
2550
m
Clay &
Silt
F
M
C
Surai Khola
Bridge
SKA10
Opposite Surai
Khola sign
2650
2645
2640
2635
2630
2625
2620
2615
2610
2605
2600
TCL
PCL
MSPebbles348
TCB
2700
2695
2690
2685
2680
2675
2670
2665
2660
2655
2650
TCB

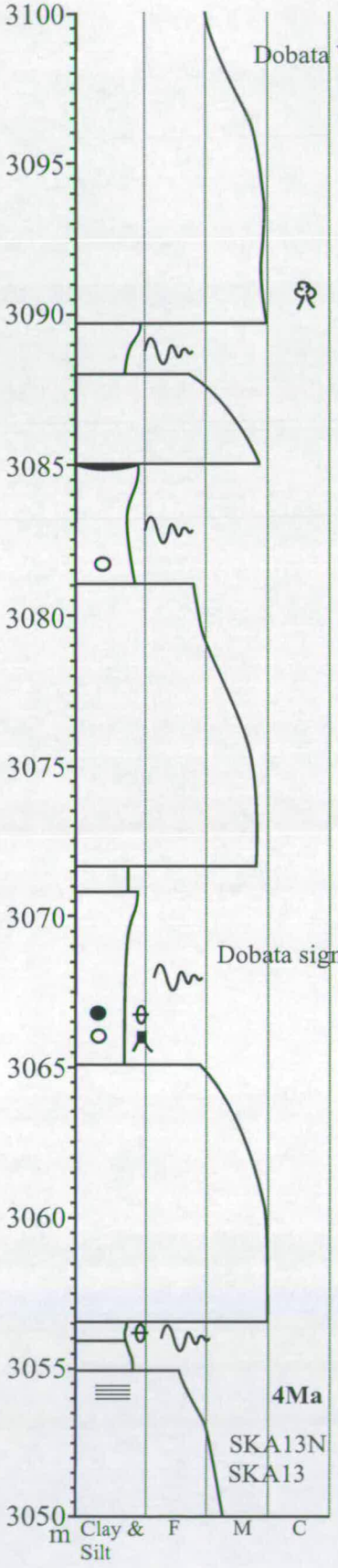

2750
2745
2740
2735
2730
2725
2720
2715
2710
2705
2700
m
Clay & Silt
F
M
C
White bridge, gorge
TCB
Bend in road, then follows road to Nala - wide gorge.
2800
2795
2790
2785
2780
2775
2770
2765
2760
2755
2750
m
Clay & Silt
F
M
C
2850
2845
2840
2835
2830
2825
2820
2815
2810
2805
2800
m
Clay & Silt
F
M
C
Gorge

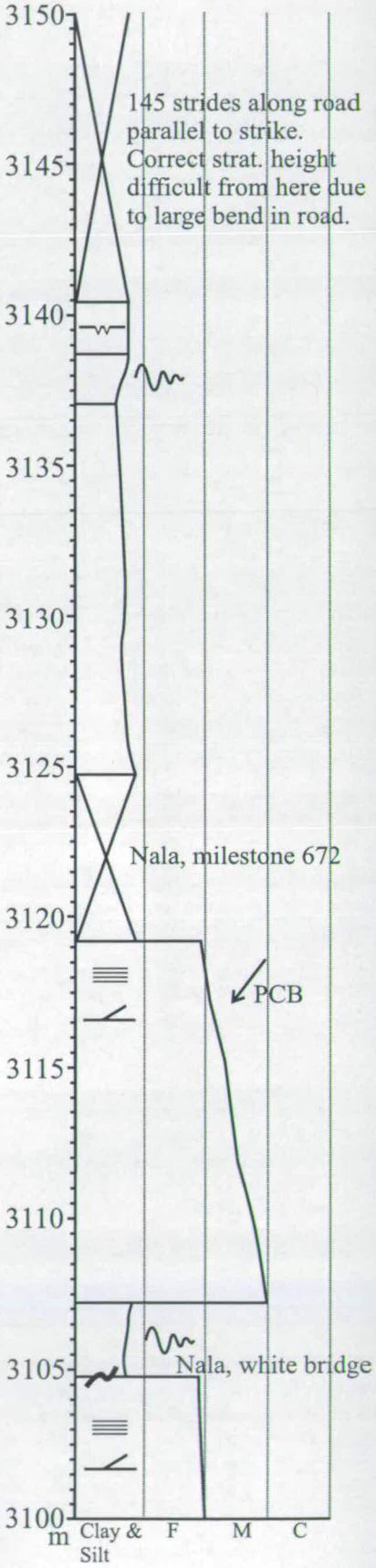

2900
2895
2890
2885
2880
2875
2870
2865
2860
2855
2850
Gorge
Small plantation
m
Clay &
Silt
F
M
C

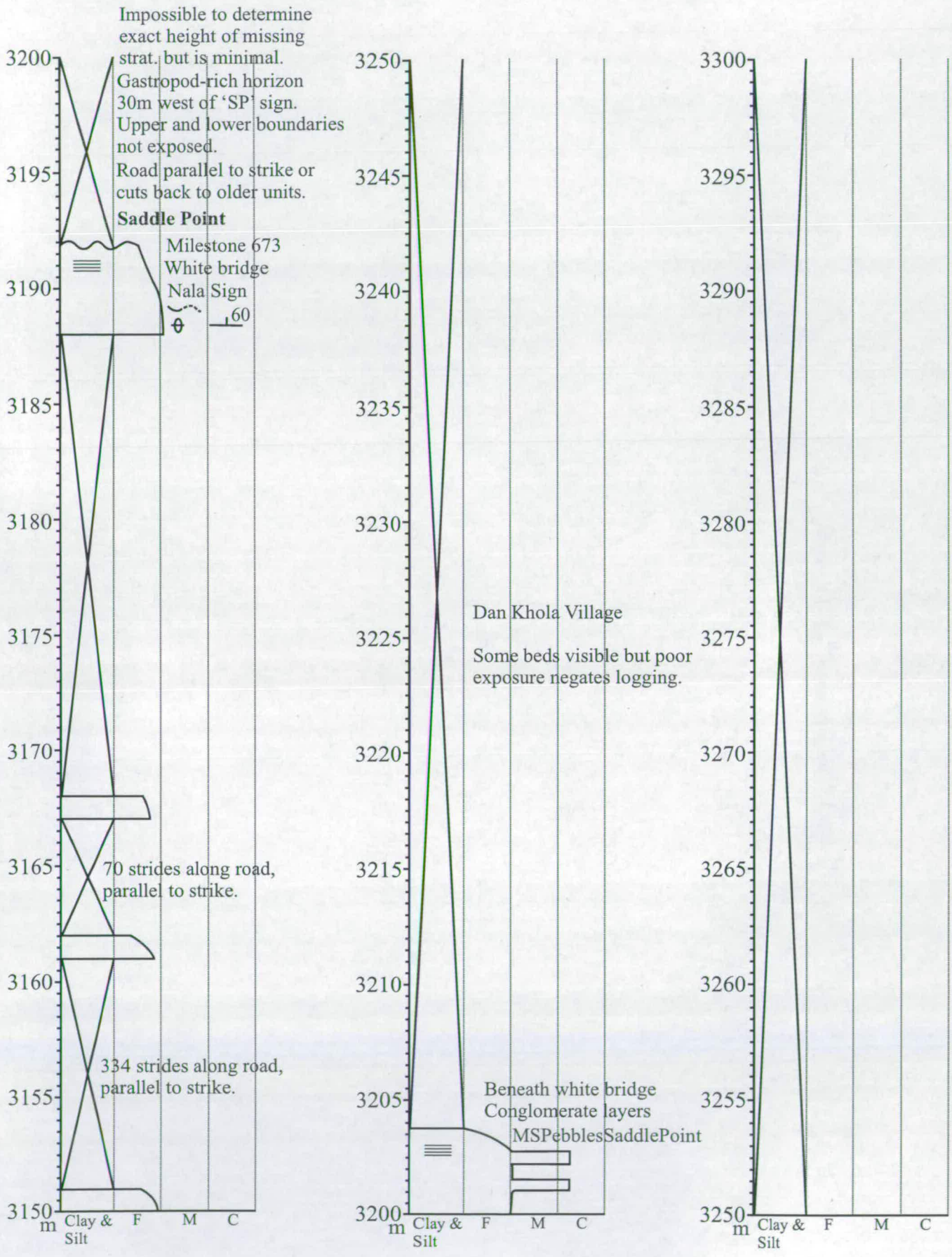

2950
2945
2940
2935
2930
2925
2920
2915
2910
2905
2900
50
TCB
PCB
m
Clay &
Silt
F
M
C

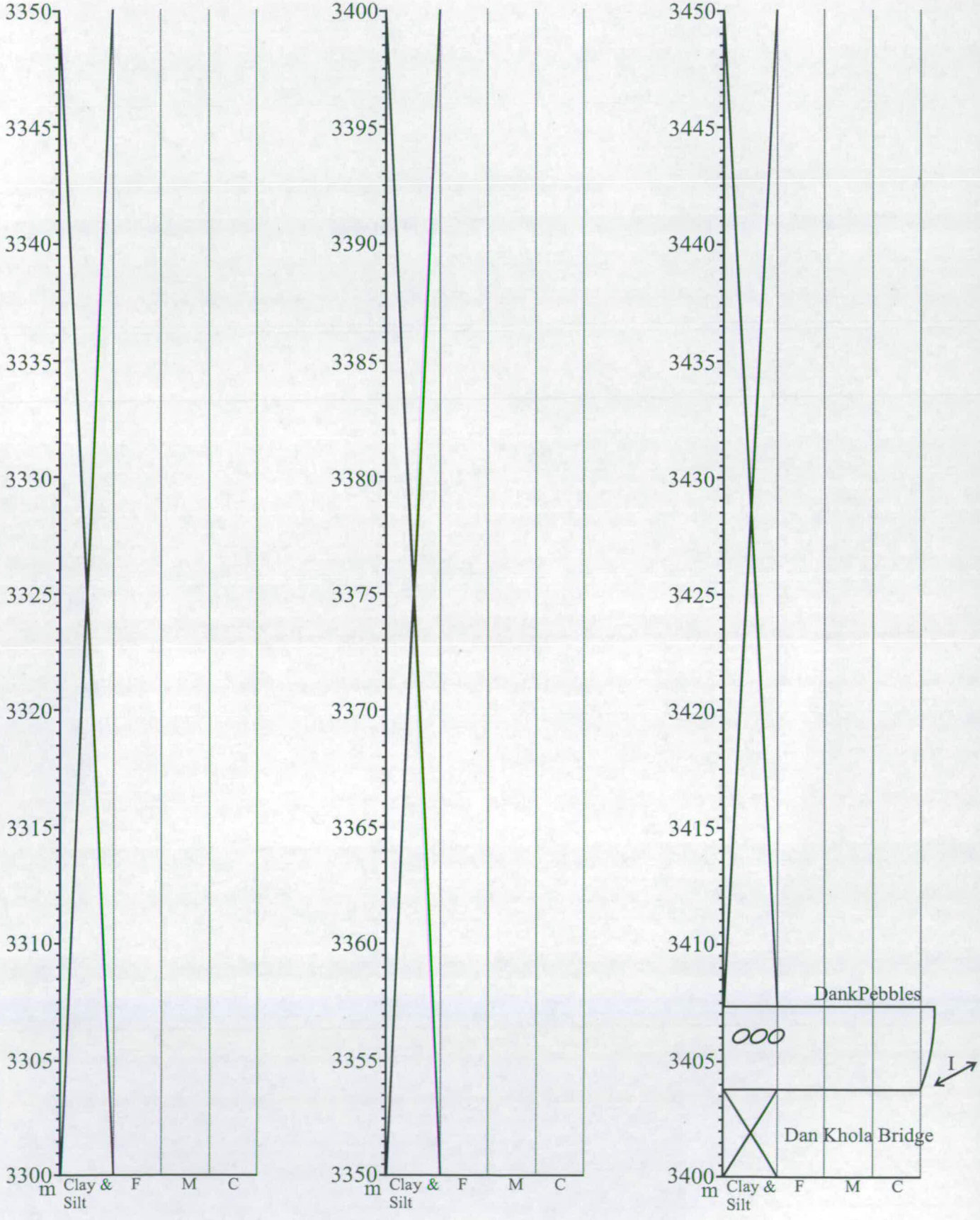

3000
2995
2990
2985
2980
2975
2970
2965
2960
2955
2950
m
Clay &
Silt
F
M
C

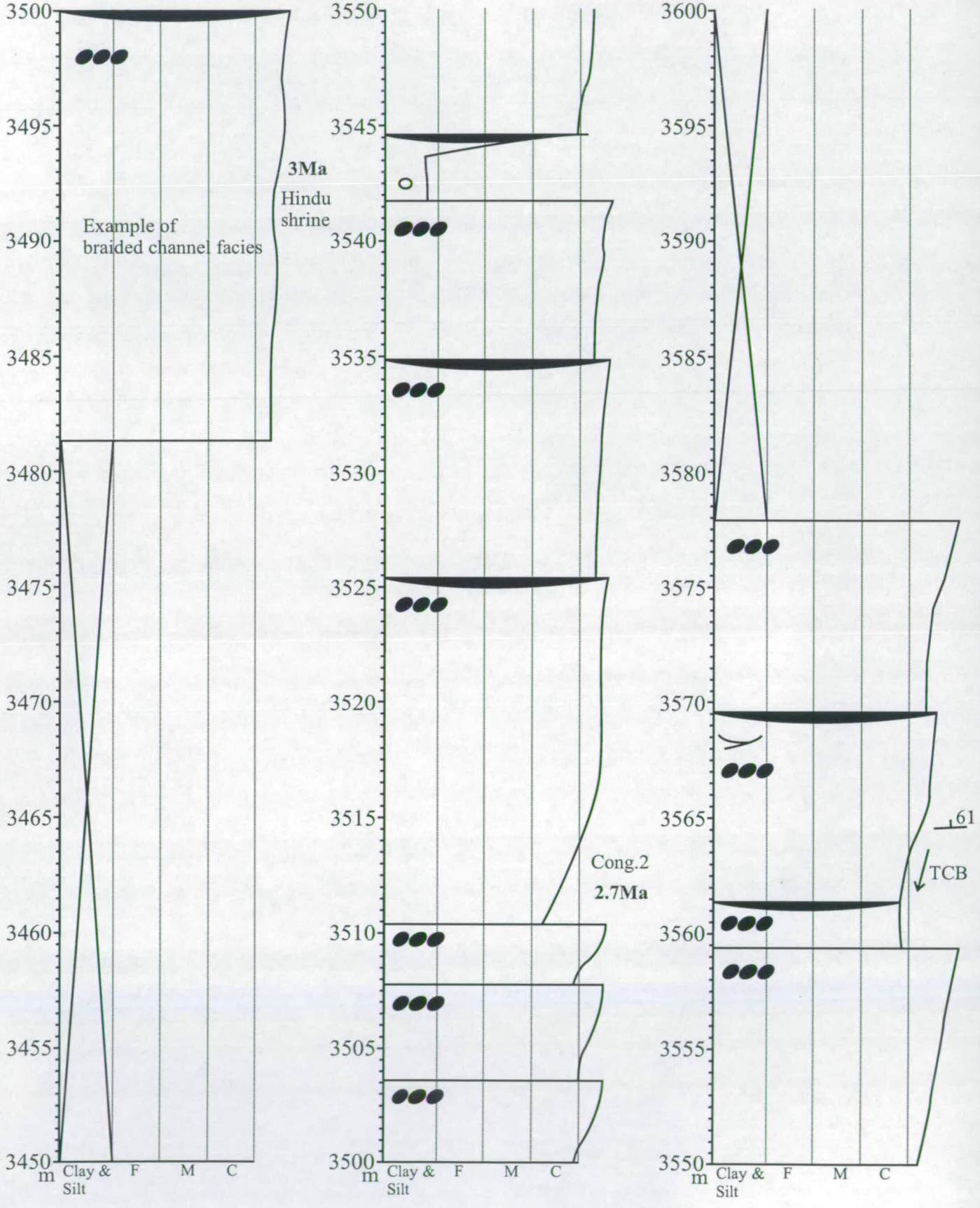

3050
3045
3040
3035
3030
3025
3020
3015
3010
3005
3000
TCL
R
TCL
R
m
Clay &
Silt
F
M
C

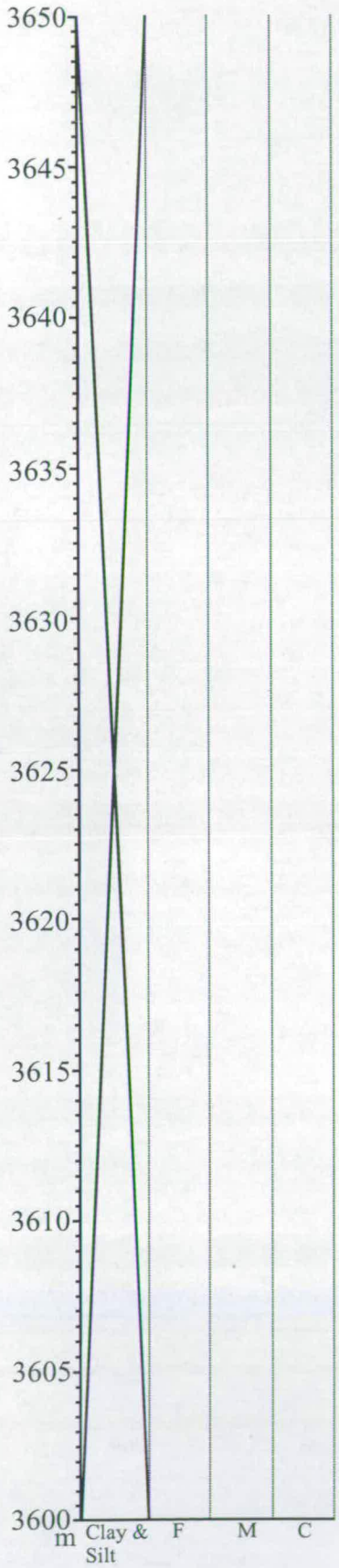

3100
3095
3090
3085
3080
3075
3070
3065
3060
3055
3050
Dobata Village
Dobata sign
4Ma
SKA13N
SKA13
m
Clay &
Silt
F
M
C

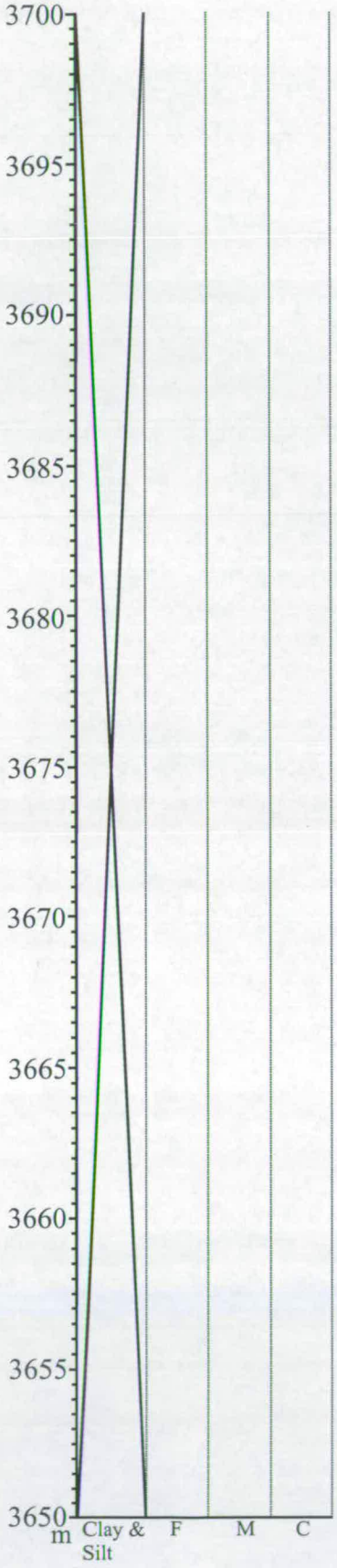

3150
3145
3140
3135
3130
3125
3120
3115
3110
3105
3100
145 strides along road
parallel to strike.
Correct strat. height
difficult from here due
to large bend in road.
Nala, milestone 672
PCB
Nala, white bridge
m
Clay &
Silt
F
M
C

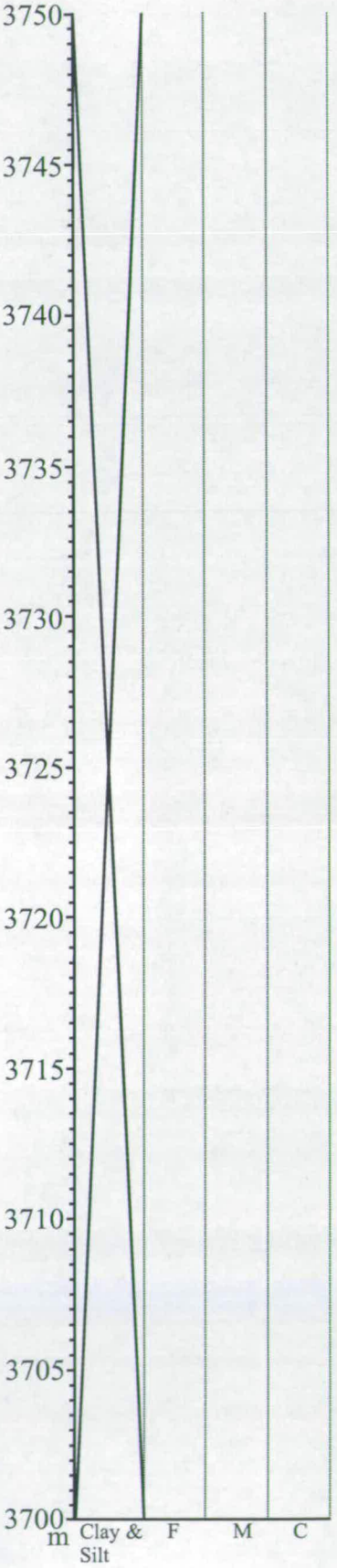

Impossible to determine exact height of missing strat. but is minimal.
Gastropod-rich horizon 30m west of 'SP' sign.
Upper and lower boundaries not exposed.
Road parallel to strike or cuts back to older units.
Saddle Point
Milestone 673
White bridge
Nala Sign
60
70 strides along road, parallel to strike.
334 strides along road, parallel to strike.
Dan Khola Village
Some beds visible but poor exposure negates logging.
Beneath white bridge
Conglomerate layers
MSPebblesSaddlePoint
3200
3195
3190
3185
3180
3175
3170
3165
3160
3155
3150
3250
3245
3240
3235
3230
3225
3220
3215
3210
3205
3200
3300
3295
3290
3285
3280
3275
3270
3265
3260
3255
3250
m
Clay & Silt
F
M
C

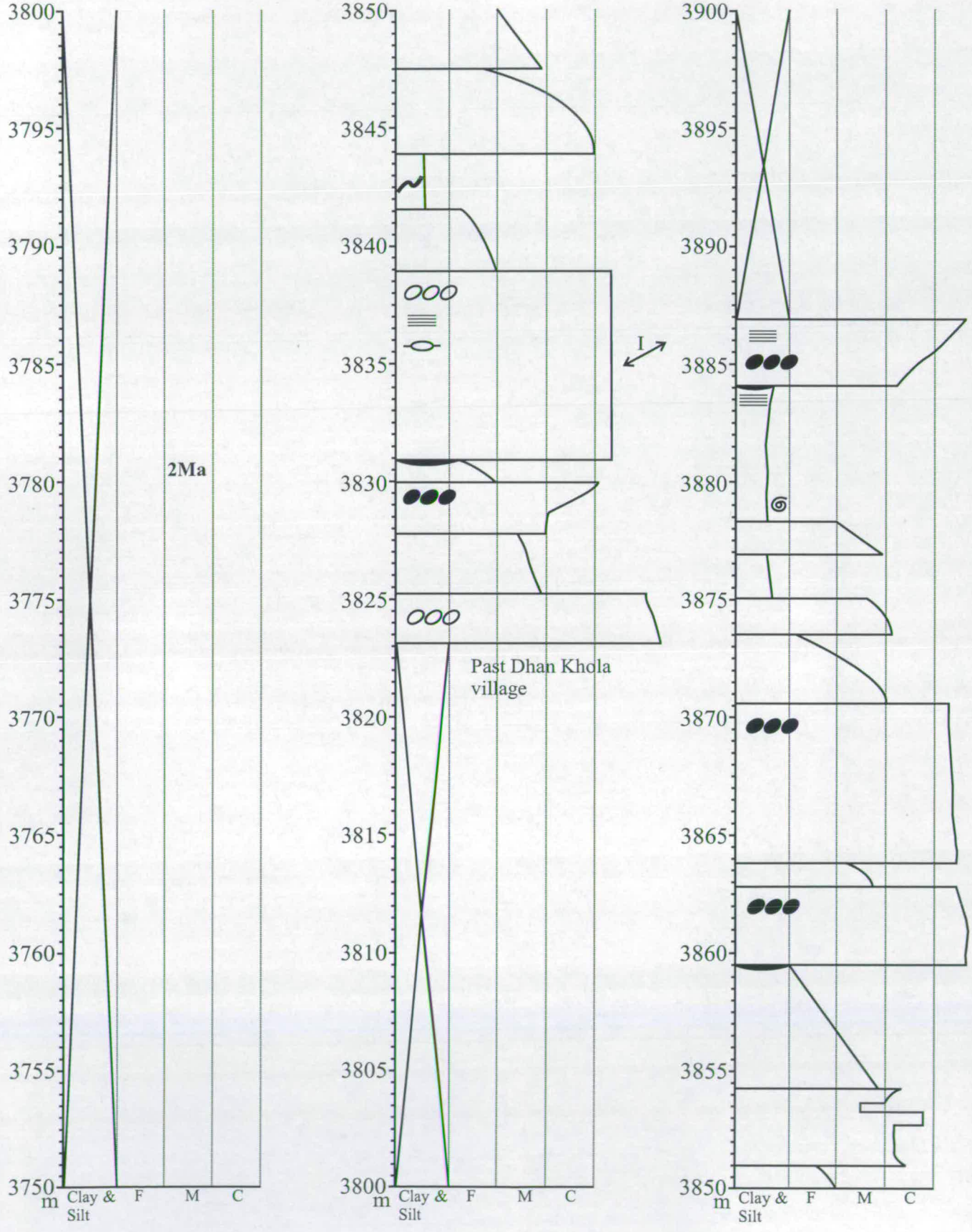

3350
3345
3340
3335
3330
3325
3320
3315
3310
3305
3300
m
Clay &
Silt
F
M
C
3400
3395
3390
3385
3380
3375
3370
3365
3360
3355
3350
m
Clay &
Silt
F
M
C
3450
3445
3440
3435
3430
3425
3420
3415
3410
3405
3400
m
Clay &
Silt
F
M
C
DankPebbles
I
Dan Khola Bridge

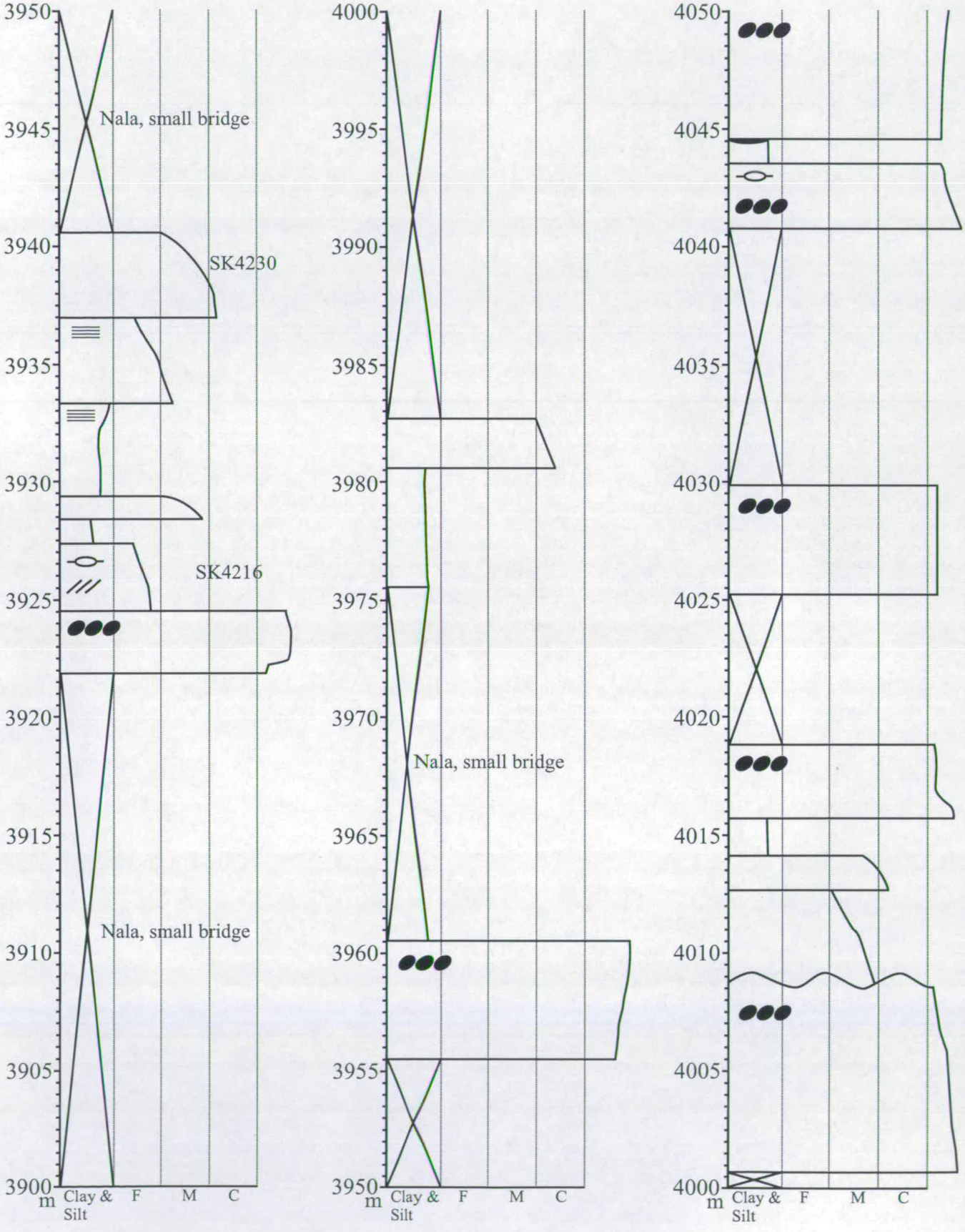

3500
3495
3490
3485
3480
3475
3470
3465
3460
3455
3450
m
Clay & Silt
F
M
C
Example of braided channel facies
3Ma
Hindu shrine
3550
3545
3540
3535
3530
3525
3520
3515
3510
3505
3500
Cong.2
2.7Ma
3600
3595
3590
3585
3580
3575
3570
3565
3560
3555
3550
61
TCB

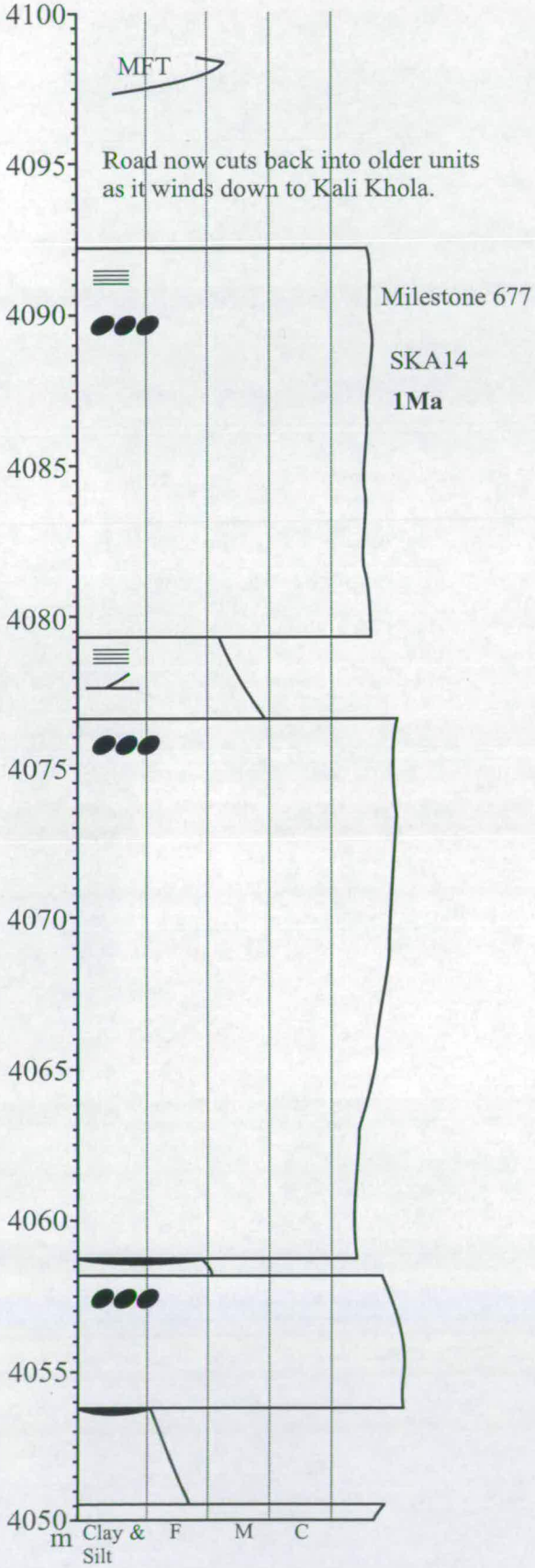

3650
3645
3640
3635
3630
3625
3620
3615
3610
3605
3600
m
Clay & Silt
F
M
C


3700
3695
3690
3685
3680
3675
3670
3665
3660
3655
3650
m
Clay & Silt
F
M
C


3750
3745
3740
3735
3730
3725
3720
3715
3710
3705
3700
m
Clay & Silt
F
M
C


3800
3795
3790
3785
3780
3775
3770
3765
3760
3755
3750
m
Clay &
Silt
F
M
C
2Ma
3850
3845
3840
3835
3830
3825
3820
3815
3810
3805
3800
I
Past Dhan Khola
village
3900
3895
3890
3885
3880
3875
3870
3865
3860
3855
3850


3950
3945
3940
3935
3930
3925
3920
3915
3910
3905
3900
m
Clay & Silt
F
M
C
Nala, small bridge
SK4230
SK4216
Nala, small bridge
4000
3995
3990
3985
3980
3975
3970
3965
3960
3955
3950
m
Clay & Silt
F
M
C
Nala, small bridge
4050
4045
4040
4035
4030
4025
4020
4015
4010
4005
4000
m
Clay & Silt
F
M
C

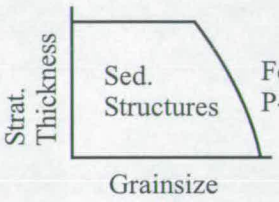

4100
4095
4090
4085
4080
4075
4070
4065
4060
4055
4050
m
MFT
Road now cuts back into older units
as it winds down to Kali Khola.
Milestone 677
SKA14
1Ma
Clay &
Silt
F
M
C

Karnali Section Sedimentary Log

Sedimentary Structures

- Bed boundary
- Lamination
- Planar Cross-Stratification
- Trough Cross-Stratification
- Load Structure
- Asymmetric Ripples
- Lateral Accretion
- Erosional Contact
- 40 — Strike and Dip of Bed (Dip value)
- Parting Lineation
- Clasts/Imbrication (If P-current is shown)
- Flutes
- C — Calcareous
- Channel(s)
- Convolute Bedding
- Dessication Cracks
- No Exposure
- Flaser Bedding
- Bioturbation (Assumed for P-Soils)
- Water Escape Structures
- Oxidised nodule
- Calcareous nodule
- Slump Structures
- Crevasse Splay
- Grooves
- xxx — Tool Marks
- Climbing Ripples
- Palaeosol

Log Format



Symbols refer to bed as a whole unless drawn in a specific location. Sandstones, Siltstones and Mudstones are distinguished by grainsize only.

Palaeocurrent Information

- ↔ Palaeoflow, direction unknown (assumed towards foreland)
- → Palaeoflow, direction known
- PCL — Planar Cross-Lamination
- TCL — Trough Cross-Lamination
- C — Channel
- T — Tools
- G — Grooves
- I — Imbrication
- R — Ripples
- Flutes
- PL — Parting Lineation
- CR — Climbing Ripples

Fossils

- Burrows
- Roots
- Bones
- Leaves
- Wood
- Shell
- Molluscs
- Trace Fossils

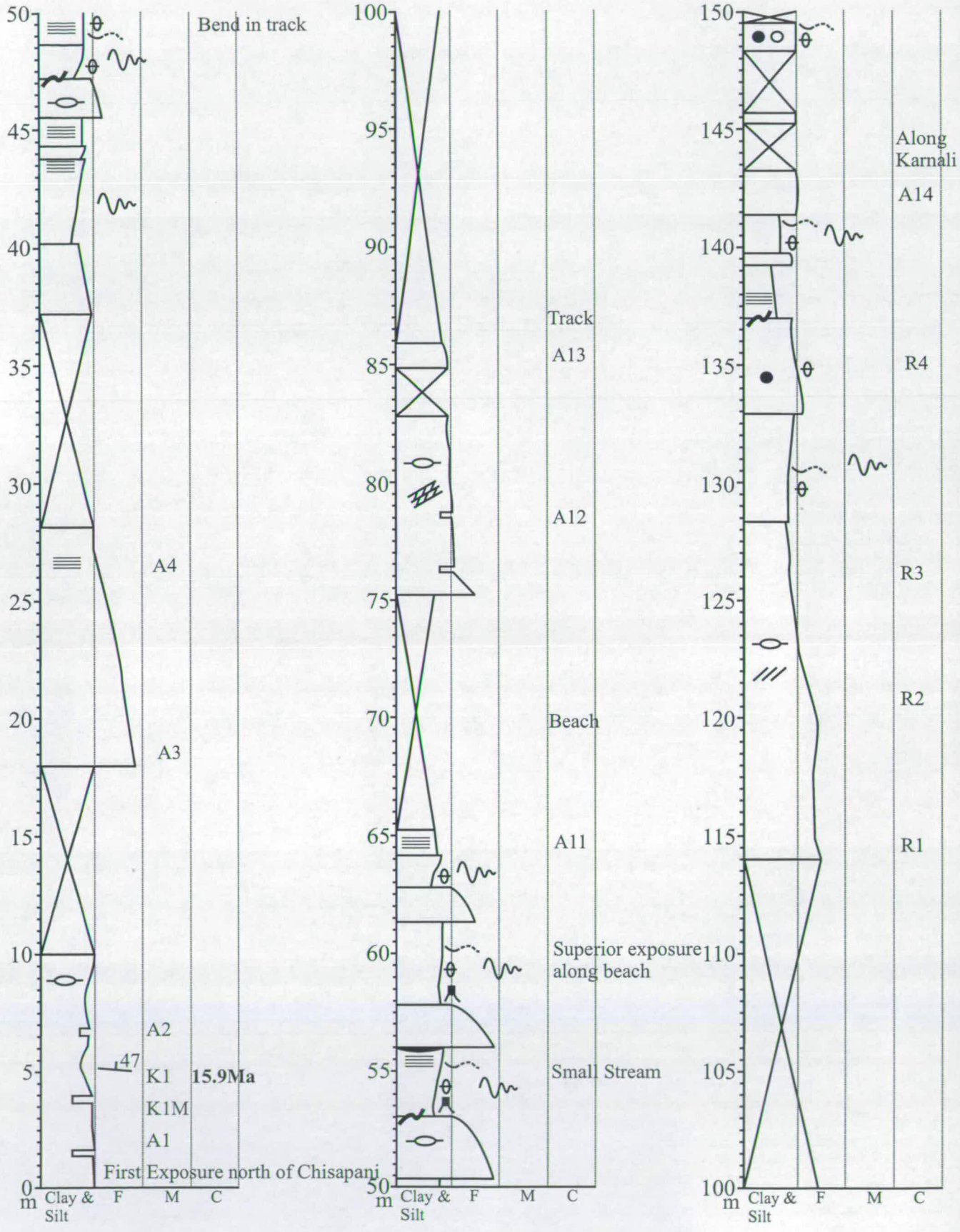
Grainsize (mm)

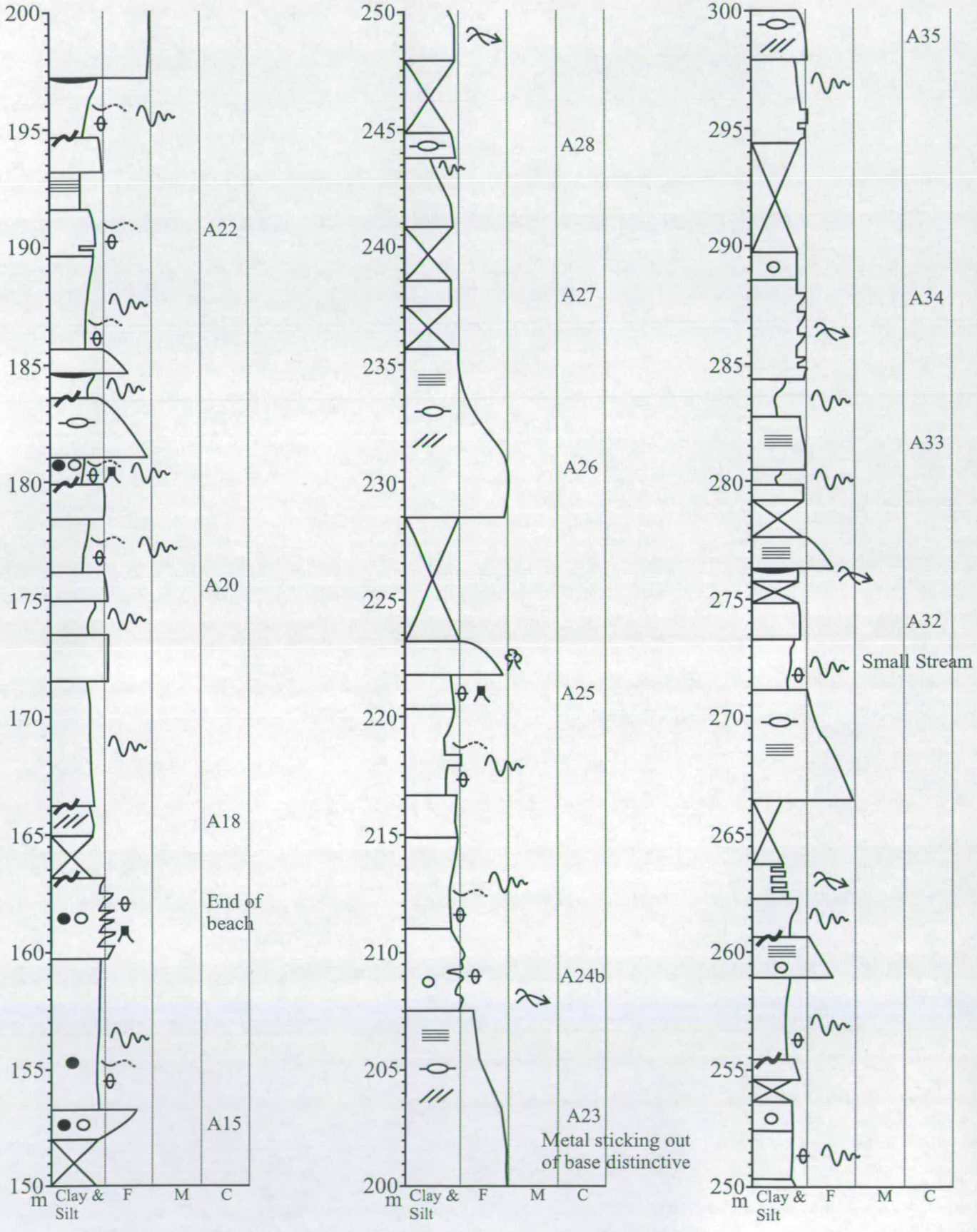
Clay	<0.002
Silt	0.002-0.06
Fine	0.06-0.2
Medium	0.2-0.6
Coarse	0.6-2

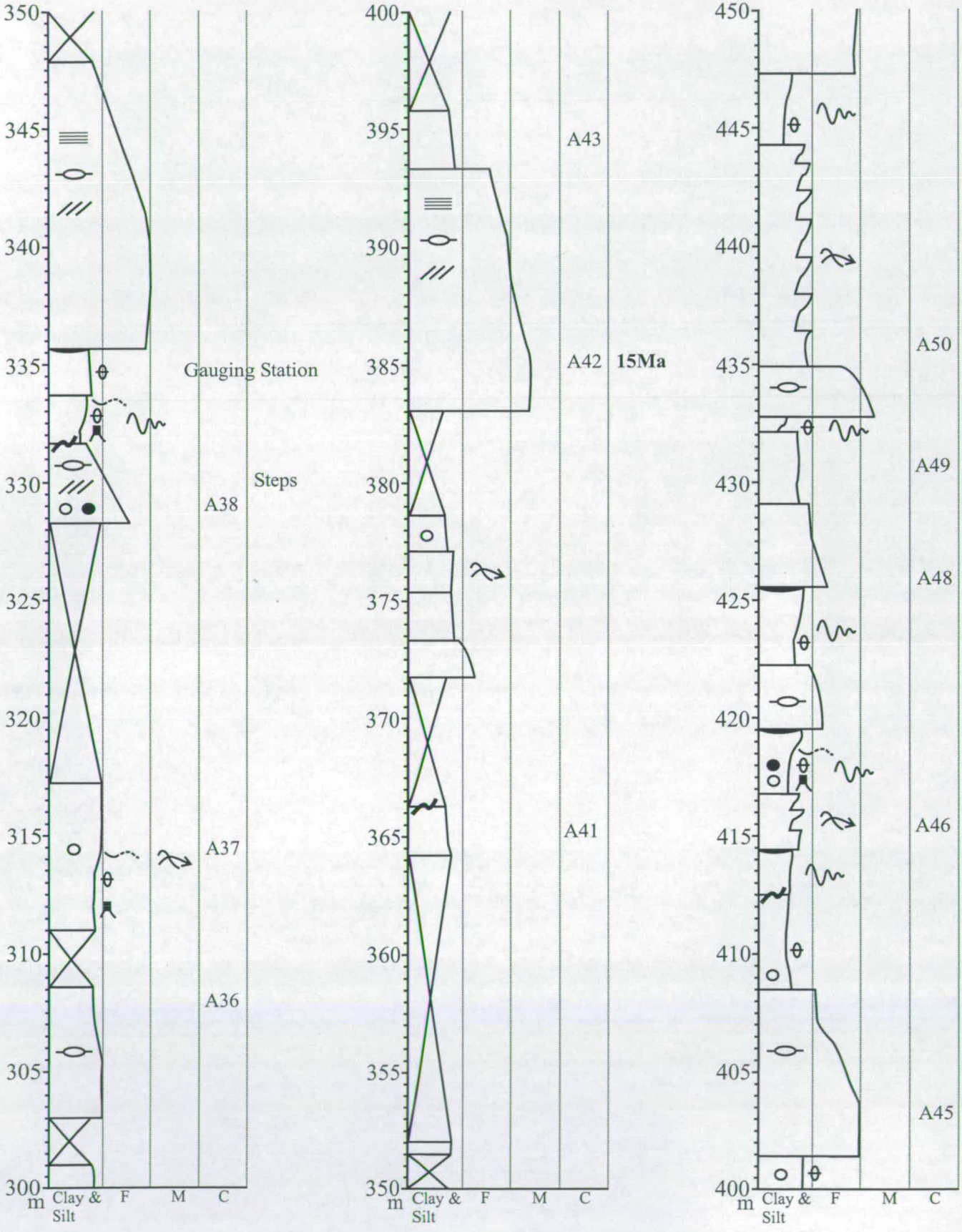
When concerning conglomerates, grainsize refers to the matrix.

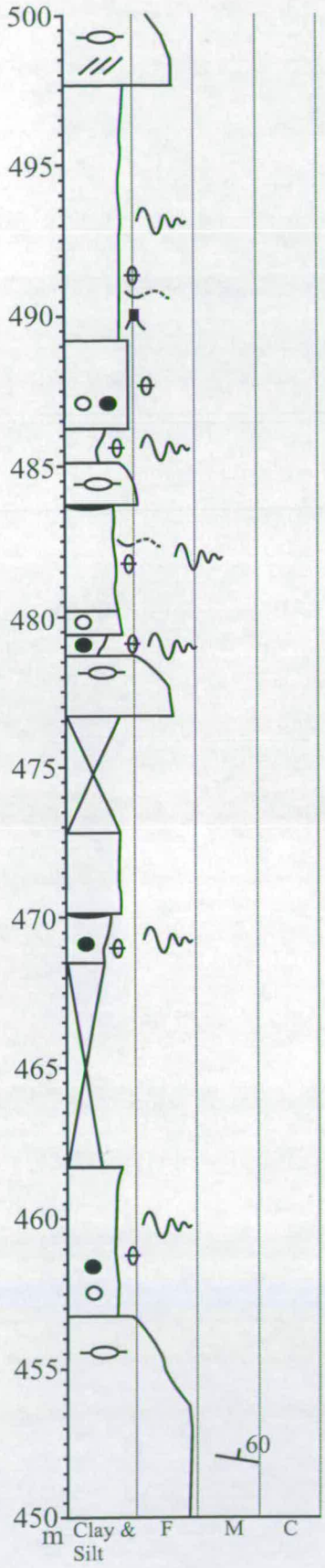
Others

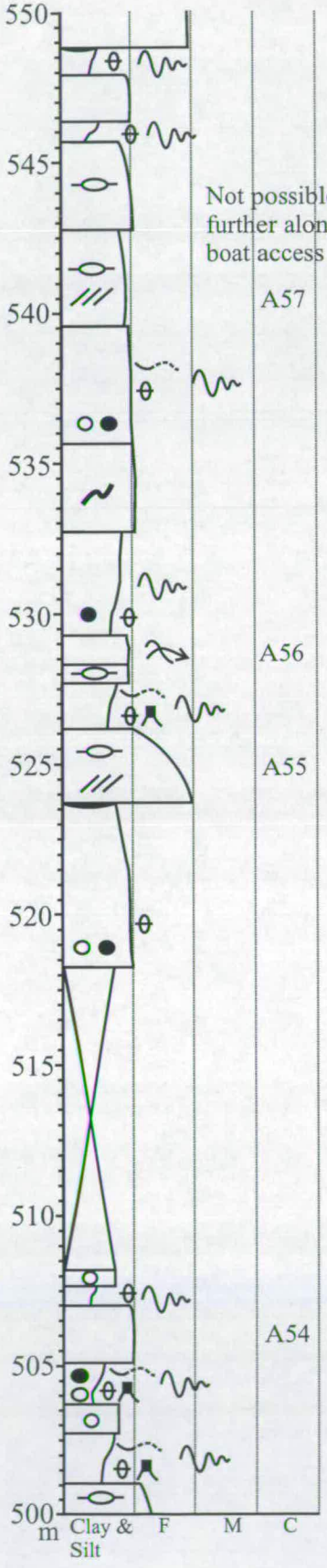
UA	P-Mag. Samples
TA18A	Sample No.
LMB	Lower-Middle Siwalik Boundary
MS2	Middle Siwalik 2 (Pebbly)

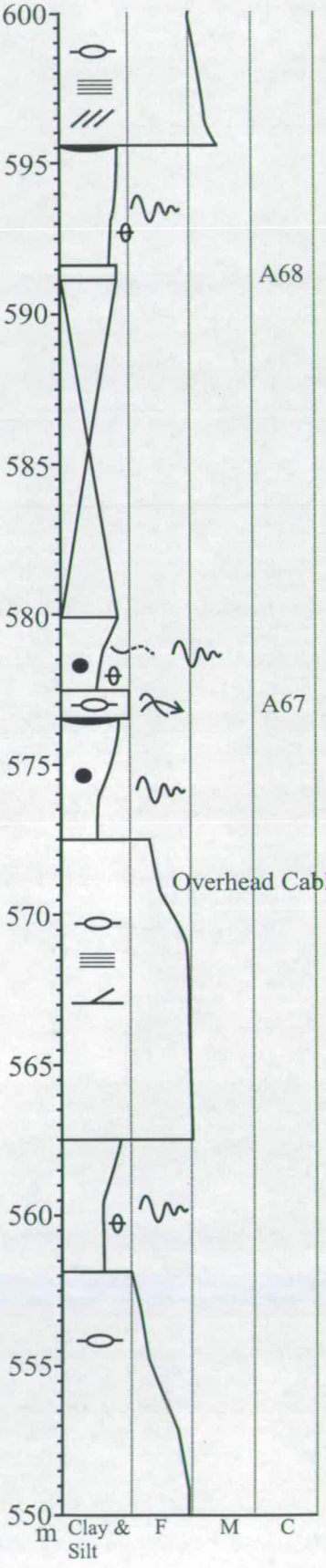

Bend in track
A4
A3
A2
47
K1
15.9Ma
K1M
A1
First Exposure north of Chisapani
Clay & Silt
F
M
C
m
Track
A13
A12
Beach
A11
Superior exposure along beach
Small Stream
Along Karnali
A14
R4
R3
R2
R1

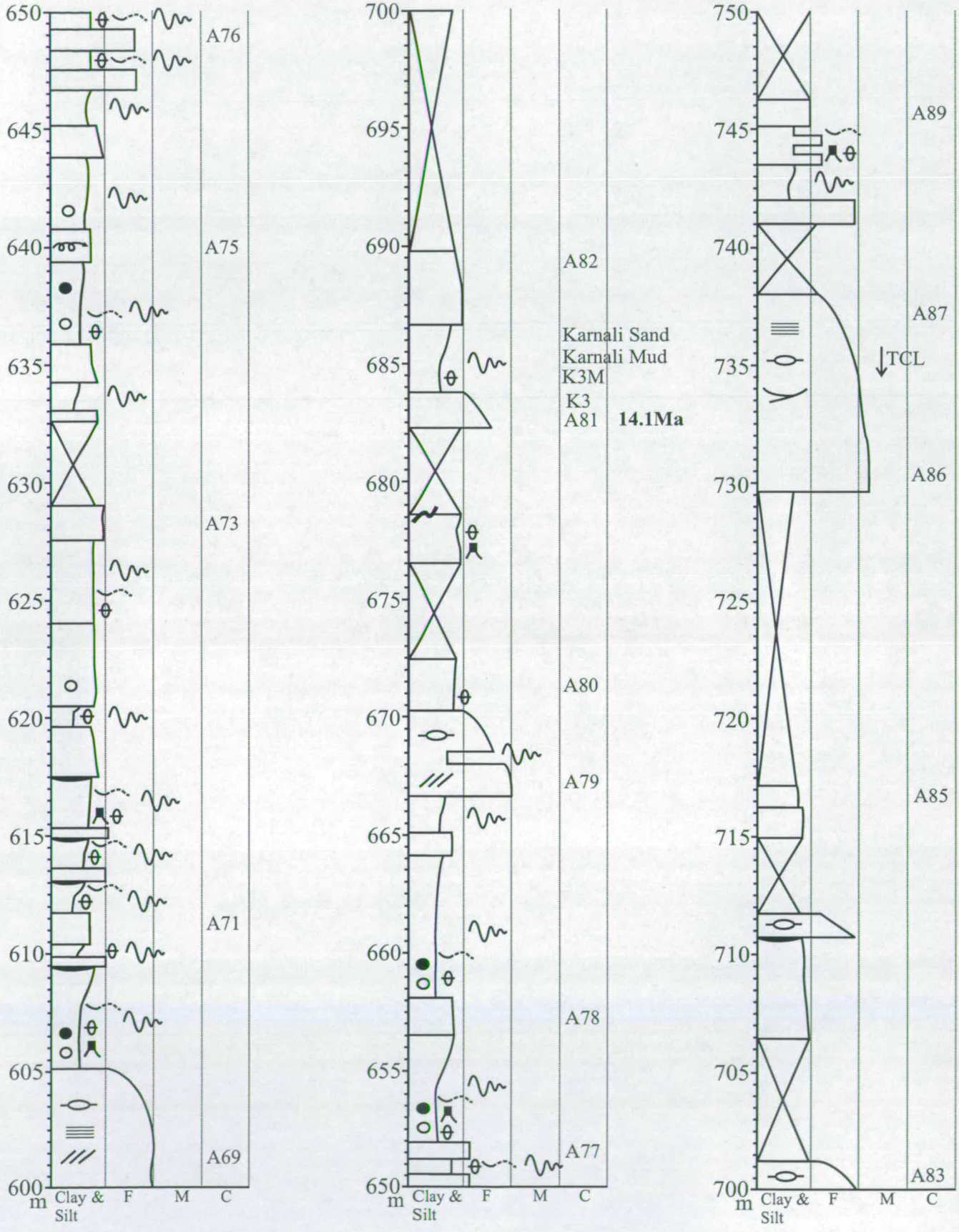

200
195
190
185
180
175
170
165
160
155
150
m
Clay & Silt
F
M
C
A22
A20
A18
End of beach
A15
250
245
240
235
230
225
220
215
210
205
200
A28
A27
A26
A25
A24b
A23
Metal sticking out of base distinctive
300
295
290
285
280
275
270
265
260
255
250
A35
A34
A33
A32
Small Stream

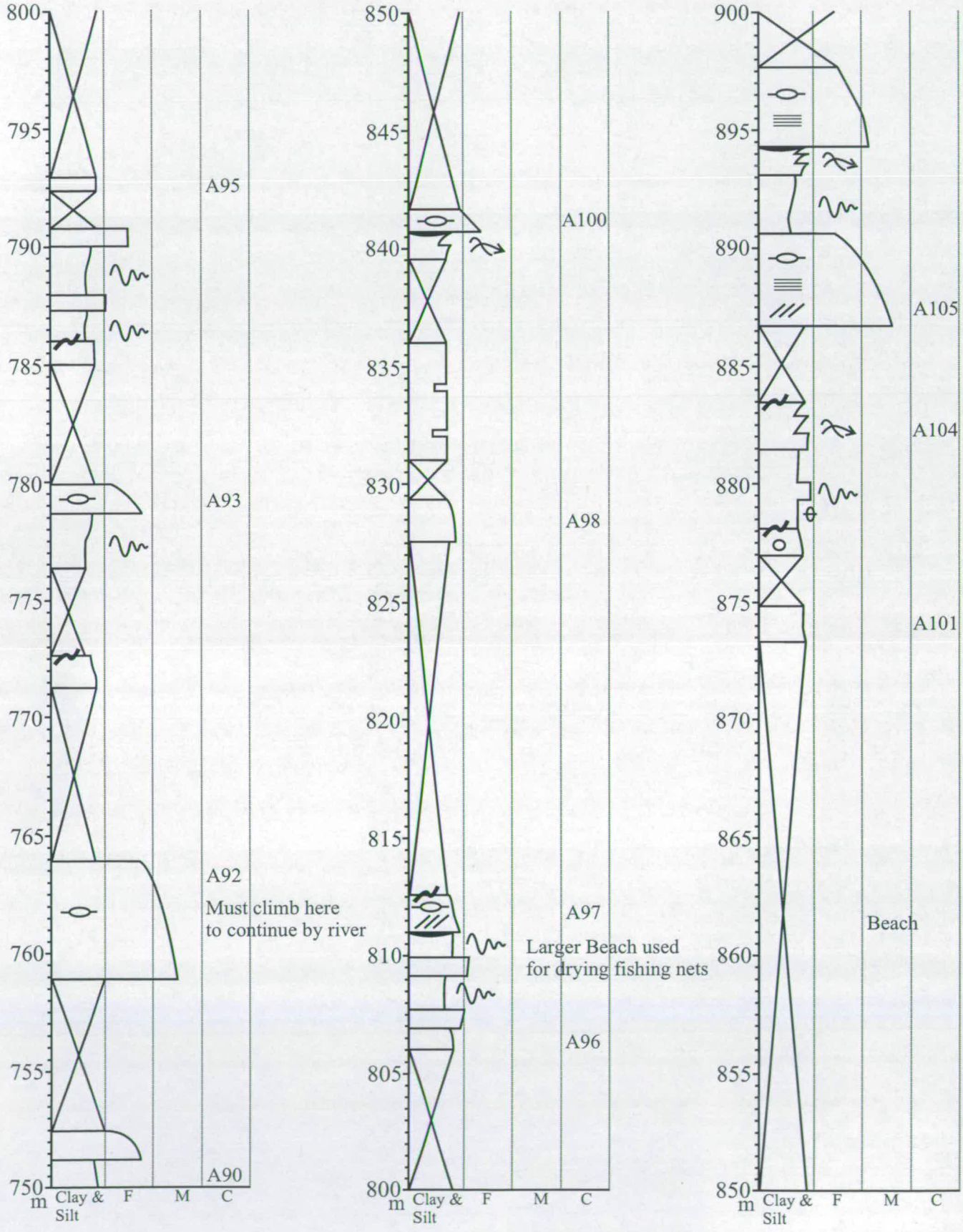

350
345
340
335
330
325
320
315
310
305
300
m
Clay & Silt
F
M
C
Gauging Station
Steps
A38
A37
A36
400
395
390
385
380
375
370
365
360
355
350
A43
A42
15Ma
A41
450
445
440
435
430
425
420
415
410
405
400
A50
A49
A48
A46
A45

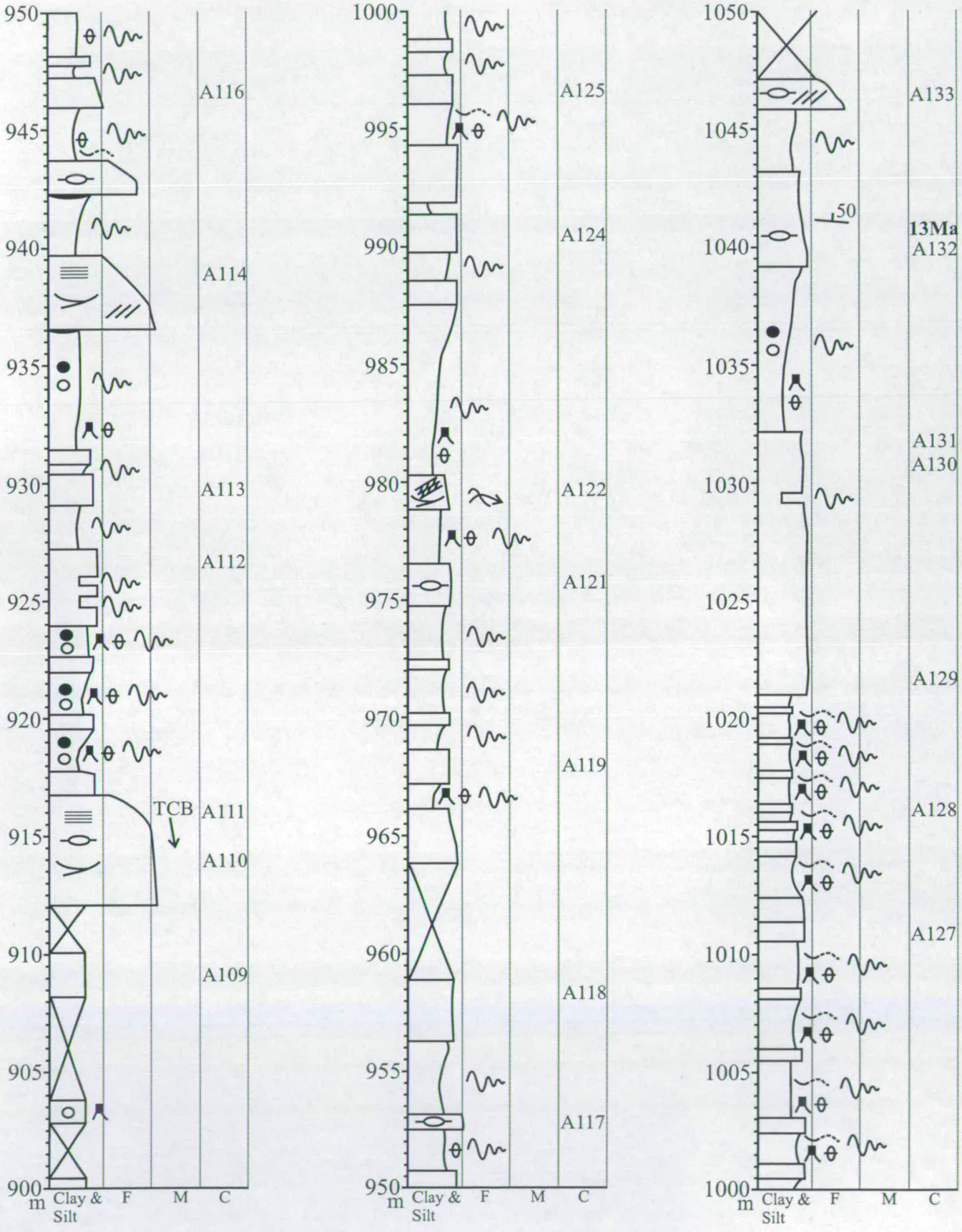

500
495
490
485
480
475
470
465
460
455
450
m
Clay &
Silt
F
M
C
60

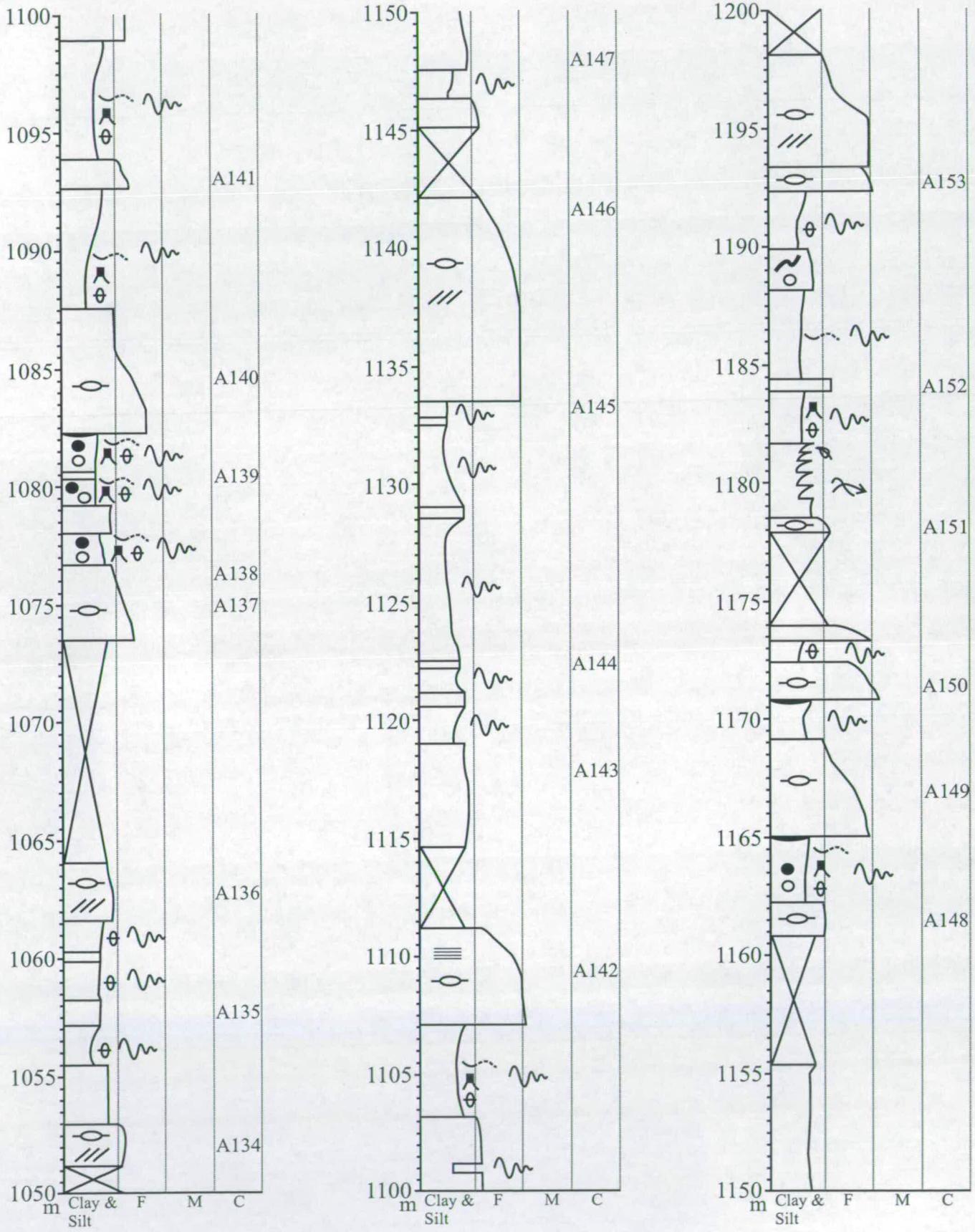

550
545
540
535
530
525
520
515
510
505
500
m
Clay &
Silt
F
M
C
Not possible to walk
further along river -
boat access only
A57
A56
A55
A54

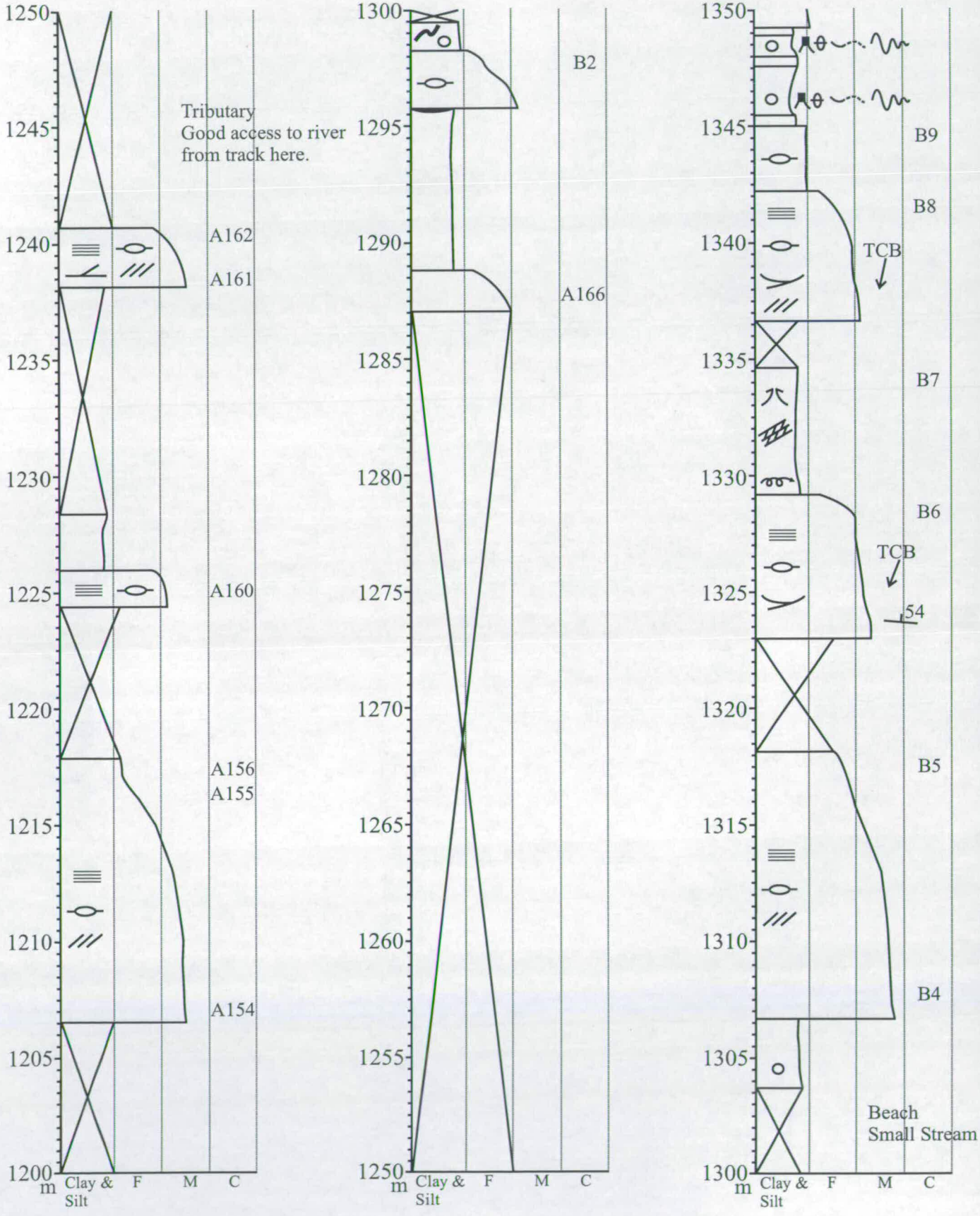

600
595
590
585
580
575
570
565
560
555
550
m
Clay &
Silt
F
M
C
A68
A67
Overhead Cable

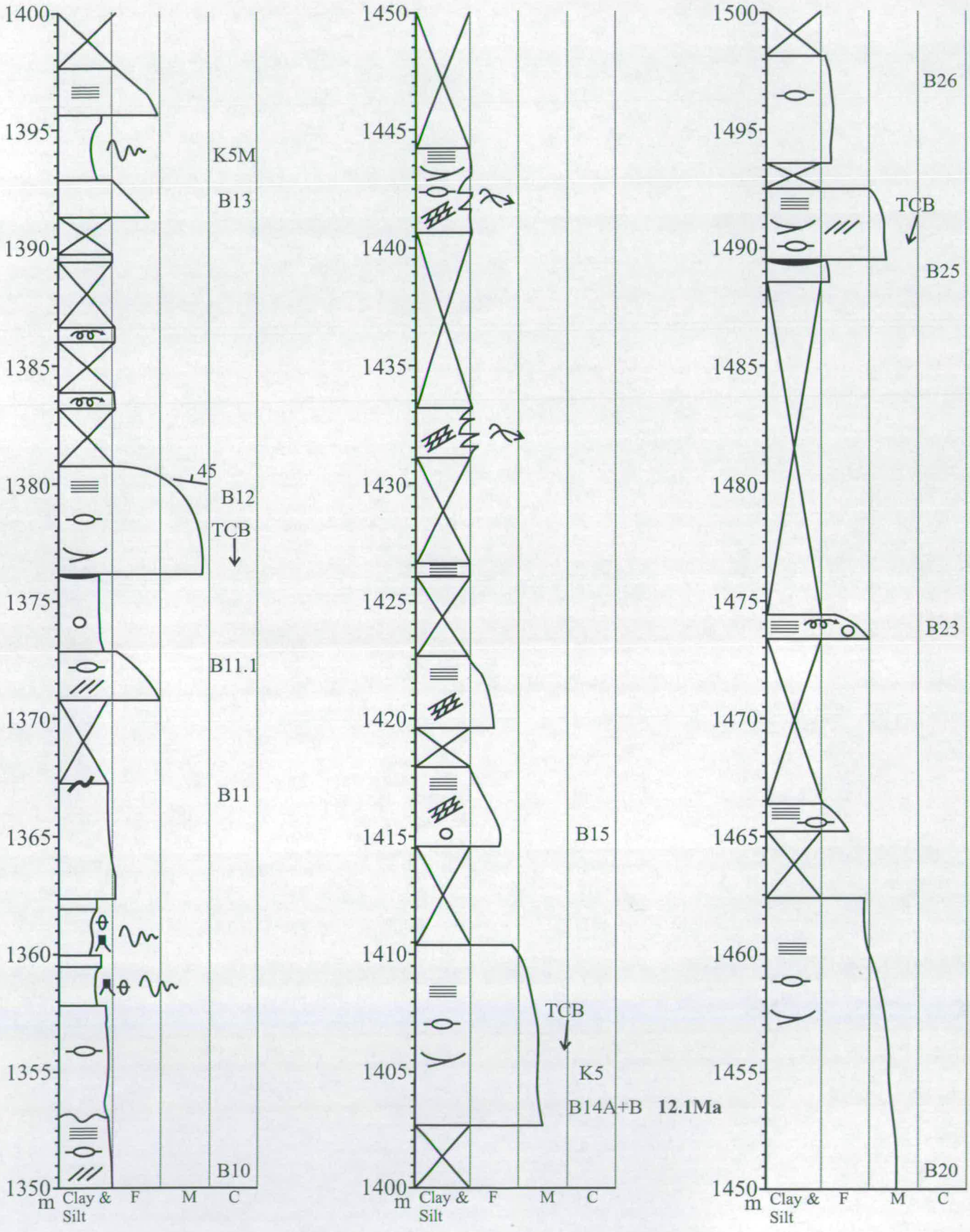

650
645
640
635
630
625
620
615
610
605
600
m
Clay & Silt
F
M
C
A76
A75
A73
A71
A69
700
695
690
685
680
675
670
665
660
655
650
A82
Karnali Sand
Karnali Mud
K3M
K3
A81
14.1Ma
A80
A79
A78
A77
750
745
740
735
730
725
720
715
710
705
700
A89
A87
TCL
A86
A85
A83

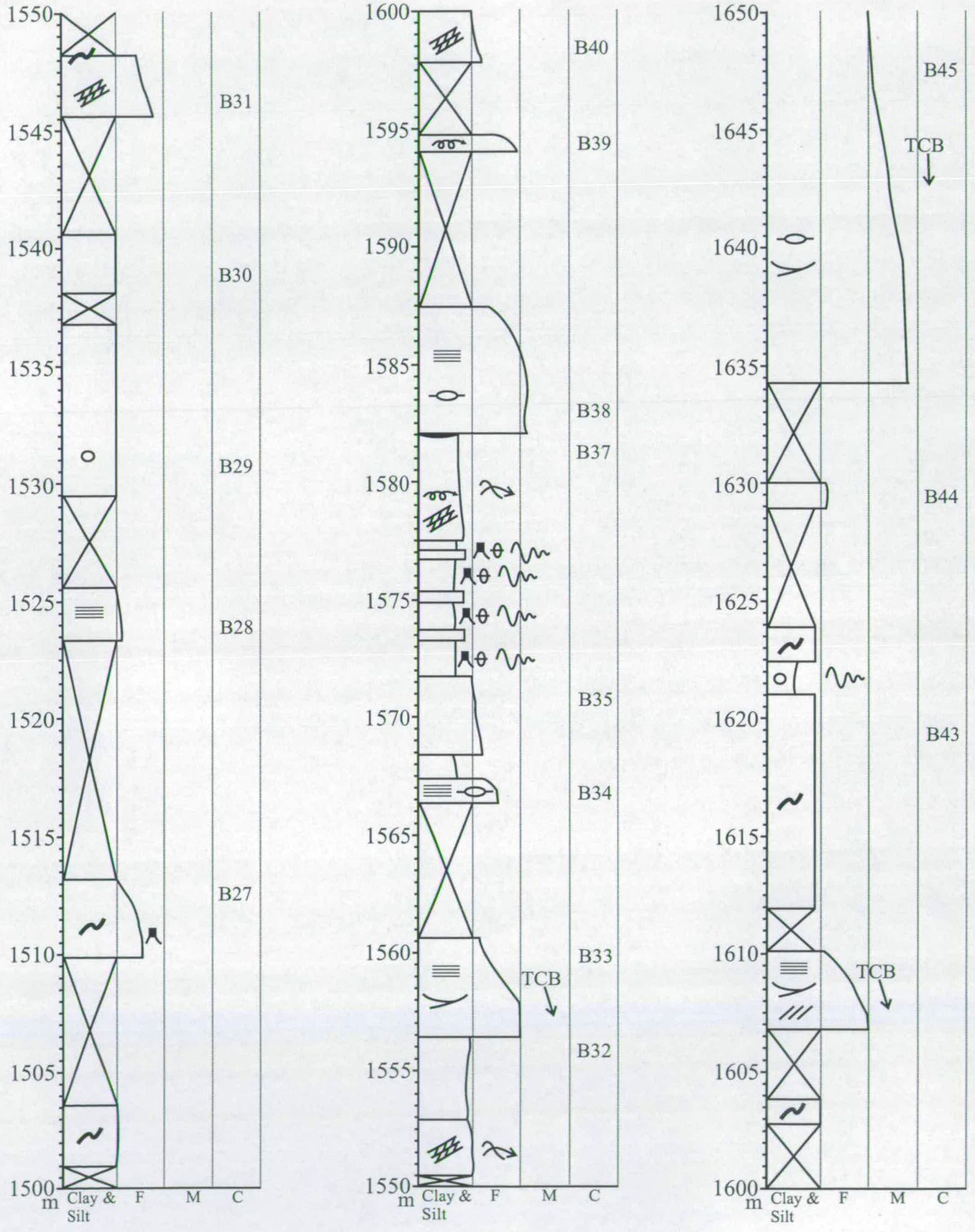

800
795
790
785
780
775
770
765
760
755
750
m
Clay &
Silt
F
M
C
A95
A93
A92
Must climb here
to continue by river
A90
850
845
840
835
830
825
820
815
810
805
800
A100
A98
A97
Larger Beach used
for drying fishing nets
A96
900
895
890
885
880
875
870
865
860
855
850
A105
A104
A101
Beach

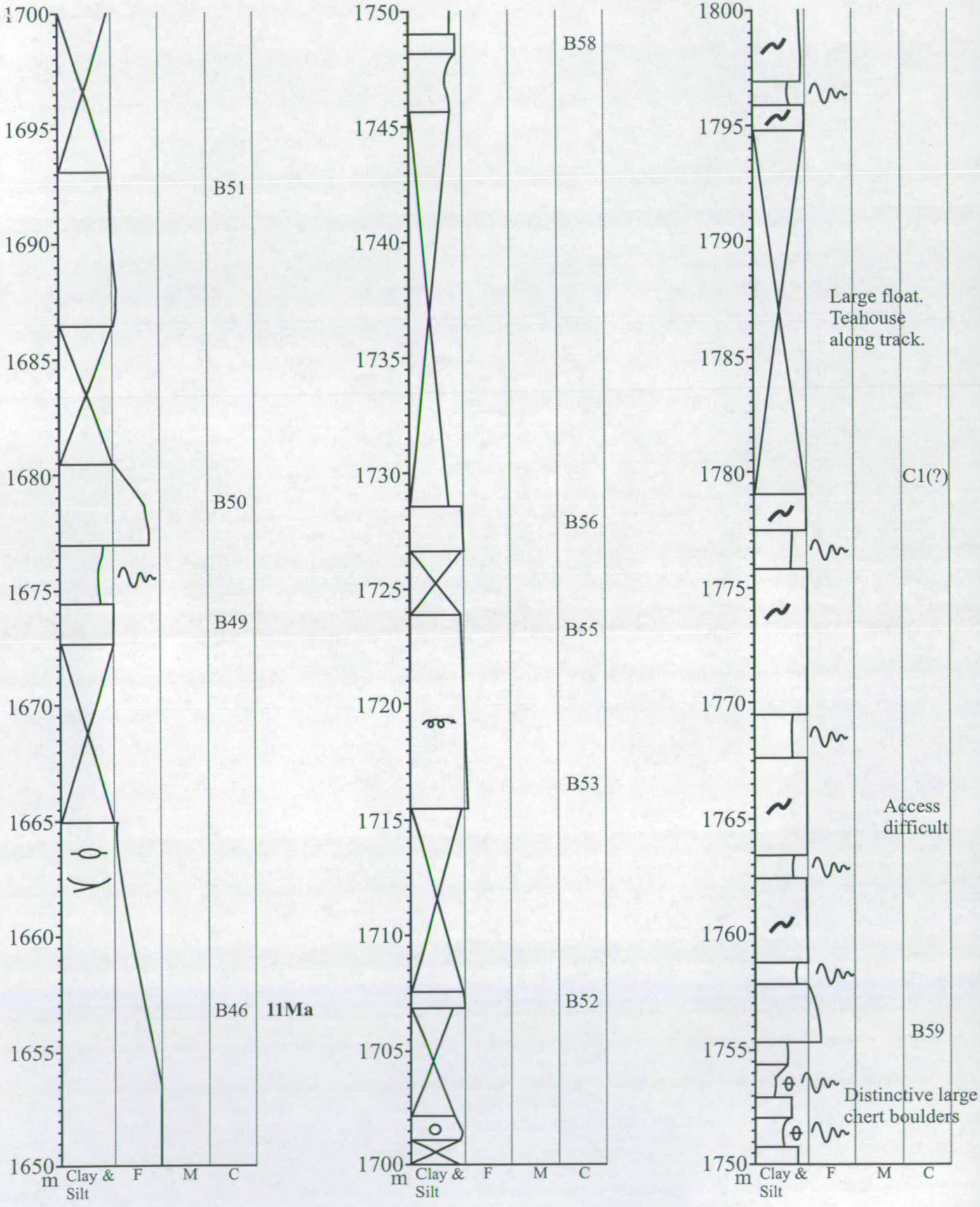

950
945
940
935
930
925
920
915
910
905
900
m
Clay &
Silt
F
M
C
A116
A114
A113
A112
TCB
A111
A110
A109
1000
995
990
985
980
975
970
965
960
955
950
A125
A124
A122
A121
A119
A118
A117
1050
1045
1040
1035
1030
1025
1020
1015
1010
1005
1000
50
13Ma
A133
A132
A131
A130
A129
A128
A127

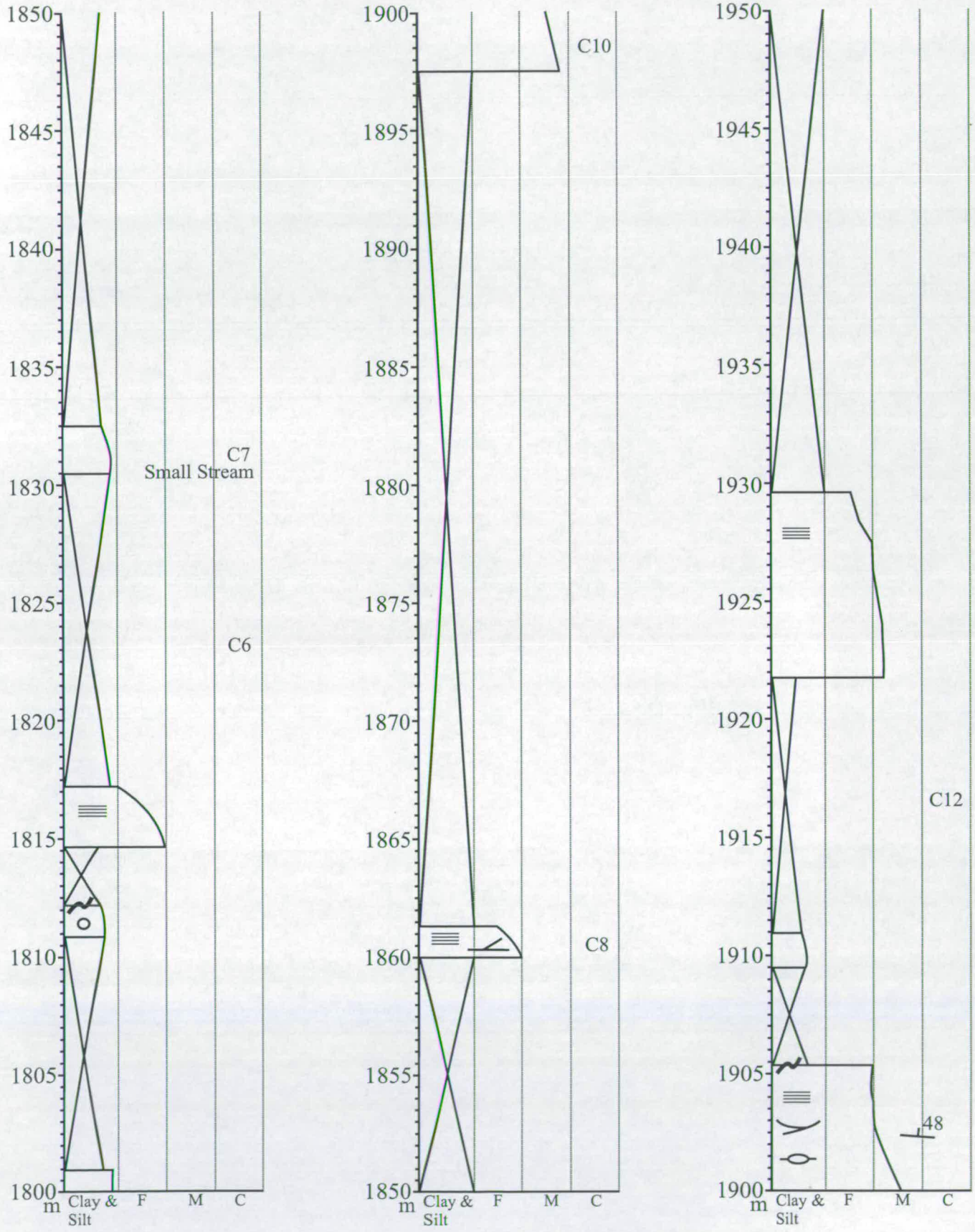

1100
1095
1090
1085
1080
1075
1070
1065
1060
1055
1050
A141
A140
A139
A138
A137
A136
A135
A134
m
Clay & Silt
F
M
C
1150
1145
1140
1135
1130
1125
1120
1115
1110
1105
1100
A147
A146
A145
A144
A143
A142
m
Clay & Silt
F
M
C
1200
1195
1190
1185
1180
1175
1170
1165
1160
1155
1150
A153
A152
A151
A150
A149
A148
m
Clay & Silt
F
M
C

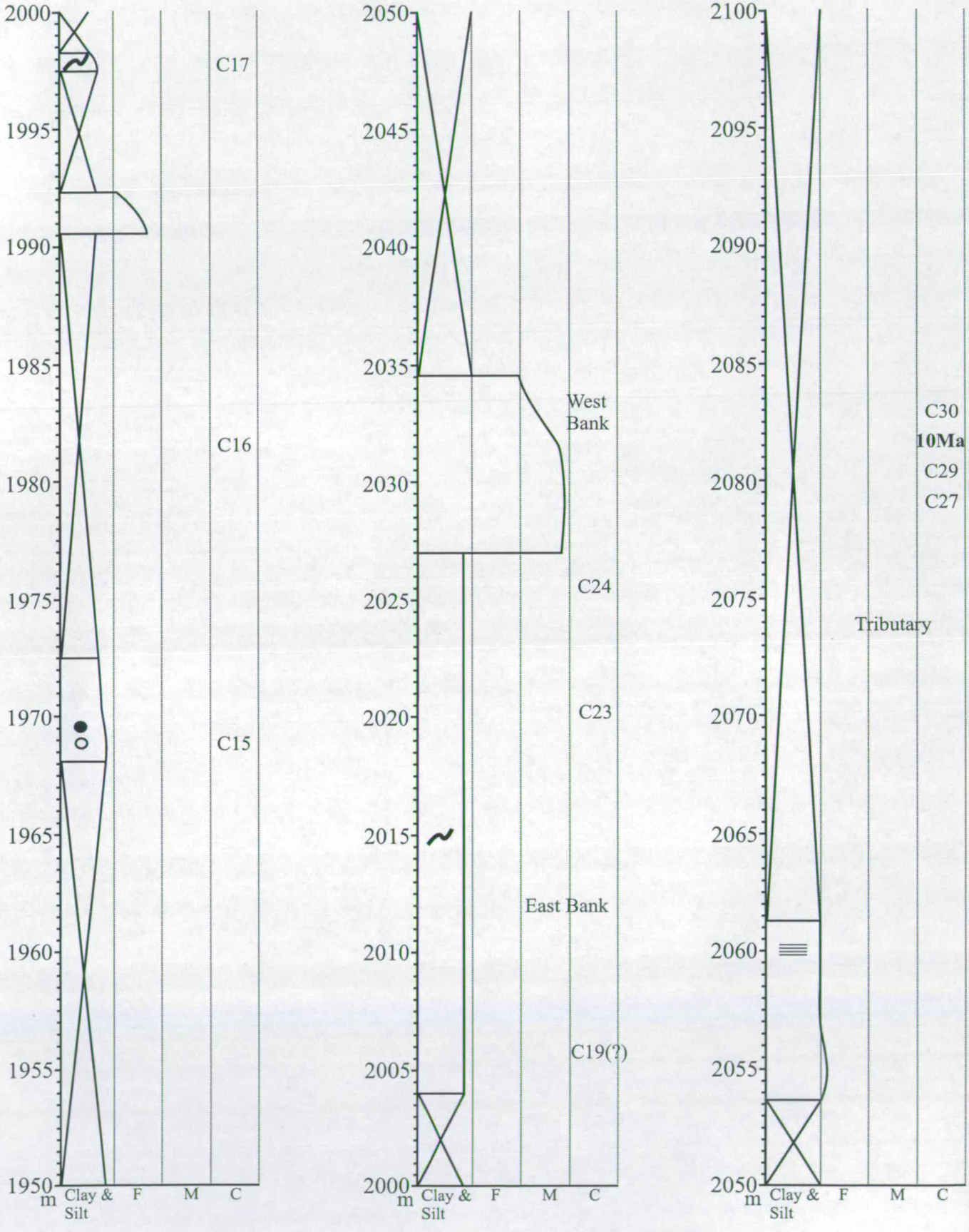

1250
1245
1240
1235
1230
1225
1220
1215
1210
1205
1200
m
Clay & Silt
F
M
C
Tributary
Good access to river from track here.
A162
A161
A160
A156
A155
A154
1300
1295
1290
1285
1280
1275
1270
1265
1260
1255
1250
B2
A166
1350
1345
1340
1335
1330
1325
1320
1315
1310
1305
1300
B9
B8
TCB
B7
B6
TCB
54
B5
B4
Beach
Small Stream

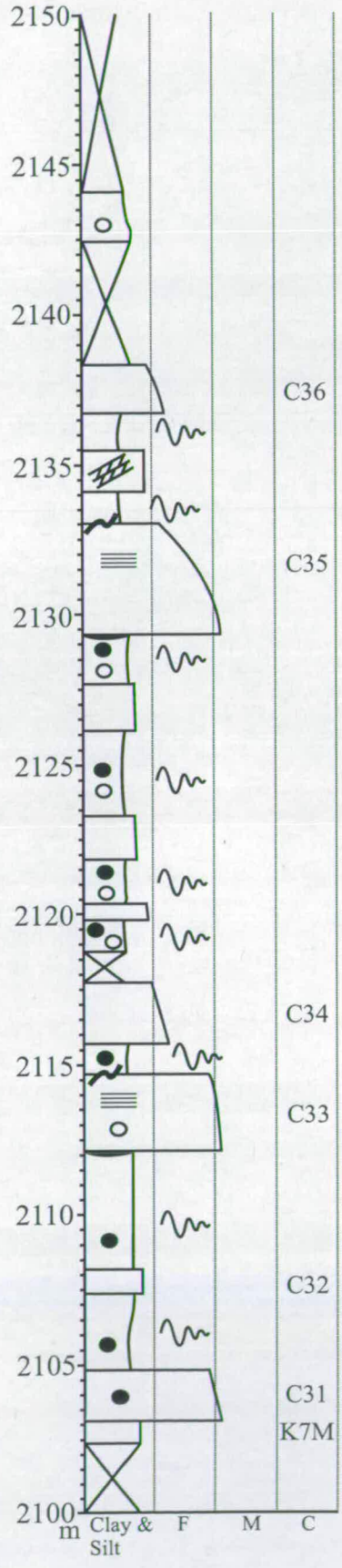

1400
1395
1390
1385
1380
1375
1370
1365
1360
1355
1350
K5M
B13
45
B12
TCB
B11.1
B11
B10
m
Clay &
Silt
F
M
C
1450
1445
1440
1435
1430
1425
1420
1415
1410
1405
1400
B15
TCB
K5
B14A+B
12.1Ma
1500
1495
1490
1485
1480
1475
1470
1465
1460
1455
1450
B26
TCB
B25
B23
B20

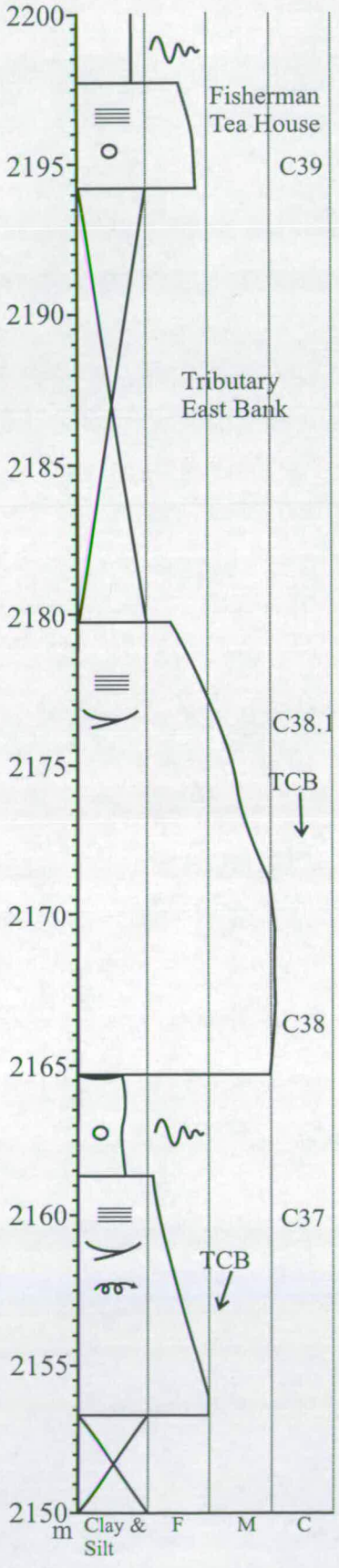

1550
1545
1540
1535
1530
1525
1520
1515
1510
1505
1500
B31
B30
B29
B28
B27
m
Clay &
Silt
F
M
C
1600
1595
1590
1585
1580
1575
1570
1565
1560
1555
1550
B40
B39
B38
B37
B35
B34
B33
B32
TCB
1650
1645
1640
1635
1630
1625
1620
1615
1610
1605
1600
B45
B44
B43

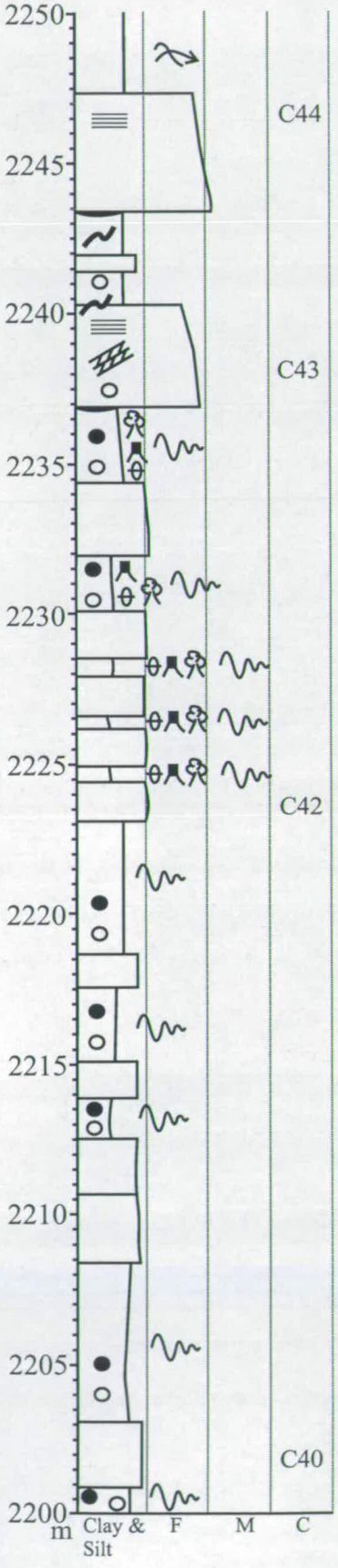

1700
1695
1690
1685
1680
1675
1670
1665
1660
1655
1650
B51
B50
B49
B46
11Ma
m
Clay & Silt
F
M
C
1750
1745
1740
1735
1730
1725
1720
1715
1710
1705
1700
B58
B56
B55
B53
B52
1800
1795
1790
1785
1780
1775
1770
1765
1760
1755
1750
Large float.
Teahouse
along track.
C1(?)
Access
difficult
B59
Distinctive large
chert boulders

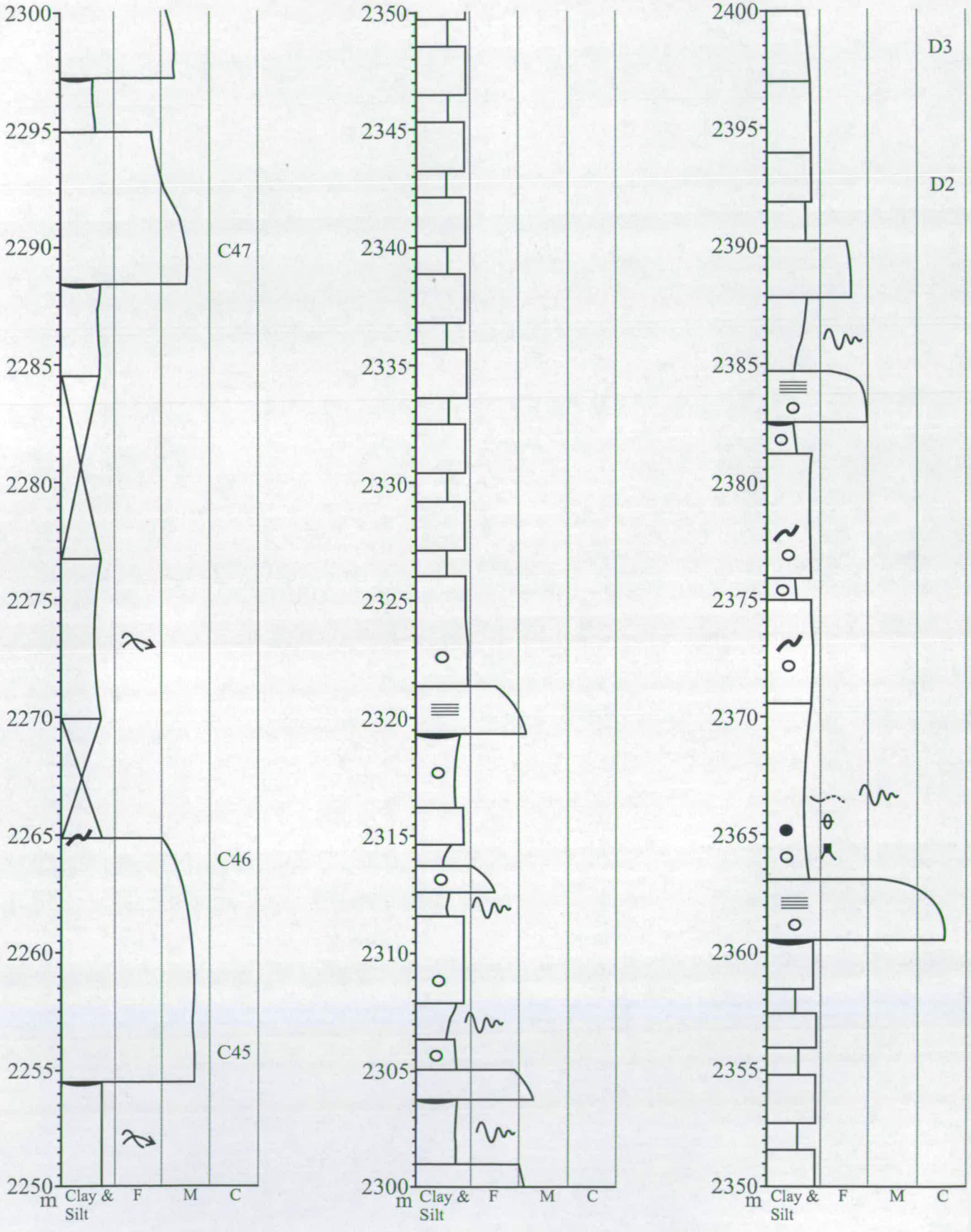

1850
1845
1840
1835
1830
1825
1820
1815
1810
1805
1800
m
Clay & Silt
F
M
C
C7
Small Stream
C6
1900
1895
1890
1885
1880
1875
1870
1865
1860
1855
1850
C10
C8
1950
1945
1940
1935
1930
1925
1920
1915
1910
1905
1900
C12
48

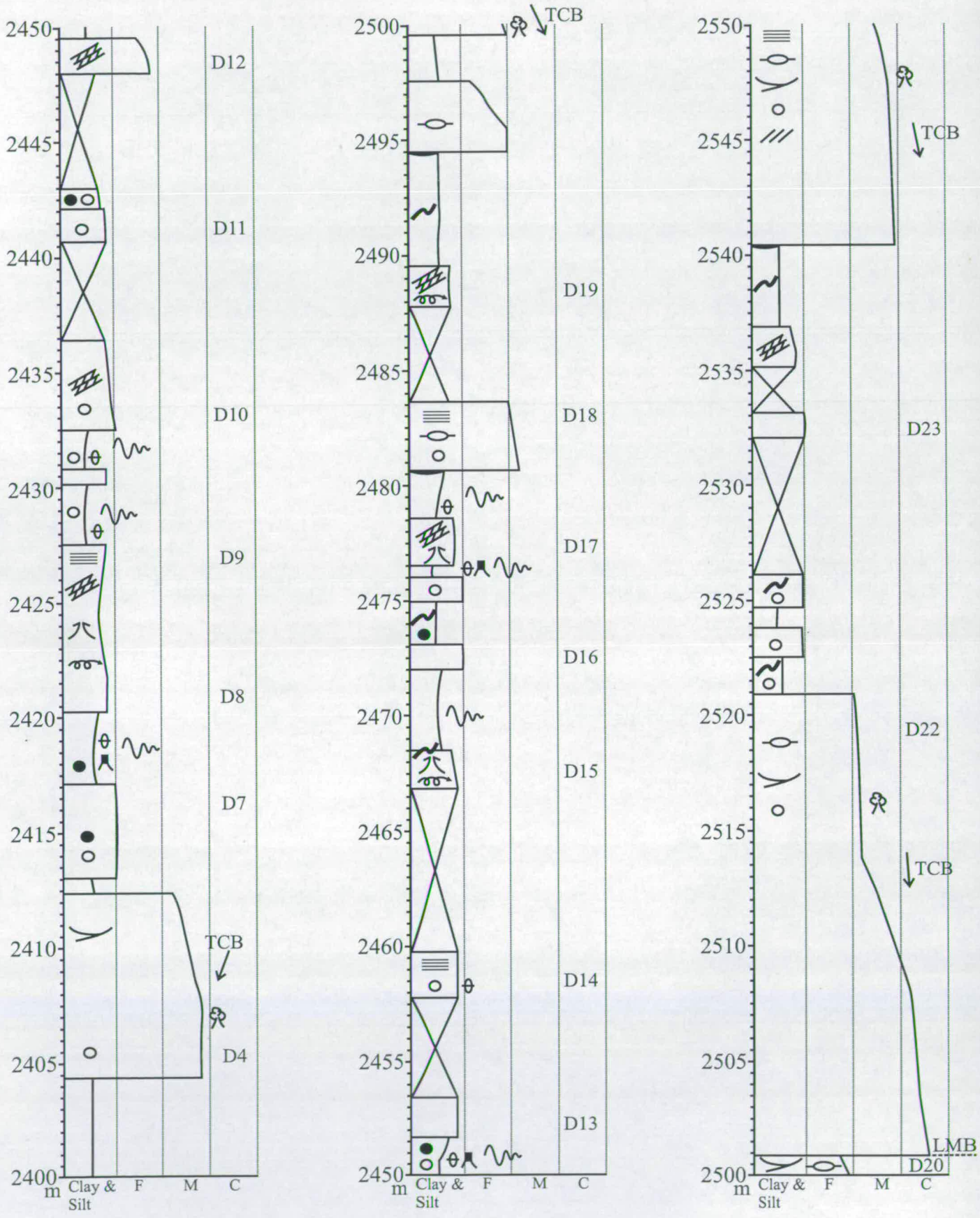

2000
1995
1990
1985
1980
1975
1970
1965
1960
1955
1950
m
Clay &
Silt
F
M
C
C17
C16
C15
2050
2045
2040
2035
2030
2025
2020
2015
2010
2005
2000
West
Bank
C24
C23
East Bank
C19(?)
2100
2095
2090
2085
2080
2075
2070
2065
2060
2055
2050
C30
10Ma
C29
C27
Tributary

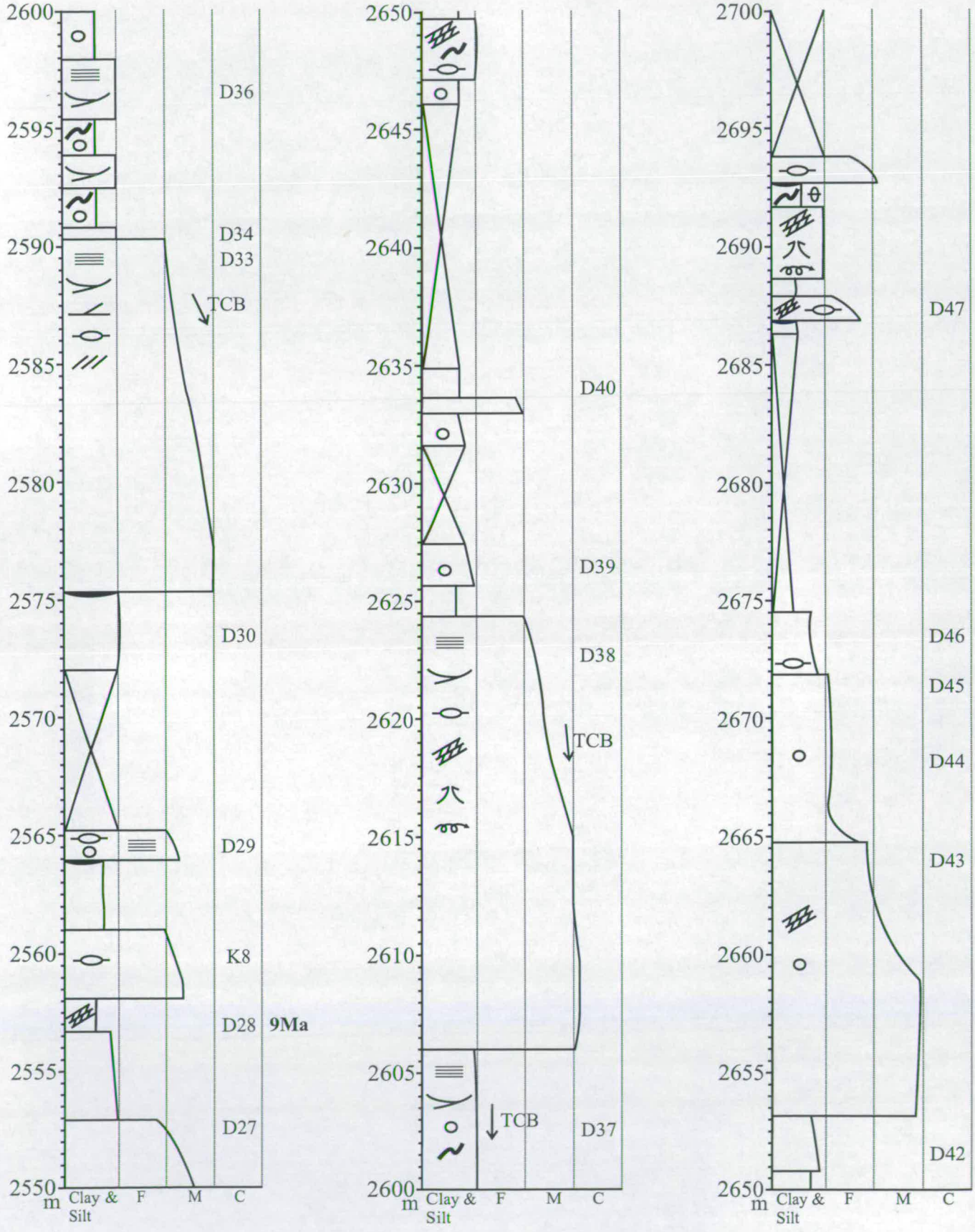

2150
2145
2140
2135
2130
2125
2120
2115
2110
2105
2100
C36
C35
C34
C33
C32
C31
K7M
m
Clay &
Silt
F
M
C

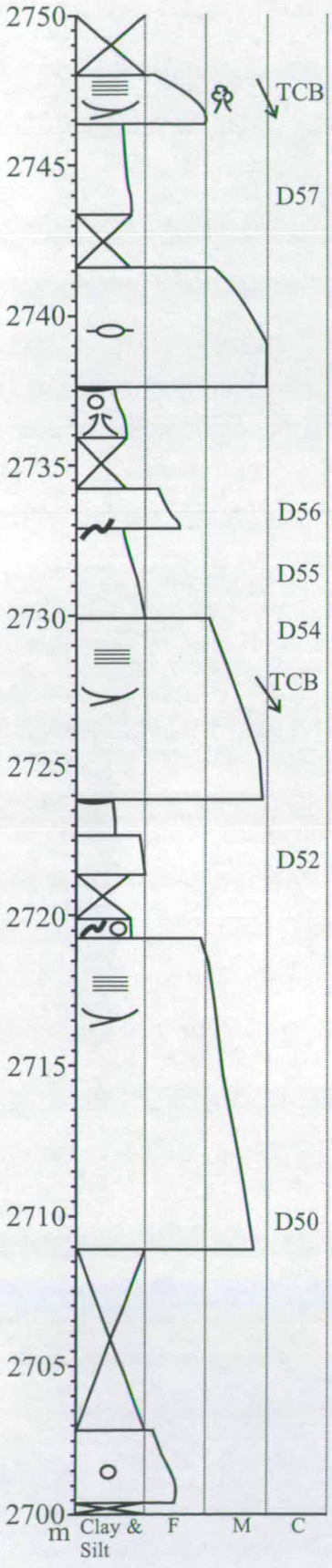

2200
2195
2190
2185
2180
2175
2170
2165
2160
2155
2150
Fisherman
Tea House
C39
Tributary
East Bank
C38.1
TCB
C38
C37
TCB
m
Clay &
Silt
F
M
C

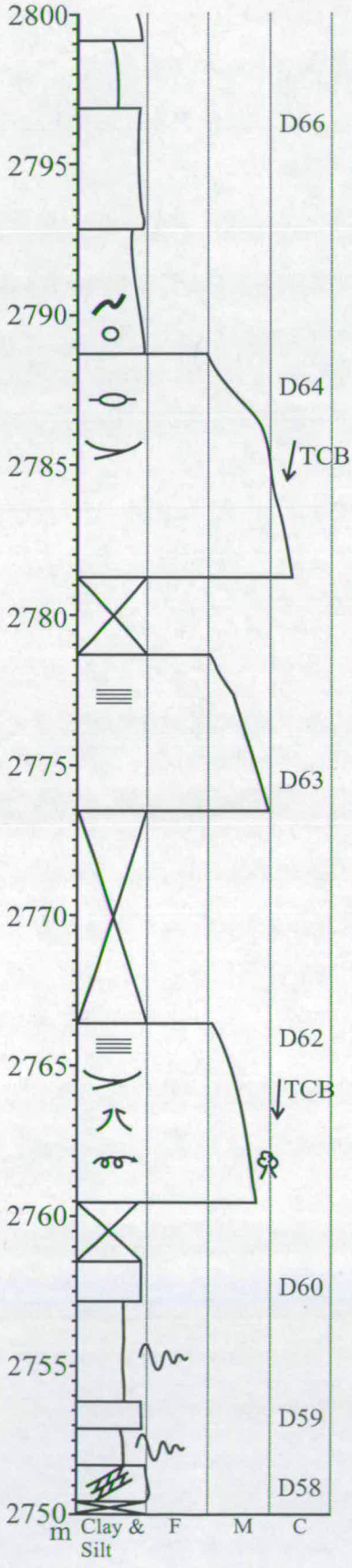

2250
2245
2240
2235
2230
2225
2220
2215
2210
2205
2200
C44
C43
C42
C40
m
Clay &
Silt
F
M
C

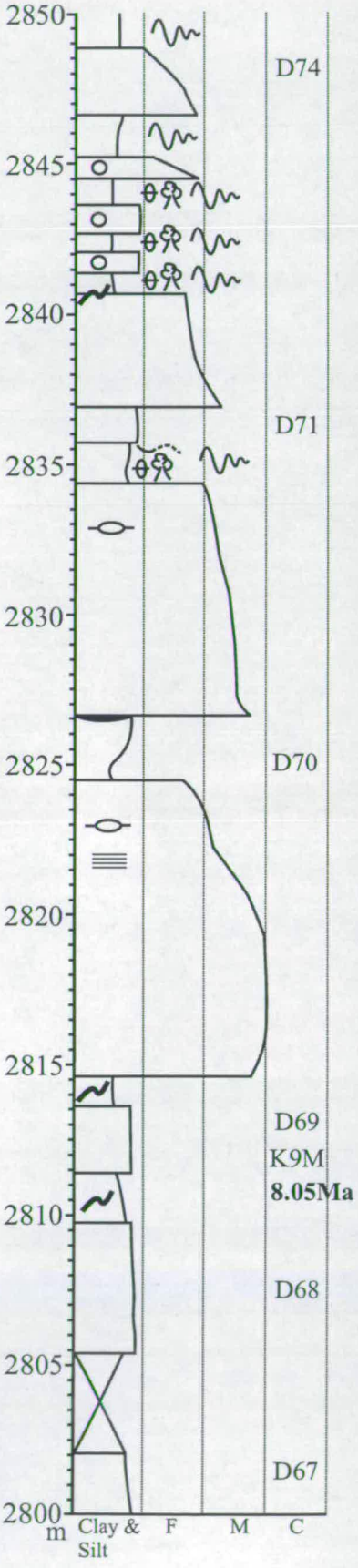

2300
2295
2290
2285
2280
2275
2270
2265
2260
2255
2250
C47
C46
C45
m
Clay &
Silt
F
M
C
2350
2345
2340
2335
2330
2325
2320
2315
2310
2305
2300
2400
2395
2390
2385
2380
2375
2370
2365
2360
2355
2350
D3
D2

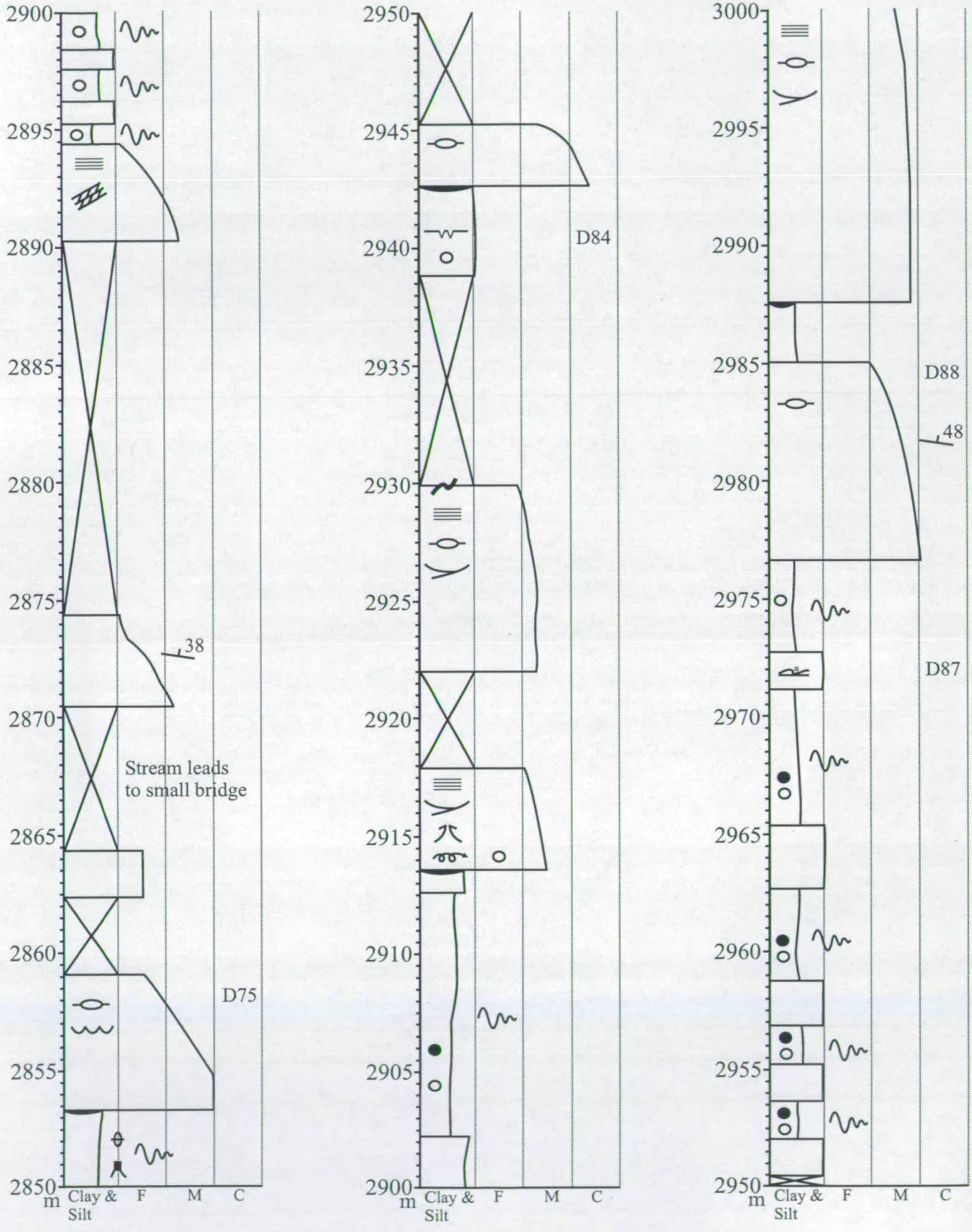

2450
2445
2440
2435
2430
2425
2420
2415
2410
2405
2400
m
Clay &
Silt
F
M
C
D12
D11
D10
D9
D8
D7
TCB
D4
2500
2495
2490
2485
2480
2475
2470
2465
2460
2455
2450
TCB
D19
D18
D17
D16
D15
D14
D13
2550
2545
2540
2535
2530
2525
2520
2515
2510
2505
2500
TCB
D23
D22
TCB
LMB
D20

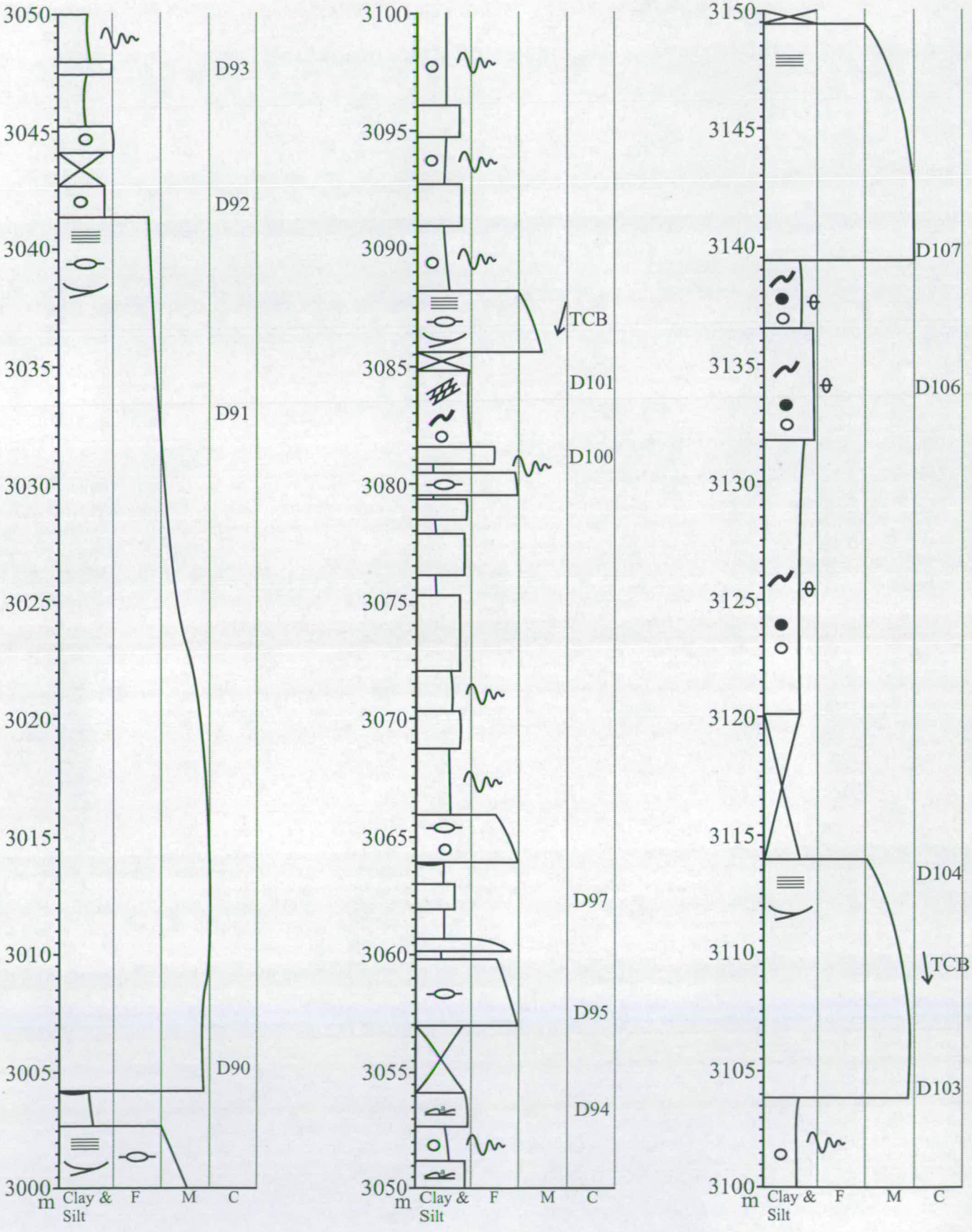

2600
2595
2590
2585
2580
2575
2570
2565
2560
2555
2550
m
Clay & Silt
F
M
C
D36
D34
D33
TCB
D30
D29
K8
D28
9Ma
D27
2650
2645
2640
2635
2630
2625
2620
2615
2610
2605
2600
D40
D39
D38
TCB
TCB
D37
2700
2695
2690
2685
2680
2675
2670
2665
2660
2655
2650
D47
D46
D45
D44
D43
D42

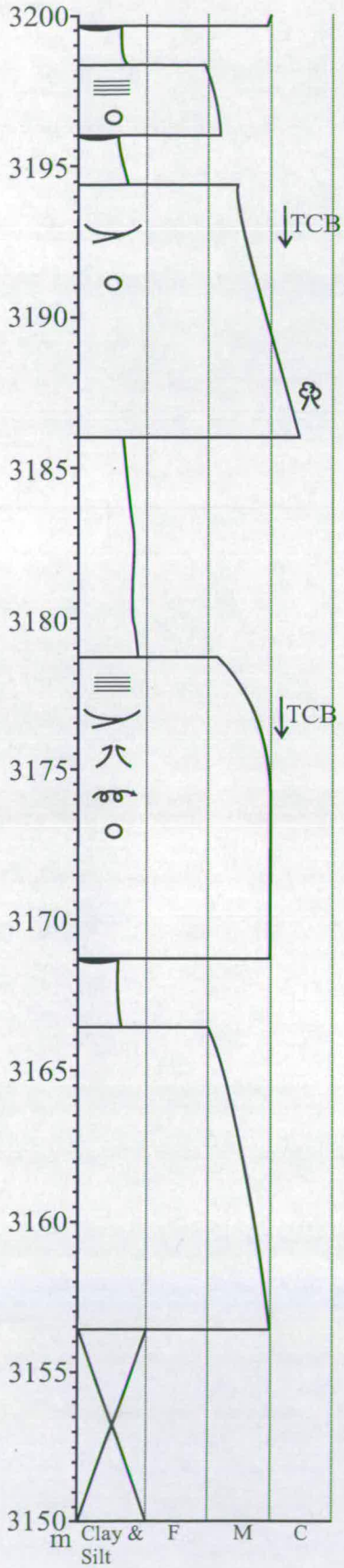

2750
2745
2740
2735
2730
2725
2720
2715
2710
2705
2700
m
Clay &
Silt
F
M
C
TCB
D57
D56
D55
D54
TCB
D52
D50

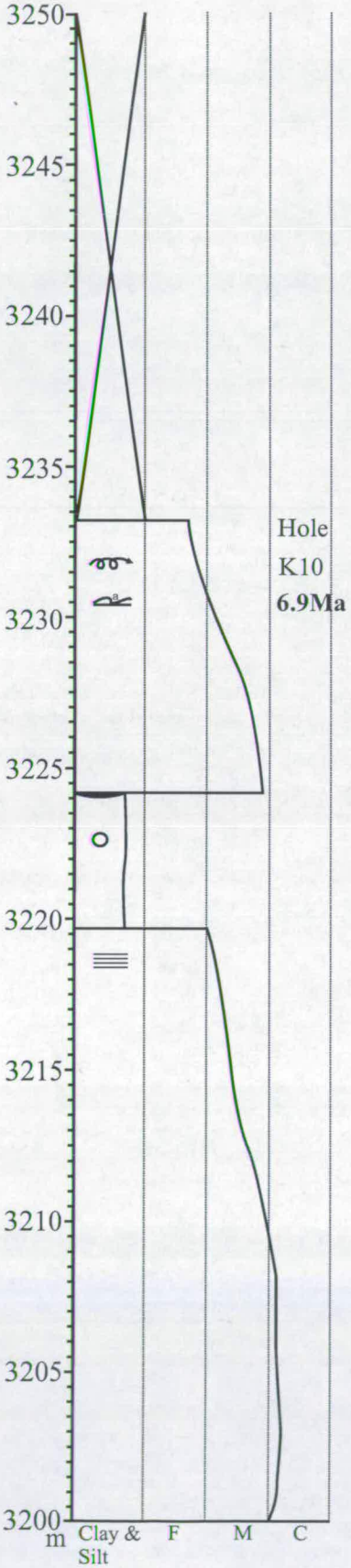

2800
2795
2790
2785
2780
2775
2770
2765
2760
2755
2750
m
Clay &
Silt
F
M
C
D66
D64
TCB
D63
D62
TCB
D60
D59
D58

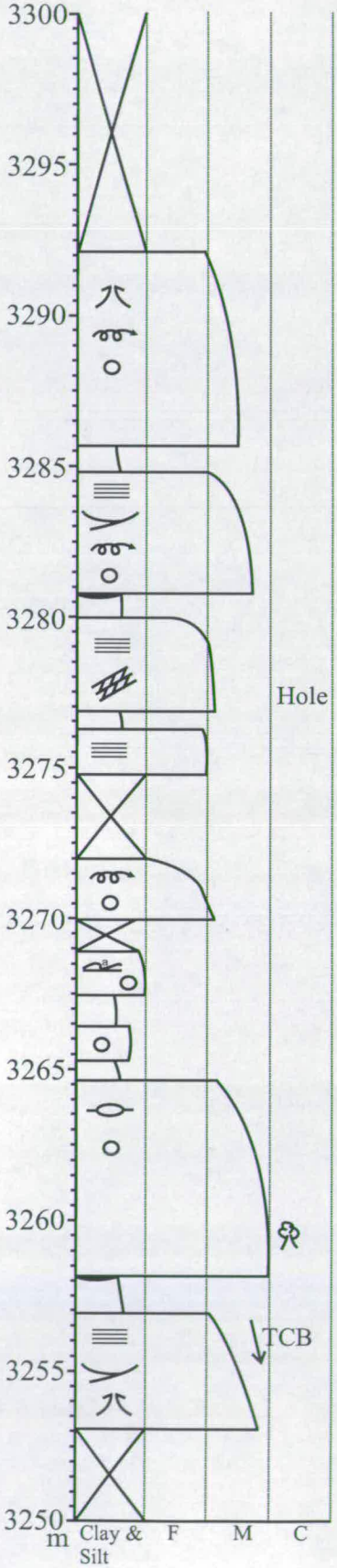

2850
2845
2840
2835
2830
2825
2820
2815
2810
2805
2800
m
Clay &
Silt
F
M
C
D74
D71
D70
D69
K9M
8.05Ma
D68
D67

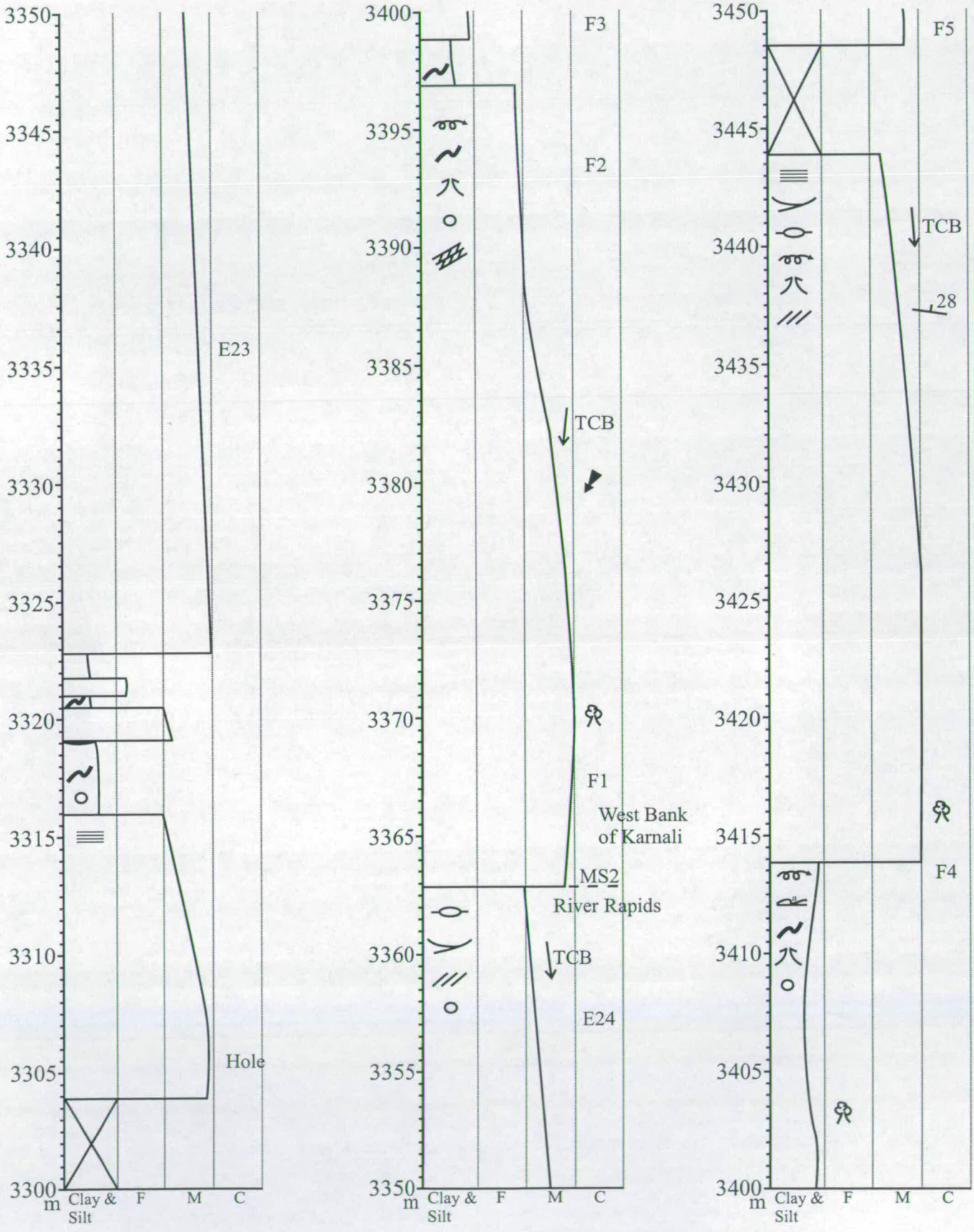

2900
2895
2890
2885
2880
2875
2870
2865
2860
2855
2850
m
Clay &
Silt
F
M
C
38
Stream leads
to small bridge
D75
2950
2945
2940
2935
2930
2925
2920
2915
2910
2905
2900
D84
3000
2995
2990
2985
2980
2975
2970
2965
2960
2955
2950
D88
48
D87

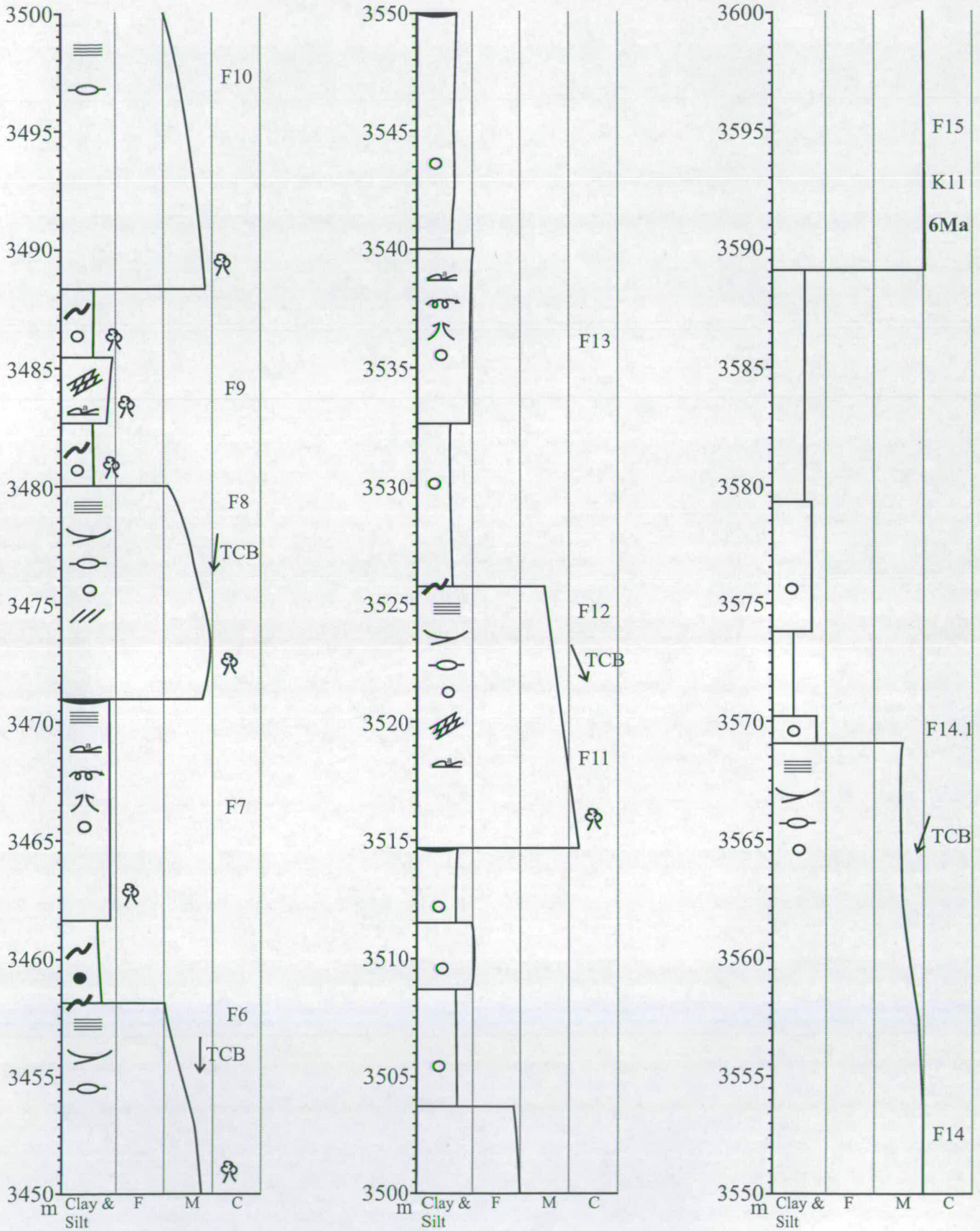

3050
3045
3040
3035
3030
3025
3020
3015
3010
3005
3000
m
Clay &
Silt
F
M
C
D93
D92
D91
D90
3100
3095
3090
3085
3080
3075
3070
3065
3060
3055
3050
TCB
D101
D100
D97
D95
D94
3150
3145
3140
3135
3130
3125
3120
3115
3110
3105
3100
D107
D106
D104
TCB
D103

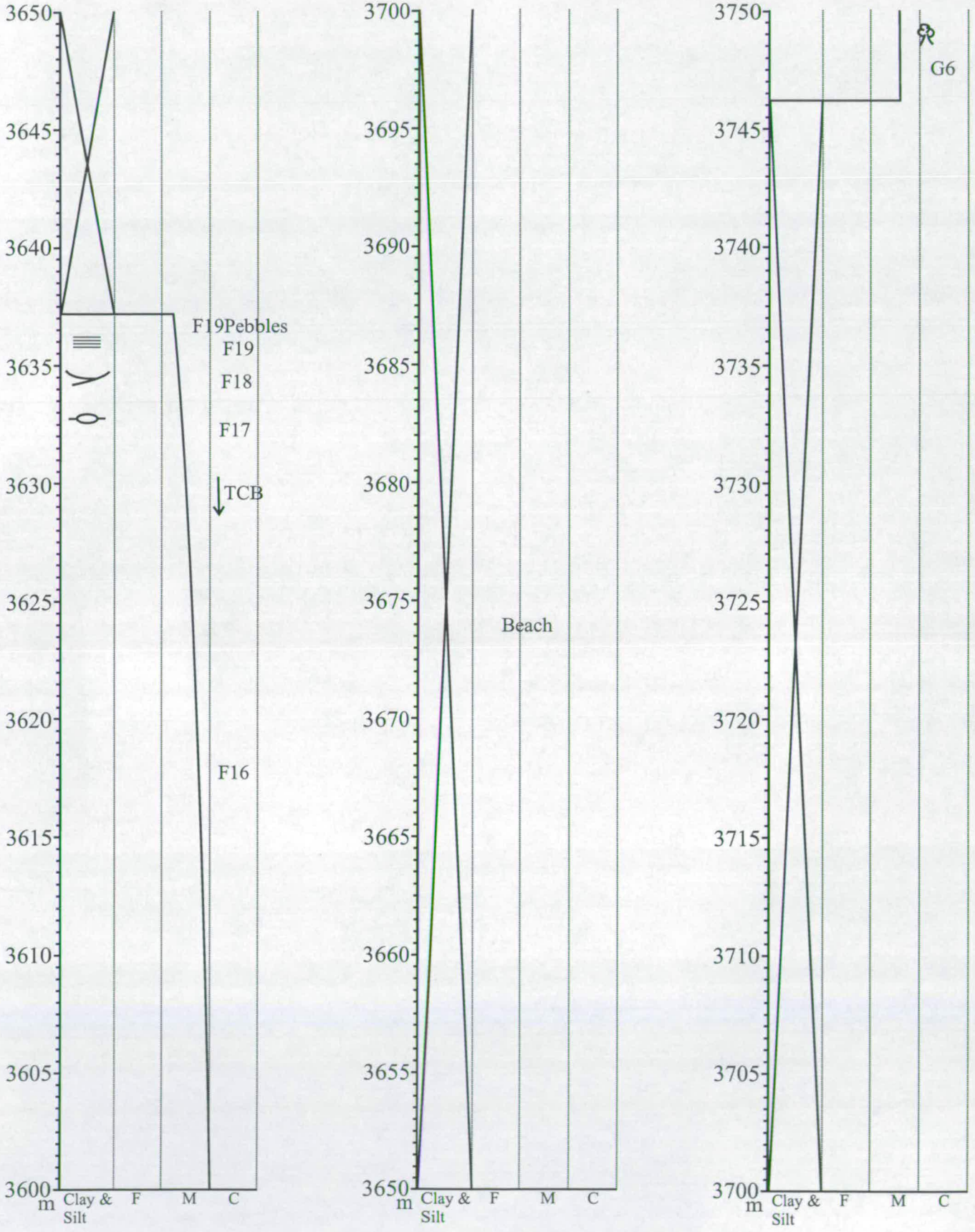

3200
3195
3190
3185
3180
3175
3170
3165
3160
3155
3150
TCB
TCB
m
Clay &
Silt
F
M
C

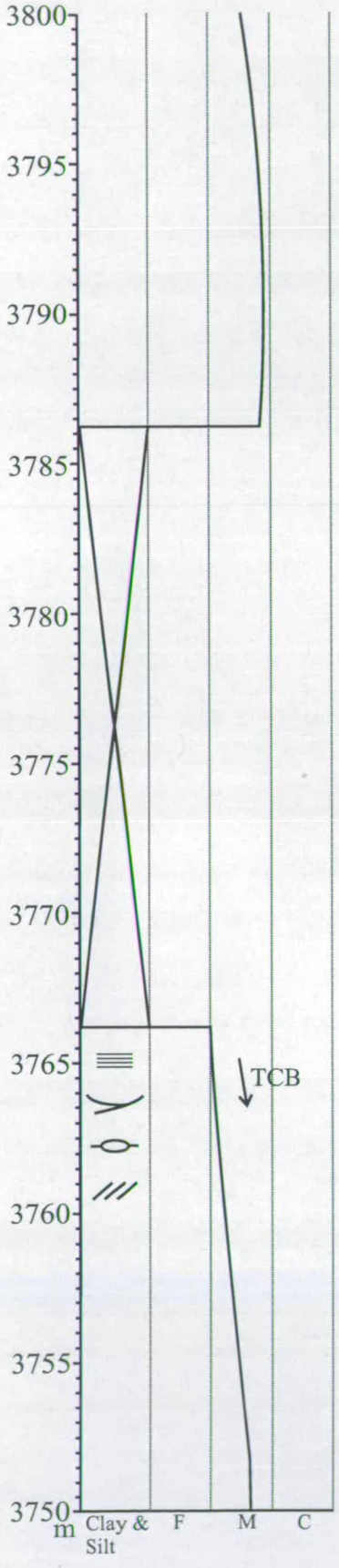

3250
3245
3240
3235
3230
3225
3220
3215
3210
3205
3200
Hole
K10
6.9Ma
m
Clay &
Silt
F
M
C

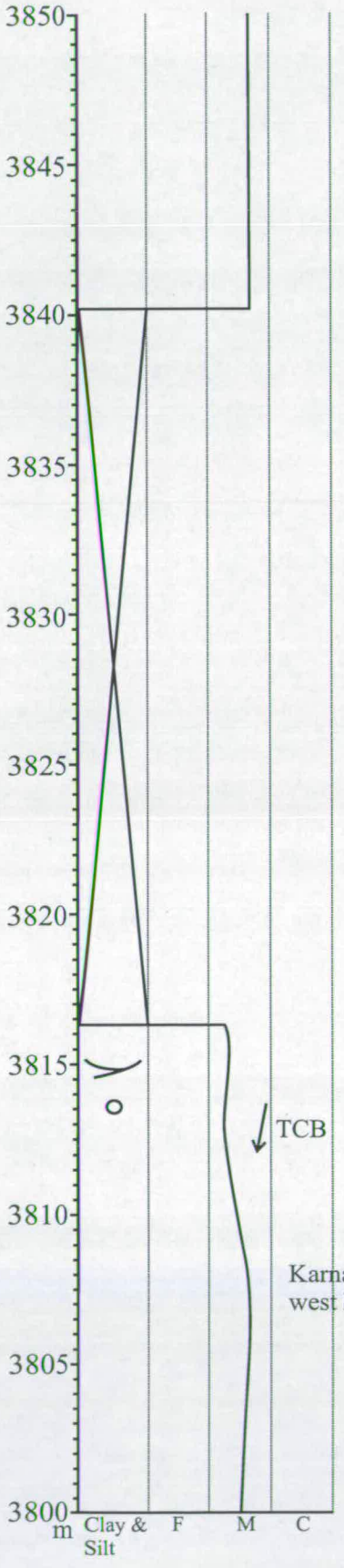

3300
3295
3290
3285
3280
3275
3270
3265
3260
3255
3250
Hole
TCB
m
Clay &
Silt
F
M
C

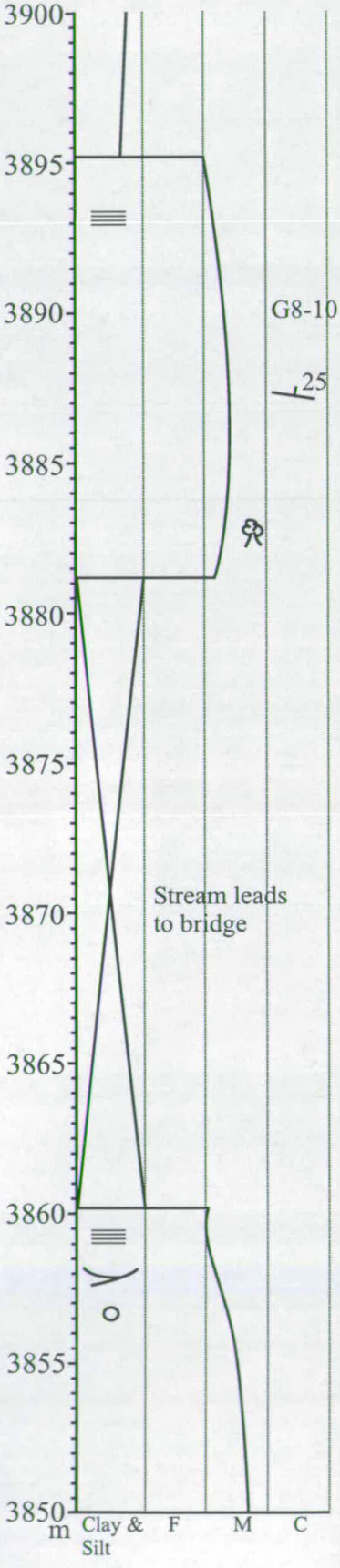

3350
3345
3340
3335
3330
3325
3320
3315
3310
3305
3300
m
Clay & Silt
F
M
C
E23
Hole
3400
3395
3390
3385
3380
3375
3370
3365
3360
3355
3350
F3
F2
TCB
F1
West Bank of Karnali
MS2
River Rapids
TCB
E24
3450
3445
3440
3435
3430
3425
3420
3415
3410
3405
3400
F5
TCB
28
F4

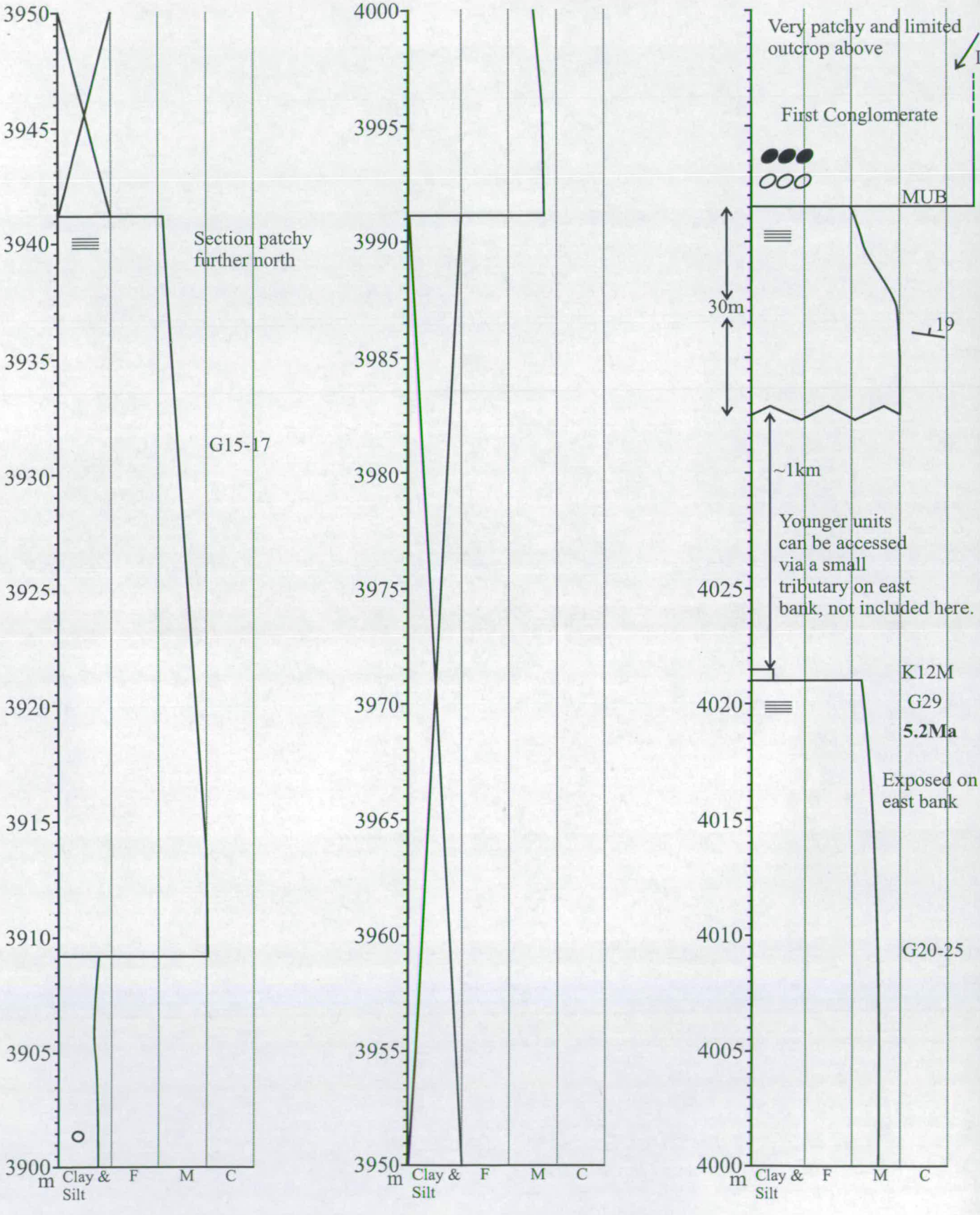

3500
3495
3490
3485
3480
3475
3470
3465
3460
3455
3450
F10
F9
F8
TCB
F7
F6
TCB
m
Clay &
Silt
F
M
C
3550
3545
3540
3535
3530
3525
3520
3515
3510
3505
3500
F13
F12
TCB
F11
m
Clay &
Silt
F
M
C
3600
3595
3590
3585
3580
3575
3570
3565
3560
3555
3550
F15
K11
6Ma
F14.1
TCB
F14
m
Clay &
Silt
F
M
C


3650
3645
3640
3635
3630
3625
3620
3615
3610
3605
3600
m
Clay & Silt
F
M
C
F19Pebbles
F19
F18
F17
TCB
F16
3700
3695
3690
3685
3680
3675
3670
3665
3660
3655
3650
Beach
3750
3745
3740
3735
3730
3725
3720
3715
3710
3705
3700
G6


3800
3795
3790
3785
3780
3775
3770
3765
3760
3755
3750
m
Clay &
Silt
F
M
C
TCB


3850
3845
3840
3835
3830
3825
3820
3815
3810
3805
3800
m
Clay &
Silt
F
M
C
TCB
Karnali bends
west here


3900
3895
3890
3885
3880
3875
3870
3865
3860
3855
3850
m
Clay &
Silt
F
M
C
G8-10
25
Stream leads
to bridge


3950
3945
3940
3935
3930
3925
3920
3915
3910
3905
3900
m
Clay & Silt
F
M
C
Section patchy further north
G15-17
4000
3995
3990
3985
3980
3975
3970
3965
3960
3955
3950
Very patchy and limited outcrop above
First Conglomerate
MUB
30m
19
~1km
Younger units can be accessed via a small tributary on east bank, not included here.
4025
4020
4015
4010
4005
4000
K12M
G29
5.2Ma
Exposed on east bank
G20-25

IV Whole-rock Nd-Sr geochemistry notes

The Siwalik mudstone samples were reduced in size using a hydraulic rock breaker and then reduced to flour in a ball mill (agate balls to limit contamination). After chemical dissolution the samples are ready for mass spectrometry.

Thermal ionisation mass spectrometry (TIMS) was used to calculate the relative abundances of isotopes. In TIMS the analyte is emitted from a heated metal filament (we used Ta and Re filaments), welded onto steel posts and set into a ceramic insulator. The filaments were heated under vacuum to remove volatile contaminants. A chemically purified salt of the analyte is evaporated onto the filament. During analysis the filament is heated to cause evaporation of the neutral atoms from the filament, accompanied by positive ions. The ratio of ions produced to atoms loaded is known as the ionisation efficiency, a principal limitation on the sensitivity of TIMS. Depending on the ionisation efficiency of the element, single, double or triple filament arrangements can be used. The ions are accelerated towards the mass analyser by a high voltage applied between the source and an accelerator slit, and collimated into a tight ion beam by applying smaller potentials to a series of slits. The TIMS source is coupled to an evacuated analyser tube that is curved into an arc between the poles of an electromagnet. The ability of the mass spectrometer to resolve adjacent ion beams depends on the width of the ion beam. The main requirement is that the ion beams create signals with flat peaks. This means that the entire ion beam of a specific isotope should pass into the collector over a significant range of magnetic flux density. The ion current will then remain constant despite

small fluctuations in accelerating voltage and magnetic field. The beams enter the ion current detector (Faraday Cup or Electron Multiplier) through a slit, a narrow slit gives better mass resolution whilst a wider slit gives greater sensitivity.

Once isotopic abundances have been measured the results are normalised into epsilon notation (ε_{Nd}) (DePaolo & Wasserburg, 1976) so that they can be directly compared with other studies using the equation:

$$\varepsilon_{Nd} = ((^{143}Nd/^{144}Nd) / (^{143}Nd/^{144}Nd) \text{ (in chondrites)} - 1) \times 10^4$$

Epsilon notation is when the measured $^{143}Nd/^{144}Nd$ ratio is portrayed relative to the composition of chondritic meteorites (CHUR) (thought to approximate the $^{143}Nd/^{144}Nd$ isotopic composition of the bulk earth) and is expressed in parts per 10^4. It is a measure of the deviation of a sample or sample suite from the expected value in a uniform reservoir, and is a normalising parameter for samples of different age. Chondritic normalisation eliminates the abundance variation between elements with odd and even atomic numbers and allows relative fractionation to be identified (Rollinson, 1993). A negative epsilon value implies source areas with a lower Sm/Nd ratio than CHUR, i.e. an enriched source. For example, the Sm/Nd ratio of continental crust is highly fractionated (< 1) relative to CHUR.

V ^{40}Ar-^{39}Ar dating notes

The ^{40}Ar-^{39}Ar dating technique involves a number of steps, each with their own potential for error. The main steps and the more important technical aspects behind them are dealt with here in the order they are carried out.

The Siwalik samples were initially cleaned and broken up using a circular saw and occasionally a hydraulic rock breaker. In order to break up the individual grains to be able to pick out white micas the broken down samples were then put in a swing mill with a little water. The water and a short crushing time means individual grains are not reduced to flour. The crushing puck was made of agate and so any contamination should have been minor. The samples are sieved into main size fractions prior to hand picking.

The white micas were hand picked using tweezers under a binocular microscope. Grains were chosen for size, thickness, and freshness. The main requirement when sampling white micas is that the physical size of the grain is greater than the distance an argon atom has to diffuse to be effectively released from the mineral structure. The effective diffusion radius for argon is commonly much less than the physical dimensions of rock crystals.

The ^{40}Ar-^{39}Ar method requires a sample of precisely known K/Ar age for an indirect determination of the integrated neutron flux (fluence) the sample has received (in our case sanidines from the Fish Canyon tuff and Taylor Creek rhyolite). These samples have a uniform 40Ar* to 40K ratio so that errors related to sample inhomogeneity are

minimised. They are also of a similar age to those expected for the white micas we were dating. The optimum irradiation for a sample is dependent mainly upon its age and K/Ca ratio and so it is beneficial for the monitor and sample to be similar in these properties.

The picked white micas were sealed in aluminium foil pots and sent to the reactor. The main nuclear reaction utilised in the ^{40}Ar-^{39}Ar technique involves the interaction of a neutron with the ^{39}K nucleus, which is transmuted to ^{39}Ar with emission of a proton. Fast neutrons are required for the reaction to proceed and to produce sufficient ^{39}Ar in a reasonable amount of time. Therefore irradiations are carried out in a nuclear reactor (preferably in the core for the highest fast-neutron flux), where fast-neutron fluxes of 10^{12}-10^{14} n/cm^2/s are possible.

Apart from ^{39}Ar, other isotopes of argon can be produced associated with the interaction of neutrons with isotopes of calcium, potassium, argon, and chlorine (Merrihue & Turner, 1966). However, these reactions are usually minor and can be accounted for, especially when using white mica, which has a relatively high K/Ca ratio. The process of obtaining the correct isotopic weights therefore involves a series of corrections for isotopes that would otherwise induce erroneous age values. For example atmospheric ^{40}Ar is corrected for by using ^{36}Ar. If excess ^{36}Ar is produced from reaction with calcium and is not taken into account there will be overcorrection for atmospheric ^{40}Ar, resulting in low apparent ages. ^{37}Ar can be used to correct for both reactor induced ^{36}Ar and ^{39}Ar derived from calcium due to its low abundance in atmospheric argon and low production rates in the reactor. Reactor

induced ^{40}Ar and ^{36}Ar (the main interferences to the technique) can be minimised by careful selection of the neutron flux (fluence) to which the sample is subjected. Because the nuclear reactor will have a neutron flux gradient across it, monitor minerals were placed in known geometric relation to the unknown samples, so that it was possible to interpolate J (irradiation parameter) values for each unknown.

The irradiated white micas were placed in copper trays and vaporised using a continuous-wave laser to extract the argon, which is then purified. Following isolation of the mass spectrometer from its pumps, the purified gas sample is admitted to the mass spectrometer to be analysed isotopically. By this method the relative abundances of the different argon isotopes provide the necessary information for age calculation using the equation:

$$t = 1/\lambda \ln (1 + J^{40}Ar^{*}/^{39}Ar_{K})$$

where t is the age of the white mica, λ is a constant of proportionality known as the decay constant (the probability of any particular atom decaying per unit time), J is the irradiation parameter, $^{40}Ar^{*}$ is the amount of radiogenic argon, and $^{39}Ar_{K}$ is the ^{39}Ar produced from ^{39}K during the irradiation.

Every fifth run was a blank, meaning that the mass spectrometer was set to calculate isotopic weights but no sample was heated by the laser. The smaller the blank, the smaller the amount of argon that can be used to derive satisfactorily accurate ages. As expected, we found the blank to gradually decrease during successive sample runs and then increase each time a new tray of white micas was added.

VI Fission-track dating notes

Fission-tracks are damaged zones of a crystal's lattice, caused by the spontaneous nuclear fission of ^{238}U (Fleischer et al., 1975). The tracks are linear trails of disrupted atoms which result when charged nuclear particles travel through insulating solids (Fleischer et al., 1975). They occur exclusively by the spontaneous fission of ^{238}U in geological samples. The preferred analytical method is the external detector zeta calibration. The mineral surface is polished and chemically etched to enlarge spontaneous surface tracks so that they can be counted. Confined tracks below the surface are also revealed if the etchant can travel through surface tracks, cleavage, or fractures. A uranium-free detector (plastic foil or muscovite) is sealed against the polished surface, and the detector and mineral grain are sent for irradiation. Irradiation induces fission in ^{235}U. During fission, some heavy particles cross the interface between the mineral and the detector, producing a mirror image of the original grain. The detector is then etched to reveal the induced tracks, which allows an estimation of the uranium parent concentration of the mineral grain. Comparison with the number of spontaneous tracks, which are a proxy for the concentration of the daughter product, allows a fission-track age to be calculated using the equation:

$$t = 1/\lambda d \, Ln \, (\lambda d \, \rho s/\rho i \, \rho d \zeta g + 1)$$

where t = age; ρs and ρi are the spontaneous and induced track densities (number of tracks/unit area); λd is the α decay constant of ^{238}U; ρd is the track density in a

dosimeter (a glass of known uranium concentration), which is used to monitor the neutron flux in the reactor; g is known as the geometry factor (allows for the fact that the spontaneous tracks intersecting the surface represent a sample from twice the effective volume than the induced tracks represent); and ζ is a constant of proportionality made up of the other parameters, including the fission decay constant and neutron capture cross-section.

Fission-tracks are metastable features that fade or anneal and shorten over time. Therefore fission-track length is an important measurement. The probability of a longer track intersecting the polished surface is greater than that for a shorter track. Therefore the apparent sample age should be older for a sample with longer tracks with all else being equal. As tracks are shortened with increasing temperature, the probability of seeing them decreases and so does the sample age.